

María del Rosario Flórez García

High spectral and spatial
resolution for the direct elemental
and isotopic analysis of solid
samples and complex matrices

Departamento
Química Analítica

Director/es
Resano Ezcaray, Martín
Vanhaecke, Frank

<http://zaguan.unizar.es/collection/Tesis>



Universidad
Zaragoza

Tesis Doctoral

HIGH SPECTRAL AND SPATIAL RESOLUTION FOR
THE DIRECT ELEMENTAL AND ISOTOPIC
ANALYSIS OF SOLID SAMPLES AND COMPLEX
MATRICES

Autor

María del Rosario Flórez García

Director/es

Resano Ezcaray, Martín
Vanhaecke, Frank

UNIVERSIDAD DE ZARAGOZA

Química Analítica

UNIVERSITY OF ZARAGOZA
DEPARTMENT OF ANALYTICAL CHEMISTRY
&
GHENT UNIVERSITY
DEPARTMENT OF ANALYTICAL CHEMISTRY



Departamento de
Química Analítica
Universidad Zaragoza



High spectral and spatial
resolution for the direct elemental
and isotopic analysis of solid
samples and complex matrices

DISSERTATION

María del Rosario Flórez García

Zaragoza, 2014

The current doctoral thesis is presented as a compendium of the following articles:

M. Aramendía, M.R. Flórez, M. Piette, F. Vanhaecke, M. Resano. **Al determination in whole blood samples as AlF via high-resolution continuum source graphite furnace molecular absorption spectrometry: potential application to forensic diagnosis of drowning.** *Journal of Analytical Atomic Spectrometry* 26 (2011) 1964-1973

M. Resano, M.R. Flórez. **Direct determination of sulfur in solid samples by means of high-resolution continuum source graphite furnace molecular absorption spectrometry using palladium nanoparticles as chemical modifier.** *Journal of Analytical Atomic Spectrometry* 27 (2012) 401-412

M.R. Flórez, M. Resano. **Direct determination of bromine in plastic materials by means of solid sampling high-resolution continuum source graphite furnace molecular absorption spectrometry.** *Spectrochimica Acta Part B* 88 (2013) 32-39

M. Resano, M.R. Flórez, E. García-Ruiz. **Progress in the determination of metalloids and non-metals by means of high-resolution continuum source atomic or molecular absorption spectrometry. A critical review.** *Analytical and Bioanalytical Chemistry* 406 (2014) 2239-2259

M. Resano, L. Rello, M. Flórez, M.A. Belarra. **On the possibilities of high-resolution continuum source graphite furnace atomic absorption spectrometry for the simultaneous or sequential monitoring of multiple atomic lines.** *Spectrochimica Acta Part B* 66 (2011) 321-328

M. Resano, M.R. Flórez, E. García-Ruiz. **High-resolution continuum source atomic absorption spectrometry for the simultaneous or sequential monitoring of multiple lines. A critical review of current possibilities.** *Spectrochimica Acta Part B* 88 (2013) 85-97

R. Evens, K.A.C. De Schamphelaere, L. Balcaen, Y. Wang, K. De Roy, M. Resano, M.R. Flórez, P. Van der Meeren, N. Boon, F. Vanhaecke, C.R. Jansen. **Liposomes as an alternative delivery system for investigating dietary metal toxicity to *Daphnia magna*.** *Aquatic Toxicology* 105 (2011) 661-668

R. Evens, K.A.C. De Schamphelaere, L. Balcaen, Y. Wang, K. De Roy, M. Resano, M.R. Flórez, N. Boon, F. Vanhaecke, C.R. Jansen. **The use of liposomes to differentiate between the effects of nickel accumulation and altered food quality in *Daphnia magna* exposed to dietary nickel.** *Aquatic Toxicology* 109 (2012) 80-89

M.R. Flórez, M. Aramendía, M. Resano, A.C. Lapeña, L. Balcaen, F. Vanhaecke. **Isotope ration mapping by means of laser ablation-single collector-ICP-mass spectrometry: Zn tracer studies in thin sections of *Daphnia magna*.** *Journal of Analytical Atomic Spectrometry* 28 (2013) 1005-1015



Departamento de
Química Analítica
Universidad Zaragoza



Dr. D. Martín Resano Ezcaray, Profesor Titular del Departamento de
Química Analítica de la Universidad de Zaragoza

y

Dr. D. Frank Vanhaecke, Catedrático del Departamento de Química
Analítica de la Universidad de Gante

CERTIFICAN

Que la presente Memoria para optar al grado de Doctor en Ciencias,
titulada:

**“High spectral and spatial resolution for the direct elemental and
isotopic analysis of solid samples and complex matrices”**

Se ha realizado en los Laboratorios del Departamento de Química
Analítica de la Universidad de Zaragoza y del Departamento de Química
Analítica de la Universidad de Gante, bajo nuestra inmediata dirección,
autorizando su presentación en la modalidad de **tesis como compendio
de publicaciones** para proseguir los trámites oportunos en orden a su
calificación por el Tribunal correspondiente.

Zaragoza, a 22 de mayo de 2014

Fdo. Dr. D.
Martín Resano Ezcaray

Fdo. Dr. D.
Frank Vanhaecke

AGRADECIMIENTOS / ACKNOWLEDGEMENTS

Reconozco que, aunque estas sean las primeras hojas, han sido las últimas en las que me he puesto a trabajar escribiendo esta memoria. Si ya es difícil resumir casi cinco años de trabajo experimental en unas pocas hojas, mucho más es encontrar una manera de, con pocas palabras, agradecer tanto y a tantos.

Voy a comenzar, como es de justicia, agradeciendo a mis directores de tesis, Martín Resano y Frank Vanhaecke, que han sido el motor de todo esto. Pienso, sinceramente, que no podía haber caído en mejores manos.

Martín Resano me acogió en su grupo de investigación sin saber muy bien quién iba a aparecer. Así y todo, desde un principio, me recibió con la confianza y la cercanía que han hecho que todo este trabajo haya salido adelante con mucho esfuerzo pero muy poca angustia. Bajo su dirección y motivación, he conseguido interesarme aún más por la química analítica y he aprendido a desarrollar una mente más práctica y más metodológica.

Frank Vanhaecke put his trust in me to be involved in this cotutelle project and has, since then, been welcoming me to his laboratories every summer for my research stays at Ghent University. It has been a great pleasure for me to be so friendly accepted in a representative group in ICPMS and have had the opportunity of getting in touch with the technique with already the best resources.

Me gustaría también agradecer especialmente a Maite Aramendía, cuyos conocimientos y experiencia tienen también su huella en mi formación, y cuya amistad y apoyo me han sido de gran ayuda a lo largo de todo el desarrollo de este trabajo.

Pero, por supuesto, a lo largo de estos años ha habido muchas personas que de una manera u otra han sido para mí imprescindibles y me gustaría mencionar y agradecer:

Al resto de mis compañeros de M.A.R.T.E.: Esperanza García, Miguel Ángel Belarra, Jorge Briceño, Engracia Mozas, Luis Rello, Ana Cris Lapeña y la recientemente abducida, Águeda Cañabate, por su amistad y por formar parte de esta peculiar familia en Zaragoza. Y a todo el departamento de Química Analítica de la Universidad de Zaragoza.

I also would like to thank my colleagues at A&MS group and the S12, those who were before and those who are still: Lieve Balcaen (I'll never forget that I started my research life by your hand), Lara Lobo, Marta Costas, Ana Rúa y Eduardo Bolea ("Frank's Spanish Armada"), Eleonora Balliana and the rest of the people I had the opportunity to meet there during the last three summers: Andrei, Deepti, Winfried, Kris, Lana, Asha, Steven, Veerle, Stepan, Björn, Dmitry, Karen, Karel, Roger, Chantal, Harry, Tine, ... I am sure I'm forgetting somebody and I will be very sorry whenever I find out.

No puedo olvidarme de mencionar al personal de Inycom: Luis de Miguel, Ramón Esteban, Pilar Sariñena, Manuel León y, por supuesto, Fernando Latorre y Sonia Lizondo, que me ayudaron mucho y con paciencia en mis comienzos a entender más a fondo los entresijos del ContrAA 700.

Laboratorios aparte, me gustaría agradecer al personal del C.M.U. Pedro Cerbuna, muy especialmente a Irene, Javier, Mónica y Manu, por toda su ayuda y cariño durante mi estancia en el colegio.

Pero sin el constante apoyo y presencia de mis amigos y mi familia, esto se hubiera hecho muy, muy difícil. Muchísimas gracias a mis padres y a mi hermano, que son mi equilibrio y mi soporte más sólido, de cerca y de lejos. Y muchísimas gracias a Luismi, por aguantarme en los momentos fáciles y, sobretodo, llamar a la cordura y seguir ahí durante y después de los difíciles.

También se lo debo a mis abuelos, a mis tíos y a mis primos. Al resto de las Vs que, aunque cada vez más desperdigadas, seguimos siendo una red segura. A la nueva generación: Elvira, Nahia, Ane y Arán, por la energía con la que llegan y nos contagian a los que ya la vamos perdiendo un poco. A Irene y Elena, por tantos momentos y tantos lacasitos®. Sólo acordarme de todos vosotros me hace sonreír.

Muchas gracias a todos. / Thank you all very much.

This work has been funded by:

- **The Spanish Ministry of Economy and Competitiveness (projects CTQ2009-08606, CTQ2012-33494)**
- **The Aragón Government (Fondo Social Europeo, Fundación ARAID and “Obra Social de IberCaja”)**
- **Ghent University (project BOF 01SB0309)**

STRUCTURE OF THE THESIS

This monograph is presented in the modality of compendium of publications in accordance with the structure established in the Regulations of Doctoral Theses (December 20, 2013 agreement of the Governing Council of the University of Zaragoza). The aforementioned structure is as follows:

- An initial page stating that the current doctoral thesis is a compendium of already published articles. **Complete references** to the articles are herein included.
- **Authorisation** for presenting the thesis as compendium of publications.
- A **general introduction** presenting the works and justifying their **thematic unity**.
- A **dissertation** specifying the goals, methodologies and final conclusions of the research based in the contributions of the doctoral student.
- A **copy** of the articles.
- An **appendix** including the journal's impact factor and thematic area(s) of each of the articles presented, as well as a **justification of the contribution of the doctoral student** if any of the work was carried out in co-authorship.

LIST OF ABBREVIATIONS

AAS	Atomic Absorption Spectrometry
A_{int}	Integrated absorbance
BAM	Bundesanstalt für Materialforschung und -prüfung / Federal Institute for Materials Research and Testing (Berlin, Germany)
BAS	Bureau of Analysed Samples Ltd. (Newby, UK)
BCR	Bureau Communautaire de Références / Community Bureau of Reference (Geel, Belgium)
BFR	Brominated Flame Retardant
c_0	Characteristic concentration
CCD	Charge-coupled device
CRM	Certified Reference Material
FAAS	Flame Atomic Absorption Spectrometry
GFAAS	Graphite Furnace Atomic Absorption Spectrometry
GFMAS	Graphite Furnace Molecular Absorption Spectrometry
HCL	Hollow-Cathode Lamp
HR CS AAS	High-Resolution Continuum Source Atomic Absorption Spectrometry
HR CS GFAAS	High-Resolution Continuum Source Graphite Furnace Atomic Absorption Spectrometry
HR CS GFMAS	High-Resolution Continuum Source Graphite Furnace Molecular Absorption Spectrometry
IBC	Iterative Baseline Correction
IRMM	Institute for Reference Materials and Measurements (Geel, Belgium)
IS	Internal Standard
K-S	Kolmogorov-Smirnov (nonparametric test)
LA-ICPMS	Laser Ablation-Inductively Coupled Plasma Mass Spectrometry

LA-SC-ICPMS	Laser Ablation-Single Collector-Inductively Coupled Plasma Mass Spectrometry
LA-SF-ICPMS	Laser Ablation-Sector Field-Inductively Coupled Plasma Mass Spectrometry
LOD	Limit of Detection
LS AAS	Line Source Atomic Absorption Spectrometry
LSBC	Least-Squares Background Correction
m_0	Characteristic mass
MAS	Molecular Absorption Spectrometry
MAT	Modern Analytical Techniques (Hillsborough, USA)
MS	Mass Spectrometry
NIST	National Institute of Standards and Technology (Gaithersburg, USA)
NPs	Nanoparticles
RSD	Relative Standard Deviation
S/N	Signal-to-Noise Ratio
SEM	Scanning Electron Microscope
SS	Solid Sampling
SS HR CS GFAAS	Solid Sampling High-Resolution Continuum Source Graphite Furnace Atomic Absorption Spectrometry
UV	Ultraviolet

CONTENTS

THEMATIC UNITY	1
I. INTRODUCTION	5
I.1. INSTRUMENTAL CHARACTERISTICS OF HIGH-RESOLUTION CONTINUUM SOURCE ATOMIC ABSORPTION SPECTROMETRY	7
I.1.1. Radiation source	8
I.1.2. Atomization unit	8
I.1.3. Monochromator	8
I.1.4. Detection system	9
I.2. METHODOLOGICAL POSSIBILITIES OF HR CS AAS	9
I.2.1. Multi-line monitoring	10
I.2.1.1. Simultaneous multi-elemental determination	10
I.2.1.2. Monitoring multiplets.....	13
I.2.1.3. Background correction.....	14
I.2.2. Monitoring molecular transitions	15
I.2.3. Direct solid sampling graphite furnace atomic absorption spectrometry applied to the analysis of micro-samples.....	19
I.3. REFERENCES	24
II. DISSERTATION	33
II.1. GENERAL GOALS	35
II.2. INSTRUMENTATION	37
I.2.1. High-resolution continuum source atomic absorption spectrometry - ContrAA 700	37

II.2.2. Laser ablation-single collector-inductively coupled plasma mass spectrometry - UP193HE laser coupled to Element XR	38
II.2.3. Additional instrumentation.....	40
II.3. METHODOLOGY AND DISCUSSION OF RESULTS	41
II.3.1. Monitoring of non-metals	41
II.3.1.1. Al determination in whole blood samples as AlF <i>via</i> high-resolution continuum source graphite furnace molecular absorption spectrometry: potential application to forensic diagnosis of drowning.....	41
II.3.1.2. Direct determination of S in solid samples by means of high-resolution continuum source graphite furnace molecular absorption spectrometry using Pd nanoparticles as chemical modifier	52
II.3.1.3. Direct determination of Br in plastic materials by means of solid sampling high-resolution continuum source graphite furnace molecular absorption spectrometry	66
II.3.1.4. Progress in the determination of metalloids and non-metals by means of high-resolution continuum source atomic or molecular absorption spectrometry. A critical review	77
II.3.2. Multi-line monitoring.....	79
II.3.2.1. On the possibilities of high-resolution continuum source graphite furnace atomic absorption spectrometry for the simultaneous or sequential monitoring of multiple atomic lines	79
II.3.2.2. High-resolution continuum source atomic absorption spectrometry for the simultaneous or sequential monitoring of multiple lines. A critical review of current possibilities.....	88
II.3.3. Microsampling	89
II.3.3.1. Simultaneous direct determination of Ni and Cd in <i>Daphnia magna</i> specimens by means of high-resolution continuum source graphite furnace atomic absorption spectrometry for eco-toxicological assessment purposes.....	89

II.3.3.2. Isotope ratio mapping by means of laser ablation-single collector-ICP-mass spectrometry: Zn tracer studies in thin sections of <i>Daphnia magna</i>	98
II.4. CONCLUSIONS.....	109
II.5. REFERENCES.....	111
III. PUBLICATIONS	123
Al determination in whole blood samples as AlF <i>via</i> high-resolution continuum source graphite furnace molecular absorption spectrometry: potential application to forensic diagnosis of drowning	125
Direct determination of sulfur in solid samples by means of high-resolution continuum source graphite furnace molecular absorption spectrometry using palladium nanoparticles as chemical modifier	135
Direct determination of bromine in plastic materials by means of solid sampling high-resolution continuum source graphite furnace molecular absorption spectrometry	147
Progress in the determination of metalloids and non-metals by means of high-resolution continuum source atomic or molecular absorption spectrometry. A critical review	155
On the possibilities of high-resolution continuum source graphite furnace atomic absorption spectrometry for the simultaneous or sequential monitoring of multiple atomic lines.....	177
High-resolution continuum source atomic absorption spectrometry for the simultaneous or sequential monitoring of multiple lines. A critical review of current possibilities	185
Liposomes as an alternative delivery system for investigating dietary metal toxicity to <i>Daphnia magna</i>	199
The use of liposomes to differentiate between the effects of nickel accumulation and altered food quality in <i>Daphnia magna</i> exposed to dietary nickel.....	207

Isotope ration mapping by means of laser ablation-single collector-ICP- mass spectrometry: Zn tracer studies in thin sections of <i>Daphnia magna</i>	217
GENERAL OUTLINE AND CONCLUSIONS	229
General outline and conclusions	231
Resumen y conclusiones generales	235
Algemeen overzicht en conclusies	241
APPENDIX	247

THEMATIC UNITY

The work presented in this dissertation has been developed within the area of expertise and analytical resources of both M.A.R.T.E. (Métodos de Análisis Rápidos con Técnicas Espectroscópicas), research group of the Department of Analytical Chemistry of the University of Zaragoza, and A&MS (Atomic and Mass Spectroscopy), research group of the department of Analytical Chemistry of Ghent University.

The work carried out focused on the potential of atomic techniques for the direct analysis of solid samples and complex matrices. Within this scheme, it has been structured in two main blocks of study supported by the compendium of nine publications: i) the exploration of the analytical benefits introduced by high-resolution continuum source atomic absorption spectrometry (HR CS AAS) in terms of spectral resolution; and ii) the improvement of spatial resolution in the direct analysis of solid micro-samples.

The first block, regarding AAS applications with high spectral resolution, covered the possibilities opened with the introduction of commercially available HR CS AAS instruments for multi-line monitoring and multi-element determination as well as the suitability for monitoring broad molecular spectra, which has demonstrated to be particularly beneficial for the determination of non-metals.

Regarding the evaluation of direct solid sampling applied to the determination of micro-samples, the benefits of HR CS AAS have been investigated and complemented with an application developed by means of laser ablation inductively coupled plasma mass spectrometry (LA-ICPMS) to collect isotopic information in order to produce isotope ratio images with high spatial resolution, which is obviously possible only when using MS.

Schematically, the enclosed articles may be assembled as follows:

A) Evaluation of the spectral resolution featured by HR CS AAS

a.i) Monitoring of non-metals by means of HR CS MAS

a.i.1) M. Aramendía, M.R. Flórez, M. Piette, F. Vanhaecke, M. Resano. **Al determination in whole blood samples as AIF via high-resolution continuum source graphite furnace molecular absorption spectrometry: potential application to forensic diagnosis of drowning.** *Journal of Analytical Atomic Spectrometry* 26 (2011) 1964-1973

a.i.2) M. Resano, M.R. Flórez. **Direct determination of sulfur in solid samples by means of high-resolution continuum source graphite furnace molecular absorption spectrometry using palladium nanoparticles as chemical modifier.** *Journal of Analytical Atomic Spectrometry* 27 (2012) 401-412

a.i.3) M.R. Flórez, M. Resano. **Direct determination of bromine in plastic materials by means of solid sampling high-resolution continuum source graphite furnace molecular absorption spectrometry.** *Spectrochimica Acta Part B* 88 (2013) 32-39

a.i.4) M. Resano, M.R. Flórez, E. García-Ruiz. **Progress in the determination of metalloids and non-metals by means of high-resolution continuum source atomic or molecular absorption spectrometry. A critical review.** *Analytical and Bioanalytical Chemistry* 406 (2014) 2239-2259

a.ii) Multi-line monitoring

a.ii.1) M. Resano, L. Rello, M. Flórez, M.A. Belarra. **On the possibilities of high-resolution continuum source graphite furnace atomic absorption spectrometry for the simultaneous or sequential monitoring of multiple atomic lines.** *Spectrochimica Acta Part B* 66 (2011) 321-328

a.ii.2) M. Resano, M.R. Flórez, E. García-Ruiz. **High-resolution continuum source atomic absorption spectrometry for the simultaneous or sequential monitoring of multiple lines. A critical review of current possibilities.** *Spectrochimica Acta Part B* 88 (2013) 85-97

B) Spatial resolution in the direct determination of solid micro-samples

b.i) Direct determination of *Daphnia magna* specimens by means of HR CS AAS

b.i.1) R. Evens, K.A.C. De Schamphelaere, L. Balcaen, Y. Wang, K. De Roy, M. Resano, M.R. Flórez, P. Van der Meer, N. Boon, F. Vanhaecke, C.R. Jansen. **Liposomes as an alternative delivery system for investigating dietary metal toxicity to *Daphnia magna*.** *Aquatic Toxicology* 105 (2011) 661-668

b.i.2) R. Evens, K.A.C. De Schamphelaere, L. Balcaen, Y. Wang, K. De Roy, M. Resano, M.R. Flórez, N. Boon, F. Vanhaecke, C.R. Jansen. **The use of liposomes to differentiate between the effects of nickel accumulation and altered food quality in *Daphnia magna* exposed to dietary nickel.** *Aquatic Toxicology* 109 (2012) 80-89

b.ii) Isotope ratio mapping of thin sections of *Daphnia magna* specimens by means of LA-single collector-ICPMS (LA-SC-ICPMS)

M.R. Flórez, M. Aramendía, M. Resano, A.C. Lapeña, L. Balcaen, F. Vanhaecke. **Isotope ratio mapping by means of laser ablation-single collector-ICP-mass spectrometry: Zn tracer studies in thin sections of *Daphnia magna*.** *Journal of Analytical Atomic Spectrometry* 28 (2013) 1005-1015

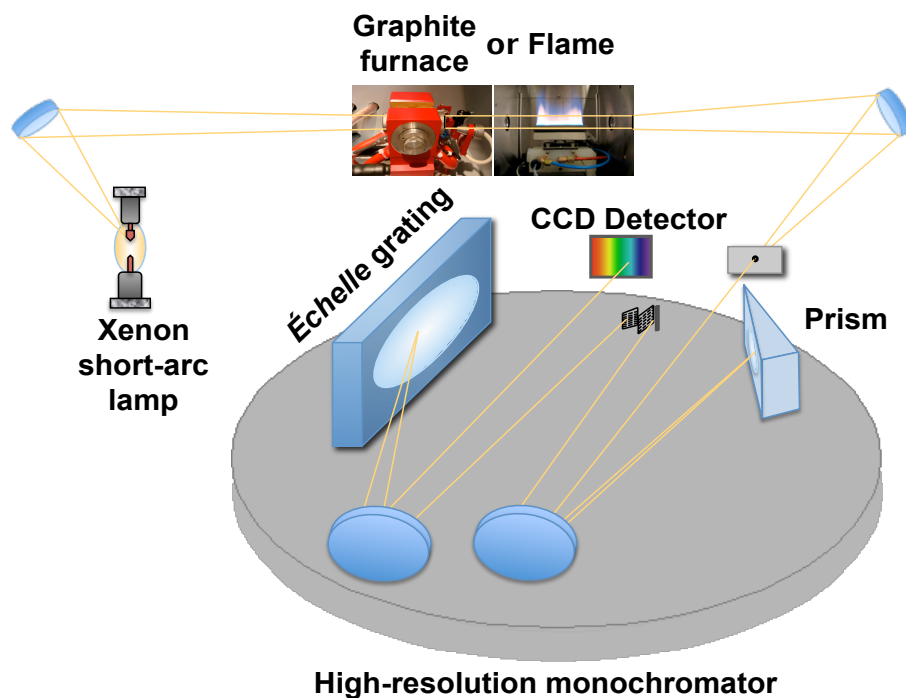


I. Introduction

Several studies have been carried out to date regarding the capabilities of HR CS AAS since the development of the first instrumental prototype proposed by Becker-Ross and co-workers [1,2] at the beginning of this last century and, more extensively, since its appearance on the market. Comparative advantages over classic line source AAS (LS AAS) instruments become evident when paying attention to its instrumental setup:

I.1. INSTRUMENTAL CHARACTERISTICS OF HIGH-RESOLUTION CONTINUUM SOURCE ATOMIC ABSORPTION SPECTROMETRY

Figure I.1. Setup of a high-resolution continuum source atomic absorption spectrometer.



I.1.1. Radiation source

The radiation source was replaced by a sole high-energy Xe short arc lamp, working under “hot-spot” mode, that reaches temperatures of about 10,000 K. The intensity gain for most of the elements (at least 1 or 2 orders of magnitude higher) allow better detection limits facing hollow-cathode lamps (HCL). Also advantageous is the fact that with just one lamp a spectral range from the far ultraviolet region (185 nm) to the near infrared (900 nm) is covered, making it possible to explore elements for which no HCL is available.

I.1.2. Atomization unit

The instrument may be equipped with both flame and/or graphite furnace atomization systems. In this work only the graphite furnace device was employed for all AAS measurements due to its potential to deal with direct solid sampling (SS) analyses. Therefore, all the discussions of this work will be referred to graphite furnace AAS (GFAAS), unless noted otherwise.

I.1.3. Monochromator

The monochromation system is composed of a 300 mm quartz prism and a 400 mm focal length echelle grating monochromator. This double monochromator is necessary to ensure a resolution power in the range of 140,000 (spectral band width of less than 2 pm for 200 nm), for it to be capable of achieving comparable sensitivities to those of the LS instruments for each element and, therefore, optimum signal-to-noise ratios (S/N). An internal Ne lamp is responsible of an active wavelength-stabilization attaining precision better than ± 0.2 pm.

I.1.4. Detection system

The greater methodological potential of the instrument however lies in the detection system: that is a charge-coupled device (CCD) array with typically 588 pixels, of which just 200 are used for analytical purposes while the rest remains available for the correction of all the wavelength-independent spectral events recorded in each pixel at the same time (lamp's flickering, variations in the transmission of the atomizer...).

As every pixel is illuminated simultaneously and read out and evaluated independently, the system essentially works with 200 independent detectors. The recorded spectral range varies from 0.2 to 1.0 nm depending on the wavelength. Within that spectral window, just a few pixels (normally 3) are used to measure atomic absorption, so the rest of the 200 pixels can be devoted to correction purposes. Besides, information of not only the line of interest but of its environment is always available, and an important portion of the work presented in this dissertation is based on making the most out of this aspect.

I.2. METHODOLOGICAL POSSIBILITIES OF HR CS AAS

Of all advantages that the HR CS AAS instrumentation incorporates in comparison with LS AAS (improved signal stability, superior potential for background correction, improved linearity...) [3] this work is partially focused on those regarding the new methodological possibilities derived from the fact that a 200 pixels spectral window is recorded in each measurement. Most specifically the main topics to be covered are:

- i) Multi-line monitoring of absorption lines for either the same or different analytes

- ii) Monitoring of molecular transitions
- iii) Direct solid sampling. Analysis of microsamples.

I.2.1. Multi-line monitoring

I.2.1.1. Simultaneous multi-elemental determination

One of the main handicaps of LS AAS was its poor potential for carrying out multi-element analyses. HR CS AAS brings up the opportunity to fully exploit the fact that a range of the spectrum is monitored in each measurement and therefore any information gathered within that spectral window may be used for analytical purposes.

There is however an important instrumental limitation and that is precisely the very small portion of the spectrum that can be simultaneously monitored: from 0.2-0.3 nm in the far-UV region (where most of the main resonant atomic lines are found) until 0.5 nm approaching the visible region up to almost 1 nm at 800 nm wavelength [4-7].

In this way, the possibilities for developing truly simultaneous multi-element determinations are subject to the compliance with the following premises:

- The atomic lines of the analytes of interest should be located close enough to fit within the spectral window allowing proper baseline adjustment but separate enough not to pose a spectral interference with each other if, for instance, broadening of one of the lines of interest happens when high amounts of one of the elements monitored are present.
- The sensitivity of the lines has to be adequate to the expected content of the corresponding element in the samples under study. That is, the sensitivity ratio between lines of the target elements must be of the

same order as the concentration ratio for those elements in the sample. It might be considered that the election of the pixels for acquiring the analytical signal can be done so to adapt the sensitivity of one line without affecting the others (*e.g.* if a line is quite wide, maybe side pixels would be preferred over centre pixels for that particular line).

Finding lines for several elements within the same spectral window is easier when the determination of elements with a great amount of usable lines along the spectrum, such as Co, Cr, Fe, Ni or Ti [6] is aimed at. With this instrumentation, use of secondary lines is very suitable as, differently from line sources, the available source intensity of this continuum lamp is practically the same for the whole spectrum [6,8]. This implies that better S/N are to be achieved when measuring secondary lines compared to line sources, ultimately resulting in better limits of detection (LODs).

At this point, two possible situations may appear:

- The target elements show similar thermochemical behaviour. Given this case, as their volatilities will be similar, the same optimum temperature program and chemical modifier/s (if needed) could be applied [9-11].
- The elements under study show different thermochemical behaviour. In this situation the use of compromise conditions would be needed. The pyrolysis temperature has to be adjusted so to avoid losses of the most volatile elements while assuring the removal of the potential matrix interferences. Besides, the atomization temperature must be sufficiently high to atomize the most refractory element without decreasing too much the signal of the most volatile analyte. Additionally, a chemical modifier could be selected on in order to

stabilize volatile analytes, taking care not to over-stabilize the refractory ones [12].

It is worth mentioning that for the latter case, a sequential approach may also be considered [13-16], where not only the optimal chemical modifier amount and temperature program for each line could be chosen (the atomization temperature of the most volatile may act as pyrolysis temperature of the following) but also the wavelength can be rapidly changed, allowing to measure each analyte under adequate sensitivity conditions. This sequential approach for multi-line monitoring is the one usually preferred when flame is used as the atomization unit as, unlike with a graphite furnace, a continuous signal is obtained and flame conditions can be changed relatively fast [17].

Taking the simultaneous approach into account, the use of internal standards (IS) for this analytical technique might also be implemented. The conditions that need to be fulfilled for the successful use of an IS are: i) the IS should be an element not present in the sample at a significant level; ii) the thermochemical behaviour of the IS should be similar to that of the analyte/s; iii) the signal of the IS, as well as the signal of the analyte, should lie within the linear range, and the ratio analyte/IS should be as close to the unity as possible. In addition, it is preferable to simultaneously monitor both IS and analyte in the same spectral window in order to properly compensate for any fluctuation occurring during the measurements or for any wavelength-dependant matrix effect. Nevertheless, the use of internal standardization with HR CS AAS has only been explored before in few papers, mainly based on flame AAS (FAAS) by means of a fast sequential mode [18-21].

This doctoral thesis will evaluate and compare strategies for determining simultaneously or sequentially two elements of different volatility by means of HR CS AAS.

I.2.1.2. Monitoring multiplets

This is another advantageous situation derived from monitoring a portion of the spectrum in which several lines of the same analyte are available within the spectral window.

This case is frequent when aiming to determine non-metals [22] by means of molecular absorption spectrometry (MAS) as it is further discussed in the following section. However, is not infrequent to encounter multiplets of atomic lines, particularly when targeting transition metals such as Co, Cr, Fe, Mn, Ni or Ti.

Again, a couple of different beneficial situations may occur:

- Different relative sensitivities between the lines of the multiplet [23]. The linear behaviour for each atomic line would be significantly different and so the global linear range attainable could be increased. In this case, the optimum analytical line may be chosen in order to adequately adapt the sensitivity to the analyte content in the sample, avoiding further sample treatments such as dilution, which is very hard to carry out when aiming at direct analysis of solid samples.
- Similar relative sensitivities between the lines of the multiplet. The most direct advantage given this case is the chance to improve the reliability of the results, identifying potential spectral overlaps. An approach to improve limits of detection may also be applied in this situation by summing the intensity values of the lines to provide a higher sensitivity [24]. This strategy would be counter-productive in

the case of lines with very different sensitivity as the addition of the least sensitive lines would significantly increase the noise level.

This doctoral thesis will try to demonstrate these potential capabilities in the context of direct analysis of solid samples and complex matrices.

I.2.1.3. Background correction

The main improvement featured by this three-dimensional detection system is the capability for evidencing spectral interferences in the vicinity of the analytical absorption line, as all the transitions are simultaneously monitored.

In most cases, it is possible to avoid the interferences by carefully optimizing the temperature program and/or by addition of a chemical modifier. However, there are situations when mathematical approaches need to be applied in order to correct for the interfering signal. This is particularly common when the interfering species is a stable diatomic molecule such as CS, NO, PO or SiO, highly prone to be formed in a graphite furnace, which generates a rapidly changing and structured background along the monitored spectral range. It is possible then to proportionally subtract the interfering signal from the obtained spectrum by applying a least-squares algorithm (Least-Squares Background Correction, LSBC) [2,6,25-27]. This approach is feasible providing that a reference spectrum is available, that is a clean absorption spectrum of the interfering species without any contribution from the analyte/s.

To apply this strategy it is essential as well that the interfering species, whether it be molecular or atomic, shows, at least, a second interference-free line available within the analytical window. This is because the LSBC

algorithm is based on the assumption that the relation between the intensities of the interfering transitions should always be constant [6].

This doctoral thesis will apply this methodology in different situations where it could prove beneficial, both when monitoring atomic or molecular spectra.

I.2.2. Monitoring molecular transitions

Determination of non-metals by means of AAS has always been a challenge. Primarily because most of the main resonant lines for non-metals lie in the vacuum-UV region below 190 nm, out of reach for the currently available commercial spectrometers [28]. P is the only element of this group that offers the possibility for direct determination based on the presence of a non-resonance line (the doublet at 213.547/213.618) suitable for AAS monitoring [29] that, although not free of spectral overlaps, may offer sufficient sensitivity for some applications [30,31].

Alternative methods to determine non-metals by means of AAS were based on indirect determinations, whereas the species of interest reacts with another one which is easier to monitor [32,33], or on MAS [22].

Regarding the latter, with LS instrumentation there was the need of finding a HCL of an element that emits radiation somewhere within the area where the molecular transition was expected to occur, and taking into account that, when using low resolution monochromators, this molecular transitions will appear as broad absorption bands, it was quite feasible to find a suitable lamp. However the background correction issue supposes an important hurdle to this strategy, as the rest of the absorption monitored within the region of the monochromator not overlapping with the narrow emission line of the HCL will be dealt with as if it was background signal

(i.e. it will be subtracted from the absorbance measured with the HCL) [22].

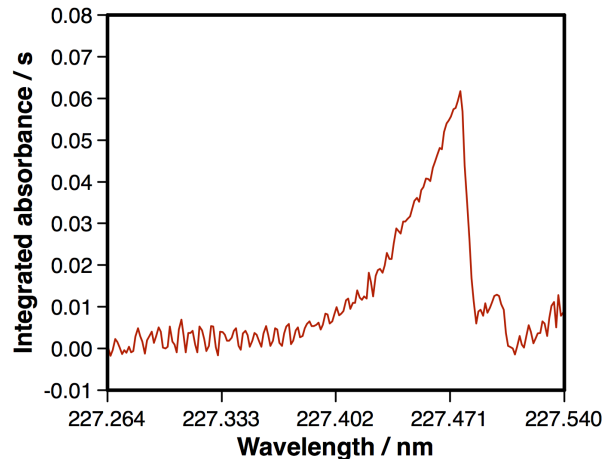
Although HR CS AAS instrumentation still cannot achieve sufficient intensity to measure in the vacuum-UV region, it has introduced important novelties for MAS methodologies, particularly due to its detection system.

At volatilization temperatures high enough a few diatomic molecules, stable in gas phase, may be produced. Some of these molecules could be spontaneously formed in the atomization unit (for instance, CS, which may serve to determine S, or PO, which may serve to determine P) while in many other situations the addition of a reagent will be needed in order to generate the desired molecule (for instance, when halogens are to be determined) [34]. Enough time and optimum ramps of temperature will be needed so to assure an adequate interaction between the species. Selectivity has to be taken into account as well when developing a MAS method. The stability of the molecules in gas phase depends on their bond strength; so, in principle, a higher bond strength should translate into higher selectivity. Most metals form stable diatomic molecules with all the halogens, therefore competition for the formation of the molecules might occur when more than one halogen is present in the samples under analysis, but usually the bond strength decreases when increasing the diameter of the halogen involved, that is, following the order $F > Cl > Br > I$ [35].

These diatomic molecules experience different possible electronic transitions, each of them presenting several vibrational transitions with superimposed rotational transitions [8]. For practical purposes, these absorption structures may be classified following three different patterns:

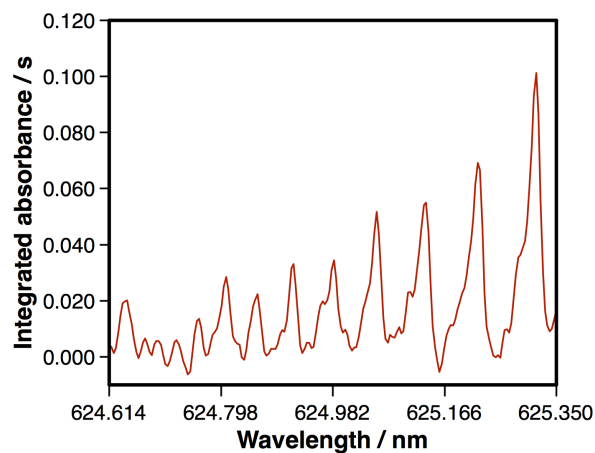
- A very dense and not completely resolved rotational spectrum. Then a quite broad band will be registered. This situation is typical for the UV systems of Al-based or Ga-based molecules [36].

Figure I.2. AlF time-integrated molecular absorbance spectrum obtained vaporizing 500 pg Al in excess of F by means of HR CS GFMS.



- Rotational spectrum evidencing several entirely resolved bands of different sensitivities. This is typically the case for those transitions registered in the visible region of the spectrum, such as the Ca-based molecules. As it was discussed in previous sections, this situation may allow to extend the linear range [37].

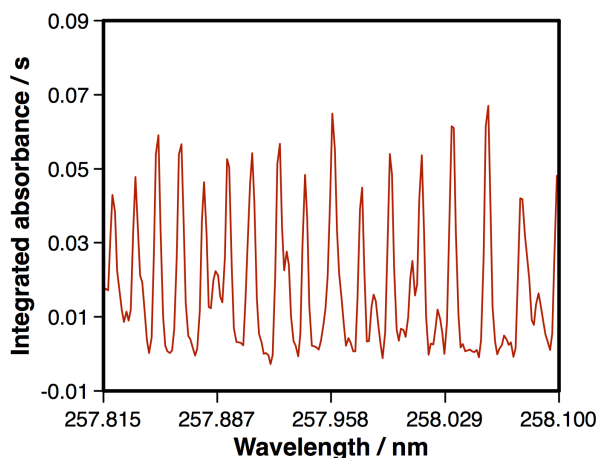
Figure I.3. CaBr time-integrated molecular absorbance spectrum obtained vaporizing 100 ng Br in excess of Ca by means of HR CS GFMS.



- A quite dense but resolved rotational spectrum, presenting a great amount of transitions practically as narrow as atomic lines and all

with similar sensitivities. This is for instance the case of CS, NO or PO, already mentioned when talking about background correction. Combining the signal for some of those lines may improve the sensitivity and therefore lead to achieve better LODs [31,38,39].

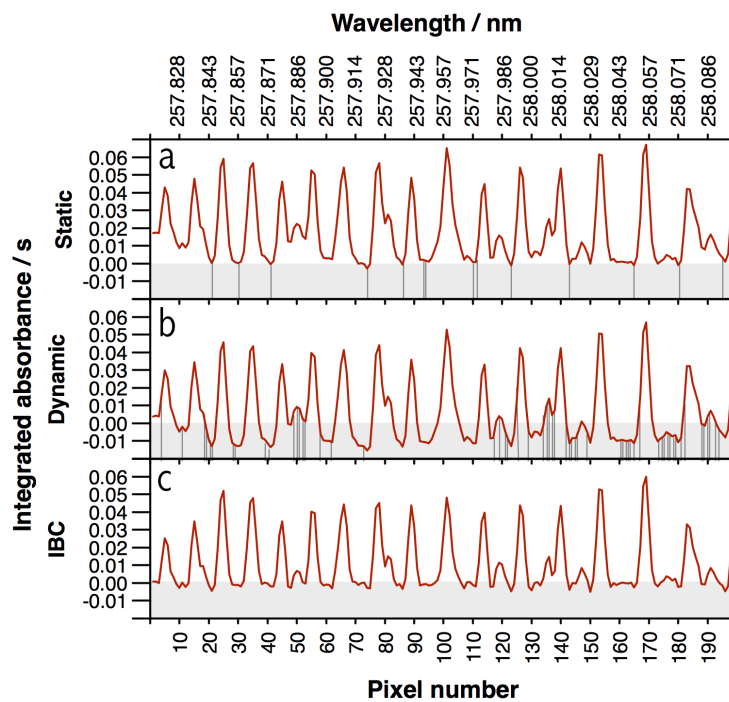
Figure I.4. CS time-integrated molecular absorbance spectrum obtained vaporizing 50 ng S by means of HR CS GFMS.



A difficulty when dealing with this sort of complex spectra may arise when it comes to fixing the baseline. The dynamic mode applied automatically by the software will most normally set the valleys between the peaks wrongly, particularly when the lines are very closely situated. It is recommended then to set the pixels for the baseline correction manually. A recent implementation in the software included a new baseline correction mode based on an algorithm named IBC (iterative baseline correction). Applying this algorithm results in narrower spectrum lines and a more defined baseline, though also the sensitivity is somewhat reduced. This correction method is especially useful when the pattern of molecular transitions is particularly complex and choosing the suitable correction pixels is not clear. In this way a potential source of error due to the baseline correction can be avoided. A comparison between these three different modes for fixing the baseline is illustrated in Figure I.5.

It constitutes an important part of this doctoral thesis to investigate the possibilities of HR CS GFMS for the direct determination of non-metals. In this regard, the work will focus not only in applying the most suitable strategy to quantify the spectrum obtained, but also in achieving proper stabilization and formation of the target molecules, during the pyrolysis and vaporization steps, respectively.

Figure I.5. CS time-integrated spectrum obtained after vaporization of 50 ng S by means of HR CS GFMS using different approaches for baseline adjustment: a) correction pixels fixed manually by the analyst under “static” working mode; b) correction pixels automatically set by the software working under “dynamic” working mode; and c) use of IBC mode for baseline correction



I.2.3. Direct solid sampling graphite furnace atomic absorption spectrometry applied to the analysis of micro-samples

Being able to perform the direct analysis of the target samples offers some significant advantages. For instance, higher sensitivity and speed in every

measurement can be achieved, as well as reducing to the minimum the use of hazardous reagents.

Another advantage, particularly important when dealing with ubiquitous or volatile analytes, is that risks of contamination or losses are also highly reduced, being this issue one of the main concerns when carrying out sample digestions.

GFAAS has proven all since the 1980s to possess a great potential for SS applications [40], sharing all the advantageous features already pointed out among all SS techniques. However it also shares some weak points. Most of them have been dealt with or even overcome with the successive improvements to the commercially available instruments. For instance, the difficulty in the handling and insertion of the solid samples into the graphite tubes [41] has been overcome with the development of auto-sampling systems equipped with a pair of tweezers for transporting the sample platforms. Automatic versions even include a microbalance for acquiring the sample weight prior to carry the platform to the graphite tubing.

Another drawback accompanying SS techniques is the need for adequate materials for calibration purposes, materials that should matrix match the samples as much as possible. This is no longer critical for GFAAS as several works already demonstrated that with a careful optimization of the furnace conditions and by measuring integrated peak areas, providing isothermal conditions are achieved during the atomization step, it is possible to successfully employ aqueous standards for calibration in most situations [42,43].

However, the most relevant disadvantage is still the large uncertainty that typically affects the results obtained. This detriment to the precision is due to the natural lack of homogeneity of the samples and the fact that very

small amount of sample is tolerated in each platform load (normally around 1 mg) [44]. To deal with this poor precision the only option to date is to increase the number of measurements for each sample, depending on the level of inhomogeneity. In general, monitoring at least 5 solid doses of each sample is rather typical and a relative standard deviation between 5%-15% is considered normal. It is worth mentioning here that employing the median as the estimate of the value of the analyte is often preferred as a way of ruling out the frequently appearing outliers associated with this technique [45].

When dealing with direct analysis of solid samples it is necessary to take into account that the whole matrix will be present within the atomization device and the analyte and the matrix will be simultaneously vaporized, giving rise to potential spectral interferences, *e.g.* owing to high background signals that may be generated by radiation scattering due to the presence of particles in the atomic vapour or to molecular absorption signals in the analytical region. To minimize this risk of interferences, some approaches are usually applied for establishing of the optimum conditions: i) in a situation where the volatility of the matrix is higher than that of the analyte, a thorough optimization of the pyrolysis stage is essential to eliminate as much matrix as possible; ii) if, on the contrary, the volatility of the analyte is higher, the pyrolysis stage is not critical, and most of the efforts should be devoted to finding an adequate atomization/vaporization temperature to selectively monitor the analyte; and iii) if analyte and matrix show similar volatilities, use of matrix modifiers and/or maintenance of Ar flow during the atomization/vaporization would be necessary to reach one of the previously discussed situations.

However, in some applications, temperature program optimization and matrix modifiers cannot completely overcome all spectral interferences. HR

CS AAS had represented a step forward in SS applications due to its superior potential facing background correction, related to the monitoring of a portion of the spectral environment of the analytical line [46,47]. An enhanced detection power, improved signal stability, the possibility of choosing the analytical pixels for the adjustment of the sensitivity and the capability for monitoring non-metals are also advantages of HR CS AAS that can be applied to SS [7].

So far, the fact that only a small amount of sample can be loaded into the sample platform has been regarded as a handicap. However, some interesting applications may derive from this fact, as it is the potential for carrying out homogeneity studies [12,48,49] or the possibility of developing analytical methods for micro-samples [50].

An important part of this thesis work has been focused on the handling and analysis of *Daphnia magna* specimens, small planktonic crustaceans of size normally around 0.2-5 mm long, used as test-organisms for ecotoxicological studies, each of them weighing just a few tens of micrograms.

Bringing this kind of samples into solution for analytical purposes entails the combination of several specimens in order to attain a detectable analytical signal. This process not only represents a potential increase in the risk of contamination but also causes the lost of information regarding the variation among individuals.

For most elements, GFAAS offers the possibility to determine total body burdens within each *D. magna* individually with a suitable sensitivity. As each invertebrate represents an individual sample, the information gathered in each determination is unique and no replicates are possible. It is clear that, in this context, the multi-elemental capabilities of HR CS AAS

technique could be particularly valuable, and so is the possibility for offline data post-processing.

The research stays at the A&MS group in the Analytical Chemistry department of Gent University in the context of this PhD had offered the possibility of further exploring the analysis of micro-samples. LA-sector field-ICPMS (LA-SF-ICPMS) allows to perform direct solid analysis for elemental and isotopic determinations with a high spatial resolution (due to the ablation process), a good spectral resolution and a high sensitivity (due to the detection system). Basically, a short laser pulse hits the surface of the sample under study promoting a small amount of sample into a vapour (dry aerosol) that is immediately led to the entrance of the plasma torch. Once inside the plasma, the particles generated in the ablation process are ionized and guided through the mass spectrometer to be adequately discriminated and further amplified when reaching the detection system in order to obtain highly selective and sensitive analytical signals. The parameters of the laser can be appropriately optimized in order to establish a good agreement between sensitivity and spatial resolution, whether lateral or in depth [51]. LA-ICPMS, as all ICPMS-based techniques, presents the capability of providing isotopic information of the samples. In this compendium of works, a study based on the combination of both features (that is, the generation of isotopic spatial information) is presented focused on the mapping of isotope ratios in thin sections of *D. magna* specimens, as a way of providing spatially-resolved the data for following tracer experiments with stable isotopes.

I.3. REFERENCES

- [1] U. Heitmann, M. Schütz, H. Becker-Ross, S. Florek, Measurements on the Zeeman-splitting of analytical lines by means of a continuum source graphite furnace atomic absorption spectrometer with a linear charge coupled device array, *Spectrochimica Acta Part B: Atomic Spectroscopy* 51 (1996) 1095–1105.
- [2] H. Becker-Ross, S. Florek, U. Heitmann, Observation, identification and correction of structured molecular background by means of continuum source AAS—determination of selenium and arsenic in human urine, *Journal of Analytical Atomic Spectrometry* 15 (2000) 137–141.
- [3] B. Welz, High-resolution continuum source AAS: the better way to perform atomic absorption spectrometry, *Analytical and Bioanalytical Chemistry* 381 (2005) 69–71.
- [4] J.M. Harnly, The future of atomic absorption spectrometry: a continuum source with a charge coupled array detector, *Journal of Analytical Atomic Spectrometry* 14 (1999) 137–146.
- [5] H. Becker-Ross, S. Florek, U. Heitmann, M.D. Huang, M. Okruss, B. Radziuk, Continuum source atomic absorption spectrometry and detector technology: A historical perspective, *Spectrochimica Acta Part B: Atomic Spectroscopy* 61 (2006) 1015–1030.
- [6] B. Welz, S. Morés, E. Carasek, M.G.R. Vale, M. Okruss, H. Becker-Ross, High-Resolution Continuum Source Atomic and Molecular Absorption Spectrometry—A Review, *Applied Spectroscopy Reviews* 45 (2010) 327–354.

-
- [7] M. Resano, E. García-Ruiz, High-resolution continuum source graphite furnace atomic absorption spectrometry: Is it as good as it sounds? A critical review, *Analytical and Bioanalytical Chemistry* 399 (2011) 323–330.
- [8] B. Welz, H. Becker-Ross, S. Florek, U. Heitmann, *High-Resolution Continuum Source AAS, The Better Way to Do Atomic Absorption Spectrometry*, Wiley-VCH, Weinheim, 2005.
- [9] I.M. Dittert, J.S.A. Silva, R.G.O. Araujo, A.J. Curtius, B. Welz, H. Becker-Ross, Direct and simultaneous determination of Cr and Fe in crude oil using high-resolution continuum source graphite furnace atomic absorption spectrometry, *Spectrochimica Acta Part B: Atomic Spectroscopy* 64 (2009) 537–543.
- [10] I.M. Dittert, J.S.A. Silva, R.G.O. Araujo, A.J. Curtius, B. Welz, H. Becker-Ross, Simultaneous determination of cobalt and vanadium in undiluted crude oil using high-resolution continuum source graphite furnace atomic absorption spectrometry, *Journal of Analytical Atomic Spectrometry* 25 (2010) 590–595.
- [11] D.P.C. Quadros, E.S. Chaves, F.G. Lepri, D.L.G. Borges, B. Welz, H. Becker-Ross, A.J. Curtius, Evaluation of Brazilian and Venezuelan Crude Oil Samples by Means of the Simultaneous Determination of Ni and V as Their Total and Non-volatile Fractions Using High-Resolution Continuum Source Graphite Furnace Atomic Absorption Spectrometry, *Energy & Fuels* 24 (2010) 5907–5911.
- [12] M. Resano, E. Bolea-Fernández, E. Mozas, M.R. Flórez, P. Grinberg, R.E. Sturgeon, Simultaneous determination of Co, Fe, Ni

- and Pb in carbon nanotubes by means of solid sampling high-resolution continuum source graphite furnace atomic absorption spectrometry, *Journal of Analytical Atomic Spectrometry* 28 (2013) 657–665.
- [13] L.M.G. dos Santos, R.G.O. Araujo, B. Welz, S. do C. Jacob, M.G.R. Vale, H. Becker-Ross, Simultaneous determination of Cd and Fe in grain products using direct solid sampling and high-resolution continuum source electrothermal atomic absorption spectrometry, *Talanta* 78 (2009) 577–583.
- [14] L.M.G. dos Santos, B. Welz, R.G.O. Araujo, S. do C. Jacob, M.G.R. Vale, A. Martens, I.B.G. Martens, H. Becker-Ross, Simultaneous Determination of Cd and Fe in Beans and Soil of Different Regions of Brazil Using High-Resolution Continuum Source Graphite Furnace Atomic Absorption Spectrometry and Direct Solid Sampling, *Journal of Agricultural and Food Chemistry* 57 (2009) 10089–10094.
- [15] F. Vignola, D.L.G. Borges, A.J. Curtius, B. Welz, H. Becker-Ross, Simultaneous determination of Cd and Fe in sewage sludge by high-resolution continuum source electrothermal atomic absorption spectrometry with slurry sampling, *Microchemical Journal* 95 (2010) 333–336.
- [16] A.T. Duarte, M.B. Dessuy, M.G.R. Vale, B. Welz, J.B. de Andrade, Sequential determination of Cd and Cr in biomass samples and their ashes using high-resolution continuum source graphite furnace atomic absorption spectrometry and direct solid sample analysis, *Talanta* 115 (2013) 55–60.

-
- [17] M.B. Dessuy, R.M. de Jesus, G.C. Brandao, S.L.C. Ferreira, M.G.R. Vale, B. Welz, Fast sequential determination of antimony and lead in pewter alloys using high-resolution continuum source flame atomic absorption spectrometry, *Food Additives & Contaminants: Part A* 30 (2013) 202–207.
- [18] H.-D. Projahn, U. Steeg, J. Sanders, E. Vanclay, Application of the reference-element technique for fast sequential flame atomic-absorption spectrometry, *Analytical and Bioanalytical Chemistry* 378 (2004) 1083–1087.
- [19] J.L. Raposo Jr., S.R. Oliveira, J.A. Nóbrega, J.A. Gomes Neto, Internal standardization and least-squares background correction in high-resolution continuum source flame atomic absorption spectrometry to eliminate interferences on determination of Pb in phosphoric acid, *Spectrochimica Acta Part B: Atomic Spectroscopy* 63 (2008) 992–995.
- [20] S.L.C. Ferreira, A.S. Souza, G.C. Brandao, H.S. Ferreira, W.N.L. dos Santos, M.F. Pimentel, M.G.R. Vale, Direct determination of iron and manganese in wine using the reference element technique and fast sequential multi-element flame atomic absorption spectrometry, *Talanta* 74 (2008) 699–702.
- [21] K. Miranda, A.G.G. Dionísio, E.R. Pereira-Filho, Copper determination in sugar cane spirits by fast sequential flame atomic absorption spectrometry using internal standardization, *Microchemical Journal* 96 (2010) 99–101.
- [22] B. Welz, F.G. Lepri, R.G.O. Araujo, S.L.C. Ferreira, M.-D. Huang, M. Okruss, H. Becker-Ross, Determination of phosphorus, sulfur

and the halogens using high-temperature molecular absorption spectrometry in flames and furnaces—A review, *Analytica Chimica Acta* 647 (2009) 137–148.

- [23] F.G. Lepri, D.L.G. Borges, R.G.O. Araujo, B. Welz, F. Wendler, M. Krieg, H. Becker-Ross, Determination of heavy metals in activated charcoals and carbon black for Lyocell fiber production using direct solid sampling high-resolution continuum source graphite furnace atomic absorption and inductively coupled plasma optical emission spectrometry, *Talanta* 81 (2010) 980–987.
- [24] U. Heitmann, B. Welz, D.L.G. Borges, F.G. Lepri, Feasibility of peak volume, side pixel and multiple peak registration in high-resolution continuum source atomic absorption spectrometry, *Spectrochimica Acta Part B: Atomic Spectroscopy* 62 (2007) 1222–1230.
- [25] B. Welz, M.G.R. Vale, M.M. Silva, H. Becker-Ross, M.-D. Huang, S. Florek, U. Heitmann, Investigation of interferences in the determination of thallium in marine sediment reference materials using high-resolution continuum-source atomic absorption spectrometry and electrothermal atomization, *Spectrochimica Acta Part B: Atomic Spectroscopy* 57 (2002) 1043–1055.
- [26] D. Bohrer, U. Heitmann, M.-D. Huang, H. Becker-Ross, S. Florek, B. Welz, D. Bertagnolli, Determination of aluminum in highly concentrated iron samples: Study of interferences using high-resolution continuum source atomic absorption spectrometry, *Spectrochimica Acta Part B: Atomic Spectroscopy* 62 (2007) 1012–1018.

-
- [27] R.G.O. Araujo, B. Welz, F. Vignola, H. Becker-Ross, Correction of structured molecular background by means of high-resolution continuum source electrothermal atomic absorption spectrometry—Determination of antimony in sediment reference materials using direct solid sampling, *Talanta* 80 (2009) 846–852.
- [28] D.A. McGregor, K.B. Cull, J.M. Gehlhausen, A.S. Viscomi, M. Wu, L. Zhang, J.W. Carnahan, Direct Determination of Nonmetals in Solution with Atomic Spectrometry, *Analytical Chemistry* 60 (1988) 1089A–1098A.
- [29] B.V. L'vov, A.D. Khartsyzov, Atomic absorption determination of sulphur, phosphorus, iodine and mercury from resonance lines in the far ultraviolet region, *Zhurnal Prikladnoi Spektroskopii* 11 (1969) 413–416.
- [30] I. López-García, P. Viñas, R. Romero-Romero, M. Hernández-Córdoba, Fast determination of phosphorus in honey, milk and infant formulas by electrothermal atomic absorption spectrometry using a slurry sampling procedure, *Spectrochimica Acta Part B: Atomic Spectroscopy* 62 (2007) 48–55.
- [31] M. Resano, J. Briceño, M.A. Belarra, Direct determination of phosphorus in biological samples using a solid sampling-high resolution-continuum source electrothermal spectrometer: comparison of atomic and molecular absorption spectrometry, *Journal of Analytical Atomic Spectrometry* 24 (2009) 1343–1354.
- [32] G.F. Kirkbright, H.N. Johnson, Application of indirect methods in analysis by atomic-absorption spectrometry, *Talanta* 20 (1973) 433–451.

- [33] P. Bermejo-Barrera, M. Aboal-Somoza, A. Bermejo-Barrera, Atomic absorption spectrometry as an alternate technique for iodine determination (1968–1998), *Journal of Analytical Atomic Spectrometry* 14 (1999) 1009–1018.
- [34] D.J. Butcher, Molecular absorption spectrometry in flames and furnaces: A review, *Analytica Chimica Acta* 804 (2013) 1–15.
- [35] D.R. Lide (Ed.), *CRC Handbook of Chemistry and Physics*, 89th ed., CRC Press/Taylor & Francis group, Boca Raton, FL, 2008–2009.
- [36] H. Gleisner, B. Welz, J.W. Einax, Optimization of fluorine determination *via* the molecular absorption of gallium mono-fluoride in a graphite furnace using a high-resolution continuum source spectrometer, *Spectrochimica Acta Part B: Atomic Spectroscopy* 65 (2010) 864–869.
- [37] T. Limburg, J.W. Einax, Determination of bromine using high-resolution continuum source molecular absorption spectrometry in a graphite furnace, *Microchemical Journal* 107 (2013) 31–36.
- [38] U. Heitmann, H. Becker-Ross, S. Florek, M.-D. Huang, M. Okruss, Determination of non-metals *via* molecular absorption using high-resolution continuum source absorption spectrometry and graphite furnace atomization, *Journal of Analytical Atomic Spectrometry* 21 (2006) 1314–1320.
- [39] R. Mior, S. Morés, B. Welz, E. Carasek, J.B. de Andrade, Determination of sulfur in coal using direct solid sampling and high-resolution continuum source molecular absorption spectrometry of

- the CS molecule in a graphite furnace, *Talanta* 106 (2013) 368–374.
- [40] M. Resano, F. Vanhaecke, M.T.C. de Loos-Vollebregt, Electrothermal vaporization for sample introduction in atomic absorption, atomic emission and plasma mass spectrometry—a critical review with focus on solid sampling and slurry analysis, *Journal of Analytical Atomic Spectrometry* 23 (2008) 1450–1475.
- [41] C. Bendicho, M.T.C. de Loos-Vollebregt, Solid Sampling in Electrothermal Atomic Absorption Spectrometry Using Commercial Atomizers. A Review, *Journal of Analytical Atomic Spectrometry* 6 (1991) 353–374.
- [42] U. Kurfürst (Ed.), *Solid Sample Analysis. Direct and Slurry Sampling using GF-AAS and ETV-ICP*, Springer-Verlag, Berlin Heidelberg, 1998.
- [43] M.A. Belarra, M. Resano, F. Vanhaecke, L. Moens, Direct solid sampling with electrothermal vaporization/atomization: what for and how?, *Trends in Analytical Chemistry* 21 (2002) 828–839.
- [44] M.A. Belarra, M. Resano, J.R. Castillo, Discrimination of the causes of imprecision in the direct determination of metals in organic solid samples by electrothermal atomization atomic absorption spectrometry, *Journal of Analytical Atomic Spectrometry* 13 (1998) 489–494.
- [45] M.A. Belarra, M. Resano, J.R. Castillo, Theoretical evaluation of solid sampling-electrothermal atomic absorption spectrometry for screening purposes, *Journal of Analytical Atomic Spectrometry* 14 (1999) 547–552.

- [46] B. Welz, M.G.R. Vale, D.L.G. Borges, U. Heitmann, Progress in direct solid sampling analysis using line source and high-resolution continuum source electrothermal atomic absorption spectrometry, *Analytical and Bioanalytical Chemistry* 389 (2007) 2085–2095.
- [47] B. Welz, D.L.G. Borges, F.G. Lepri, M.G.R. Vale, U. Heitmann, High-resolution continuum source electrothermal atomic absorption spectrometry—An analytical and diagnostic tool for trace analysis, *Spectrochimica Acta Part B: Atomic Spectroscopy* 62 (2007) 873–883.
- [48] U. Bagschik, D. Quack, M. Stoepler, Homogeneity studies in a variety of reference materials using solid sampling Zeeman graphite furnace AAS, *Analytical and Bioanalytical Chemistry* 338 (1990) 386–389.
- [49] M. Rossbach, K.-H. Grobecker, Homogeneity studies of reference materials by solid sampling - AAS and INAA, *Accreditation and Quality Assurance* 4 (1999) 498–503.
- [50] L. Ebdon, E.H. Evans, Determination of copper in biological microsamples by direct solid sampling graphite furnace atomic absorption spectrometry, *Journal of Analytical Atomic Spectrometry* 2 (1987) 317–320.
- [51] B. Fernández, F. Claverie, C. Pécheyran, O.F.X. Donard, Direct analysis of solid samples by fs-LA-ICP-MS, *Trends in Analytical Chemistry* 26 (2007) 951–966.



II. Dissertation

II.1. GENERAL GOALS

Our research groups have a long experience in the development of analytical methods for the direct analysis of solid samples using GF-AAS and ICPMS. These methods try to provide analytical information in a more direct and simple way, relying in simple calibration approaches whenever feasible. This PhD continues further this tradition and aims at developing new methods taking advantage of the existing improvements in terms of instrumentation.

In this regard, all the determinations attempted (*e.g.*, Al in blood, S in various materials, Br in polymers) present challenges when following the common digestion approaches, such that exploring direct analysis may bring in significant advantages.

In addition to this goal of developing straightforward methods, the systematic exploration of the capabilities of a high-resolution continuum source atomic absorption spectrometer is a major objective of this work. This instrumentation provides spectrally resolved information that can help in detecting and correcting for interferences, carry out multi-element determinations or monitor molecular spectrum quantitatively. This second aspect should not be seen as a separate topic, since these characteristics are the ones that might make feasible to develop the direct methods discussed above.

Finally, a third goal arises after examination of the benefits and disadvantages of direct SS analysis. These techniques typically offer spatially resolved information, which might be problematic when aiming at achieving a mean value for inhomogenous samples, but can be a very significant advantage when the goal is to obtain information from micro-samples. Thus, this work will also explore the potential of HR CS AAS and

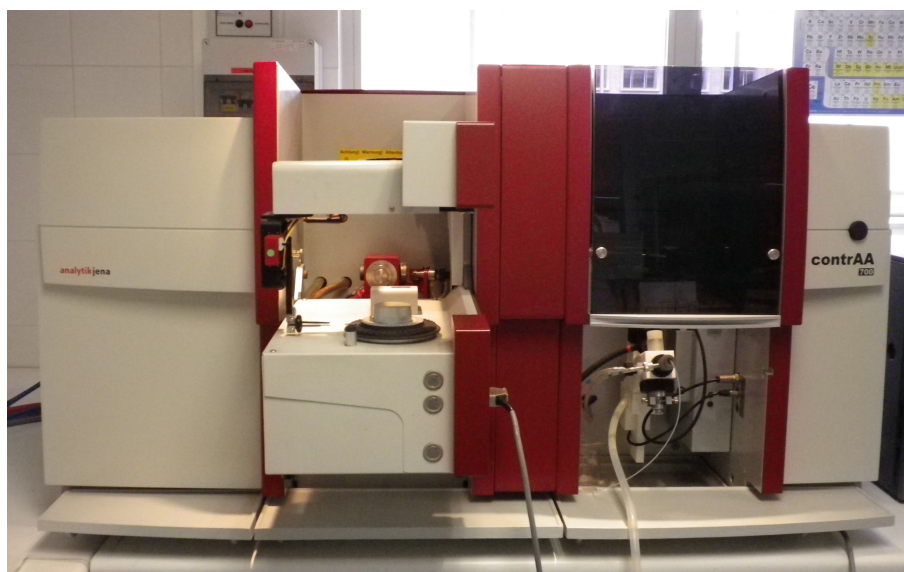
LA-ICPMS to obtain information that can be of ecotoxicological relevance, focusing on analysis of *D. magna* specimens.

II.2. INSTRUMENTATION

II.2.1. High-resolution continuum source atomic absorption spectrometry - ContrAA 700

All the works described from now on in sections II.3.1, II.3.2 and II.3.3.1 were carried out using a HR CS AAS instrument (ContrAA 700). This instrument, commercially available from Analytik Jena AG (Jena, Germany), is equipped with both flame and graphite furnace atomizers, a Xenon short-arc lamp (GLE, Berlin, Germany) operating in “hot-spot” mode as the radiation source, a high-resolution double echelle monochromator (DEMON) and a linear CCD array detector with 588 pixels, 200 of which are used for monitoring the analytical signal and performing BG corrections, while the rest are used for internal functions such as correcting for fluctuations in the lamp intensity, as further described in the introduction section. The furnace atomizer of the HR CA AAS instrument is a transversely heated graphite tube atomizer, equipped with pyrolytic graphite tubes and platforms for solid sampling and sample introduction, and an automated solid sampling accessory (SSA 600). This solid sampling device allows for automatic weighing and transport of the samples to the furnace by means of a pair of tweezers and incorporates a microbalance with a readability of 1 µg. After first taring the empty sample platform, an appropriate amount of sample is deposited onto the platform to be weighed. Subsequently, all the required chemical modifiers are added to the sample prior to be transferred into the graphite furnace to be subjected to the corresponding optimized temperature program in every case. All these operations are fully controlled by the instrument software, with exception of the sample deposition and the addition of the modifier, which need to be carried out manually.

Figure I.6. AnalytikJena ContrAA 700 HR CS AAS instrument used throughout this doctoral thesis



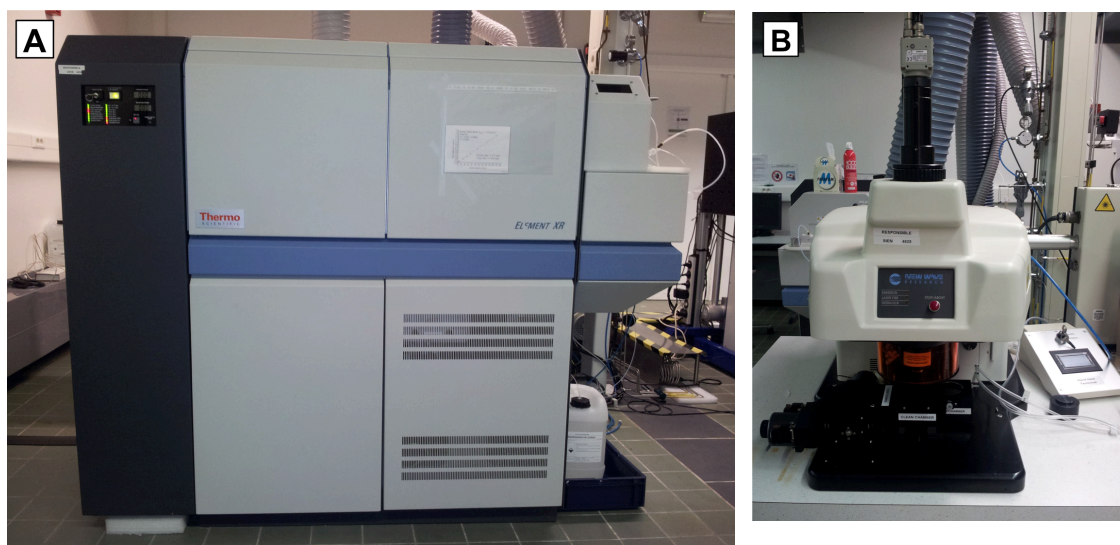
II.2.2. Laser ablation single collector inductively coupled plasma mass spectrometry - UP193HE laser coupled to Element XR

In section II.3.3.2 another instrumentation for the analysis of microsamples was regarded as an implementation on the study of the enhancement of the spatial resolution. For the work presented, a New Wave Research 193 nm wavelength ArF* excimer-based laser ablation system (UP193HE, New Wave Research, CA, USA) was coupled to a sector field-based ICP-MS instrument (Element XR, Thermo Scientific, Bremen, Germany). The LA unit is equipped with an ablation cell mounted on a tri-translational stage. A teardrop-shaped ablation cell [1], built by Axel Gerdes at the University of Frankfurt based on the work of Bleiner and Günther [2], was used throughout the work. This cell has an internal volume of *circa* 2.5 cm³, which, compared with the standard cell (30 cm³ volume), reduces the washout time significantly, allowing improved time-resolved elemental and isotopic information [3] and, therefore, better spatial resolution.

A quartz dual pass cyclonic spray chamber with two inlet ports (Elemental Scientific Inc., Omaha, NE, USA) was included in the setup for simultaneous nebulization of a solution with the ablated aerosol (“wet plasma” mode). The aerosols coming from the spray chamber and the laser ablation cell were mixed by means of a Y-shaped connection. The benefits of this setup are discussed in the corresponding methodological section devoted to this study.

A new slit system provided by Thermo Fisher Scientific (Bremen, Germany) for the Element XR, which generates flat top peaks at a mass resolution of $m/\Delta m \approx 2000$ (20% ion transmission with respect to that observed at low resolution mode) [4], was used. These mass spectral characteristics are realized *via* a wider exit slit than the conventional medium resolution slit (offering a resolution of $m/\Delta m \approx 4000$ at 10% ion transmission with respect to low resolution mode), which generates triangular shaped peaks.

Figure I.7. **A)** Thermo Element XR SF-ICPMS instrument and **B)** New Wave Research UP193HE laser ablation unit used in the work described in the experimental section II.3.3.2



II.2.3. Additional instrumentation

For the CS molecular absorption monitoring study, a Scanning Electron Microscope (SEM) JEOL (Tokyo, Japan) JSM-6400, configured with an energy dispersive X-ray analyser INCA 300 X-Sight from Oxford Instruments (Abingdon, UK), was used for the examination of the graphite platforms. This instrument was available through the Research Support Services of the University of Zaragoza.

For the Zn isotope ratio imaging of *D. magna* specimens, a SLEE (Mainz, Germany) CUT 4060 rotatory microtome was used for cutting the 20 µm sagittal sections of each sample individual. Access to this instrument was possible at the Department of Basic Medical Sciences of Ghent University.

II.3. METHODOLOGY AND DISCUSSION OF THE RESULTS

II.3.1. Monitoring of non-metals

II.3.1.1. Al determination in whole blood samples as AlF via high-resolution continuum source graphite furnace molecular absorption spectrometry: potential application to forensic diagnosis of drowning

Goals

The final goal of this work was to assess the validity of Al as a chemical proxy to complement the forensic diagnosis of death-by-drowning in contaminated fresh waters.

Diagnosis of true drowning is still one of the most common challenges in forensic pathology [5]. Physiological signs have a limited validity, especially when the body exhibits putrefaction evidences. Additional chemical and biochemical tests are needed in order to offer a reliable way of discern between true drowning and a different lethal cause. Traditionally, the diatom test, based in the finding of diatom algae in a sufficiently high concentration within the organs of the dead body [6] was used as powerful indicator of drowning. However, nowadays some species of these organisms are being gradually extinct in polluted waters, compromising the applicability of this popular test. Therefore, the finding of (bio)chemical markers for drowning diagnosis is still a field of interest in Forensic Science.

Monitoring of Al may be an alternative approach worth exploring, as it complies well with the premises for a suitable marker: i) to be present in large amounts in the drowning water and absent or present in very small amounts in the blood of a healthy person (Al levels in the blood of healthy people are usually low, at the $10 \mu\text{g L}^{-1}$ level or lower) [7,8], and ii) to enter

the blood circulation only by the alveolo-capillary membrane during the agony period of the drowning event.

From a methodological point of view, a comparison between the direct determination of Al in blood samples by means of AAS and the monitoring of the AlF absorption band after the addition of a fluorinating agent by means of MAS was explored in order to develop a straightforward analytical method enabling the monitoring of Al in suspects of drowning.

Methodology

Direct determination of Al by means of GFAAS in such a complex matrix as whole blood is not free of hindrances. Occurrence of non-spectral interferences usually implies sample dilution with different reagents [8-10] and even so, standard addition method would still be required for calibration. Moreover, also spectral interferences take place, the most problematic one being the Fe line appearing at 309.278 nm [11], located just between the Al duplet at 309.271/309.284 nm, which is impossible to be separated in time and that overlaps significantly for samples containing more than 0.5 g Fe L⁻¹ (as it is the case for blood samples [12]). This issue, however, can be avoided by measuring in the 396.152 nm line, which offers slightly less sensitivity.

The formation of stable Al diatomic molecules and the recording of its molecular transitions has been used in several works particularly for the quantification of non-metals by both flame and graphite furnace MAS [13]. In this work, HR CS MAS is used to further study the absorption spectra of the AlF molecule, although aiming at Al determination.

Several blood samples for cadavers found in water media (named as DS-1 to DS-8) along with water collected from the locations where those bodies

were found were provided for this study. Also blood from corpses not found in water was available to use as control samples, CTRL-1 and CTRL-2. Both groups of samples were stabilized with lithium heparine and were collected around Ghent (Belgium) and its district, where high levels of Al was expected to be found in water accumulations due to the intense industrial activity of the area.

With regards to the method validation, a blood reference sample was analysed. Seronorm trace element human whole blood level II was purchased from Sero (Billingstad, Norway), which provides an indicative value for Al content. This sample comes as powder that needs to be reconstituted in purified water. A certified reference material for water (BCR-610 Ground water, high contents) purchased from the Institute of Reference Materials and Measurements (IRMM; Geel, Belgium) was also analysed.

Besides, two blood samples collected from Miguel Servet Hospital in Zaragoza (Spain) and stabilized with potassium-EDTA were also available to compare the effects of different matrices on the method. These two blood samples, referred to as LS-1 and LS-2, along with the Seronorm and one of the drowning suspects were also analysed by means of SF-ICPMS, with the Thermo Element XR, after sample digestion with HNO_3 and H_2O_2 heating on a hot plate, for a further validation of the results.

For the determination on the atomic line 396.152 nm, samples were diluted a factor of 1:4 with ultrapure water and the standard addition method (of 50, 100 and 200 pg Al added with a diluted aqueous standard) was applied for calibration and five replicate measurement of each point were performed.

In the case of the AlF molecular transition, sample dilution was only carried out in order to improve the precision of the method. However, this step would not be strictly necessary, as the fluorinating agent also promotes the decomposition of the organic sample, helping to reduce matrix effects as well as avoiding accumulation of residues in the platform after vaporization. External calibration was carried out *versus* daily prepared aqueous Al standard solutions.

NH₄F·HF was selected as fluorinating agent due both to its high degree of purity and its relatively high thermal stability (decomposes at 240°C, therefore resisting the drying stage and becoming active during the pyrolysis). Optimization of the quantity of NH₄F·HF was essential in order to find the lowest amount needed to properly promote the AlF molecule and to remove the sample matrix as much as possible, while minimizing the detrimental effects of high contents of F over the optical components. 10 µL of an aqueous 5% NH₄F·HF solution was proven to be suitable.

As for the optimization of the temperature program, for the formation and monitoring of the AlF molecule, it had to be taken into account that: i) enough drying time and stages are needed in order to allow proper interaction between the fluorinating reagent and the blood samples, so to favour matrix removal and avoid sample spilling at the beginning of the pyrolysis, ii) adequate pyrolysis temperatures to remove most matrix components while ensuring measurement repeatability are required and iii) vaporization temperatures high enough to have the atoms in gas phase available to form the diatomic molecule, but mild enough to avoid breaking the molecular bond, are essential.

Optimized instrumental parameters and conditions for the analysis for both AAS and MAS methods are summarized in Tables II.1 and II.2.

Table II.1. Instrumental parameters used for direct Al determination by means of HR CS GFAAS in blood and water samples.

Wavelength	396.152 nm			
Number of detector pixels summed (C±1)	3 (5.3 pm)			
Ar gas flow during atomization	Stop-Flow			
Modifier	No			
Sample volume	10 µL			
Temperature program				
Step	Temperature/°C	Ramp/°C s ⁻¹	Hold time/s	Gas flow rate/ L min ⁻¹
Drying	100	6	30	2.0
Drying	160	6	30	2.0
Drying	200	6	20	2.0
Pyrolysis	1000	40	40	2.0
Auto zero	1000	0	5	0.0
Atomization	2500	600	6	0.0
Cleaning	2600	500	4	2.0

Table II.2. Instrumental parameters for Al determination by means of HR CS GFMAAS based in the formation of the diatomic AlF molecule in blood and water samples.

Wavelength at central pixel*	227.402 nm			
Wavelength of the peak maximum (C)	227.477 nm			
Number of detector pixels summed (C±2)	5 (5.5 pm)			
Ar gas flow during atomization	Stop-Flow			
Modifier	10 µL NH ₄ F HF (5%)			
Sample volume	10 µL			
Temperature program				
Step	Temperature/°C	Ramp/°C s ⁻¹	Hold time/s	Gas flow rate/ L min ⁻¹
Drying	100	6	50	2.0
Drying	160	6	60	2.0
Drying	200	6	20	2.0
Pyrolysis	1000	40	40	2.0
Auto zero	1000	0	5	0.0
Atomization	2300	600	4	0.0
Cleaning	2600	500	4	2.0

*The central pixel is not positioned at the peak maximum to achieve proper baseline definition.

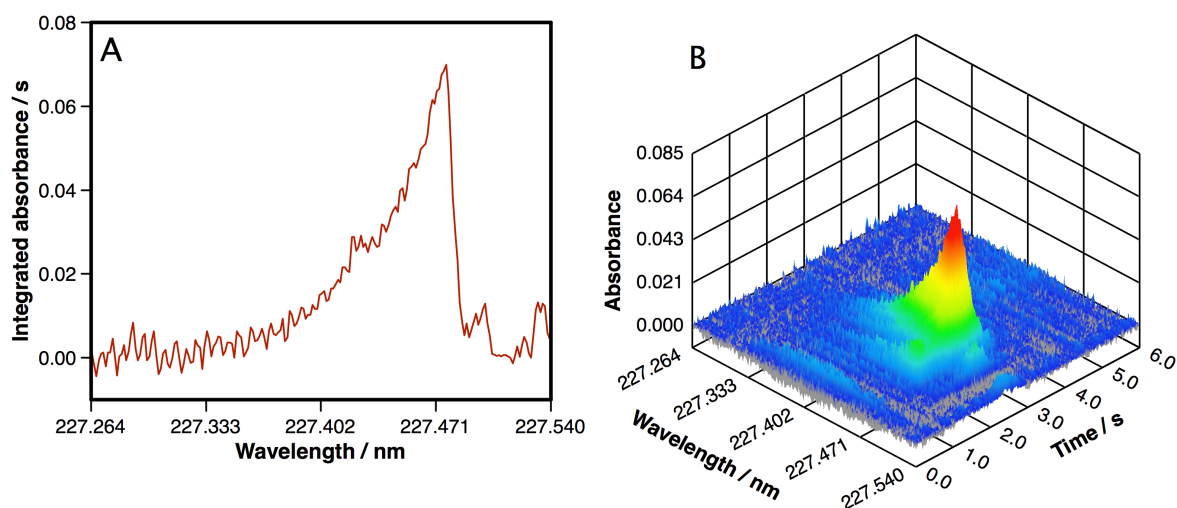
The analytical result was obtained summing the A_{int} for the 3 central pixels of the transition peak registered at 396.152 nm (for the AAS determination) and the 5 central pixels of the transition band registered at 227.477 nm (for the MAS determination). Each sample was analysed in a different session. For each water and blood sample, three and five replicates were measured, respectively. The average was taken as the estimate value of the total Al content in the samples.

Results and discussion

As it was mentioned in previous sections, in order to develop a method based in a molecular absorption band it is desirable to have a molecule available with a bond strength above 500 KJ mol⁻¹, to be capable to resist the temperatures required within the graphite furnace without decomposing [13]. On the other hand, it was also alluded before to the decreasing stability of the binary compounds containing halogens with an increasing atomic number. Therefore, F was chosen to form the diatomic molecule with Al, with a bond strength of 664 KJ mol⁻¹ [14], favourably competing with other halogens present in blood (particularly Cl, that forms AlCl with a bond strength of 511 KJ mol⁻¹) [14].

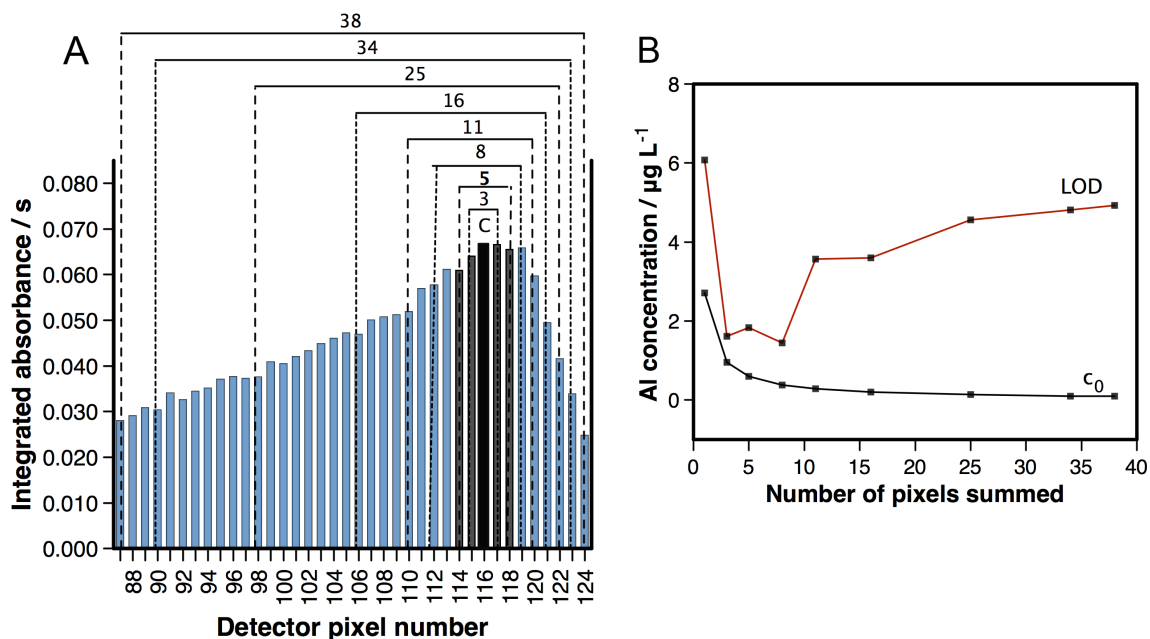
AlF shows its main resonance system in the middle-ultraviolet region, with a maximum absorbance at 227.477 nm, being part of a quite broad and asymmetrical absorption band [15]. In order to correctly monitor this band it is necessary to fix the central pixel of the analytical window so to have a sufficient number of baseline pixels at both sides of the band. In Figure II.1 a typical molecular absorbance spectrum for AlF acquired under the conditions listed in Table II.2 is presented.

Figure II.1. Overview of the AlF molecular absorption structure around 227.402 nm (central pixel) for the vaporization of 0.5 ng Al added as Al standard solution, plus 10 μL of a 5% $\text{NH}_4\text{F}\cdot\text{HF}$ fluorinating solution under the furnace conditions listed in Table II.2. **A** shows a wavelength resolved time-integrated spectrum, while in **B** the three-dimensional time and wavelength resolved spectrum is presented.



Also, the number of pixels summed for obtaining the analytical absorbance value is a parameter to be optimized due to the pronounced asymmetry of the band. The selection of this peak volume is based both in the best S/N (and therefore, best LODs) achieved and best accuracy with the informative values of the Seronorm reference sample. Taking this into account, the sum of 5 pixels centred in the peak maximum at 227.477 nm and symmetrically distributed at both of its sides was found optimal, as it is illustrated in Figure II.2.

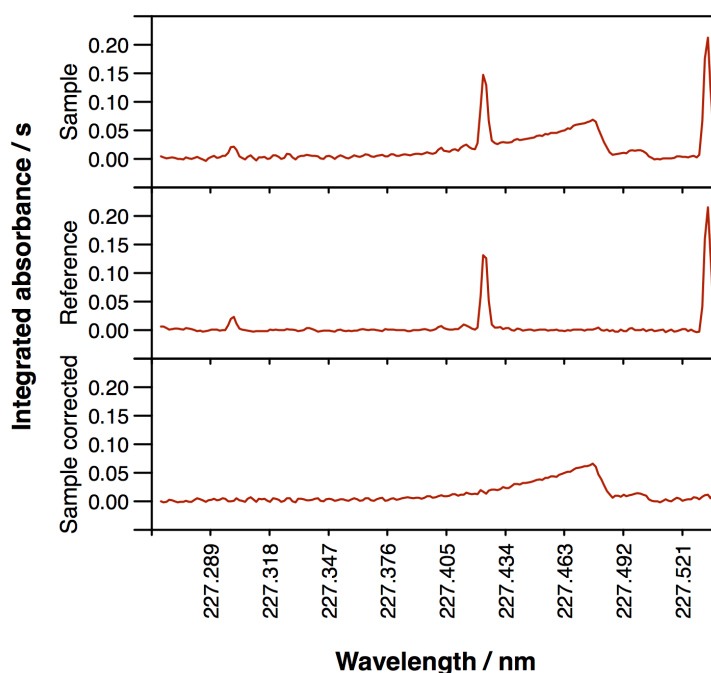
Figure II.2. Optimization of the number of pixels summed for data acquisition. **A)** Pixel representation of the most sensitive portion of the AlF molecular band. The pixel combinations evaluated are indicated with the number of pixels summed in each case. **B)** LOD and characteristic concentration (c_0 , the concentration that provides a signal equal to 0.0044) calculated for each pixel combination evaluated. The error bars have been omitted, as their magnitude is similar to that of the markers used in the figure.



With such a broad band the possibilities of encountering spectral interferences increase. In this particular case a triplet appears with narrow absorption peaks at 227.300 nm, 227.423 nm and 227.534 nm when blood samples are dosed into the furnace. Plasus SpecLine database [16] was consulted in order to identify the origin and it hints at a N_2 system as the potential interference. Anyhow, the appearance of this system does not significantly affect the final results as the analytical region of the AlF band lies between two of those interfering peaks.

However, it is worth mentioning that it is easy in this case to obtain a “pure” interfering spectrum, just by not adding the fluorinating agent to the sample and therefore avoiding the formation of the AlF molecular species.

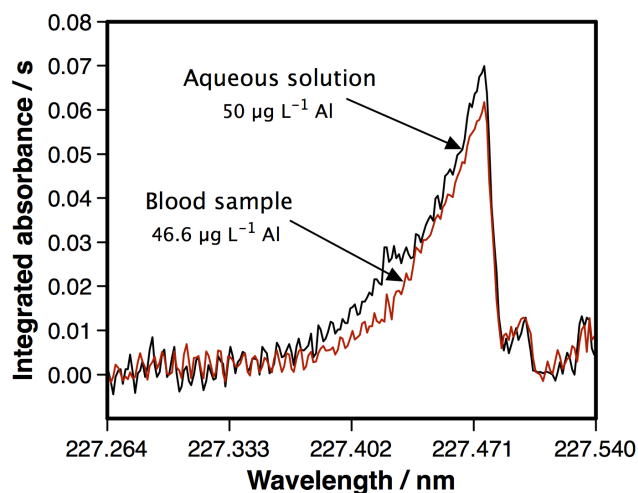
Figure II.3. Wavelength resolved time-integrated spectrum recorded in the analytical region of AlF molecular absorbance for a blood sample under the conditions listed in table II.2., with (Sample) and without (Reference) the addition of the fluorinating agent, and after the application of the LSBC methodology for spectral interference correction (Sample corrected).



Then a reference spectrum of the interference is obtained and the least-squares algorithm can be applied to satisfactory correct for the overlap. The application of the LSBC correction method is illustrated in Figure II.3.

Under optimum conditions, very similar signal profiles for the Al aqueous standards and the blood samples could be obtained, thus enabling the use of a simple calibration strategy, as illustrated in Figure II.4.

Figure II.4. Comparison of a wavelength-resolved time integrated AIF molecular absorbance signal recorded in the vicinity of 227.4 nm for the vaporization of a similar amount of Al from an aqueous solution and directly from a blood sample under the conditions listed in table II.2.



The reproducibility of the MAS method was evaluated by analysing the Seronorm reference sample in four different days under optimized conditions, then the mean of the results for these four different sessions was calculated obtaining a value of $57.5 \pm 3.4 \mu\text{g L}^{-1}$ (reference value for Seronorm, $58.9 \pm 9.9 \mu\text{g L}^{-1}$), which was considered as very satisfactory in terms of precision and accuracy.

A comparison of the performances of the MAS and AAS techniques was also carried out. While in the case of AAS the need for sample dilution of at least a factor of 1:4 cannot be avoided, the limits of detection for both MAS and AAS are rather similar ($1.5 \mu\text{g L}^{-1}$ for AAS and $1.8 \mu\text{g L}^{-1}$ for MAS), due mainly to the fact that the measurement of the molecular band introduces a higher level of noise to the signal. Regarding the precision, however, better figures are obtained for the MAS method than for the AAS one. Besides, higher temperatures are needed for the AAS technique (optimum atomization temperature of 2500°C), which negatively affects the

perishable components of the instrument, particularly the sample platform and the graphite tubes, and even under these conditions matrix removal is not complete and a mechanical cleaning of the platform between samples is needed, making the AAS method more prone to contamination problems.

In spite of that, results were obtained using both methods for the samples for which SF-ICPMS values were available. All the obtained values are presented in Table II.3, where a good agreement between the results for all the techniques is shown. It is important to stress that MAS was the only technique for which it was not necessary to use standard additions for calibration.

Table II.3. Comparison of the Al concentration values obtained for the Seronorm reference material and three blood samples by means of SF-ICPMS, AAS and MAS. Uncertainties are expressed as 95% confidence intervals (calculated as $\pm ts/\sqrt{n}$, where t, s and n have their usual meanings).

	Reference / $\mu\text{g L}^{-1}$	SF-ICPMS / $\mu\text{g L}^{-1}$ (n=3)	AAS / $\mu\text{g L}^{-1}$ (n=5)	MAS / $\mu\text{g L}^{-1}$ (n=5)
Seronorm	58.9 \pm 9.9	60.1 \pm 6.1	56.9 \pm 8.1	57.5 \pm 3.4 ^a
LS-1	--	46.8 \pm 9.2	46.6 \pm 5.7	45.0 \pm 4.6
LS-2	--	96.5 \pm 10.4	100.3 \pm 9.2	96.4 \pm 7.6
DS-5	--	23.7 \pm 6.0	24.6 \pm 8.8	24.3 \pm 5.3

The rest of the blood samples of drowning suspects were analysed just applying the MAS methodology. Results are gathered in Table II.4.

The Spearman rank correlation coefficient method [17] reveals a positive correlation between the Al content in the blood of the drowning suspects and the water media in which they were found at a 95% significance level ($\rho=0.952$; $\rho_c=0.738$). This correlation supports the validity of Al as a drowning marker for deaths occurring in water media with high Al concentrations. The number of subjects in this study is however insufficient to extract more sound conclusions from a forensic point of view, since there

are additional factors affecting the total amount of Al entering the bloodstream that need to be taken into account (*e.g.*, duration of the agony). But in general, from these results it can be inferred that for water samples with concentrations of Al of around 200 $\mu\text{g L}^{-1}$ (and higher), the concentration of Al in the blood of the drowning bodies would at least double the “basal” level (considering “basal” level a concentration of 10-15 $\mu\text{g L}^{-1}$ Al, based in the control samples and the samples for which the corresponding water media is “Al-clean”).

Table II.4. Al concentration results obtained for the eight samples of blood and water for drowning suspect cases and the two control blood samples by means of HR CS GFMS. Uncertainties are expressed as 95% confidence intervals (calculated as $\pm ts/\sqrt{n}$, where t, s and n have their usual meanings).

	Al content in water / $\mu\text{g L}^{-1}$	Al content in blood / $\mu\text{g L}^{-1}$
DS-1	2.31 \pm 0.24	4.32 \pm 0.82
DS-2	412 \pm 14	94.3 \pm 6.8
DS-3	296 \pm 12	37.1 \pm 3.7
DS-4	483 \pm 18	38.9 \pm 3.1
DS-5	195 \pm 11	24.3 \pm 5.3
DS-6	505 \pm 14	133 \pm 9
DS-7	14.9 \pm 1.0	12.9 \pm 2.1
DS-8	30.1 \pm 1.7	11.9 \pm 1.7
CTRL-1	--	6.5 \pm 1.0
CTRL-2	--	10.5 \pm 1.8

II.3.1.2. Direct determination of S in solid samples by means of high-resolution continuum source graphite furnace molecular absorption spectrometry using Pd nanoparticles as chemical modifier

Goals

The ultimate aim of this work was to develop a direct and straightforward method for the determination of S in a variety of solid materials, relying only in calibration *versus* aqueous standard solutions.

S is widely present in nature and essential for all life, being part of the structure of several enzymes, vitamins and all proteins. In the industry is extensively used in the production of many products, such as fertilizers, pesticides and fungicides, food additives, pharmaceutical formulations, depending on its chemical form [18]. Due to the aforementioned spreadability, simple analytical methods for S determination capable of dealing with different types of samples are to be pursued.

In this work, the potential of HR CS MAS for the determination of S in direct solid samples, based in the formation of the diatomic CS molecule and the monitoring of its molecular spectra is evaluated. Particular attention was paid to find a suitable combination of chemical modifiers to achieve proper formation and stabilization of the target molecule, as well as a signal independent of the exact chemical form in which S is found in the sample. In this way, calibration with aqueous standards may enable accurate results to be obtained.

Methodology

Determination of atomic S is, as usual when dealing with most non-metals, not a feasible approach due to the lack of atomic lines within the UV-visible region for this element (in fact, its main resonant line appears at 180.7 nm) for atomic absorption/emission spectrometry techniques [19].

Several sulfide species are known to be formed and are available for MAS evaluation (*e.g.*, CS, GeS, SH, S₂, ...) [20,21], but most of the previous works are focused on the study of the CS molecule in the region of 258.0 nm due to its superior performance [13].

Although the CS molecular system exhibits a structure of well-defined peaks of similar sensitivity [22], in this work the transition peak appearing

at 257.958 nm was chosen to be monitored with the central pixel of the spectral window, since no spectral overlaps were previously reported and a better baseline stability was obtained for this peak.

A series of solid samples, all of them certified reference materials (CRMs), of very different nature, were selected in order to assess the validity of the method. The materials available were: i) two polyethylene CRMs with different concentration of S, ERM-EC680 and ERM-EC681, produced by the Institute for Reference Materials and Measurements (IRMM, Geel, Belgium) and presented in granular form; ii) Mild Steel 453 and High-speed steel 482, purchased from the Bureau of Analysed Samples Ltd. (BAS, Newby, UK), available in small chips; iii) two biological reference materials, CRM 129 Elements in hay powder (Community Bureau of Reference, BCR, Geel, Belgium) and 1566a Oyster tissue (National Institute of Standards and Technology, NIST, Gaithersburg, USA), both presented as powders; and iv) NIST 2718 Green petroleum coke, also available in powder form.

The samples were cut into fragments of adequate mass making use of a ceramic knife, and deposited onto the platform, along with the corresponding amount of chemical modifier. The platform was subsequently transported to the graphite tube to be subjected to the optimized temperature programme. Table II.5 presents a summary of the instrumental parameter used in the determination.

Ru was employed as permanent modifier. The procedure described by Vale *et al.* [23] for thermal deposition onto the platform furnace was followed. 40 µg of Pd were added in the form of a hydroalcoholic suspension of Pd nanoparticles to properly stabilize S [24].

Table II.5. Instrumental parameters used in the determination of S by means of HR CS GFMA for the promotion and monitor of the CS molecule in gas phase

Electronic transition used	$\Delta v=0, X \ ^1\Sigma^+ \rightarrow A \ ^1\Pi$ of CS molecule			
Wavelength / nm	Main lines of CS in the vicinity of 258 nm (central pixel = 257.958 nm)			
Number of detector pixels summed per line	3 (~4.3 pm)			
Ar gas flow during atomization / mL min ⁻¹	Stop-flow conditions			
Chemical modifiers	Ru (permanent modifier) + Pd (40 µg) nanoparticles			
Sample mass / mg	0.5-2.0 (BAS 482, BAS 453)			
	0.1-0.3 (BCR 129, NIST 1566a)			
	0.3-1.0 (ERM-EC680)			
	1.5-3.5 (ERM-EC681)			
	0.04-0.05 (NIST 2718)			
Temperature program				
Step	Temperature/ °C	Ramp/ °C s ⁻¹	Hold time/ s	Gas flow rate/ L min ⁻¹
Drying	110	2	10	2.0
Pyrolysis	800	50	20	2.0
Auto Zero	800	0	5	0.0
Vaporization	2400	2000	5	0.0
Cleaning	2600	1000	5	2.0

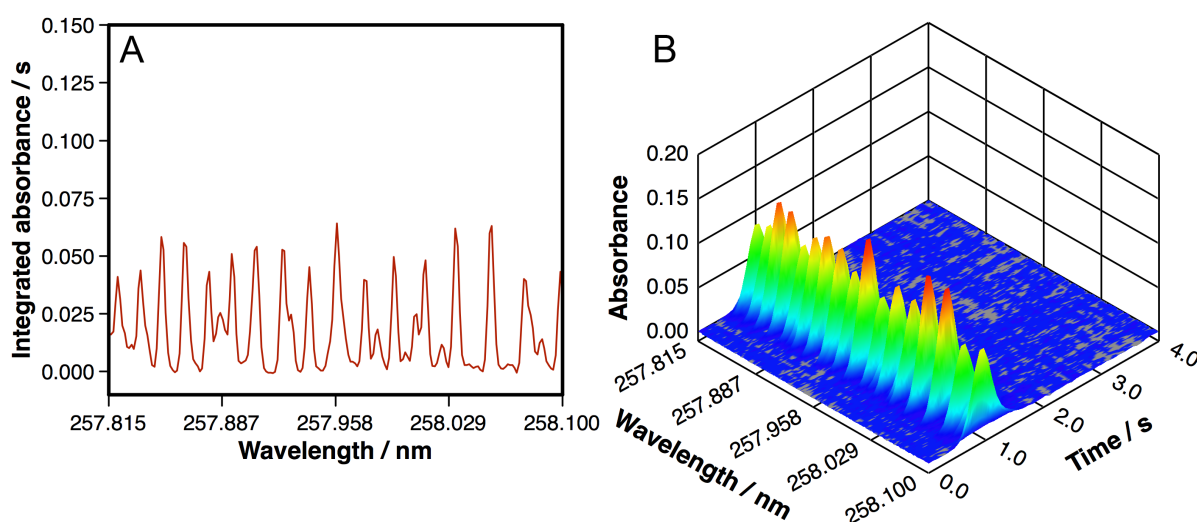
Calibration was carried out *versus* daily prepared aqueous S standard solutions (as Na₂SO₄). The analytical result was obtained summing the A_{int} for the 3 central pixels of each one of the transition peaks registered in the vicinity of 258 nm. For each sample, eight determinations (in total) were carried out, and for each determination, five solid replicates were measured. The median was taken as the estimate value of the total S content in the samples.

Results and discussion

A graphite furnace is particularly suitable for the promotion of the CS molecule due to the obviously high availability of C atoms. This, along with the high stability of the CS bond (714.1 KJ mol⁻¹) [14] makes this molecule very fit for purpose.

The molecular spectrum of CS (Figure II.5) presents several sharp rotational transitions with a width of just a few picometers, similar to that of an atomic line [25]. The sensitivities for these peaks are quite similar and therefore, while not suitable for linear range expansion, it can be feasible to improve the LOD by combining the signal for some of the most sensitive ones.

Figure II.5. Overview of the CS molecular absorption structure around 257.958 nm (central pixel) for the vaporization of 500 ng S added as Na₂SO₄ solution under the furnace conditions listed in Table II.5. **A** shows a wavelength resolved time-integrated spectrum, while in **B** the three-dimensional time and wavelength resolved spectrum is presented.

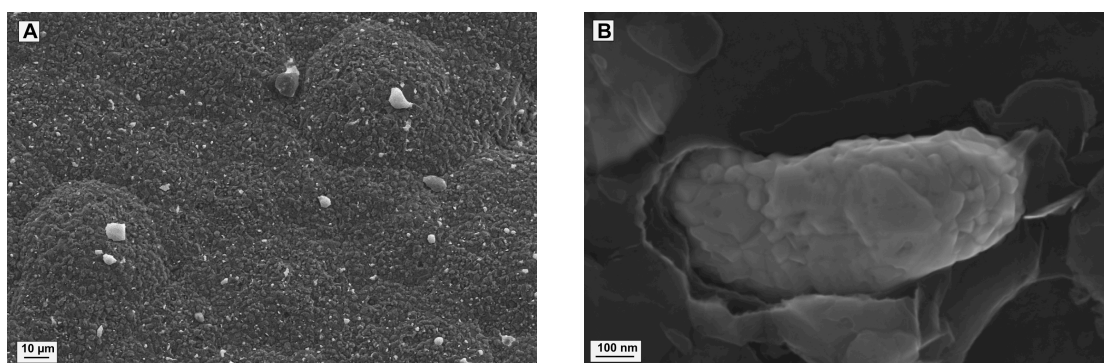


Due to the lack of agreement among the previous works dealing with CS monitoring by means of HR CS MAS [25-27] concerning the use of chemical modifiers, special attention was paid to this issue in the present work. In fact, choosing the adequate/s chemical modifier/s is crucial if proper stabilization of the CS molecule, regardless of the particular chemical form in which S is found, is aimed at.

The use of permanent modifiers was already been reported as recommended in the bibliography to obtain a better sensitivity. In this

work, the permanent modifiers most typically used, W, Zr and Ru, were tested and, although the results were not significantly different, Ru provided somewhat better results in terms of sensitivity (by a 15-20% higher) and better defined temporal profiles. It was observed, by acquiring SEM images, that Ru particles are randomly distributed all across the surface of the graphite sample platforms, in the form of large agglomerates of approximately 0.5-1 μm length, as it is shown in Figure II.6.

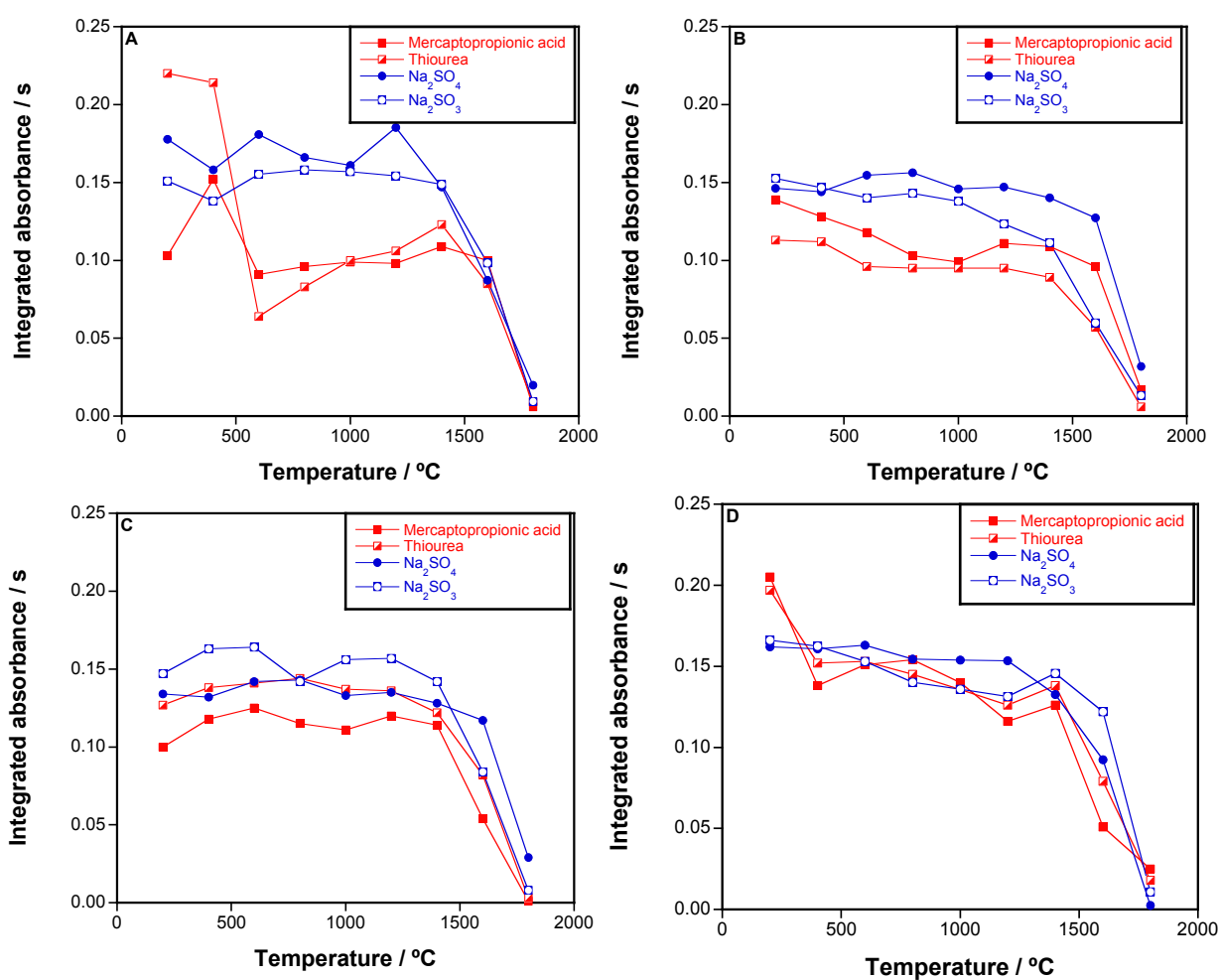
Figure II.6. SEM images of: **A**) an overview of the graphite surface of a solid sampling platform with Ru permanent coating (1 000x magnification). The unevenly distributed pale masses correspond to Ru depositions; and **B**) a closer view of one of the Ru agglomerates (80 000x magnification).



In combination with Ru, and based in previous experiences [28], Pd was also tested as chemical modifier in order to interact with S, hopefully breaking its original bonds within the sample structure and helping in stabilizing it until favourable conditions for the promotion of CS in the graphite furnace are reached. For this purpose the chemical form in which Pd was added to the samples was carefully evaluated over four different S species (sodium sulfite, sodium sulfate, thiourea and 3-mercaptopropionic acid) using Ru as permanent modifier in all the experiments. Pyrolysis curves, plotted in Figure II.7, were obtained for 500 ng of S as each of the four S species adding 40 μg of Pd in different ways: i) as Pd nitrate a good stabilization of the less volatile species up to 1200°C was achieved, while

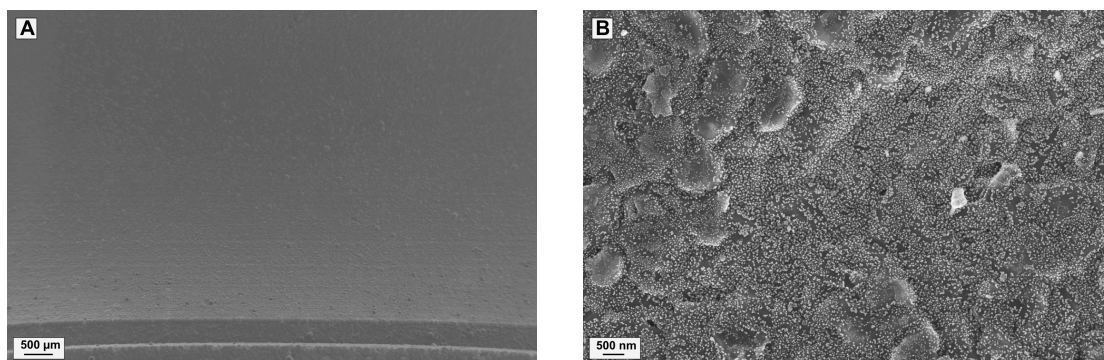
the more volatile species are clearly suffering from signal losses; ii) as thermally pre-reduced Pd nitrate, using a prior 1000°C heating step, the same situation occurs although the differences between less and more volatile species are not as pronounced as they were in the first case; iii) as pre-reduced Pd nitrate by previous addition of an excess of citric acid, only the signal for the most volatile compound (3-mercaptopropionic acid) remains slightly reduced in comparison with the other three species; and iv) as a Pd nanoparticles suspension produced in-house, providing the best results with similar responses for all the four species up to 1000°C pyrolysis temperature.

Figure II.7. Pyrolysis curves obtained for 500 ng of S introduced in different chemical forms when monitoring the 257.958 nm molecular CS line in the presence of Ru as permanent modifier plus 40 µg of Pd, added in different forms: **A)** as Pd(NO₃)₂; **B)** as Pd(NO₃)₂, but thermally pre-reduced using a previous 1000°C pyrolysis step; **C)** as Pd(NO₃)₂ together with an excess of citric acid; **D)** as Pd nanoparticles.



Volynsky and Krivan [29,30] already introduced the principles of the use of colloidal Pd as chemical modifier in graphite furnace techniques, which is the same situation as the current case except for the fact that the particle size used for this work is smaller (of approximately 20 nm size). SEM photographs are presented in Figures II.8 and II.9 comparing the coating of the sample platform with Pd nitrate and Pd nanoparticles after subjecting them to a 600°C pyrolysis temperature. The addition of nanoparticles provides a homogeneously distributed coating of metallic and highly reactive Pd nanoparticles throughout the bed of the platform (see Figures II.8.A, II.8.B and II.9.B). These particles are available for interaction already during the drying step, offering a large surface due to the small particle size attained. In the case of Pd nitrate, the distribution is not homogeneous but instead it tends to diffuse towards the edges of the platforms (see Figure II.8.C). Moreover a thin layer is formed very prone to crack as the temperature rises during the pyrolysis step (see Figures II.8.D and II.9.C).

Figure II.8. SEM images of the sample surface of a graphite platform subjected to a 600°C pyrolysis stage under the following conditions: **A** and **B**) with 40 µg Pd previously deposited as an in-house synthesised suspension of Pd nanoparticles (acquired with a 25x and a 10 000x magnification, respectively); **C** and **D**) with 40 µg Pd previously deposited as Pd(NO₃)₂ solution (acquired with a 25x and a 10 000x magnification, respectively).



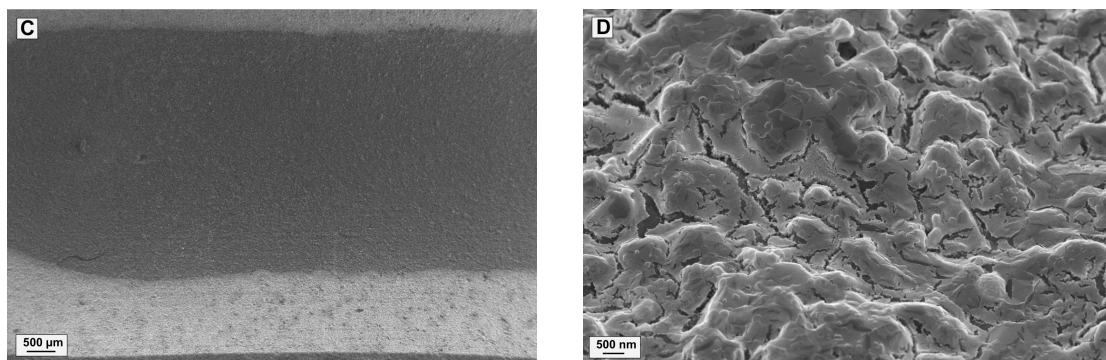
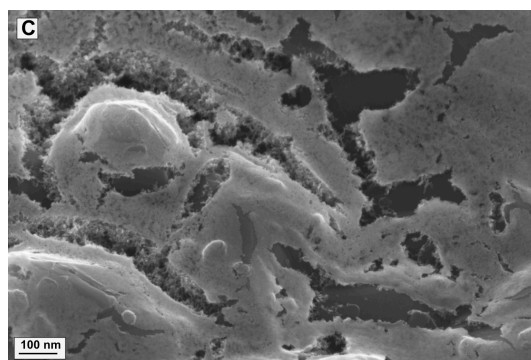
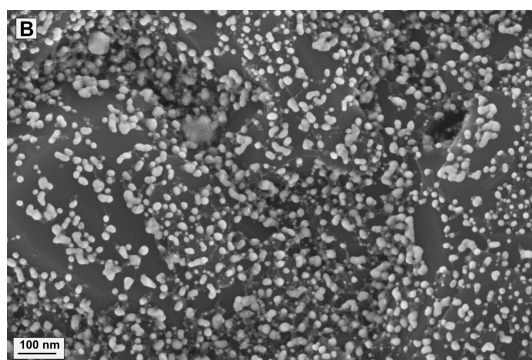
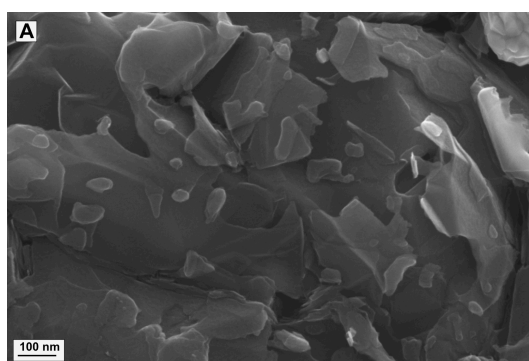


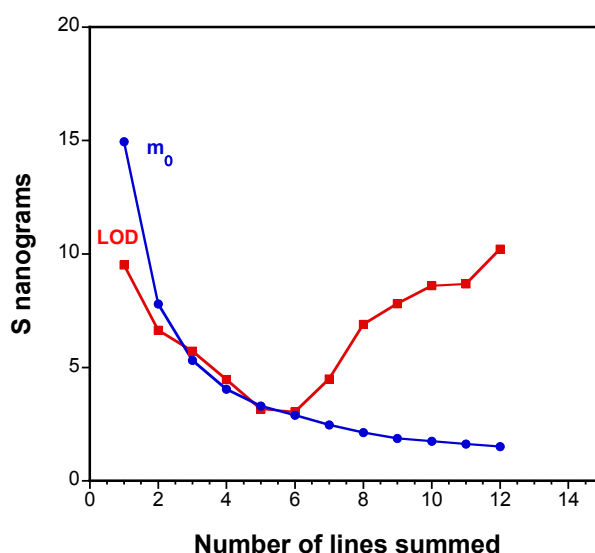
Figure II.9. SEM images acquired with 50 000X magnification of the sample surface of a graphite platform subjected to a 600°C pyrolysis stage under the following conditions: **A)** empty sample platform; **B)** with 40 µg Pd previously deposited as an in-house synthesised suspension of Pd nanoparticles; **C)** with 40 µg Pd previously deposited as Pd(NO₃)₂ solution.



A temperature of 2400°C was preferred for atomization and measurement of the signal based on a better peak definition rather than the greatest peak area (achieved at 2200°C). Under these conditions of temperature and chemical modifiers, the analytical figures of the method were evaluated: i) a wide range of linearity was obtained for the 12 more sensitive transitions

(from 50 to 2500 ng S); and ii) for the 257.958 nm peak a LOD of 9 ng and a characteristic mass (m_0) of 14 ng were calculated, although combining the signal for the six main lines within the recorded spectral window, both the LOD and the characteristic mass (m_0) decrease down to 3 ng. Figure II.10 represents the influence of summing the signal for different line combinations tested on the LOD and on the m_0 .

Figure II.10. Influence of simultaneous multi-line evaluation of several CS lines on the m_0 and the LOD, calculated from a series of 15 replicates. The summation was performed following the order of sensitivity, starting with the molecular line located at 257.958 nm.



The method then was applied to the determination of the very different types of solid samples listed before. The suspension of Pd nanoparticles proved to perform satisfactory also with direct solid sampling, providing a uniform response despite the chemical form in which S is available. The behaviour of the different matrices is not the same, as expected when dealing with solid samples. The signal appears normally delayed in comparison with an aqueous standard and, when dealing with refractory matrices, broadened (as it is the case of the steel samples and petroleum coke). However, a good correspondence in terms of A_{int} between the

samples and S aqueous standards was attained for all cases, allowing the use of the latter for calibration purposes, as illustrated in Figures II.11 and II.12.

Figure II.11. Time- and wavelength-resolved absorbance spectra obtained after the vaporization of approximately 500 ng S under the furnace conditions listed in Table II.5 from: **A)** a polyethylene CRM (ERM-EC680) without the addition of Pd nanoparticles; **B)** a polyethylene CRM (ERM-EC680) with the addition of Pd nanoparticles as chemical modifier; **C)** a biological CRM (BCR 129 Hay powder) with the addition of Pd nanoparticles as chemical modifier; and **D)** a steel CRM (BAS high-speed steel 482) with the addition of Pd nanoparticles as modifier.

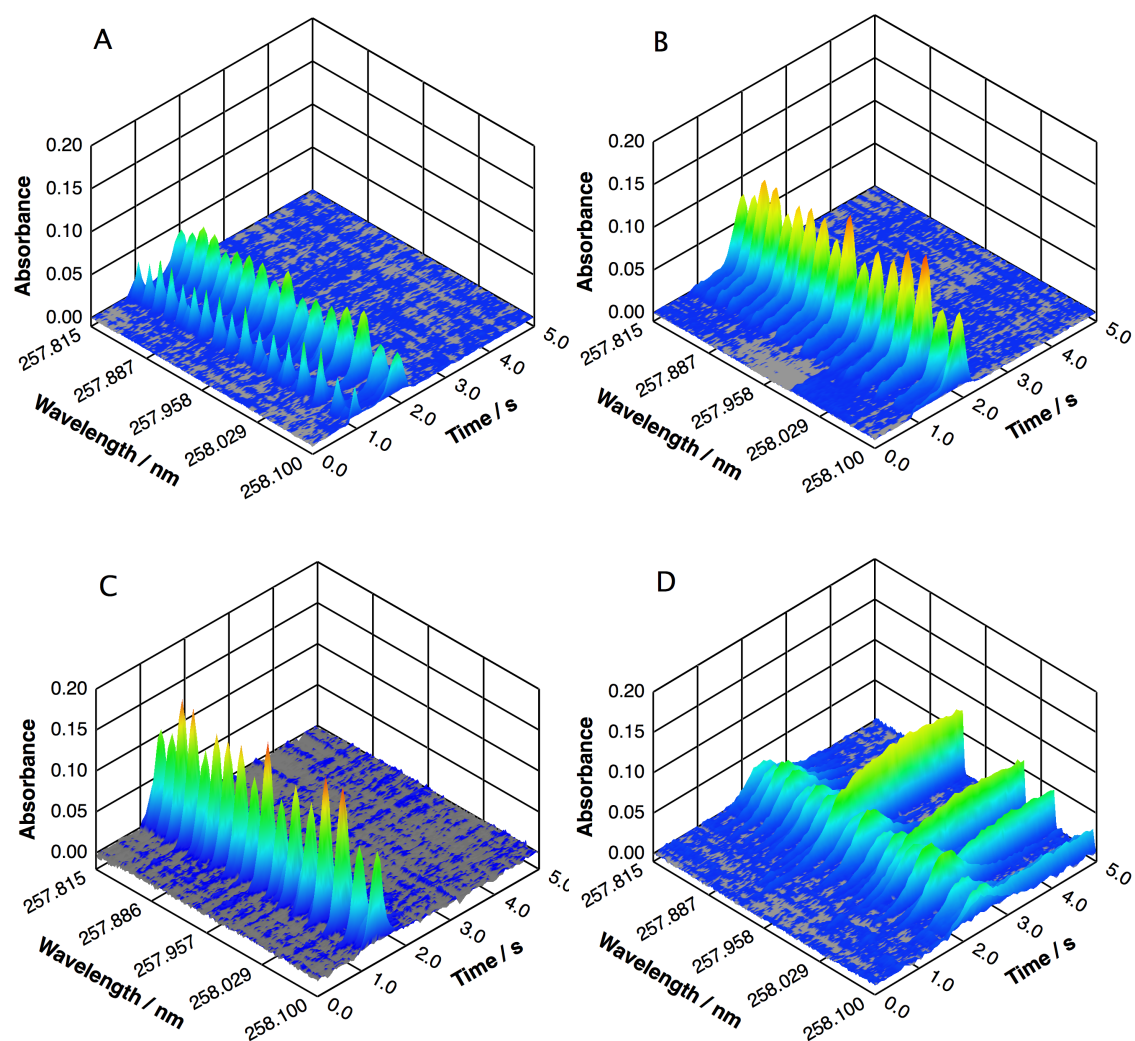
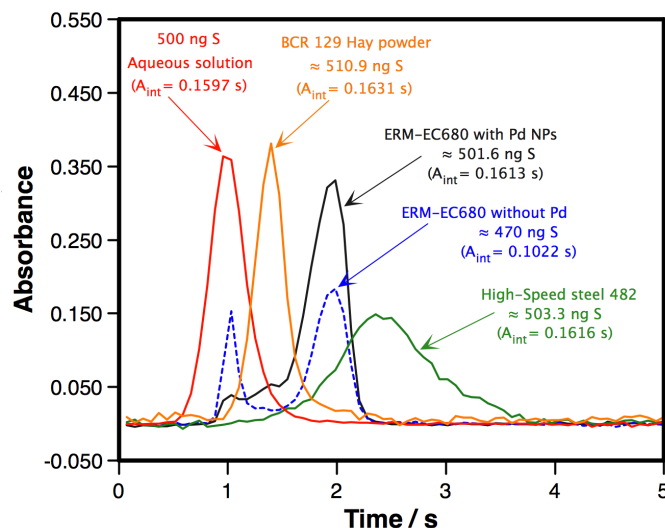


Figure II.12. Time-resolved absorbance signals measured at 257.958 nm (as sum of the 3 central pixels) and under the conditions listed in Table II.5 for a similar amount of S in aqueous solution and directly from several different solid samples, for comparison purposes



Each sample was subjected to eight determinations carried out in three different days. Every determination (15-20 min of work) consisted in five replicate solid doses and the median calculated for these five values was considered as representative value. Results for the six main transitions and the combination of all of them are reported in Table II.6.

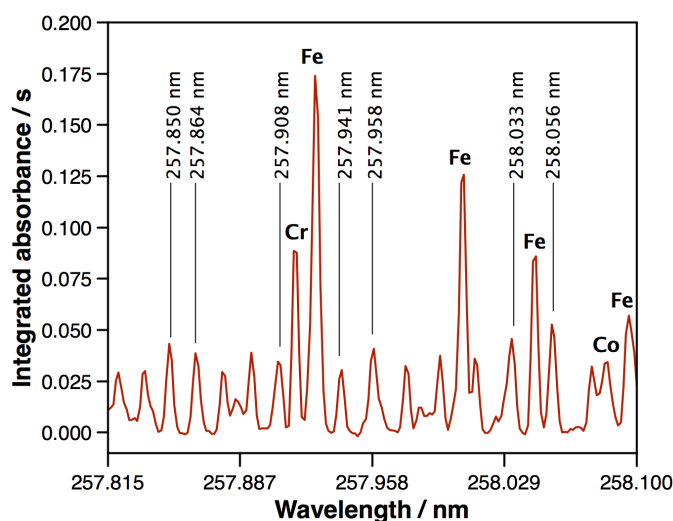
Excellent agreement with the certified reference values was achieved with the central line as well as with the average for all samples, providing precisions between 5-10% for individual lines and down to 3-5% for the total average. Also, based in the polyethylene ERM-EC681 sample, a LOD of $3 \mu\text{g g}^{-1}$ was calculated for the central line while $1 \mu\text{g g}^{-1}$ can be achieved when summing the signal for the six main lines under study.

Table II.6. Determination of S in different CRMs by means of HR CS GFMS (n=8) using different lines in the vicinity of 258 nm. Uncertainties are expressed as 95% confidence intervals (calculated as $\pm ts/\sqrt{n}$, where t, s and n have their usual meanings) and as relative standard deviation (RSD) values.

Sample	Reference value	257.958 nm (Central line)							Average (All lines)
		257.850 nm	257.864 nm	257.908 nm	258.033 nm	258.056 nm	258.056 nm		
ERM-EC680 polyethylene	S content/ $\mu\text{g g}^{-1}$ RSD/%	644 \pm 43 (8.0)	643 \pm 32 (6.0)	631 \pm 35 (6.6)	701 \pm 37 6.3)	698 \pm 43 (7.3)	665 \pm 32 (4.6)		
ERM-EC681 polyethylene	S content/ $\mu\text{g g}^{-1}$ RSD/%	78 \pm 4 (6.9)	77 \pm 5 (7.8)	82 \pm 5 (7.8)	79 \pm 5 (7.8)	81 \pm 4 (6.1)	80 \pm 2 (2.7)		
BAS High-speed steel 482	S content/ $\mu\text{g g}^{-1}$ RSD/%	251 \pm 15 (7.1)	235 \pm 14 (7.2)	242 \pm 15 (7.3)	257 \pm 16 (7.5)	267 \pm 13 (6.1)	251 \pm 12 (4.4)		
BAS Mid steel 453	S content/ $\mu\text{g g}^{-1}$ RSD/%	347 \pm 24 (8.1)	346 \pm 24 (8.4)	325 \pm 23 (8.5)	356 \pm 21 (7.0)	375 \pm 21 (6.6)	346 \pm 19 (5.3)		
BCR 129 Hay powder	S content/ $\mu\text{g g}^{-1}$ RSD/%	3120 \pm 240 (9.2)	3200 \pm 250 (9.3)	3140 \pm 170 (6.4)	2970 \pm 200 (8.1)	3060 \pm 250 (9.7)	3080 \pm 90 (2.8)		
NIST 1566a Oyster tissue	S content/ $\mu\text{g g}^{-1}$ RSD/%	8360 \pm 420 (6.0)	8790 \pm 370 (5.0)	8870 \pm 340 (4.6)	8700 \pm 470 (6.4)	8890 \pm 340 (4.6)	8670 \pm 240 (2.6)		
NIST 2718 Green petroleum coke	S content/ $\mu\text{g g}^{-1}$ RSD/%	45140 \pm 3380 (9.0)	45560 \pm 3270 (8.6)	46550 \pm 3350 (8.6)	43540 \pm 3560 (9.7)	45380 \pm 3110 (8.2)	45750 \pm 1680 (3.5)		

It needs to be mentioned that for the steel samples, spectral interferences occur in the region monitored due to the high amounts of Fe, Cr and Co present in the matrix (see Figure II.11.D). However, as illustrated in Figure II.13, those lines do not overlap with any of the selected six main lines [27], but depending on the amount of analyte and/or of the interfering Fe, it may be problematic to fix the baseline for the 258.056 nm peak. For this reason, this transition was not considered in the total average signal for the BAS Mild steel material, with an approximately 99% of Fe.

Figure II.13. Wavelength resolved time-integrated CS absorbance spectrum obtained after the vaporization of 1.300 mg of BAS High-speed steel 482 (325 ng S), showing the interfering peaks for Fe (960 μg), Cr (53 μg) and Co (3 μg) within the analytical region.



To conclude, this work presented a simple and fast method for the determination of S as CS by means of HR CS MAS based in an appropriate combination of chemical modifiers (Ru as permanent platform coating and metallic Pd added as a suspension of Pd nanoparticles) providing normalized analytical responses for a variety of samples and regardless of the particular chemical form in which S is found in the samples.

II.3.1.3. Direct determination of Br in plastic materials by means of solid sampling high-resolution continuum source graphite furnace molecular absorption spectrometry

Goals

The aim of this work was to study the potential of HR CS GFMAS for the determination of halogens while developing an analytical method for the direct determination of Br in polymeric samples.

This application was chosen because of the growing interest in controlling the toxicity and environmental impact of the great amount of plastic waste generated nowadays.

There is a group of additives, particularly used in the production of plastics intended for electronic devices, electrical appliances, clothing and furniture, known as brominated flame retardants (BFRs), whose function is to modify the behaviour of the host materials against fire [31,32]. These sorts of additives are normally organic compounds containing various Br atoms within their molecular structure, and they tend to be bonded to the polymeric material in such a weakly way that they are quite easy to be released into the environment becoming a potential risk to the ecosystem [33-35].

Strict regulations and restrictions have been established then regarding the use of BFRs, leading to the need for robust analytical methods capable of monitoring the presence of these compounds in plastics and ensure whether or not the legal limits are met [36,37].

HR CS GFMAS may offer a simple, fast and sensitive enough approach for the direct determination of Br in plastic samples within such a context based on its potential for solid sampling and the capabilities to monitor

molecular transitions along a narrow spectral window, as it was discussed in the previous section.

Methodology

The method developed is based on the formation of the diatomic molecule CaBr in gas phase and the monitoring of its molecular spectra in the vicinity of 625.315 nm.

Six reference materials (comprising polyethylene, polypropylene and ABS resin) with different certified contents in Br were analysed in order to validate the method. Table II.7 below provides some information on each one of those materials, such as type of plastic, Br content and physical form.

Each plastic material was cut in fragments of appropriate mass according to its Br content using a ceramic knife. After weighing the sample, the required chemical modifiers were added to the platform in order to form and stabilise the CaBr molecule (that is, 30 µg Pd as Pd(NO₃)₂ solution and 300 µg Ca as CaCO₃ solution). The sample platform was then transported to the graphite furnace to be subjected to the optimized temperature program.

Table II.7. List of polymeric CRMs analysed for Br

	Type of material	Certified Br content /mg kg ⁻¹	Physical form	Availability
ERM-EC680	High density polyethylene	808 ± 19	Granules (aprox. 10 mg weight)	IRMM
ERM-EG681	High density polyethylene	98 ± 5	Granules (aprox. 10 mg weight)	IRMM
PE-H-11A	High density polyethylene	1100 ± 44	Discs (aprox. 31 mm diameter and 13 mm thickness)	MAT
PE-L-11A	Low density polyethylene	500 ± 20	Discs (aprox. 31 mm diameter and 13 mm thickness)	MAT
ERM-EC591	Polypropylene	2080 ± 70	Granules (aprox. 10 mg weight)	IRMM
BAM-H010	Acrylonitrile butadiene styrene	240 ± 21	Discs (aprox. 40 mm diameter and 6 mm thickness)	BAM

Institute for Reference Materials and Measurements (IRMM, Geel, Belgium)

Modern Analytical Techniques (MAT, Hillsborough, USA)

Federal Institute for Materials Research and Testing (BAM, Berlin, Germany)

Table II.8 summarizes the instrumental conditions and temperature program used for this application.

Table II.8. Instrumental parameters used in the determination of Br by means of HR CS GFMS

Electronic transition	Red system, $\Delta v=0$, $X^2\Sigma^+ \rightarrow A^2\Pi$ (CaBr)	
Central wavelength	625.315 nm	
Spectral window	0.73 nm	
Number of detector pixels summed per line	3 (≈ 11 pm)	
Chemical modifiers	Ca (300 μ g) Pd (30 μ g)	
Sample mass range	ERM-EC680	0.1 mg - 0.2 mg
	ERM-EC681	0.7 mg - 1.0 mg
	PE-H-11A	0.1 mg - 0.2 mg
	PE-L-11A	0.1 mg - 0.4 mg
	ERM-EC591	0.1 mg - 0.15 mg
	BAM-H010	0.3 mg - 1.0 mg

Temperature program

Step	Temperature/ $^{\circ}\text{C}$	Ramp/ $^{\circ}\text{C s}^{-1}$	Hold time/ s	Gas flow rate/ L min^{-1}
Drying	90	5	20	2.0
Drying	120	5	30	2.0
Pyrolysis	1000	50	30	2.0
Auto Zero	1000	0	5	0.0
Vaporization	2100	3000	6	0.0
Cleaning	2500	1000	4	2.0

Optimizing the amount of Ca was required in order to ensure complete interaction with all Br species present in the samples and therefore maximize the sensitivity. It has to be taken into consideration that Ca forms stable diatomic molecules with most non-metals and association of Ca with F and Cl gives rise to more stable mono-halides than CaBr. Therefore, if a material with high contents of F and/or Cl is to be determined, a direct method without any prior sample treatment, like the one optimized in this work, would not be suitable. Anyway, 300 μ g Ca has proven to be a

sufficient amount to ensure a complete reaction when 100 ng of Br or lower amounts are present.

Pd was used as chemical modifier in order to stabilize the analyte during the pyrolysis step and best results were obtained when added in masses above 10 µg for a 100 ng Br solution.

Paying attention to the temperature program, the CaBr molecule allows for pyrolysis temperatures up to 1400-1500°C. After this temperature, the signal drop is rather abrupt, and so is the growth for the signal when monitoring the vaporization temperature, reaching a maximum at 1900-2200°C. This is a very positive situation, where a pyrolysis temperature high enough to allow most matrix removal can be used and, at the same time, a rather mild vaporization temperature can be applied during the measurement, resulting in a beneficial effect over the lifetime of all perishable components of the furnace.

Calibration was carried out *versus* daily prepared aqueous Br standard solutions. The analytical result was obtained summing the A_{int} for the 3 central pixels of the transition peak registered at 625.315 nm. Each sample was analysed in a different session. For each sample, seven determinations (in total) were carried out, and for each determination, three solid replicates were measured. The median was taken as the estimate value of the total Br content in the samples.

Results and discussion

As it was already mentioned in the introduction chapter, the main atomic absorption lines of Br lie within the vacuum-UV region. The principal line is located at 148.845 nm [38]. Because it is not possible to measure in such short wavelength with the instrumentation currently available, it is

necessary to search for an alternative. Just a couple of previous works were published using HR CS AAS for studying the absorption spectra of Br-based molecules. Huang *et al.* [39] made a general study comparing the formation and absorption structures of Br binary compounds with Al, Sr and Ca, further focusing in the AlBr and CaBr molecules. Limburg and Einax [40] optimized an analytical method for the determination of Br as CaBr in water solutions and organic solvents.

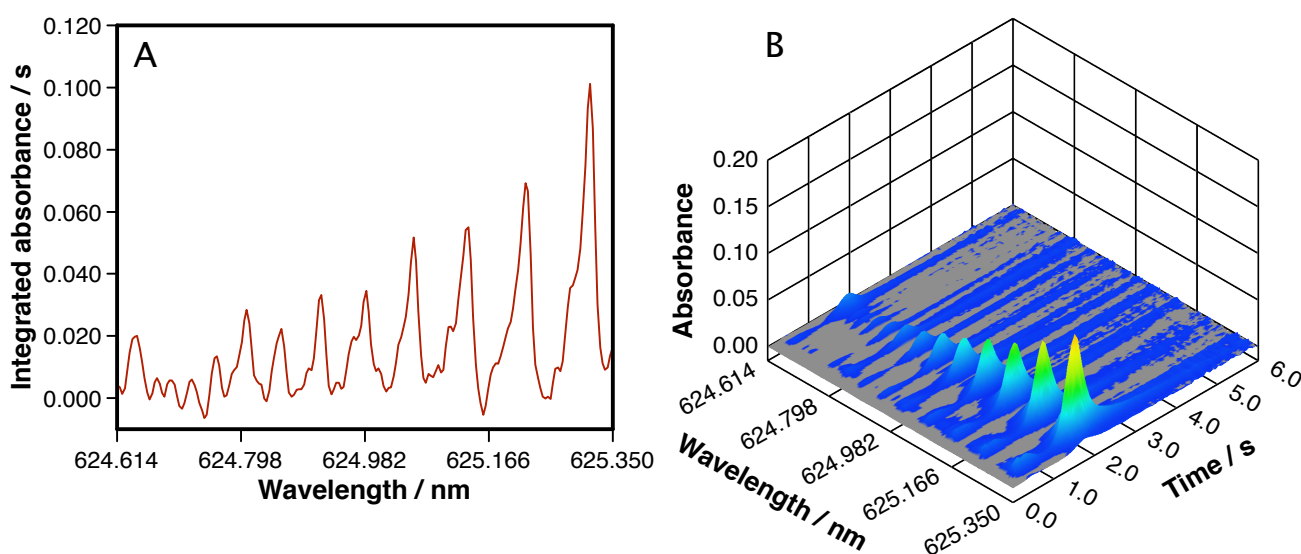
In this work, and based on those previous studies, Ca was preferred over Al for mainly two reasons: i) CaBr is less volatile than AlBr [39]. In monitoring CaBr, it is possible to use pyrolysis temperatures up to 1400°C-1500°C (up to 900°C in the case of AlBr), assuring a better removal of the matrix, and this is particularly important when the direct analysis of solid samples is intended; and ii) the resolved structure of its spectrum opposite to the broad band of AlBr.

CaBr has its main resonance system between 625 and 628 nm, consisting on a structure of fine rotational lines that are well resolved and show a maximum peak at 625.315 nm [22]. This kind of molecular absorption structure greatly simplifies the selection of pixels for baseline correction, providing the method with a suitable robustness.

In Figure II.14 a typical absorption profile for CaBr is depicted. In this work, only the four more sensitive peaks were taken into account to be studied in detail. These transitions appearing at 625.315 nm, 625.223 nm, 625.135 nm and 625.058 nm are close and distant enough in sensitivity to make it feasible to explore the possibility of improving the LOD as well as expanding the linear range [41,42]. Indeed, if the intensity of all four main lines is combined, it is possible to reduce the LOD by a factor of three (1.8

$\mu\text{g g}^{-1}$ Br in comparison to $5.4 \mu\text{g g}^{-1}$, attainable when monitoring only the most sensitive peak).

Figure II.14. Overview of the CaBr molecular absorption structure around 624.982 nm (central pixel) for the vaporization of 100 ng Br, plus 300 μg Ca and 30 μg Pd under the furnace conditions listed in Table II.8. **A** shows a wavelength resolved time-integrated spectrum, while in **B** the three-dimensional time and wavelength resolved spectrum is presented.



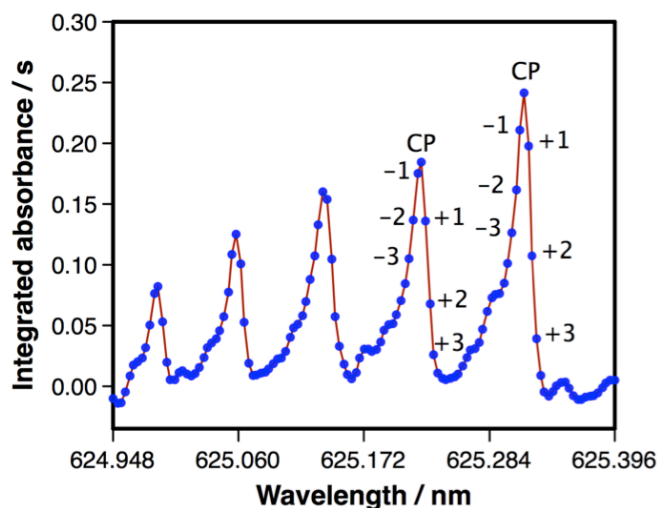
On the other hand, the difference in sensitivity between the four lines allows for the expansion of the linear range along almost three orders of magnitude, as it is presented in Table II.9. Of course, making use of the signal for less sensitive peaks would increase the linear range even further, but that would be of no interest for the current application.

Table II.9. Analytical features for the four main CaBr rotational transitions monitored under the conditions summarized in Table II.8. Characteristic mass values were calculated as 0.0044 divided by the slope of the calibration curve. LODs values were calculated as three times the standard deviation of the blank (n=10) divided by the slope of the calibration curve.

Wavelength/ nm	m ₀ / ng	LOD / ng	Linear range	R ²
625.315	1.32	5.4	Up to 300 ng	0.999
625.223	1.77	7.3	Up to 300 ng	0.999
625.135	2.42	12.7	Up to 700 ng	0.996
625.058	3.00	18.2	50 – 2000 ng	0.997

It is worth mentioning that an alternative to increase the linear range always available when using HR CS AAS is the possibility to select side pixels, instead of using the central pixel plus the two adjacent ones (CP \pm 1), which is the option recommended for achieving the best LOD [42-44]. This strategy to expand linearity has been successfully used in previous works [42,45,46], but seems to be limited in this particular case by i) the proximity of the adjacent lines and ii) the asymmetry of the peaks, as shown in Figure II.15. This aspect is relevant because if the signal is symmetrical, as it is most often the case for atomic lines, by using two side pixels located at the same distance from the CP (*e.g.* +3 and -3), the overall signal may remain constant even if there are some spectral drifts during the measurements (the increase in one pixel would be balanced by the decrease in the other one). However, that is clearly not the case for CaBr lines, as the signal becomes very asymmetric when moving more than 2 pixels away from the central pixel. Thus, monitoring side pixels is not recommended in this case. Fortunately, the availability of less sensitive CaBr makes it easier to accommodate the sensitivity of the method to that of the sample and that should be the preferred solution for monitoring high Br amounts.

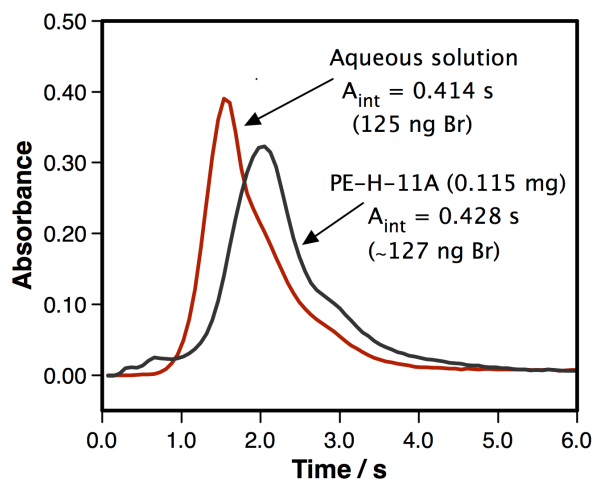
Figure II.15. Wavelength resolved time-integrated absorbance spectrum obtained by vaporization of approximately 250 ng of Br (0.310 mg of sample ERM-EC680). The signal only shows the region where the main CaBr molecular absorption lines are located. The signal recorded by every individual detector pixel is highlighted (blue dots).



Monitoring several absorption peaks is also an advantage for better assessing the reliability of the results, permitting to directly detect any spectral overlap affecting one of the peaks. Therefore, the determination of the plastic samples was carried out in all of the four main sensitive lines of the CaBr molecular system following the methodological procedure described before.

It is important to emphasize that in these optimal conditions the signals obtained for the solid samples and for aqueous standard solutions were always comparable in terms of peak area. Figure II.16 shows an example of the typical temporal signal profile found for polymers and for solutions.

Figure II.16. Comparison of a time-resolved molecular absorbance signal recorded at the 625.315 nm CaBr transition (sum of three central pixels) after vaporizing a similar amount of Br from an aqueous solution and directly from a polyethylene material under the conditions listed in Table II.8.



The results obtained for the CRMs listed in Table II.7 and for each of the absorption peaks listed in Table II.9 are displayed in Table II.10. In all of the cases, a good agreement with the reference values was found. Anyhow, best results are obtained when combining the values of the four transitions studied, which brings about also the best precision (RSD values between 3 and 7 %).

It can be concluded that HR CS GFMA offers a fast and simple method for determining total Br content in polymers, which is sensitive enough to comply with regulations. This method can be useful for screening purposes with the idea of filtering out most of the samples prior to be subjected to more time-consuming techniques that may selectively analyse the target brominated compounds in each of those in which the total Br content is high enough to be of concern.

Table II.10. Determination of Br in different CRMs by means of SS HR CS GFAAS ($n=7$) using different lines in the vicinity of 625.2 nm. Uncertainties are expressed as 95% confidence intervals (calculated as $\pm t_s/\sqrt{n}$, where t_s and n have their usual meanings) and as RSD values.

Sample	Reference value	625.315 nm	625.223 nm	625.135 nm	625.058 nm	Average (all lines)
ERM-EC680	Br content/mg kg ⁻¹ (RSD/%)	808 ± 19 (4.6)	784 ± 33 (4.5)	809 ± 30 (4.0)	843 ± 37 (4.7)	810 ± 40 (3.1)
ERM-EC681	Br content/mg kg ⁻¹ (RSD/%)	98 ± 5 (9.1)	91.2 ± 6.4 (7.6)	95.7 ± 6.5 (7.4)	108.0 ± 7.0 (7.0)	98.7 ± 11.3 (7.2)
PE-H-11A	Br content/mg kg ⁻¹ (RSD/%)	1100 ± 44 (4.3)	1100 ± 57 (5.5)	1090 ± 66 (6.6)	1140 ± 52 (5.0)	1130 ± 49 (2.7)
PE-L-11A	Br content/mg kg ⁻¹ (RSD/%)	500 ± 20 (4.6)	475 ± 13 (2.9)	516 ± 18 (3.4)	514 ± 16 (3.1)	502 ± 30 (3.7)
ERM-EC591	Br content/mg kg ⁻¹ (RSD/%)	2080 ± 70 (7.6)	1920 ± 160 (8.7)	1940 ± 150 (8.5)	2160 ± 160 (7.8)	2030 ± 180 (5.7)
BAM-H010	Br content/mg kg ⁻¹ (RSD/%)	240 ± 21 (6.7)	211 ± 13 (6.8)	227 ± 18 (8.5)	245 ± 9 (4.0)	232 ± 26 (7.1)

II.3.1.4. Progress in the determination of metalloids and non-metals by means of high-resolution continuum source atomic or molecular absorption spectrometry. A critical review

This article reviews all the literature available based on the use of HR CS AAS for the determination of metalloids and non-metals. In particular, the advantages of the techniques for the monitoring of metalloids are highlighted, since these analytes (B, Si, Ge, As, Se, Sb and Te) share that their resonance lines are always located at short wavelengths and they do not typically show suitable alternative lines. At these wavelengths (below 260 nm) the potential for suffering from spectral overlaps significantly increases as ubiquitous diatomic molecules such as PO, CS, NO or SiO absorb radiation. Thus, the benefits of HR CS AAS to detect and correct for interferences is discussed, and examples found in the literature are presented. Figure II.17 shows an example of the application of the least-squares algorithm permitting the isolation of a measured Sb signal in a urine sample surrounded by the PO hyperfine molecular structure that was presented in the review.

Despite of the improved performance of the technique for metalloids, perhaps its most remarkable feature is the new potential to directly determine non-metals by means of the monitoring of the molecular spectra of diatomic species. Figure II.18 indicates how authors are increasingly making use of this possibility for research.

In this regard, the article presents a tutorial discussion on the right strategy to produce the species of interest in a furnace and to take advantage of the type of spectrum typically obtained, proposing a practical classification of three types of spectra (of which AlF, CS and CaBr, shown in the previous chapters, are good examples). The article also indicates some basic differences when using a flame as atomizer. Finally, the work devotes a

specific section to the works published to date describing the determination of P, S, halogens and N-containing species, respectively. Since, the majority of the aspects related to monitoring of molecular species have been already described in the introduction and in the previous sections, no more details will be provided herein.

Figure II.17. Application of the LSBC algorithm for isolating the Sb atomic absorption signal from the PO molecular structure in the vicinity of 217.6 nm. **A)** Time-resolved absorption spectrum obtained from the measurement of a 1:2 diluted urine sample containing $45.9 \mu\text{g L}^{-1}$ Sb by means of HR CS AAS; **B)** Sb absorption signal resulting from applying LSBC on the signal obtained in A; **C)** Time-integrated absorbance spectra of a) the urine sample recorded in **A**; b) a 1% (m/v) $\text{NH}_4\text{H}_2\text{PO}_4$ solution; and c) spectrum result from the subtraction of the reference spectrum (b) to the urine sample signal (a) using LSBC.

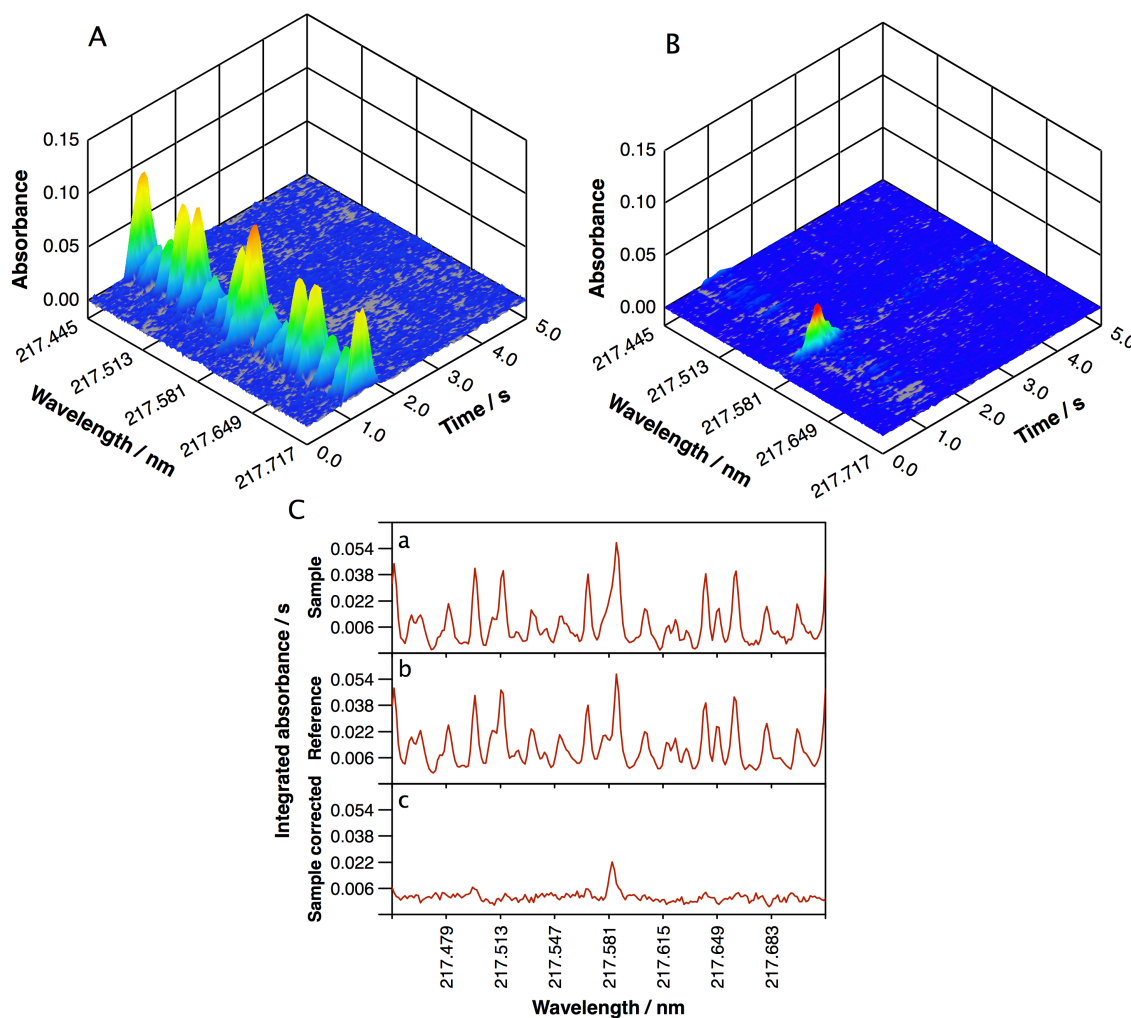
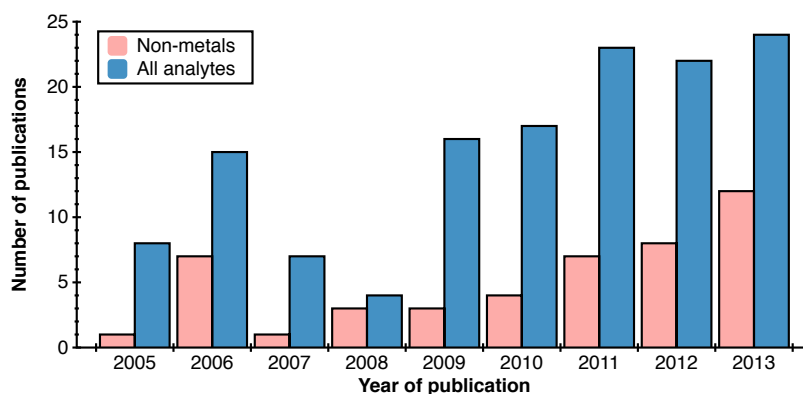


Figure II.18. Number of publications that have reported the use of high-resolution continuum source atomic (or molecular) absorption spectrometry for the determination of non-metals, or of any type of analyte. Source: ISI Web of Science. Papers that appeared in proceedings and book chapters are not included.



II.3.2. Multiline monitoring

II.3.2.1. On the possibilities of high-resolution continuum source graphite furnace atomic absorption spectrometry for the simultaneous or sequential monitoring of multiple atomic lines

Goals

The aim of this work was to evaluate the potential of the nowadays commercially available HR CS AAS instrumentation to perform simultaneous or sequential monitoring of multiple atomic lines to fully exploit the analytical advantages derived from this strategy and investigate under which circumstances it may allow to expand the linear range and, particularly, to develop multi-element methods.

Methodology

All the measurements presented in this work were carried out using HR CS GFAAS.

The direct determinations of Co, Fe and Ni in NIST SRM 1566a Oyster tissue (National Institute of Standards and Technology, Gaithersburg,

USA) and Ni and Cd in BCR CRM 679 White cabbage (Community Bureau of Reference, Geel, Belgium) were carried out in the conditions summarized in Tables II.11 and II.12, respectively.

Table II.11. Instrumental parameters used for the simultaneous determination of Co, Fe and Ni in NIST SRM 1566a Oyster tissue by means of solid sampling HR CS GFAAS

Analyte	Ni	Fe	Fe	Co
Wavelength / nm	352.454	352.604	352.617	352.685
Number of pixels summed	3 (≈ 5.9 pm)	3 (≈ 5.9 pm)	3 (≈ 5.9 pm)	3 (≈ 5.9 pm)
Sample mass / mg	2-3			
Chemical modifier	5 μg Pd (added as $\text{Pd}(\text{NO}_3)_2$ solution)			
Temperature program				
Step	Temperature / $^\circ\text{C}$	Ramp / $^\circ\text{C s}^{-1}$	Time /s	Gas flow rate /L min $^{-1}$
Drying	150	5	35	2.0
Pyrolysis	1000	50	30	2.0
Auto-zero	1000	0	5	0.0
Atomization	2500	1200	6	0.0
Cleaning	2600	500	4	2.0

Table II.12. Instrumental parameters used for the multi-elemental determination of Cd and Ni in BCR CRM 679 White cabbage by means of solid sampling HR CS GFAAS using **a)** a simultaneous approach and **b)** a sequential approach

a) Simultaneous determination of Cd and Ni				
Analyte	Cd	Ni		
Wavelength / nm	228.802	228.998		
Number of pixels summed	3 (≈ 3.7 pm)	3 (≈ 3.7 pm)		
Sample mass / mg	0.3 – 0.5			
Chemical modifier	1 μg Pd (added as $\text{Pd}(\text{NO}_3)_2$ solution)			
Temperature program				
Step	Temperature/ $^\circ\text{C}$	Ramp/ $^\circ\text{C s}^{-1}$	Time/s	Gas flow rate/L min $^{-1}$
Drying	150	5	35	2.0
Pyrolysis	800	50	30	2.0
Auto-zero	800	0	5	0.1
Atomization	2300	1200	7	0.1
Cleaning	2600	500	4	2.0

b) Sequential determination of Cd and Ni				
Analyte	Cd		Ni	
Wavelength / nm	228.802		234.554	
Number of pixels summed	3 (≈ 3.7 pm)		3 (≈ 3.7 pm)	
Sample mass / mg	0.1 – 0.3			
Temperature program				
Step	Temperature/°C	Ramp/°C s ⁻¹	Time/s	Gas flow rate/L min ⁻¹
Addition of 10 μ L of chemical modifier (Pd, 30 mg L ⁻¹)				
Drying	150	5	35	2.0
Pyrolysis	700	300	30	2.0
Auto-zero	700	0	5	0.1
Atomization	1300	1200	5	0.1
Cool down	20	100	10	2.0
Addition of 10 μ L of chemical modifier (Pd, 100 mg L ⁻¹)				
Drying	150	10	35	2.0
Pyrolysis	1300	500	1	2.0
Gas adapt	1300	0	5	0.1
Atomization	2500	1200	5	0.1
Cleaning	2600	500	4	2.0

Samples were directly analysed, without any previous treatment. Calibration was carried out *versus* daily prepared aqueous standard solutions in all cases. The analytical result was obtained summing the A_{int} for the 3 central pixels of the transition peaks monitored. For each sample, five replicate measurements were performed. The median was taken as the representative value of the total analyte content in the samples.

Results and discussion

As it was already discussed in the introduction section, when simultaneously monitoring multiple lines of the same element within the same analytical spectral window two situations may arise: i) if the sensitivities of the atomic lines are similar, combining the analytical signal for all of them may somehow improve the LOD [41,42]; and ii) if the sensitivity of the lines is

significantly different it is not advisable to sum their signals, as the less sensitive ones will moderately improve the analytical signal while contributing to increase the noise level. However, in this last situation an easy expansion of the linearity is feasible, as each of the lines should cover a very different linear range.

Two clear examples of these situations were already presented when dealing with molecular absorption structures (CS and CaBr, representing i) and ii) cases, respectively). In this work the Ni triplet appearing in the 234.6 nm region is evaluated in order to further illustrate the situation in which atomic lines with different sensitivities are at disposal. Figure II.19 displays the spectrum recorded from 234.533 nm to 234.792 nm, where three lines of Ni appear (at 234.554, 234.663 and 234.751 nm) with a representation of their linear ranges. Table II.13 summarizes the analytical features of each of these lines.

Figure II.19. Wavelength-resolved time-integrated spectrum showing the Ni triplet in the vicinity of 234.6 nm of 10 ng Ni added as an elemental aqueous solution by means of HR CS AAS. The linear range of each of the three lines is also shown.

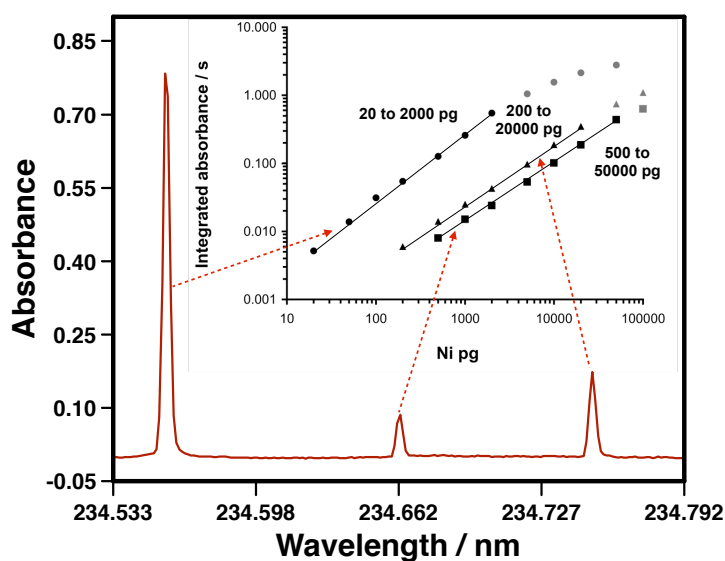


Table II.13. Analytical features of the three lines of the Ni triplet found in the vicinity of 234.6 nm

Wavelength/ nm	m_0/pg	LOD/pg	Linear range/pg	R^2
234.554	16	11	Up to 2,000	0.998
234.663	260	210	Up to 50,000	0.999
234.751	140	160	Up to 20,000	0.999

The three lines exhibit very different sensitivities and therefore very different linear behaviour, permitting to cover a range from 20 to 50,000 pg. In this way, the line that fits best for every sample can be chosen *a posteriori* without modifying the experimental conditions or repeating any measurements.

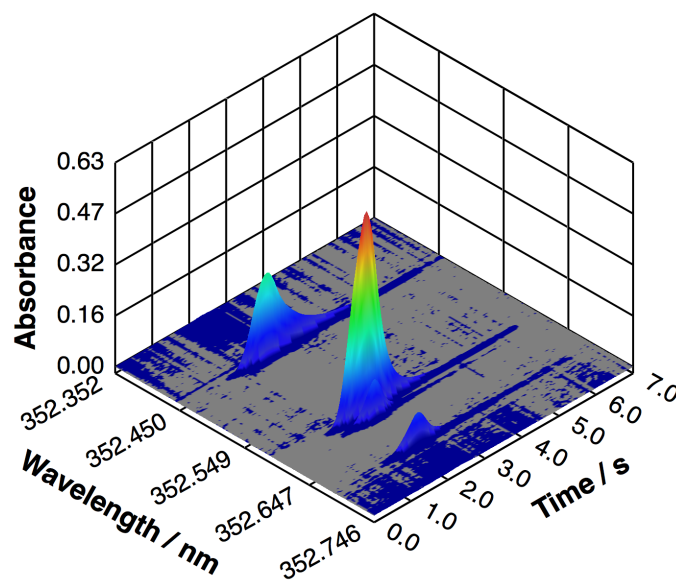
Concerning the multi-elemental capabilities of the HR CS AAS technique, it was also previously discussed how, when lines of different elements lie close enough to be recorded within the same spectral window, two situations may be encountered: i) that the elements of interest show similar volatilities; and ii) that the elements show very different thermal behaviour.

In this work, both situations were studied and illustrated with examples.

In the situation where the volatilities are similar it is rather simple to optimize a temperature program that suits all the elements for an almost simultaneous atomization. The neighbouring of 352.5 nm, where an atomic line for Ni (352.454 nm, with a m_0 of 30 pg), a duplet for Fe (352.604/352.617 nm, with m_0 of 3 and 27 ng, respectively) and a line for Co (352.685 nm, with a m_0 of 75 pg) are found, was further studied in this work. Direct solid determination of a biological CRM, NIST 1566a Oyster tissue, was investigated under the instrumental parameters listed in Table II.11. It is important to stress that there is an adequate correspondence between the sensitivities of these lines and the analyte contents in this sample, which is a requisite for simultaneous multi-element analysis using

HR CS GFAAS. The organic sample matrix is easy to remove at moderate pyrolysis temperatures, avoiding analyte losses as well as minimizing potential matrix interferences, which makes this kind of sample ideal for SS HR CS GFAAS analysis. A three-dimensional spectrum recorded for one of the sample replicates is presented in Figure II.20.

Figure II.20. Three-dimensional time- and wavelength-resolved absorbance spectrum obtained for the simultaneous determination of Co (352.685 nm), Fe (352.604/352.617 nm) and Ni (352.454 nm) in 2.795 mg of NIST SRM 1566a Oyster tissue by means of SS HR CS GFAAS under the instrumental conditions listed in Table II.11.



As can be seen, well-defined unimodal signal profiles were obtained for all analytes, which were actually very similar both in terms of shape and, most important, in terms of sensitivity to those obtained for aqueous standard solutions, thus enabling simple calibration just by constructing the curve with aqueous standard solutions.

The results for this determination are presented in Table II.14, which proved the validity of the method to obtain accurate multi-element values in a fast and simple way.

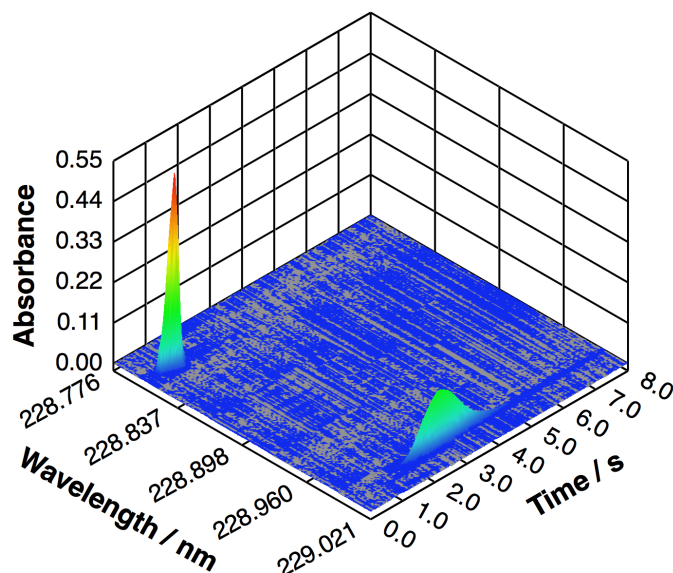
Table II.14. Results obtained for the simultaneous multi-element determination of Co, Fe and Ni (n=5) in NIST SRM 1566a Oyster Tissue by means of solid sampling HR CS GFAAS. Uncertainties are expressed as 95% confidence intervals (calculated as $\pm ts/\sqrt{n}$, where t, s and n have their usual meanings)

Wavelength / nm	Analyte	Result / $\mu\text{g g}^{-1}$	Certified value / $\mu\text{g g}^{-1}$
352.454	Ni	2.08 ± 0.20	2.25 ± 0.45
352.604	Fe	557 ± 23	539 ± 32
352.617	Fe	567 ± 31	539 ± 32
352.685	Co	0.59 ± 0.06	0.57 ± 0.11

When the elements of interest show very different volatilities, two possibilities can be considered. If a simultaneous determination is preferred, compromise conditions of temperature and chemical modifier/s have to be employed. However, in this case a sequential approach is also possible programming a different atomization step for each of the analytes [47-50]. Moreover, also the spectral region can be modified for each atomization step, and so are the Ar flow conditions and the chemical modifier/s, allowing for the determination of each analyte in its optimum conditions.

To compare these two approaches, a biological reference material, BCR 679 White cabbage was analysed for Cd and Ni contents. In the region of 228.9 nm, two lines that are sufficiently close to be recorded simultaneously appear, corresponding to the main Cd atomic line (228.802 nm) and a secondary Ni atomic line (228.998 nm). Compromise furnace conditions were developed in order to simultaneously monitor both signals, using an atomization temperature high enough to atomize both elements but without decreasing too much the sensitivity for the most volatile one (Cd). In addition, the amount of chemical modifier was also optimized, paying special attention to the stabilization of Cd during the pyrolysis. The conditions finally used are summarized in Table II.12(a) and the three-dimensional spectrum obtained is presented in Figure II.21.

Figure II.21. Three-dimensional time- and wavelength-resolved absorbance spectrum obtained for the simultaneous determination of Cd (228.802 nm) and Ni (228.998 nm) in 0.453 mg of BCR CRM 679 White cabbage by means of solid sampling HR CS GFAAS under the instrumental conditions listed in Table II.12(a).



However, by selecting two different atomic absorption lines for Ni and Cd for this sample and the optimum conditions for each one of them it is possible to subject the sample to two temperature programs consecutively and obtain sequential results for Cd and Ni (the optimum atomization temperature for Cd would be suitable for Ni pyrolysis), but from the same sample replicate. Conditions for the analysis are presented in Table II.12(b) and an illustrative bi-dimensional plot of both signals in time is deployed in Figure II.22.

Results obtained for both approaches along with the certified reference values are presented in Table II.15 for comparison purposes. An excellent agreement with the expected values is reported in both situations. Again, it was feasible to carry out the calibration with aqueous standard solutions.

Figure II.22. Time profile for the sequential and selective atomization of Cd and Ni in 0.266 mg of BCR CRM 679 White cabbage by means of SS HR CS GFAAS under the instrumental conditions listed in Table II.12(b).

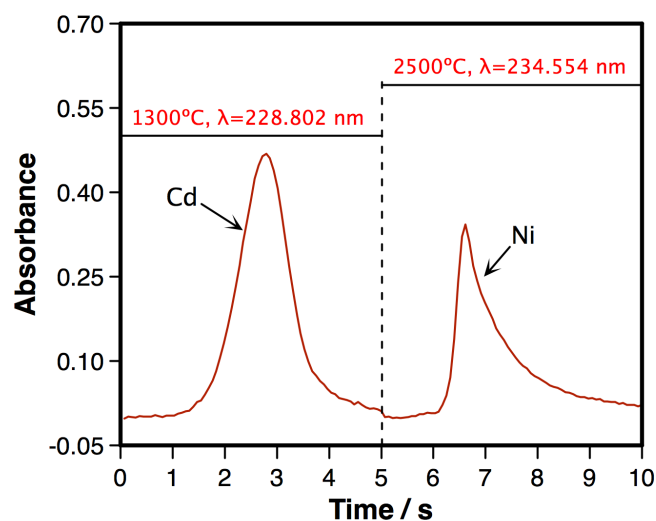


Table II.15. Comparative results obtained for the simultaneous (using the conditions listed in Table II.12(a)) and sequential (using the conditions listed in II.12(b)) multi-element determination of Cd and Ni (n=5) in BCR CRM 679 White cabbage by means of SS HR CS GFAAS. Uncertainties are expressed as 95% confidence intervals (calculated as $\pm ts/\sqrt{n}$, where t, s and n have their usual meanings)

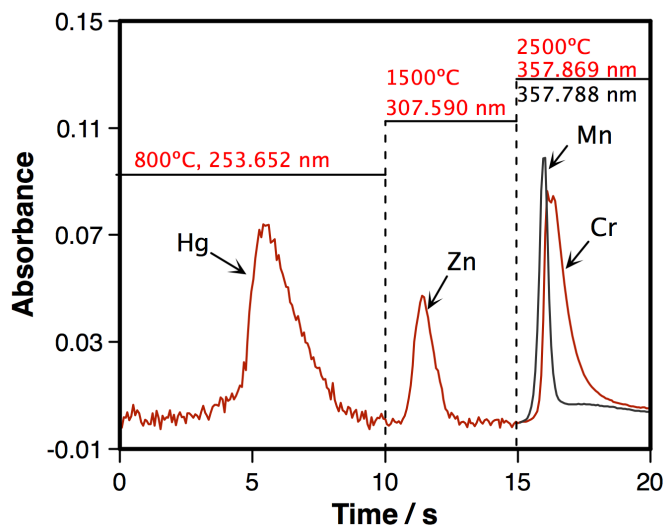
Analyte	Simultaneous method/ $\mu\text{g g}^{-1}$	Sequential method/ $\mu\text{g g}^{-1}$	Certified value / $\mu\text{g g}^{-1}$
Cd	1.69 ± 0.13	1.60 ± 0.14	1.66 ± 0.07
Ni	27.3 ± 1.7	27.6 ± 1.9	27.0 ± 0.8

Figure II.23 presents an example of the sequential situation further expanded when a highly volatile element (Hg) wants to be determined along with an element with medium volatility (Zn) and two of low volatility (Cr and Mn). The last two elements show closely adjacent lines such that they are simultaneously monitored.

In summary, although limited when comparing with other multi-element techniques, the commercially available HR CS AAS instrumentation offers a potential possibility for performing multi-line monitoring and direct

multi-element analysis, which represents a key improvement in the trajectory of AAS techniques.

Figure II.23. Sequential and selective atomization of Hg (5 ng), Zn (20 ng) and Cr (40 pg) added as a multi-element aqueous standard solution by means of HR CS GFAAS. The signal of Mn, due to the use of KMnO_4 as chemical modifier for Hg, was divided by a factor of 5 to keep the same scale



II.3.2.2. High-resolution continuum source atomic absorption spectrometry for the simultaneous or sequential monitoring of multiple lines. A critical review of current possibilities

This review work critically examines the potential of HR CS AAS for multi-line monitoring, discussing in detail the possible strategies to develop multi-element methods, considering the requirements and limitations of the technique.

Moreover, the article also discusses other advantages deriving from multi-line monitoring, such as: i) the expansion of the linear range by measuring multiplets; ii) the possible improvements in the LOD and in precision by summing the signals from different lines of the same element or molecule; iii) the possibilities to correct for matrix effects by selecting an IS; and iv) the accurate mathematical correction of spectral overlaps by simultaneous

monitoring of other lines of the interfering molecule or element that are free of interferences. All these aspects are illustrated with examples found in the literature, stressing their importance for the straightforward analysis of solid samples and complex materials.

Finally, the differences found when the flame is used as an atomization unit, thus resulting in quasi-stable signals, are also addressed.

Since the majority of these aspects have been already commented extensively in the introduction and in the previous section, they will not be repeated herein.

II.3.3. Microsampling

II.3.3.1. Simultaneous direct determination of Ni and Cd in *Daphnia magna* specimens by means of high-resolution continuum source graphite furnace atomic absorption spectrometry for eco-toxicological assessment purposes

Goals

This work is part of a broader cooperation study with the Laboratory of Environmental Toxicology and the Laboratory of Microbial Ecology and Technology of Ghent University.

In this work, the capabilities of SS HR CS GFAAS for the direct determination of the total Ni body burden in individual specimens of *D. magna* (small aquatic invertebrates of approx. 2 mm length that are widely used in eco-toxicological research) were investigated.

Out of the interpretation of the obtained results from the eco-toxicological point of view two papers were published. A first one is based in the study of the potential of using metal-contaminated liposomes as an alternative delivery system of dietary metals rather than the usually employed metal-

exposed algae. A reduction in the content of some of the essential nutrients (*e.g.* fatty acids) has been reported for the latter to be influenced by this metal exposure, resulting in equivocal results. A second paper was presented establishing an experiment for the quantification of the contribution of the aforementioned nutritional quality shifts to the toxic effects when metal-contaminated algae are used as food vectors.

While the toxicity experiment was only focused on Ni exposure and only the concerning results were published in the aforementioned articles, basal concentrations of Cd were also of interest in view of future eco-toxicological studies based on Cd-stress [51,52].

In this doctoral thesis only the analytical aspects of the method developed will be further discussed, stressing the suitability of SS HR CS GFAAS for the direct determination of unique individual specimens of small size.

Methodology

An analytical multi-element method was developed in order to monitor the Ni body content (analyte of interest) as well as Cd basal concentrations in a batch of 192 *D. magna* specimens divided in different lots. The members of each lot were subjected to different dietary and waterborne conditions.

The spectral analytical window was then centered on 228.899 nm so to properly monitor both Ni and Cd atomic lines. The spectral region has been already described in Section II.3.2.1 to illustrate the possibilities of HR CS AAS for simultaneous multi-element determinations when dealing with analytes of very different volatilities and applied to the analysis of BCR CRM 679 White cabbage. The furnace conditions for the determination of Cd and Ni in *D. magna* samples were slightly modified, though. As the main interest was focused on Ni, a maximum sensitivity had to be assured for this

element. To this aim, atomization temperature of 2400°C was preferred and additional Ar gas flow in this step was suppressed. Pyrolysis stage was fixed in 700°C. Instrumental conditions are listed in Table II.16.

Table II.16. Instrumental parameters used for the simultaneous multi-elemental determination of Cd and Ni in *D. magna* by means of SS HR CS GFAAS

Analyte	Cd	Ni		
Wavelength / nm	228.802	228.998		
Number of pixels summed	3 (≈ 3.7 pm)	3 (≈ 3.7 pm)		
Chemical modifier	1 μ g Pd (added as Pd(NO ₃) ₂ solution)			
Temperature program				
Step	Temperature/°C	Ramp/°C s ⁻¹	Time/s	Gas flow rate/L min ⁻¹
Drying	150	5	35	2.0
Pyrolysis	700	50	30	2.0
Auto-zero	700	0	5	0.0
Atomization	2400	1500	10	0.0
Cleaning	2600	500	4	2.0

Pd modifier was needed in order to stabilize Cd during the pyrolysis. However, it is worth pointing out here that the 10 μ L Pd(NO₃)₂ solution also fulfils the role of preventing the ejection of the sample from the furnace during the drying step due to the sweeping effect of the Ar flow over the very light invertebrate individuals, as already recommended in a previous work [45].

D. magna individuals were collected after being subjected to a 21-day toxicity test. Performance [53] and culture conditions can be found elsewhere [54]. Individuals were exposed to two different diet combinations:

- 10:1 w/w of control algae and Ni-exposed liposomes at 5 different levels (variations should only be observed for Ni content).

- 10:1 w/w of Ni-exposed algae at 5 different levels and control liposomes (variations in Ni content might be accompanied by variations in nutritional quality).

Simultaneously, some daphnids were fed with control algae and liposomes but exposed to a water medium with enriched Ni concentrations of 25, 50 and 75 $\mu\text{g L}^{-1}$, to assess the implications of the exposure of the invertebrates to a polluted waterborne media due to the release of the metal from the algae and the liposomes.

Each dried individual *D. magna* specimen was previously weighed in the microbalance of the automatic SS device and, after the addition of the chemical modifier with a micro-pipette, it was transferred to the graphite furnace to be subjected to the temperature program. The typical dry weigh of the adult control samples was about 300 μg , while for individuals exposed to high Ni concentrations, it was typically not higher than 100 μg .

Calibration was carried out *versus* daily prepared aqueous Ni and Cd standard solutions. The analytical result was obtained summing the A_{int} for the 3 central pixels of the transition peaks monitored. Samples were divided in different groups regarding type of metal exposure and results were presented aiming to establish statistical comparisons between the different populations.

Results and discussion

The expanded possibilities offered by HR CS AAS for multi-element determinations are especially interesting when dealing with individual micro-samples. In this case, the whole sample needs to be subjected to the temperature programme at once and no replicates are possible, as each

individual may respond to the culture and exposure conditions in a unique way.

Moreover, SS methods are particularly suitable for micro-samples analysis, as any method that involves putting the sample into solution would require the combination of several specimens in order to achieve an acceptable analyte signal. In this way, not only the risk of contamination would be much higher, but the information in the variation between different individuals would be lost.

A Cd-Ni multi-element method was then optimized for SS HR CS GFAAS in order to be applied to individual invertebrate samples.

As it was already mentioned in previously presented works on multi-element determinations, when analytes with very different volatilities are aimed to be simultaneously monitored, compromise furnace temperature conditions are needed. Pyrolysis and atomization curves for both Ni and Cd are presented in Figure II.24.

Eventually, a pyrolysis temperature of 700°C and an atomization stage of 2400°C were selected as optimum for the simultaneous determination.

Analytical figures for both lines are summarized in Table II.17.

The available within the spectral window line for Ni is, in view of the features presented, suitable for this application, taking as reference the total Ni body burden found in *D. magna* individuals exposed to high concentrations of Ni through diet in a previous experiment carried out by Evens *et al.* [54] under similar culture/exposure conditions.

Figure II.24. Pyrolysis and atomization curves for: **A)** Ni, measured at 228.998 nm for 10 μL of a 300 $\mu\text{g L}^{-1}$ Ni standard solution; and **B)** Cd, measured at 228.802 nm, for 10 μL of a 10 $\mu\text{g L}^{-1}$ Cd standard solution.

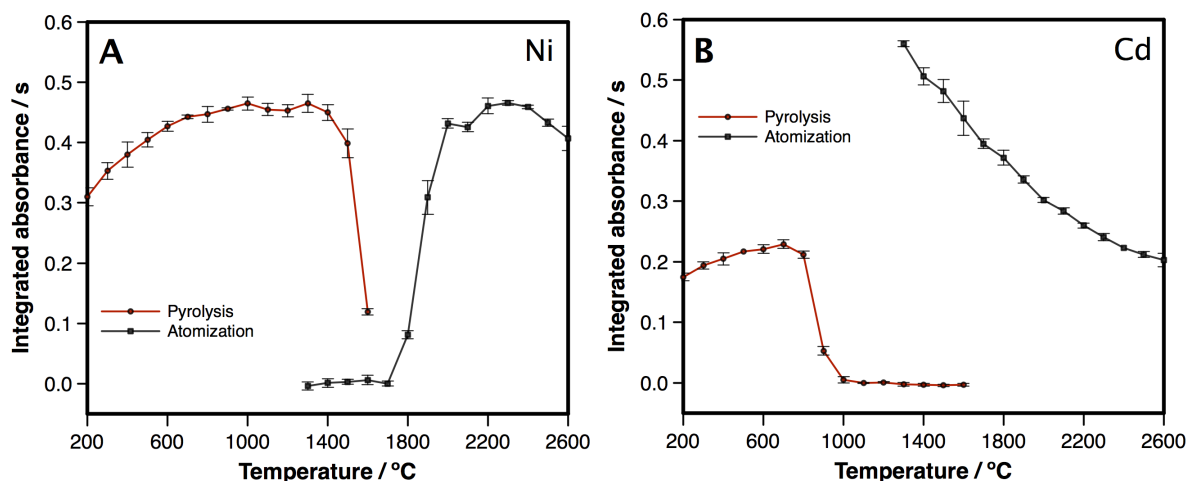
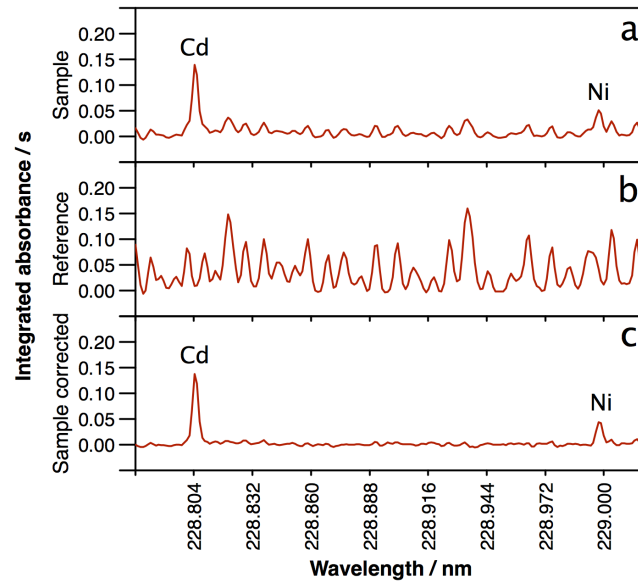


Table II.17. Analytical performance of the Cd and Ni lines found in the vicinity of 228.9 nm

Wavelength /nm	Relative sensitivity	m_0 /pg	LOD /pg	Linear range /pg	R^2
228.802 (Cd)	100	1.1	2.2	Up to 350	0.994
228.998 (Ni)	25	35.2	151.4	Up to 10,000	0.995

The spectral range between 228.776 nm and 229.021 nm is strongly affected by a background of PO molecular absorption transitions, whenever a source of phosphorus is introduced into the furnace, as it is the case for most biological matrices. Moreover, in this case stop flow furnace conditions during atomization are essential to have an adequate sensitivity for Ni and under the optimized furnace conditions both analyte and interfering signals coincide in time. In this way, LSBC remains the only possible approach to both preserve the highest sensitivity attainable for Ni and successfully correct any potential spectral overlap coming from the structured molecular background. Result of the application of the LSBC algorithm is illustrated in Figure II.25.

Figure II.25. Wavelength resolved time-integrated spectrum recorded in the analytical region of 228.9 nm by means HR CS GFAAS under the conditions listed in Table II.16 for: **a**) a *D. magna* specimen exposed to high dietary Ni contents (Sample); **b**) a 1% (m/v) $\text{NH}_4\text{H}_2\text{PO}_4$ solution (Reference); and **c**) after the application of the LSBC methodology for spectral interferences correction (Sample corrected)



Comparative results obtained by applying the developed method to the different exposure groups of *D. magna* samples are presented in Table II.18. From these results it can be observed that Ni bioaccumulation increase with the increasing level of diet exposure either being liposomes or algae and no appreciable change is observed when the metal exposure is performed *via* the water medium for the concentrations tested. Cd basal concentrations remain below $1 \mu\text{g g}^{-1}$ in all cases. The test of Kolmogorov-Smirnov [17] was applied to each of the groups and confirmed a normal distribution of the population (or not significant deviations from normality) in every case with exception of the control group of samples.

Table II.18. Results obtained in the analysis of each *D. magna* Ni exposure population by means of SS HR CS GFAAS.

Ni	Ni-exposed liposomes / Control algae				Control liposomes / Ni-exposed algae				Waterborne Ni-exposure				
	Control	Level1	Level2	Level3	Level4	Level1	Level2	Level3	Level4	Level1	Level2	Level3	Level4
Average / $\mu\text{g g}^{-1}$	1.7	8.2	14.3	15.8	53.3	2.8	4.7	13.8	79.9	1.3	1.0	1.6	
Median / $\mu\text{g g}^{-1}$	0.5	5.6	13.3	15.3	42.0	2.0	2.8	11.6	44.7	1.2	1.0	1.1	
Standard deviation / $\mu\text{g g}^{-1}$	3.9	8.0	7.8	8.8	30.9	2.1	4.3	10.8	90.0	0.5	0.4	0.8	
RSD /%	224.7	98.4	54.2	55.9	57.9	74.1	91.2	78.3	112.6	35.3	45.1	49.5	
Minimum value / $\mu\text{g g}^{-1}$	0.1	1.1	5.7	4.4	23.2	0.9	1.7	3.4	10.9	0.9	0.3	0.8	
Maximum value / $\mu\text{g g}^{-1}$	19.5	30.3	30.7	36.1	115.0	8.4	20.7	45.4	365.9	2.1	1.5	2.5	
Number of samples	24	23	14	15	11	24	23	21	18	6	6	5	
Kurtosis	21.1	2.7	-0.2	0.4	0.0	1.6	7.9	2.9	5.9	1.5	0.0	-3.1	
Asymmetry coefficient	4.5	1.7	0.7	0.8	1.0	1.5	2.6	1.7	2.4	1.3	-0.5	0.5	
K-S* experimental value	0.319	0.175	0.142	0.184	0.207	0.275	0.287	0.199	0.267	0.179	0.139	0.320	
K-S* critical value	0.269	0.275	0.349	0.338	0.391	0.269	0.275	0.287	0.309	0.519	0.519	0.563	
Cd													
Average / $\mu\text{g g}^{-1}$	0.6	0.7	0.3	0.4	0.4	1.0	0.5	0.4	0.3	0.8	0.9	0.7	
Median / $\mu\text{g g}^{-1}$	0.6	0.7	0.2	0.4	0.4	0.8	0.5	0.4	0.2	0.8	0.8	0.6	
Standard deviation / $\mu\text{g g}^{-1}$	0.2	0.3	0.3	0.2	0.3	0.6	0.2	0.2	0.2	0.3	0.4	0.2	
RSD /%	32.9	42.3	123.6	50.3	75.2	55.7	43.6	49.3	90.6	32.3	49.5	27.4	
Minimum value / $\mu\text{g g}^{-1}$	0.3	0.3	-0.005	0.03	0.03	0.3	0.2	0.2	0.0001	0.5	0.3	0.5	
Maximum value / $\mu\text{g g}^{-1}$	1.0	1.5	1.3	0.7	1.2	2.6	1.1	0.9	0.8	1.2	1.6	1.0	
Number of samples	24	23	14	15	11	24	23	21	18	6	6	5	
Kurtosis	-0.1	0.4	7.1	-0.1	1.4	1.2	0.1	-0.5	0.5	-1.2	0.6	4.0	
Asymmetry coefficient	0.6	0.8	2.5	-0.3	1.2	1.2	0.5	0.6	1.1	0.4	0.7	1.9	
K-S* experimental value	0.127	0.115	0.248	0.120	0.175	0.228	0.114	0.144	0.197	0.180	0.190	0.392	
K-S* critical value	0.269	0.275	0.349	0.338	0.391	0.269	0.275	0.287	0.309	0.519	0.519	0.563	

* K-S stands for Kolmogorov-Smirnov

Apart from this study, a batch of *D. magna*'s ehippia (winter-seasonal eggs of the specie of barely 1 mm length) were analysed for Ni making use of the Ni-triplet appearing at 234 nm already described in Section II.3.2.1. The eggs were collected at different depths in an artificial reference lake to be compared with another batch of eggs collected from an actual lake highly contaminated with Ni. Results are presented in Table II.19.

Table II.19. Results obtained in the analysis of all the ehippia populations found at different levels of both a Ni-polluted lake and an artificial reference lake by means of solid sampling HR CS GFAAS. At every depth level, 10 individuals were collected and analysed.

Hourglass lake (Canada)		
<u>Sampling depth</u>	<u>Average content / $\mu\text{g g}^{-1}$</u>	<u>RSD / %</u>
0-1 cm	634.4	34.2
1-2 cm	1310.4	38.9
2-3 cm	1499.9	31.5
3-4 cm	893.2	45.1
4-6 cm	799.1	46.4
6-21 cm	570.2	51.3
Reference lake		
<u>Sampling depth</u>	<u>Average content / $\mu\text{g g}^{-1}$</u>	<u>RSD / %</u>
0.4 cm	95.9	62.6
4-6 cm	150.7	34.0
6-7 cm	238.5	40.8
7-9 cm	154.8	20.9
9-10 cm	103.1	33.9
10-12 cm	126.3	50.4
12-17 cm	138.8	56.9

From the average content of each sampling depth the high actual Ni contamination in the real lake is confirmed and it can be inferred that Ni bioaccumulation increases until a certain depth in a factor of 2.5 the level present in the more superficial samples, and then decreases again. This behaviour seems to be the tendency for both artificial and actual environments.

II.3.3.2. Isotope ratio mapping by means of laser ablation-single collector-ICP-mass spectrometry: Zn tracer studies in thin sections of *Daphnia magna*

Goals

Taking advantage of the possibility of working with different instrumental setups offered by this co-tutelage work, LA-SC-ICPMS was also studied as a complementary technique for microsampling.

In this work, two important features of LA-ICPMS were combined: i) its capability for providing isotopic information [55], and ii) the high spatial resolution reported for elemental mapping [56]. While both characteristics are increasingly addressed in the literature in a separate way, very few studies have reported on the use of LA-ICPMS for acquiring isotope ratio mappings [57], and none based on the use of more easily accessible SC-ICPMS

In order to evaluate the capabilities of LA-SC-ICPMS for filling this methodological gap, the use of this technique for developing a tracer experiment in *D. magna* individuals exposed to increased dissolved Zn concentrations with different isotopic composition was optimized so to offer a way for presenting the data as Zn isotopic ratio images of thin sections.

The development of this methodological approach included: i) the evaluation of the performance of a new entrance/exit slit combination available for the Thermo Element XR instrument capable of providing flat-topped spectral peaks and better enhanced ion transmission when operating at higher mass resolution ($m/\Delta m \approx 2000$) in comparison with the conventional medium resolution one ($m/\Delta m \approx 4000$, triangular shaped peaks); ii) the use of a wet plasma set-up for improving plasma robustness; iii) thorough optimization of the ablation conditions and data acquisition

parameters in order to attain the best precision possible; and iv) adequate data treatment.

Methodology

After culturing *D. magna* specimens from a monoclonal in-house laboratory population under the normal dietary and waterborne conditions, that may be found elsewhere [58], 21 days old individuals were collected and exposed to a water medium fortified with a Zn spike, isotopically enriched in ^{64}Zn and ^{67}Zn for a total Zn concentration of 1 mg L^{-1} . The isotopic composition of the Zn spike was determined to be ^{64}Zn (50.52%), ^{66}Zn (2.12%), ^{67}Zn (44.79%), ^{68}Zn (2.52%) and ^{70}Zn (0.05%) [59]. The Zn exposure lasted for 24 hours without any further feeding or aeration, then the individuals were properly rinsed and dehydrated to be embedded in cubes filled with molten paraffin for, once cold, being cut in $20 \mu\text{m}$ thickness sagittal sections using a rotary microtome. The fine sections were then adhered to glass plates for ablation. Measurement conditions and instrumental parameters used for sample ablation are summarized in Table II.20.

“Wet plasma” conditions were achieved by simultaneously nebulizing a $5 \mu\text{g L}^{-1}$ Cu isotopic standard solution (NIST SRM 976, National Institute of Standards and Technology, MD, USA) with the dry aerosol generated in the ablation. In this way, Cu isotope ratio was monitored and used as internal standard for mass bias correction.

NIST SRM 612 Trace elements in glass reference material was used for optimizing the instrumental settings at the beginning of every measurement session so to maximize the Zn signal intensity, to obtain good peak shapes and attain a stable U/Th ratio close to unity, minimizing the formation of oxides and doubly-charged ions [60].

Table II.20. Instrumental settings and data acquisition parameters for the ablation of thin sections of *D. magna* individuals by means of LA-SF-ICPMS

LA unit parameters: New Wave Research UP193HE	
Wavelength	193 nm
Cell volume	$\approx 2.5 \text{ cm}^3$
Spot size	30 μm
Repetition rate	10 Hz
Scanning speed	60 $\mu\text{m s}^{-1}$
Energy density	1.8-2.1 J cm^{-2}
Laser warm-up time	10 s
ICPMS instrumental parameters: Thermo Element XR	
Mass resolution, $m/\Delta m$	2000
RF power	1120 W
Auxiliary gas flow rate (Ar)	0.70 L min^{-1}
Nebulizer gas flow rate (Ar)	0.75 L min^{-1}
Carrier (He) gas flow rate through cell	0.60 L min^{-1}
Data acquisition parameters	
Scanning mode	E-Scan
Settling time	1 ms
Samples per peak	50
Mass window	10%
Sample time	3 ms
Segment duration (total dwell time per nuclide)	15 ms
Runs/passes	600/1
Nuclides monitored	$^{63}\text{Cu}^+$, $^{64}\text{Zn}^+$, $^{65}\text{Cu}^+$, $^{66}\text{Zn}^+$, $^{67}\text{Zn}^+$, $^{68}\text{Zn}^+$

Concerning data handling, rejection of spiky signals (about 0.5% of the acquired points or less) was done manually by spotting the signals exceeding the level of the 10 adjacent points by more than 3 times their standard deviation. On the other hand, the first 10 seconds of laser's warm-up were considered gas blank signal and subtracted from every data point. If the Zn net signal laid beneath the blank value plus three times the standard deviation for the gas blank, the Zn concentration was considered too low for providing reliable isotope ratios and these values were disregarded for constructing the final isotope ratio image.

The isotope ratios considered for image composition were $^{66}\text{Zn}/^{64}\text{Zn}$, $^{68}\text{Zn}/^{64}\text{Zn}$, $^{66}\text{Zn}/^{67}\text{Zn}$ and $^{68}\text{Zn}/^{67}\text{Zn}$. A point-by-point mass bias correction was applied for each isotope ratio by applying the empirical strategy proposed by Longerich *et al.* [61] and improved by Maréchal *et al.* [62] and Woodhead [63]. Estimation of the K-factor was done by the exponential model of Russell *et al.* [64].

Results and discussion

During the whole process of optimization for developing a method to acquire Zn isotope ratio images in such thin sections of a *D. magna* specimen particular attention was paid to three main aspects [65]: i) maximization of sensitivity; ii) reduction of the occurrence of spiky signals; and iii) improvement of precision by trying to achieve quasi-simultaneous measurement conditions.

The parameters affecting these factors are all interrelated and, therefore, the optimization requires to find compromise conditions in most cases. It is firstly necessary to point out that the Zn concentration in the samples is expected to be quite low (approximately $80 \mu\text{g g}^{-1}$ in base level populations) [45]. Moreover, Zn presents several potential spectral interferences. In this type of samples the most problematic ones are due to the formation of polyatomic species based on P and Ca (mainly present in the exoskeleton of the crustaceans) and on S and Cl (essential elements for all living organisms). For this reason, a sector field instrument capable of working under medium resolution conditions would be required [66,67]. The use of a conventional medium resolution slit ($m/\Delta m \approx 4000$) completely overcome these interferences but at the same time entails a significant drop in sensitivity as well as triangular-shaped peaks which also negatively affects the precision of the isotope ratio measurements. To cope with these

detrimental effects a new medium resolution slit system based on a wider exit slit was used in this work, providing a 50% decrease in resolution (though sufficient for finding an interference-free region in the centre of the peak, as it is shown in Figure II.26) but flat-topped peaks (leading to higher precision) and enhanced ion transmission efficiency (leading to higher sensitivity, approx. a factor of 2).

Regarding the laser parameters for the ablation, the spot size of the laser beam had to be optimized in order to achieve an adequate compromise between sensitivity and spatial resolution considering the small dimensions of the samples under study. Also the scan speed needed to be adjusted, in accordance with the laser energy and repetition rate, so to minimize sample acquisition time without sacrificing the sensitivity and spatial resolution achieved. In this case, 30 μm spot size resulted in a good agreement between resolution and signal intensity, with a 10 Hz repetition rate, a laser fluence of 1.8-2.1 J cm^{-2} (for ablating the total thickness of the sample without inflicting damage to the glass) and a 60 $\mu\text{m s}^{-1}$ scan speed (for a reasonable total acquisition time).

A teardrop ablation cell [1-3] with a reduce volume of 2.5 cm^3 was used in this work to reduce as much as possible the required washout time and therefore, minimize the signal expansion.

As for the achievement of more robust plasma conditions, wet plasma conditions are known to provide higher robustness towards matrix effects [65,68] and more stable signals with a significantly reduced amount of spikes, as shown in Figure II.27. In this work, a setup was developed based on an experimental setting presented by O'Connor *et al.* [68]. A Y-shaped joint was used to connect the liquid aerosol coming from a dual-pass spray chamber to the stream of the dry aerosol coming from the ablation cell,

where both merge and flow toward the plasma torch. A diagram giving an outline of this disposition is presented in Figure II.28.

Figure II.26. Mass spectra in the vicinity of ^{64}Zn and ^{68}Zn when simultaneously nebulizing high concentrations of Cl and S, using different mass resolution slit systems. **A)** Mass spectrum in the vicinity of ^{64}Zn for a solution containing $3\ \mu\text{g L}^{-1}\ \text{Zn}$ and $10\ \text{mg L}^{-1}\ \text{S}$ using a conventional medium resolution slit system ($m/\Delta m \approx 4000$). **B)** Mass spectrum in the vicinity of ^{64}Zn for a solution containing $3\ \mu\text{g L}^{-1}\ \text{Zn}$ and $10\ \text{mg L}^{-1}\ \text{S}$ using a new medium resolution slit system (flat-topped peaks, $m/\Delta m \approx 2000$). **C)** Mass spectrum in the vicinity of ^{68}Zn for a solution containing $3\ \mu\text{g L}^{-1}\ \text{Zn}$ and $4.25\ \text{g L}^{-1}\ \text{Cl}$ using a conventional medium resolution slit system ($m/\Delta m \approx 4000$). **D)** Mass spectrum in the vicinity of ^{68}Zn for a solution containing $3\ \mu\text{g L}^{-1}\ \text{Zn}$ and $4.25\ \text{g L}^{-1}\ \text{Cl}$ using a new medium resolution slit system (flat-topped peaks, $m/\Delta m \approx 2000$).

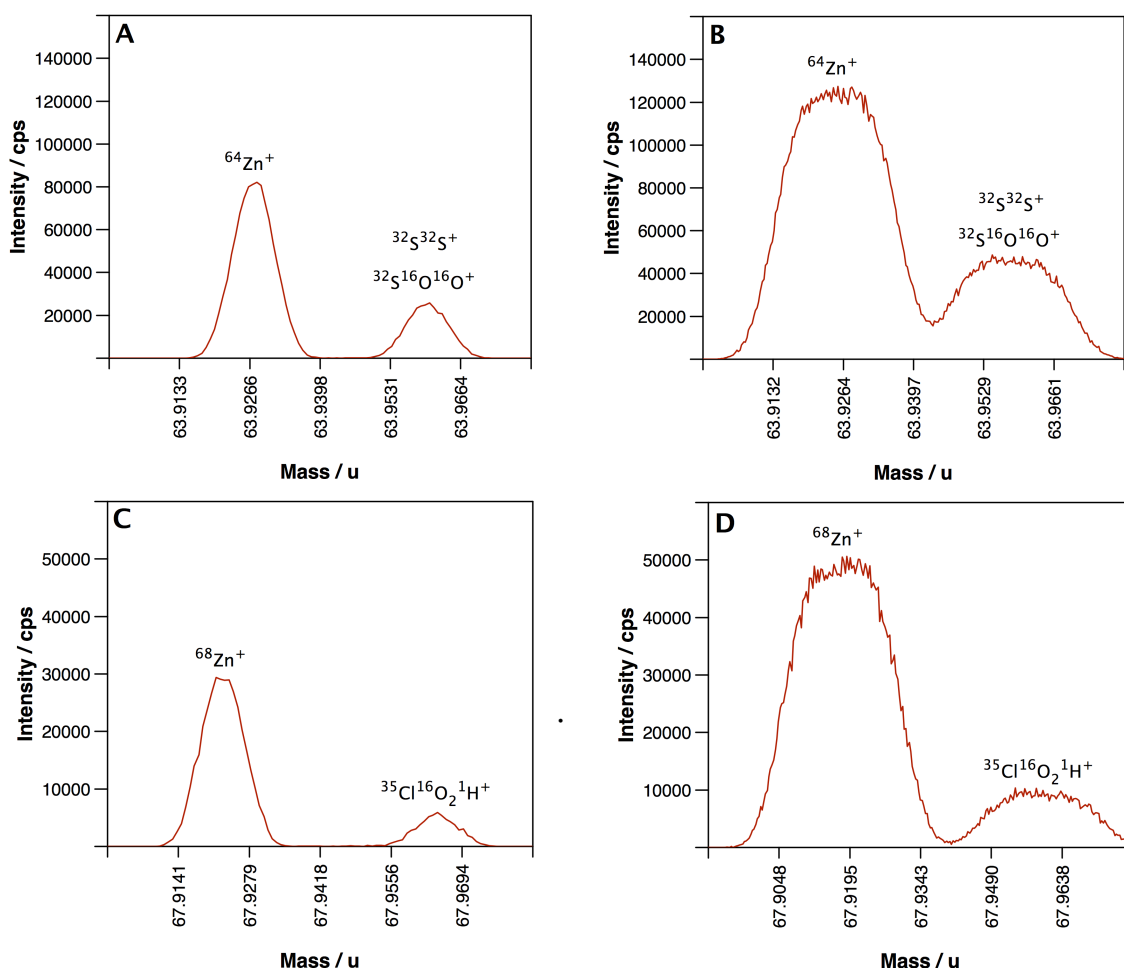


Figure II.27. Comparison between the ^{64}Zn signals obtained upon ablation of NIST SRM 612 glass (400 μm , 20 Hz, 10 $\mu\text{m s}^{-1}$, 10 J cm^2) measured in both dry and wet (through nebulization of a 0.14 M HNO_3 solution) plasma conditions.

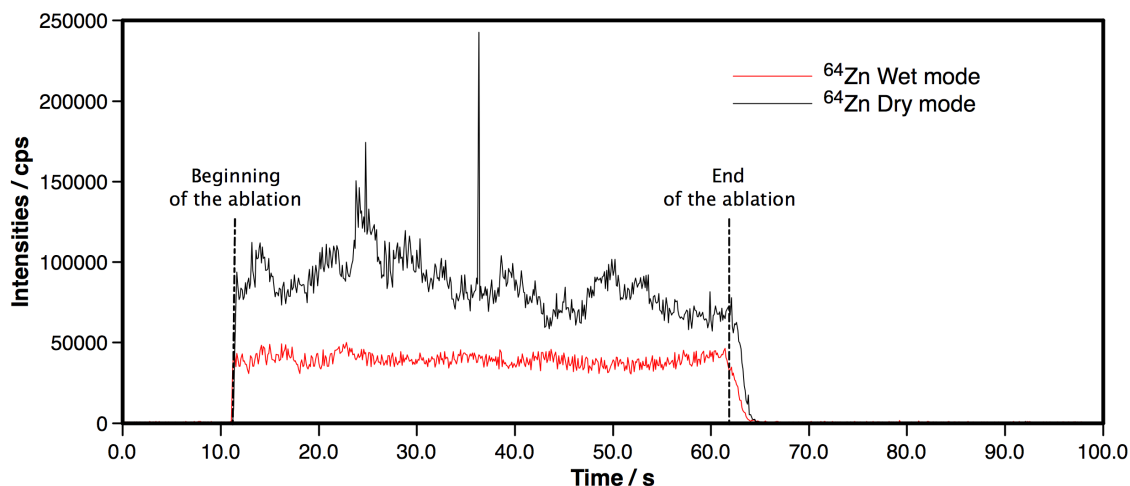
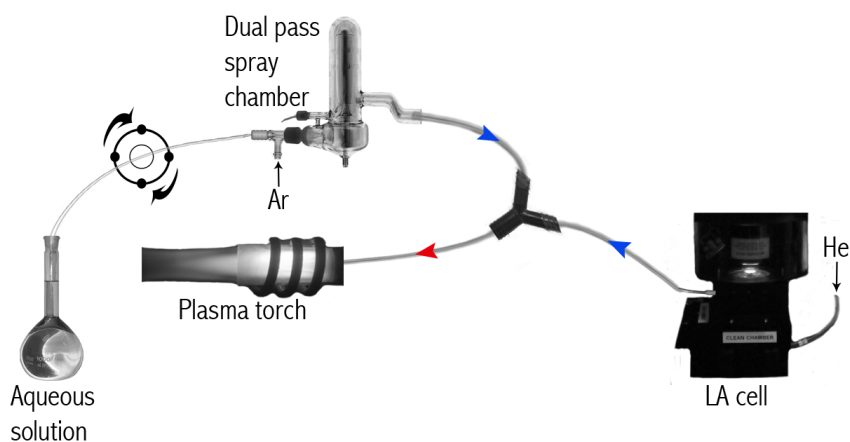


Figure II.28. Wet plasma setup used for the acquisition of Zn isotope ratio images



This approach permitted to nebulize a Cu isotopic standard solution for the generation of the wet plasma and be able to use it afterward for mass bias correction purposes in data treatment.

On the other hand, in order to attain a situation as close as possible to the ideally simultaneous detection of the isotopes monitored, the mass

spectrometer acquisition parameters had to be studied, particularly paying attention to the nuclides monitored (they should be as close as possible), the settling time and the total dwell time. An internal standard (Cu) was selected that allowed for scanning of all nuclides only by changing the accelerating voltage, under a fixed magnet mass. In this way, the settling time could be set at 1 ms, the minimum allowed by the instrument software. To establish an adequate total dwell time, an homogeneous material for Zn (NIST SRM 612 glass) [69] was measured under the same conditions of mass window (central 10% of the peak), samples per peak (50) and settling time (1 ms) but varying the time spent at each sample from 1 ms (5 ms dwell time per nuclide) to 16 ms (83 ms dwell time per nuclide) in order to evaluate its influence on the measurement precision. Data points were averaged every approximately 500 ms, so to obtain 30 x 30 μm square pixels, and the point-by-point RSD was compared for every isotope ratio measured. Both medium resolution slits systems were tested for this optimization, as illustrated in Figure II.29. It was concluded that the one providing flat-topped peaks led to improved isotope ratio precisions in all cases. Moreover, best precision was obtained when using from 15 ms to 27 ms acquisition time (5% RSD or better for the most favourable ratios, $^{66}\text{Zn}/^{64}\text{Zn}$ and $^{68}\text{Zn}/^{64}\text{Zn}$).

Under these optimized conditions the images were generated ablating 30 μm vertically adjacent rasters. Approximately 50 scan lines of about 50 s duration each were needed to cover the whole sample section. As the ablation moved at 60 $\mu\text{m s}^{-1}$ with a 10 Hz repetition rate, a pace of 6 μm per laser shot (0.1 s) was established. Measuring 50 samples per peak and measuring just in the central 10% portion of the nominal peak, 5 points per nuclide were registered every 0.5 s (30 μm spot size), which means 1 point every 0.1 s. That means that a signal intensity value for every target nuclide

was actually obtained for every laser shot. With every laser shot, only 6 μm of new material are sampled, together with 24 μm of an already ablated area. In this way, the moving average of 5 data points was used for processing the collected data under these conditions, as it perfectly simulate the ablation process.

Figure II.29. Measurement precision (%RSD) for Zn isotope ratios as a function of the total dwell time selected per nuclide, obtained for the ablation of NIST SRM 612 glass (200 μm , 20 Hz, 10 $\mu\text{m s}^{-1}$, 10 J cm^2) under wet plasma conditions, using **A**) a new medium resolution slit system (flat-topped peaks, $m/\Delta m \approx 2000$) and **B**) a conventional medium resolution slit system (triangular peaks, $m/\Delta m \approx 4000$). The number between brackets next to each dwell time value indicates the number of points averaged for obtaining a single isotope ratio value every 500 ms. Natural values for the isotope ratios showed in the charts: $^{66}\text{Zn}/^{64}\text{Zn}=0.564$, $^{68}\text{Zn}/^{64}\text{Zn}=0.375$, $^{67}\text{Zn}/^{66}\text{Zn}=0.146$, $^{68}\text{Zn}/^{67}\text{Zn}=4.567$.

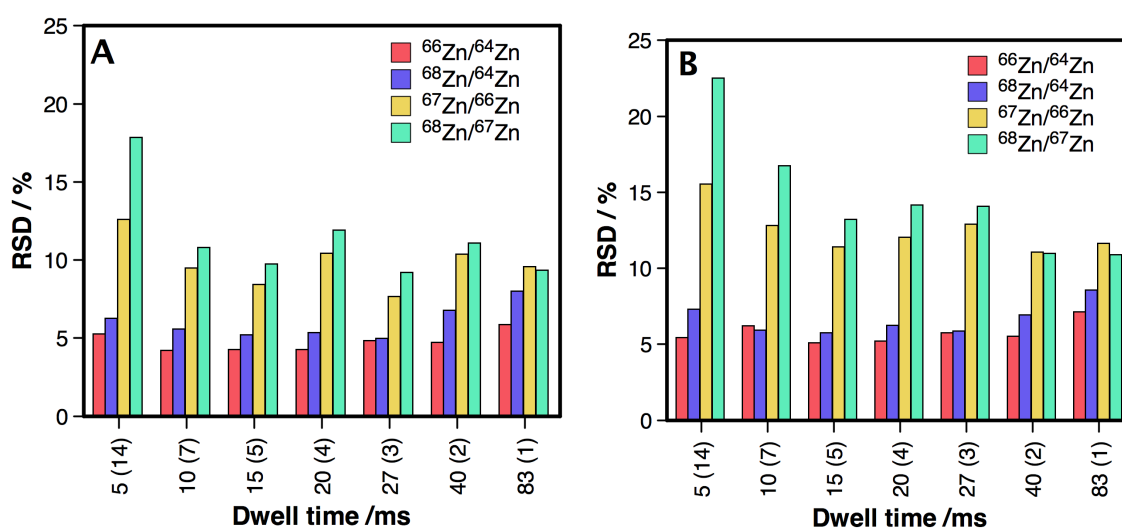
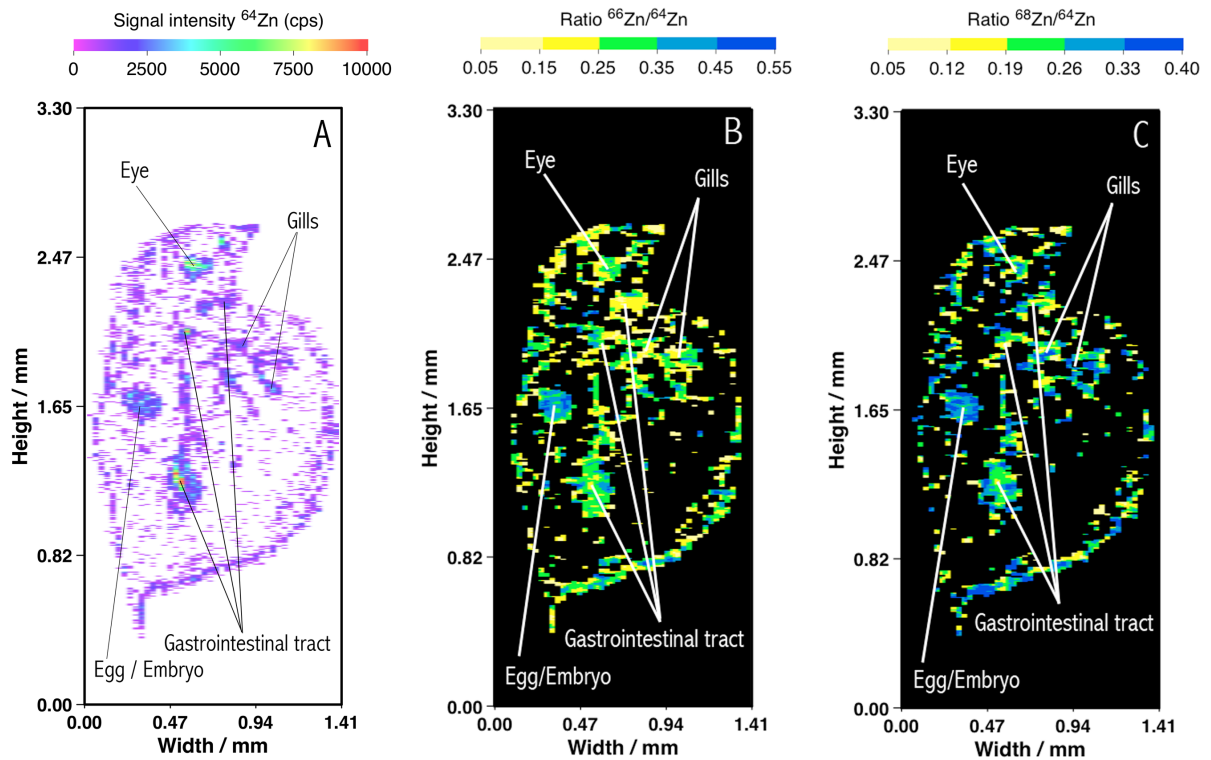


Figure II.30.A shows the ^{64}Zn body distribution image of a *D. magna* specimen exposed to ^{64}Zn -enriched water medium. It can be observed how Zn preferentially accumulates in the eye, the gastrointestinal tract, the gills and the egg/embryo, as it was expected from previous findings presented in the literature [70]. Figures II.30.B and II.30.C show the $^{66}\text{Zn}/^{64}\text{Zn}$ and

$^{68}\text{Zn}/^{64}\text{Zn}$ isotope ratio images, respectively, obtained after transforming the elemental images for the same 20 μm section of a *D. magna*.

Figure II.30. Isotope mapping of ^{64}Zn (A), $^{66}\text{Zn}/^{64}\text{Zn}$ isotope ratio (B) and $^{68}\text{Zn}/^{64}\text{Zn}$ isotope ratio (C) distribution over a 20 μm section of a *D. magna* specimen exposed to a ^{64}Zn -enriched water medium obtained by LA-SC-ICPMS

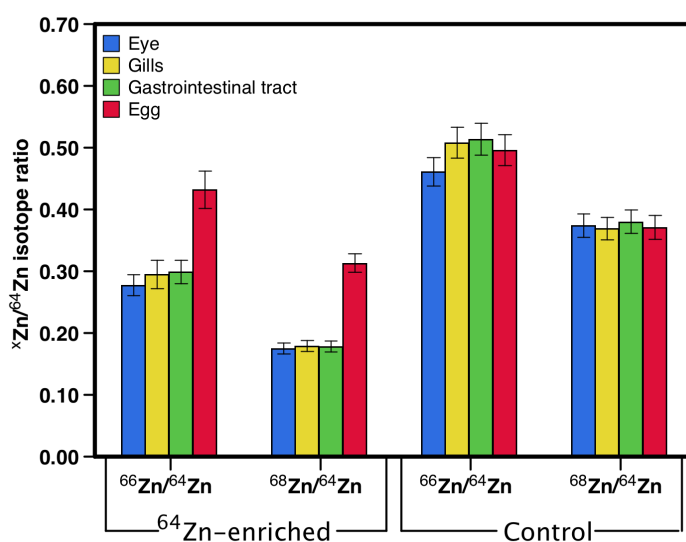


Average isotope ratios were calculated for the different mentioned regions for both control and exposed *D. magna* individuals. The analytical uncertainty was estimated by ablating 4 contiguous sections of the same specimen in each case (control and exposed). Results are illustrated in Figure II.31.

From this figure it can be seen that in the control specimen no significant difference was encountered between the body areas of accumulation, with isotope ratio values close to the expected for Zn of isotopic natural abundance ($^{66}\text{Zn}/^{64}\text{Zn}=0.564$ and $^{68}\text{Zn}/^{64}\text{Zn}=0.375$). However, exposed specimens record isotope ratios close to natural values only in the

egg/embryo area, while the other accumulation areas present significantly lower values for both $^{66}\text{Zn}/^{64}\text{Zn}$ and $^{68}\text{Zn}/^{64}\text{Zn}$, indicating that ^{64}Zn coming from the spiked water was being incorporated into those organs, as it could be deduced from Figure II.30.

Figure II.31. Mean $^{66}\text{Zn}/^{64}\text{Zn}$ and $^{68}\text{Zn}/^{64}\text{Zn}$ isotope ratio values for the main Zn body accumulation areas in four contiguous sections of the same *D. magna* specimens, one exposed to a ^{64}Zn -enriched medium and one control specimen. Analytical uncertainty, u , is given as the standard deviation between sections ($n=4$). Isotope ratio values expected for a Zn of natural isotopic composition are $^{66}\text{Zn}/^{64}\text{Zn}=0.564$ and $^{68}\text{Zn}/^{64}\text{Zn}=0.375$, while isotope ratio values for the Zn isotopic spike used for enriching the water medium are $^{66}\text{Zn}/^{64}\text{Zn}=0.042$ and $^{68}\text{Zn}/^{64}\text{Zn}=0.050$



In view of all the results, it can be concluded that this work presents a way for optimizing the development of tracer experiments with views to acquire the data as isotope ratio images by means of LA-SC-ICPMS in thin sections of biological samples containing the elements of interest in very low amounts, so to be able to access to not only elemental but also isotopic information. This approach permits visualizing not only where the target element is present (as it is the case in elemental imaging), but also, specifically, where the tracer is truly accumulated, facilitating the elucidation of, for instance, element uptake routes.

II.4. CONCLUSIONS

As discussed before, this doctoral thesis has been carried out having three main goals in mind. Below, the main conclusions obtained are listed.

1. In all cases, it was possible to develop straightforward methods for the direct determination of the analytes of interest in the samples evaluated. These methods required minimal to no sample preparation and relied in the use of aqueous standards to construct the calibration curves (or, in the case of isotopic analysis, to correct for mass bias), thus offering substantial advantages in comparison with traditional methodologies based on sample digestion.
2. The potential of HR CS AAS to evaluate multiple lines has been investigated in detail. Despite the limitations found owing to the narrow spectral range that can be monitored simultaneously, this technique offers significant advantages in comparison with line sources.
 - 2.1. It is possible to carry out the simultaneous determination of several elements, if these show adjacent suitable lines. On the other hand, if the elements show a very different thermal behaviour, a sequential approach that still permits to obtain all the information from the same sample replicate is also possible.
 - 2.2. The mathematical correction of interferences, even of rapidly changing and highly structured background, is feasible as long as it is possible to obtain a clean reference spectrum. Different examples where this strategy (LSBC) is valid have been shown (AlF in blood, Ni in *D. magna*, Sb in urine), as well as several approaches to obtain the reference spectrum.
 - 2.3. The availability of several lines of the same species permits obtaining further information that can help in detecting interferences, expanding the linear range or improving the LOD and the

precision. Several examples of these benefits have been presented throughout the work.

2.4. These benefits not only apply to the monitoring of atomic but also of molecular spectra, which can be used to obtain quantitative information on non-metals (*e.g.*, Br or S) or even of metals in situations where the usual lines may be affected by interferences (Al). Strategies to better evaluate different types of molecular spectra are also presented. In addition, successful approaches have been developed to stabilize volatile species in the furnace and to produce the target molecules.

3. *D. magna* specimens were selected as target sample to evaluate the potential of HR CS GFAAS and LA-ICPMS for micro sampling. It was demonstrated that HR CS GFAAS can be a very appropriate technique for the direct elemental analysis of such type of sample, as Ni and Cd could be determined simultaneously in individual specimens. On the other hand, use of LA-ICPMS offers additional possibilities for direct analysis of these small crustaceans, owing to its potential to achieve even higher spatial resolution, together with isotopic information. In this context, isotopic analysis may permit to identify if the target element shows an exogenous or endogenous nature. A methodology to detect Zn in daphnids has been proposed, enabling a resolution of 30 μm and precision values around 5% RSD to be achieved, even when using a SC-ICPMS device.

II.5. REFERENCES

- [1] D. Frei, A. Gerdes, Precise and accurate *in situ* U–Pb dating of zircon with high sample throughput by automated LA-SF-ICP-MS, *Chemical Geology* 261 (2009) 261–270.
- [2] D. Bleiner, D. Günther, Theoretical description and experimental observation of aerosol transport processes in laser ablation inductively coupled plasma mass spectrometry, *Journal of Analytical Atomic Spectrometry* 16 (2001) 449–456.
- [3] M.S.A. Horstwood, G.L. Foster, R.R. Parrish, S.R. Noble, G.M. Nowell, Common-Pb corrected *in situ* U-Pb accessory mineral geochronology by LA-MC-ICP-MS, *Journal of Analytical Atomic Spectrometry* 18 (2003) 837–846.
- [4] T. Lindemann, M. Hamester, J. Hinrichs, L. Rottmann, J.D. Wills, Improved isotope ratio precision at high mass resolution with sector field ICP-MS, *Federation of Analytical Chemistry and Spectroscopy Societies (FACSS)*, 2009.
- [5] M.H.A. Piette, E.A. De Letter, Drowning: Still a difficult autopsy diagnosis, *Forensic Science International* 163 (2006) 1–9.
- [6] J. Hürlimann, P. Feer, F. Elber, K. Niederberger, R. Dirnhofer, D. Wyler, Diatom detection in the diagnosis of death by drowning, *International Journal of Legal Medicine* 114 (2000) 6–14.
- [7] J.-P. Goullé, L. Mahieu, J. Castermant, N. Neveu, L. Bonneau, G. Lainé, D. Bouige, C. Lacroix, Metal and metalloid multi-elementary ICP-MS validation in whole blood, plasma, urine and hair. Reference values, *Forensic Science International* 153 (2005) 39–44.

- [8] K.G. Ljunggren, V. Lidums, B. Sjögren, Blood and urine concentrations of aluminium among workers exposed to aluminium flake powders, *British Journal of Industrial Medicine* 48 (1991) 106–109.
- [9] W. Frech, A. Cedergren, C. Cederberg, J. Vessman, Evaluation of some critical factors affecting determination of aluminum in blood, plasma or serum by electrothermal atomic absorption spectrometry, *Clinical Chemistry* 28 (1982) 2259–2263.
- [10] P.C. D'Haese, F.L. Van de Vyver, F.A. De Wolff, M.E. De Broe, Measurement of Aluminum in serum, blood, urine, and tissues of chronic hemodialyzed patients by use of electrothermal atomic absorption spectrometry, *Clinical Chemistry* 31 (1985) 24–29.
- [11] D. Bohrer, U. Heitmann, M.-D. Huang, H. Becker-Ross, S. Florek, B. Welz, D. Bertagnolli, Determination of aluminum in highly concentrated iron samples: Study of interferences using high-resolution continuum source atomic absorption spectrometry, *Spectrochimica Acta Part B: Atomic Spectroscopy* 62 (2007) 1012–1018.
- [12] I. Rodushkin, F. Ödman, S. Branth, Multielement analysis of whole blood by high resolution inductively coupled plasma mass spectrometry, *Fresenius' Journal of Analytical Chemistry* 364 (1999) 338–346.
- [13] B. Welz, F.G. Lepri, R.G.O. Araujo, S.L.C. Ferreira, M.-D. Huang, M. Okruss, H. Becker-Ross, Determination of phosphorus, sulfur and the halogens using high-temperature molecular absorption spectrometry in flames and furnaces—A review, *Analytica Chimica*

Acta 647 (2009) 137–148.

- [14] D.R. Lide (Ed.), CRC Handbook of Chemistry and Physics, 89th ed., CRC Press/Taylor & Francis group, Boca Raton, FL, 2008–2009.
- [15] B. Welz, H. Becker-Ross, S. Florek, U. Heitmann, High-Resolution Continuum Source AAS, The Better Way to Do Atomic Absorption Spectrometry, Wiley-VCH, Weinheim, 2005.
- [16] Plasus SpecLine Database, version 2.1, Plasus, Königsbrunn, Germany.
- [17] J.N. Miller, J.C. Miller, Statistics and Chemometrics for Analytical Chemistry, 5th ed., Pearson Education Limited, Essex, 2005.
- [18] The Sulfur Institute, <http://www.sulphurinstitute.org/index.cfm>
- [19] B. Welz, M. Sperling, Atomic Absorption Spectrometry, 3rd ed., Wiley-VCH, Weinheim, 1999.
- [20] K. Dittrich, B. Vorberg, Molecular absorption spectrometry with electrothermal volatilization in a graphite tube. Part 8. A study of molecular absorption of GeS and determination of sulphur Species *via* GeS, *Analytica Chimica Acta* 152 (1983) 149–161.
- [21] P. Tittarelli, G. Lavorato, Determination of sulphur in fuel oils by absorption spectrometry of electrothermally generated carbon sulphide molecules, *Analytica Chimica Acta*. 201 (1987) 59–65.
- [22] R.W.B. Pearse, A.G. Gaydon, The Identification Of Molecular Spectra, 4th ed., John Wiley & Sons Inc., New York, NY, 1976.

- [23] M.G.R. Vale, M.M. Silva, B. Welz, R. Nowka, Control of spectral and non-spectral interferences in the determination of thallium in river and marine sediments using solid sampling electrothermal atomic absorption spectrometry, *Journal of Analytical Atomic Spectrometry* 17 (2002) 38–45.
- [24] A.B. Volynsky, Mechanisms of action of platinum group modifiers in electrothermal atomic absorption spectrometry, *Spectrochimica Acta Part B: Atomic Spectroscopy* 55 (2000) 103–150.
- [25] Z. Kowalewska, Feasibility of high-resolution continuum source molecular absorption spectrometry in flame and furnace for sulphur determination in petroleum products, *Spectrochimica Acta Part B: Atomic Spectroscopy* 66 (2011) 546–556.
- [26] U. Heitmann, H. Becker-Ross, S. Florek, M.-D. Huang, M. Okruss, Determination of non-metals *via* molecular absorption using high-resolution continuum source absorption spectrometry and graphite furnace atomization, *Journal of Analytical Atomic Spectrometry* 21 (2006) 1314–1320.
- [27] H.S. Ferreira, F.G. Lepri, B. Welz, E. Carasek, M.-D. Huang, Determination of sulfur in biological samples using high-resolution molecular absorption spectrometry in a graphite furnace with direct solid sampling, *Journal of Analytical Atomic Spectrometry* 25 (2010) 1039–1045.
- [28] M. Resano, M. Verstraete, F. Vanhaecke, L. Moens, J. Claessens, Direct determination of sulfur in Bisphenol A at ultratrace levels by means of solid sampling-electrothermal vaporization-ICP-MS, *Journal of Analytical Atomic Spectrometry* 16 (2001) 793–800.

-
- [29] A.B. Volynsky, V. Krivan, Comparison of various forms of palladium used as chemical modifiers for the determination of selenium by electrothermal atomic absorption spectrometry, *Journal of Analytical Atomic Spectrometry* 11 (1996) 159–164.
- [30] A.B. Volynsky, V. Krivan, Colloidal palladium—a promising chemical modifier for electrothermal atomic absorption spectrometry, *Spectrochimica Acta Part B: Atomic Spectroscopy* 52 (1997) 1293–1304.
- [31] H. Zweifel, R.D. Maier, M. Schiller (Eds.), *Plastics Additives Handbook*, 6th ed., Hanser Publications, Cincinnati, OH, 2009.
- [32] E. Eljarrat, D. Barceló (Eds.), *Brominated Flame Retardants*, The handbook of environmental chemistry 16, Springer-Verlag, Berlin Heidelberg, 2011.
- [33] M. Alae, R.J. Wenning, The significance of brominated flame retardants in the environment: current understanding, issues and challenges, *Chemosphere* 46 (2002) 579–582.
- [34] P.O. Darnerud, Toxic effects of brominated flame retardants in man and in wildlife, *Environment International* 29 (2003) 841–853.
- [35] L.S. Birnbaum, D.F. Staskal, Brominated flame retardants: cause for concern? *Environmental Health Perspectives* 112 (2004) 9–17.
- [36] Directive 2002/95/EC of the European Parliament and of the Council of 27 January 2003 on the restriction of the use of certain hazardous substances in electrical and electronic equipment (RoHS), *Official Journal of the European Union* (2003), L 37/19–L 37/23.

- [37] Commission Decision of 18 August 2005 amending Directive 2002/95/EC of the European Parliament and of the Council for the purpose of establishing the maximum concentration values for certain hazardous substances in electrical and electronic equipment (2005/618/EC), Official Journal of the European Union (2005), L 214/65.
- [38] NIST Atomic Spectra Database Lines Form, http://physics.nist.gov/PhysRefData/ASD/lines_form.html
- [39] M.-D. Huang, H. Becker-Ross, S. Florek, U. Heitmann, M. Okruss, High-resolution continuum source electrothermal absorption spectrometry of AlBr and CaBr for the determination of bromine, *Spectrochimica Acta Part B: Atomic Spectroscopy* 63 (2008) 566–570.
- [40] T. Limburg, J.W. Einax, Determination of bromine using high-resolution continuum source molecular absorption spectrometry in a graphite furnace, *Microchemical Journal* 107 (2013) 31–36.
- [41] M. Resano, J. Briceño, M.A. Belarra, Direct determination of phosphorus in biological samples using a solid sampling-high resolution-continuum source electrothermal spectrometer: comparison of atomic and molecular absorption spectrometry, *Journal of Analytical Atomic Spectrometry* 24 (2009) 1343–1354.
- [42] U. Heitmann, B. Welz, D.L.G. Borges, F.G. Lepri, Feasibility of peak volume, side pixel and multiple peak registration in high-resolution continuum source atomic absorption spectrometry, *Spectrochimica Acta Part B: Atomic Spectroscopy* 62 (2007) 1222–1230.

-
- [43] M. Resano, J. Briceño, M.A. Belarra, Direct determination of Hg in polymers by solid sampling-graphite furnace atomic absorption spectrometry. A comparison of the performance of line source and continuum source instrumentation, *Spectrochimica Acta Part B: Atomic Spectroscopy* 64 (2009) 520–529.
- [44] M. Aramendía, M.R. Flórez, M. Piette, F. Vanhaecke, M. Resano, Al determination in whole blood samples as AlF *via* high-resolution continuum source graphite furnace molecular absorption spectrometry: potential application to forensic diagnosis of drowning, *Journal of Analytical Atomic Spectrometry* 26 (2011) 1964–1973.
- [45] J. Briceño, M.A. Belarra, K.A.C. De Schamphelaere, S. Vanblaere, C.R. Janssen, F. Vanhaecke, M. Resano, Direct determination of Zn in individual *Daphnia magna* specimens by means of solid sampling high-resolution continuum source graphite furnace atomic absorption spectrometry, *Journal of Analytical Atomic Spectrometry* 25 (2010) 503–510.
- [46] M. Resano, A.C. Lapeña, M.A. Belarra, Potential of solid sampling high-resolution continuum source graphite furnace atomic absorption spectrometry to monitor the Ag body burden in individual *Daphnia magna* specimens exposed to Ag nanoparticles, *Analytical Methods* 5 (2013) 1130–1139.
- [47] F. Vignola, D.L.G. Borges, A.J. Curtius, B. Welz, H. Becker-Ross, Simultaneous determination of Cd and Fe in sewage sludge by high-resolution continuum source electrothermal atomic absorption spectrometry with slurry sampling, *Microchemical Journal* 95 (2010) 333–336.

- [48] L.M.G. dos Santos, B. Welz, R.G.O. Araujo, S. do C. Jacob, M.G.R. Vale, A. Martens, I.B.G. Martens, H. Becker-Ross, Simultaneous Determination of Cd and Fe in Beans and Soil of Different Regions of Brazil Using High-Resolution Continuum Source Graphite Furnace Atomic Absorption Spectrometry and Direct Solid Sampling, *Journal of Agricultural and Food Chemistry* 57 (2009) 10089–10094.
- [49] L.M.G. dos Santos, R.G.O. Araujo, B. Welz, S. do C. Jacob, M.G.R. Vale, H. Becker-Ross, Simultaneous determination of Cd and Fe in grain products using direct solid sampling and high-resolution continuum source electrothermal atomic absorption spectrometry, *Talanta* 78 (2009) 577–583.
- [50] B. Welz, S. Morés, E. Carasek, M.G.R. Vale, M. Okruss, H. Becker-Ross, High-Resolution Continuum Source Atomic and Molecular Absorption Spectrometry—A Review, *Applied Spectroscopy Reviews* 45 (2010) 327–354.
- [51] M. Messiaen, C.R. Janssen, O. Thas, K.A.C. De Schamphelaere, The potential for adaptation in a natural *Daphnia magna* population: broad and narrow-sense heritability of net reproductive rate under Cd stress at two temperatures, *Ecotoxicology* 21 (2012) 1899–1910.
- [52] M. Messiaen, C.R. Janssen, L. De Meester, K.A.C. De Schamphelaere, The initial tolerance to sub-lethal Cd exposure is the same among ten naïve pond populations of *Daphnia magna*, but their micro-evolutionary potential to develop resistance is very different, *Aquatic Toxicology* 144-145 (2013) 322–331.
- [53] Organisation for Economic Co-operation Development (OECD)

- guidelines for testing of chemicals. Guideline 211: *Daphnia magna* reproduction test, OECD Publication Service, Paris, 2012.
- [54] R. Evens, K.A.C. De Schamphelaere, C.R. Janssen, The effects of dietary nickel exposure on growth and reproduction of *Daphnia magna*, *Aquatic Toxicology* 94 (2009) 138–144.
- [55] J.S. Becker, State-of-the-art and progress in precise and accurate isotope ratio measurements by ICP-MS and LA-ICP-MS, *Journal of Analytical Atomic Spectrometry* 17 (2002) 1172–1185.
- [56] I. Konz, B. Fernández, M. Luisa Fernández, R. Pereiro, A. Sanz-Medel, Laser ablation ICP-MS for quantitative biomedical applications, *Analytical and Bioanalytical Chemistry* 403 (2012) 2113–2125.
- [57] D.S. Urgast, S. Hill, I.-S. Kwun, J.H. Beattie, H. Goenaga-Infante, J. Feldmann, Zinc isotope ratio imaging of rat brain thin sections from stable isotope tracer studies by LA-MC-ICP-MS, *Metallomics* 4 (2012) 1057–1063.
- [58] B.T.A. Muysen, K.A.C. De Schamphelaere, C.R. Janssen, Mechanisms of chronic waterborne Zn toxicity in *Daphnia magna*, *Aquatic Toxicology* 77 (2006) 393–401.
- [59] F. Vanhaecke, L. Balcaen, D. Malinovsky, Use of single-collector and multi-collector ICP-mass spectrometry for isotopic analysis, *Journal of Analytical Atomic Spectrometry* 24 (2009) 863–886.
- [60] B. Hattendorf, C. Latkoczy, D. Günther, Peer Reviewed: Laser Ablation-ICPMS, *Analytical Chemistry* 75 (2003) 341A–347A.

- [61] H.P. Longerich, B.J. Fryer, D.F. Strong, Determination of lead isotope ratios by inductively coupled plasma-mass spectrometry (ICP-MS), *Spectrochimica Acta Part B: Atomic Spectroscopy* 42 (1987) 39–48.
- [62] C.N. Maréchal, P. Télouk, F. Albarède, Precise analysis of copper and zinc isotopic compositions by plasma-source mass spectrometry, *Chemical Geology* 156 (1999) 251–273.
- [63] J. Woodhead, A simple method for obtaining highly accurate Pb isotope data by MC-ICP-MS, *Journal of Analytical Atomic Spectrometry* 17 (2002) 1381–1385.
- [64] W.A. Russell, D.A. Papanastassiou, T.A. Tombrello, Ca isotope fractionation on the Earth and other solar system materials, *Geochimica et Cosmochimica Acta* 42 (1978) 1075–1090.
- [65] M. Aramendía, M. Resano, F. Vanhaecke, Isotope ratio determination by laser ablation-single collector-inductively coupled plasma-mass spectrometry. General capabilities and possibilities for improvement, *Journal of Analytical Atomic Spectrometry* 25 (2010) 390–404.
- [66] L. Moens, P. Verrept, R. Dams, U. Greb, G. Jung, B. Laser, New high-resolution inductively coupled plasma mass spectrometry technology applied for the determination of V, Fe, Cu, Zn and Ag in human serum, *Journal of Analytical Atomic Spectrometry* 9 (1994) 1075–1078.
- [67] F. Vanhaecke, L. Moens, Overcoming spectral overlap in isotopic analysis *via* single- and multi-collector ICP-mass spectrometry,

Analytical and Bioanalytical Chemistry 378 (2004) 232–240.

- [68] C. O'Connor, B.L. Sharp, P. Evans, On-line additions of aqueous standards for calibration of laser ablation inductively coupled plasma mass spectrometry: theory and comparison of wet and dry plasma conditions, *Journal of Analytical Atomic Spectrometry* 21 (2006) 556–565.
- [69] S.M. Eggins, J.M.G. Shelley, Compositional Heterogeneity in NIST SRM 610-617 Glasses, *Geostandards Newsletter* 26 (2002) 269–286.
- [70] B. De Samber, R. Evens, K. De Schamphelaere, G. Silversmit, B. Masschaele, T. Schoonjans, B. Vekemans, C.R. Janssen, L. Van Hoorebeke, I. Szalóki, F. Vanhaecke, G. Falkenberg, L. Vincze, A combination of synchrotron and laboratory X-ray techniques for studying tissue-specific trace level metal distributions in *Daphnia magna*, *Journal of Analytical Atomic Spectrometry* 23 (2008) 829–839.

III. Publications

Cite this: *J. Anal. At. Spectrom.*, 2011, **26**, 1964

www.rsc.org/jaas

PAPER

Al determination in whole blood samples as AlF via high-resolution continuum source graphite furnace molecular absorption spectrometry: potential application to forensic diagnosis of drowning

Maite Aramendía,^{*a} María R. Flórez,^b Michel Piette,^c Frank Vanhaecke^d and Martín Resano^{*b}

Received 17th June 2011, Accepted 9th August 2011

DOI: 10.1039/c1ja10183h

In this work, a new methodology for direct determination of Al in whole blood samples by means of high-resolution continuum source graphite furnace molecular absorption spectrometry has been developed, based on the formation of the AlF diatomic molecule in the graphite furnace and the subsequent monitoring of its molecular absorption. The proposed methodology provides an alternative method to conventional atomic absorption, solving most of the problems related to the latter technique, particularly matrix effects, providing a straightforward alternative for blood analysis. The addition of NH₄F·HF, which is required for promotion of the AlF molecule, was found to improve sample matrix removal for whole blood samples, whether they contain EDTA or heparin as anticoagulant agents. Besides minimizing residues in the graphite platform, this circumstance enabled the use of aqueous standards to build a calibration curve, avoiding the need for the cumbersome method of standard additions, while not affecting significantly detection capabilities (1.8 µg L⁻¹ LOD). The method developed was also used for exploring the possibilities of Al as a chemical marker assisting forensic diagnosis of death-by-drowning. For this purpose, a set of samples (water and blood) obtained from 8 drowning suspects and two controls were analysed for their Al levels. Although additional studies with a large number of samples would be needed in order to draw definitive conclusions from a forensic point of view, a positive correlation between Al concentration in the drowning water and Al concentration in the blood of drowning suspects was found, supporting the validity of Al as a marker for drowning diagnosis.

1 Introduction

Drowning is the second leading cause of death from unintentional injury, and accounts for more than half a million deaths annually worldwide.¹ However, the post-mortem diagnosis of drowning continues to be one of the most difficult in forensic pathology, especially when it comes to differentiate between “true drowned” bodies and corpses recovered out of water but with a different cause of death.² In fact, in spite of the extensive discussions about the topic found in the medico-legal literature of the last 20 years,^{3,4} the ideal test for this purpose still needs to be established.⁴

Besides the physiopathological alterations induced by this picture, diagnosis of death-by-drowning is usually supported by additional tests (none of them definitive), based on the fact that the water and, thus, the particles, microorganisms and chemical substances it contains, will enter the blood circulation by different processes at the moment of death. As a result, detection and/or quantification of these water components in the blood and/or certain parts of the dead bodies can help in arriving at a reliable diagnosis of drowning. The diatom test, for instance, looks for the presence of diatom algae in different organs of the body that are irrigated with water-contaminated blood during the agony, such as brain, liver or kidneys.⁵ The applicability of this popular method is, however, compromised due to the gradual extermination of diatom algae in contaminated waters, and that is why finding alternative (bio)chemical markers is still a hot research topic in forensic science.

Any candidate marker should fulfil three requirements: (i) the marker should have the possibility to pass the alveolo-capillary membrane to get into the blood circulation in the agony period; (ii) it should be present in large amounts in the drowning water while being absent or present in very small amounts in the blood/body of healthy persons; and (iii) there should be no

^aCentro Universitario de la Defensa-Academia General Militar de Zaragoza, Carretera de Huesca s/n, 50090 Zaragoza, Spain. E-mail: maiteam@unizar.es

^bUniversity of Zaragoza, Faculty of Sciences, Department of Analytical Chemistry, Pedro Cerbuna 12, Zaragoza, E-50009, Spain

^cDepartment of Forensic Medicine, Ghent University, J. Kluykensstraat 29, 9000 Ghent, Belgium

^dDepartment of Analytical Chemistry, Ghent University, Krijgslaan 281-S12, 9000 Ghent, Belgium

entering into the circulation by other ways such as the gastrointestinal tract or due to post-mortem diffusion.² In this context, different elements have been evaluated as potential markers. In particular, F,⁶ Na, Cl, Mg, Ca⁷ and especially Sr^{8,9} have proved to be helpful in a variety of situations, although their applicability is far from being universal due to different factors such as, e.g., different dietary habits⁸ or insufficient levels of the marker in the water media.¹⁰

The use of Al as an alternative chemical marker could be an interesting possibility in cases involving contaminated fresh water media for which applicability of other common markers might be compromised. In fact, and in spite of its ubiquity in the earth's crust, Al levels in the blood of healthy people are usually very low, in the range of 2–5 ppb.^{11,12} Although Al levels in surface waters are also expected to be low, an exponential increase in Al concentration can be expected if the water pH falls below 6.0,¹³ which can be the case for areas of intense industrial activity. An adequate analytical method for use in the medico-legal practice, *i.e.* reliable, relatively simple and cost-effective, enabling Al determination in water and blood samples, would be therefore needed to test the validity of this metal as a drowning marker.

Unfortunately, finding an analytical method fulfilling these requirements is not an easy task. While the determination of Al in water samples is not problematic, direct determination of Al traces in a complex matrix such as whole blood is particularly challenging. Among other technique-dependent issues (*e.g.*, occurrence of spectral interferences), one of the main general problems related to trace Al determination is the occurrence of severe contamination issues, often obliging to work under clean room conditions, if sample digestion is intended.^{14,15} Taking this into account, development of a method based on the use of graphite furnace atomic absorption spectrometry (GFAAS) with the potential for direct analysis of blood samples without the need for sample digestion could be advantageous.

However, direct Al determination in whole blood samples by means of this technique is also not straightforward, mainly due to the occurrence of both spectral and non-spectral interferences. Concerning spectral interferences, problems have been reported for either of the two more sensitive atomic lines available for this element, one at 309.3 nm (doublet 309.271/309.284 nm) and another at 396.152 nm, in a variety of analytical situations.^{16–18} Using high-resolution continuum source graphite furnace atomic absorption spectrometry (HR-CS GFAAS), Bohrer and co-workers could properly characterize what is probably the most problematic spectral interference affecting the determination of Al in blood samples.¹⁸ In fact, there is an Fe line (309.278 nm) situated just between the Al duplet at 309.271/309.284 nm. Due to their similar behaviour in the graphite furnace, Al and Fe signals cannot be temporally separated at any atomization temperature and, even if the Fe line is much weaker than that of Al, the interference becomes significant for samples containing more than 0.5 g Fe L⁻¹, the typical Fe level in whole blood samples.¹⁹ As indicated by these authors, the problem can be solved by using the line at 396.152 nm, slightly less sensitive but not interfered with Fe, or working with a HR-CS GFAAS instrument and using only the central pixel of the Al line at 309.271 nm for quantification purposes, which results, however, in worse signal-to-noise (*S/N*) ratios.

Nevertheless, and even if these measures are implemented, the occurrence of non-spectral interferences is probably a more serious problem that needs to be taken into account. In this regard, analysis of whole blood samples usually implies sample dilution with different diluents (*e.g.*, Triton X-100, ammonia, nitric acid or sulfuric acid) in order to avoid build-up of carbonaceous residues in the atomizers and other deleterious effects produced by such a heavy matrix.^{11,20,21} In all cases, even after sample dilution, direct calibration with aqueous or matrix-matched standards leads to erroneous results for Al determination, and the use of the inconvenient method of standard additions remains necessary. In fact, due to these difficulties, the routine control of Al levels in, *e.g.*, the blood of haemodialysis patients, is normally carried out in serum or plasma after sample centrifugation, even if a significant part of the Al remains in the precipitate²⁰ and the need for sample dilution and/or standard addition calibration is not fully avoided.^{20,21}

Taking all these into account, it is evident that Al determination in whole blood samples by means of GFAAS could be improved in several aspects. Until recently, margin for improvement was very limited in AAS, mainly due to instrumental restrictions. However, the arrival of HR-CS GFAAS instrumentation^{22–25} has opened up new possibilities in this field that are particularly relevant for analysis of complex matrices, such a significantly improved potential for detection and correcting for spectral overlaps^{26,27} and matrix effects.²⁸ Moreover, this type of instrumentation also permits the quantitative monitoring of the molecular absorption of diatomic molecules,²⁹ which might be interesting in this particular case, as an alternative technique for overcoming the existing problems when using the atomic lines for Al determination in whole blood. Molecular absorption of Al diatomic molecules has been used for quantification of S, F, Cl and Br, both in flame and GF, as recently reviewed by Welz *et al.*;³⁰ however, to the best of our knowledge, formation of these diatomic molecules and monitoring of their molecular absorption for the determination of Al have not been tested so far.

This paper aims at evaluating the possibilities of HR-CS graphite furnace spectrometry for monitoring molecular absorption of Al diatomic molecules (AIF molecules in particular) with quantitative purposes, applying it for the first time to the direct determination of Al in a complex organic sample such as whole blood. Advantages and disadvantages of this methodology compared with the traditional use of atomic lines will be evaluated and discussed in detail. This evaluation has been carried out with the final goal of developing a suitable method for assessing the possibilities of Al as a chemical marker for drowning diagnosis in contaminated fresh waters. For this purpose, a series of blood and water samples from drowning suspects and other control corpses found around the Belgian city of Ghent and its district (with an intensively exploited industrial area for which elevated Al levels in surface waters could be expected) has been collected for analysis. Evaluation of the results obtained for these samples is also presented.

2 Experimental

2.1. Instrumentation

Atomic and molecular absorption experiments were carried out using a high-resolution continuum source atomic absorption

spectrometer (HR-CS AAS), ContraAA 700, commercially available from Analytik Jena AG (Jena, Germany). The optical system comprises: a xenon short-arc lamp (GLE, Berlin, Germany) operating in “hot-spot” mode as the radiation source, a high resolution double echelle monochromator (DEMON) and a linear CCD array detector with 588 pixels, 200 of which are used for analytical purposes (monitoring of the analytical signal and BG correction), while the rest are used for internal functions, such as correcting for fluctuations in the lamp intensity. More details on this instrument can be found elsewhere.^{22,31} The instrument is equipped with a transversely heated graphite tube atomizer, pyrolytic graphite tubes for solid sampling (without dosing hole) and an automated solid sampling accessory (SSA 600), which incorporates a microbalance with a readability of 1 µg. The samples were introduced using solid sampling graphite platforms.

Dissolution of the blood samples used for validation purposes was carried out in a class-10 clean room. Subsequent analysis of the digests was carried out with an Element XR (Thermo Electron, Bremen, Germany) sector field (SF)-ICPMS instrument.

2.2. Samples and standards

2.2.1. Standards and reagents. Purified water was obtained from a Milli-Q system (Millipore, Billerica, USA). Al solutions were prepared daily from commercially available 1 g L⁻¹ single-element standard (CertiPUR®, Merck, Darmstadt, Germany), by appropriate dilution with 0.14 mol L⁻¹ HNO₃. Ammonium hydrogen difluoride solutions were prepared daily by dissolving an adequate amount of this reagent (99.999% purity), available from Sigma-Aldrich (Steinheim, Germany), in purified water. 14 mol L⁻¹ HNO₃ of analytical grade was purchased from Merck. 30% ultrapure H₂O₂ was purchased from Fluka (Sigma-Aldrich, Steinheim, Germany).

2.2.2. Samples. Blood samples from a total of 10 cadavers (8 found in water media and 2 found in other circumstances and used as controls) were available for the investigation. The samples from drowning suspects are referred to in this work as DS-1 to DS-8, while the samples from cadavers found in other circumstances are referred to as CTRL-1 and CTRL-2. All of these samples were collected in 7.5 mL Li heparinized Monovette® tubes for metal analysis available from Sarstedt (Essen, Belgium), ensuring a maximum Al content of 40 ng per tube (equivalent to 5.3 µg g⁻¹ Al in the final sample), and were stored at -20 °C until analysis. A blood reference sample with indicative values for Al, Seronorm Trace Element Human Whole Blood, level II (batch 0503109, Sero, Billingstad, Norway), was also analysed for validation purposes. This sample is available as a powder and was reconstituted in purified water. Additionally, two blood samples from living subjects available from the Hospital Miguel Servet (Zaragoza, Spain) were also analysed as a means to validate the performance of the method proposed for blood samples containing other anticoagulant reagents. These samples are referred to as LS-1 and LS-2, and were collected in 3.0 mL BD Vacutainer® tubes (BD, Franklin Lakes, NJ, USA) containing 5.4 mg potassium-EDTA per tube.

Water samples for the eight drowning suspects were collected in previously cleaned 30 mL PE vials. These samples were

acidified after collection with ultrapure nitric acid to reach a final acid concentration of ~0.14 mol L⁻¹ BCR-610 Ground water (high contents) available from the Institute for Reference Materials and Measurements (IRMM) (Geel, Belgium) was analysed for validation purposes.

2.2.3. Procedure for direct analysis of the blood and water samples by means of HR-CS GFMS and/or HR-CS GFAAS. Blood samples were analysed either directly or after proper dilution with purified water in 3 mL pre-cleaned polyethylene autosampler vials. Before analysis or dilution, the collecting tubes containing the blood samples were gently mixed for ensuring sample homogeneity. The solid sampling device used allows for automatic transporting of the samples into the furnace.^{25,32} The empty graphite platform was first transported to the dispensing platform using a pair of tweezers. 10 µL of the blood sample (diluted or undiluted) plus 10 µL of the NH₄F·HF modifier solution (when needed) were placed onto the platform using a calibrated micropipette. The platform was then transferred into the graphite furnace and subsequently subjected to the temperature program. All these operations were fully controlled by the computer, except for the deposition of the sample and the modifier solutions onto the platform, which was carried out manually.

The operating conditions used are summarized in Tables 1 and 2. Integrated absorbance (A_{int}) was selected as the measurement mode in all cases. For the atomic line evaluated (396.152 nm), the values obtained for three detector pixels (the central pixel plus the adjacent ones, CP ± 1), corresponding to a spectral interval of 5.3 pm, were summed. For the molecular line evaluated (AlF at 227.5 nm), the values obtained for five detector pixels, corresponding to a spectral interval of 5.5 pm, were summed. In the latter case, this summing operation was performed offline, using an Excel spreadsheet. More details on the quantification procedure used for this line are provided in Section 3.1.

For the atomic line, samples were diluted with ultrapure water before analysis (1 : 4 dilution factor), and the method of standard additions was used for calibration. For this purpose, three additions of 10 µL of aqueous solutions of 5, 10 and 20 µg L⁻¹ Al were carried out by depositing the standard solutions onto the sampling platforms, already containing the diluted blood sample, with a calibrated micropipette. Five replicate measurements of each point of the calibration curve were performed, representing approximately 1 h of work per sample.

For the molecular line, sample dilution was not strictly necessary and external calibration with aqueous standards was feasible. In any case, most samples were diluted with ultrapure water before analysis (1 : 4 dilution factors) in order to improve repeatability. Only samples for which Al concentration values below 10 ppb were obtained in the first replicate were finally analysed undiluted. Every working session consisted of the measurement of one calibration curve plus four sample determinations. The 3-point calibration curve (covering the range between 5 and 50 µg L⁻¹ Al) was constructed by pipetting 10 µL of aqueous solutions of appropriate concentration plus 10 µL of the modifier and depositing them onto the sampling platform, while every sample determination was calculated as the mean of five replicate measurements. The full process represents approximately 90 min of work.

Table 1 Instrumental parameters used in the determination of Al by means of HR-CS electrothermal molecular absorption spectrometry after formation of the AlF molecule

Wavelength at central pixel ^a	227.402 nm
Wavelength of the peak maximum (C)	227.477 nm
Number of detector pixels summed (C ± 2)	5 (5.5 pm)
Ar gas flow during atomization	Stop-flow
Modifier	10 µL NH ₄ F·HF (5%)
Sample volume	10 µL

Temperature program

Step	Temperature/°C	Ramp/°C s ⁻¹	Hold time/s
Drying	100	6	50
Drying	160	6	60
Drying	200	6	20
Pyrolysis	1000	40	40
Auto zero	1000	0	5
Atomization	2300	600	4
Cleaning	2600	500	4

^a The central pixel is not positioned at the peak maximum to obtain proper baseline definition.

Table 2 Instrumental parameters used in the determination of Al by means of HR-CS electrothermal atomic absorption spectrometry in water and blood samples

Wavelength	396.152 nm
Number of detector pixels summed (C ± 1)	3 (5.3 pm)
Ar gas flow during atomization	Stop-flow
Modifier	No
Sample volume	10 µL

Temperature program

Step	Temperature/°C	Ramp/°C s ⁻¹	Hold time/s
Drying	100	6	30
Drying	160	6	30
Drying	200	6	20
Pyrolysis	1000	40	40
Auto zero	1000	0	5
Atomization	2500	600	6
Cleaning	2600	500	4

Water samples were also analysed either directly or after proper dilution with purified water in order to adjust sensitivity. Samples were introduced into the graphite furnace following the same methodology described above. The operating conditions used are summarized in Table 2 and are similar to the conditions used for the analysis of the blood samples by using the atomic line, except for the drying and pyrolysis stages that could be considerably shortened for the analysis of water. External calibration with aqueous standards was used in this case.

2.2.4. Procedure for analysis of the blood samples by means of SF-ICPMS for comparison purposes. Analysis of part of the blood samples available was also carried out by means of SF-ICPMS after sample digestion, in order to obtain additional reference values and further validate the proposed methodology. In particular, four samples were analysed: the Seronorm reference sample, one of the samples from drowning suspects collected in Liheparinized tubes (DS-5) and the two samples from living patients collected in EDTA containing tubes (LS-1 and LS-2). An

adaptation of the analysis method proposed by Rodushkin *et al.* in ref. 19 was used for this purpose: 0.5 mL of blood were placed on 10 mL Savillex beakers to which 2 mL of ultrapure 14 M HNO₃ was added. The closed beakers were heated on a hot plate at 120 °C for 90 min. Then, 0.5 mL ultrapure 30% H₂O₂ was added and the mixture was heated for an additional 30 min. Samples were diluted to 20 mL. Two procedural blanks were prepared using 1 mL of water instead of blood. At this point, Sc was added to the solution to be used as an internal standard. Analysis of the resulting solution was carried out using SF-ICPMS.

3 Results and discussion

3.1. Selection of the Al diatomic molecule for analysis

The use of molecular absorption of Al diatomic molecules for quantitative purposes is not very novel. In fact, formation and monitoring of molecular absorption for AlF, AlCl, AlBr, AlI and AlS for the determination of sulfur and the halogens, both for flame and graphite furnace AA instruments, have been investigated in the literature since the 70's, as recently reviewed by Welz and coworkers in ref. 30 even though, before the development of HR-CS, the instrumentation typically available (line sources designed to measure narrow atomic lines) represented a serious limitation for the monitoring of these and other molecules. Although this working methodology has never been used for the quantification of Al, some of the conclusions drawn in those works can be used for the development of the analytical method in this case. First of all, selection of the most suited molecule from the ones listed before is needed. As indicated by Welz in his review, data of the bond strength of diatomic molecules are a helpful orientation for finding molecules well suited for molecular absorption spectrometry (MAS). Molecules with bond strength above 500 kJ mol⁻¹ are easier to form and have better chances of surviving at the elevated temperatures of the graphite furnaces, and thus are ideal candidates for this purpose.³⁰ Taking this into account, the use of AlF (664 kJ mol⁻¹) for MAS is particularly favored if compared with AlCl (511 kJ mol⁻¹), AlBr (429 kJ mol⁻¹), AlI (370 kJ mol⁻¹) and AlS (373 kJ mol⁻¹).³³ Moreover, another effect has to be considered. Formation of any of these molecules in the gas phase would imply the addition of an excess of a halide- or sulfide-forming agent to the liquid phase, which very likely will result in the transformation (in the liquid phase) of, at least part of the Al present in the sample, into the corresponding aluminium halide/sulfide. In this regard, the use of F is again advantageous, as aluminium trifluoride is much more thermally stable than aluminium sulfide or the rest of the Al-halogenides (boiling points: AlF₃ 1290 °C; AlCl₃ 180 °C; (AlBr₃)₂ 255 °C; (AlI₃)₂ 382 °C; and Al₂S₃ 150 °C),³³ permitting the use of higher pyrolysis temperatures without the risk for analyte losses. Promotion of the AlF molecule and detection of its molecular absorption were therefore the working methodology selected in the current work for attempting direct Al quantification in the blood samples by means of graphite furnace (GF) MAS.

3.2. Formation of the AlF molecule in the graphite furnace and monitoring of its molecular absorption: preliminary experiments

The first experiments for the optimization of the working conditions were carried out with Al aqueous solutions, and 10 µL

of a 50 ng mL⁻¹ Al standard were used for this purpose. After the first experiments were carried out, it became obvious that working with the liquid autosampler was problematic as it increased substantially the degree of Al contamination. Working with the solid sampling device permitted a better control for this level of contamination, as the vials containing the samples/reagents/standards were only opened before injection and pipette tips could be easily replaced when needed. Therefore, the solid sampling device was used for further experiments. In spite of this fact, volume related concentrations were always used and the instrument built-in microbalance was not deployed.

Based on our previous experience with fluorinating agents in the graphite furnace,³⁴ NH₄F·HF was first tested for promoting the formation of AIF. This reagent can be obtained with a high degree of purity (crucial in this case) and has a relatively high thermal stability (decomposes at 240 °C (ref. 33)), which enables its activity beyond the drying step and explains its high efficiency as a fluorinating agent in the graphite furnace. Addition of 10 µL of a 5% NH₄F·HF solution, which had given good results in our previous investigations, was also tested in this case.

Before starting the construction of the pyrolysis and vaporization curves, spectral settings for monitoring the AIF molecular absorption were chosen. The main resonance system for AIF lies in the far ultra-violet, and results from a $\Delta\nu = 0$ sequence of the X¹Σ⁺-A¹Π electronic transition.²² The most sensitive band head for this system, located at 227.47 nm, is considerably broader than a typical atomic line and, unlike them, presents a pronounced dissymmetry, as seen in Fig. 1, where a typical absorption profile around the AIF band head at 227.47 nm for 10 µL of a 50 ng g⁻¹ Al solution + 10 µL of the fluorinating agent is presented.

As can be seen in this figure, the bandwidth of the absorption head at 227.47 nm occupies a significant portion of the spectral window offered by our instrument detector at this wavelength (around 0.3 nm). For accurate monitoring of molecular bands, it is very important to obtain a sufficient number of baseline pixels both to the right and to the left of this band. In order to achieve this goal, and as a direct consequence of the dissymmetry of the band, the typical way of working for CS AAS spectrometers, *i.e.*, using the central pixel of the detector for monitoring the peak maximum so that the absorbance value is automatically recorded by the instrument, is not recommended in this case. In fact, if the peak maximum is monitored with the central pixel, the left flank of the absorbance peak would be “cut”, making impossible to achieve a proper baseline definition. Instead, the central detector pixel was positioned to monitor a wavelength of 227.402 nm, which permitted the detection of the full AIF absorption band located to the right, leaving enough pixels at both sides for the definition of the baseline. The signal was then exported and treated off-line with an Excel spreadsheet, as the software of the instrument only allows direct integration of a defined number of pixels surrounding the central pixel. Optimization of the offline data treatment protocol was next considered.

For HR-CS instruments like the one used in this work, with a pixel detector, absorbance values are obtained as the sum of the individual integrated (in time) absorbance values of the selected pixels (wavelengths), which results in a volume under the absorbance 3D peak. Selection of the peak volume giving the best *S/N* ratios is an important parameter that needs to be

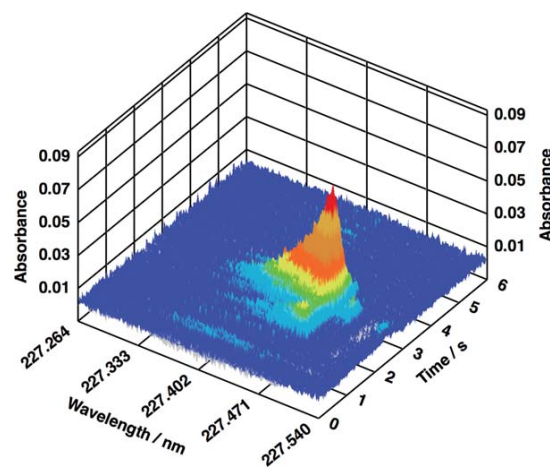


Fig. 1 3D Time and wavelength resolved absorbance spectrum for 10 µL of a 50 ng mL⁻¹ Al standard solution + 10 µL of a 5% NH₄F·HF fluorinating solution.

optimized. While for atomic lines, this issue is well studied and clear conclusions are readily available,³⁵⁻³⁸ the same cannot be said for such a broad and asymmetrical absorption peak like the one obtained for the AIF molecule and, thus, further optimization was carried out in this case. For this purpose, a series of 10 replicate measurements of the blank (just the fluorinating agent) and 5 replicate measurements of a 50 ppb Al standard solution + fluorinating agent were measured. The integrated absorbance values for gradually growing peak volumes, as shown in Fig. 2A, were calculated. These integrated absorbance values were then used for calculating the characteristic concentration and the LOD for each pixel combination, and the results are summarized in Fig. 2B.

Self evidently, the characteristic concentration decreases with every new pixel included in the calculation. In spite of this fact, the use of a number of pixels larger than 8 degrades the *S/N* ratios and results in worse LODs. As seen in Fig. 2, the best LODs were achieved when using signals corresponding to the sum of 3 to 8 pixels in the centre of the absorption peak. In the end, the sum of 5 pixels symmetrically distributed around the peak maximum at 227.477 nm was used for further experiments, as it provided results in better agreement with the expected values for the analysis of the Seronorm reference blood sample.

With this working methodology, the pyrolysis and vaporization curves for the aqueous solutions under fluorinating conditions, shown in Fig. 3A, could be finally acquired.

Two different processes affect the formation and detection of the AIF molecule in the graphite furnace; on the one hand, as indicated by Tsunoda and co-workers in their pioneering work,³⁹ AIF formation seems to be only possible if free Al atoms are available in the gaseous phase, for which high temperatures are required. On the other hand, if too high temperatures are used, dissociation of the AIF molecule formed will occur, with the subsequent signal reduction. As a result, compromise conditions need to be used. In order to monitor and minimize the possible molecule dissociation occurring at high temperatures, atomic

absorbance at 396.152 nm was also measured for the mixture Al standard + fluorinating agent. This curve is also included in Fig. 3A.

As seen in this figure, pyrolysis temperatures up to 1400 °C can be used for recording the molecular absorption of AIF without significant effects on the signal. The use of pyrolysis temperatures below 1200 °C is, however, recommended, as measurement repeatability for the molecular line seems to degrade for temperatures beyond this value.

As for the vaporization, as could be expected and as a consequence of the two competing processes mentioned above, the vaporization curve for the molecular line does not show a plateau after the signal has reached its maximum. Increasing the temperature well above 2100 °C results in a net signal reduction probably due to AIF dissociation, as supported by the higher

atomic absorption values recorded for the atomic line at 396.152 nm at these temperatures. In this case, however, slightly higher vaporization temperatures, in the range of 2200–2300 °C, are recommended. At these temperatures, AIF dissociation (and Al atomic absorption) is still not significant; but in contrast, the signal profile for AIF is better defined and a significant improvement in measurement repeatability is obtained (see Fig. 3A).

3.3. Direct analysis of the blood samples by HR-CS GFMS

Once the optimum conditions for the formation and detection of the AIF molecule for aqueous standards had been found, optimization of the working protocol for the analysis of the blood samples was carried out. A reference material (Serorm Trace Element Human Whole Blood, Level II) and three real samples (DS-5, LS-1 and LS-2, see Section 2.2.2. for details) were used during the optimization experiments. As indicated in the Introduction, one of the crucial issues that needs to be addressed when working with whole blood samples is sample matrix removal for

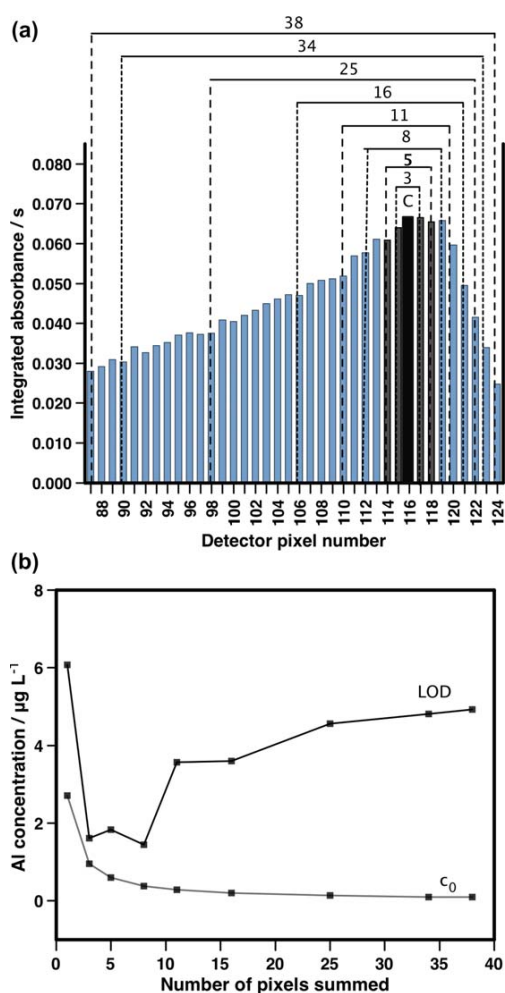


Fig. 2 Optimization of the data acquisition methodology. (A) Pixel combinations tested. The numbers indicated over each pixel combination indicate the number of pixels summed in each case. (B) Limit of detection (LOD) and characteristic concentration (c_0) calculated for the pixel combinations indicated in (A). The number of pixels summed (as indicated in (A)) is included on the x-axis. The error bars have been omitted, as their magnitude is similar to that of the markers used in the figure.

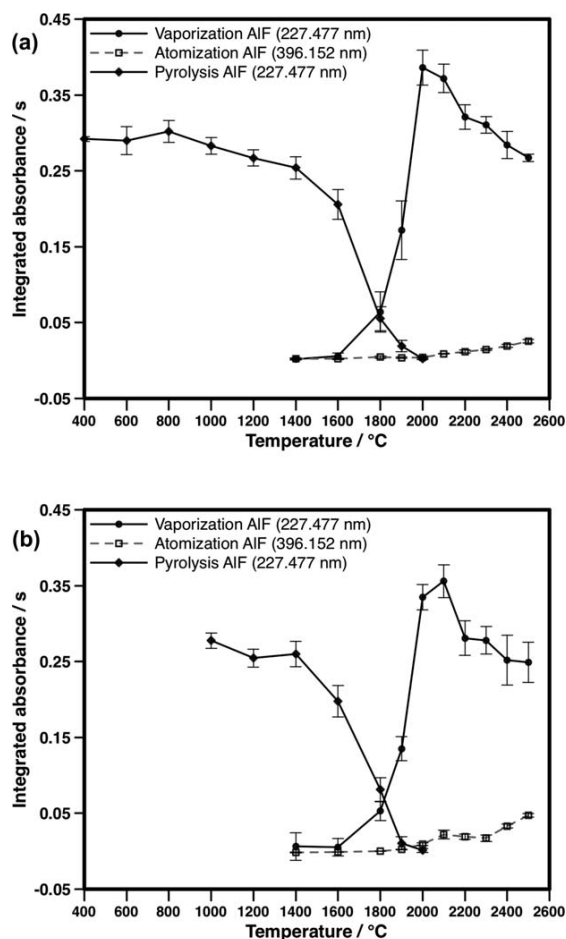


Fig. 3 Pyrolysis and atomization/vaporization curves, measured at 396.152 nm (Al atomic line) and 227.477 nm (AIF molecular band), for (A) 10 µL of a 50 ppb Al solution + 10 µL of a 5% $\text{NH}_4\text{F}\cdot\text{HF}$ solution and (B) 10 µL of a blood sample containing 46.6 µg L⁻¹ Al + 10 µL of a 5% $\text{NH}_4\text{F}\cdot\text{HF}$ solution.

avoiding or minimizing the occurrence of matrix effects. Although matrix removal is generally carried out during the pyrolysis step, the importance of the drying step in this regard cannot be underestimated in cases like the one considered here, where achieving proper interaction between the modifier and the analyte from the beginning is critical. As previously described for the direct analysis of organic samples by means of ETV-ICPMS,³⁴ addition of $\text{NH}_4\text{F}\cdot\text{HF}$, on top of providing the F atoms needed for promotion of the AIF molecule, could actually help digesting the blood sample in the graphite furnace, therefore helping to reduce one of the main problems reported for direct analysis of whole blood samples. In this case, the use of a drying stage in three phases (see Table 1) ensured a proper interaction between modifier and sample and avoided spilling at the beginning of the pyrolysis step. As for the pyrolysis temperature, the use of 1000 °C, guaranteeing a proper promotion of the AIF molecule without premature analyte losses, as shown in Fig. 3B for one of the blood samples analysed, proved to be the best solution for (i) avoiding residue build-up after the vaporization of any of the undiluted blood samples tested and (ii) minimizing matrix effects (although not fully avoiding them, as discussed below). For the vaporization step, and similarly to what had been observed for the aqueous solutions, best results in terms of sensitivity–repeatability were obtained at a temperature of 2300 °C (see Fig. 3B).

Next, further optimization of the amount of $\text{NH}_4\text{F}\cdot\text{HF}$ added was performed. The goal of this optimization was finding the minimum quantity needed for ensuring the proper promotion of the AIF molecule as well as a complete matrix removal, while minimizing the potentially deleterious effects that exposure to too high a fluoride concentration could have on the optical components (*e.g.*, in the quartz window). The quantity used for the preliminary experiments, *i.e.*, 10 μL of a 5% $\text{NH}_4\text{F}\cdot\text{HF}$ solution, proved to be the optimum value and was used for further experiments.

3.3.1. Spectral interference evaluation. One of the potential disadvantages of working with relatively broad molecular lines such as the one considered in this work is the increased probability of finding spectral interferences within the wavelength range recorded. However, using the proposed methodology, where addition of an external reagent is needed in order to promote the formation of the molecule for which the absorbance is being measured, has additional advantages in this regard and offers a powerful diagnostic tool. In fact, by simply monitoring the absorption spectrum at the wavelength of interest for the sample under analysis, but without the addition of the molecule-forming agent ($\text{NH}_4\text{F}\cdot\text{HF}$ in this case), one can actually “look under the line” for interfering species originating from the sample matrix.²² The absorption spectrum without the addition of the fluorinating agent was therefore recorded at the beginning of every sample analysis for detecting matrix-related spectral interferences. No significant influence of the relatively strong atomic lines for Co (227.452 nm) and Ni (227.467 nm) that have been reported to overlap with the peak maximum⁴⁰ was detected for any of the blood samples under analysis. In every case, however, a structured background showing three sharp band heads was recorded, partially overlapping with the AIF band monitored as shown in Fig. 4 (reference spectrum).

The Plasus SpecLine database⁴¹ hints at the $a^1\Pi_g-X^1\Sigma_g^+ \text{N}_2$ system as the potential interference, although only two of the three lines observed were actually identified by this software. It can also be mentioned that the spectra of other more typical molecular systems that appear in this spectral region, *e.g.*, SiO or NO, do not match that of the interference at all. In order to reduce or eliminate this overlap, modification of the temperature program was attempted, but no significant improvement was obtained. Correction of this kind of background spectrum can be performed, however, using a least-squares algorithm included in the software of the HR-CS AAS instrument for this purpose. Implementation of this correcting algorithm is very simple, and only requires the acquisition of one reference spectrum for the observed interfering structures (*i.e.*, acquisition of the spectrum for one of the blood samples vaporized with no fluorinating agent). More details for this approach can be found elsewhere.²⁶ The benefits of this correction approach can be appreciated in Fig. 4 for one of the real blood samples analysed. As seen in this figure, a clean spectrum for the sample affected by the interferences is obtained after application of the algorithm.

Although this working methodology is very interesting and can be of capital importance for other analytical situations,^{18,42,43} it is fair to stress the fact that, in this case, its use does not significantly affect the final quantitative results. As seen in Fig. 4, the part of the interference spectrum that actually overlaps with the peak volume used for quantification is minimal, and the direct use of the uncorrected signals did not provide significantly different results from those obtained after the least squares correction was applied, in all of the cases investigated. In any case, and taking into account that implementation of this correction method is automatically done by the instrument by simply selecting the reference spectrum, recording the absorbance profile of the sample alone at the beginning of the determination procedure is always recommended, keeping the

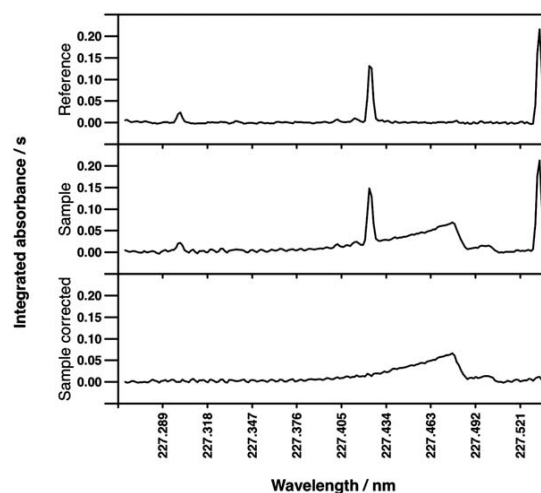


Fig. 4 Wavelength resolved time-integrated absorbance spectrum for 10 μL EDTA containing blood sample: without the addition of $\text{NH}_4\text{F}\cdot\text{HF}$ (reference); with the addition of 10 μL of a 5% $\text{NH}_4\text{F}\cdot\text{HF}$ solution (sample); and after application of the LSBC methodology for correction of the spectral interferences (sample corrected).

possibility for evaluating and correcting for the influence of these interferences *a posteriori*.

3.3.2. Analysis of the blood samples for method validation.

Once the working conditions had been optimized, analysis of the blood samples mentioned before was carried out. Under the working conditions described in the previous sections, very similar signal profiles for the Al aqueous standards and the blood samples could be obtained, as seen in Fig. 5. This enables the use of direct external calibration for quantification purposes, making the use of cumbersome standard addition methodology unnecessary. Although sample dilution is not strictly necessary, better repeatability can be obtained if samples are diluted 1 : 4 with ultrapure water, especially for the real samples that contain heparin or EDTA to prevent coagulation, probably due to a better interaction of the chemical modifier with the sample. For samples containing low amounts of Al, however, direct analysis of the undiluted samples is still possible and offers acceptable results.

Results for the analysis of the validation samples (after 1 : 4 dilution), obtained following the experimental procedure described in Section 2.2.3, are summarized in Table 3. As seen in this table, good agreement between the values obtained with the proposed methodology and the reference values was obtained in all cases, and adequate figures in terms of result precision and accuracy were obtained for this working methodology in all of the cases. In order to check method reproducibility, the Seronorm sample was analysed in four different days following the aforementioned experimental procedure, and the final result displayed in Table 3 was calculated as the mean of these four determinations. As seen in the table, very satisfactory results were also obtained in this regard.

3.4. Analysis of the blood samples by HR-CS GFAAS and comparison with the MAS method

Analysis of the same samples (Seronorm, DS-5, LS-1 and LS-2) was carried out by means of SF-ICPMS, as described in Section 2.2.4, to obtain truly independent values. Furthermore, analysis by means of HR-CS GFAAS using the atomic line at 396.152 nm was also carried out to compare the performances of the MAS and AAS techniques. The optimized temperature program used in this case is shown in Table 2. The main differences with the program used for the analysis based on the use of the molecular band lie in the atomization (or vaporization) and drying steps. In the case of the atomization/vaporization, the use of the atomic line requires higher temperatures (2500 °C) than that of the molecular band, which could result in a reduced lifetime for the graphite tubes in the former case. A three-step drying stage was also necessary in this case in order to avoid spilling of the sample at the beginning of the pyrolysis step, although the length of the stages could be somewhat reduced.

As previously commented, the influence of non-spectral interferences is severe for the direct determination of Al in whole blood, and sample dilution was needed to reduce matrix effects and residue build-up in the graphite furnace. In spite of this fact, matrix effects could not be fully avoided, even for 1 : 9 dilution factors, and the use of standard additions for calibration was necessary. Implementation of this measure for dealing with matrix effects did not avoid the need for dilution, as acceptable results could only be obtained for 1 : 4

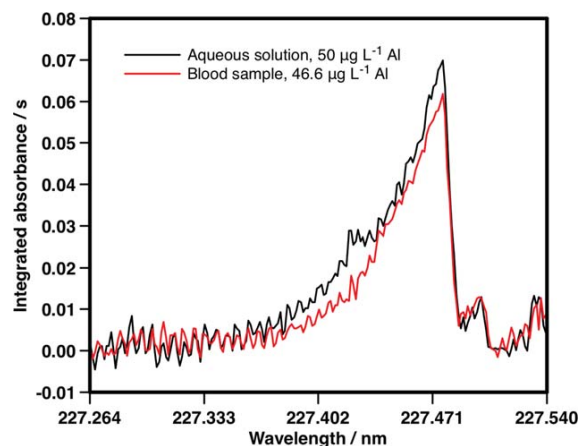


Fig. 5 Comparison of wavelength resolved time-integrated absorbance spectra for the vaporization of 10 μL of a 50 $\mu\text{g L}^{-1}$ Al aqueous solution and 10 μL of a blood sample containing 46.6 $\mu\text{g L}^{-1}$ Al and EDTA, using the working conditions summarized in Table 1.

dilution factors or above. This, self-evidently, has a negative influence on the minimum Al concentration values that can be determined in blood samples by using this method. In spite of this fact, and even if the MAS method permitted the direct analysis of the undiluted blood samples, the detection capabilities of both methodologies are very similar, with LODs of 1.5 $\mu\text{g L}^{-1}$ for the AAS method and 1.8 $\mu\text{g L}^{-1}$ for the MAS method, respectively. In reality, sensitivity for the atomic line and the molecular band are similar, but evaluation and measurement of the molecular band introduces more noise. As a consequence, the LOD for the MAS method is poorer than that of the AAS method, although the need for dilution in the latter case compensates for this difference. Besides, matrix removal was not complete with the AAS technique and mechanical removal of the residues had to be carried out after every determination, which obviously increases the risk for contamination.

For the rest, and as shown in Table 3, good agreement with the results obtained for the molecular band and the reference values available were also obtained in this case for the validation samples, although with poorer precision figures than those obtained with the MAS technique (as could be expected for the standard addition methodology). Considering the total analysis time, performance of the MAS technique is also better than that of the AAS technique due to the need for standard addition calibration in the latter case, which represents a significant decrease in sample throughput as detailed in Section 2.2.3.

Summarizing, while both techniques offer rather similar figures of merit regarding detection capabilities, the MAS technique solves the existing problems related to matrix effects, residue build-up and calibration observed for the AAS technique, which results in a methodology less prone to contamination and much easier to use, and a remarkable improvement in sample throughput.

3.5. Suitability of the determination of Al levels in blood and water samples for diagnosis of drowning

Finally, analysis of the drowning suspect samples was carried out with the AIF-MAS methodology described in the previous

Table 3 Comparison of the reference and determined Al concentration values for the validation samples. SF-ICPMS, AAS and MAS results were obtained following the experimental procedures included in Sections 2.2.3 and 2.2.4. Uncertainties are expressed as 95% confidence intervals

	Reference/ $\mu\text{g L}^{-1}$	SF-ICPMS/ $\mu\text{g L}^{-1}(n = 3)$	AAS/ $\mu\text{g L}^{-1}(n = 5)$	MAS/ $\mu\text{g L}^{-1}(n = 5)$
Seronorm	58.9 ± 9.9	60.1 ± 6.1	56.9 ± 8.1	57.5 ± 3.4^a
LS-1	—	46.8 ± 9.2	46.6 ± 5.7	45.0 ± 4.6
LS-2	—	96.5 ± 10.4	100.3 ± 9.2	96.4 ± 7.6
DS-5	—	23.7 ± 6.0	24.6 ± 8.8	24.3 ± 5.3

^a This result was calculated as the mean of four different determinations carried out in four different days.

sections. A series of 10 blood samples were analysed, 8 obtained from drowning suspects and 2 from bodies recovered under different circumstances and used as controls. 8 water samples taken from the water media where the drowning suspects had been found were also analysed following the methodology described in Section 2.2.3. Results for all of these analyses are gathered in Table 4.

From these data, some general ideas about the utility of the proposed methodology for drowning diagnosis can be extracted. First of all, application of the Spearman rank correlation coefficient method⁴⁴ reveals a positive correlation between the Al content in water and Al content in blood of the drowning suspects at a 95% significance level ($r = 0.952$; $r_{\text{critical}} = 0.738$), supporting the validity of Al as a drowning marker. Establishing an Al threshold concentration in blood for indicating a clear drowning diagnosis is, however, quite risky at this point, although some indications can be given in this regard. Firstly, and as revealed by the results obtained for samples CTRL-1, CTRL-2, DS-1, DS-7 and DS-8, Al levels up to $10\text{--}15 \mu\text{g L}^{-1}$ found in the blood samples can be considered as “normal” or “basal” levels. Translating this Al result into clear answers for drowning diagnosis obviously depends on the Al content found in the water media: if low Al concentration values are found in the drowning media (like for cases DS-1, DS-7 and DS-8), the validity of Al as a drowning marker is obviously inexistent. On the other hand, if high Al concentrations are found in the water, Al values below this limit should indicate a cause of death different from drowning. In this regard, determining an Al concentration threshold in the water high enough to induce a clear increase in the “basal” Al levels in blood is difficult, as additional factors such as, *e.g.*, duration of the agony would certainly have a significant influence on the total amount of Al entering the bloodstream. This idea is supported by the fact that, as observed when comparing cases DS-2 and DS-4, a higher Al level in the water media does not immediately result in a higher Al level in the blood of the suspect. However, it is also true that for all water samples showing $200 \mu\text{g Al}$ per litre or higher, an Al blood level at least twice as high as the “basal” level has been found.

From all of the above, it seems clear that the method proposed has some potential as a valid marker for drowning diagnosis, although an extensive study investigating a large number of suspects and controls would be needed in order to extract clearer conclusions from a forensic point of view. Carrying out this study is probably worth trying, considering the few diagnostic

Table 4 Al concentration levels found in the blood and drowning water of eight drowning suspects collected in the area of Gent (DS-1 to DS-8) plus two control corpses collected in the same geographical area under other circumstances different from drowning (CTRL-1 and -2). Uncertainties are expressed as 95% confidence intervals (3 and 5 replicates were measured for water and blood samples, respectively)

	Al content in water/ $\mu\text{g L}^{-1}$	Al content in blood/ $\mu\text{g L}^{-1}$
DS-1	2.31 ± 0.24	4.32 ± 0.82
DS-2	412 ± 14	94.3 ± 6.8
DS-3	296 ± 12	37.1 ± 3.7
DS-4	483 ± 18	38.9 ± 3.1
DS-5	195 ± 11	24.3 ± 5.3
DS-6	505 ± 14	133 ± 9
DS-7	14.9 ± 1.0	12.9 ± 2.1
DS-8	30.1 ± 1.7	11.9 ± 1.7
CTRL-1	—	6.5 ± 1.0
CTRL-2	—	10.5 ± 1.8

tools that forensic doctors have at their disposal when dealing with death by drowning.

4 Conclusions

The use of HR-CS GFMS for determination of Al in blood samples *via* formation of the AIF molecule in the graphite furnace and monitoring of its molecular absorption provides an alternative method to conventional atomic absorption, resolving most of the problems related to the latter technique. Addition of $\text{NH}_4\text{F}\cdot\text{HF}$ required for promotion of the AIF molecule has the advantage of improving sample matrix removal and minimizing residues in the graphite platform that, otherwise, need to be removed mechanically increasing the risk for contamination. As a result, with this method it is possible to construct the calibration curve with aqueous standards, avoiding the need for the cumbersome method of standard additions, while detection capabilities are essentially maintained ($1.8 \mu\text{g L}^{-1}$ vs. $1.5 \mu\text{g L}^{-1}$ LODs for the MAS and AAS methods, respectively).

Application of this cost-effective and relatively easy to use methodology for Al determination in the blood of drowning suspects, on the other hand, has shown some potential to be used as a valid marker for drowning diagnosis, as a positive correlation between Al concentration in drowning water and Al concentration in the blood of drowning suspects seems to be present. Additional studies with a large number of corpses and controls would be, however, needed in order to draw more definitive conclusions from a forensic point of view.

Acknowledgements

This work has been funded by the Spanish Ministry of Science and Innovation (Project CTQ2009-08606) and the Aragon Government (Departamento de Ciencia, Tecnología y Universidad del Gobierno de Aragón y Fondo Social Europeo and Fundación ARAID and “Obra Social de IberCaja”, with additional support from Inycom). Maite Aramendía thanks the FWO-Vlaanderen for her postdoctoral grant. María del Rosario Flórez thanks the Spanish Ministry of Science and Innovation for her doctoral grant.

Notes and references

- M. D. Pérez-Cárceles, A. Sibón, M. L. Gil del Castillo, M. A. Vizcaya, E. Osuna, T. Casas, J. L. Romero and A. Luna, *Biol. Trace Elem. Res.*, 2008, **126**, 27–37.
- M. H. A. Piette and E. A. De Letter, *Forensic Sci. Int.*, 2006, **163**, 1–9.
- J. Timperman, *Forensic Sci.*, 1972, **1**, 397–409.
- B. Ludes and P. Fornes, Drowning, in *Forensic Medicine: Clinical and Pathological Aspects*, ed. J. Payne-James, A. Busuttill and W. Smock, Greenwich Medical Media Ltd., London, San Francisco, 2003, pp. 247–257.
- J. Hürlimann, P. Feer, F. Elber, K. Niederberger, R. Dirrhofer and D. Wyler, *Int. J. Leg. Med.*, 2000, **114**, 6–14.
- C. Yu-Chuan, D. Zhao-Ke and Z. Jia-Zhen, *Forensic Sci. Int.*, 1990, **46**, 289–294.
- B.-L. Zhu, K. Ishida, M. Taniguchi, L. Quan, S. Oritani, K. Tsuda, Y. Kamikodai, M. Q. Fujita and H. Maeda, *Leg. Med.*, 2003, **5**, S298–S301.
- M. Piette, B. Desmet and R. Dams, *Sci. Total Environ.*, 1994, **141**, 269–273.
- J. E. Azparren, E. Perucha, P. Martínez, R. Muñoz and G. Vallejo, *Forensic Sci. Int.*, 2007, **168**, 138–142.
- J. E. Azparren, A. Fernandez-Rodriguez and G. Vallejo, *Forensic Sci. Int.*, 2003, **137**, 55–59.
- K. G. Ljunggren, V. Lidums and B. Sjögren, *Br. J. Ind. Med.*, 1991, **48**, 106–109.
- J.-P. Goullé, L. Mahieu, J. Castermant, N. Neveu, L. Bonneau, G. Lainé, D. Bouige and C. Lacroix, *Forensic Sci. Int.*, 2005, **153**, 39–44.
- C. T. Driscoll and W. D. Schecher, *Environ. Geochem. Health*, 1990, **12**, 28–49.
- E. M. Skelly and F. T. DiStefano, *Appl. Spectrosc.*, 1988, **42**, 1302–1306.
- I. Rodushkin, E. Engström and D. C. Baxter, *Anal. Bioanal. Chem.*, 2010, **396**, 365–377.
- S. Salomon, P. Giamarchi, A. Le Bihan, H. Becker-Ross and U. Heitmann, *Spectrochim. Acta, Part B*, 2000, **55**, 1337–1350.
- S. Tang, P. J. Parsons and W. Slavin, *Spectrochim. Acta, Part B*, 1997, **52**, 1351–1365.
- D. Bohrer, U. Heitmann, M. Huang, H. Becker-Ross, S. Florek, B. Welz and D. Bertagnolli, *Spectrochim. Acta, Part B*, 2007, **62**, 1012–1018.
- I. Rodushkin, F. Ödman and S. Branth, *Fresenius J. Anal. Chem.*, 1999, **364**, 338–346.
- P. C. D'Haese, F. L. Van de Vyver, F. A. de Wolff and M. E. De Broe, *Clin. Chem. (Washington, D. C.)*, 1985, **31**, 24–29.
- W. Frech, A. Cedergren, C. Cederberg and J. Vessman, *Clin. Chem. (Washington, D. C.)*, 1982, **28**, 2259–2263.
- B. Welz, H. Becker-Ross, S. Florek and U. Heitmann, *High Resolution Continuum Source AAS—the Better Way to do Atomic Absorption Spectrometry*, Wiley-VCH, Weinheim, 2005.
- B. Welz, *Anal. Bioanal. Chem.*, 2005, **381**, 69–71.
- B. Welz, D. L. G. Borges, F. G. Lepri, M. G. R. Vale and U. Heitmann, *Spectrochim. Acta, Part B*, 2007, **62**, 873–883.
- M. Resano, F. Vanhaecke and M. T. C. de Loos-Vollebregt, *J. Anal. At. Spectrom.*, 2008, **23**, 1450–1475.
- H. Becker-Ross, S. Florek and U. Heitmann, *J. Anal. At. Spectrom.*, 2000, **15**, 137–142.
- M. Resano and E. García-Ruiz, *Anal. Bioanal. Chem.*, 2011, **399**, 323–330.
- M. Resano, L. Rello, M. Flórez and M. A. Belarra, *Spectrochim. Acta, Part B*, 2011, **66**, 321–328.
- B. Welz, S. Morés, E. Carasek, M. G. R. Vale, M. Okruss and H. Becker-Ross, *Appl. Spectrosc. Rev.*, 2010, **45**, 327–354.
- B. Welz, F. G. Lepri, R. G. O. Araujo, S. L. C. Ferreira, M. D. Huang, M. Okruss and H. Becker-Ross, *Anal. Chim. Acta*, 2009, **647**, 137–148.
- U. Heitmann, M. Schütz, H. Becker-Ross and S. Florek, *Spectrochim. Acta, Part B*, 1996, **51**, 1095–1105.
- M. G. R. Vale, N. Oleszczuk and W. N. L. dos Santos, *Appl. Spectrosc. Rev.*, 2006, **41**, 377–400.
- CRC Handbook of Chemistry and Physics*, ed. D. R. Lide, CRC Press, Boca Raton, 74th edn, 1994.
- M. Resano, M. Aramendia and F. Vanhaecke, *J. Anal. At. Spectrom.*, 2006, **21**, 1036–1044.
- U. Heitmann, B. Welz, D. L. G. Borges and F. G. Lepri, *Spectrochim. Acta, Part B*, 2007, **62**, 1222–1230.
- M. Resano, J. Briceño and M. A. Belarra, *Spectrochim. Acta, Part B*, 2009, **64**, 520–529.
- M. Resano, J. Briceño and M. A. Belarra, *J. Anal. At. Spectrom.*, 2009, **24**, 1343–1354.
- J. Briceño, M. A. Belarra, K. A. C. De Schampelaere, S. Vanblaere, C. R. Janssen, F. Vanhaecke and M. Resano, *J. Anal. At. Spectrom.*, 2010, **25**, 503–510.
- K. Tsunoda, K. Fujiwara and K. Fuwa, *Anal. Chem.*, 1977, **49**, 2035–2039.
- M. D. Huang, H. Becker-Ross, S. Florek, U. Heitmann and M. Okruss, *Spectrochim. Acta, Part B*, 2006, **61**, 572–578.
- Plasus SpecLine Database, version 2.1*, Plasus, Königsbrunn, Germany.
- M. Resano, E. Mozas, C. Crespo, J. Briceño, J. del Campo Menoyo and M. A. Belarra, *J. Anal. At. Spectrom.*, 2010, **25**, 1864–1873.
- R. G. O. Araujo, B. Welz, F. Vignola and H. Becker-Ross, *Talanta*, 2009, **80**, 846–852.
- J. N. Miller and J. C. Miller, *Statistics and Chemometrics for Analytical Chemistry*, Pearson Education Limited, Essex, England, 5th edn, 2005.

Cite this: *J. Anal. At. Spectrom.*, 2012, **27**, 401

www.rsc.org/jaas

PAPER

Direct determination of sulfur in solid samples by means of high-resolution continuum source graphite furnace molecular absorption spectrometry using palladium nanoparticles as chemical modifier

Martín Resano* and María R. Flórez

Received 4th November 2011, Accepted 16th December 2011

DOI: 10.1039/c2ja10322b

This work investigates the potential benefits of using Pd nanoparticles, in combination with Ru as permanent modifier, for sulfur monitoring as CS by means of high-resolution continuum source graphite furnace molecular absorption spectrometry. Upon heating, these small (approx. 20 nm diameter) Pd nanoparticles are evenly distributed over the platform surface, offering a larger surface for interaction with the analyte during the drying and pyrolysis steps. In this way, a more efficient stabilization of sulfur species can be achieved. Furthermore, a similar analytical response is obtained regardless of the chemical form in which sulfur species are originally found, thus making it easier to develop quantitative analytical methods for this analyte. When using these modifiers, and under optimized working conditions, it is possible to use this technique for direct analysis of different types of solid samples (biological, petroleum coke, polyethylene and steel CRMs), thus circumventing the traditional drawbacks associated with sample digestion when sulfur determination is aimed at. Accurate results are obtained using only the central CS line found at 257.958 nm, with precision values in the 5–10% RSD range (14 ng characteristic mass; 9 ng limit of detection). Moreover, the combined use of the main six CS lines available in the spectral area simultaneously monitored by the detector permits to further improve precision to 3–5% RSD, while decreasing the limit of detection down to 3 ng (the characteristic mass is also 3 ng), which represents a relative limit of detection of approx. $1 \mu\text{g g}^{-1}$, as calculated for the sample with the lowest sulfur content. In all cases, straightforward calibration with aqueous standards was proved to be feasible, and the sample throughput is of 3–4 samples per hour (5 replicates per sample).

1. Introduction

Sulfur is an abundant element on earth's crust (0.044%) and can be considered as one of the main building blocks for life in our planet, owing to its presence in proteins. Furthermore, sulfur, in different chemical forms, is an important raw material for a wide variety of industries and products, being currently used in fertilizers (mainly as sulfate), fungicide and pesticide formulations (as elemental sulfur), pharmaceuticals (organic sulfur), as an additive of foodstuffs (as SO_2), among many other applications.¹

Given the importance of this element, and considering its extensive use in many fields, the development of fast and straightforward methods for its determination in various types of samples is of great interest. However, for various reasons, such as lack of atomic lines in the UV-visible region when opting for atomic absorption or atomic emission spectrometry (AAS or AES),² or spectral overlaps when using inductively coupled

plasma mass spectrometry (ICP-MS),³ sulfur is not simple to determine at trace levels even with the most sensitive of the atomic spectrometry techniques. Still today, cumbersome and not very selective spectrophotometric methods are widely used, in addition to the so-called dedicated analyzers,⁴ which are costly and often specific for particular types of samples.

Regarding the use of graphite furnace (GF) atomic absorption spectrometers, despite the lack of suitable atomic lines in the spectral region that is typically accessible, the determination of sulfur was already evaluated in the 80s based on the formation of different sulfide species (*e.g.*, GeS or CS) and the monitoring of their molecular absorption using a hollow cathode lamp (HCL) of another element that emitted light in the spectral area of interest, as reported by Dittrich and Vorberg⁵ and Tittarelli and Lavorato.⁶ These early applications are reviewed in a recent work.⁷ Obviously, the performance of such technique could not be very satisfactory, owing to the poor suitability of the HCL source and the low resolution of "classic" AAS, which resulted in insurmountable problems when dealing with molecular sharp lines showing structured background.

This situation has changed very significantly upon arrival of high-resolution continuum source (HR CS) GFAAS

University of Zaragoza, Faculty of Sciences, Department of Analytical Chemistry, Pedro Cerbuna 12, Zaragoza, E-50009, Spain. E-mail: mresano@unizar.es

instrumentation, which has opened up new possibilities in this field.^{8–12} In addition to offering several advantages for the measurement of atomic absorption, this type of instrumentation permits the reliable quantitative monitoring of the molecular absorption of diatomic molecules, owing to the continuous nature and the high intensity of the radiation source (Xe lamp), and the excellent spectral resolution provided (better than 2 pm at 200 nm). In this way, new methods for the determination of sulfur, phosphorus and the halogens using graphite furnace molecular absorption spectrometry (GFMS) have been proposed, as reviewed by Welz *et al.*⁷ This GFMS technique can also offer some advantages for the determination of metals, in some particular situations.¹³

However, despite these new possibilities, one of the main reasons to opt for the use of graphite furnace-based techniques is the potential to carry out direct analysis of solid samples, thus improving sensitivity and expeditiousness. This aspect is even more relevant in the case of sulfur determination, as the ubiquity of the element, the high volatility of many of its compounds, and the obvious impossibility to use sulfuric acid as reagent to help dissolve the sample, make it difficult to obtain reliable results when digestion approaches are attempted. In particular, the potential for suffering from analyte losses can be very serious, and it is not surprising that protocols for sulfur determination often include many steps (*e.g.*, reduction to hydrogen sulfide, trapping of the latter in a solution by precipitation, and re-dissolution of the formed compound) to minimize this risk,¹⁴ at the cost of sample throughput.

The potential of GFMS has, however, been very seldom evaluated for direct analysis of solid samples. The only two works reporting on this topic so far have investigated the determination of phosphorus¹⁵ and, precisely, of sulfur,¹⁶ in biological samples, in both cases. There may be reasons for this limited number of works, as the process of formation of suitable diatomic molecules from a solid sample is, *a priori*, more complex than the process of atomization. Moreover, a review of the few works devoted to sulfur monitoring by GFMS¹⁷ clearly indicates remaining problems for achieving proper stabilization of this element, as well as for obtaining an analytical signal that is independent of the chemical form in which the analyte is found. It is clear that more work is required to expand the field of applications for this element, as will be discussed in Section 3.

The aim of this work is to further investigate the potential of GFMS for sulfur monitoring, evaluating more efficient ways to add the chemical modifier (*e.g.*, Pd as nanoparticles), in an attempt to develop suitable methods for the direct determination of sulfur in very different types of solid samples, namely biological materials, petroleum coke, polyethylene and steel. The ultimate goal is always to develop simple procedures relying only on the use of aqueous standards for calibration.

2. Experimental

2.1. Instrumentation

All the experiments in this work were carried out using a HR CS AAS, ContrAA 700, commercially available from Analytik Jena AG (Jena, Germany) and equipped with both graphite furnace and flame atomizers. The optical system comprises a xenon

short-arc lamp (GLE, Berlin, Germany) operating in “hot-spot” mode as the radiation source, a high-resolution double echelle monochromator (DEMON) and a linear CCD array detector with 588 pixels, 200 of which are used for analytical purposes (monitoring of the analytical signal and BG correction), while the rest are used for internal functions, such as correcting for fluctuations in the lamp intensity. More details on this type of instrumentation can be found elsewhere.^{18,19}

This HR CS AAS instrument is equipped with a transversely heated graphite tube atomizer and both solid sampling and liquid sampling autosamplers. The solid sampling device (SSA 600) incorporates a microbalance with a readability of 1 µg.²⁰ Pyrolytic graphite tubes were used in all experiments. Solid samples were introduced using solid sampling graphite platforms.

A transmission electron microscope JEOL (Tokyo, Japan) JEM 2000 FX II was used for estimating the size of the nanoparticles, and a Scanning Electron Microscope JEOL JSM-6400, configured with an energy dispersive X-ray analyzer INCA 300 X-Sight from Oxford Instruments (Abingdon, UK), was used for examination of the graphite platforms.

2.2. Reagents and standards

2.2.1. Reagents and chemical modifiers. Purified water was obtained from a milli-Q system (Millipore, Billerica, USA). Pd, Ru and Zr solutions were prepared from commercially available 1 g L⁻¹ single-element standards (Merck, Darmstadt, Germany), by appropriate dilution with 0.14 mol L⁻¹ HNO₃. Citric acid (3 g in 100 mL) and Na₂WO₄ · 2H₂O (7.8 g in 100 mL) were also prepared from the solid reagents (Merck) dissolved in milli-Q water. 14 mol L⁻¹ HNO₃ was purchased from Merck. All the reagents were of analytical grade purity or higher.

Pd nanoparticles were prepared as follows: 11 mL of a 10 g L⁻¹ standard solution of Pd (as Pd(NO₃)₂) were mixed with 20 mL of an aqueous solution of polyvinylpyrrolidone (PVP, *M_w* ≈ 58 000, Alfa Aesar, Karlsruhe, Germany), which was prepared dissolving 264 mg of PVP in 100 mL of milli-Q water, and with 25 mL of ethanol (grade 90%, Alfa Aesar, Karlsruhe). The mixture was stirred and allowed to reflux for 3 hours under air resulting in a dark brown solution. This procedure is described in more detail elsewhere.²¹

2.2.2. Standards. S aqueous solutions (100 mg L⁻¹) were prepared by dissolving in milli-Q water suitable amounts of Na₂SO₄, Na₂SO₃, thiourea (Panreac, Barcelona, Spain) and 3-mercaptopropionic acid (Alfa Aesar, Karlsruhe, Germany). A 1 g L⁻¹ S solution (S as NH₄SO₄) was also purchased from SPEX CertiPrep (Metuchen, USA). All the reagents were of analytical grade purity or higher.

2.3. Samples

In order to assess the validity of the method developed, four different certified reference materials (CRMs) were used for analysis. ERM-EC680 and ERM-EC681 are polyethylene CRMs produced by BCR (Community Bureau of Reference, Geel, Belgium). These samples are available in granular form, with each granule weighing 8–13 mg. CRM Mild Steel 453 and High-speed steel 482 were available from the Bureau of Analysed

Samples Ltd. (BAS, Newby, UK). These samples are available in small chips, with each chip weighing 10–13 mg.

The rest of the CRMs investigated were available as fine powders: BCR CRM 129 Elements in Hay powder, as well as NIST (National Institute of Standards and Technology, Gaithersburg, USA) Standard Reference Materials 1566a Oyster tissue and 2718 Green petroleum coke.

2.4. Procedure for determination of S by solid sampling HR CS GFMS

2.4.1. Impregnation of the tube and platform with Ru.

Thermal deposition was chosen as the method for coating the sample platforms with Ruthenium as a permanent modifier, following the procedure described by Vale *et al.*²² In this procedure, 10 repetitive injections of 40 μL of a 1 g L⁻¹ standard solution of Ru were carried out, and after each injection the temperature program shown in Table 1 was applied.

A single extra injection, followed by the full temperature program used for the impregnation, was also applied after every run of 20 sample replicates, in order to avoid coating losses that may result in sensitivity variations during analyses.

2.4.2. Sample analysis. No sample pretreatment was needed, other than cutting the samples into fragments of appropriate mass (see Table 2) using a ceramic knife, when necessary (polyethylene and steel materials). The solid sampling device used allows for automatic weighing and transport of the samples into the furnace. The empty platform was first transported to the microbalance using a pair of tweezers. After taring, an appropriate amount of sample was deposited onto the platform and weighed. The corresponding amount of the chemical modifier was added afterwards. The platform was then transferred to the graphite furnace and subsequently subjected to the temperature program. All these operations were fully controlled by the computer except for the deposition of the sample and the modifier, which were carried out manually.

The operating conditions are summarized in Table 2. For every line evaluated, the values obtained for three detector pixels (the central pixel plus the adjacent ones, CP \pm 1), corresponding to a spectral interval of 4.3 pm, were summed.

The calibration was carried out using 10 μL of an S aqueous solution of the appropriate concentration and 20 μL of the Pd nanoparticle suspension as modifier (40 μg of Pd), deposited with a micropipette onto the solid sampling platform. For every

Table 1 Temperature program used for the thermal deposition of Ru as a permanent modifier in the solid sample platforms. In total, 10 injections of modifier solution were carried out. However, after each of the first 9 injections, only stages from 1 to 5 were applied. The complete temperature program was only applied after the last injection²²

Stage	Temperature/ $^{\circ}\text{C}$	Ramp/ $^{\circ}\text{C s}^{-1}$	Hold time/s	Gas flow rate/L min ⁻¹
(1) Drying	100	7	10	2.0
(2) Drying	130	7	40	2.0
(3) Drying	160	100	60	2.0
(4) Pyrolysis	1000	100	20	2.0
(5) Pyrolysis	1400	100	5	0.1
(6) Pyrolysis	2000	100	5	0.1

Table 2 Instrumental parameters used in the determination of sulfur by means of HR CS GFMS

Electronic transition used	$\Delta v = 0, X^1\Sigma^+ \rightarrow A^1\Pi$ of CS molecule
Wavelength/nm	Main lines of CS in the vicinity of 258 nm (central pixel = 257.958 nm)
Number of detector pixels summed per line	3 (\sim 4.3 pm)
Ar gas flow during atomization/mL min ⁻¹	Stop-flow conditions
Chemical modifiers	Ru (permanent modifier) + Pd (40 μg) nanoparticles
Sample mass/mg	0.5–2.0 (BAS 482, BAS 453) 0.1–0.3 (BCR 129, NIST 1566a) 0.3–1.0 (ERM-EC680) 1.5–3.5 (ERM-EC681) 0.04–0.05 (NIST 2718)

Temperature program

Step	Temperature/ $^{\circ}\text{C}$	Ramp/ $^{\circ}\text{C s}^{-1}$	Hold time/s
Drying	110	2	10
Pyrolysis	800	50	20
Auto Zero	800	0	5
Vaporization	2400	2000	5
Cleaning	2600	1000	5

determination, five solid samples were analyzed and the median of the five results was taken as representative value.²³ Integrated absorbance (A_{int}) was selected as the measurement mode in all the circumstances.

3. Results and discussion

3.1. Sulfur monitoring by means of graphite furnace molecular absorption spectrometry

3.1.1. Wavelength selection. As discussed in the Introduction, the use of HR CS AAS instrumentation, either with a flame atomizer or with a graphite furnace, also permits the monitoring of molecular lines, opening new possibilities for sulfur determination. In particular, of the different options available (*e.g.*, CS, SH, S₂, *etc.*), there seems to be an agreement in the literature on the superior performance obtained when monitoring the spectrum of the CS molecule around 258.0 nm, which corresponds with the $\Delta v = 0$ vibrational sequence of the electronic transition $X^1\Sigma^+ \rightarrow A^1\Pi$.¹⁷ This spectrum shows many sharp rotational lines, of a width similar to that typically observed for atomic lines (a few picometers), which are characterized by similar sensitivity, even though the most sensitive “lines” have been reported to be found exactly at 257.593 nm, 257.958 nm and 258.056 nm.^{24–29} In addition to the good sensitivity, selection of CS is also preferable owing to the high stability of the CS bond (714.1 kJ mol⁻¹), which makes formation of this molecule to be highly favored in a graphite furnace,^{17,25} where carbon is obviously highly available.

Of these lines mentioned above, different authors have used several of them in their works.^{16,17,27} In our case, centering the spectra around the strong line of 257.958 nm was decided, since potential spectral overlaps with an Fe line have been reported for the other most sensitive line of 258.056 nm,¹⁶ which may hamper its use, in particular, for analysis of steel, as will be discussed later

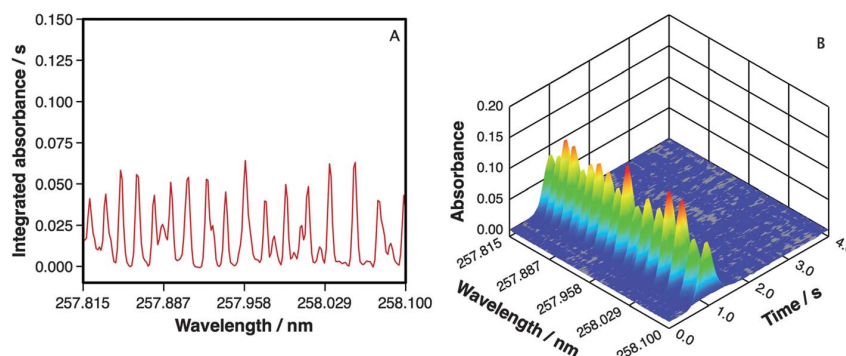


Fig. 1 (A) Wavelength resolved time-integrated absorbance spectrum obtained after the vaporization of 500 ng of sulfur (as Na_2SO_4) recorded when monitoring the spectral region in the vicinity of 258 nm by means of high-resolution continuum source graphite furnace molecular absorption spectrometry under the conditions described in Table 2. (B) Time and wavelength resolved absorbance spectrum obtained after the vaporization of 500 ng of sulfur (as Na_2SO_4) in the same conditions as (A).

on. Besides, better baseline stability was obtained in this spectral area in our working conditions. An example of the spectrum obtained for vaporization of a sulfur solution with the instrument used in this work is shown in Fig. 1a, where this sharp rotational structure mentioned before can be clearly appreciated. Fig. 1b shows the temporal evolution of the signal, which, as expected, is exactly the same for all the “lines” monitored, confirming its correspondence with the same CS molecule.

Finally, it can also be mentioned that a recent work published by Jim *et al.*, using a home-made continuum source AAS instrument (characterized by lower resolution but a wider spectral window in comparison with the instrument used in the current work), has preferred the monitoring of a broad absorption band, not reported before and located between 200 and 210 nm, for S determination in coal using the slurry technique.³⁰ The attribution of this band to a particular species is not evident, but it is suggested to be related with both C and S, and its signal is strengthened by the fact that a filter furnace atomizer (offering a porous graphite structure and, thus, a large C surface for C and S interaction) was used in that work. Since the filter furnace device does not really permit direct solid sampling analysis, this approach will not be investigated in the present work.

3.1.2. Selection of chemical modifier. While regarding the selection of the best molecule for sulfur monitoring and of the spectral area of most interest there is a good agreement among researchers, the same can hardly be said concerning the use of chemical modifier(s), as discussed in more detail by Kowalewska.¹⁷

If we focus on the three only works reporting on CS monitoring by HR CS GFMA to date, Heitmann *et al.* recommended the use of methane during pyrolysis and addition of Ca for S stabilization,²⁷ while Ferreira *et al.* did not see any change when adding methane and demonstrated superior performance of Pd in comparison with Ca,¹⁶ particularly when analyzing solid samples. In both cases, however, addition of Zr as permanent modifier was recommended. Ferreira *et al.* stated that this could be possibly explained because otherwise sulfur species that are in direct contact with graphite might be intercalated in its layered structure, ultimately not giving rise to CS but to the very volatile

CS_2 .¹⁶ Finally, Kowalewska opted for the combination, Pd + Mg in organic forms, for analysis of petroleum.¹⁷

The conclusion of these previous works is that the level of stabilization obtained is still not sufficient. In fact, a very dissimilar performance was reported for different sulfur species introduced as aqueous standards, by Ferreira *et al.*¹⁶ Furthermore, Kowalewska reported that light petroleum products containing volatile sulfur compounds could not be accurately analyzed.¹⁷ It appears that, while the arrival of HR CS AAS has indeed made it feasible to accurately monitor the sharp rotational structure of CS electronic transitions opening new ways for S determination, achieving proper stabilization of sulfur in a graphite furnace regardless of the chemical form in which sulfur is present still remains a challenge, as already discussed in early works with line source MAS.^{31,32} This is a situation that can only be solved by using more effective chemical modifiers.

This aspect was investigated in more detail in the current work. In agreement with the works discussed before, we also saw the benefit of using a permanent modifier to obtain more sensitivity. Zr, W and Ru were tested for this purpose, and best results were actually obtained with Ru, which is a typical permanent modifier,^{33–35} but was not reported before for S monitoring. The difference of using Ru compared with the use of W or Zr is not very significant, but approximately 15–20% more sensitivity was obtained with Ru, and peaks were better defined, showing 30–40% larger peak heights and, thus, less tailing. Ru was therefore used in all further experiments.

In addition to permanent modification with Ru, Pd was also tested as chemical modifier. This combination of a permanent modifier plus Pd has provided satisfactory results in similar situations.¹⁵ Moreover, previous results of sulfur monitoring based on graphite furnace techniques (electrothermal vaporization coupled to ICP-MS³⁶ and ICP-OES³⁷) have demonstrated a strong tendency for Pd to interact with sulfur. This aspect may be critical in the current situation in which the goal is to monitor diatomic species, which is somewhat more complicated than traditional atomic measurements. The basic idea is to add a modifier that may attract sulfur, thus helping in breaking the original sulfur bonds early in the process, and that stabilizes sulfur long enough until it can be released under furnace

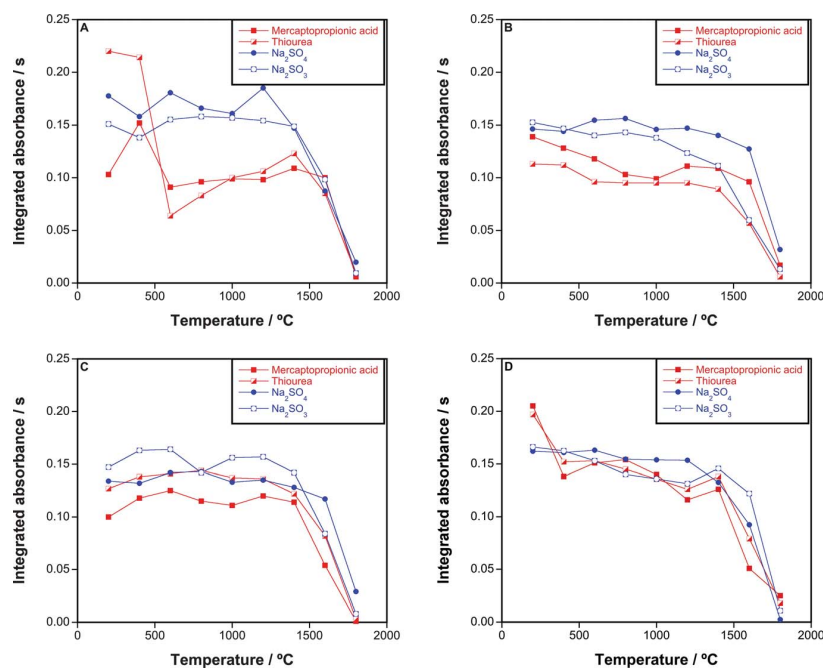


Fig. 2 Pyrolysis curves obtained for 500 ng of sulfur introduced in different chemical forms when monitoring the 257.958 nm CS molecular line (sum of 3 central pixels) in the presence of Ru as permanent modifier plus 40 μg of Pd, added in different forms: (A) as $\text{Pd}(\text{NO}_3)_2$; (B) as $\text{Pd}(\text{NO}_3)_2$, but thermally prereduced using a prior 1000 $^\circ\text{C}$ pyrolysis step; (C) as $\text{Pd}(\text{NO}_3)_2$ together with an excess of citric acid; (D) as Pd nanoparticles, produced as described in Section 2.2.1.

conditions that are favorable for the formation of the CS molecule. In this way, not only pyrolysis temperatures high enough to remove most of matrix components can be used, but also the analytical response may be normalized regardless of the chemical form in which sulfur is introduced.

Still, for optimum performance, the chemical form in which Pd is added may be critical, as well as adding an amount sufficient for efficient interaction (at least a 5/1 Pd S^{-1} molar ratio, according to our results). To compare the different responses obtained as a function of the way in which Pd is added, pyrolysis curves for four different sulfur species (sodium sulfite, sodium sulfate, thiourea and 3-mercaptopropionic acid) were monitored using Ru as chemical modifier, and adding the same amount of Pd (40 μg) in different ways. The results obtained are shown in Fig. 2.

As expected, addition of Pd as nitrate does not seem to be the most efficient approach. As can be seen in Fig. 2a, while this form seems to stabilize well the inorganic species (which are less volatile: Na_2SO_4 boiling point is 1429 $^\circ\text{C}$, while Na_2SO_3 decomposes at 593 $^\circ\text{C}$) up to 1200 $^\circ\text{C}$, it does not offer the same performance for the more volatile organic species (thiourea decomposes at 182 $^\circ\text{C}$, while the boiling point of 3-mercaptopropionic acid is 110 $^\circ\text{C}$), for which a lower signal is clearly obtained even at low pyrolysis values.

It is well known that reduction of Pd can help in achieving a better performance, since in that way metallic Pd is available earlier in the process, and that form is believed to be the most active one.^{15,38–40} This reduction can be traditionally achieved either thermally (preheating a Pd solution) or by addition of a reductant, such as citric acid. As shown in Fig. 2b and c, the

situation improves when using such approaches. In particular, the addition of citric acid seems very promising, as only the signal for the most volatile sulfur species is slightly reduced compared with the rest. In this particular case, it could be hypothesized that the addition of citric acid might not only help in producing metallic Pd earlier, but it might also release some active carbon⁴¹ during the pyrolysis, thus further helping in the formation of CS.¹⁶ However, the use of citric acid in combination with thermally prereduced Pd did not provide any improvement in the performance of this modifier, thus rendering this hypothesis as very unlikely.

There is however another possibility for providing metallic Pd that could be of interest in this context, and that is the addition of Pd nanoparticles. Contrary to the current situation in many scientific fields, the use of nanoparticles as modifiers in graphite furnace techniques has been reported very seldom. Besides, the nanoparticles investigated to date (naked Ag^{42} and Au^{43} nanoparticles) correspond with elements that are not considered as the most efficient modifiers, and were probably chosen mainly because their nanoparticles are widely available. Thus, no significant advantages have been observed in those works, other than the low blanks achieved, since in terms of analyte stabilization the values reported (*e.g.*, maximum pyrolysis temperature without losses) are comparable with those found for the most usual modifiers. There are, however, reasons to believe that the use of Pd nanoparticles may be more promising in the current case.

Pd nanoparticles can be easily produced and stabilized in the presence of a suitable agent (for instance, polyvinylpyrrolidone) in hydroalcoholic media, and, thus, can be directly added in

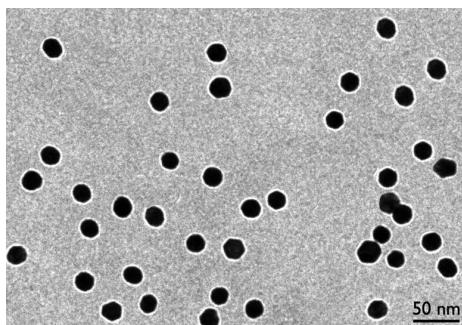


Fig. 3 Transmission electron microscopy image (50 000 \times magnification) of the Pd nanoparticles produced as described in Section 2.2.1.

solution (although the term suspension is more proper). The concept behind their use is similar to that of colloidal Pd, introduced by Volynsky and Krivan,^{44,45} except for the particle size, which is smaller in the current case. This is a critical aspect, because the smaller the particle size, the higher the surface that is available for interaction with the analyte, as demonstrated by the improved performance obtained when using nanoparticles as catalysts in synthesis processes.^{46,47} To sum up, *a priori*, the addition of Pd nanoparticles should provide a better performance because metallic and highly reactive Pd nanoparticles would be available for interaction already during the drying step.

This approach was tested in the current work. Pd nanoparticles of approx. 20 nm size (see Fig. 3), as evaluated by TEM monitoring, were synthesized as described in Section 2.2.1.,²¹ and 20 μ L of this suspension (55/45 water/ethanol mixture) were added together with the sulfur aqueous standard, in the same

way as it would be done with any Pd aqueous solution. As shown in Fig. 2d, this approach provided the best results, permitting to obtain very similar responses for all the species investigated up to pyrolysis of 1000 $^{\circ}$ C, which should be sufficient for analysis of many types of samples. Thus, these nanoparticles were used as chemical modifiers for further experiments.

In order to further explore the reasons behind the improved performance of Pd when added as nanoparticles, examination of several graphite platforms after heating at various temperatures was carried out using Scanning Electron Microscopy (SEM). First of all, it was observed that Ru particles are randomly distributed across the platform, in the form of large agglomerates (approx. 0.5–1 μ m length). Concerning Pd, when added as Pd(NO₃)₂, it was confirmed that it is not evenly distributed over the platform surface. It has already been described in the literature that this modifier tends to migrate towards the edges of the platform either during drying or pyrolysis.^{48,49} In this case, it could be seen already after drying at 200 $^{\circ}$ C that Pd is mostly found in the walls of the concave platform (boat) used in this work. In addition to this, in the area in which Pd is present, it appears as a thin layer covering the graphite (see Fig. 4b), a layer that shows some cracks that increase with higher temperatures.

As stated before, these aspects are already well-known. In fact, different ways to improve the homogeneity of Pd distribution have been discussed in the literature. The use of ascorbic acid or other reductants may help, but still the distribution of Pd agglomerates has been reported to be uneven.³⁸ Addition of Mg(NO₃)₂ (ref. 48) or electrodeposition^{49,50} have been reported to be more successful concerning the homogeneity of the Pd distribution, but Pd is still found in the form of relatively large agglomerates of approx. 1 μ m diameter.⁵⁰

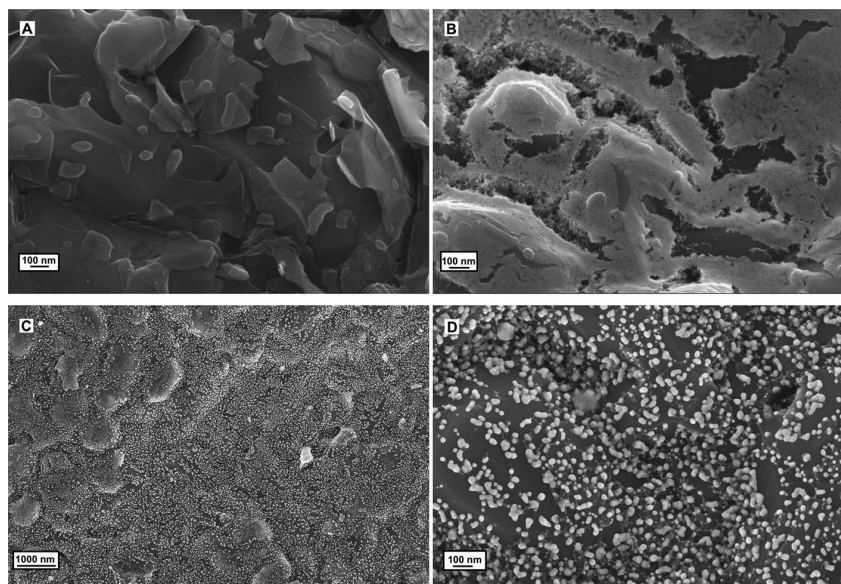


Fig. 4 Scanning electron microscopy images of: (a) an empty graphite platform (50 000 \times magnification), after pyrolysis at 600 $^{\circ}$ C; (b) a graphite platform (50 000 \times magnification) in which 40 μ g Pd has been deposited as Pd(NO₃)₂ solution, after pyrolysis at 600 $^{\circ}$ C; (c) a graphite platform (10 000 \times magnification) in which 40 μ g Pd has been deposited as Pd nanoparticles, produced as described in Section 2.2.1., after pyrolysis at 600 $^{\circ}$ C; (d) a graphite platform (50 000 \times magnification) in which 40 μ g Pd has been deposited as Pd nanoparticles, produced as described in Section 2.2.1., after pyrolysis at 600 $^{\circ}$ C.

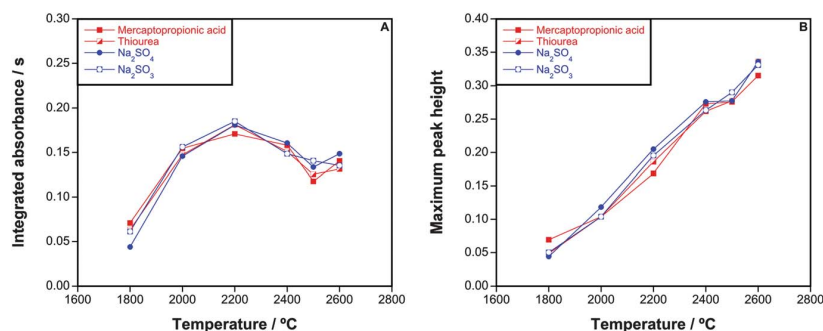


Fig. 5 Vaporization curves obtained for 500 ng of sulfur introduced in different chemical forms when monitoring the 257.958 nm CS molecular line (sum of 3 central pixels) in the presence of Ru as permanent modifier plus 40 μg of Pd, added as Pd nanoparticles. Both the integrated absorbance (A) and the maximum peak height (B) values are shown.

In contrast with this situation, when Pd is added from a nanoparticle suspension, it was observed that a very homogeneous distribution was achieved after drying. Moreover, Pd was found in the form of nanoparticles of approx. 20 nm. This form was maintained during the pyrolysis (even though the average size tends to increase a bit with temperature). Fig. 4c and d illustrate this point showing a graphite platform after pyrolysis at 600 °C, where the even distribution of spherical Pd nanoparticles can be appreciated. It should be noted that the large and bright particle that appears in the right center of Fig. 4c corresponds to a Ru agglomerate. Finally, after increasing the temperature up to 2400 °C (vaporization temperature), no indication of remaining Pd was found in the graphite furnace.

It can be concluded that the ultimate goal of attaining very small droplets of metallic Pd homogeneously distributed all over the platform, as discussed in the literature many times,^{38,48–50} seems to be better achieved when adding this modifier as a nanoparticle suspension. In this way, a larger surface for interaction with the analyte is available during drying and pyrolysis. Moreover, Pd is removed efficiently during the vaporization, thus minimizing potential memory effects.

The nanoparticle suspension showed good stability (no evidence of agglomeration) during the period in which the experiments were carried out (approx. six months) for a concentration range between 0.5 g L⁻¹ and 2.0 g L⁻¹. Obtaining higher

concentration proved more challenging, but it was not really necessary for the current (and for most) applications. These nanoparticles are simple to synthesize and use, and, thus, they may offer some potential advantages for other analytes besides sulfur, particularly for elements that owing to their high volatility and/or complex chemistry are hard to stabilize in a graphite furnace. Further work will be directed to their preparation in other alcoholic media (*e.g.*, propanol), since it has been reported that achieving even smaller particle sizes (and, thus, perhaps a better performance) may be possible in that way.²¹

3.2. Analytical performance of the procedure proposed

After selection of the chemical modifier (Ru as permanent plus Pd nanoparticles), the rest of the parameters were optimized. As can be seen in Fig. 5a, best peak area values are obtained for vaporization temperatures of 2200 °C. However, the signal is best defined (less tailing) if a higher vaporization is used, as can be deduced from the peak height values (see Fig. 5b). As a compromise, a value of 2400 °C was selected for CS vaporization.

Good linearity was obtained under these working conditions for an interval that extended from 50 to 2500 ng S, as shown in Fig. 6a, which is a wide range for GFMS, and this is an important factor for direct solid sampling analysis, owing to the

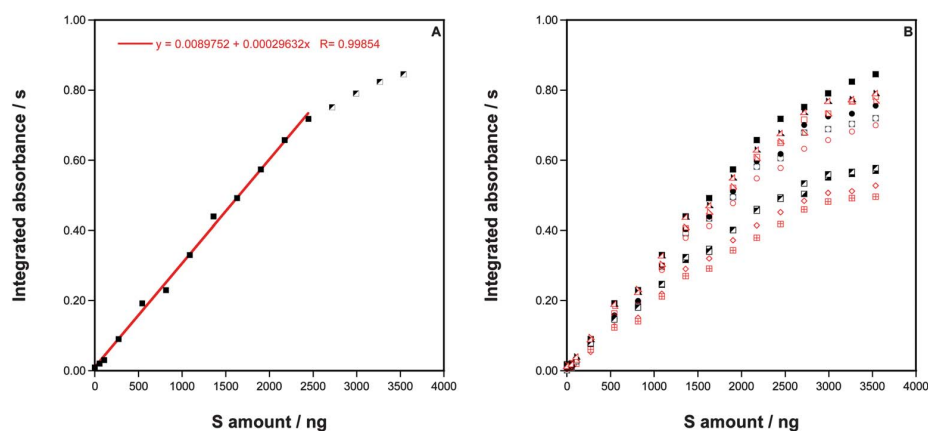


Fig. 6 (A) Linearity observed when monitoring the 257.958 nm CS molecular line under the conditions shown in Table 2. (B) Integrated area as a function of the mass of sulfur for the 12 most sensitive CS molecular lines shown in Fig. 1a, measured under the conditions listed in Table 2.

obvious difficulties for sample dilution. Moreover, a characteristic mass of 14 ng and a limit of detection (LOD) of 9 ng were calculated for the 257.958 nm line in these conditions. These values are slightly better than those reported by Kowalewska using the 258.056 nm line (12 ng as characteristic mass, but summing eleven detector pixels for signal integration instead of three as most often recommended,¹⁷ and 14 ng as LOD) and by Ferreira using the 258.033 nm line (18 ng as characteristic mass and 15 ng as LOD),¹⁶ while Heitmann *et al.* reported values that are still moderately better using the 258.056 nm line (12 ng as characteristic mass and 2.3 ng as LOD).²⁷

However, all these values were obtained using only one (the central) of the molecular lines that are simultaneously monitored. This approach, *a priori*, represents a loss of information, as some benefits may derive from the separated or combined use of various of these lines, such as an improved linear range⁵¹ or a better limit of detection.^{15,27,52} Improving the linearity is, in this case, not feasible using any of the main 12 lines displayed in Fig. 1a, as their sensitivity varies only very moderately (10–30%), and thus all of them show a remarkably similar behavior (see Fig. 6b) in terms of linearity. There are a few smaller peak profiles in the spectrum, but their use is not recommended because they are more affected by fluctuations of the baseline (it has already been discussed in the literature that it is better to select “isolated” lines, meaning lines that show a clear valley at both sides of the central pixels²⁷) and by adjacent more sensitive pixels. It is, however, feasible to combine the signal of the most sensitive of these lines to improve the limit of detection to some extent, as already reported by Heitmann *et al.* for the area surrounding the 258.056 nm line.²⁷ In this way, the detection limit could be decreased down to 3 ng only if the main six lines in the region monitored are simultaneously used, while the characteristic mass also goes down to 3 ng (see Fig. 7).

Nevertheless, when monitoring several lines it is always important to assess that there are no significant influence of spectral overlaps, especially since these spectral regions are rich in lines from various elements. Relatively insensitive lines for Fe,

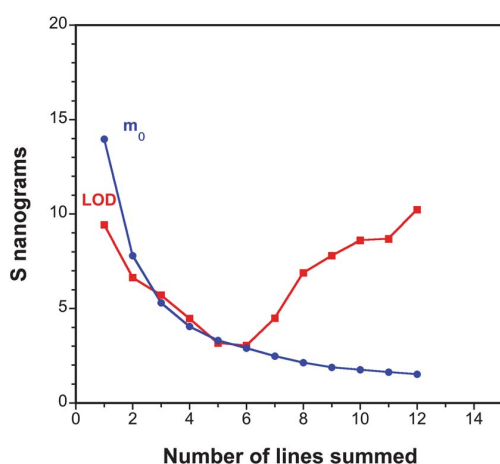


Fig. 7 Influence of simultaneous multi-line evaluation of several CS lines on the characteristic mass and the detection limit, calculated from a series of 15 replicates. The summation was performed following the order of sensitivity, starting with the molecular line located at 257.958 nm.

Cr and Co are found in this region, but since the concentration of these elements in the samples of interest may be very high, particularly in the case of steels, they might pose some problems for accurate quantification. Fortunately, with HR CS AAS instrumentation interferences are identified with ease, as it is very unlikely that the interfering element and the analyte show a complete overlap, both in spectral and temporal terms.

Fig. 8 shows a signal of a solid steel sample containing approx. 960 μg of Fe, 53 μg of Cr and 3 μg of Co. As can be seen, some lines for these elements, including several Fe lines, appear in the selected region. However, they do not seem to significantly overlap with any of the six major lines of CS, except perhaps for the line located at 258.056 nm, for which the tailing of the Fe might contribute a bit to the overall signal. In any case, the interference does not appear to be as severe as reported before,¹⁶ possibly because the resolution of the commercially available HR CS AAS instrument is known to be a bit better (approx. 1.4 pm per pixels in this spectral region) than that of the prototype used by Ferreira *et al.* Anyway, this was one of the reasons for focusing around the 257.958 nm line, as in this way good sensitivity and better selectivity is obtained.

Overall, the performance of the method proposed for solutions seems promising enough to be applied to the direct analysis of solid samples.

3.3. Direct analysis of solid samples

Direct solid sampling analysis was investigated next for very different types of samples: two polyethylene, two biological, two steel, and one petroleum coke CRMs, using the temperature program shown in Table 2.

In this context, the potential benefits of using a suspension of Pd nanoparticles as chemical modifier could be further evaluated. As shown in Fig. 9a, in the absence of Pd nanoparticles, the signal obtained for the polyethylene sample is very different from the one observed for aqueous solutions (Fig. 1b). Two different peaks can be clearly appreciated. This fact is interesting since, according to the CRM report, sulfur is expected to be present in the polyethylene samples in two different forms, as it is mostly added as sulfate (of Ba and Pb), but also as sulfide of volatile

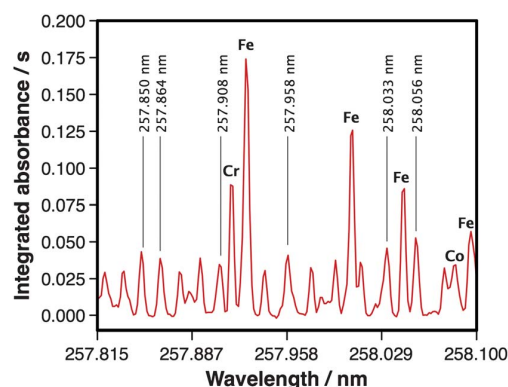


Fig. 8 Wavelength resolved time-integrated absorbance spectrum obtained after the vaporization of a solid sample (1.300 mg of BAS High-speed steel 482) showing the peak profiles for CS (325 ng S), as well as for Fe (960 μg), Cr (53 μg) and Co (3 μg).

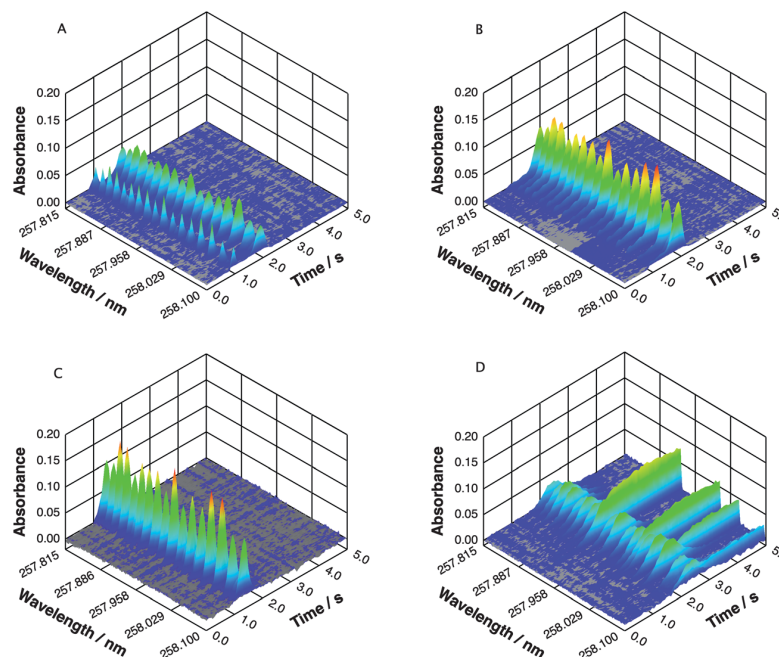


Fig. 9 Comparison of the time and wavelength resolved absorbance spectra obtained after the vaporization of a similar amount of sulfur (approx. 500 ng) from (A) a polyethylene CRM (ERM-EC680) without the addition of Pd nanoparticles; (B) a polyethylene CRM (ERM-EC680) with the addition of Pd nanoparticles as chemical modifier; (C) a biological CRM (BCR 129 Hay powder) with the addition of Pd nanoparticles as modifier; (D) a steel CRM (BAS High-speed steel 482) with the addition of Pd nanoparticles as modifier. The rest of the conditions used are shown in Table 2.

elements (Cd and Hg), which should vaporize before because of their higher volatility. However, in the presence of Pd nanoparticles, more efficient sulfur stabilization is achieved, as shown in Fig. 9b, and only one peak is obtained. This proves that the nanoparticles are capable of interacting with sulfur also when direct solid sampling is attempted, providing a more uniform response despite the chemical form in which sulfur is introduced.

Under these conditions, comparison with aqueous standards is possible. The signal is delayed compared with that of the aqueous standard and the temporal profiles are not identical (see Fig. 1b

and 9b), as it is very often the case when direct solid sampling is attempted,^{53–55} but the peak areas of both polyethylene samples and aqueous standards are equivalent, as demonstrated for the central line (257.958 nm) in Fig. 10. It can also be noted that, in the absence of the Pd modifier, the overall signal for S is lower, possibly reflecting losses of the most volatile sulfur species found in the polymer.

The biological samples (BCR 129 and NIST 1566a) proved to be relatively simple ones, rendering signal profiles very similar to those obtained for aqueous standards, only half a second delayed in time (see Fig. 9c and 10).

As for the steel samples, this is a very different type of material. Contrary to what occurs with polyethylene or biological materials, which should be very efficiently pyrolyzed at 800–1000 °C,^{56,57} the matrix for steel samples is not expected to be completely removed during the pyrolysis. Therefore, vaporization of sulfur from this matrix is anticipated to be more difficult. This is what can be observed in Fig. 9d. For these samples, the signal for sulfur is clearly delayed and broadened, in comparison with that obtained for the aqueous standard. Moreover, the expected peaks for Fe, Cr and Co mentioned in Section 3.2. appear, even though they should pose no major problem for quantification for most of the main lines, as discussed before. However, it is again remarkable that the integrated peak area for the central line (257.958 nm) is comparable to that obtained for aqueous standards, thus *a priori* permitting the use of aqueous standards for calibration, as can be observed in Fig. 10.

From a practical point of view, it can be noted that analysis of metals resulted in some deposits in the platform. They do not

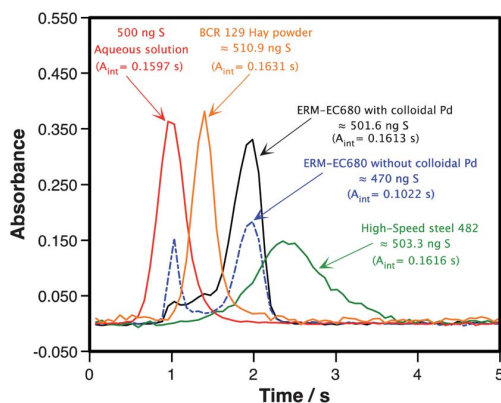


Fig. 10 Comparison of the time resolved absorbance measured at 257.958 nm (sum of 3 central pixels) obtained after the vaporization of a similar amount of sulfur from an aqueous solution or directly from various solid samples (the same solid samples as displayed in Fig. 9), under the conditions listed in Table 2.

Table 3 Determination of sulfur in different certified reference materials by means of solid sampling HR CS GFMS ($n = 8$) using different lines in the vicinity of 258 nm. Uncertainties are expressed as 95% confidence intervals (C.I.) and as relative standard deviation values. C.I. have been calculated as $\pm t/s/\sqrt{n}$ where t , s and n have their usual meanings

Sample	Reference value	257.958 nm (central line)	257.850 nm	257.864 nm	257.908 nm	258.033 nm	258.056 nm	Average (all lines)
ERM-EC680 polyethylene	670 ± 70	676 ± 41 (7.3)	644 ± 43 (8.0)	643 ± 32 (6.0)	631 ± 35 (6.6)	701 ± 37 (6.3)	698 ± 43 (7.3)	665 ± 32 (4.6)
ERM-EC681 polyethylene	78 ± 17	80 ± 5 (7.0)	78 ± 4 (6.9)	77 ± 5 (7.8)	82 ± 5 (7.8)	79 ± 5 (7.8)	81 ± 4 (6.1)	80 ± 2 (2.7)
BAS High-speed steel 482	250 ± 23	252 ± 11 (5.3)	251 ± 15 (7.1)	235 ± 14 (7.2)	242 ± 15 (7.3)	257 ± 16 (7.5)	267 ± 13 (6.1)	251 ± 12 (4.4)
BAS Mild steel 453	340 ± 10	328 ± 18 (6.7)	347 ± 24 (8.1)	346 ± 24 (8.4)	325 ± 23 (8.5)	356 ± 21 (7.0)	375 ± 21 (6.6)	346 ± 19 (5.3)
BCR129 Hay powder	3160 ± 40	3020 ± 200 (8.1)	3120 ± 240 (9.2)	3200 ± 250 (9.3)	3140 ± 170 (6.4)	2970 ± 200 (8.1)	3060 ± 250 (9.7)	3080 ± 90 (2.8)
NIST 1566a Oyster tissue	8620 ± 190	8420 ± 550 (7.5)	8360 ± 420 (6.0)	8790 ± 370 (5.0)	8870 ± 340 (4.6)	8700 ± 470 (6.4)	8890 ± 340 (4.6)	8670 ± 240 (2.6)
NIST 2718 Green petroleum coke	47 030 ± 79	48 350 ± 3230 (8.0)	45 140 ± 3380 (9.0)	45 560 ± 3270 (8.6)	46 550 ± 3350 (8.6)	43 540 ± 3560 (9.7)	45 380 ± 3110 (8.2)	45 750 ± 1680 (3.5)

represent major problems for analysis as long as the platform is substituted after analysis of 40 samples. Otherwise, some decrease in sensitivity could be observed as the platform gets covered by metal deposits, thus requiring performing more frequent recalibrations to maintain accuracy.

Finally, the last CRM investigated, NIST 2718 Green petroleum coke, showed a behavior very similar to that of the steel, which is consistent with the low volatility of this matrix. Again, signals that were delayed and broadened in comparison with those of the aqueous standards were obtained, but their peak areas remained comparable.

3.4. Sample analysis

Once the optimum conditions were established, sample analysis by means of solid sampling HR CS GFMS was undertaken using the conditions indicated in Table 2 and detailed in Section 2.4. For each sample, eight determinations (in total) were carried out on three different days. For every determination, five replicate solid samples were measured, and the median of the five was obtained as a representative value.²³ The calibration curves were always constructed using aqueous standards of sulfur (as sulfate). Sample masses were adjusted to work always within the linear range. This basically represents using relatively high masses (up to 3.5 mg) for the sample with lower contents (ERM-EC681), which is feasible since matrix removal during pyrolysis is very efficient for this type of sample, as discussed before.^{57,58} On the other hand, low samples masses were used for those samples with the higher sulfur contents. In the extreme case of NIST 2718, only approx. 50 µg of sample per replicate were subjected to analysis.

The results finally obtained are displayed in Table 3. As can be seen, a value in excellent agreement with the certified one was always achieved when using only the central line (257.958 nm). Concerning the precision of the technique, RSD values varied between 5 and 10%, values that are typical for the solid sampling technique even when elements much easier for GF monitoring are determined.^{10,20,59} It can also be stated that all the samples investigated in the work are CRMs, which are often more homogeneous than real samples. A limit of detection of 3 µg g⁻¹ was calculated for ERM-EC681.

It is also possible to evaluate more CS lines, as discussed in Section 3.2. The rest of the major lines observed in this region seem to offer a satisfactory response as well, as demonstrated by the values obtained in Table 3. By combining different lines, precision can be even further improved to values between 3 and 5% RSD, while the average values also show an exceptional agreement with the reference values. A limit of detection of only 1 µg g⁻¹ was calculated under these conditions for ERM-EC681. The only line that shows some statistically significant disagreement with the reference value (their confidence intervals do not overlap) is 250.056 nm for the BAS Mild Steel material (approx. 99% Fe), possibly as a consequence of an overlap with the Fe line, as discussed in Section 3.2. The influence of this minor disagreement on the overall result is very low, but it might be preferable to exclude this line when analyzing samples with very high iron contents.

It is remarkable that such different types of samples can be analyzed under the same conditions, achieving a very similar

performance, thus proving the robustness of the approach developed. Overall, it can be concluded that the procedure proposed fulfils the requirements for fast and routine control of sulfur in the samples investigated (every determination requires only 15–20 min of work), offering significant benefits when compared with traditional digestion approaches.

4. Conclusions

The addition of Pd nanoparticles, in combination with the use of Ru as permanent modifier, permits a more efficient stabilization of sulfur species in a graphite furnace, furthermore helping in providing a more normalized response regardless of the chemical form in which sulfur species are originally found, when monitoring CS molecular lines by means of high-resolution continuum source graphite furnace molecular absorption spectrometry. This is likely due to the fact that these small Pd nanoparticles are homogeneously distributed all over the platform, offering a larger surface for interaction with the analyte during the drying and pyrolysis steps.

Moreover, it was demonstrated that this combination of modifiers is also effective for direct analysis of very different types of solid samples, allowing for the development of fast direct solid sampling methods, which are capable of providing accurate results simply based on straightforward calibration with aqueous standards.

Preparing and using Pd nanoparticles proved very simple. It is the authors' opinion that use of Pd in this form, particularly in combination with a permanent modifier, is an interesting option, worth evaluating for those complex analytes that are typically hard to stabilize in a graphite furnace.

Acknowledgements

This work has been funded by the Spanish Ministry of Science and Innovation (Project CTQ2009-08606) and the Aragon Government ("Programa de apoyo a la I + D + I" from ARAID Foundation and "Obra social de IberCaja", with additional support from Inycom, and Fondo Social Europeo). María del Rosario Flórez thanks the Spanish Ministry of Science and Innovation for her doctoral grant.

Notes and references

- 1 <http://www.sulphurinstitute.org/index.cfm>, accessed November 2011.
- 2 B. Welz and M. Sperling, *Atomic Absorption Spectrometry*, 3rd edn, Wiley-VCH, Weinheim, Germany, 1999.
- 3 J. Riondato, F. Vanhaecke, L. Moens and R. Dams, *J. Anal. At. Spectrom.*, 1997, **12**, 933–937.
- 4 D. Lawrenz, *Phys. Status Solidi A*, 1998, **167**, 373–381.
- 5 K. Dittrich and B. Vorberg, *Anal. Chim. Acta*, 1983, **152**, 149–161.
- 6 P. Tittarelli and G. Lavorato, *Anal. Chim. Acta*, 1987, **201**, 59–65.
- 7 B. Welz, F. G. Lepri, R. G. O. Araujo, S. L. C. Ferreira, M. D. Huang, M. Okruss and H. Becker-Ross, *Anal. Chim. Acta*, 2009, **647**, 137–148.
- 8 B. Welz, *Anal. Bioanal. Chem.*, 2005, **381**, 69–71.
- 9 B. Welz, D. L. G. Borges, F. G. Lepri, M. G. R. Vale and U. Heitmann, *Spectrochim. Acta, Part B*, 2007, **62**, 873–883.
- 10 M. Resano, F. Vanhaecke and M. T. C. de Loos-Vollebregt, *J. Anal. At. Spectrom.*, 2008, **23**, 1450–1475.
- 11 B. Welz, S. Morés, E. Carasek, M. G. R. Vale, M. Okruss and H. Becker-Ross, *Appl. Spectrosc. Rev.*, 2010, **45**, 327–354.
- 12 M. Resano and E. García-Ruiz, *Anal. Bioanal. Chem.*, 2011, **399**, 323–330.
- 13 M. Aramendía, M. R. Flórez, M. Piette, F. Vanhaecke and M. Resano, *J. Anal. At. Spectrom.*, 2011, **26**, 1964–1973.
- 14 Y. D. Hong, S. W. Namgung, M. Yoshida and A. Malik, *Talanta*, 2000, **51**, 291–301.
- 15 M. Resano, J. Briceño and M. A. Belarra, *J. Anal. At. Spectrom.*, 2009, **24**, 1343–1354.
- 16 H. S. Ferreira, F. G. Lepri, B. Welz, E. Carasek and M. D. Huang, *J. Anal. At. Spectrom.*, 2010, **25**, 1039–1045.
- 17 Z. Kowalewska, *Spectrochim. Acta, Part B*, 2011, **66**, 546–556.
- 18 U. Heitmann, M. Schütz, H. Becker-Ross and S. Florek, *Spectrochim. Acta, Part B*, 1996, **51**, 1095–1105.
- 19 H. Becker-Ross, S. Florek, U. Heitmann, M. D. Huang, M. Okruss and B. Radziuk, *Spectrochim. Acta, Part B*, 2006, **61**, 1015–1030.
- 20 M. G. R. Vale, N. Oleszczuk and W. N. L. dos Santos, *Appl. Spectrosc. Rev.*, 2006, **41**, 377–400.
- 21 T. Teranishi and M. Miyake, *Chem. Mater.*, 1998, **10**, 594–600.
- 22 M. G. R. Vale, M. M. Silva, B. Welz and R. Nowka, *J. Anal. At. Spectrom.*, 2002, **17**, 38–45.
- 23 M. A. Belarra, M. Resano and J. R. Castillo, *J. Anal. At. Spectrom.*, 1999, **14**, 547–552.
- 24 M. D. Huang, H. Becker-Ross, S. Florek, U. Heitmann and M. Okruss, *Anal. Bioanal. Chem.*, 2005, **382**, 1877–1881.
- 25 M. D. Huang, H. Becker-Ross, S. Florek, U. Heitmann and M. Okruss, *Spectrochim. Acta, Part B*, 2006, **61**, 181–188.
- 26 M. D. Huang, H. Becker-Ross, S. Florek, U. Heitmann, M. Okruss and C. D. Patz, *Anal. Bioanal. Chem.*, 2008, **390**, 361–367.
- 27 U. Heitmann, H. Becker-Ross, S. Florek, M. D. Huang and M. Okruss, *J. Anal. At. Spectrom.*, 2006, **21**, 1314–1320.
- 28 A. Virgilio, J. L. Raposo, Jr, A. A. Cardoso, J. A. Nóbrega and J. A. Gomes Neto, *J. Agric. Food Chem.*, 2011, **59**, 2197–2201.
- 29 A. Baysal and S. Akman, *Talanta*, 2011, **85**, 2662–2665.
- 30 G. Jim, D. Katskov and P. Tittarelli, *Talanta*, 2011, **83**, 1687–1694.
- 31 D. A. Katskov, M. Lemme and P. Tittarelli, *Spectrochim. Acta, Part B*, 2004, **59**, 101–114.
- 32 M. Lemme, D. A. Katskov and P. Tittarelli, *Spectrochim. Acta, Part B*, 2004, **59**, 115–124.
- 33 M. G. R. Vale, M. M. Silva, B. Welz and É. C. Lima, *Spectrochim. Acta, Part B*, 2001, **56**, 1859–1873.
- 34 D. L. Tsalev, V. I. Slaveykova, L. Lampugnani, A. D'Ulivo and R. Georgieva, *Spectrochim. Acta, Part B*, 2000, **55**, 473–490.
- 35 I. López-García, R. E. Rivas and M. Hernández-Córdoba, *Anal. Bioanal. Chem.*, 2008, **391**, 1469–1474.
- 36 M. Resano, M. Verstraete, F. Vanhaecke, L. Moens and J. Claessens, *J. Anal. At. Spectrom.*, 2001, **16**, 793–800.
- 37 A. Mroczek, G. Werner, R. Wennrich and W. Schrön, *Fresenius' J. Anal. Chem.*, 1998, **361**, 34–42.
- 38 L. M. Voth-Beach and D. E. Shrader, *J. Anal. At. Spectrom.*, 1987, **2**, 45–50.
- 39 A. B. Volynsky, *Spectrochim. Acta, Part B*, 2000, **55**, 103–150.
- 40 M. A. Belarra, M. Resano, S. Rodríguez, J. Urchaga and J. R. Castillo, *Spectrochim. Acta, Part B*, 1999, **54**, 787–795.
- 41 A. B. Volynsky, E. M. Sedykh and L. N. Bannykh, *Talanta*, 1991, **38**, 761–765.
- 42 S. Gunduz, S. Akman, A. Baysal and M. Kahraman, *Spectrochim. Acta, Part B*, 2010, **65**, 297–300.
- 43 S. Gunduz, S. Akman, A. Baysal and M. Culha, *Microchim. Acta*, 2011, **172**, 403–407.
- 44 A. B. Volynsky and V. Krivan, *J. Anal. At. Spectrom.*, 1996, **11**, 159–164.
- 45 A. B. Volynsky and V. Krivan, *Spectrochim. Acta, Part B*, 1997, **52**, 1293–1304.
- 46 V. Mazumder and S. Sun, *J. Am. Chem. Soc.*, 2009, **131**, 4588–4589.
- 47 H. P. Hemantha and V. V. Sureshbabu, *Org. Biomol. Chem.*, 2011, **9**, 2597–2601.
- 48 H. Quio and K. W. Jackson, *Spectrochim. Acta, Part B*, 1991, **46**, 1841–1859.
- 49 J. P. Matousek and H. K. J. Powell, *Talanta*, 1997, **44**, 1183–1193.
- 50 E. Bulska, B. Thybusch and H. M. Ortner, *Spectrochim. Acta, Part B*, 2001, **56**, 363–373.
- 51 M. Resano, L. Rello, M. Flórez and M. A. Belarra, *Spectrochim. Acta, Part B*, 2011, **66**, 321–328.
- 52 U. Heitmann, B. Welz, D. L. G. Borges and F. G. Lepri, *Spectrochim. Acta, Part B*, 2007, **62**, 1222–1230.
- 53 M. Resano, E. García-Ruiz, C. Crespo, F. Vanhaecke and M. A. Belarra, *J. Anal. At. Spectrom.*, 2003, **18**, 1477–1484.

- 54 M. Resano, M. Aramendía, E. Garcia-Ruiz, C. Crespo and M. A. Belarra, *Anal. Chim. Acta*, 2006, **571**, 142–149.
- 55 M. Resano, J. Briceño, M. Aramendía and M. A. Belarra, *Anal. Chim. Acta*, 2007, **582**, 214–222.
- 56 F. Vanhaecke, M. Resano, M. Verstraete, L. Moens and R. Dams, *Anal. Chem.*, 2000, **72**, 4310–4316.
- 57 M. Resano, J. Briceño and M. A. Belarra, *Spectrochim. Acta, Part B*, 2009, **64**, 520–529.
- 58 M. Resano, E. Garcia-Ruiz, F. Vanhaecke, C. Crespo and M. A. Belarra, *J. Anal. At. Spectrom.*, 2004, **19**, 958–965.
- 59 M. A. Belarra, M. Resano, F. Vanhaecke and L. Moens, *TrAC, Trends Anal. Chem.*, 2002, **21**, 828–839.



Contents lists available at ScienceDirect

Spectrochimica Acta Part B

journal homepage: www.elsevier.com/locate/sab

Direct determination of bromine in plastic materials by means of solid sampling high-resolution continuum source graphite furnace molecular absorption spectrometry



M.R. Flórez, M. Resano*

Department of Analytical Chemistry, University of Zaragoza, Pedro Cerbuna 12, 50009 Zaragoza, Spain

ARTICLE INFO

Article history:

Received 14 June 2013

Accepted 25 July 2013

Available online 3 August 2013

Keywords:

Solid sampling

High-resolution continuum source graphite

furnace molecular absorption spectrometry

Bromine determination

Polymer analysis

ABSTRACT

This work investigates the potential of high-resolution continuum source graphite furnace molecular absorption spectrometry for the direct determination of bromine in polymers, which could be interesting in view of the current regulations restricting the use of organobrominated compounds. The method developed is based on the addition of Ca (300 μg) and Pd (30 μg) to favor the formation of CaBr, which is monitored at the main molecular “lines” (rotational spectra) found in the vicinity of 625.315 nm.

It was found that accurate results could be obtained for all the samples investigated (polyethylene, polypropylene and acrylonitrile butadiene styrene certified reference materials) using any of the lines studied and constructing the calibration curve with aqueous standards. Furthermore, the combined use of the main four CaBr lines available in the spectral area simultaneously monitored permits to easily expand the linear range up to 2000 ng, provides a limit of detection of 1.8 ng (1.8 $\mu\text{g g}^{-1}$ for a mass of 1 mg) and further improves precision to values between 3–7% RSD. Overall, the method proposed seems suited for the fast and simple control of these types of samples (approximately 10 min for sample are required), circumventing the traditional problems associated with sample digestion (e.g., losses of volatile compounds), and providing sufficient sensitivity to easily comply with regulations.

© 2013 Elsevier B.V. All rights reserved.

1. Introduction

The ubiquity of plastic materials and the huge amount of plastic waste generated in the modern world have led to a growing concern in terms of their environmental impact. In this context, special attention is being paid to a variety of different inorganic and organic additives incorporated to the structure of the polymers to enhance their qualities [1], and to their leakage to the environment [2].

Most polymeric materials, and particularly those aiming to be employed in the production of electronic devices, electrical appliances, clothing and furniture, are very often protected against ignition by the addition of the so-called brominated flame retardants (BFRs). The term BFRs encompass several organic compounds containing various atoms of bromine within their molecular structure, such as polybrominated diphenylethers (PBDEs), polybromobiphenyls (PBBs), tetrabromobisphenol A or hexabromocyclododecane. The function of all of these additives is to modify the behavior of the flammable host material against fire, inhibiting its combustion and significantly reducing the risk of fire-related damages. Their mechanism of action is based on the capability of the halogen to trap the oxidizing free radicals generated in the combustion, therefore, stopping the flame from propagating [3].

Unlike other types of polymer additives, flame-retardants are weakly bonded to the flammable materials, hence being highly prone to be released into the environment. Besides, two of the main characteristics of these organobrominated compounds, which make them suitable as BFRs for plastics, are their hydrophobic nature and their very long-term stability, both features being a serious problem when speaking about bioaccumulation in the ecosystem and the wildlife, categorizing them as persistent pollutants [3–5].

While new types of environmentally safe flame-retardants are investigated, regulations and restrictions on the use of BFRs are being implemented in order to lower their impact. Within the European Union, the 2002/95/EC directive on the “Restriction of the use of certain Hazardous Substances” (RoHS) restrains the use of PBBs and PBDEs in electrical and electronic equipment since July 2006 [6], and further regulations have set the maximum permitted limit for PBBs and PBDEs to 1000 mg kg^{-1} (0.1% w/w) [7]. It is essential then to have robust analytical methods for monitoring the presence of these compounds in raw plastic materials to ensure that this legal limit is met.

Several techniques have been employed to determine BFRs concentrations, either by means of speciation-based methods such as gas chromatography mass spectrometry [8] or liquid chromatography inductively coupled plasma mass spectrometry [9], or methods based in total Br determination such as X-Ray fluorescence spectrometry (XRF) [10], inductively coupled plasma mass spectrometry (ICP-MS) [11,12], ion exchange chromatography [13] and some others. However, most of the

* Corresponding author. Tel.: +34 976761634; fax: +34 976761290.
E-mail address: mresano@unizar.es (M. Resano).

applications found in the literature require extensive sample preparation in order to bring the sample into solution. These previous steps need to be thoroughly controlled in order to minimize the risk of Br losses due to its high volatility [14,15].

It can be mentioned that, owing to the large number of samples that need to be controlled on a daily basis due to the abovementioned regulations, the development of screening schemes becomes very appealing [16,17]. This means that analysis of all samples can be carried out first by means of a fast and simple method that is able to provide the total Br content, hopefully filtering out most samples, such that only in those cases in which the Br content is sufficiently high to be of concern, the application of a more time consuming method capable of providing information on the different Br species that are present in the sample becomes necessary [11].

In order to develop such fast and simple methodologies for total Br content in polymers, the use of solid sampling techniques seems promising, and it has also been demonstrated that they can be incorporated well into a screening scheme [17,18]. However, few approaches focusing on the direct determination of Br in polymers (or in solid materials in general) have been published to date.

Techniques that have been studied within this context are radio-frequency glow discharge-optical emission spectroscopy (rf-GD-OES) [19] or mass spectrometry (rf-GD-MS) [20,21], laser-induced plasma spectroscopy (LIPS) [22], laser ablation (LA)-ICP-MS [23], XRF [15,23,24], and neutron activation analysis (NAA) [25]. However, all of those techniques show some drawbacks to operate efficiently in the scheme proposed. High limits of detection (LOD) were reported in the cases of rf-GD-OES, rf-GD-MS and LIPS, while the main difficulty associated with XRF and LA-ICP-MS seems to be the limited number of reference materials available, which are typically required for calibration when using these (and most solid sampling) techniques [23,24,26]. Moreover, XRF results have been reported to be not only affected by the composition of the matrix but also by the form in which the sample is available (granulates or pucks) [24]. On the other hand, despite its detection power, NAA requires the availability of a nuclear reactor, and it is thus hardly accessible to routine and industrial laboratories.

A technique that has demonstrated potential for direct analysis of solid samples in general, and of polymers in particular, is graphite furnace atomic absorption spectrometry [27–29]. Several examples demonstrate the benefits of this technique for straightforward analysis of polymers using aqueous standards for calibration [30–33]. While traditionally this technique did not permit the direct monitoring of halogens, as their atomic lines were not accessible, the arrival of high-resolution continuum source instrumentation has opened new possibilities in this field making it possible to monitor not only atomic but also molecular “lines” [34,35]. In this regard, two recent articles by Huang et al. [36] and by Limburg and Einax [37] have demonstrated that it is feasible to determine Br using this approach, after sample dissolution. However, to the best of the authors’ knowledge, no report on the use of this technique for the direct determination of Br in solid samples has been published yet.

It is the goal of this paper to develop a simple, fast and sensitive enough to comply with regulation procedure for the direct determination of total Br content in plastic samples by means of high-resolution continuum source graphite furnace molecular absorption spectroscopy (HR CS GFMS). This method will be based in the formation of the diatomic molecule CaBr, which is stable in gas phase even at a relatively high temperature, and in the subsequent recording of its molecular spectra in the vicinity of 625.315 nm.

2. Experimental

2.1. Instrumentation

All the measurements in this work were carried out using a HR CS AAS instrument (ContrAA 700), which is commercially available from Analytik Jena AG (Jena, Germany). This instrument is equipped with

both flame and graphite furnace atomizers, in separate compartments, a Xenon short-arc lamp (GLE, Berlin, Germany) operating in “hot-spot” mode as the radiation source, a high-resolution double echelle monochromator (DEMON) and a linear CCD array detector with 588 pixels, 200 of which are used for monitoring the analytical signal and performing BG corrections, while the remainder are used for internal functions such as correcting for fluctuations in the lamp intensity. More details on this type of instrumentation can be found elsewhere [38,39].

The HR CS AAS instrument is equipped with a transversely heated graphite tube atomizer and an automated solid sampling accessory (SSA 600). This solid sampling device incorporates a microbalance with a readability of 1 µg. Pyrolytic graphite tubes and solid sampling graphite platforms were used in this work.

2.2. Samples and standards

2.2.1. Standards and reagents

Purified water was obtained from a Milli-Q system (Millipore, Billerica, USA). HNO₃ solutions were prepared from pro-analysis grade 14 mol L⁻¹ HNO₃ (Merck, Darmstadt, Germany).

Bromide aqueous solutions were prepared from commercially available 1 g L⁻¹ Br standard (CertiPUR Bromide standard solution traceable to SRM from NIST NaBr, Merck) by appropriate dilution with purified water. A 20 g L⁻¹ Ca solution was prepared from a solid CaCO₃ reagent (ACS reagent, ≥99.0%, powder, Sigma-Aldrich, St. Louis, USA) dissolved in 0.14 mol L⁻¹ HNO₃. Pd modifier was prepared from commercially available 10 g L⁻¹ single-element standard (as Pd(NO₃)₂, Merck) by appropriate dilution with 0.14 mol L⁻¹ HNO₃.

2.2.2. Samples

Six reference materials with a certified bromine content encompassing three different types of plastic materials were analyzed in order to validate the method developed. Polyethylene samples ERM-EC680 and ERM-EC681, as well as Polypropylene ERM-EC591, were purchased from the Institute for Reference Materials and Measurements (IRMM, Geel, Belgium), all of them being available in granules of approximately 10 mg weight. Polyethylene's PE-H-11A and PE-L-11A were purchased from Modern Analytical Techniques (MAT) LLC (Hillsborough, USA), and were available as plastic discs with a diameter of approximately 31 mm and 13 mm thickness. Acrylonitrile butadiene styrene resin was purchased from the Federal Institute for Materials Research and Testing (BAM, Berlin, Germany) in a disc form with 40 mm diameter and 6 mm thickness. A list collecting details for each material tested can be found in Table 1.

2.3. Procedure for the determination of Br by SS HR CS GFMS

This method does not involve any sample pre-treatment beyond cutting each plastic material into fragments of appropriate mass (see Table 2) using a ceramic knife. The solid sampling device used allows for automatic weighing and transport of the samples to the furnace by means of a pair of tweezers. After first taring the empty sample platform, an appropriate amount of sample is deposited onto the platform to be weighed. Subsequently, all the required reagents – 10 µL of a Pd(NO₃)₂ solution (30 µg Pd), plus 15 µL of a CaCO₃ solution (300 µg Ca), both prepared in 0.14 mol L⁻¹ HNO₃ – are added, and the platform

Table 1
Certified reference materials (CRMs) analyzed in this work.

	Type of polymeric material	Certified Br content/mg kg ⁻¹
ERM-EC680	High density polyethylene	808 ± 19
ERM-EC681	High density polyethylene	98 ± 5
PE-H-11A	High density polyethylene	1100 ± 44
PE-L-11A	Low density polyethylene	500 ± 20
ERM-EC591	Polypropylene	2080 ± 70
BAM-H010	Acrylonitrile butadiene styrene	240 ± 21

Table 2
Instrumental parameters used in the determination of Br by means of HR CS GFMS.

Electronic transition	Red system, $\Delta v = 0, X^2\Sigma^+ \rightarrow A^2\Pi$ (CaBr)			
Central wavelength	625.315 nm			
Spectral window	0.73 nm			
Number of detector pixels summed per line	3 (≈ 11 pm)			
Chemical modifiers	Ca (300 μg) Pd (30 μg)			
Sample mass range	ERM-EC680	0.1 mg–0.2 mg		
	ERM-EC681	0.7 mg–1.0 mg		
	PE-H-11A	0.1 mg–0.2 mg		
	PE-L-11A	0.1 mg–0.4 mg		
	ERM-EC591	0.1 mg–0.15 mg		
	BAM-H010	0.3 mg–1.0 mg		
Temperature program				
Step	Temp./ $^{\circ}\text{C}$	Ramp/ $^{\circ}\text{C s}^{-1}$	Hold time/s	Ar flow rate/L min $^{-1}$
Drying	90	5	20	2.0
Drying	120	5	30	2.0
Pyrolysis	1000	50	30	2.0
Auto zero	1000	0	5	0.0
Vaporization	2100	3000	6	0.0
Cleaning	2500	1000	4	2.0

is finally introduced into the graphite furnace to be subjected to the temperature program. All these operations are fully controlled by the instrument software, with exception of the sample deposition and the addition of the reagents, which need to be carried out manually.

The instrumental conditions and the temperature program used were carefully optimized (see Section 3.1.2. for details) and are summarized in Table 2. The central pixel (101) of the detector was positioned at 625.315 nm, and the resulting spectral window that was simultaneously monitored ranged from 624.948 nm to 625.678 nm (0.730 nm in total), a region where the main lines of CaBr appear.

Calibration was carried out against aqueous standard solutions. 10 μL of a $\text{Pd}(\text{NO}_3)_2$ solution (30 μg Pd), plus 15 μL of a CaCO_3 solution (300 μg Ca), both prepared in 0.14 mol L $^{-1}$ HNO_3 were deposited onto the graphite platform with a micropipette, together with 10 μL of a Br aqueous solution of the appropriate concentration (0, 5, 10 and 30 mg L $^{-1}$ Br).

For every determination, three solid samples were analyzed and the median of the three results was taken as representative value [18]. In all cases, integrated absorbance (A_{int}) was selected as measurement mode and the sum of the signals obtained for 3 pixels (the central pixel of each line plus the two adjacent ones, $\text{CP} \pm 1$) was considered as the analytical result for each line studied, unless otherwise stated.

3. Results and discussion

3.1. Monitoring of Br by means of high-resolution continuum source graphite furnace molecular absorption spectrometry (HR CS GFMS)

3.1.1. Selection of the molecule and of the spectral region

All main atomic absorption lines of bromine are located in the vacuum ultraviolet region, with its principal line occurring at 148.845 nm [40], making it necessary to search for alternatives. A few attempts were carried out in the past to investigate the molecular absorbance of Br when combined with several elements from the IIa and IIIa groups using the conventional line source absorption spectrometers [41–43].

However, the introduction of HR CS AAS has substantially expanded the potential of the technique, whether it is using a flame or a graphite furnace as atomization unit [44]. This technology has opened up new possibilities in this field that are particularly relevant for analysis of complex matrices, such a significantly improved potential for detecting and correcting for spectral overlaps [45,46] and matrix effects [47]. Moreover, this type of instrumentation provides a continuous and

high intensity emission over a broad spectral interval (190–900 nm) and permits the monitoring of molecular or atomic absorption with high spectral resolution (a few picometers). Thus, it is much more suited for the quantitative monitoring of the molecular absorption of diatomic molecules than any of the line devices explored in the works mentioned above, as demonstrated in several recent articles, primarily directed towards the determination of non-metals (Cl, F, P or S) [34,35,48–54].

Concerning Br, it seems that this element has been a bit overlooked, as only two articles have studied the absorption spectra of Br-based molecules using HR CS AAS. In the first and most general work, Huang et al. [36] reported that good results in terms of sensitivity were only achieved when forming binary compounds with Al, Sr and Ca. Sr however, was left aside due to its very similar behavior with Ca and a comparative study between AlBr and CaBr molecular absorption structures was carried out, concluding that both methods could provide reliable results for Br determination and the decision of using one or the other should be made based on the nature of the samples. Very recently, Limburg and Einax [37] optimized an analytical method for the quantification of bromine as CaBr in water solutions and organic solvents.

Based on these results, in the present work the possibility of monitoring either AlBr or CaBr was evaluated. While the sensitivity for both AlBr and CaBr was found to be similar, the addition of Ca was finally preferred over Al to form the diatomic molecule with Br, because: i) CaBr is less volatile than AlBr [36]. In monitoring CaBr, it is possible to use pyrolysis temperatures up to 1400 $^{\circ}\text{C}$ –1500 $^{\circ}\text{C}$ (up to 900 $^{\circ}\text{C}$ in the case of AlBr), assuring a better removal of the matrix, and this is particularly important when the direct analysis of solid samples is intended; and ii) the structure of the CaBr absorption spectrum consists of mostly well defined individually isolated lines of different sensitivities, which may bring some advantages to define the baseline properly and to adapt the sensitivity, as detailed below.

The main resonance system of CaBr appears between 625 and 628 nm. This diatomic molecule has a bond dissociation energy [55] of approximately 339 KJ mol $^{-1}$ and its absorbance spectrum presents a structure of fine rotational lines with its maximum peak at 625.315 nm, corresponding to the $\Delta v = 0$ vibrational band of the electronic transition $X^2\Sigma^+ \rightarrow A^2\Pi$, the so-called red system [56]. This well-resolved fine structure simplifies the selection of pixels to fix the baseline, therefore potentially leading to more robustness in comparison with the use of molecules that provide very dense unresolved molecular structures giving rise to broad bands [57], such as the case for AlBr [36]. A typical absorption profile of the CaBr molecule is shown in Fig. 1A. This spectrum was obtained vaporizing a Br aqueous solution in the conditions listed in Table 2, but centering the spectral window in 624.982 nm in order to have the broadest overview of the molecular transitions that is attainable with our instrumentation. Fig. 1B shows the three-dimensional spectrum of the signal, where the temporal profile can be seen. In both Figs. 1A and 1B the fine rotational structure can be clearly observed and it is also worth mentioning that the line-up appearance of individual narrow molecular transitions decreasing in. Sensitivity along the recorded spectral window allows to perform the determination using several of these lines simultaneously and opens up the possibility of enhancing the sensitivity of the method, as well as of extending the linear range, as will be discussed in detail in Section 3.2.

3.1.2. Optimization of the reagents and of the temperature program

Ca is able to form stable diatomic molecules with most non-metals. In fact, the association of Ca with F or Cl gives rise to more stable mono-halides than CaBr, with bond dissociation energies [55] of 529 and 409 KJ mol $^{-1}$, respectively. It is then worth mentioning here that, for plastics with high F or Cl content, as it is the case of polyvinyl chloride, this procedure for determining Br as CaBr without any prior sample treatment would not be suitable and a new strategy should be designed, possibly using procedures based on digestion and separation.

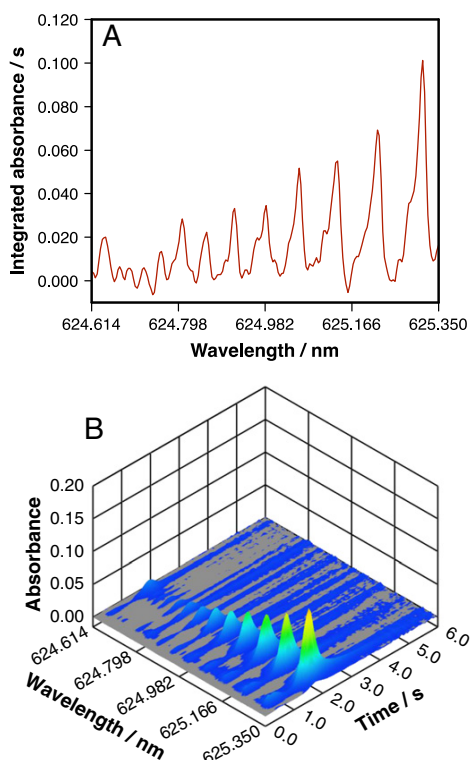


Fig. 1. A) Wavelength resolved time-integrated molecular absorbance spectrum of CaBr obtained for the vaporization of 100 ng of Br, with the addition of 300 μg Ca and 30 μg Pd, by means of HR CS GFMS with the spectral window centered in 624.982 nm. B) Time and wavelength resolved spectrum obtained after vaporization of 100 ng of Br in the same conditions as in A).

In any case, Ca should be in a great excess over Br to ensure a complete reaction and maximize the sensitivity. Therefore, an optimization of the amount of Ca (prepared from CaCO_3 dissolved in $0.14 \text{ mol L}^{-1} \text{ HNO}_3$) was carried out for 10 μL of a 10 mg L^{-1} Br solution (100 ng Br) in the presence of Pd as chemical modifier and measuring in the most sensitive line of the resonance system, i.e. 625.315 nm. Fig. 2A shows the evolution of the curve towards higher Ca amounts. 300 μg of Ca was selected as the optimum amount and was further used in all experiments.

On the other hand, Pd (as $\text{Pd}(\text{NO}_3)_2$) was chosen as chemical modifier to stabilize the analyte during the pyrolysis step. Fig. 2B shows the absorbance observed for 100 ng Br as a function of the amount of Pd used. Best results were obtained when Pd was added in masses above 10 μg and it was decided to carry on further studies using 30 μg Pd. It is worth mentioning here that Limburg and Einax [37] observed an improvement of approximately 20% in terms of sensitivity when using Zr-coated graphite tubes while measuring the molecular CaBr spectrum, but only in the absence of a platform, which is always needed for direct solid sampling. No positive effect was noticed in our case when testing the method with permanently modified graphite tubes and platforms. In this regard, our results seem to be in good agreement with the previous observations of Huang et al. [36]. Therefore, no permanent modifier was used in this study.

With these optimized amounts of Ca and Pd, pyrolysis and vaporization temperature curves were investigated. Fig. 3 shows the evolution of both curves. As can be seen, the signal for CaBr remains fairly stable until pyrolysis temperatures were up to 1400–1500 $^\circ\text{C}$, after which the drop of the signal is rather abrupt. At the same time, the growth of the signal for the vaporization curve is also quite fast, reaching its maximum peak area values at temperatures between 1900 and 2200 $^\circ\text{C}$. It is relatively

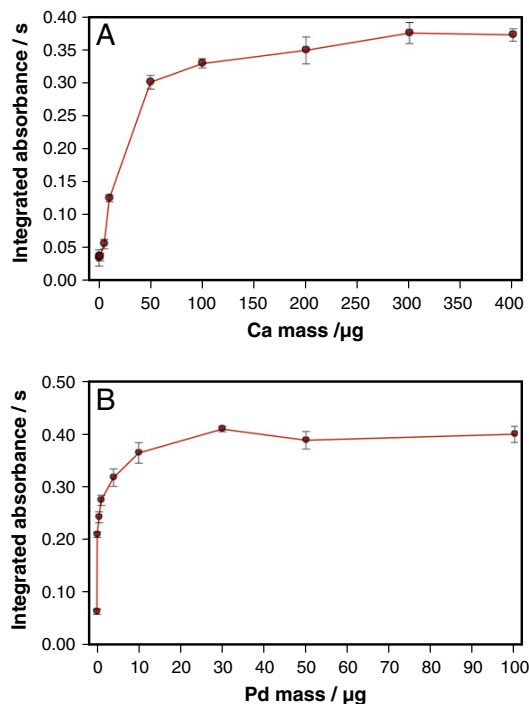


Fig. 2. A) Optimization of the amount of Ca added. This curve was obtained upon vaporization of 100 ng of Br, with the addition of 30 μg Pd as chemical modifier, by monitoring the 625.315 nm CaBr molecular absorption line. B) Optimization of the amount of Pd added. This curve was obtained in the same conditions as in A), but fixing the amount of Ca added to 300 μg , while varying the amount of Pd added. Uncertainties are expressed as the standard deviation of three replicates.

rare to achieve such a positive behavior in any AAS method, as it permits the use of pyrolysis temperatures high enough to remove most matrix components and, at the same time, does not require using a very high temperature during the measurement step. This is one of the advantages of developing a method where only vaporization and no atomization is required [48].

No significant differences were observed regarding the temporal profiles of the signals, and a vaporization temperature of 2100 $^\circ\text{C}$ was finally chosen for further work. The pyrolysis temperature was fixed at 1000 $^\circ\text{C}$, which proved adequate to successfully decompose the polymeric matrixes studied in this work.

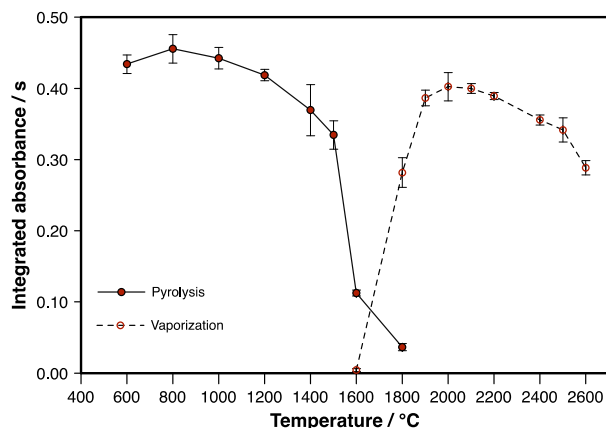


Fig. 3. Pyrolysis and vaporization curves obtained for 100 ng of Br with the addition of 300 μg Ca and 30 μg Pd when monitoring the 625.315 nm CaBr molecular absorption line. Uncertainties are expressed as the standard deviation of three replicates.

The use of this mild temperature program has a positive effect on the lifetime of all the perishable components of the furnace, particularly on the graphite tubes and sample platforms, as the latter can last for more than 200 heating cycles, while the same graphite tube could be used for all the experiments.

3.2. Selection of lines and analytical properties of the method

Having various analytical lines available to choose from is in principle always beneficial, as it may lead to improvements in the LOD or in the working linear range [47,58]. And this aspect is particularly interesting when monitoring the rotational structure of a molecular band, as in many cases the number of analytically useful lines is higher in comparison with the monitoring of atomic lines, whereas only doublets or triplets are usually available.

From the whole spectrum recorded in Fig. 1, only the four more sensitive lines of the resonance system were studied in detail for method development (i.e. 625.315 nm, 625.223 nm, 625.135 nm and 625.058 nm). Less sensitive lines were dismissed as the limits of detection achievable in such conditions would be too high to be useful in the context of this study.

A priori, if the goal is to improve the LOD, only lines with similar sensitivity should be evaluated, as weaker lines may contribute more to the noise than to the overall signal [48,51,58]. On the other hand, if the goal is to expand the linear range, the use of lines with dissimilar sensitivity seems more useful [47]. However, in this particular case, the four molecular lines are close and distant enough in terms of sensitivity, making it feasible to explore both strategies.

It was observed that it is possible to reduce the limit of detection by a factor of three when combining the signal of all the main four lines (1.8 ng, which represents $1.8 \mu\text{g g}^{-1}$ Br for 1 mg of sample) in comparison to the LOD obtained when monitoring the most sensitive CaBr line only (625.315 nm, $5.4 \mu\text{g g}^{-1}$ Br). This value is similar to that reported by Huang et al. (2 ng Br, for both CaBr and AlBr) [36]. In comparison with other direct solid sample techniques that have been used for polymer analysis, the value is significantly better than those reported by means of rf-GD-OES ($440 \mu\text{g g}^{-1}$ in the best case) [19], of LIPS ($500 \mu\text{g g}^{-1}$) [22], and of rf-GD-MS ($2000 \mu\text{g g}^{-1}$ in Ar and $5000 \mu\text{g g}^{-1}$ in He in ref. [20], although improved results, between 370 and $3580 \mu\text{g g}^{-1}$ depending on the species monitored, were reported more recently in ref. [21]). Only XRF has been reported to provide a similar LOD for the direct determination of Br in plastics ($1.5 \mu\text{g g}^{-1}$ for samples in the form of granulates and $1.2 \mu\text{g g}^{-1}$ for puks) [24]. On the other hand, while in ref. [25] no LOD was indicated for NAA, the analysis of samples containing $25 \mu\text{g g}^{-1}$ of Br by means of this technique was demonstrated. In any case, it is clear that the use of HR CS GFMAS permits to comfortably comply with legal requirements regarding Br determination in polymers.

On the other hand, the differences in sensitivity between the four molecular lines make it possible to easily expand the linear range along almost three orders of magnitude (see Table 3). In this way, the two most sensitive lines (625.315 nm and 625.223 nm) provide a linear range up to 300 ng, while the middle line (625.135 nm) extends it up to 700 ng and the less sensitive one (625.058 nm) shows linear behavior between 100 and 2000 ng Br. Further expansion using less sensitive lines is feasible but, as stated before, not very useful for polymer analysis, where the legal limits set the maximum content of PBBs and PBDEs to 1000 mg kg^{-1} (0.1% w/w). Anyway, Limburg and Einax further explored this feature and reported that the linear range can be expanded up to $10,000 \text{ ng Br}$ [37], using the lines found at 624.984, 624.917, 624.858 and 624.806 nm (see Fig. 1).

3.3. Direct analysis of solid samples

Another advantage of monitoring several absorption lines is the fact that it can help improve the reliability of the results, since any spectral

Table 3

Characteristic mass, limit of detection and linear range for the CaBr rotational lines monitored under the conditions listed in Table 2. LODs were calculated as three times the standard deviation of the blank ($n = 10$) divided by the slope of the calibration curve. The characteristic masses were calculated as 0.0044 divided by the slope of the calibration curve.

Wavelength/nm	m_0/ng	LOD/ng	Linear range	R^2
625.315	1.32	5.4	Up to 300 ng	0.999
625.223	1.77	7.3	Up to 300 ng	0.999
625.135	2.42	12.7	Up to 700 ng	0.996
625.058	3.00	18.2	50–2000 ng	0.997

overlap affecting only some of them would be detected. Therefore, Br determination was carried out using the four more sensitive lines of the molecular absorption spectra of CaBr, in order to better assess the quality of the results obtained with each one of them.

With the optimum experimental conditions listed in Table 2, solid sampling HR CS GFMAS was used for Br determination in the six certified reference materials (CRMs) listed in Table 1, using the procedure described in Section 2.3. Each sample was analyzed in a different session, always measuring a new calibration curve, with daily prepared aqueous standards, at the beginning of each session.

As an example, Fig. 4 shows the comparison of the temporal signal profiles obtained for similar amounts of Br introduced as an aqueous standard solution and as a solid sample, both of them measured at the 625.315 nm absorption line. As can be seen, the signal for the solid sample is unimodal and well defined, but it appears to be a bit delayed and exhibits some more tailing in comparison with the signal obtained for aqueous standard solutions. A similar situation was observed for all samples, which is certainly not unusual when attempting direct solid sampling analysis by graphite furnace-based techniques [51,59]. Despite this (moderately) dissimilar signal profiles, providing complete vaporization is attained and the temperature of the furnace does not change significantly over the duration of the signals, the use of integrated peak areas often makes it feasible to calibrate with aqueous standards. That was found to be the case in this application, as equivalent peak area values were always found for solid samples and aqueous standard solutions, as illustrated in Fig. 4.

For each sample, seven determinations (in total) were carried out, and, for every determination, three replicate solid samples were measured. Sample masses were adapted for each CRM (see Table 2) in order to obtain signal intensities that were within the linear range of every absorption line under study (50–300 ng Br).

The results obtained for each of the main four CaBr lines and for the six samples analyzed are displayed in Table 4. A good agreement with the certified reference values was found for every line and every sample,

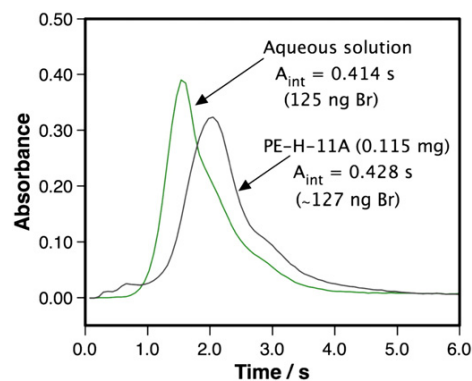


Fig. 4. Comparison of the time-resolved absorbance measured at 625.315 nm CaBr line (sum of three central pixels) obtained after vaporization of a similar amount of Br from an aqueous standard solution or directly from a polymeric material, under the conditions listed in Table 2.

as in all cases the confidence intervals overlapped with those available as reference. In principle, some trend could be observed (e.g., the tendency of 625.058 nm to provide slightly higher results). However, the analysis of the results by means of paired *t*-test did not permit to establish any significant difference for any of the four lines evaluated, so all the lines can be considered as equally suitable for analysis.

In any case, best results were obtained by combining the values of all the four lines. Not only the average values show an exceptional agreement with the reference values in all cases, but also the precision can be even further improved to values between 3 and 7% RSD. These RSDs are certainly low for direct solid sampling, and reflect the good level of homogeneity of the samples studied (CRMs). As a rule, polymers are more homogenous than other types of samples, and the fact that BFRs are added in significant amounts probably helps as well. For this reason, carrying out only three replicates per determination was proposed, while in other cases the use of at least five replicates is recommended [18].

As discussed before, sample masses were adapted to work in the linear range for all the lines and samples evaluated. However, for samples with even higher Br levels, reducing the sample mass even further is not recommended as it becomes uncomfortable to operate with masses below 0.1 mg. In such case, the use of only the less sensitive absorption line (625.058 nm) seems to be the simplest solution as it permits to quantitatively monitor up to 2 μg (2% Br for a sample mass of 0.1 mg), which should be more than enough for the application proposed.

It is worth mentioning that an alternative to increase the linear range always available when using HR CS AAS is the possibility to select side pixels, instead of using the central pixel plus the two adjacent ones (CP ± 1), which is the option recommended for achieving the best LOD [32,57,58]. This strategy to expand linearity has been successfully used in previous works [58,60,61], but seems to be limited in this particular case by i) the proximity of the adjacent lines and ii) the asymmetry of the peaks, as shown in Fig. 5. This aspect is relevant because if the signal is symmetrical, as it is most often the case for atomic lines, by using two side pixels located at the same distance from the CP (e.g. +3 and -3), the overall signal may remain constant even if there are some spectral drifts during the measurements (the increase in one pixel would be balanced by the decrease in the other one). However, that is clearly not the case for CaBr lines, as the signal becomes very asymmetric when moving more than 2 pixels away from the central pixel. Thus, monitoring side pixels is not recommended in this case. Fortunately, the availability of less sensitive CaBr makes it easier to accommodate the sensitivity of the method to that of the sample, as discussed before, and that should be the preferred solution for monitoring high Br amounts.

4. Conclusions

A method was developed for the direct determination of Br, as CaBr, in polymers by means of high-resolution continuum source graphite

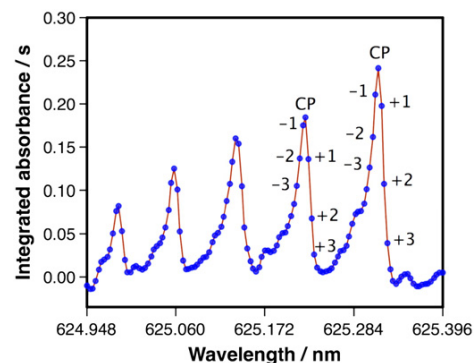


Fig. 5. Wavelength resolved time-integrated absorbance spectrum obtained by vaporization of approximately 250 ng of Br (0.310 mg of sample ERM-EC680). The signal only shows the region where the main CaBr molecular absorption lines are located. The signal recorded by every individual detector pixel is highlighted (blue dots).

furnace molecular absorption spectrometry. Using Ca as reagent, Pd as chemical modifier and a suitable temperature program it was possible to develop a straightforward procedure with aqueous standards for calibration. Moreover, by taking advantage of the structure of the CaBr molecular spectrum, and using the four main CaBr lines combined, it is possible to achieve limits of detection of 1.8 ng Br (1.8 $\mu\text{g g}^{-1}$ for a sample mass of 1 mg) and to easily extend the linear range up to 2000 ng Br, which is a suitable range to comply with regulations.

Six different CRMs featuring different polymers (polyethylene, polypropylene and acrylonitrile butadiene styrene), with certified Br contents ranging from 100 to 2000 $\mu\text{g g}^{-1}$, were analyzed in order to validate the method. The results obtained are in a very good agreement with the reference values with imprecision values between 3.0 and 7.0% RSD.

It can be concluded that the procedure proposed fulfils the requirements for fast control of Br in the polymers (every determination requires only 10 min of work), offering significant benefits when compared with traditional digestion approaches.

Acknowledgments

This work has been funded by the Spanish Ministry of Economy and Competitiveness (project CTQ2012-33494) and the Aragón Government (Fondo Social Europeo). María del Rosario Flórez thanks the Spanish Ministry of Economy and Competitiveness for her doctoral grant (project CTQ2009-08606).

Table 4

Determination of Br in different certified reference materials by means of solid sampling HR CS GFMS ($n = 7$) using different lines in the vicinity of 625.2 nm. Uncertainties are expressed as 95% confidence intervals (C.I.) and as relative standard deviation values. C.I. has been calculated as $\pm ts/\sqrt{n}$ where t , s and n have their usual meanings.

Sample	Reference value	625.315 nm	625.223 nm	625.135 nm	625.058 nm	Average (all lines)
ERM-EC680	Br content/mg kg ⁻¹ (RSD %)	808 \pm 19 (4.6)	784 \pm 33 (4.5)	809 \pm 30 (4.0)	843 \pm 37 (4.7)	810 \pm 40 (3.1)
ERM-EC681	Br content/mg kg ⁻¹ (RSD %)	98 \pm 5 (9.1)	99.8 \pm 8.4 (7.6)	91.2 \pm 6.4 (5.5)	95.7 \pm 6.5 (7.4)	108.0 \pm 7.0 (7.0)
PE-H-11A	Br content/mg kg ⁻¹ (RSD %)	1100 \pm 44 (4.3)	1160 \pm 46 (4.3)	1110 \pm 57 (5.5)	1090 \pm 66 (6.6)	1140 \pm 52 (5.0)
PE-L-11A	Br content/mg kg ⁻¹ (RSD %)	500 \pm 20 (4.6)	502 \pm 23 (2.9)	475 \pm 13 (4.6)	516 \pm 18 (3.4)	514 \pm 16 (3.1)
ERM-EC591	Br content/mg kg ⁻¹ (RSD %)	2080 \pm 70 (7.6)	2100 \pm 150 (7.6)	1920 \pm 160 (8.7)	1940 \pm 150 (8.5)	2160 \pm 160 (7.8)
BAM-H010	Br content/mg kg ⁻¹ (RSD %)	240 \pm 21 (6.7)	246 \pm 15 (6.8)	211 \pm 13 (6.8)	227 \pm 18 (8.5)	245 \pm 9 (4.0)
						232 \pm 26 (7.1)

References

- [1] In: H. Zweifel, R.D. Maier, M. Schiller (Eds.), *Plastics Additives Handbook*, 6th ed., Hanser Publications, Cincinnati, USA, 2009.
- [2] L.S. Birnbaum, D.F. Staskal, Brominated flame retardants: cause for concern? *Environ. Health Perspect.* 112 (2004) 9–17.
- [3] E. Eljarra, D. Barceló, Brominated Flame Retardants, *The handbook of environmental chemistry*, vol. 16, Springer, Berlin, Germany, 2011.
- [4] P.O. Darnerud, Toxic effects of brominated flame retardants in man and in wildlife, *Environ. Int.* 29 (2003) 841–853.
- [5] M. Alaee, R.J. Wenning, The significance of brominated flame retardants in the environment: current understanding, issues and challenges, *Chemosphere* 46 (2002) 579–582.
- [6] Directive 2002/95/EC, Off. J. Eur. Union (2003), (L 37/19-L 37/23).
- [7] Commission Decision 2005/618/EC, Off. J. Eur. Union (2005), (L214/65).
- [8] T.P.J. Linsinger, A. Birgersson-Liebich, A. Lamberty, F. Pellizzato, T. Venelinov, S. Voorspoels, Development of the first certified reference materials for solid brominated flame retardants in polymers, *Anal. Chem.* 81 (2009) 3792–3800.
- [9] S. Mingwu, W. Chao, J. Yongjuan, D. Xinhua, F. Xiang, Determination of selected polybrominated diphenylethers and polybrominated biphenyl in polymers by ultrasonic-assisted extraction and high-performance liquid chromatography-inductively coupled plasma mass spectrometry, *Anal. Chem.* 82 (2010) 5154–5159.
- [10] H. Fink, U. Panne, M. Theisen, R. Niessner, T. Probst, X. Lin, Determination of metal additives and bromine in recycled thermoplasts from electronic waste by TXRF analysis, *Fresenius J. Anal. Chem.* 368 (2000) 235–239.
- [11] A. Solà Vazquez, J.M. Costa-Fernández, J. Ruiz Encinar, R. Pereiro, A. Sanz-Medel, Bromine determination in polymers by inductively coupled plasma-mass spectrometry and its potential for fast first screening of brominated flame retardants in polymers and paintings, *Anal. Chim. Acta* 623 (2008) 140–145.
- [12] Y. Okamoto, H. Komori, H. Kataoka, S. Tsukahara, T. Fujiwara, Direct determination of bromine in plastics by electrothermal vaporization/inductively coupled plasma mass spectrometry using a tungsten boat furnace vaporizer and an exchangeable sample cuvette system, *Rapid Commun. Mass Spectrom.* 24 (2010) 1265–1270.
- [13] E. Dimitrakakis, A. Janz, B. Bilutewski, E. Gidararakos, Determination of heavy metals and halogens in plastics from electric and electronic waste, *Waste Manage.* 29 (2009) 2700–2706.
- [14] F. Cordeiro, P. Bouchou, T. Linsinger, B. de la Calle, Determination of brominated flame retardants: a proficiency test, *Accred. Qual. Assur.* 17 (2012) 439–444.
- [15] A. Lamberty, W. Van Borm, P. Quevaullier, Collaborative study to improve the quality control of trace element determinations in polymers. Part 2. Certification of polyethylene reference materials (CRMs 680 and 681) for As, Br, Cd, Cl, Cr, Hg, Pb, and S content, *Fresenius J. Anal. Chem.* 370 (2001) 811–818.
- [16] M. Valcárcel, S. Cárdenas, M. Gallego, Sample screening systems in analytical chemistry, *Trends Anal. Chem.* 18 (1999) 685–694.
- [17] M. Resano, E. García-Ruiz, M. Aramendia, M.A. Belarra, Solid sampling-graphite furnace atomic absorption spectrometry for Hg monitoring in soils. Performance as a quantitative and as a screening method, *J. Anal. At. Spectrom.* 20 (2005) 1374–1380.
- [18] M.A. Belarra, M. Resano, J.R. Castillo, Theoretical evaluation of solid sampling-electrothermal atomic absorption spectrometry for screening purposes, *J. Anal. At. Spectrom.* 14 (1999) 547–552.
- [19] A. Solà Vazquez, A. Martín, J.M. Costa-Fernández, J. Ruiz Encinar, N. Bordel, R. Pereiro, A. Sanz-Medel, Quantification of bromine in flame-retardant coatings by radiofrequency glow discharge-optical emission spectrometry, *Anal. Bioanal. Chem.* 389 (2007) 683–690.
- [20] L. Li, C.M. Barshick, J.T. Millay, A.V. Welty, F.L. King, Determination of bromine in flame-retardant plastics using pulsed glow discharge mass spectrometry, *Anal. Chem.* 75 (2003) 3953–3961.
- [21] C. González de Vega, L. Lobo, B. Fernández, N. Bordel, R. Pereiro, A. Sanz-Medel, Pulsed glow discharge time of flight mass spectrometry for the screening of polymer-based coatings containing brominated flame retardants, *J. Anal. At. Spectrom.* 27 (2012) 318–326.
- [22] I. Radivojevic, R. Niessner, C. Haisch, S. Florek, H. Becker-Ross, U. Panne, Detection of bromine in thermoplasts from consumer electronics by laser-induced plasma spectroscopy, *Spectrochim. Acta Part B* 59 (2004) 335–343.
- [23] C. Simons, C. Mans, S. Hanning, A. Janßen, M. Radtke, U. Reinholz, M. Ostermann, M. Michaelis, J. Wienold, D. Alber, M. Kreyenschmidt, Study on microscopic homogeneity of polymeric candidate reference materials BAM H001–BAM H010 by means of synchrotron m-XRF and LA-ICP-MS, *J. Anal. At. Spectrom.* 25 (2010) 40–43.
- [24] C. Mans, S. Hanning, C. Simons, A. Wegner, A. Janßen, M. Kreyenschmidt, Development of suitable plastic standards for X-ray fluorescence analysis, *Spectrochim. Acta Part B* 62 (2007) 116–122.
- [25] I.J. Kim, K.S. Lee, E. Hwang, H.S. Min, Y.H. Yim, Accurate measurement of bromine contents in plastic samples by instrumental neutron activation analysis, *Anal. Chim. Acta* 769 (2013) 22–29.
- [26] M. Resano, E. García-Ruiz, F. Vanhaecke, Laser ablation-inductively coupled plasma-dynamic reaction cell-mass spectrometry for the multi-element analysis of polymers, *Spectrochim. Acta Part B* 60 (2005) 1472–1481.
- [27] M.G.R. Vale, N. Oleszczuk, W.N.L. dos Santos, Current status of direct solid sampling for electrothermal atomic absorption spectrometry – a critical review of the development between 1995 and 2005, *Appl. Spectrosc. Rev.* 41 (2006) 377–400.
- [28] M.A. Belarra, M. Resano, F. Vanhaecke, L. Moens, Direct solid sampling with electrothermal vaporization/atomization: what for and how? *Trends Anal. Chem.* 21 (2002) 828–839.
- [29] M. Resano, F. Vanhaecke, M.T.C. de Loos-Vollebregt, Electrothermal vaporization for sample introduction in atomic absorption, atomic emission and plasma mass spectrometry – a critical review with focus on solid sampling and slurry analysis, *J. Anal. At. Spectrom.* 23 (2008) 1450–1475.
- [30] M. Resano, M.A. Belarra, J.R. Castillo, F. Vanhaecke, Direct determination of phosphorus in two different plastic materials (PET and PP) by solid sampling-graphite furnace atomic absorption spectrometry, *J. Anal. At. Spectrom.* 15 (2000) 1383–1388.
- [31] M. Resano, M. Aramendia, A.B. Volynsky, M.A. Belarra, Solid sampling-graphite furnace atomic absorption spectrometry for the direct determination of trace amounts of silicon in polyamide. Comparison of the performance of platinum and palladium as chemical modifiers, *Spectrochim. Acta Part B* 59 (2004) 523–531.
- [32] M. Resano, J. Briceño, M.A. Belarra, Direct determination of Hg in polymers by solid sampling-graphite furnace atomic absorption spectrometry. A comparison of the performance of line source and continuum source instrumentation, *Spectrochim. Acta Part B* 64 (2009) 520–529.
- [33] A.T. Duarte, M.B. Dessuy, M.M. Silva, M.G.R. Vale, B. Welz, Determination of cadmium and lead in plastic material from waste electronic equipment using solid sampling graphite furnace atomic absorption spectrometry, *Microchem. J.* 96 (2010) 102–107.
- [34] U. Heitmann, H. Becker-Ross, S. Florek, M.D. Huang, M. Okruss, Determination of non-metals via molecular absorption using high-resolution continuum source absorption spectrometry and graphite furnace atomization, *J. Anal. At. Spectrom.* 21 (2006) 1314–1320.
- [35] B. Welz, F.G. Lepri, R.G.O. Araujo, S.L.C. Ferreira, M.D. Huang, M. Okruss, H. Becker-Ross, Determination of phosphorus, sulfur and the halogens using high-temperature molecular absorption spectrometry in flames and furnaces – a review, *Anal. Chim. Acta* 647 (2009) 137–148.
- [36] M.D. Huang, H. Becker-Ross, S. Florek, U. Heitmann, M. Okruss, High-resolution continuum source electrothermal absorption spectrometry of AlBr and CaBr for the determination of bromine, *Spectrochim. Acta Part B* 63 (2008) 566–570.
- [37] T. Limburg, J.W. Einax, Determination of bromine using high-resolution continuum source molecular absorption spectrometry in a graphite furnace, *Microchem. J.* 107 (2013) 31–36.
- [38] B. Welz, H. Becker-Ross, S. Florek, U. Heitmann, High-Resolution Continuum Source AAS: The Better Way to Do Atomic Absorption Spectrometry, Wiley-VCH, Weinheim, Germany, 2005.
- [39] U. Heitmann, M. Schütz, H. Becker-Ross, S. Florek, Measurements on the Zeeman-splitting of analytical lines by means of a continuum source graphite furnace atomic absorption spectrometer with a linear charge coupled device array, *Spectrochim. Acta Part B* 51 (1996) 1095–1105.
- [40] NIST Atomic Spectra Database Lines Form, http://physics.nist.gov/PhysRefData/ASD/lines_form.html, (last accessed June 2013).
- [41] P. Parvinen, L.H.J. Lajunen, Determination of bromine by aluminium monobromide molecular absorption spectrometry using arsenic atomic lines, *Spectrosc. Lett.* 23 (1990) 1321–1330.
- [42] K. Dittrich, B. Vorberg, J. Funk, V. Beyer, Determination of some nonmetals by using diatomic molecular absorbance in a hot graphite furnace, *Spectrochim. Acta Part B* 39 (1984) 349–363.
- [43] K. Tsunoda, K. Fujiwara, K. Fuwa, Determination of chlorine and bromine by molecular absorption of aluminum monohalides at high temperature, *Anal. Chem.* 50 (1978) 861–865.
- [44] B. Welz, S. Morés, E. Carasek, M.G.R. Vale, M. Okruss, H. Becker-Ross, High-resolution continuum source atomic and molecular absorption spectrometry – a review, *Appl. Spectrosc. Rev.* 45 (2010) 327–354.
- [45] H. Becker-Ross, S. Florek, U. Heitmann, Observation, identification and correction of structured molecular background by means of continuum source AAS – determination of selenium and arsenic in human urine, *J. Anal. At. Spectrom.* 15 (2000) 137–141.
- [46] M. Resano, E. García-Ruiz, High-resolution continuum source graphite furnace atomic absorption spectrometry: is it as good as it sounds? A critical review, *Anal. Bioanal. Chem.* 399 (2011) 323–330.
- [47] M. Resano, L. Rello, M. Flórez, M.A. Belarra, On the possibilities of high-resolution continuum source graphite furnace atomic absorption spectrometry for the simultaneous or sequential monitoring of multiple atomic lines, *Spectrochim. Acta Part B* 66 (2011) 321–328.
- [48] M. Resano, J. Briceño, M.A. Belarra, Direct determination of phosphorus in biological samples using a solid sampling-high resolution-continuum source electrothermal spectrometer: comparison of atomic and molecular absorption spectrometry, *J. Anal. At. Spectrom.* 24 (2009) 1343–1354.
- [49] H. Gleisner, B. Welz, J.W. Einax, Optimization of fluorine determination via the molecular absorption of gallium mono-fluoride in a graphite furnace using a high-resolution continuum source spectrometer, *Spectrochim. Acta Part B* 65 (2010) 864–869.
- [50] Z. Kowalewska, Feasibility of high-resolution continuum source molecular absorption spectrometry in flame and furnace for sulphur determination in petroleum products, *Spectrochim. Acta Part B* 66 (2011) 546–556.
- [51] M. Resano, M.R. Flórez, Direct determination of sulfur in solid samples by means of high-resolution continuum source graphite furnace molecular absorption spectrometry using palladium nanoparticles as chemical modifier, *J. Anal. At. Spectrom.* 27 (2012) 401–412.
- [52] Z. Qin, D. McNeel, H. Gleisner, A. Raab, K. Kyeremeh, M. Jaspars, E. Krupp, H. Deng, J. Feldmann, Fluorine speciation analysis using reverse phase liquid chromatography coupled off-line to continuum source molecular absorption spectrometry (CS-MAS): identification and quantification of novel fluorinated organic compounds in environmental and biological samples, *Anal. Chem.* 84 (2012) 6213–6219.
- [53] M.A. Bechlin, J.A. Gomes Neto, J.A. Nóbrega, Evaluation of lines of boron, phosphorus and sulfur by high-resolution continuum source flame atomic absorption spectrometry for plant analysis, *Microchem. J.* 109 (2013) 134–138.
- [54] R. Mior, S. Morés, B. Welz, E. Carasek, J.B. de Andrade, Determination of sulfur in coal using direct solid sampling and high-resolution continuum source molecular

- absorption spectrometry of the CS molecule in a graphite furnace, *Talanta* 106 (2013) 368–374.
- [55] In: D.R. Lide, D.R. Lide (Eds.), *CRC Handbook of Chemistry and Physics*, 89th ed., CRC Press/Taylor and Francis, Boca Raton, USA, 2008–2009.
- [56] R.W.B. Pearse, A.G. Gaydon, *The Identification of Molecular Spectra*, 4th ed. John Wiley & Sons Inc., New York, USA, 1976.
- [57] M. Aramendía, M.R. Flórez, M. Piette, F. Vanhaecke, M. Resano, Al determination in whole blood samples as AlF via high-resolution continuum source graphite furnace molecular absorption spectrometry: potential application to forensic diagnosis of drowning, *J. Anal. At. Spectrom.* 26 (2011) 1964–1973.
- [58] U. Heitmann, B. Welz, D.L.G. Borges, F.G. Lepri, Feasibility of peak volume, side pixel and multiple peak registration in high-resolution continuum source atomic absorption spectrometry, *Spectrochim. Acta Part B* 62 (2007) 1222–1230.
- [59] M. Resano, E. Bolea-Fernández, E. Mozas, M.R. Flórez, P. Grinberg, R.E. Sturgeon, Simultaneous determination of Co, Fe, Ni and Pb in carbon nanotubes by means of solid sampling high-resolution continuum source graphite furnace atomic absorption spectrometry, *J. Anal. At. Spectrom.* 28 (2013) 657–665.
- [60] J. Briceño, M.A. Belarra, K.A.C. De Schampelaere, S. Vanblaere, C.R. Janssen, F. Vanhaecke, M. Resano, Direct determination of Zn in individual *Daphnia magna* specimens by means of solid sampling high-resolution continuum source graphite furnace atomic absorption spectrometry, *J. Anal. At. Spectrom.* 25 (2010) 503–510.
- [61] M. Resano, A.C. Lapeña, M.A. Belarra, Potential of solid sampling high-resolution continuum source graphite furnace atomic absorption spectrometry to monitor the Ag body burden in individual *Daphnia magna* specimens exposed to Ag nanoparticles, *Anal. Methods* 5 (2013) 1130–1139.

Progress in the determination of metalloids and non-metals by means of high-resolution continuum source atomic or molecular absorption spectrometry. A critical review

M. Resano · M. R. Flórez · E. García-Ruiz

Received: 16 October 2013 / Revised: 14 November 2013 / Accepted: 18 November 2013 / Published online: 7 December 2013
© Springer-Verlag Berlin Heidelberg 2013

Abstract This work examines the new possibilities introduced with the arrival of commercially available high-resolution continuum source atomic absorption spectrometers for the determination of metalloids (B, Si, Ge, As, Se, Sb and Te) and non-metals (P, S, F, Cl, Br, I and N-based species), such as the improved potential to detect and correct for spectral overlaps and the strategies available to correct for matrix effects. In particular, and considering the increasing number of papers reporting on the use of molecular absorption spectrometry using graphite furnaces and flames as vaporizers, the work discusses in detail the advantages and limitations derived from the monitoring of molecular spectra from a practical point of view, in an attempt to guide future users of the technique.

Keywords High-resolution continuum source · Atomic absorption spectrometry · Molecular absorption spectrometry · Graphite furnace · Flame · Determination of non-metals · Determination of metalloids

Introduction

Metalloids and non-metals are the most challenging elements to be determined by means of atomic absorption spectrometry (AAS). These elements show high electronegativity, which leads to high ionization potentials and resonance lines that appear at very short wavelengths [1], making their determination problematic not only for AAS, but for most atomic techniques [2].

In the case of AAS, the problem is that, at short wavelengths, the possibilities to suffer from spectral interferences (e.g., overlap of molecular species, radiation scattering, emission from the atomizer) significantly increase. Moreover, these elements also show a very complex chemistry, such that the potential for chemical interferences is also considerable.

This situation is further aggravated in the case of non-metals. The main resonance lines for most of these elements fall below 190 nm and are thus not accessible for conventional optical spectrometers. In fact, with a few exceptions (e.g., phosphorus), the direct determination of non-metals is not possible using AAS. Instead, use of indirect methods [3], or of methods based on the formation of diatomic molecules that are stable in flames or graphite furnaces, was proposed already in the 70s and 80s [4–6], even though the typical line source (LS)-AAS devices available at the time showed significant limitations for the quantitation of this type of spectrum. The theory and developments related with the measurement of these molecules in atomizers using what is termed as medium resolution spectrometers is extensively covered in the review of Welz et al. [7].

During the last decade, the introduction of high-resolution continuum source atomic absorption spectrometry (HR CS AAS) has substantially expanded the potential of the technique, whether it be using a flame (F) or a graphite furnace (GF) as atomizer [8–11]. This idea, the use of a continuum source device, was investigated by different authors (and particularly by J. Harnly) over the years [12–16], but it was finally Becker-Ross and co-workers [17–19] who presented a device that proved sufficiently successful to be commercialized by Analytik Jena in 2003 equipped with a flame as atomizer, and, since 2007, incorporating also a graphite furnace. This instrument is based on: (1) a high-pressure xenon short-arc lamp operating at brightness temperatures of approximately 10,000 °C, capable of providing a high intensity in the visible and (far) UV region; (2) an optical system based on an

M. Resano (✉) · M. R. Flórez · E. García-Ruiz
Department of Analytical Chemistry, University of Zaragoza,
Pedro Cerbuna 12, 50009 Zaragoza, Spain
e-mail: mresano@unizar.es

echelle monochromator dispersing radiation in two steps (by using a prism first and an echelle grating afterwards); and (3) a linear CCD array for detection. The schematics of this instrument are shown in Fig. 1.

This technology has opened up new possibilities in this field that, in principle and considering the aspects mentioned before, should be particularly relevant for the determination of metalloids and non-metals, such a significantly improved potential for detecting and correcting for both spectral overlaps [9, 19, 20] and matrix effects [20]. It is important to stress that this type of instrumentation provides a continuous and high intensity emission over a large spectral interval (from 190 to 900 nm), allowing for the monitoring of either molecular or atomic absorption with high spectral resolution (a few picometers), even though only a narrow spectral region (from 0.2 to 1.0 nm, depending on the wavelength) can be simultaneously monitored [11]. Thus, it is much more suited for the quantitative monitoring of the molecular absorption of diatomic molecules than any of the line devices used in previous decades.

A review of the HR CS AAS literature can illustrate this point. As shown in Fig. 2, the number of papers making use of this instrumentation for the determination of non-metals, since the first article published in 2005 [21], shows a clear trend upwards. Moreover, the percentage of HR CS AAS papers devoted to non-metals is also growing, to the point that it corresponds with approximately 50 % of the total number of HR CS AAS papers published during the last year.

It is the purpose of this article to critically examine the potential of HR CS AAS for the determination of metalloids and non-metals. In this regard, no previous review was found in the literature discussing the situation for metalloids. For non-metals, the review published by Welz et al. in 2009 and focused on phosphorus, sulfur and the halogens is certainly noteworthy [7]. As indicated before, such review contains

comprehensive information on the theory behind the monitoring of molecular spectra in atomizers and a historical discussion on results obtained with medium resolution devices, as well as on the few articles available at the time using HR CS molecular absorption spectrometry (MAS). In addition, a very recent article on MAS in flames and furnaces has been published by Butcher [22]. This article also devotes a significant portion to these fundamental and historical aspects. Therefore, for such topics, the reader is kindly referred to these articles. The current article will focus only on recent applications obtained with the commercially available HR CS AAS instrumentation. However, a few previous seminal papers will be included in the tables/discussion for comparison purposes.

HR CS AAS for the determination of metalloids

The term metalloid is commonly used in Chemistry for those elements that show intermediate characteristics between those of metals and those of non-metals. Different authors have proposed different elements as metalloids, based on properties such as ionization energies, electronegativity and conductivity (metalloids tend to be semi-conductors), but the elements most commonly accepted as such are B, Si, Ge, As, Se, Sb and Te [23].

As stated in the introduction, these elements show properties that made their determination difficult by means of AAS. Some of them are relatively specific (e.g., Se can form very volatile compounds while B and Si may form carbides in a graphite furnace [24, 25]), but they all share that their resonance lines are always located at short wavelengths. In fact the most sensitive lines for these elements are: 193.696 nm (As), 196.026 nm (Se), 214.281 nm (Te), 217.581 nm (Sb), 249.772/249.677 nm (B), 251.611/251.432 nm (Si) and 265.157 nm (Ge). Thus, with the exception of Ge, all these elements showed lines that are found below 252 nm. It is precisely in this area where it is more frequent to find spectral overlaps with diatomic molecules such as PO, CS, NO or SiO. Moreover, radiation scattering effects become significantly more pronounced in this region, since the coefficient of scattering obeys Rayleigh's law and it is inversely proportional to the fourth power of the wavelength [26]. Furthermore, unlike transition metals, metalloids do not show usable lines in other spectral regions.

Therefore, the use of HR CS AAS should represent a step forward for determination of these elements. As discussed in the "Introduction", this instrument provides a continuous and high emission in all the range 190–900 nm. It is true that the spectral radiance of the Xe lamp decreases below 230 nm [8], but the remaining radiance is always 2 orders of magnitude higher than that of hollow cathode lamps, even in this region.

This instrumentation is equipped with a detector with 588 individual pixels that are monitored truly simultaneously. Of

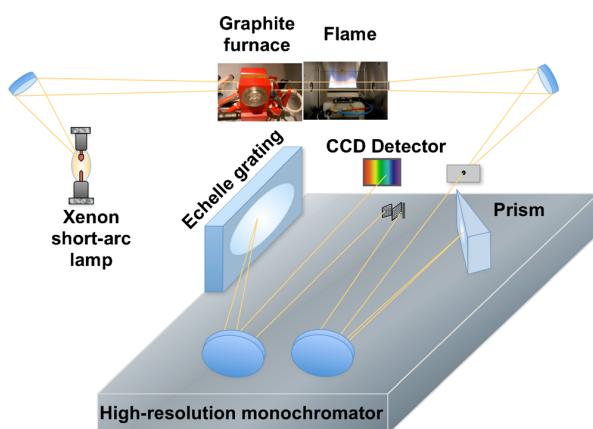
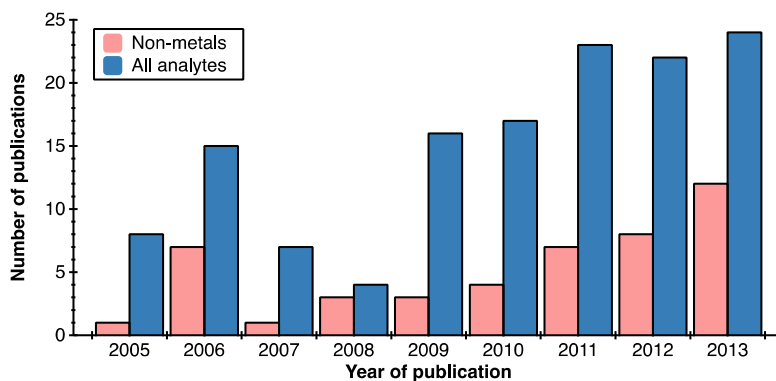


Fig. 1 Setup of a high-resolution continuum source atomic absorption spectrometer. Reproduced with permission of Springer (doi:10.1007/s00216-010-4105-x) [10]

Fig. 2 Number of publications that have reported the use of high-resolution continuum source atomic (or molecular) absorption spectrometry for the determination of non-metals, or of any type of analyte. Source: ISI Web of Science. Papers that appeared in proceedings and book chapters are not included



these, the signal of only 200 pixels is displayed (see Fig. 3a). In this way, a truly 3D signal can be obtained, when considering the time scale (see Fig. 3b). The instrument features high-resolution (pm level), because the spectral region that is simultaneously monitored is narrow (0.2 nm around 200 nm, which increases up to 1.0 nm around 800 nm). This aspect limits its applicability for simultaneous multi-element analysis, as discussed in more detail elsewhere [20, 27]. However, it is important to indicate that the remaining detector pixels are used for corrections. As stressed several times in the literature, this instrument operates like a double-beam device, such that all the events that affect the flux of radiation of all the pixels simultaneously and to the same extent are automatically compensated [9]. That means that all those events that can be considered as continuous in the short wavelength interval that is measured, such as radiation scattering, lamp flickering or temporal changes in the transmittance of the gas phase, can be effectively corrected for, leading to a much more stable baseline, which is a remarkable feature when lines located in the far UV need to be monitored [28]. This reason combined with the high intensity of the Xe-lamp permits this instrumentation to typically achieve a better detection limit (3-5 times) than a line source device [9, 29].

Another critical feature that HR CS AAS instrumentation provides is the potential to mathematically correct for spectral overlaps in a simple and accurate way, as long as it is feasible to obtain a suitable reference spectrum, which means a spectrum in which only the interfering species is present.

Figs. 4 and 5 show an example on how this feature works. A determination of Sb in urine is intended using the main absorption line for Sb (217.581 nm). However, as can be seen in Fig. 4a, there is a structured background appearing in this area that seems to overlap with the target line, which should appear in the center of the spectrum (in fact, it can be seen that in the center the signal appears a bit earlier, which indicates the presence of another species compared with the rest of the spectrum). The first clear benefit of HR CS AAS is that it is possible to appreciate any concomitant interference. In some situations, it may be feasible to avoid the observed spectral

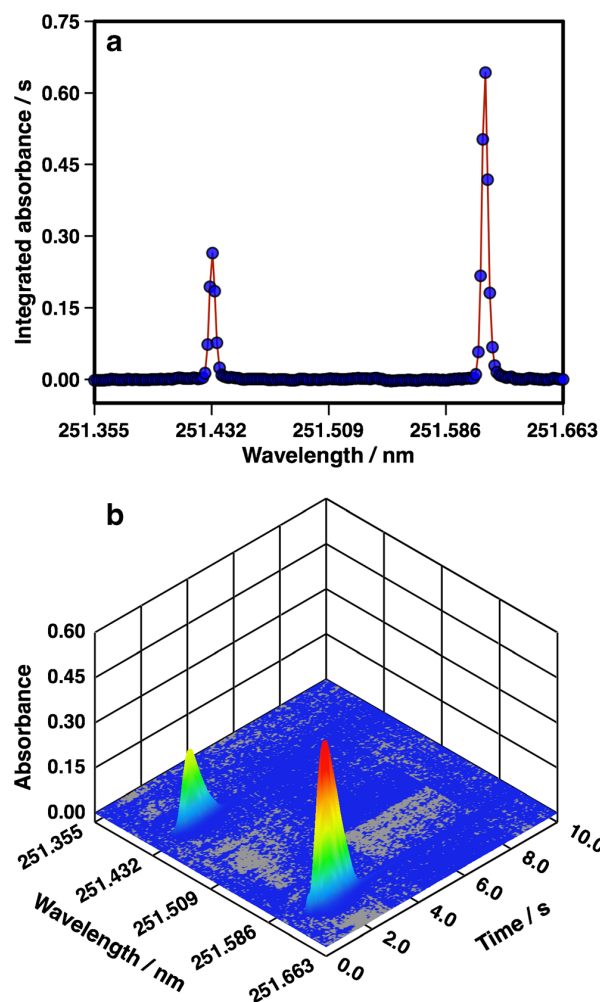


Fig. 3 a Time-integrated absorbance profiles in the vicinity of the 251.432/251.611 nm Si doublet as obtained by HR CS GFAAS monitoring of a $500 \mu\text{g L}^{-1}$ solution. The signal recorded by every individual detector pixel is shown (blue dots). b Same signal as in (a), but time-resolved

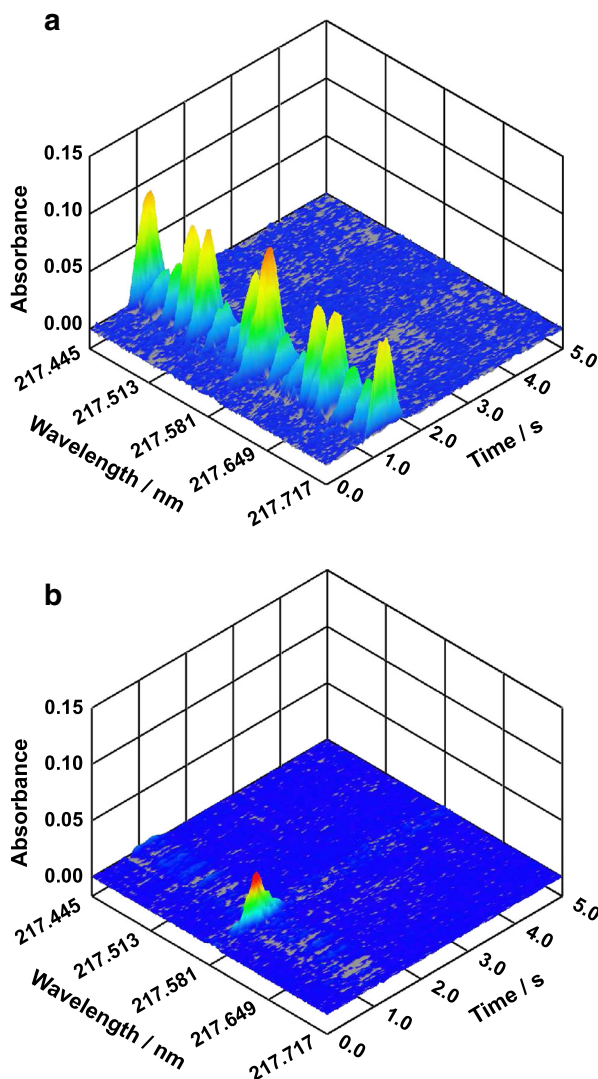


Fig. 4 **a** Time-resolved absorption spectrum as obtained after HR CS GFAAS measurement of a urine sample (diluted 1:2) containing $45.9 \mu\text{g L}^{-1}$ of Sb; **b** Same signal as in (a) after subtraction of the reference spectrum using least-squares background correction

overlap by further optimization of the temperature program or by addition of a suitable chemical modifier. However, in some other situations this may not be sufficient or it may require too much work for a routine lab. Even if that is the case, it is often possible to correct for the interference and achieve accurate results in situations that are beyond the capabilities of traditional BG correction systems (e.g., deuterium or Zeeman-effect based).

When this type of structured background is found, it can be usually attributed to the absorption spectrum of a diatomic species. In fact, in this particular region, it is known that PO absorbs, and therefore a reference spectrum was obtained with a phosphate solution. The 2D spectrum of the sample is shown

in Fig. 5a and the PO spectrum is shown in Fig. 5b. Obviously, there is a good correspondence between the peaks of the interference found in the sample and those of the reference spectrum (except for the central part, in which also the Sb signal should be found), which serves to confirm the identity of the interfering molecule. In fact, what is being monitored in this area is the rotational hyperfine structure of a PO molecular electronic transition, which might be used to determine P, as will be discussed in the next section. Thus, since the relation between the intensities of all these PO “lines” should always be constant (only subject to small experimental errors), based on the signals obtained for the PO lines that do not overlap with Sb, it is possible to proportionally subtract the portion of the PO signal that overlaps with Sb using a least squares algorithm. In this way, the resulting corrected spectrum shows only the atomic absorption of the target analyte, with a stable baseline, which is shown in 3D in Fig. 4b and in 2D in Fig. 5c.

The software of the HR CS AAS instrument can perform this least-squares background correction (LSBC) in a fast and simple way, and this approach has been demonstrated to work efficiently, even in situations in which the signal of the interference is quite significant compared with that of the analyte. The main reason for this efficacy is that all the different lines are truly simultaneously read out, because if a sequential method would be used any variations occurring during the alternate measurements would have an effect on the results. And this approach is particularly useful for the determination of metalloids since, as discussed before, absorption of diatomic molecules is very frequent at short wavelengths.

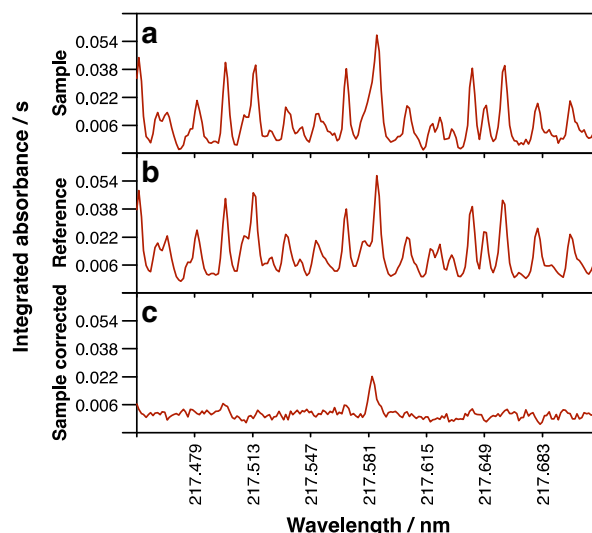


Fig. 5 Time-integrated absorbance spectra obtained after HR CS GFAAS measurement of (a) a urine sample (diluted 1:2) containing $45.9 \mu\text{g L}^{-1}$ of Sb; (b) a 1 % (m/v) $\text{NH}_4\text{H}_2\text{PO}_4$ solution; c same signal as in (b), after subtraction of the reference spectrum (shown in b) using least-squares background correction

Table 1 presents the examples found in the literature that are devoted to the determination of metalloids using HR CS AAS. As can be seen, several of them have made use of this feature. In fact, the first article reporting on the use of LSBC with HR CS AAS investigated the determination of As and Se in urine [19] using a graphite furnace. The work clearly shows the difficulties that would be found with conventional line source AAS as not only one, but two different species overlap with the signal of the analytes. As signal was affected by the presence of NaCl and PO in gas phase, while Se signal overlapped with those of NO and PO. It can be mentioned that it is possible to correct for spectral overlaps with this approach even when there is more than one interfering species. In such case, the sequential subtraction of every reference spectrum should provide the net atomic absorption signal, as demonstrated in the above-referred work by accurate analysis of a urine reference material.

Araujo et al. encountered a similar problem when attempting the direct determination of Sb in sediments by means of solid sampling HR CS GFAAS [30]. Obviously, direct solid sampling is attractive as it permits obtaining faster results but, by eliminating any previous analytical step (e.g., sample digestion), the whole matrix will be present, thus enhancing the risk of suffering from spectral overlaps. Moreover, another issue associated with direct solid sampling is that it is not comfortable to dilute the sample, such that if the analyte levels are not very low the use of an alternative less sensitive line could be recommended. This work clearly shows the benefits of HR CS AAS for such situation. This technique makes the use of alternative lines more suitable, because all of them will have practically the same lamp energy, as opposed to hollow cathode lamps, where weaker lines are noisier [9]. Sb shows several usable lines, even though all of them are located at a low wavelength. For this work, the one located at 231.147 nm was found adequate in terms of sensitivity. However, in this region interferences owing to the presence of both SiO and PO species were found. Sequential application of the LSBC approach allowed the accurate quantification of the target analyte (Sb) in all the samples investigated [30]. Another work presented by the same research group further investigated the determination of Sb in airborne particulate matter collected on glass fiber filters [31]. In this case, use of the LSBC approach was not found necessary, but the authors state that while the procedure developed was straightforward when using HR CS GFAAS, attempts to translate it to a line source device failed, because the line selected (another Sb less sensitive line, 212.739 nm) is very weak (20 times less sensitive than the main line) and the spectrum obtained was too noisy.

The examples shown above are all based on the use of a graphite furnace as atomizer, but LSBC can also be used for flames. Raposo et al. [32] determined Si in lubricant oil and used LSBC for correction of the interference caused by the

absorption of CS molecules in the area surrounding the main Si line (251.611 nm). Moreover, these authors also proved another potential benefit of this instrument, which is the use of an internal standard (IS) to correct for matrix effects. Even though for best results ideally the signal of the IS should be monitored truly simultaneously together with that of the analyte (and that is certainly the case if HR CS GFAAS is used [20]), in the case of HR CS FAAS, since the signal is quasi stable and it is possible to change the analytical line in a few seconds, it is not always necessary to do so. The authors evaluated different IS, and finally opted for W, which was (sequentially) monitored at the 255.135 nm line.

A very different type of application that also made use of an IS was developed by Wiltsche et al. [33]. These authors evaluated the possibilities of HR CS FAAS for B isotopic analysis. This is in principle possible because the atomic lines for pure ^{10}B and pure ^{11}B (the only two stable boron isotopes) are slightly different: 208.95898 nm for ^{10}B and 208.95650 nm for ^{11}B , as measured by emission techniques. The authors used this alternative line because the isotopic shift observed for the main B line is too small (0.85 pm) to be appreciated with a HR CS FAAS instrument. Still, the difference at 208.9 nm (approx. 2.5 pm) is not sufficiently large to observe two fully resolved peaks with this instrumentation. However, what can be appreciated is that the position of the B absorption profile varies as a function of the boron isotopic ratio. The maximum of the boron peak profile shifts towards higher wavelengths when the % of ^{10}B increases. Thus, there is still potential to determine the B isotopic composition. However, since this isotopic shift is very small, it is absolutely essential to correct for possible instabilities of the monochromator in order to achieve sufficient precision and accuracy. In principle, this can be done using a suitable IS that is monitored truly simultaneously. Thus, an element that exhibits lines that are close enough to that of B, such that both can be monitored at the same time, needs to be selected. For this purpose, the authors evaluated the performance of Fe and Ni, with satisfactory results for both of them. The authors conclude that, while use of HR CS FAAS cannot rival mass spectrometric approaches in terms of accuracy and precision, it is an inexpensive and simple alternative suitable to distinguish different enrichment levels of ^{10}B (within 5 %) in steel samples [33].

Another interesting feature that can be used for determination of some metalloids is the possibility to monitor multiple lines of the same analyte. In this regard, it can be mentioned that the main lines for both B (249.772/249.677 nm) and Si (251.611/251.432 nm) are in fact doublets, two lines that are very closely located and that exhibit different sensitivity (approx. a factor of 2 for boron, and a factor of 3 for Si [8]). Occurrence of close lines of the analyte was typically a problem when using line source AAS devices, since both of them were actually measured and the resulting combined signal exhibited limited linearity. The situation is totally the opposite

Table 1 Applications reporting on the determination of metalloids using HR CS AAS

Atomizer	Analyte	Wavelength (nm)	Limit of detection/ characteristic mass or concentration	Modifier	Sample	Remarks	Reference
Graphite Furnace	As	193.696	25 pg/74 pg	Pd	Urine	Use of LSBC to correct for the spectral interferences caused by NaCl and PO	[19]
Graphite Furnace	As	193.696	0.08 $\mu\text{g g}^{-1}$ /N.A.	Pd	Multivitamin dietary supplements	Slurry sampling. Sequential determination of various metals	[92]
Flame	¹⁰ B ¹¹ B	208.959 208.957	Not available Not available		Steel samples	Quick method for estimation of B isotope ratios. Internal isotopic standards (Fe, Ni) used to compensate for monochromator instability	[33]
Flame	B	249.773 249.677	0.5 mg L ⁻¹ /8.5 mg L ⁻¹ 2.9 mg L ⁻¹ /16.5 mg L ⁻¹ $\Sigma = 1.0 \text{ mg L}^{-1}/5.6 \text{ mg L}^{-1}$		Medicinal plants	Comparison of performance using different detector pixels and/or summing (Σ) the signal of the two lines	[35]
Graphite Furnace	Sb	231.147	0.02 $\mu\text{g g}^{-1}$ /28 pg	Ir coating	Sediment reference materials	Direct solid sampling. Calibration with aqueous standards. Use of LSBC to solve the spectral overlap caused by PO and SiO molecules	[30]
Graphite Furnace	Sb	212.739	15 $\mu\text{g g}^{-1}$ /0.7 ng	Ru coating	Airborne particulate matter on glass filters	Direct solid sampling. Calibration with aqueous standards	[31]
Flame	Sb	212.739	5.7 mg L ⁻¹ /8.9 mg L ⁻¹		Pewter alloy cups	Fast sequential determination of Pb and Sb	[93]
Graphite Furnace	Sb	217.582	15 $\mu\text{g g}^{-1}$ /38 pg	Ru coating	Dust deposited on tree leaves and CRM of urban particulate matter	Direct solid sampling. Calibration with aqueous standards	[94]
Graphite Furnace	Sb	231.147	0.06 mg kg ⁻¹ /35 pg	Pd + Mg + Triton X-100	Polymers from waste electronic equipment	Direct solid sampling. Calibration with aqueous standards. Cr was determined sequentially in the samples	[95]
Graphite Furnace	Se	196.026	38 pg/113 pg	Ni	Urine	Use of LSBC to correct for the spectral interferences caused by NO and PO	[19]
Graphite Furnace	Se	196.027	0.06 $\mu\text{g g}^{-1}$ /N.A.	Pd	Multivitamin dietary supplements	Slurry sampling. Sequential determination of various metals	[92]
Flame	Si	251.611	40 ng g ⁻¹ /1.2 mg kg ⁻¹		Lubricating oil	Al, Ba, Mo and V sequentially determined in the samples	[96]
Flame	Si	251.611	8.4 $\mu\text{g L}^{-1}$ /N.A.		Lubricant oil	Use of LSBC to solve the spectral overlap caused by CS molecules. Use of W as an internal standard to correct for matrix effects	[32]
Flame	Si	251.611	0.60 mg kg ⁻¹ /0.63 mg L ⁻¹		Vegetable oil and biodiesel	Dilution of the samples with xylene	[97]
Graphite Furnace	Si	251.611	3.2 ng/130 pg	Pd + Mg(NO ₃) ₂	Etching solutions of silicon wafers	Due to the high concentration of Si, less expensive wall atomization was used	[77]

when using HR CS AAS, because these lines are simultaneously but separately recorded, such that the more suitable line can be selected every time, permitting to actually expand the linear range [20, 34]. Bechlin et al. evaluated both B lines for plant analysis by means of HR CS FAAS [35].

Finally, it can be mentioned that no article has reported on the determination of Ge or Te using HR CS AAS so far. This is not very surprising, as these elements are not very commonly determined by AAS. Some basic information (the characteristic mass obtained with HR CS GFAAS and the characteristic concentration obtained with HR CS FAAS) can be found in the book by Welz et al. [8] devoted to this technique.

Additionally, a recent article has evaluated the use of graphite tubes with smaller inner diameters (thus, leading to a lower volume and, conversely, to higher sensitivity), taking advantage of the fact that the Xe lamp, operated in hot spot mode, concentrates its energy in a small plasma with a diameter of less than 0.2 mm. Thus, only a small portion of the typical graphite tube (6.0 mm of inner diameter) is really illuminated. The authors succeeded in decreasing the limits of detection (LODs) by using a 2 mm (inner diameter) tube. The degree of improvement varied for different elements, being of 6-7 for Ge, Sb and Te, and only of 3-5 for As, B and Se. Si was not measured [36].

Overall, it can be concluded that HR CS AAS provides some significant advantages for the monitoring of metalloids, of which the potential to correct for continuous events that cause background and to correct for structured background signals that are produced in the presence of diatomic molecules are particularly noteworthy, considering the spectral region in which the lines of these elements appear. In addition, other advantages that are more generic can be exploited as well (use of an internal standard, monitoring of multiplets). Finally, the potential to determine the B isotopic composition, is certainly an appealing but niche feature.

HR CS AAS and HR CS MAS for the determination of non-metals

If determination of metalloids can be considered as challenging using conventional line source AAS instrumentation, the determination of non-metals is even more difficult. As briefly discussed in the “Introduction”, the main resonance lines of these elements are located below 190 nm, such that they are out of reach for commercially available spectrometers [37]. Phosphorus, however, exhibits a non-resonance line (the doublet at 213.547/213.618 nm) suitable for AAS monitoring, as already reported by L'vov and Khartsyzov [38], that can offer sufficient sensitivity for some applications [39], even though its use was problematic due to the occurrence of spectral overlaps, as will be discussed later [40].

The alternatives available for the rest of the elements include either indirect determination, in which the species of interest react with another one, typically a metal that can be easily determined by AAS [3, 37]. Obviously such strategy requires high selectivity in all the reactions carried out and it is generally much more laborious than a direct determination. Alternatively, the use of molecular absorption spectrometry, but using the potential of flames and furnaces to attain a sufficiently high temperature to produce gaseous diatomic molecules, was explored. Quantitative determinations were reported already in the 70s, and this type of work has continued until recently [41]. As discussed in the “Introduction”, quantification of the type of spectrum provided by gaseous molecules was very difficult using line source instrumentation. Among other aspects, it has to be considered that the main reason for success in terms of selectivity of line source AAS is the almost perfect correspondence between the emission line of the hollow cathode lamp and the atomic absorption line. Such perfect matching is not possible in the case of molecular spectra, where authors have to rely on the use of hollow cathode lines of elements that emit radiation in the area where the molecular transition is expected to be found. It has to be considered that with monochromators of low resolution the rotational structure of the molecules will not be fully resolved, resulting in absorption bands rather than in fine lines. Thus, it is in principle possible to find a hollow cathode lamp whose emission overlaps with a portion of one of the analyte broad molecular absorption bands. But the major problem will be background correction, because the remaining area of this broad band or of any other analyte molecular band that does not overlap with the narrow emission profile of the hollow cathode lamp (but still falls within the wide region monitored by the monochromator, typically 0.2 nm or more) will be considered as background by the correction system and, thus, will be subtracted from the absorption measured with the hollow cathode lamp. For a detailed discussion on the evolution of these early works, the reader is kindly referred to the work of Welz et al. [7].

With the introduction of HR CS AAS instrumentation the situation has changed significantly. Still, atomic lines for these elements are not accessible (except for those of phosphorus referred before), but the characteristics of this instrumentation already discussed in previous sections are much more suited for the quantification of the complex spectra obtained when diatomic molecules absorb in a flame or in a graphite furnace. Still, the determination of some non-metals is hardly feasible (e.g. noble gases). No paper has reported so far on the determination of C or O. This is normal, owing to the ubiquity of these elements in graphite furnaces and flames. However, determination of the rest of stable non-metals (P, S, all the halogens and even some N species) has been reported using HR CS AAS instrumentation, by means of molecular absorption spectrometry [22].

The determination of these elements is, however, not equally easy or feasible, as different aspects have to be taken into account. A general discussion on these aspects is provided below, while specific sections will be devoted to the non-metals more commonly determined (P, S, halogens and some nitrogen-containing species).

General considerations for the determination of non-metals in furnaces and flames using MAS

As discussed before, at the typical temperatures existing in a flame or a graphite furnace, only some diatomic molecules and a few triatomic ones are stable. The stability of these molecules essentially depends on their bond strength. It has already been recommended to use molecules with bond strengths higher than 500 kJ mol^{-1} for HR CS MAS monitoring [7]. Molecules with lower bond strengths might also be formed, but it has to be kept in mind that selectivity decreases with the bond strength.

Overall, the process is more complicated than in AAS, where the relatively high temperature of the atomizer ensures that, at some point, atoms will be formed. When MAS is attempted, it is necessary to ensure that the targeted molecules are formed, and there might be competition with other molecules. For instance, some molecules are spontaneously formed in a graphite furnace or a flame, owing to their high stability and the availability of the needed reagents. If S is introduced into an atomizer, CS (714 kJ mol^{-1}) will most likely be formed at some point (C is certainly available), and if P is introduced into an atomizer, PO (599 kJ mol^{-1}) will also be formed at some point (there is always O as well). In fact, it was already discussed in the previous sections that CS and PO are responsible for many spectral overlaps when attempting to determine metals. Thus, it makes sense to use the ubiquity of these signals to our advantage and develop methods based on them to quantify S or P. That does not mean that these methods will be totally free from interferences. Even for these molecules, formation of other competing compounds has been reported (e.g., formation of CS₂, which is very volatile, instead of CS [42]).

However, in many other cases a reagent needs to be added to obtain the desired molecule. That is typically the case for the determination of halogens. That means that, if direct analysis of solid samples or of complex matrixes in a graphite furnace is intended, the temperature program needs to be carefully optimized to permit a suitable interaction between the analyte species and this reagent at some point, which may be difficult in some cases. Again, the bond strength is very important for these elements, because in many samples not only one halogen but several of them will be present. It is typically the case that most metals form bonds in decreasing order of strength with F, Cl, Br and I. That means that developing methods for F may be relatively simple, but

determining I or Br in a matrix that contains significant amounts of F or Cl can be very challenging, and may require some separation step [43]. It is thus not so surprising to confirm that most of the papers devoted to determination of non-metals have investigated either P, S or F, which are the elements giving rise to more stable, and thus, more selective molecules.

Finally, even if one molecule is selectively formed, that does not guarantee that the sensitivity obtained will be sufficient. Typically, the absorptivity of these molecules does not provide LODs as low as those available with AAS for metals, with one exception: some F-based molecules can be determined with excellent sensitivity.

In this context, it has to be mentioned that use of a graphite furnace is certainly preferable over a flame, not only because it provides superior sensitivity, but also because it permits to control the chemistry more carefully, with an optimized temperature program and the addition of chemical modifiers, which may be critical to ensure that the desired molecule is formed regardless of the chemical form in which the analyte is present in the sample [44, 45], and also that no losses occur during pyrolysis. In this regard, most articles devoted to HR CS FMAS have determined molecules that are spontaneously formed in a flame (e.g. CS, PO or SH), with only a few exceptions [46–48].

Despite this increased complexity, a positive aspect of GFMAAS in comparison with GFAAS is that, since only vaporization is required, a relatively low vaporization temperature can be used (in fact a very high one might be detrimental as the molecular bond may be broken), as it occurs when electrothermal vaporization is used for sampling coupled to inductively coupled plasma techniques [49, 50]. This is an advantage to determine hardly volatiles elements, such as P [51], and could also open possibilities to determine refractory metals in molecular form [52].

Finally, some considerations on the type of spectrum offered by these molecules can be made. These diatomic molecules will show different possible electronic transitions, and each of them several vibrational transitions with superimposed rotational transitions. Thus, it is typically the rotational spectra what is going to be appreciated with the resolution available (pm level) in a HR CS AAS instrument. A more detailed discussion on this point is provided elsewhere [7]. However, from a practical point of view, focusing on how the molecular spectrum will look and should be treated in a HR CS AAS instrument, after reviewing the examples found in the literature, a distinction can be made between essentially three different types of signal.

If the rotational spectrum is very dense, it may not be fully resolved with the resolution available. Then a broad band will be observed, as it is typical of the ultraviolet systems of Al-based molecules such as AlF, AlCl or AlBr. An example for the AlF spectrum is shown in Fig. 6a. This type of spectrum

does not pose too many issues for the instrument to set the baseline, as long as the band is positioned properly, leaving sufficient detector pixels at both sides. Considering that the band is often quite asymmetrical, that means that it may not be recommended to always position the peak maximum in the center of the detector (pixel 101 of the 200 pixels available). For the signal shown in Fig. 6a, if the peak maximum is monitored with the central pixel, the left flank of the absorbance peak would be cut off, making impossible to achieve a proper baseline definition [52]. It also needs to be considered that the width of such band is significantly higher than the typical width of an atomic line (see Fig. 3a or 5c for comparison). Thus, if for an atomic line it is typically recommended to use only the three central pixels for quantification in order to obtain the best LOD (the rest of the pixels offer a lower

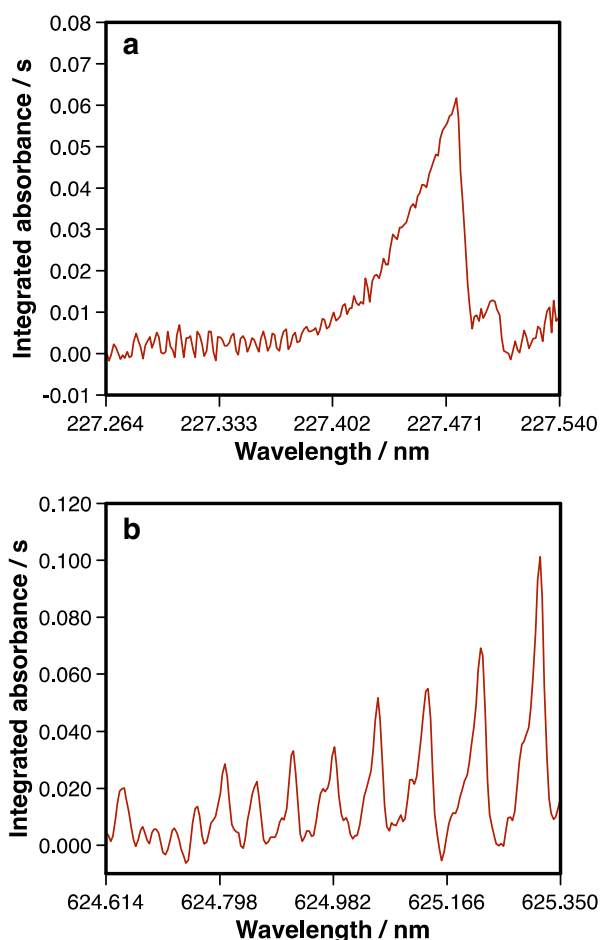


Fig. 6 **a** Time-integrated molecular absorbance spectrum of AlF as obtained by HR CS GFMS. The signal corresponds with the vaporization of 500 pg of Al, in excess of F. **b** Time-integrated molecular absorbance spectrum of CaBr as obtained by HR CS GFMS. The signal corresponds with the vaporization of 100 ng of Br, in excess of Ca. Reproduced with permission from Elsevier <http://www.sciencedirect.com/science/article/pii/S058485471300222X> [43]

signal to noise ratio) [34], for these broad bands, the use of 5 or 7 central pixels can still provide a better LOD [52, 53].

For other molecules (and typically for those monitored in the visible region of the spectrum), various totally resolved bands of different sensitivity are obtained, as shown in Fig. 6b for CaBr. This is a favorable situation, because it is simple to set the baseline properly. Moreover, such system permits expanding the working range easily, as it is possible to select the transition that is more suitable for the analyte content in every case [43, 54].

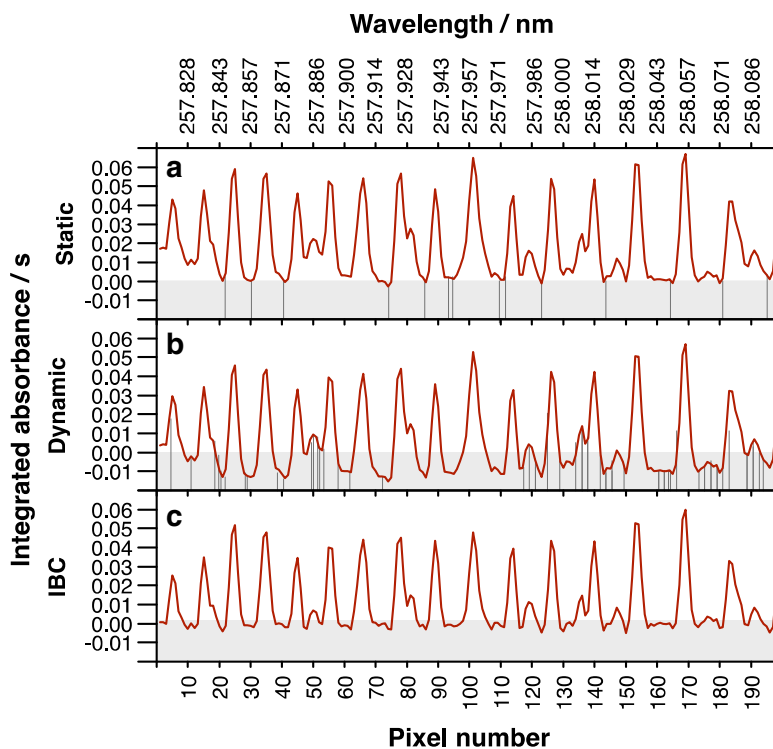
Finally, a third situation occurs when the rotational spectrum is dense but can be resolved by the instrument, such that many transitions that show a width similar to that of atomic lines are observed. The UV spectra of CS, NO or PO are clear examples of this situation. Figure 7 shows the typical signal obtained for CS. This case poses some advantages as well. Since various transitions of relatively similar sensitivity are available, there is no need to restrict analysis to only one of them. In fact, combining the signal of several of these lines may serve to improve the LOD [44, 51, 55] to some extent (up to a factor of 3, depending on the number of lines summed). It is always necessary to make sure that the selected lines do not suffer from spectral overlaps [42, 44]. However, again, this case is advantageous from this point of view because, while overlap of some particular transition may occur, it is hard to envision a case where all these transitions suffer from interferences, at least from atomic lines. If the interference is produced by a molecular spectrum, LSBC may be applied.

The difficulty in monitoring these signals is that there are so many and they are so close that the software of the instrument may have difficulties in properly setting the baseline if the automatic (named dynamic) mode is chosen [56] (see Fig. 7b). Thus the manual (or static) mode, where the analyst defines the valleys of the peaks, is preferred (see Fig. 7a). In this regard it can also be mentioned that a recent software update provides a new baseline correction algorithm call IBC (iterative baseline correction). While the exact details of this algorithm are not available, its application helps in reducing the width of the lines at the cost of also lowering their maximum value, as shown in Fig. 7c. Thus, it becomes simpler to set the baseline for the software. Moreover, this approach may be recommended to avoid some spectral overlaps, even though no article has yet reported on its use, but this may simply be because it is a novel feature.

Determination of phosphorus: MAS or AAS?

As discussed before, P is the only non-metal that could be determined via AAS, not by means of its resonance lines, but by using a less sensitive doublet located at 213.547/213.618 nm, as proposed already by L'vov and Khartsyzov [38]. In this way, some successful determinations of P were

Fig. 7 Time-integrated absorbance spectra obtained when monitoring CS transitions by HR CS GFMAAS using different approaches to set the baseline for 50 ng of S. The zero level and the area below are highlighted in *grey*. The pixels that the analyst (static mode) or the software (dynamic mode) select to define the baseline are indicated by vertical lines



reported even using direct solid sampling [39] or slurries [57]. However, for GFAAS, it was clear that the use of a suitable chemical modifier was critical to achieve accurate results [58], and different combinations were tested for this analyte, including Ca, La, NaF and Pd, alone, or in combination with other substances [40].

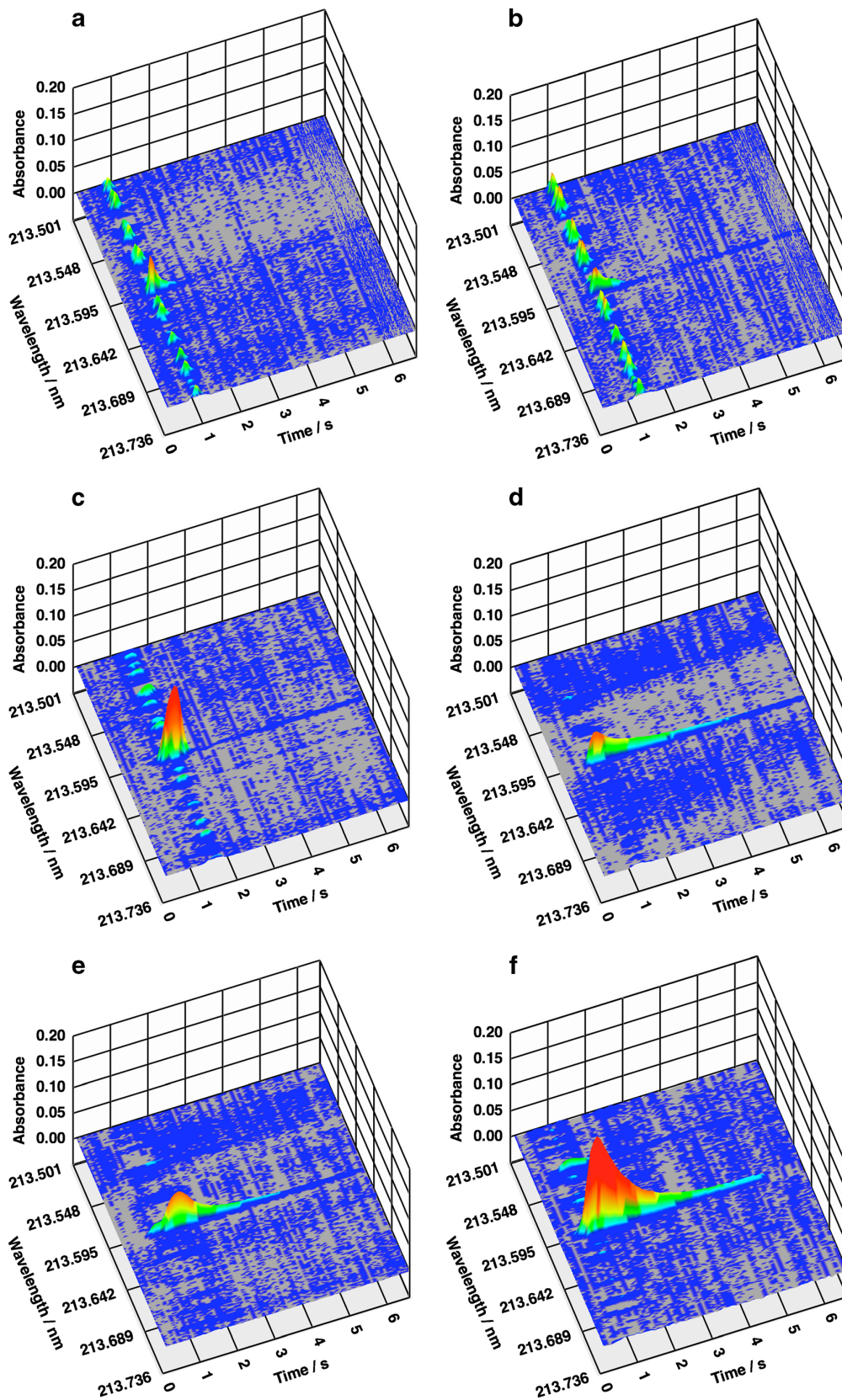
The real reason for this somewhat strange response observed for P as a function of the chemical modifier used was not evident until the arrival of HR CS GFAAS instrumentation. The determination of P by AAS is not only problematic because this is an element showing complex chemistry, capable of both forming volatile compounds but also of penetrating into the graphite structure to form refractory carbides [59]. The main issue was discovered and investigated in detail in a series of articles published by the group of B. Welz [40, 59–61]. The key aspect is that, depending on the chemical modifier used and on the temperature conditions, PO will be formed together with or instead of P, and PO molecular transitions overlap with the P lines mentioned above. In a way, the own analyte is creating spectral interferences hampering its determination by AAS, which is quite unique. The advantage of using HR CS GFAAS for this element is very significant, not only because the possible presence of PO species will be clearly observed, but also because this PO overlap can be efficiently corrected using LSBC, as discussed in “HR CS AAS for the determination of metalloids”, which resulted critical for investigation of the atomization

mechanism of phosphorus in GFAAS in the absence of a chemical modifier [59]. Overall, it can be concluded that use of Pd, alone or together with Ca or ascorbic acid, is preferred to mainly form P [40]. And also, it appears that the Zeeman-effect BC system is more adequate than the use of a deuterium lamp when dealing with PO structures [60, 61].

Resano et al. also investigated the performance of several modifiers for P direct determination in biological solid samples [51]. Figure 8 shows a summary of the results, in which the aspects discussed before can be appreciated. If no modifier is used, a significant amount of P is found as PO. Use of a permanent modifier (W), while it may be desirable to avoid P intercalation into the graphite structure, does not improve this situation, but the addition of Pd alleviates this issue to a large extent. In the end, best sensitivity was found using Pd plus ascorbic acid in addition to W as permanent modifier [51].

However, instead of using a relatively complex mixture of modifiers and a high atomization temperature (2600 °C), it

Fig. 8 Time-resolved absorbance spectrum for 600 ng of phosphorus recorded by means of HR CS GFAAS in the vicinity of the 213.547/213.618 nm atomic doublet with an atomization temperature of 2600 °C in the presence of various chemical modifiers. **a** No chemical modifier; **b** Tungsten coating; **c** 10 µg of palladium; **d** 300 µg of ascorbic acid; **e** 10 µg of palladium plus 300 µg of ascorbic acid; **f** Tungsten coating, 10 µg of palladium and 300 µg of ascorbic acid. Reproduced with permission from the Royal Society of Chemistry <http://pubs.rsc.org/en/content/articlelanding/2009/ja/b907937h> [51]



was demonstrated that it is also feasible to use a simpler modifier and milder conditions to favor the production of PO (W as permanent modifier only and a vaporization temperature of 1900 °C) and it was feasible to determine P in the same biological solid samples in both ways, measuring either atomic P or PO. The detection limit for PO is a bit worse ($5 \mu\text{g g}^{-1}$ for AAS vs. $20 \mu\text{g g}^{-1}$ for MAS, which was obtained combining the signal achieved at 9 of the transitions that were simultaneously monitored), but the lifetime of the graphite parts can be significantly improved [51].

It has to be mentioned that the first article to report determination of P via quantification of PO by HR CS GFMS was published by Heitmann et al. [55]. In such paper the authors investigated various non-metals (Cl, F, P and S) and for P they did not need to use any chemical modifier for analysis of a digested reference material (rye flour). Still, other authors have preferred to determine P in atomic form, using Pd or Pd plus $\text{Mg}(\text{NO}_3)_2$ as modifiers, for analysis of digested biological materials [62] and biodiesel [63], respectively.

Finally, it is important to stress that the use of HR CS AAS instrumentation has opened new possibilities for the determination of P in air-acetylene flames as well, where formation of PO has been preferred [35, 64–66], while the monitoring of atomic P requires a nitrous-acetylene flame [66]. The complete spectrum of PO recorded with air-acetylene was published by Huang et al. [64], followed by a study of the main chemical interferences (Ca, Mg) and a proposal to correct for them (addition of Ti to form Ca or Mg titanates, which are more stable than the corresponding interfering phosphates) [65].

The main characteristics of all the methods discussed are summarized in Table 2.

Determination of sulfur

This is one of the elements for which the use of HR CS AAS instrumentation has clearly brought new possibilities. Even though it was already well-known that S could form diatomic molecules with different metals that absorb radiation in the UV–Vis [67, 68], most of the authors have preferred monitoring the molecule CS, which exhibits a rich rotational structure around 258.0 nm, belonging to the electronic transition $X^1\Sigma^+ \rightarrow A^1\Pi$, as shown in Fig. 7.

Use of graphite furnace as atomizer has demonstrated advantageous, permitting the direct analysis of solid samples (biological [42, 44, 69], plastics and metals [44] or coal [45, 70]) or of complex liquid samples (petroleum products [56]). However, careful optimization of the temperature program and addition of the optimum chemical modifier seems required, not only because sulfur can form volatile compounds that can be easily lost during the pyrolysis [56], but because a different analytical response can be observed for different sulfur species (e.g. organic versus inorganic sulfur [45]). As

can be seen from the summary presented in Table 3, most authors have opted for the addition of a permanent modifier (Ir, Ru, W or Zr) together with Pd (or Ca). But even the form in which Pd is added can play a relevant role in the results obtained, as addition of Pd in the form of nanoparticles (approx. 20 nm) has shown superior performance in terms of stabilization of species during pyrolysis, helping in providing a similar signal regardless of the chemical form in which sulfur species are originally found in the sample [44].

Besides this aspect, it is important to consider possible spectral overlaps when selecting a CS transition in this region, since various atomic lines appear (e.g., for Cr, Co or Fe [42, 44]), and that is one of the reasons why different authors opted for the use of either 257.958 nm [44], 258.033 nm [42] or 258.056 nm [55] as the main transition, although the combination of various of them can lead to a better LOD, as discussed in “General considerations for the determination of non-metals in furnaces and flames using MAS”, and even to a better precision [44, 55]. A more detailed discussion on the benefits of multi-line evaluation is presented elsewhere [11].

A recent work of Baumbach et al. [71] has investigated the monitoring of SnS as a way to quantify S, reporting better LODs than those obtained with CS, although the presence of Ni can result in interferences, which does not pose a serious threat for water samples, as evaluated in that work, but might be a factor for other samples. Finally, a recent work published by Jim et al. can also be mentioned, even though it has not been carried out with high-resolution CS AAS, but using a home-made lower-resolution continuum source AAS instrument. The authors performed S determination in coal using the slurry technique, and preferred the monitoring of a broad absorption band located between 200 and 210 nm, which is not attributed to a particular species, but it is suggested to be related with both C and S [72].

Several authors have also explored the possibilities of the flame as vaporizer for S quantitation. Most of them have also selected CS as the molecule to focus on. In fact, the first paper to report on monitoring of molecular species using HR CS AAS instrumentation was devoted to S determination in wine [21]. This article was later followed by a more general work where the complete CS (and SH) spectrum in an air-acetylene flame was shown [73], and possible interferences were evaluated (e.g., Pb, which led to lead sulfate formation, or Fe, which might overlap with some CS transitions). The need to use an extremely rich fuel flame was also emphasized, owing to the reactivity of CS with atomic oxygen. Finally, these authors demonstrated the potential of the HR CS FMAS technique to determine different sulfur species (free SO_2 , total SO_2 , bound SO_2 , total S, and sulfate) in wine, based on their different sensitivity, and also making use of the addition of various reagents (1 % HCl, iodine, 20 % HCl or nitrogen) [74].

Table 2 Applications reporting on P determination using HR CS AAS or HR CS MAS

Atomizer	Species monitored	Wavelength (nm)	Limit of detection/ characteristic mass or concentration	Modifier	Sample	Remarks	Reference
Graphite Furnace	PO	246.40	0.9 ng/4.4 ng		CRM IAEA-V-8 rye flour	No modifier needed	[55]
Graphite Furnace	P	213.617	Not available	NaF, La, Pd Pd + Ascorbic acid, Pd + Ca		Investigation of chemical modifiers for the determination of P by atomic absorption. Without the addition of a modifier no atomic P is formed and at this wavelength the absorption measured is due to PO, Pd alone or with Ca or ascorbic acid provide predominantly P atoms	[40]
Graphite Furnace	P	213.617	Not available	NaF		Study of atomization for P proposing a two-step mechanism. Use of LSBC to subtract reliably the molecular absorption due to PO	[59]
Graphite Furnace	P	213.618	Not available	NaF, La, Pd Pd + Ca		Systematic study of the artifacts created when monitoring P using LS-GFAAS and D ₂ background correction	[60]
Graphite Furnace	P PO	213.618 Σ 9 transitions in the vicinity of 213.561	4.9 μg g ⁻¹ /4.6 ng 20.8 μg g ⁻¹ /4.7 ng	Pd, Ascorbic acid, Pd + Ascorbic acid, W coating, W coating + Pd + Ascorbic acid	Biological CRMs	Direct solid sampling. Calibration with aqueous standards. Comparison of advantages a drawbacks when monitoring P or PO	[51]
Graphite Furnace	P	213.618	N.A./11 ng	NaF, Pd Pd + Ca		Systematic study of the potential of Zeeman-effect background correction to deal with PO structures	[61]
Graphite Furnace	P	213.614	0.5 μg g ⁻¹ /N.A.	Pd + Mg(NO ₃) ₂	Biodiesel sample	Importance of slow heating during the drying step. External calibration with organic P standard solutions	[63]
Graphite Furnace	P	213.618	0.06 μg g ⁻¹ /0.4 ng	Pd	Biological CRMs	Investigation of wall and platform atomization. Preconcentration procedure using ionic liquid assisted cloud point extraction	[62]
Flame	PO	246.40 247.78	Not available Not available		Cast iron CRMs	PO band heads systematically evaluated for the determination of P in an air-acetylene flame. Although 246.40 provides best sensitivity, 324.62 offers a better LOD owing to higher lamp intensity	[64]
Flame	PO	324.62 327.04	1.3 mg L ⁻¹ /N.A. Not available			Study of chemical interferences (Ca and Mg)	[65]
Flame	P PO	213.618 246.400	55 mg L ⁻¹ /140 mg L ⁻¹ 20 mg L ⁻¹ /128 mg L ⁻¹		Pine needles and super phosphate CRMs Liquid fertilizer and NIST 120c phosphate rock	Determination of atomic P requires a nitrous oxide-acetylene flame.	[66]

Table 2 (continued)

Atomizer	Species monitored	Wavelength (nm)	Limit of detection/ characteristic mass or concentration	Modifier	Sample	Remarks	Reference
	PO	247.620	17 mg L ⁻¹ /192 mg L ⁻¹			PO can be monitored in an air-acetylene flame	
	PO	247.780	12 mg L ⁻¹ /173 mg L ⁻¹				
	PO	324.616	18 mg L ⁻¹ /217 mg L ⁻¹				
	PO	327.040	20 mg L ⁻¹ /233 mg L ⁻¹				
Flame	PO	246.400	27.2 mg L ⁻¹ /211.3 mg L ⁻¹		Medicinal plants	Comparison of performance using different detector pixels and/or summing (Σ) the signal of three lines	[35]
	PO	247.620	16.4 mg L ⁻¹ /251.1 mg L ⁻¹				
	PO	247.780	39.3 mg L ⁻¹ /358.0 mg L ⁻¹				
			$\Sigma = 15.6 \text{ mg L}^{-1}/135 \text{ mg L}^{-1}$				

Virgilio et al. evaluated different CS and SH transitions for analysis of mineralized agricultural samples [75]. As already reported in [73], SH bands are much less sensitive. Kowalewska presented a thorough work discussing the problems associated with S determination in petroleum products using both HR CS GFMAS and HR CS FMAS, and succeeded in determining S in heavy oils and crude oil, but not in light petroleum products [56]. Other applications are summarized in Table 3.

Determination of halogens

The number of articles reporting on the determination of halogens depends very much on the halogen considered. In fact, most of the works published to date have been devoted to F. This can be explained to some extent taking into account that, while for most of non-metals it is only possible to achieve LODs at the low ng level when using HR CS GFMAS, for F LODs at the low pg level have been reported. In fact such LODs are more typical of AAS than of MAS, and may be difficult to match by means of alternative technique. Finally, as already discussed in “General considerations for the determination of non-metals in furnaces and flames using MAS”, F is the halogen that typically forms the strongest bonds with metals, such that its determination may be more selective.

As can be seen in Table 4, the preferred molecule to determine F by HR CS GFMAS seems to be GaF, owing to its good selectivity and robustness concerning interferences, as stated in the first article on this topic published by Heitmann et al. [55], a procedure that was further optimized later on [53, 76], since a relatively complex mixture of modifiers seems necessary for best performance when targeting this molecule. However, other possibilities have also been explored such as AlF [52, 77], CaF [78, 79] or SrF [80, 81]. Certainly, having such variety of choices is positive, because the reagent can be adapted to the sample. For instance, if a sample is very rich in Ca (e.g. milk [79]), it may be advisable to take advantage of this aspect and generate CaF, rather than suffering the competing interference from this element. Moreover, more simple temperature programs can be developed with AlF, CaF or SrF [52, 78, 80], because of the higher thermal stability of these compounds.

As discussed before, the LODs reported using F-based molecules are so competitive that even determination of a metal using HR CS GFMAS has been proposed. The article intended the determination of Al in blood samples, which may help in diagnose drowning. Al determination via AAS is complicated by spectral overlaps from Fe, hampering the use of the most sensitive Al lines. The formation of AlF and its quantification by HR CS GFMAS permitted direct determination of Al in the blood samples, still providing a satisfactory LOD for the application intended [52].

Table 3 Applications reporting on the determination of S by means of HR CS MAS

Atomizer	Species monitored	Wavelength (nm)	Limit of detection/ characteristic mass or concentration	Modifier	Sample	Remarks	Reference
Graphite Furnace	CS	258.056	2.3 ng/12 ng	Zr coating + Ca + methane	CRM NIST1570A Spinach and 1547 Peach leaves	Summation of various transitions to improve precision	[55]
Graphite Furnace	CS	258.033	15 ng/18 ng	W coating + Pd	Biological CRMs	Direct solid sampling. Calibration with aqueous standards prepared from thiourea	[42]
Graphite Furnace	CS	257.958 257.850	9 ng/14 ng	Ru coating + Pd nanoparticles	Polymer, steel, petroleum, coke and biological CRMs	Use of Pd nanoparticles permits an efficient stabilization of sulfur species during the pyrolysis and provides a normalized response for them. Direct solid sampling. Calibration with aqueous standards	[44]
Graphite Furnace	CS	257.864 257.908 258.033 258.056					
Graphite Furnace	CS	258.033	0.1 µg/N.A.	Ru coating	Coal samples	Direct solid sampling. Aqueous standards prepared with L-cysteine for calibration. Double peaks observed	[45]
Graphite Furnace	CS	258.056	3.5 ng/8.1 ng	Ir coating + Pd	Food samples	Direct solid sampling. Calibration with aqueous standards	[69]
Graphite Furnace	CS	257.592	0.15 mg L ⁻¹ /N.A.		Coal and ashes	Slurry sampling. Calibration with aqueous standards	[70]
Graphite Furnace	SnS	271.578	0.16 ng/N.A.	Zr coating	Water and CRMs of leaves and bushes	Measurements without platform	[71]
Graphite Furnace	CS	258.056	14 ng/12 ng	Pd + Mg in acetylacetonate	Fuel and crude oils	Comparative performance for light and heavy petroleum products	[56]
Flame	CS	258.056	18 mg kg ⁻¹ /104 mg kg ⁻¹		Wine	Different response for sulfite and sulfate observed. Oxidation to sulfate required for determination of total S	[21]
Flame	CS	258.056	Not available				
Flame	CS	257.593 257.959	4.4 mg L ⁻¹ /90 µg g ⁻¹ N.A./120 µg g ⁻¹		Cast iron CRMs	Study of the main CS transitions found in an air-acetylene flame. The need for a fuel-rich flame is emphasized	[73]
Flame	CS	258.056	2.4 mg L ⁻¹ /125 µg g ⁻¹		Wine	Determination of sulfur forms (free SO ₂ , total SO ₂ , bound SO ₂ , total S and sulfate)	[74]
Flame	CS	258.056	1.8 mg L ⁻¹ free SO ₂ /N.A.		Plant leaves	Comparison of the influence of different organic solvents	[98]
Flame	CS	257.961	14 mg L ⁻¹ /N.A.		Fungicides and fertilizers	Evaluation of the usefulness of molecular absorption of CS and SH for the determination of total S. Monitoring of CS leads to significantly lower LOD	[75]
Flame	CS	257.595 257.958	13.4 mg L ⁻¹ /393.9 mg L ⁻¹ 22.5 mg L ⁻¹ /412.5 mg L ⁻¹				
Flame	SH	258.056	30.0 mg L ⁻¹ /400.3 mg L ⁻¹				
Flame	CS	323.658 324.064	2.80 g L ⁻¹ /10.8 g L ⁻¹ 1.70 g L ⁻¹ /13.1 g L ⁻¹				
Flame	CS	327.990	0.78 g L ⁻¹ /5.17 g L ⁻¹				
Flame	CS	258.056	0.01 %(w/w)/N.A.		Coal samples	Study of calibrants among sulfuric acid, sodium sulfide, sodium thiosulfate and ammonium sulfate. The most appropriate calibrant was H ₂ SO ₄	[99]
Flame	CS	257.595	38.7 mg L ⁻¹ /636.3 mg L ⁻¹		Medicinal plants	Comparison of performance using different detector pixels and/or summing (Σ) the signal of the two lines	[35]
Flame	CS	257.958	54.9 mg L ⁻¹ /1006.2 mg L ⁻¹ Σ = 31.2 mg L ⁻¹ /416.3 mg L ⁻¹				

Table 4 Applications reporting on the determination of halogens by means of HR CS MAS

Atomizer	Species monitored	Wavelength (nm)	Limit of detection/characteristic mass or concentration	Modifier	Sample	Remarks	Reference
Graphite Furnace	GaF	211.248	9 pg/13 pg	Zr coating + Mg	CRM BCR109 (Zinc ore)	Recommends GaF over AlF because of narrower profile and freedom from spectral overlaps	[55]
Graphite Furnace	GaF	211.248	5.2 pg/7.4 pg	Zr coating + Pd + Zr + NaAc + Ru(III) nitrosyl nitrate	BCR274 (single cell protein) Drinking and mineral water	Modifier Pd/Zr thermally pretreated before each sample introduction together with the Ga reagent at 1100 °C NaAc + Ru(III) nitrosyl nitrate as additional modifiers plus more Ga are injected with the sample after cooling down	[53]
Graphite Furnace	GaF	211.248	5.2 pg/N.A.	Zr coating + Pd + Zr + NH ₄ H ₂ PO ₄	Toothpaste	Modifier Pd/Zr thermally pretreated before each sample introduction together with Ga at 1100 °C Cool down step, addition of sample plus Ga and NH ₄ H ₂ PO ₄ Use of LSBC to subtract PO bands from the GaF spectrum	[76]
Graphite Furnace	CaF	606.440	1.6 ng/2.5 ng		Tea	Ca acts both as molecule forming reagent and chemical modifier, so no other reagent has to be added Ca has a negative influence on graphite tube lifetime compared with Ca	[78]
Graphite Furnace	AlF	227.477	1.8 µg L ⁻¹ Al/N.A.	NH ₄ F.HF	Blood	Addition of NH ₄ F.HF, required for promotion of AlF molecule, was found to also improve sample matrix removal for whole blood samples Use of aqueous standards for calibration	[52]
Graphite Furnace	SrF	651.187	0.36 ng/0.55 ng		Water	Sr acts both as molecule forming reagent and as chemical modifier	[80]
Graphite Furnace	GaF	211.248	33 pg/N.A.	Zr coating + Ca	Cancer cells	Determination of F containing in the drug 5-fluorouracil GaF and PO signals can be separated in time	[84]
Graphite Furnace	AlF	227.46	145 pg/13 pg	Ba	Etching solutions of silicon wafers	Best results obtained when the reagent is pre-dried before both sample and modifier are added to the furnace	[77]
Graphite Furnace	GaF	211.248	4 pg/N.A.	Zr coating + Pd/Zr/Mg + CH ₃ COONa	Novel fluorinated compounds environmental and biological	F speciation using HPLC coupled off-line to HR-CS GFMAS	[82]
Graphite Furnace	GaF	211.248	Not available	Zr coating + Pd/Zr/Mg + CH ₃ COONa	Novel fluoro compounds in microorganisms	F speciation using HPLC coupled off-line to HR-CS GFMAS	[83]
Graphite Furnace	SrF	651.187	Not available			Investigation of the mechanism of SrF molecule formation	[81]
Graphite Furnace	CaF	606.440	0.26 ng/0.13 ng	Zr coating	Milk and waste water CRM	Calibration by means of the standard addition method	[79]
Flame	GaF	211.248	1 mg L ⁻¹ /N.A.		BCR33 (Super-phosphate)	GaF band heads systematically evaluated for F determination in air-acetylene flame	[46]
Flame	AlF	227.461	5.5 mg L ⁻¹ /72.8 mg L ⁻¹		Toothpaste and waste water	Measurement of the AlF molecular absorption generated in an C ₂ H ₂ /N ₂ O flame	[48]
Graphite Furnace	AlCl	261.42	70 pg/300 pg	Sr	IAEA-V-8 (Rye flour) CRM	AlCl selected over InCl owing to higher bond strength and narrower, clearly isolated band heads	[55]
Graphite Furnace	AlCl	261.418	1.2 ng/N.A.	Al + Ag + Sr	Bovine muscle and Milk powder	Spectral interference due to the use of the modifier was corrected by LSBC Ag	[86]

Table 4 (continued)

Atomizer	Species monitored	Wavelength (nm)	Limit of detection/characteristic mass or concentration	Modifier	Sample	Remarks	Reference
Flame	InCl	267.24	3 mg L ⁻¹ /N.A.		BCR151 (Milk powder), HISS-1 and PACS-2 (Marine sediments) Salt and pharmaceutical product	added prior to sample digestion to avoid Cl losses Owing to significant chemical interferences, the method of standard additions should be used for calibration Comparison of the performance obtained with AlBr and CaBr: CaBr absorption is affected by Cl, Al, K and Na ions, while only inorganic acids affect the absorption of AlBr	[47]
Graphite Furnace	AlBr CaBr	278.914 625.315	2 ng/N.A. 2 ng/N.A.			Evaluation of the linear range obtained with different CaBr transitions that are simultaneously monitored Best performance obtained without platform	[87]
Graphite Furnace	CaBr	625.315	78 pg/N.A.	Zr coating + Pd + Mg	Polybrominated flame retardants	Direct solid sampling Use of aqueous standards for calibration Using various CaBr transitions it is possible to improve the LOD and expand linearity	[54]
Graphite Furnace	CaBr	625.315 625.223 625.135 625.058	5.4 ng/1.32 ng 7.3 ng/1.77 ng 12.7 ng/2.42 ng 18.2 ng/3.00 ng	Pd	Plastic CRMs materials	Study of the molecular absorption spectra of the diatomic molecules AlI, GaI, InI, TlI, MgI, CaI, SrI and BaI Similar sensitivity for different I-containing species observed when monitoring BaI and no additional modifier is needed	[43]
Graphite Furnace	BaI BaI BaI BaI BaI BaI BaI BaI BaI BaI	538.308 538.139 537.972 537.804 537.638 561.127 560.950 560.772 560.595 560.421	0.6 ng/1.0 ng N.A./1.3 ng N.A./1.6 ng N.A./2.1 ng N.A./2.8 ng N.A./1.4 ng N.A./1.6 ng N.A./2.0 ng N.A./2.5 ng N.A./3.0 ng		Thyroid hormone pills		[88]

Table 5 Applications reporting on the determination of N-containing species by HR CS MAS

Atomizer	Species monitored/Analyte	Wavelength (nm)	Limit of detection/characteristic mass or concentration	Modifier	Sample	Remarks	Reference
Flame	NO/Nitrate	215.360				Study of the molecular absorption of NO produced by HNO ₃	
Graphite Furnace	NO/Nitrate	214.526	N.A./10 pg N	Ca	Water CRMs and a nitrate fertilizer CRM	Different sensitivities for nitrite and nitrate observed. The method is also applicable to the determination of nitrite after oxidation to nitrate	[90]
		214.587	N.A./10 pg N				
		214.744	N.A./8 pg N				
		214.904	N.A./7 pg N				
		215.195	N.A./11 pg N				
Graphite Furnace	NO/Nitric acid	215.360	5 ng N/7 pg N		Etching solutions of silicon wafers	Addition of La necessary to avoid losses during drying in acidic medium	[77]
		214.803	96 ng NO ₃ ⁻ /20 ng NO ₃ ⁻	La			
Quartz cell	NO/Nitrite	215.360	0.045 µg mL ⁻¹ NO ₂ /N.A.		Water samples	NO is generated by the reduction of nitrite in acidic media with ascorbic acid and then transferred to the quartz cell with Ar	[91]
						Measurement of signal peak height	

Another noteworthy type of application has been reported recently, using HR CS GFMS for off-line detection and quantification of novel fluorine containing compounds, after HPLC separation [82, 83]. The compounds are also monitored in parallel with electrospray ionization mass spectrometry to obtain structural information as well. Traditionally, this type of speciation study is best carried out using techniques that can work on-line, such as inductively coupled plasma mass spectrometry. However, the high ionization potential of F (higher than that of Ar) hampers the use of such technique. Thus, HR CS GFMS appears as one of the few sensitive and fluorine-specific technique suitable for these studies.

Other applications of HR CS GFMS for F determination include analysis of toothpaste [76], tea [78], water [80], cancer cells containing a fluorinated drug [84], etching solutions from the photovoltaic industry [77] and milk [79]. It could be mentioned that no application reporting on direct solid sampling analysis of F has been published yet, except for one article that did not use a HR CS device, but a line source instrument [41].

On the other hand, the number of articles to date devoted to monitoring of F by HR CS FMAS is very limited. Huang et al. explored the main bands of GaF in an air/acetylene flame [46], while Ozbek and Akman explored the monitoring of AlF in a nitrous oxide/acetylene flame [48].

As for the rest of the halogens, the number of articles focused on them is significantly lower. This aspect is normal, to some extent, for elements for which competing techniques exist (e.g. I can be detected with high sensitivity by means of inductively coupled plasma mass spectrometry [85]). However, the situation is a bit surprising for Cl, since this is an important element that may show difficulties for its determination at trace levels by means of other techniques. Yet there are only three articles investigating the use of HR CS MAS for this element: one based on work with flame [47] exploring InCl bands, and the remaining ones with GF focused on AlCl [55, 86]. Moreover, while the strength of Cl bonds with metals is not as high as those of F, they are still high enough, in fact above the suggested optimum value of 500 kJ mol⁻¹ in the case of AlCl [7]. This limited number of successful works may indicate that some problems have arisen when attempting Cl determination by means of HR CS MAS in other samples, probably due to chemical interferences. A more systematic research on the different options available for Cl determination by MAS seems to be required.

Regarding Br, three articles on this element using HR CS GFMS have been published so far. In the first article, Huang et al. compared the performance of CaBr and AlBr and found both systems suitable and capable of providing a similar sensitivity, and in fact they are complementary as they seem to be affected by potential interferences in a different way [87]. Later works have focused on the monitoring of CaBr. Since several transitions of various sensitivity are found for

this molecule (see Fig. 6b), it is possible to obtain a wide linear range (up to five orders of magnitude, from 100 pg to 10 µg) [54]. Moreover, using this strategy of monitoring CaBr, a fast and simple approach permitting the direct determination of Br in solid plastic materials by HR CS GFMS has been developed, which may be of relevance according to current regulations on control of organobrominated compounds in polymers (e.g., 2002/95/EC directive) [43].

Finally, for I, different diatomic molecules were investigated by Huang et al. using HR CS GFMS, but the most promising results were obtained when monitoring BaI [88], which shows enough stability to avoid the addition of any chemical modifier. No further work has reported results on this element.

Determination of N-containing species

The determination of some nitrogen-containing species has proven feasible as well. The applications reported so far are collected in Table 5. Huang et al. used HR CS FMAS (a prototype that permits the simultaneous monitoring of a large spectral region, from 200 nm to 465 nm [89]) to evaluate the main NO band heads, in order to focus in the most sensitive area for the determination of nitrate by means of HR CS GFMS [90]. Best sensitivity was reported at 215.360 nm, even though information of other similar transitions is provided as well. The authors point to the volatility of N-based species as both a problem (losses may occur for pyrolysis temperatures over 150 °C in acidic medium) and as an advantage (a vaporization of only 700 °C is required, thus ensuring a long lifetime for graphite components). Moreover, a different sensitivity for nitrite (25 % of that of nitrate) is reported, hinting at potential for the development of a speciation method. Accurate values for the nitrate determination in water samples and in a fertilizer (calcium ammonium nitrate) were presented, while noting that ammonia does not produce NO, so it does not interfere during analysis of the fertilizer.

Determination of nitric acid in etching solutions of the photovoltaic industry using HR CS GFMS has been demonstrated [77], using a slightly different transition (214.803 nm). In this work, addition of La to stabilize the analyte during the drying step is proposed, since the sample is very acidic.

Finally, a method for the determination of nitrite has been published. In such approach, the analyte is reduced in acidic media with ascorbic acid and then transferred by a stream of Ar into a quartz cell, where NO is monitored by HR CS MAS using the 215.360 nm transition. Different water samples were successfully analyzed using this approach [91].

Conclusions

Use of HR CS AAS provides very relevant advantages for the accurate quantification of metalloids, even in the presence of

potentially overlapping molecular structures. Furthermore, this type of instrumentation has brought new possibilities for the quantification of molecular spectra, allowing for the direct monitoring of several non-metals (P, S, F, Cl, Br, I and N-containing species), which could be determined only with great difficulties with line source-AAS devices, if at all.

Despite these improvements, still more work seems to be needed in HR CS MAS since the number of diatomic species investigated is relatively limited and the chemical modifiers used so far are relatively conventional (e.g., a permanent modifier plus Pd). Furthermore, the potential of the technique for speciation studies has only been hinted at, and thus more work in this area can be anticipated.

Acknowledgments This work has been funded by the Spanish Ministry of Economy and Competitiveness (project CTQ2012-33494) and the Aragón Government (Fondo Social Europeo). MRF thanks the Spanish Ministry of Economy and Competitiveness for her PhD grant (project CTQ2009-08606).

References

- McGregor DA, Cull KB, Gehlhausen JM, Viscomi AS, Wu M, Zhang L, Camahan JW (1988) *Anal Chem* 60:1089A–1098A
- Mello PA, Barin JS, Duarte FA, Bizzi CA, Diehl LO, Muller EI, Flores EMM (2013) *Anal Bioanal Chem* 405:7615–7642
- Kirkbright GF, Johnson HN (1973) *Talanta* 20:433–451
- Tsunoda K, Fujiwara K, Fuwa K (1978) *Anal Chem* 50:861–865
- Tsunoda K, Haraguchi H, Fuwa K (1980) *Spectrochim Acta B* 35:715–729
- Dittrich K, Vorberg B, Funk J, Beyer V (1984) *Spectrochim Acta B* 39:349–363
- Welz B, Lepri FG, Araujo RGO, Ferreira SLC, Huang MD, Okruss M, Becker-Ross H (2009) *Anal Chim Acta* 647:137–148
- Welz B, Becker-Ross H, Florek S, Heitmann U (2005) *High-Resolution Continuum Source AAS. The Better Way to Do Atomic Absorption Spectrometry*. Wiley-VCH, Weinheim
- Welz B, Morés S, Carasek E, Vale MGR, Okruss M, Becker-Ross H (2010) *Appl Spectrosc Rev* 45:327–354
- Resano M, García-Ruiz E (2011) *Anal Bioanal Chem* 399:323–330
- Resano M, Flórez MR, García-Ruiz E (2013) *Spectrochim Acta B* 88:85–97
- Keliher PN, Wohlers CC (1974) *Anal Chem* 46:682–687
- Zander AT, O'Haver TC, Keliher PN (1976) *Anal Chem* 48:1166–1175
- Jones BT, Smith BW, Winefordner JD (1989) *Anal Chem* 61:1670–1674
- Harnly JM (1996) *Fresenius J Anal Chem* 355:501–509
- Harnly JM (1999) *J Anal At Spectrom* 14:137–146
- Becker-Ross H, Florek S, Heitmann U, Weisse R (1996) *Fresenius J Anal Chem* 355:300–303
- Becker-Ross H, Florek SV (1997) *Spectrochim Acta B* 52:1367–1375
- Becker-Ross H, Florek S, Heitmann U (2000) *J Anal At Spectrom* 15:137–141
- Resano M, Rello L, Flórez M, Belarra MA (2011) *Spectrochim Acta B* 66:321–328
- Huang MD, Becker-Ross H, Florek S, Heitmann U, Okruss M (2005) *Anal Bioanal Chem* 382:1877–1881
- Butcher DJ (2013) *Molecular absorption spectrometry in flames and furnaces: A review*. *Anal Chim Acta* 804:1–15

23. Masterton WL, Slowinski EJ, Stanitski CL (1985) *Chemical Principles*, 6th edn. Saunders College Publishing, Philadelphia
24. Resano M, Briceño J, Aramendía M, Belarra MA (2007) *Anal Chim Acta* 582:214–222
25. Resano M, Aramendía M, Volynsky AB, Belarra MA (2004) *Spectrochim Acta B* 59:523–531
26. Welz B, Sperling M (1999) *Atomic Absorption Spectrometry*, 3rd edn. Wiley-VCH, Weinheim
27. Resano M, Bolea-Fernández E, Mozas E, Flórez MR, Grinberg P, Sturgeon RE (2013) *J Anal At Spectrom* 28:657–665
28. Gallindo Borges DL, Furtado da Silva A, Welz B, Curtius AJ, Heitmann U (2006) *J Anal At Spectrom* 21:763–769
29. Resano M, Briceño J, Belarra MA (2009) *Spectrochim Acta B* 64: 520–529
30. Araujo RGO, Welz B, Vignola F, Becker-Ross H (2009) *Talanta* 80: 846–852
31. Araujo RGO, Welz B, Castilho INB, Vale MGR, Smichowski P, Ferreira SLC, Becker-Ross H (2010) *J Anal At Spectrom* 25:580–584
32. Raposo JL Jr, Oliveira SR, Gomes Neto JA, Nóbrega JA, Jones BT (2011) *Anal Lett* 44:2150–2161
33. Wilsche H, Prattes K, Zischka M, Knapp G (2009) *Spectrochim Acta B* 64:341–346
34. Heitmann U, Welz B, Borges DLG, Lepri FG (2007) *Spectrochim Acta B* 62:1222–1230
35. Bechlin MA, Gomes Neto JA, Nóbrega JA (2013) *Microchem J* 109: 134–138
36. Huang MD, Becker-Ross H, Okruss M, Geisler S, Florek S (2012) *J Anal At Spectrom* 27:982–988
37. Bernejo-Barrera P, Aboal-Somoza M, Bernejo-Barrera A (1999) *J Anal At Spectrom* 14:1009–1018
38. L'vov BV, Khartsyzov AD (1969) *Zh Prikl Spektrosk* 10:413
39. Resano M, Belarra MA, Castillo JR, Vanhaecke F (2000) *J Anal At Spectrom* 15:1383–1388
40. Lepri FG, Dessuy MB, Vale MGR, Borges DLG, Welz B, Heitmann U (2006) *Spectrochim Acta B* 61:934–944
41. de Moraes Flores EL, Barin JS, de Moraes Flores EM, Dressler VL (2007) *Spectrochim Acta B* 62:918–923
42. Ferreira HS, Lepri FG, Welz B, Carasek E, Huang MD (2010) *J Anal At Spectrom* 25:1039–1045
43. Flórez MR, Resano M (2013) *Spectrochim Acta B* 88:32–39
44. Resano M, Flórez MR (2012) *J Anal At Spectrom* 27:401–412
45. Mior R, Morés S, Welz B, Carasek E, de Andrade JB (2013) *Talanta* 106:368–374
46. Huang MD, Becker-Ross H, Florek S, Heitmann U, Okruss M (2006) *Spectrochim Acta B* 61:572–578
47. Huang MD, Becker-Ross H, Florek S, Heitmann U, Okruss M (2006) *Spectrochim Acta B* 61:959–964
48. Ozbek N, Akman S (2012) *Talanta* 94:246–250
49. Resano M, Vanhaecke F, de Loos-Vollebregt MTC (2008) *J Anal At Spectrom* 23:1450–1475
50. Aramendía M, Resano M, Vanhaecke F (2009) *Anal Chim Acta* 648: 23–44
51. Resano M, Briceño J, Belarra MA (2009) *J Anal At Spectrom* 24: 1343–1354
52. Aramendía M, Flórez MR, Piette M, Vanhaecke F, Resano M (2011) *J Anal At Spectrom* 26:1964–1973
53. Gleisner H, Welz B, Einax JW (2010) *Spectrochim Acta B* 65:864–869
54. Limburg T, Einax JW (2013) *Microchem J* 107:31–36
55. Heitmann U, Becker-Ross H, Florek S, Huang MD, Okruss M (2006) *J Anal At Spectrom* 21:1314–1320
56. Kowalewska Z (2011) *Spectrochim Acta B* 66:546–556
57. López-García I, Viñas P, Romero-Romero R, Hernández-Córdoba M (2007) *Spectrochim Acta B* 62:48–55
58. Curtius AJ, Schlemmer G, Welz B (1987) *J Anal At Spectrom* 2:115–124
59. Dessuy MB, Vale MGR, Lepri FG, Welz B, Heitmann U (2007) *Spectrochim Acta B* 62:429–434
60. Dessuy MB, Vale MGR, Lepri FG, Borges DLG, Welz B, Silva MM, Heitmann U (2008) *Spectrochim Acta B* 63:337–348
61. Lepri FG, Welz B, Dessuy MB, Vale MGR, Bohrer D, de Loos-Vollebregt MTC, Huang MD, Becker-Ross H (2010) *Spectrochim Acta B* 65:24–32
62. Kumar SJ, Meeravali NN, Manjusha R (2013) *J Anal At Spectrom* 28:585–592
63. de Campos RC, Correia CLT, Vieira F, Saint'Pierre TD, Oliveira AC, Gonçalves R (2011) *Spectrochim Acta B* 66:352–355
64. Huang MD, Becker-Ross H, Florek S, Heitmann U, Okruss M (2006) *J Anal At Spectrom* 21:338–345
65. Huang MD, Becker-Ross H, Florek S, Heitmann U, Okruss M (2006) *J Anal At Spectrom* 21:346–349
66. Ferreira RB, Oliveira SR, Franzini VP, Virgilio A, Raposo JL Jr, Gomes Neto JA (2011) *Atom Spectrosc* 32:56–61
67. Parvinen P, Lajunen LHJ (1994) *Anal Chim Acta* 295:205–210
68. DA K, Lemme M, Tittarelli P (2004) *Spectrochim Acta B* 59:101–114
69. Ozbek N, Akman S (2013) *J Agric Food Chem* 61:4816–4821
70. Nakadi FV, Rosa LR, da Veiga MAMS (2013) *Spectrochim Acta B* 88:80–84
71. Baumbach G, Limburg T, Einax JW (2013) *Microchem J* 106:295–299
72. Jim G, Katskov D, Tittarelli P (2011) *Talanta* 83:1687–1694
73. Huang MD, Becker-Ross H, Florek S, Heitmann U, Okruss M (2006) *Spectrochim Acta B* 61:181–188
74. Huang MD, Becker-Ross H, Florek S, Heitmann U, Okruss M, Patz CD (2008) *Anal Bioanal Chem* 390:361–367
75. Virgilio A, Raposo JL Jr, Cardoso AA, Nóbrega JA, Gomes Neto JA (2011) *J Agric Food Chem* 59:2197–2201
76. Gleisner H, Einax JW, Morés S, Welz B, Carasek E (2011) *J Pharm Biomed Anal* 54:1040–1046
77. Bücker S, Acker J (2012) *Talanta* 94:335–341
78. Morés S, Monteiro GC, da Silva SF, Carasek E, Welz B (2011) *Talanta* 85:2681–2685
79. Ozbek N, Akman S (2013) *Food Chem* 138:650–654
80. Ozbek N, Akman S (2012) *Spectrochim Acta B* 69:32–37
81. Ozbek N, Akman S (2013) *Anal Sci* 29:741–746
82. Qin Z, McNee D, Gleisner H, Raab A, Kyeremeh K, Jaspars M, Krupp E, Deng H, Feldmann J (2012) *Anal Chem* 84:6213–6219
83. Qin Z, Raab A, Krupp E, Deng H, Feldmann J (2013) *J Anal At Spectrom* 28:877–882
84. Krüger M, Huang MD, Becker-Ross H, Florek S, Ott I, Gust R (2012) *Spectrochim Acta B* 69:50–55
85. Resano M, Garcia-Ruiz E, Moens L, Vanhaecke F (2005) *J Anal At Spectrom* 20:81–87
86. Fechetia M, Tognon AL, da Veiga MAMS (2012) *Spectrochim Acta B* 71–72:98–101
87. Huang MD, Becker-Ross H, Florek S, Heitmann U, Okruss M (2008) *Spectrochim Acta B* 63:566–570
88. Huang MD, Becker-Ross H, Florek S, Okruss M, Welz B, Morés S (2009) *Spectrochim Acta B* 64:697–701
89. Becker-Ross H, Okruss M, Florek S, Heitmann U, Huang MD (2002) *Spectrochim Acta B* 57:1493–1504
90. Huang MD, Becker-Ross H, Florek S, Heitmann U, Okruss M, Welz B, Ferreira HS (2010) *J Anal At Spectrom* 25:163–168
91. Brandao GC, Lima DC, Ferreira SLC (2012) *Talanta* 98:231–235
92. Krawczyk M (2014) *J Pharm Biomed Anal* 88:377–384
93. Dessuy MB, de Jesus RM, Brandao GC, Ferreira SLC, Vale MGR, Welz B (2013) *Food Addit Contam A* 30:202–207
94. Shaltout AA, Welz B, Castilho INB (2013) *Atmos Environ* 81:18–24

95. Tavares Duarte A, Dessuy MB, Vale MGR, Welz B (2013) Determination of chromium and antimony in polymers from electrical and electronic equipment using high-resolution continuum source graphite furnace atomic absorption spectrometry. *Anal Methods* 5: 6941–6946
96. Amorim Filho VR, Gomes Neto JA (2009) *Anal Sci* 25:95–100
97. de Oliveira LCC, Vieira MA, Ribeiro AS, Lisboa MT, Gonçalves RA, de Campos RC (2012) *Energy Fuels* 26:7041–7044
98. Wang Y, Li JX (2009) *Spectrosc Spectr Anal* 29:1418–1421
99. Baysal A, Akman S (2011) *Talanta* 85:2662–2665



Contents lists available at ScienceDirect

Spectrochimica Acta Part B

journal homepage: www.elsevier.com/locate/sab

On the possibilities of high-resolution continuum source graphite furnace atomic absorption spectrometry for the simultaneous or sequential monitoring of multiple atomic lines

M. Resano ^{a,*}, L. Rello ^{a,b}, M. Flórez ^a, M.A. Belarra ^a

^a Department of Analytical Chemistry, University of Zaragoza, Pedro Cerbuna 12, 50009 Zaragoza, Spain

^b Department of Clinical Biochemistry, "Miguel Servet" University Hospital, Paseo Isabel La Católica 1–3, 50009 Zaragoza, Spain

ARTICLE INFO

Article history:

Received 29 December 2010

Accepted 24 March 2011

Available online 2 April 2011

Keywords:

Solid sampling

High-resolution continuum source graphite furnace atomic absorption spectrometry

Multi-element analysis

Internal standardization

Monitoring of multiplets

ABSTRACT

This paper explores the potential of commercially available high-resolution continuum source graphite furnace atomic absorption spectrometry instrumentation for the simultaneous or sequential monitoring of various atomic lines, in an attempt to highlight the analytical advantages that can be derived from this strategy. In particular, it is demonstrated how i) the monitoring of multiplets may allow for the simple expansion of the linear range, as shown for the measurement of Ni using the triplet located in the vicinity of 234.6 nm; ii) the use of a suitable internal standard may permit improving the precision and help in correcting for matrix-effects, as proved for the monitoring of Ni in different biological samples; iii) direct and multi-element analysis of solid samples may be feasible on some occasions, either by monitoring various atomic lines that are sufficiently close (truly simultaneous monitoring, as demonstrated in the determination of Co, Fe and Ni in NIST 1566a Oyster tissue) or, alternatively, by opting for a selective and sequential atomization of the elements of interest during every single replicate. Determination of Cd and Ni in BCR 679 White cabbage is attempted using both approaches, which permits confirming that both methods can offer very similar and satisfactory results. However, it is important to stress that the second approach provides more flexibility, since analysis is no longer limited to those elements that show very close atomic lines (closer than 0.3 nm in the ultraviolet region) with a sensitivity ratio similar to the concentration ratio of the analytes in the samples investigated.

© 2011 Elsevier B.V. All rights reserved.

1. Introduction

The recent commercial release of high-resolution continuum source atomic absorption spectrometers (HR CS AAS) represents a revolution in this field, in particular when aiming at the direct analysis of complex samples. This type of instrumentation, based on the prototype developed by Becker-Ross and co-workers [1,2], brings about very significant improvements in comparison with traditional line source devices. The main advantages of HR CS AAS can be summarized as follows [3]:

- (a) Improved signal stability. The array detector used in the device commercially available permits the simultaneous monitoring of two hundred "wavelength sectors" (pixels), enabling efficient correction for many unwanted spectroscopical events (e.g., lamp flicker noise, temporal changes in the transmittance of the gas phase, etc.). This aspect, in combination with the higher radiation intensity of the Xe lamp compared with that of

traditional line sources, makes it feasible to obtain better-defined signals at lower analyte levels, and results in better limits of detections (a factor of 3 to 5).

- (b) Superior background correction potential. This technique allows monitoring the spectral neighborhood of the analyte lines, thus permitting to detect potential interferences. In the case that these interferences cannot be resolved in time (by optimization of the temperature program combined with the use of chemical modifiers), the technique still offers a considerably superior approach for the mathematical correction of complex, high and even rapidly changing backgrounds, since they are monitored simultaneously with the atomic absorption lines [1,4–7].
- (c) Expanded linear range. It is possible to decrease the sensitivity and therefore expand the working range by measuring the absorbance at the wings of absorption lines [8,9].
- (d) Potential to monitor molecular lines. This fact opens the doors to determine relatively low levels of non-metals, such as Cl, F, P or S, for which using narrow molecular absorption "lines" may be an appealing alternative since the most sensitive atomic lines for these elements are situated in the far UV region, which is not accessible for line source AAS instrumentation [10,11].

* Corresponding author. Tel.: +34 976761634; fax: +34 976761290.
E-mail address: mresano@unizar.es (M. Resano).

- (e) Only one lamp source is needed. Self-evidently, this is an important practical advantage, as traditional line source AAS required the acquisition of many lamps, some of which were often seldom used.

It is necessary to say that there are still some traditional disadvantages of the technique that persists (e.g., difficulties in achieving good sensitivity for refractory analytes and memory effects when using a graphite furnace atomizer), but, overall, the development of HR CS instrumentation represents a significant step forward for AAS. However, despite of these important advantages, there is one aspect notoriously lacking in the previous discussion. That is the potential for multi-element analysis. Obviously, this aspect can be considered as one of the driving forces behind the development of continuum source-based AAS. However, despite of the promising characteristics of the HR CS AAS technique, it seems that the currently available detectors do not permit to easily implement this important characteristic in an AAS instrument, as discussed in various reviews [12–15]. The instrumentation currently available features a detector with 588 pixels, but only 200 of those pixels are used for analytical purposes (the rest are used for internal corrections). This instrument provides exceptional resolution, and every one of those pixels monitors a range of only 1 to 2 pm, but that also means that such instrument only allows for the simultaneous monitoring of much less than 1 nm of spectrum (0.2–0.3 nm in the UV region and up to 0.5 nm in the visible region). This bandwidth is very narrow, which seriously limits the potential for simultaneous multi-elemental analysis with graphite furnace AAS (GFAAS). It has to be mentioned that this limitation is not very relevant for flame AAS, since multi-elemental analysis based on a fast sequential operation mode can be more easily performed with this technique.

Despite this important limitation, Welz and co-workers have succeeded in developing some applications in which two elements were determined simultaneously using GFAAS [16–20], which represents an obvious improvement in comparison with typical line source AAS possibilities. Moreover, in addition to multi-element analysis, there are other aspects of analytical interests that the use of HR CS AAS makes possible, such as the use of an internal standard or the individual monitoring of all the lines available in multiplets that, to the best of the authors' knowledge, have not been systematically investigated.

This work aims at evaluating the performance of commercially available HR CS AAS instrumentation for the simultaneous or sequential monitoring of multiple lines, in an attempt to obtain analytical improvements such as an extended linear range, a mean to correct for matrix-effects, to improve precision or to obtain multi-element information. The work will emphasize these aspects in the context of direct analysis of solid samples and complex materials and will focus on GFAAS, owing to its superior potential to perform in such a context [21–24].

2. Experimental

2.1. Apparatus

All the experiments in this work were carried out using a HR CS AAS, ContrAA 700, commercially available from Analytik Jena AG (Jena, Germany) and equipped with both graphite furnace and flame atomizers. The optical system comprises a xenon short-arc lamp (GLE, Berlin, Germany) operating in "hot-spot" mode as the radiation source, a high-resolution double echelle monochromator (DEMON) and a linear CCD array detector with 588 pixels, 200 of which are used for analytical purposes (monitoring of the analytical signal and BG correction), while the rest are used for internal functions, such as correcting for fluctuations in the lamp intensity. More details on this type of instrumentation can be found elsewhere [2].

The HR CS AAS instrument is equipped with a transversely heated graphite tube atomizer and both solid sampling and liquid sampling autosamplers. The solid sampling device (SSA 600) incorporates a microbalance with a readability of 1 μg [24]. Pyrolytic graphite tubes were used in all experiments. Solid samples were introduced using solid sampling graphite platforms.

2.2. Standard solutions and reagents

Purified water was obtained from a Milli-Q system (Millipore, Billerica, USA). Ag, Cd, Co, Ni, Fe, and Pd solutions were prepared daily by diluting a commercially available 1 g L^{-1} standards (Merck, Darmstadt, Germany).

2.3. Samples

Two biological reference materials produced by NIST (National Institute of Standards and Technology, Gaithersburg, USA) and BCR (Community Bureau of Reference, Geel, Belgium) were analyzed in this work. The materials investigated were: SRM 1566a Oyster tissue from NIST and CRM 679 White cabbage from BCR. Both were available as powders.

Blood and urine standards of known Ni contents were prepared by addition of suitable quantities of Ni solution to Ni-free (meaning that the Ni level was below the LOD of the standard GFAAS method) venous blood samples and urine samples.

2.4. Procedure for solid sampling HR CS GFAAS analysis

Samples were directly analyzed without any prior preparation step. The solid sampling device used allows for automatic weighing and transporting of the samples into the furnace [25]. The empty platform was first transported to the microbalance using a pair of tweezers. After taring, an appropriate amount of sample was placed on the platform and weighed. The corresponding amount of chemical modifier, if needed, was added afterwards. Finally, the platform was transferred into the graphite furnace and subsequently subjected to the temperature program. All these operations were fully controlled from the computer, except for the deposition of the sample and the modifier solutions onto the platform, which was carried out manually.

The operating conditions are summarized in the Tables shown in Section 3.3. Integrated absorbance was selected as the measurement mode in all cases. For every line evaluated, the values obtained for three detector pixels (the central pixel plus the adjacent ones, $\text{CP} \pm 1$), were summed.

The calibration was performed using 10 μL of an aqueous solution of the appropriate concentration added with a micropipette, together with the modifier solutions if needed, onto the sampling platform. Five replicate measurements (representing approximately 15–20 min of work) were carried out for each determination and the median was taken as the representative value, in order to minimize the possible influence of outliers [26].

3. Results and discussion

3.1. Benefits derived from the monitoring of multiplets

One of the main obvious advantages of HR CS AAS is that all absorption lines of all elements that fall within the spectral range of the spectrometer (from 190 to 900 nm) are accessible. Moreover, the radiation intensity of the continuum source used in this device is, on average, about two orders of magnitude higher than that of the narrow emission lines of a hollow cathode lamp over that spectral range. [27]. In the words of Welz et al., "this means that there are no more "weak lines"; that is, lines with low emission intensity and hence a poor signal to noise ratio [12]." Thus, the situation for using

less sensitive lines has improved considerably. This aspect is important to develop direct solid sampling applications, because it is not simple to dilute the samples and, quite often, if the analyte is present in the sample at relatively high levels, the use of alternative lines becomes a need [21,22,24,28]. Moreover, this aspect may be even further improved if the transition selected shows a multiplet.

This fact represents a significant difference compared with the situation typically found when using line sources. In that case, whenever a multiplet was monitored, actually the combined absorption of all the multiplet lines was typically measured (unless the difference between the lines was high enough such that the resolution of the monochromator allowed for the selection of only one of them), which often translated into poor linearity.

The use of HR CS AAS has reverted this situation, making it more appealing to monitor multiplets. With this instrumentation, it is now possible to get all the information on every line of the multiplet separately. If the sensitivities of these lines are similar, it has already been demonstrated by Heitmann et al. (who monitored the Mn –279.482/279.827/280.108 nm- and V –318.341/318.397/318.538 nm- triplets) that using all the lines and summing their signals improves a bit (less than a factor of two for those cases) the limit of detection (LOD) [8]. This effect can be increased even further when monitoring molecular “lines” (corresponding with the rotational hyperfine structure of molecular electronic transitions), as in that case the number of lines with similar sensitivity can be much higher (e.g., up to 10 for the monitoring of PO lines in the vicinity of 213.618 nm [29]), making this aspect more appealing (LOD improved a factor of 3 in that situation). In any case, using all the information of these lines enhances the reliability of the analytical results, as it serves to detect potential interferences (e.g., if different lines provide significantly different analytical results).

However, another advantageous situation occurs when the sensitivity of the lines forming the multiplet is significantly different. In this case, it does not make much sense to combine the signals obtained for all the lines, since the addition of the least sensitive lines would improve the overall analytical signal only very moderately, causing at the same time an increase in the noise level and, thus, degrading the final LOD. Instead, this situation represents a very simple way to expand the linear range, because the linearity of every one of these lines should be very different. Fig. 1 shows an example of this situation. In this case, a Ni triplet (234.554/234.663/234.751 nm) is being measured. Ni is one of the elements that show more atomic lines, including various multiplets [12].

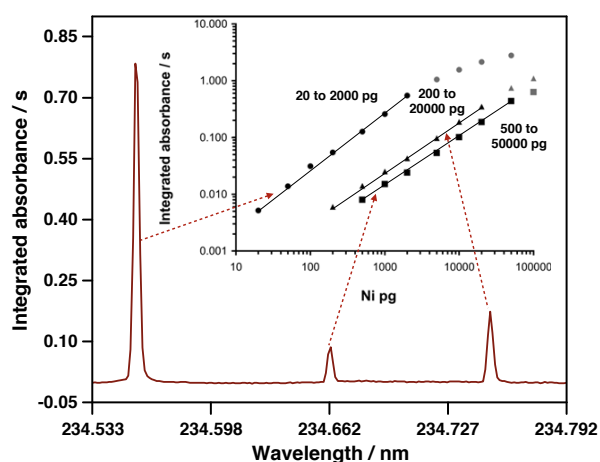


Fig. 1. Wavelength-resolved time-integrated absorbance spectrum showing the Ni triplet located in the vicinity of 234.6 nm, as obtained after HR CS GFAAS measurement of an aqueous solution containing 10 ng of Ni. The linear range of every line of the triplet is also shown.

Table 1

Analytical performance of the lines that compose the Ni triplet found in the vicinity of 234.6 nm.

Wavelength/nm	Characteristic mass/pg	LOD/pg	Linear range ^a /pg	R ²
234.554	16	11	Up to 2000	0.998
234.663	260	210	Up to 50,000	0.999
234.751	140	160	Up to 20,000	0.999

^a The upper limit of the linear range was calculated by applying the Dixon-Q test to the residuals of the calibration points in order to confirm if a suspected value was significantly different at the 95% confidence level.

As can be seen in Table 1, these lines show very different sensitivity. The slope of the most sensitive line of the triplet (234.554 nm) is approximately thirty times higher than the slope of the least sensitive one (234.663 nm). In fact, the 234.554 nm line is only a factor of three less sensitive than Ni main line (232.003 nm), which makes the use of this triplet useful for trace analysis. Fig. 1 shows the linear ranges of every one of these lines, which are very wide for AAS (two orders of magnitude per line). Moreover, since all these lines are always simultaneously measured with the HR CS AAS instrument, depending of the analyte concentration of every sample, the analyst can use the most adequate of these lines in every case, therefore covering in practice a range between 20 and 50,000 pg, without the need to modify any experimental conditions and remeasure any sample. This aspect is very important in the context of solid sampling analysis, and even more important if the samples that are being investigated can only be measured once (e.g., direct analysis of individual invertebrates, as described elsewhere [9]).

There are many other elements that show multiplets that can also be used to expand the linearity in this simple and straightforward way. It is necessary to be cautious, however, when dealing with lines that are too close (e.g., less than 30 pm distance), as it has to be mentioned that the peak width of the atomic lines (which is typically around 10 pm) tend to increase with an increasing concentration of analyte, such that eventually both lines may overlap, which would affect very significantly the analytical response of the least sensitive line.

3.2. Use of an internal standard

One of the best-known strategies for the correction of possible variations occurring during a series of measurements is the use of an internal standard. This approach, widely used in inductively coupled plasma-based methods, for instance, is not typically used in the case of atomic absorption, mostly owing to the limited potential for multi-element monitoring that characterizes this technique when a line source is used.

A few papers have investigated the benefits of using an internal standard with flame AAS, even using a HR CS AAS device [30], by means of a fast sequential mode [30–33]. However, the best performance for an internal standard can only be achieved when the internal standard and the analyte are truly simultaneously monitored. This aspect has been demonstrated for GFAAS analysis in a number of works using the simultaneous line-source spectrometer SIMAA 6000 [34–39], which was designed to combine and detect the radiation originating from up to four hollow cathode lamps, such that several elements could be measured at the same time. This instrument is no longer commercially available and shows many differences with HR CS GFAAS instrumentation, such that it seems relevant to investigate the performance of the latter instrumentation in detail.

The first obvious difference is that, for truly simultaneous monitoring using HR CS AAS, the line of the analyte and that of the internal standard need to be within the narrow spectral bandwidth that is possible to visualize with such an instrument (0.2–0.3 nm in the UV region, as discussed in the introduction). Even though this is a clear limitation, it is not so severe in this case, because the internal

standard is an element that the analyst can select, and there are a number of elements with hundreds of atomic lines (e.g., Co, Cr, Fe, Ni or Ti) that could be used for the purpose. Moreover, it is always positive to select a line for the internal standard that is close to that of the analyte, because there are some matrix-effects that are wavelength dependent (e.g., scattering of radiation) and that could otherwise affect them in a different way.

Besides that condition, there are a number of additional requirements, the most important being: i) the internal standard should not be present at significant levels in the sample (or, if it is present, its content should be known in advance, and then it would not be necessary to spike the sample with a solution of the internal standard); ii) the ratio between the signals of the internal standard and the analyte should be close to unity; and iii) the physicochemical properties of both the internal standard and the analyte should be as similar as possible, to ensure that they endure exactly the same conditions during the measurements. The latter aspect is particularly important in the case of GFAAS analysis because, if the elements do not show similar volatilities in a graphite furnace, they will be vaporized and atomized at different times, such that the correlation between their respective sources of uncertainties will be poor. This aspect has already been demonstrated in the works referred before by using the SIMAA 6000 instrument [36–38], and the situation found with HR CS GFAAS is no different.

To illustrate this point, Table 2 shows the results obtained for the measurement of fifteen consecutive firings for Ag and Ni using or not using Ni or Co, respectively, as internal standards. In both cases, a line for the internal standard sufficiently close to that of the analyte could be found. Amounts of both the analyte and the internal standard that provide signals sufficiently high (integrated absorbance in the range 0.3–0.5 s) and with a ratio close to unity were chosen, such that optimal precision can, in principle, be obtained. As can be seen, in fact, the precision obtained when using typical working conditions (10 μL for sampling) is fairly good (better than 2% RSD) in the absence of an internal standard. It is obviously difficult to improve such values, and, in fact, the use of an internal standard is (slightly) detrimental when Ni is used as such to monitor Ag. This reflects the point discussed before. Ni and Ag are not vaporized and atomized simultaneously (see Fig. 2A), so the variations occurring during these processes may affect them in a different way. This is clearly indicated by the poor correlation coefficients for their signals (see Table 2). As a result of this, the final uncertainty of the measurement has now two contributions instead of only one.

The case for Ni and Co is different. These elements behave very similarly in a graphite furnace and their atomization occurs simultaneously (see Fig. 2B), which translates into a very good correlation between the signals for both elements. As a consequence, Co performs very well as internal standard for Ni, helping to correct for measurement drifts and improving the overall precision for Ni monitoring below 1% RSD in optimal conditions, a value uncharacteristically low for GFAAS and, in practice, out of reach without the use of an internal standard.

However, the use of an internal standard can also be beneficial even when the electrothermal behavior of the analyte and of the internal standard are not so similar, if conditions are such that the

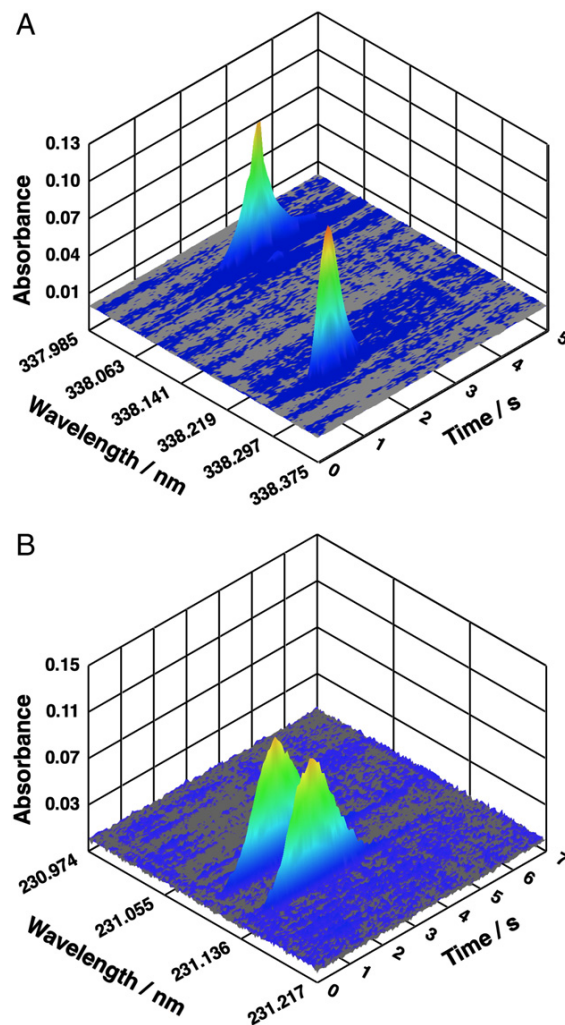


Fig. 2. A) Time- and wavelength-resolved absorbance spectra obtained upon HR CS GFAAS measurement of an aqueous solution containing Ag (400 pg) and Ni (40 ng). The atomic lines of 338.289 nm (Ag) and 338.057 nm (Ni) were selected for the measurements; B) Time- and wavelength-resolved absorbance spectra obtained upon HR CS GFAAS measurement of an aqueous solution containing Ni (1 ng) and Co (400 ng). The atomic lines of 231.096 nm (Ni) and 231.136 nm (Co) were selected for the measurements.

main source of uncertainty affects both in a similar way. For instance, if owing to low sample availability it is necessary to work with lower volumes (2 μL is the minimal amount that our autosampler can deliver), the variation in the sampling is expected to become the main source of uncertainty, and it should affect both the internal standard and the analyte in the same way, providing they are found in the primary sample solution. This effect is shown in Table 2. As can be seen, when delivering only 2 μL of sample, precision degrades to 7–8%

Table 2

Comparison of the precision achieved for the monitoring of aqueous standard solutions by means of HR CS GFAAS, with and without the use of an internal standard (IS). Fifteen consecutive measurements were carried out in each case.

Analyte amount	IS amount	Analyte line/nm	IS line/nm	Volume/ μL	%RSD (without IS)	%RSD (with IS)	R value ^a	F value ^b
400 pg Ag	40 ng Ni	338.289	338.057	10	1.7	2.1	0.0885	1.53
400 pg Ag	40 ng Ni	338.289	338.057	2	7.5	3.1	0.9390	5.85
1 ng Ni	400 ng Co	231.096	231.136	10	1.7	0.8	0.9469	4.52
1 ng Ni	400 ng Co	231.096	231.136	2	7.3	3.3	0.9638	4.89

^a Correlation coefficient between the signal of the analyte and that of the internal standard.

^b Critical value of the F test = 2.47.

RSD in both cases (the main uncertainty source is the same), and the use of an internal standard is beneficial, significantly (as proved by F test values) improving this value down to 3% RSD. A similar effect can be expected to occur in real-life applications when analyzing viscous samples, such that variations in the sampling efficiency may degrade precision significantly.

But obviously, the main motivation for using an internal standard is correcting for matrix-effects and making it easier to develop calibration approaches when analyzing complex samples, as already described in the literature for the determination of Pb in vinegar [34], Se in sparkling water [35], Cd and Pb in blood [36], Pb in various biological samples [37], As and Se in urine [38] and As, Cu and Pb in sugar-cane [39], using the SIMAA 6000 device in all the cases. The same principle can be applied to HR CS GFAAS, using the same Ni and Co lines already shown in Fig. 2B.

When aiming at analysis of biological samples, matrix-effects are not infrequent. A comparison of calibration curves obtained for Ni when measuring aqueous standards, urine samples (diluted only 1:1) and blood samples (diluted 1:3) was carried out, and differences in the analytical responses were appreciated. In particular, for blood, the slope was 18% lower than that obtained with aqueous standards. This matrix-effect could be efficiently corrected for when using the signal for Co as internal standard, which permitted obtaining practically identical calibration curves, regardless of the matrix (less than 2% difference in the slopes, see Fig. S-1 – Supplementary data in Appendix A – for more details). Moreover, this situation represents the case described above where matrix-effects and irreproducible sampling degrade the precision. In fact, precision for 15 replicate measurements of urine and blood was characterized by RSD values of 6.8% and 8.4%, respectively, values which could be improved to 1.8% and 2.9% when Co was used as internal standard, owing to the correlation found between Ni and Co signals ($r = 0.961$ and $r = 0.947$, respectively). This aspect is illustrated in Fig. 3, where the individual values for Ni and Co in urine, as well as their respective ratios, are displayed.

Overall, it is these authors' opinion that the use of an internal standard in connection with HR CS AAS instrumentation should be encouraged, as it may help in solving some frequent problems and in improving precision in many real-life situations.

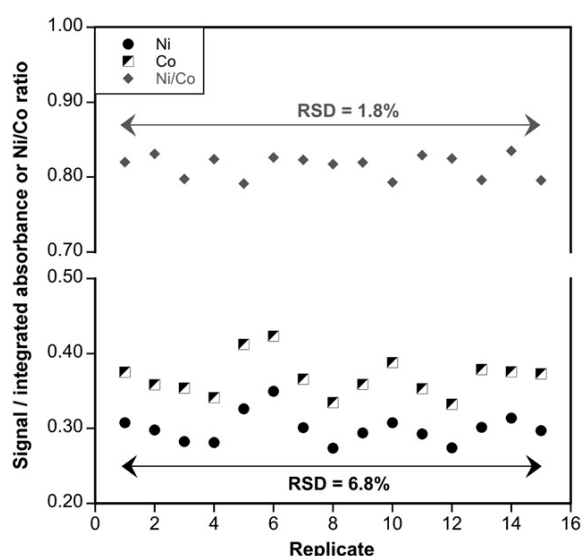


Fig. 3. Evolution of the Ni and Co signals obtained upon HR CS GFAAS measurement of a urine sample spiked with 1 ng Ni and 400 ng Co, showing the improved precision obtained when using the Co signal as internal standard for Ni. The same spectral interval shown in Fig. 2B was monitored.

3.3. Multi-element analysis

As stated in the introduction, *a priori*, the current potential for multi-element analysis of the HR CS GFAAS technique is limited owing to the narrow spectral bandwidth that is simultaneously monitored. However, it should be taken into account that, very often, the most important aspect is not to measure all the elements simultaneously, but instead to measure all the elements of interest from the same sample replicate (the same tube firing), which opens possibilities for sequential monitoring.

In practice, there are two possible situations only, either the elements of interest show similar volatilities or not. If the elements of interest show similar volatilities, it seems simple to use the same temperature program to vaporize them and atomize almost simultaneously. Then, truly simultaneous monitoring can be accomplished providing that i) there are atomic lines for these elements that are closely located and ii) the sensitivity ratio between these lines is of the same order as the concentration ratio in the samples of interest, as discussed recently by Welz et al. [12]. It is certainly not so frequent that both criteria can be met, but Welz and coworkers have used this approach to determine Co and V [17] and Cr and Fe [20] in crude oil.

In this work, we have investigated this possibility for the direct determination of a biological certified reference material (NIST 1566a Oyster tissue). Elements such as Co, Fe or Ni show many atomic lines and it seems feasible to determine them simultaneously, as all of them are non-volatile. Actually, this is a relative simple sample for direct analysis, since it is feasible to use a pyrolysis temperature sufficiently high to remove most matrix components (of organic nature) without risking analyte losses, such that the resulting analyte signals should not be significantly affected by matrix interferences [21,22,28]. Ni and Co showed atomic lines in the vicinity of 352.6 nm (Ni 352.454 nm, characteristic mass 30 pg; and Co 352.685 nm, characteristic mass 75 pg) that are suitable for determinations at the $\mu\text{g g}^{-1}$ level using 2–3 mg of sample, while Fe shows a doublet (352.604 and 352.617 nm, see Fig. S-2) that is much less sensitive (characteristic masses, 3 and 27 ng, respectively), which is fit for purpose in this case as the Fe content in the sample is much higher (approx. $500 \mu\text{g g}^{-1}$).

Thus, analysis of the sample was undertaken, using the conditions shown in Table 3 and the methodology discussed in Section 2.4. As shown in Fig. 4, well-defined unimodal signals were obtained for the solid samples, signals that were very similar in shape and in peak area values to those obtained for aqueous standards, such that straightforward calibration with aqueous standard seemed to be feasible. The results presented in Table 4 proved that it is possible to obtain accurate values in this simple way, confirming the potential of HR CS GFAAS for direct and simultaneous multi-element analysis (three elements in this case) of solid samples, as long as the conditions discussed in the second paragraph of this section are fulfilled.

Table 3

Instrumental parameters used in the simultaneous determination of Co, Fe and Ni in NIST SRM 1566a Oyster tissue by means of solid sampling HR CS GFAAS.

Analyte	Ni	Fe	Fe	Co
Wavelength/nm	352.454	352.604	352.617	352.685
Number of pixels summed	3 (≈ 5.9 pm)	3 (≈ 5.9 pm)	3 (≈ 5.9 pm)	3 (≈ 5.9 pm)
Sample mass/mg	2–3			
Chemical modifier	5 μg Pd (added as $\text{Pd}(\text{NO}_3)_2$ solution)			
Temperature program				
Step	Temperature/ $^{\circ}\text{C}$	Ramp/ $^{\circ}\text{C s}^{-1}$	Time/s	Gas flow/ L min^{-1}
Drying	150	5	35	2
Pyrolysis	1000	50	30	2
Auto-zero	1000	0	5	0
Atomization	2500	1200	6	0
Cleaning	2600	500	4	2

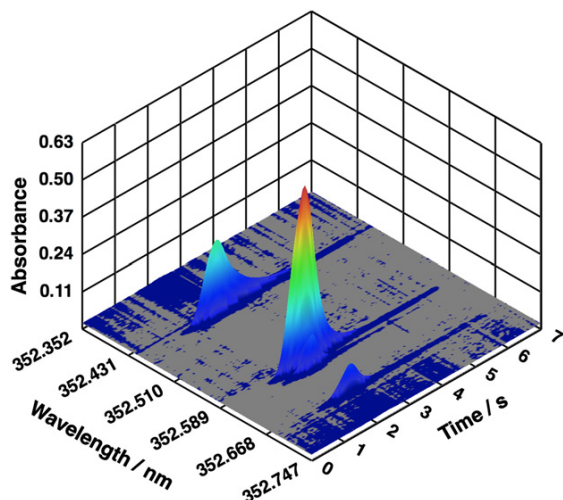


Fig. 4. Time- and wavelength-resolved absorbance spectra obtained upon the direct analysis of 2.795 mg of NIST SRM 1566a Oyster tissue by means of HR CS GFAAS using the conditions shown in Table 3.

The second situation, determination of elements showing very different volatilities, seems more complicated *a priori*. Indeed, if the idea is to use one atomization program only, compromise conditions have to be used owing to the different electrothermal behavior of the analytes. That is the reason why, when tackling this situation (determination of Cd and Fe in various types of samples [16,18,19]), Welz and coworkers proposed the use of two atomization temperatures, such that every analyte can be determined using its optimal atomization temperature.

In the current work, it is investigated if that situation (used of two atomization steps) can be taken even further. In fact, if two atomization steps are to be used, there is no actual need to use atomic lines that are closely located since wavelength modification has already been reported to take only 2 s for an HR CS AAS instrument, including all correction and optimization steps [12]. Thus, in theory, every element can be determined at the atomic line of choice, using the Ar flow conditions that fit better, and even using different chemical modifiers, or different amounts of the same chemical modifier, if needed (the sample can be cooled down and a second modifier solution can be added).

Again, a solid sample was selected to evaluate the feasibility of this strategy. A biological reference material with certified values for Cd and Ni was chosen, BCR 679 White cabbage. Obviously, Cd and Ni are elements of very different volatility. In fact, the use of the optimal atomization temperature for Ni represents an almost two-fold decrease in the sensitivity for Cd (see Fig. S-3), which could be expected since the residence time of a volatile element typically decreases with increasing temperatures, owing to diffusional losses. Still, there is a Ni atomic line (228.998 nm) that is very close to the main Cd atomic line (228.802 nm), such that it seems possible to try

Table 4

Results obtained for the simultaneous determination ($n=5$) of Co, Fe and Ni in NIST SRM 1566a Oyster tissue by means of solid sampling HR CS GFAAS.

Wavelength/nm	Analyte	Result/ $\mu\text{g g}^{-1}$	Certified value/ $\mu\text{g g}^{-1}$
352.454	Ni	2.08 ± 0.20	2.25 ± 0.45
352.604	Fe	557 ± 23	539 ± 32
352.617	Fe	567 ± 31	539 ± 32
352.685	Co	0.59 ± 0.06	0.57 ± 0.11

The confidence intervals (C.I.) have been calculated as $\pm ts/\sqrt{n}$, where t is the Student's t -distribution value for a probability level of 95%, s is the standard deviation and n is the number of replicate determinations.

Table 5

Instrumental parameters used in the simultaneous determination of Cd and Ni in BCR CRM 679 White cabbage by means of solid sampling HR CS GFAAS.

Analyte	Cd	Ni		
Wavelength/nm	228.802	228.998		
Number of pixels summed	3 (≈ 3.7 pm)	3 (≈ 3.7 pm)		
Sample mass/mg	0.3–0.5			
Chemical modifier	1 μg Pd (added as $\text{Pd}(\text{NO}_3)_2$ solution)			
Temperature program				
Step	Temperature/ $^{\circ}\text{C}$	Ramp/ $^{\circ}\text{C s}^{-1}$	Time/s	Gas flow/ L min^{-1}
Drying	150	5	35	2
Pyrolysis	800	50	30	2
Auto-zero	800	0	5	0.1
Atomization	2300	1200	7	0.1
Cleaning	2600	500	4	2

to simultaneously monitor both signals, using suitable sample masses (approx. 0.5 mg), mini-flow conditions to adjust the sensitivity and a temperature high enough to atomize both elements. The detailed absorption profiles can be obtained from the solid samples (as shown in Fig. 5), and their areas are comparable with those observed for aqueous standards.

Alternatively, a sequential approach can be used, selecting now two lines that cannot be monitored simultaneously (228.802 nm for Cd and 234.554 nm for Ni, another Ni line that shows appropriate sensitivity for this sample). The working conditions are shown in Table 6. In this case, atomization of Cd is undertaken first at 1300 $^{\circ}\text{C}$ (a temperature that is appropriate for Ni pyrolysis) and then the conditions are modified, the temperature increases up to 2500 $^{\circ}\text{C}$ (the optimal temperature to achieve the best temporal definition, with minimum tailing, for Ni atomic signal profiles) and Ni can be measured at the new wavelength, as illustrated in Fig. 6. In this case, and owing to the large difference in the analyte contents, a different and optimal amount of chemical modifier (Pd) was added before every step. Again, this approach provided well-defined signal profiles for solid standards and aqueous solutions, with comparable peak areas.

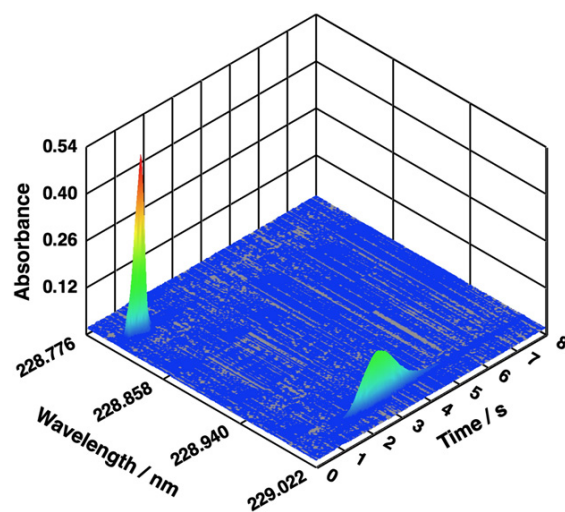


Fig. 5. Time- and wavelength-resolved absorbance spectra obtained upon the direct measurement of 0.453 mg of BCR CRM 679 White cabbage by means of HR CS GFAAS using the conditions shown in Table 5. The signal that appears on the left side corresponds to Cd (228.802 nm) and the signal on the right side with Ni (228.998 nm).

Table 6

Instrumental parameters used in the determination of Cd and Ni in BCR CRM 679 White cabbage by means of solid sampling HR CS GFAAS using a sequential monitoring approach (two different atomization steps during every tube firing).

Analyte	Cd	Ni		
Wavelength/nm	228.802	234.554		
Number of pixels summed	3 (≈ 3.7 pm)	3 (≈ 3.7 pm)		
Sample mass/mg	0.1–0.3			
Temperature program				
Step	Temperature/ $^{\circ}$ C	Ramp/ $^{\circ}$ C s $^{-1}$	Time/s	Gas flow/L min $^{-1}$
Addition of 10 μ L of chemical modifier (Pd, 30 mg L $^{-1}$)				
Drying	150	5	35	2
Pyrolysis	700	300	30	2
Auto-zero	700	0	5	0.1
Atomization	1300	1200	5	0.1
Cool down	20	100	10	2
Addition of 10 μ L of chemical modifier (Pd, 100 mg L $^{-1}$)				
Drying	150	5	35	2
Pyrolysis ^a	1300	500	1	2
Auto-zero	1300	0	5	0.1
Atomization	2500	1200	5	0.1
Cleaning	2600	500	4	2

^a This second pyrolysis step would not be really necessary from a scientific point of view, but it is compulsory due to the configuration of the software of the instrument.

Table 7 shows the results obtained for Cd and Ni using both approaches. As can be seen, in both cases the agreement with the reference values is excellent, such that it is possible to use any of them. However, the second approach can be much more flexible for multi-element analysis, as there are no more requirements to find close lines characterized by a suitable sensitivity ratio. Instead, every element can be determined under optimal conditions. The only requirement that is necessary to fulfill is that the volatilities of the elements of interest should be different enough such that no losses of the less volatile element occur during atomization of the most volatile analyte. This aspect can also be further ensured using chemical modifiers.

Moreover, the sequential approach can be expanded even further if the difference in the analyte volatilities is sufficiently high. Fig. 7 shows how it is possible to sequentially and selectively monitor, during every single replicate, a very volatile analyte (Hg), an element of medium volatility (Zn) and two elements of low volatility that showed closed lines (Mn and Cr), using a triple atomization program with different wavelengths. In fact, MnO_4^- is used as chemical

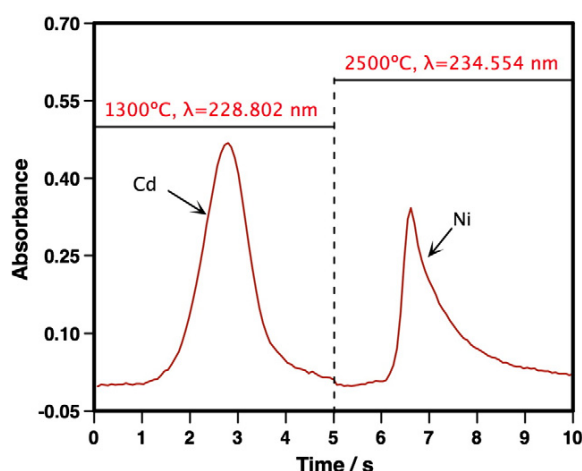


Fig. 6. Sequential and selective atomization of Cd and Ni as obtained for the direct measurement of a solid sampling replicate (0.266 mg of BCR CRM 679 White cabbage) by means of HR CS GFAAS using the conditions shown in Table 6.

Table 7

Results obtained for the determination ($n=5$) of Cd and Ni in BCR CRM 679 White cabbage by means of solid sampling HR CS GFAAS using two different approaches, truly simultaneous monitoring (conditions shown in Table 5), or sequential monitoring (use of two different atomization steps, as shown in Table 6). In both cases, Cd and Ni were always monitored from every sample replicate.

Analyte	Result simultaneous method/ $\mu\text{g g}^{-1}$	Result sequential method/ $\mu\text{g g}^{-1}$	Certified value/ $\mu\text{g g}^{-1}$
Cd	1.69 ± 0.13	1.60 ± 0.14	1.66 ± 0.07
Ni	27.3 ± 1.7	27.6 ± 1.9	27.0 ± 0.8

The confidence intervals (C.I.) have been calculated as $\pm ts/\sqrt{n}$, where t is the Student's t -distribution value for a probability level of 95%, s is the standard deviation and n is the number of replicate determinations.

modifier for Hg [40–42], and that is the reason why Mn signal appears in the Figure, as there is a very insensitive Mn line close to the main atomic line for Cr.

4. Conclusions

While obviously the current configuration of commercially available HR CS GFAAS instrumentation has not been designed having multi-line monitoring in mind, there is still potential to do so. Monitoring various atomic lines of the same element or of different elements is sometimes possible, which provides a mean for expanding the linear range (e.g., monitoring of multiplets), or for improving precision and correcting for matrix-effects (use of an internal standard).

Furthermore, direct and multi-element analysis of solid samples is also possible on some occasions, as demonstrated in the current work, either by monitoring various atomic lines that are sufficiently close (truly simultaneous monitoring) or, if these are lacking, by opting for a selective and sequential atomization of the elements of interest during every single replicate, which seems to be a more flexible approach.

Overall, the potential of HR CS GFAAS instrumentation to monitor multiple lines may seem limited when compared with other multi-element techniques (e.g., inductively coupled plasma-based methods), but it represents a significant step forward if compared with traditional line source AAS devices. It is these authors' opinion that the current owners of HR CS GFAAS instrumentation may find

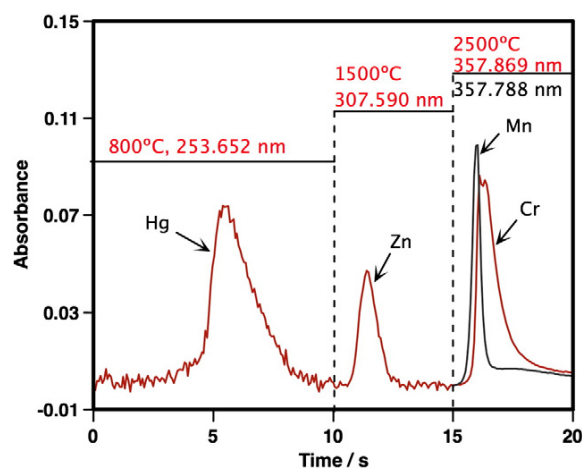


Fig. 7. Example of sequential and selective atomization of Hg (5 ng), Zn (20 ng) and Cr (40 pg) as obtained for a single HR CS GFAAS replicate of an aqueous standard solution. KMnO_4 and Pd were used as chemical modifiers. The signal of Mn was also simultaneously monitored with that of Cr owing to the proximity of their atomic lines, but was actually divided by a factor of 5 to keep the same scale.

favorable situations to profit from some of the multi-line features discussed before, which are currently underused.

Supplementary materials related to this article can be found online at doi:10.1016/j.sab.2011.03.008.

Acknowledgments

This work has been funded by the Spanish Ministry of Science and Innovation (Project CTQ2009-08606) and the Aragon Government (“Programa de apoyo a la I + D + I” from ARAID Foundation and “Obra Social de IberCaja”, with additional support from Inycom).

References

- H. Becker-Ross, S. Florek, U. Heitmann, Observation, identification and correction of structured molecular background by means of continuum source AAS – determination of selenium and arsenic in human urine, *J. Anal. At. Spectrom.* 15 (2000) 137–141.
- U. Heitmann, M. Schütz, H. Becker-Ross, S. Florek, Measurements on the Zeeman-splitting of analytical lines by means of a continuum source graphite furnace atomic absorption spectrometer with a linear charge coupled device array, *Spectrochim. Acta Part B* 51 (1996) 1095–1105.
- B. Welz, High-resolution continuum source AAS: the better way to perform atomic absorption spectrometry, *Anal. Bioanal. Chem.* 381 (2005) 69–71.
- D.L.G. Borges, A.F. da Silva, B. Welz, A.J. Curtius, U. Heitmann, Determination of lead in biological samples by high-resolution continuum source graphite furnace atomic absorption spectrometry with direct solid sampling, *J. Anal. At. Spectrom.* 21 (2006) 763–769.
- M. Resano, J. Briceño, M.A. Belarra, Direct determination of Hg in polymers by solid sampling-graphite furnace atomic absorption spectrometry. A comparison of the performance of line source and continuum source instrumentation, *Spectrochim. Acta Part B* 64 (2009) 520–529.
- R.G.O. Araujo, B. Welz, F. Vignola, H. Becker-Ross, Correction of structured molecular background by means of high-resolution continuum source electrothermal atomic absorption spectrometry. Determination of antimony in sediment reference materials using direct solid sampling, *Talanta* 80 (2009) 846–852.
- M. Resano, E. Mozas, C. Crespo, J. Briceño, J. del Campo Menoyo, M.A. Belarra, Solid sampling high-resolution continuum source graphite furnace atomic absorption spectrometry to monitor the biodistribution of gold nanoparticles in mice tissue after intravenous administration, *J. Anal. At. Spectrom.* 25 (2010) 1864–1873.
- U. Heitmann, B. Welz, D.L.G. Borges, F.G. Lepri, Feasibility of peak volume, side pixel and multiple peak registration in high-resolution continuum source atomic absorption spectrometry, *Spectrochim. Acta Part B* 62 (2007) 1222–1230.
- J. Briceño, M.A. Belarra, K.A.C. De Schampelaere, S. Vanlaere, C. Janssen, F. Vanhaecke, M. Resano, Direct determination of Zn in individual *Daphnia magna* specimens by means of solid sampling high-resolution continuum source graphite furnace atomic absorption spectrometry, *J. Anal. At. Spectrom.* 25 (2010) 503–510.
- B. Welz, F.G. Lepri, R.G.O. Araujo, S.L.C. Ferreira, M.D. Huang, M. Okruss, H. Becker-Ross, Determination of phosphorus, sulfur and the halogens using high-temperature molecular absorption spectrometry in flames and furnaces – a review, *Anal. Chim. Acta* 647 (2009) 137–148.
- U. Heitmann, H. Becker-Ross, S. Florek, M.D. Huang, M. Okruss, Determination of non-metals via molecular absorption using high-resolution continuum source atomic absorption spectrometry and graphite furnace atomization, *J. Anal. At. Spectrom.* 21 (2006) 1314–1320.
- B. Welz, S. Morés, E. Carasek, M.G.R. Vale, M. Okruss, H. Becker-Ross, High-resolution continuum source atomic and molecular absorption spectrometry – a review, *Appl. Spectrosc. Rev.* 45 (2010) 327–354.
- H. Becker-Ross, S. Florek, U. Heitmann, M.D. Huang, M. Okruss, B. Radziuk, Continuum source atomic absorption spectrometry and detector technology: a historical perspective, *Spectrochim. Acta Part B* 61 (2006) 1015–1030.
- J.M. Harnly, The future of atomic absorption spectrometry: a continuum source with a charge coupled array detector, *J. Anal. At. Spectrom.* 14 (1999) 137–146.
- M. Resano, E. García-Ruiz, High-resolution continuum source graphite furnace atomic absorption spectrometry: Is it as good as it sounds? a critical review, *Anal. Bioanal. Chem.* 399 (2011) 323–330.
- F. Vignola, D.L.G. Borges, A.J. Curtius, B. Welz, H. Becker-Ross, Simultaneous determination of Cd and Fe in sewage sludge by high-resolution continuum source electrothermal atomic absorption spectrometry with slurry sampling, *Microchem. J.* 95 (2010) 333–336.
- I.M. Dittert, J.S.A. Silva, R.G.O. Araujo, A.J. Curtius, B. Welz, H. Becker-Ross, Simultaneous determination of cobalt and vanadium in undiluted crude oil using high-resolution continuum source graphite furnace atomic absorption spectrometry, *J. Anal. At. Spectrom.* 25 (2010) 590–595.
- L.M.G. dos Santos, B. Welz, R.G.O. Araujo, S.C. Jacob, M.G.R. Vale, A. Martens, I.B. Gonzaga Martens, H. Becker-Ross, Simultaneous determination of Cd and Fe in beans and soil of different regions of Brazil using high-resolution continuum source graphite furnace atomic absorption spectrometry and direct solid sampling, *J. Agric. Food Chem.* 57 (2009) 10089–10094.
- L.M.G. dos Santos, R.G.O. Araujo, B. Welz, S.d.C. Jacob, M.G.R. Vale, H. Becker-Ross, Simultaneous determination of Cd and Fe in grain products using direct solid sampling and high-resolution continuum source electrothermal atomic absorption spectrometry, *Talanta* 78 (2009) 577–583.
- I.M. Dittert, J.S.A. Silva, R.G.O. Araujo, A.J. Curtius, B. Welz, H. Becker-Ross, Direct and simultaneous determination of Cr and Fe in crude oil using high-resolution continuum source graphite furnace atomic absorption spectrometry, *Spectrochim. Acta Part B* 64 (2009) 537–543.
- M. Resano, F. Vanhaecke, M.T.C. de Loos-Vollebregt, Electrothermal vaporization for sample introduction in atomic absorption, atomic emission and plasma mass spectrometry – a critical review with focus on solid sampling and slurry analysis, *J. Anal. At. Spectrom.* 23 (2008) 1450–1475.
- M.A. Belarra, M. Resano, F. Vanhaecke, L. Moens, Direct solid sampling with electrothermal atomization/vaporization. What for and how? *Trends Anal. Chem.* 21 (2002) 828–839.
- B. Welz, M.G.R. Vale, D.L.G. Borges, U. Heitmann, Progress in direct solid sampling analysis using line source and high-resolution continuum source electrothermal atomic absorption spectrometry, *Anal. Bioanal. Chem.* 389 (2007) 2085–2095.
- M.G.R. Vale, N. Oleszczuk, W.N.L. dos Santos, Current status of direct solid sampling for electrothermal atomic absorption spectrometry – a critical review of the development between 1995 and 2005, *Appl. Spectrosc. Rev.* 41 (2006) 377–400.
- K.-C. Friese, V. Krivan, A solid-sampling system for a transversely heated graphite furnace and its application to trace element analysis of high-purity tantalum powders by atomic absorption spectrometry, *Spectrochim. Acta Part B* 53 (1998) 1069–1078.
- M.A. Belarra, M. Resano, J.R. Castillo, Theoretical evaluation of solid sampling-electrothermal atomic absorption spectrometry for screening purposes, *J. Anal. At. Spectrom.* 14 (1999) 547–552.
- B. Welz, H. Becker-Ross, S. Florek, U. Heitmann, High-resolution continuum source AAS – the better way to do atomic absorption spectrometry, Wiley-VCH, Weinheim, 2005.
- M. Resano, M. Aramendia, E. Garcia-Ruiz, C. Crespo, M.A. Belarra, Solid sampling-graphite furnace atomic absorption spectrometry for the direct determination of silver at trace and ultratrace levels, *Anal. Chim. Acta* 571 (2006) 142–149.
- M. Resano, J. Briceño, M.A. Belarra, Direct determination of phosphorus in biological samples using a solid sampling-high resolution-continuum source electrothermal spectrometer: comparison of atomic and molecular absorption spectrometry, *J. Anal. At. Spectrom.* 24 (2009) 1343–1354.
- J.L. Raposo Jr., S.R. Oliveira, J.A. Nóbrega, J.A.G. Neto, Internal standardization and least-squares background correction in high-resolution continuum source flame atomic absorption spectrometry to eliminate interferences on determination of Pb in phosphoric acid, *Spectrochim. Acta Part B* 63 (2008) 992–995.
- S.L.C. Ferreira, A.S. Souza, G.C. Brandao, H.S. Ferreira, W.N.L. dos Santos, M.F. Pimentel, M.G.R. Vale, Direct determination of iron and manganese in wine using the reference element technique and fast sequential multi-element flame atomic absorption spectrometry, *Talanta* 74 (2008) 699–702.
- H.D. Projahn, U. Steeg, J. Sanders, E. Vanclay, Application of the reference-element technique for fast sequential flame atomic-absorption spectrometry, *Anal. Bioanal. Chem.* 378 (2004) 1083–1087.
- K. Miranda, A.G.G. Dionísio, E.R. Pereira-Filho, Copper determination in sugar cane spirits by fast sequential flame atomic absorption spectrometry using internal standardization, *Microchem. J.* 96 (2010) 99–101.
- S.R. de Oliveira, J.A.G. Neto, Evaluation of Bi as internal standard to minimize matrix effects on the direct determination of Pb in vinegar by graphite furnace atomic absorption spectrometry using Ru permanent modifier with co-injection of Pd/Mg(NO₃)₂, *Spectrochim. Acta Part B* 62 (2007) 1046–1050.
- A.P. Oliveira, J.A.G. Neto, J.A. Nóbrega, P.V. Oliveira, Use of the internal standardization for difficult sampling by graphite furnace atomic absorption spectrometry, *Talanta* 64 (2004) 334–337.
- P.R.M. Correia, P.V. Oliveira, J.A.G. Neto, J.A. Nóbrega, Silver as internal standard for simultaneous determination of Cd and Pb in whole blood by electrothermal atomic absorption spectrometry, *J. Anal. At. Spectrom.* 19 (2004) 917–922.
- B. Radziuk, N.P. Romanova, Y. Thomassen, Evaluation of internal standardisation in electrothermal atomic absorption spectrometry, *Anal. Commun.* 36 (1999) 13–16.
- P.R.M. Correia, P.V. Oliveira, Cobalt as internal standard for arsenic and selenium determination in urine by simultaneous atomic absorption spectrometry, *Talanta* 67 (2005) 46–53.
- N.M. Caldas, S.R. Oliveira, J.A.G. Neto, Feasibility of internal standardization in the direct and simultaneous determination of As, Cu and Pb in sugar-cane spirits by graphite furnace atomic absorption spectrometry, *Anal. Chim. Acta* 636 (2009) 1–5.
- A.F. da Silva, B. Welz, A.J. Curtius, Noble metals as permanent chemical modifiers for the determination of mercury in environmental reference materials using solid sampling graphite furnace atomic absorption spectrometry and calibration against aqueous standards, *Spectrochim. Acta Part B* 57 (2002) 2031–2045.
- I. López-García, M. Sánchez-Merlos, M. Hernández-Córdoba, Determination of mercury in soils and sediments by graphite furnace atomic absorption spectrometry with slurry sampling, *Spectrochim. Acta Part B* 52 (1997) 2085–2092.
- M. Resano, E. García-Ruiz, M. Aramendia, M.A. Belarra, Solid sampling-graphite furnace atomic absorption spectrometry for Hg monitoring in soils. Performance as a quantitative and as a screening method, *J. Anal. At. Spectrom.* 20 (2005) 1374–1390.



Contents lists available at ScienceDirect

Spectrochimica Acta Part B

journal homepage: www.elsevier.com/locate/sab

Review

High-resolution continuum source atomic absorption spectrometry for the simultaneous or sequential monitoring of multiple lines. A critical review of current possibilities

M. Resano*, M.R. Flórez, E. García-Ruiz

Department of Analytical Chemistry, University of Zaragoza, Pedro Cerbuna 12, 50009 Zaragoza, Spain

ARTICLE INFO

Article history:

Received 6 May 2013

Accepted 10 June 2013

Available online 15 June 2013

Keywords:

High-resolution continuum source atomic absorption spectrometry

Graphite furnace

Flame

Multi-element determination

ABSTRACT

This work examines the capabilities and limitations of commercially available high-resolution continuum source atomic absorption spectrometry instrumentation for multi-line monitoring, discussing in detail the possible strategies to develop multi-element methodologies that are truly simultaneous, or else sequential, but from the same sample aliquot.

Moreover, the simultaneous monitoring of various atomic or molecular lines may bring other important analytical advantages, such as: i) expansion of the linear range by monitoring multiplets; ii) improvements in the limit of detection and in precision by summing the signals from different lines of the same element or molecule; iii) simple correction for matrix-effects by selecting a suitable internal standard; or iv) accurate mathematical correction of spectral overlaps by simultaneous monitoring of free lines of the interfering molecule or element. This work discusses how authors have made use of these strategies to develop analytical methodologies that permit the straightforward analysis of complex samples.

© 2013 Elsevier B.V. All rights reserved.

Contents

1. Introduction	85
2. Simultaneous multi-element determinations using high-resolution continuum source graphite furnace atomic absorption spectrometry	86
2.1. Requirements, limitations and strategies to develop multi-element methods	86
3. Other advantages derived from multi-line monitoring using high-resolution continuum source graphite furnace atomic (or molecular) absorption spectrometry	89
3.1. Monitoring several lines of the same analyte	89
3.2. Use of an internal standard	90
3.3. Background correction	91
4. Multi-line monitoring in high-resolution continuum source flame atomic (or molecular) absorption spectrometry	93
5. Conclusions	95
Acknowledgments	96
References	96

1. Introduction

The introduction of high-resolution continuum source atomic absorption spectrometers (HR CS AAS) represents the most significant advance experienced by this technique in various decades [1]. This instrumentation became commercially available in 2003, equipped with a flame atomizer only, while in 2007 a spectrometer featuring

both a graphite furnace and a flame atomizer in two separate sampling compartments was released, although the research groups of Becker-Ross and Welz already published several works using prototypes of similar characteristics before those dates [2,3]. As can be seen in Fig. 1, the number of articles that evaluate the use of continuum source instruments for atomic absorption is finally growing, which is particularly obvious after the introduction of the commercial device equipped with the graphite furnace. Moreover, there is also a clear tendency to publish more applied work, even outside atomic spectroscopy journals, which demonstrates that the technique is maturing very fast and it is ready to be used in routine labs.

* Corresponding author. Tel.: +34 976761634; fax: +34 976761290.
E-mail address: mresano@unizar.es (M. Resano).

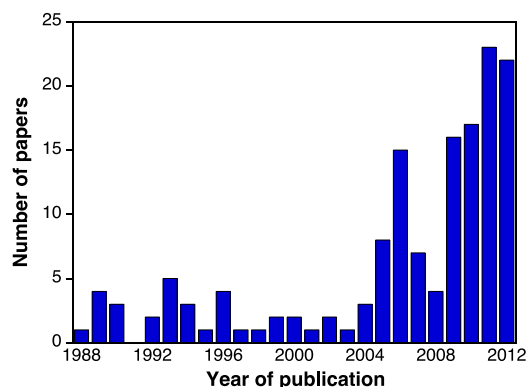


Fig. 1. Number of publications that have reported the use of continuum source atomic absorption spectrometry during the last 25 years. Papers that appeared in proceedings and book chapters are not included. Source: ISI Web of Science.

Use of continuum source-based atomic absorption equipment is not really a novel topic in the scientific literature. However, during the last five decades line source AAS was the technique of choice, following the basic idea proposed by Walsh [4]. This situation is logical because the correspondence between atomic emission and absorption lines permitted great selectivity to be attained even for instruments with limited resolution (nm level), while for successfully using a continuum source device a much better resolution was required. However, owing to the possible advantages derived from the use of a continuum source (e.g., higher multi-element capabilities), this idea was never abandoned, and several authors (notably J. Harnly) developed their own prototypes as the technical capabilities of spectrometers were improving [5–11]. These prototypes showed some limitations, and, in particular, it was difficult to find a suitable lamp with sufficient intensity in the far UV.

Becker-Ross and co-workers [12–15] presented a device based on (1) a high-pressure xenon short-arc lamp operating at brightness temperatures of approximately 10,000 °C, capable of providing a high intensity in the visible and (far) UV region, (2) an optical system based on an echelle monochromator dispersing radiation in two steps (by using a prism first and an echelle grating afterwards), and (3) a linear CCD array for detection. This configuration proved successful and the spectrometers currently commercialized by Analytik Jena are based on it, even though their characteristics are not totally identical. Fig. 2 shows the schematics of this instrument. In this regard, this review will focus on discussing the characteristics of the commercially available instrumentation.

This type of instrument provides significant advantages in comparison to traditional line source devices, such as improved signal stability, superior background correction potential, capabilities to monitor narrow molecular “lines” (the term transition is actually more correct when referring to molecular spectra, and will be used from now on), which permit the determination of non-metals, and improved linearity by making use of side pixels [16–19].

In addition, there is potential to simultaneously monitor several atomic lines, thus permitting multi-element determinations to be carried out. However, this potential is actually rather limited. The reason is that the instrumentation currently available only allows for the simultaneous monitoring of a small portion of the spectrum (0.2–0.3 nm in the UV region). This aspect does not seem to be always well understood by prospective new users of the technique that perhaps have other expectations (maybe also because some of the previous prototypes discussed before showed higher multi-element possibilities [7–11]). Thus, one of the main goals of this paper will be to further clarify this point and to discuss in detail under which circumstances it is possible to perform simultaneous multi-element

determinations with the current instrumentation commercially available.

However, there are other important advantages derived from the simultaneous monitoring of multiple atomic lines and/or molecular transitions. This review will examine them and highlight how different authors have made use of them to develop novel methodologies.

The review will be mostly focused on work carried out using a graphite furnace as atomizer, owing to its superior possibilities. Nevertheless, a specific section devoted to the peculiarities of flame (F) AAS in the context of multi-line monitoring will be presented as well.

2. Simultaneous multi-element determinations using high-resolution continuum source graphite furnace atomic absorption spectrometry

2.1. Requirements, limitations and strategies to develop multi-element methods

As discussed before, the potential of the current instrumentation to perform truly simultaneous multi-element determinations is limited. The main reason for this is that this instrumentation features a detector with 588 pixels of which only 200 are used for analytical purposes, while the remainder are used for internal corrections. This instrumentation provides an exceptional resolution, as every one of those pixels monitors a range of a few picometers only (approx. 1 pm at 200 nm), but that also means that such an instrument only allows for the simultaneous monitoring of a very small part of the spectrum: 0.2–0.3 nm in the UV region, where the most useful atomic lines are typically found, increasing in the visible region up to approx. 1.0 nm at 800 nm. Further improvements in this aspect would certainly be welcome, although they probably require the development of a suitable type of detector for this instrument (which represents a considerable investment) as the requirements of a GFAAS device (transient signals) are not the same as those for other types of optical instruments (e.g. emission devices), as discussed in various reviews [10,18,20].

Despite this limitation, there are still some possibilities to develop truly simultaneous methods. Table 1 shows a summary of the articles that have reported applications in this regard.

As discussed in these articles, there are a number of prerequisites to develop these multi-element methods. First of all, it is necessary to find atomic lines of the target elements that are sufficiently close (within 0.2–1.0 nm, depending on the wavelength). The difficulty in finding these lines depends on the target elements. There are some elements with hundreds of usable lines available in the UV–vis area, such as Co, Cr, Fe, Ni or Ti [18], and others that show at least tens of lines (e.g., Cu, Mn, Pb or Pd). Obviously, if your target analytes show many lines, chances to find some that are close enough increase.

However, not all the lines show the same sensitivity, and the lines finally selected must be suitable for the expected contents of all the target analytes. This is a severe requirement, because some solutions frequently used to adapt the sensitivity when performing mono-element determinations (e.g., diluting the sample or keeping the Ar flow during the atomization step) may not be appropriate for a simultaneous multi-element approach, as it is evident that they will have an effect on all the analytes.

Finally, the furnace conditions need to be considered. If the target elements show similar thermochemical behavior, it may be simple to develop a temperature program and use a chemical modifier that is adequate for all of them. However, if their behavior is very different (e.g., simultaneous determination of very volatile and refractory elements), compromise conditions need to be used. This last requirement does not typically represent an insurmountable problem to develop truly simultaneous methods. Such methods require the use of a chemical modifier in sufficient amount to properly stabilize the most volatile analytes (while preventing over-stabilization of the most refractories), a pyrolysis temperature low enough to avoid

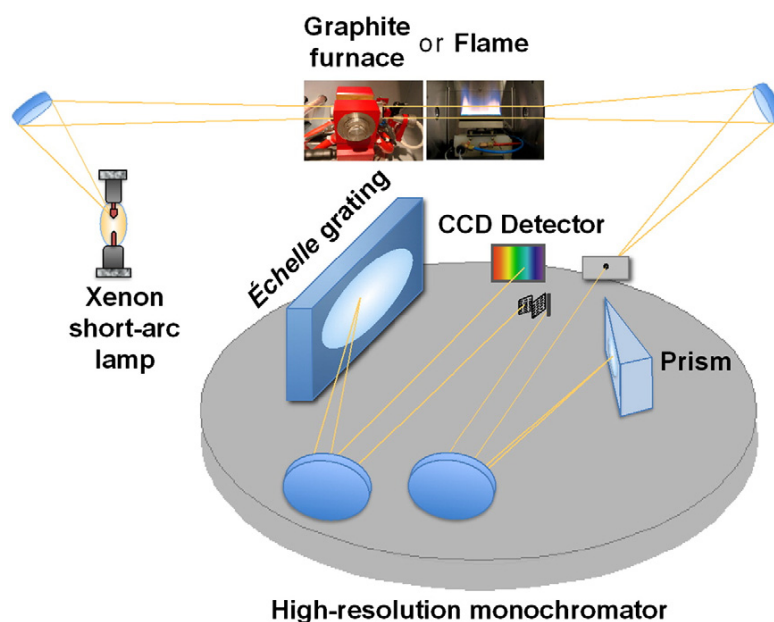


Fig. 2. Setup of a high-resolution continuum source atomic absorption spectrometer. Reproduced with permission from Springer (<http://link.springer.com/article/10.1007/s00216-010-4105-x>).

losses of these volatile analytes (but hopefully high enough to remove most matrix components whenever possible) and an atomization temperature sufficiently high to properly atomize the most refractory elements, without decreasing too much the signal intensity for the most volatile ones. For instance, in reference [21] the use of an atomization temperature of 2500 °C, needed for Co, Fe and Ni, results in a 30% decrease in sensitivity for Pb.

However, when targeting elements with very different thermal behaviors, it also needs to be considered that maybe truly simultaneous monitoring is not required. It may be possible to determine the analytes sequentially, but from the same tube firing, thus obtaining all information from the very same replicate. For instance, dos Santos et al. used this approach for the direct determination of Cd and Fe in grain products [22] and in beans and soils [23], as they proposed a method with two atomization temperatures: 1700 °C for Cd and 2600 °C for Fe. Vignola et al. also used two atomization steps for the determination of these elements in sewage sludge using slurry sampling [24].

Resano et al. explored such sequential approach a bit further, because if different atomization steps are used, then it becomes unnecessary to monitor the same spectral area all the time [25]. In this way, it was feasible to determine Cd and Ni in a biological reference material (BCR CRM 679 White cabbage) using direct solid sampling by means of two different approaches: i) truly simultaneous monitoring using the closely adjacent lines of 228.802 nm (Cd) and 228.998 nm (Ni) and a temperature program optimized for both analytes (atomization at 2300 °C) or ii) sequential atomization of Cd (1300 °C) and Ni (2500 °C). In the latter case, it is possible to use not only the optimum temperature for every analyte, but also an optimum wavelength, as different wavelengths can be monitored during each atomization step (228.802 nm for Cd and 234.554 nm for Ni). Duarte et al. have also used this sequential approach to determine both Cd (atomization at 1500 °C monitoring the 228.802 nm line) and Cr (atomization at 2600 °C monitoring either the 357.869 nm or the 428.972 nm line, depending on the analyte content) in a given aliquot of biomass and biomass samples [26].

By taking all these aspects into consideration, the possibility not only of monitoring similar elements truly simultaneously, but also

of monitoring extremely dissimilar elements in a sequential way (but from the same sample aliquot) using optimum furnace and wavelength conditions for each one of them, it may be concluded that while the (different) thermochemical characteristics of the target analytes always need to be considered, that is not the real limiting factor in developing more multi-element approaches in HR CS GFAAS (in a similar way as it occurs with electrothermal vaporization-inductively coupled plasma mass spectrometry [27]). Instead, with the instrumentation currently available, the main problem when simultaneous monitoring is intended is to find lines that are sufficiently close and that show a suitable sensitivity for the analyte content.

Thus, the recommended approach when trying to develop a multi-element method is to focus on the target analytes with less suitable lines available and evaluate if, in the vicinity of these, there are some lines of the other elements that could be used for the determination. For instance, in [21] the goal was to directly determine Co, Fe, Ni and Pb in carbon nanotubes, elements that were expected to be present at different levels ($\mu\text{g g}^{-1}$ for Pb and mg g^{-1} for the others).

To determine Pb at such levels, it is only possible to select either the most sensitive line (217.001 nm) or the alternative resonance line located at 283.306 nm, which is roughly two-times less sensitive, but actually offers a better signal-to-noise ratio and, thus, it is typically preferred for trace determinations of Pb. Therefore, the choice is limited and it is only necessary to evaluate if in the spectral area surrounding these lines there are other lines available. In fact, in the vicinity of the 283.306 nm there are secondary lines available for Co (two of them), Fe and Ni (see Fig. 3). Obviously these are not the most sensitive lines for these elements, but they are actually well suited for the high Co, Ni and Fe levels expected to be present in the carbon nanotube samples. It is only because these requirements are met, availability of close lines that show adequate sensitivity, that it was possible to develop a simultaneous method for the determination of the four target elements. Optimization of the temperature program, type and amount of chemical modifier, calibration approach, etc., is always required, but those are technical aspects that can very often be solved in a satisfactory way. Moreover, when developing a multi-element approach it is always important to make sure that the baseline is correctly defined for all the target lines, which might

Table 1

Applications reporting on multi-element determinations (from a single replicate) using high-resolution continuum source graphite furnace atomic absorption spectrometry.

Wavelength (nm)	Analyte	Limit of detection/characteristic mass	Modifier	Sample	Remarks	Reference
228.802 228.726	Cd Fe	0.6 $\mu\text{g kg}^{-1}$ /0.9 pg 0.5 mg kg^{-1} /1.2 ng	W-Ir mixture permanent modifier (200 μg each)	Grain products	Determination using two atomization temperatures (1700 °C for Cd, 2600 °C for Fe) Direct solid sampling after grinding (in case of bread and biscuits) Aqueous standards for calibration	[22]
228.802 228.726	Cd Fe	2 $\mu\text{g kg}^{-1}$ /0.7 pg 4.5 mg kg^{-1} /1.0 ng	W-Ir mixture permanent modifier (200 μg each)	Beans and soil	Determination using two atomization temperatures (1700 °C for Cd, 2600 °C for Fe) Side pixel evaluation at the line wings used to reduce sensitivity and increase dynamic range for determination of high Fe concentrations Direct solid sampling after grinding Aqueous standards for calibration	[23]
357.868 358.120	Cr Fe	1 $\mu\text{g kg}^{-1}$ /3.6 pg 0.6 mg kg^{-1} /0.5 ng	No modifier	Crude oil	Simultaneous determination Sample homogenization in an ultrasonic bath Aqueous standards for calibration	[66]
240.725 240.674	Co V	8 $\mu\text{g kg}^{-1}$ /7.2 pg 1.2 mg kg^{-1} /2.1 ng	Pd (20 μg) and Triton X-100 (20 μL 0.05%)	Crude oil	Simultaneous determination Side pixel evaluation at the line wings used to reduce sensitivity and increase dynamic range for determination of high Co concentrations Sample homogenization in an ultrasonic bath Aqueous standards for calibration	[67]
305.432 305.633	Ni V	3 $\mu\text{g g}^{-1}$ /320 pg 1 $\mu\text{g g}^{-1}$ /85 pg	HNO ₃ (0.35 mol L ⁻¹) + Triton X-100 (5% m/v)	Crude oil	Simultaneous determination Oil-in-water emulsions + HNO ₃ for total Ni and V concentration; in the absence of HNO ₃ only the thermally stable fraction is determined, such the volatile fractions can be obtained by difference	[68]
228.802 228.725	Cd Fe	0.03 $\mu\text{g g}^{-1}$ /0.9 pg 90 $\mu\text{g g}^{-1}$ /1.6 ng	Pd (5 μg), HNO ₃ (0.7 mol L ⁻¹) and HF (0.2 mol L ⁻¹)	Sewage sludge	Determination using two atomization temperatures (1300 °C for Cd, 2300 °C for Fe) Slurry sampling Aqueous standards for calibration	[24]
352.685 352.604 352.617 352.454	Co Fe Fe Ni	N.A./75 pg N.A./3 ng N.A./27 ng N.A./30 pg	Pd (5 μg)	NIST SRM 1566a Oyster tissue	Simultaneous determination Direct solid sampling Aqueous standards for calibration	[25]
228.802 228.998 234.554	Cd Ni Ni	11 pg/16 pg	Pd (1 μg)	BCR CRM 679 White cabbage	Comparison between truly simultaneous (228.802 nm and 228.998 nm) or sequential (228.802 nm and 234.554 nm) monitoring of Cd and Ni from the same sample aliquot Direct solid sampling Aqueous standards for calibration	[25]
319.397 319.200	Mo Ti	1.5 $\mu\text{g L}^{-1}$ /1.6 $\mu\text{g L}^{-1}$ 6.5 $\mu\text{g L}^{-1}$ /6.6 $\mu\text{g L}^{-1}$	Pt (1 μg)	Urine in clinical filter paper	Simultaneous determination Direct solid sampling of dried urine spots Matrix-matched standards for calibration	[69]
283.393 283.443 283.245 283.455 283.306 228.802 357.869 428.972	Co Co Fe Ni Pb Cd Cr Cr	86 ng/82 ng 440 ng/400 ng 6 ng/18 ng 65 ng/66 ng 23 pg/17 pg 1.1 $\mu\text{g kg}^{-1}$ /N.A. 21 $\mu\text{g kg}^{-1}$ /N.A. 90 $\mu\text{g kg}^{-1}$ /N.A.	Pd (100 ng)	Carbon nanotubes Biomass samples and biomass ashes	Simultaneous determination Direct solid sampling Side pixel evaluation at the line wings used to reduce sensitivity and increase dynamic range Aqueous standards for calibration Sequential determination from the same sample aliquot Determination using two atomization temperatures (1500 °C for Cd, 2600 °C for Cr) and a different wavelength for each element Direct solid sampling Aqueous standards for calibration	[21] [26]

N.A.: not available.

not be the case if one of the lines is too close to the end of the detector window, so centering this window properly becomes important.

Other examples of multi-element determinations are shown in Table 1. Apart from [25], where the direct simultaneous determination of three elements, Co, Fe and Ni, in NIST SRM 1566a Oyster tissue is reported, the rest of the studies typically involve the determination of two analytes, one showing many lines available, such as Co, Fe, Ni or Ti, together with another element for which the number of suitable lines is limited. There are a few other articles reporting simultaneous monitoring of various elements (Cd, Fe and Ni in [28]; Fe and Pt in [19]) in which no sample analysis is attempted, only aqueous standards are tested, so these are not included in the table.

It is also necessary to stress that, despite the limitations discussed earlier, the current HR CS GFAAS instrumentation brings some advantages to achieving simultaneous multi-element determinations. In particular, this instrumentation is much more suitable for monitoring of secondary lines, which is very often required in these applications. This is simply because the source intensity for all these lines is approximately the same, contrary to what occurs with a line source that provides less intensity for the secondary lines, as discussed by Welz et al. [18]. This typically results in better signal-to-noise ratio, and, eventually, in better limits of detection (LODs).

The second important aspect is the possibility to adapt the sensitivity because it is a function of the detector pixels selected, as

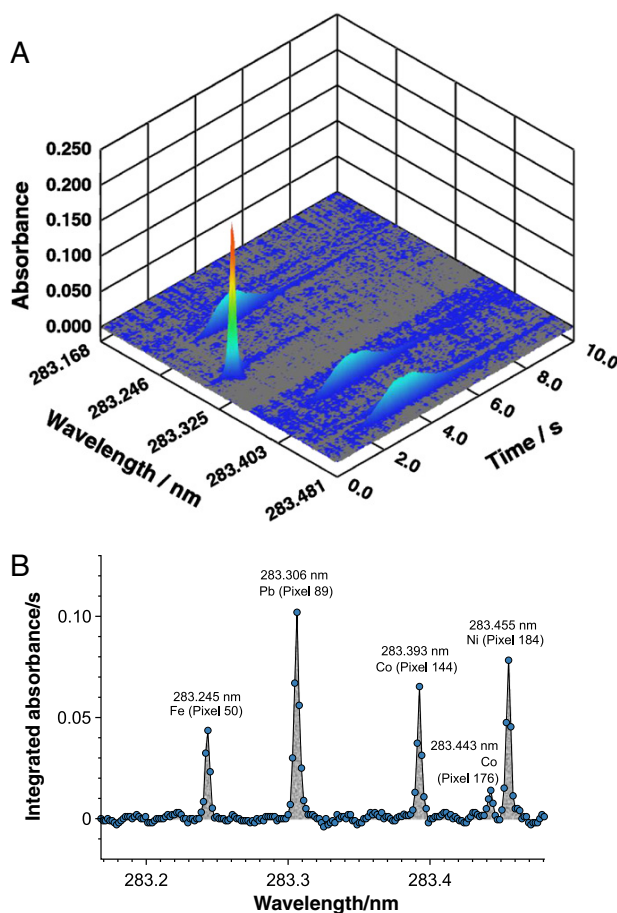


Fig. 3. (A) Time- and wavelength-resolved absorbance profiles in the vicinity of the 283.306 nm line obtained by direct atomization of a solid sample (0.151 mg of 2LV-BIO-SWCNT-1, which contains approx. 1 ng of Pb, 0.4 mg of Fe, 2.7 mg of Ni and 2.7 of mg Co). (B) Same signal as in (A), but time-integrated. The signal recorded by every individual detector pixel is shown (blue dots). Reproduced with permission from the Royal Society of Chemistry (<http://pubs.rsc.org/en/content/articlelanding/2013/ja/c3ja30377b>).

discussed by Heitmann et al. [29]. Typically, for best sensitivity and lowest detection limits, use of the central pixels is preferred. As higher analyte masses are introduced into the atomizer, at some point the signal at the center of the absorption line will start growing more slowly, losing the linear response and eventually become saturated (see Fig. 4D). However, as the analyte mass increases, the absorption line profile also becomes much broader, such that use of side pixels may become advantageous, permitting an increase in the working range. Fig. 4 shows a recent example of this strategy permitting determination of Ag in solid samples over 5 orders of magnitude (although not shown in the figure and not relevant for the work intended, it could be mentioned that even higher amounts of Ag could be determined with such an approach) [30].

This strategy becomes even more important when attempting to perform multi-element determinations, because it is practically the only approach that permits adapting (decreasing) the sensitivity for an element without affecting the sensitivity for the others. Moreover, it is simple to apply, as the information from all the 200 detector pixels is always available. The analyst can decide which ones are most suitable, even post-analyses, without the need for measuring any further replicates [21].

If this strategy is chosen it has to be ensured that the increase in the signal width for the element present at higher levels is indeed

not negatively affecting the signal of some other analyte, which may occur if the signals of both are too close (e.g., spectral overlap or issues to properly define the baseline for the smaller signal in the vicinity of the larger one). It also needs to be considered that introduction of too high masses may lead to memory effects, which can be severe for refractory elements.

In any case, it is also important to stress that most of the articles highlighted in Table 1 demonstrate the superior potential of HR CS GFAAS for the direct analysis of solid samples or of complex liquid materials, using straightforward calibration strategies [31]. Thus, the possibility to perform direct multi-element analysis, in addition to the lack of digestion/pre-concentration approaches, results in methods with a very high sample throughput.

3. Other advantages derived from multi-line monitoring using high-resolution continuum source graphite furnace atomic (or molecular) absorption spectrometry

3.1. Monitoring several lines of the same analyte

In addition to some capabilities to perform faster multi-element determinations, the simultaneous monitoring of a portion of the spectrum in which several lines may be available brings about other significant advantages that have to be taken into consideration as well.

For instance, there are situations in which different lines of the same element are available. Appearance of these multiplets is not very infrequent when monitoring atomic lines (particularly for those elements that show more lines such as Co, Cr, Fe, Mn, Ni, and Ti), but it is not the rule. However, this is in fact the most common scenario when using GF for determining non-metals (e.g., halogens, P, S), a possibility that is now available for HR CS instruments [32]. In such case, the rotational hyperfine structure of molecular electronic transitions is typically monitored. In this way, several spectral features with a width similar to that of atomic lines are often available, as shown in Fig. 5A for CS (used to determine S).

It is always beneficial to have different lines to select from. In practice, there are two possible situations: either the different lines available show similar sensitivities, or else their relative sensitivities are very different.

If the sensitivities of the different lines differ significantly, the obvious advantage is that it becomes easier to find one with a sensitivity that is suitable for the analyte content, thus avoiding dilutions (difficult to perform when direct solid sampling is intended) or use of alternative conditions. In fact, it is interesting to point out that monitoring of multiplets used to be problematic with traditional line source AAS devices, because the combined signal of all the lines was typically measured owing to the correspondence between emission and absorption lines and the low resolution of the monochromators used. This led to poor linearity. The situation has been reversed owing to the use of a continuum source with high resolution, since now every line is independently measured and the analyst can choose the most suitable one in every particular case.

For instance, Fig. 5B shows a triplet for Co that can be monitored simultaneously. The three different lines available show good linearity between 5 to 250 $\mu\text{g L}^{-1}$ (241.164 nm), 100 $\mu\text{g L}^{-1}$ to 10,000 $\mu\text{g L}^{-1}$ (241.276 nm) and 5000 to 250,000 $\mu\text{g L}^{-1}$ (241.319 nm), respectively, thus permitting coverage of a working range of almost 5 orders of magnitude with ease. Another similar example for Ni (234.554 nm, 234.663 nm and 234.751 nm lines) is reported in [25]. Lepri et al. reported simultaneous monitoring of the 344.099 nm and 344.388 nm lines for Fe, and the 232.003 nm and 232.138 nm lines for Ni, in order to expand the working linear range when carrying out the direct analysis of charcoal and carbon black [33]. Limburg and Einax recently discussed how the use of different molecular CaBr transitions can be used to determine Br, achieving a 5 orders of magnitude working

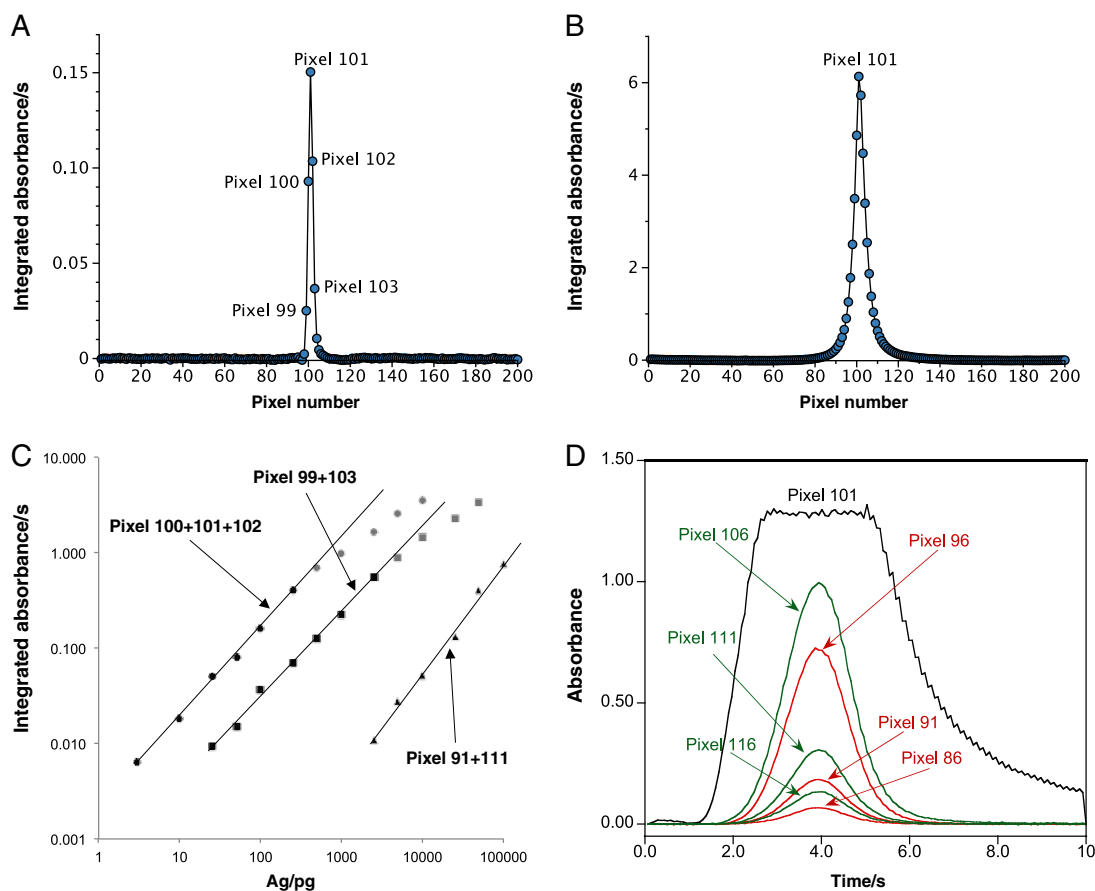


Fig. 4. (A) Absorption line profiles obtained for 250 pg of Ag at 328.068 nm, showing the signal recorded by every individual detector pixel (blue dots). (B) Absorption line profiles obtained for 100,000 pg of Ag at 328.068 nm. (C) Linearity observed when monitoring the Ag 328.068 nm atomic line as a function of the detector pixels selected. Gray points fall outside the linear range. (D) Time-resolved absorbance signal measured at Ag 328.068 nm obtained upon the atomization of Ag 100,000 pg as a function of the detector pixel selected.

Reproduced with permission from the Royal Society of Chemistry (<http://pubs.rsc.org/en/content/articlelanding/2013/ay/c2ay26456k>).

range (from $10 \mu\text{g L}^{-1}$ to 1g L^{-1}) [34]. Some further examples of doublets and triplets can be seen in chapter 6 of [3].

The other situation, having several lines available exhibiting relatively similar sensitivity, is more frequent when monitoring molecular transitions. This topic, determination of non-metals using molecular spectra by means of HR CS MAS is clearly receiving more attention, as some of these elements are determined with great difficulties by means of other techniques. It is beyond the scope of this review to examine this aspect in detail and the reader can find more information in a dedicated review [32]. However, it is important to stress that in this case, while evaluation of the analytical performance of the different transitions is always recommended [35,36], there is no need for using only one for quantitation. The use of several of these transitions will always improve the reliability of results (e.g., if good agreement is found among them) and can serve to detect potential spectral overlaps [37,38].

In addition, it has already been demonstrated by Heitmann et al. that monitoring several strong lines and summing their signals increases the sensitivity and can, consequently, improve the limit of detection (LOD) [29]. In that work the improvement obtained was limited (less than a factor of two), because only triplets were investigated (Mn 279.482/279.827/280.108 nm; and V 318.341/318.397/318.538 nm). Information on the characteristic masses of the V triplet is also available in [39].

In the case of molecular transitions, their number with similar sensitivity and a favorable signal-to-noise ratio can be higher. For instance, use

of 9 transitions for the monitoring of PO in the vicinity of 213.618 nm results in a 3-fold improvement in terms of LOD [40], while monitoring of the six strongest CS transitions in the vicinity of 258 nm also decreased the LOD by a factor of 3 [37]. Heitmann et al. also showed that an improvement in terms of precision can be achieved for CS monitoring (from 4% to 2% RSD) when summing the 5 strongest transitions found in this spectral region [41]. A similar improvement (a factor of 2 in % RSD) is reported in ref. [37] for direct analysis of solid samples.

3.2. Use of an internal standard

Another interesting option that is available when using HR CS AAS instrumentation is the possibility to use an internal standard (IS). This strategy is considered as almost mandatory to achieve accurate results with some techniques, but its use in atomic absorption has never been popular owing to the obvious limitations of line source based instruments.

However, there are still very few studies making use of this possibility when using HR CS GFAAS [25], while there are a few more using it for HR CS FAAS methods. Those will be discussed in a subsequent section.

The reasons for this limited use are varied. On the one hand, lack of tradition may play a role. On the other hand, there are some requirements that an ideal internal standard should fulfill, the main being:

- i) the IS should not be present in the sample at significant levels;
- ii) the IS should be truly simultaneously monitored together with

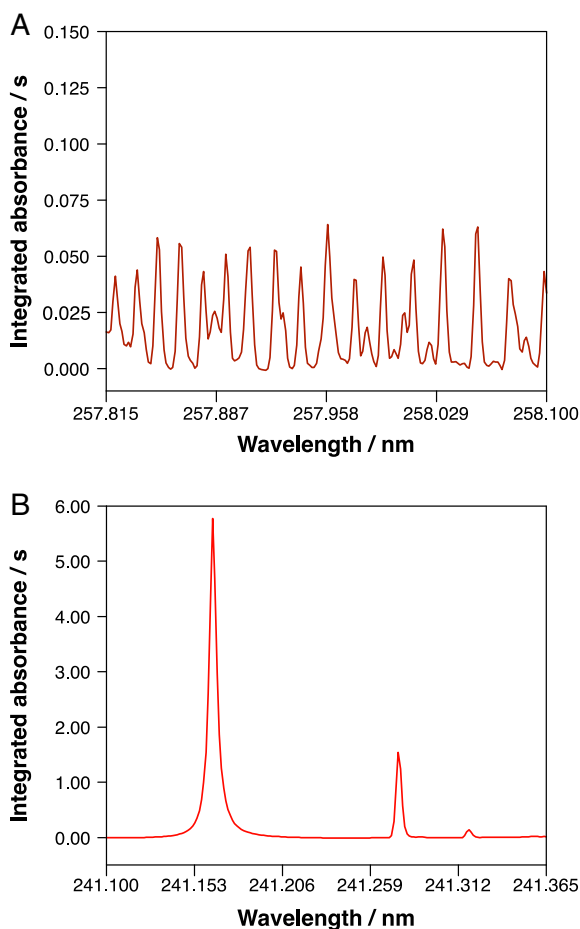


Fig. 5. (A) Wavelength resolved time-integrated absorbance spectrum obtained after the vaporization of 500 ng of sulfur (as Na_2SO_4) recorded when monitoring the spectral region in the vicinity of 258 nm by means of high-resolution continuum source graphite furnace molecular absorption spectrometry. (B) Wavelength-resolved time-integrated absorbance spectrum showing the Co triplet located in the vicinity of 241.2 nm, as obtained after HR CS GFAAS measurement of an aqueous solution containing 1 μg of Co.

(A) Reproduced with permission from the Royal Society of Chemistry (<http://pubs.rsc.org/en/content/articlelanding/2012/ja/c2ja10322b>).

- the analyte(s), such that all the fluctuations occurring during the measurements are properly compensated for;
- iii) the signals of both analyte(s) and IS should be within the linear range, and their ratio as close to unity as possible.

Complying with requisite ii) is perhaps the most difficult, because it means that the IS should possess a line that is close enough (0.2–1.0 nm, see Section 2) to that of the analyte, so both can be simultaneously monitored. Moreover, the thermochemical characteristics of both the IS and the analyte should be similar, otherwise their atomization will take place at different times, and thus both elements will not endure exactly the same conditions during the measurements.

Despite these limitations, it is noteworthy that the IS can be chosen by the analyst from all the elements that are not expected to be present in the samples, and its concentration can also be chosen, thus making the use of less sensitive lines always possible. Therefore, these requirements are not as difficult to meet as those discussed earlier for multi-element determinations, so it is the authors' opinion that more determinations could make use of this strategy, which can serve to correct for matrix or sampling effects in a simple way, or compensate for variations (e.g., tube and/or platform deterioration)

occurring during long measurement sessions (e.g., determination of the degree of homogeneity of a sample, which may require hundreds of replicate values [42]).

An example of the benefits of this strategy is shown in Fig. 6 [25]. As shown in Fig. 6A, the determination of Ni in biological samples (urine and blood) using line 231.096 nm is obviously affected by matrix effects that may lead to the use of cumbersome calibration approaches (e.g., standard addition) or to the use of time consuming sample pretreatment procedures. Alternatively, addition of Co to the samples may help in solving the problem. There is a Co line (231.136 nm) that is close enough to that of Ni so both can be simultaneously monitored. Moreover, Co behaves very similarly to Ni in a graphite furnace, so their signals follow an almost identical temporal evolution (see Fig. 6B). As shown in Fig. 6C, simply by using Co as IS it is possible to obtain a similar response (Ni/Co ratio) from aqueous standards, blood or urine samples, thus allowing for the development of a straightforward “dilute and shoot” method for analysis of such samples.

It is interesting to note that, while work on use of IS in connection with HR CS GFAAS instrumentation is so limited, a few more articles were published in the past using a simultaneous line-source spectrometer (SIMAA 6000) [43–50], proving the benefits of using an IS when carrying out a GFAAS determination, in particular for correcting for matrix effects [43,45,47–50]. Such an instrument is no longer commercially available, but it was designed to combine the radiation originating from up to four hollow cathode lamps and direct it through the graphite furnace, such that several elements could be measured at the same time but at different wavelengths. Thus, perhaps selecting an IS was easier with such a device, because there was no need to look for adjacent lines. However, while this requirement of using adjacent lines may be a limitation, the use of an IS with HR CS GFAAS instrumentation can lead to even better results because, in principle, it is preferable to use an IS with a line that is found in the same spectral region as that of the analyte, with a common baseline defined for both lines, to better compensate for some aspects that might be wavelength dependent (lamp fluctuations, light scattering, etc.).

In any case, it is clear from these studies that it is important to find an internal standard that possesses thermochemical characteristics similar to that of the analyte, such that the sources of noise for the IS and the analyte are well correlated and the overall uncertainty of the measurements decreases. However, there are situations in which the main reason for signal variation is not the measurement but the sampling error, because the volume of sample available is very low (e.g., 2 μL) or the sample contains a high amount of gaseous bubbles [44]. In such case, the criteria for finding an IS can be relaxed, and an improvement in the results can be obtained even if the IS does not perfectly match the thermochemical behavior of the analyte [25].

3.3. Background correction

Finally, another important advantage derived from the simultaneous monitoring of multiple lines is the potential to mathematically correct for spectral overlaps, as long as it is possible to obtain a suitable reference spectrum, that is a spectrum in which only the interfering species is present.

Fig. 7 shows such an example. A simultaneous determination of Cd and Ni in a biological sample (*Daphnia magna* [51,52]) is intended. The signal from the sample shows that it is possible to see adjacent Cd (228.802 nm) and Ni (228.998 nm) lines simultaneously, but there is a structured background appearing in this area and it may overlap with the target lines, particularly with Ni since its signal is smaller (see Fig. 7A). This is one of the most important advantages of HR CS AAS instrumentation, that it is possible to clearly see any concomitant interference. In some cases, it may be feasible to avoid the spectral overlap simply by optimization of the temperature program or by addition of a chemical modifier, but in other situations

this may be more difficult. But even then, it is often possible to correct for the interference and achieve accurate results in situations that are beyond the capabilities of traditional BG correction systems (e.g., deuterium or Zeeman).

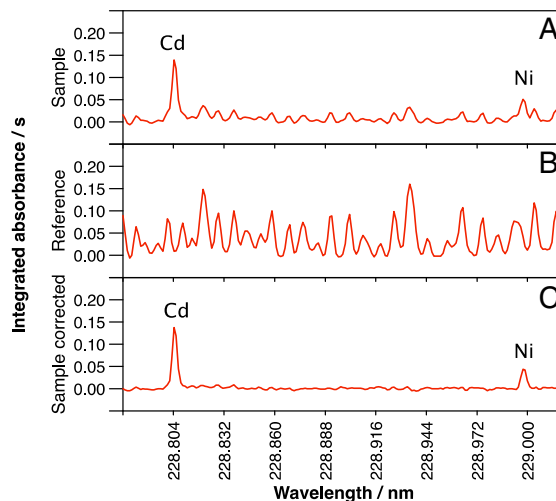
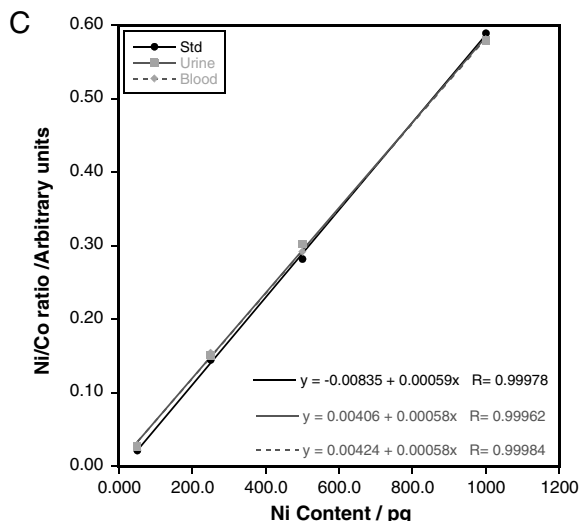
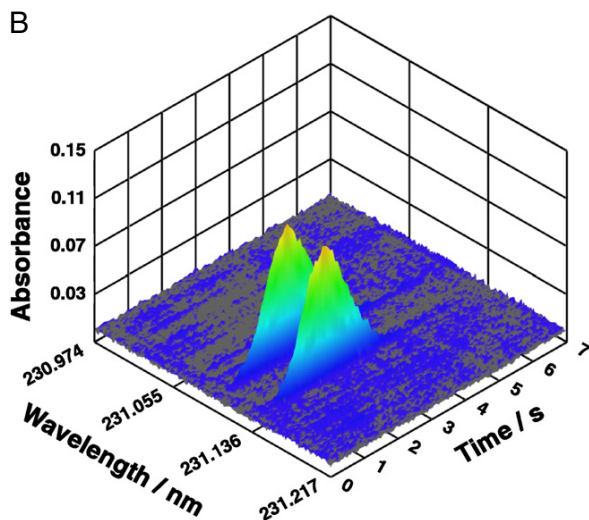
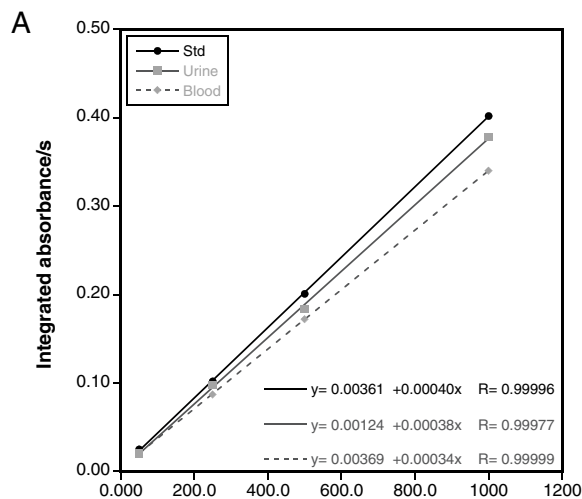


Fig. 7. Wavelength-resolved time-integrated absorbance spectra obtained after HR CS GFAAS measurement of (A) a *Daphnia magna* specimen cultured in a media exposed to Cd and Ni; (B) a 1% (m/v) $\text{NH}_4\text{H}_2\text{PO}_4$ solution; and (C) same signal as in (A), after subtraction of the reference spectrum (shown in B) using least-squares background correction.

When this type of structured background is found, it is typically attributed to the absorption spectrum of diatomic species (rotational hyperfine structure of molecular electronic transitions, as discussed in Section 3.1). In this spectral region, it is well-known that PO may absorb, so a reference spectrum was obtained with a phosphate solution. Such a spectrum is shown in Fig. 7B and it can be seen that there is a good correspondence between the peaks of the interference present in the sample (Fig. 7A) and those of the reference spectrum, confirming the identity of the interfering molecule. Thus, since the relation between the intensities of all the PO transitions should always be constant (only subject to small experimental errors), based on the signals obtained for PO transitions that do not overlap with Cd and Ni atomic lines, it is possible to proportionally subtract the portion of the PO signal that overlaps with the Cd and Ni signals in every sample replicate using a least squares algorithm. In this way, the corrected spectrum shows only the atomic absorption of the target analytes, with a stable baseline, as shown in Fig. 7C.

This least-squares background correction (LSBC) approach has been demonstrated to work very efficiently, even in situations in which the signal of the interference is significantly higher than that of the analyte. Obviously, the reason for this efficacy is that all the transitions are simultaneously monitored, because if a sequential method would be used any variations occurring during the alternate measurements would affect the final results.

Table 2 shows several examples found in the literature reporting on the use of LSBC since the first article published by Becker-Ross et al. [15]. It should be mentioned that it is possible to correct for spectral overlaps with this approach even when there is more than one interfering species. In such case, the sequential subtraction of every

Fig. 6. (A) Calibration curves for aqueous standard solutions, for blood and for urine samples spiked with a known amount of Ni obtained upon HR CS GFAAS monitoring of the 231.096 nm Ni atomic line. (B) Time- and wavelength-resolved absorbance spectra obtained upon HR CS GFAAS measurement of an aqueous solution containing Ni (1 ng) and Co (400 ng) showing the atomic lines of 231.096 nm (Ni) and 231.136 nm (Co). (C) Same curves as in (A) when using the signal obtained for Co as internal standard. All solutions and samples were spiked with a fixed amount of Co (40 mg L^{-1}). Urine and blood samples were diluted with milli-Q water 1:1 and 1:3, respectively. Reproduced with permission from Elsevier (<http://www.sciencedirect.com/science/article/pii/S0584854711000590>).

Table 2

Applications reporting on the use of least-squares background correction (LSBC) in connection with high-resolution continuum source graphite furnace atomic (or molecular) absorption spectrometry.

Target analyte	Wavelength (nm)	Interfering species	Sample	Other comments	Reference
As	193.696	NaCl, PO	Human urine		[15]
Se	196.026	NO, PO			
Tl	276.787	SO ₂	Marine sediments	Solid sampling	[70]
Pb	217.001	PO	Biological CRMs	Solid sampling	[71]
Ni	232.003/ 232.138	C ₂		Filter furnace	[28]
P	213.547/ 213.618	PO		Evaluation of different sources, correction systems and chemical modifiers	[72–74]
Al	396.152	Unidentified (caused by presence of sugar and Fe)	Pharmaceutical products		[75]
Ag	328.068 338.289	SO	Rock and ores	Solid sampling	[76]
Sb	231.147	SiO, PO	Sediments	Solid sampling	[53]
Ni	232.003/ 232.138	SiO	Coal CRMs, activated charcoal, black carbon	Solid sampling	[33]
V	318.341/ 318.397/ 318.538	Unidentified (S-based)			
Au	242.795	PO	Mouse tissues	Solid sampling	[54]
Zn	213.856	Fe			[18]
AlF	227.477	Unidentified, possibly N-based molecule	Whole blood		[55]

reference spectrum should provide the net atomic absorption signal. This was, in fact, demonstrated with the first example published [15], since As was corrected for the presence of both NaCl and PO in urine, while NO and PO interfered with the determination of Se in the same sample. In both cases, it was possible to attain accurate results after LSBC for analysis of a reference material. A similar case was discussed by Araujo et al. [53] for analysis of sediments, in which the sequential correction for both SiO and PO species permitted a clean spectrum in which it was possible to quantify the target analyte (Sb) to be obtained.

It is also important to mention that this strategy may also be used to correct for overlaps from atomic lines, but only if the interfering element shows another atomic line in the vicinity that is free from interferences, as needed for proportionally subtracting the effect of the interfering line. Such a situation has been described for overcoming the interference of Fe on Zn [18]. Determination of Zn may be difficult in samples with high Fe level because the main line for Zn (213.856 nm) is severely overlapped by a secondary Fe line (213.859 nm). However, there is another Fe line that is close enough (213.970 nm) such that it can also be simultaneously monitored, and therefore LSBC can be successfully applied.

Obviously, the key to apply LSBC is to have a suitable reference spectrum. This is very easy when the interfering species is produced by the own atomizer because a blank can readily provide a reference spectrum. That was the case when evaluating HR CS GFAAS with a filter furnace atomizer, as C₂ species overlapping with Ni lines appeared at high temperatures (higher than 2500 °C) [28].

Unfortunately, this is not the most frequent situation. In most cases, and in particular when using GFAAS for analysis of complex materials or solid samples, the interference is produced by the matrix. However, even then it is not difficult to find out which species is (are) interfering, because there are only a few molecules that are stable enough at high temperatures and can absorb in the region of interest. As can be seen from Table 2, formation of CS, NO, PO, or SiO is frequently the reason for the interference, although for some particular samples other molecules should be considered as well (e.g., NaCl in urine).

Finally, in some cases it is even simpler to obtain a proper reference if a material similar to the sample but not containing the analyte can be obtained. For instance, in [54], analysis of tissues from mouse exposed to Au nanoparticles was performed. In this case, it was also possible to obtain tissues of animals not exposed to Au, and then

their spectrum should only show the interference. In other cases, if the analyte is very volatile, it may be present in the sample, but could be removed during the pyrolysis in the absence of any chemical modifier, thus again permitting the reference spectrum to be obtained with ease.

Reference [55] reports on a singular case, determination of Al in blood by monitoring AlF. In such case, the analyte is always present in the sample but, if no fluorinating agent is added, Al will not form AlF, so no analyte signal will be observed. Thus, it was again easy to obtain a perfect reference spectrum from the sample and correct for the spectral overlap of a molecule, even though the interfering molecule could not be identified.

4. Multi-line monitoring in high-resolution continuum source flame atomic (or molecular) absorption spectrometry

The situation for FAAS is very different from that discussed for GFAAS. Since the nature of the signals obtained in FAAS is not transient, but instead a steady-state signal can be obtained, most authors aiming at multi-element determinations have opted for a fast sequential mode. Wavelengths and flame conditions can be changed quickly (about 20 s [56]) and it is thus possible to determine every element under optimum conditions in a single run. Several of these examples are summarized in Table 3.

As discussed earlier, use of less sensitive lines in HR CS FAAS is favorable because the intensity of the Xe lamp is practically the same for all of them, thus leading to better signal-to-noise ratios in comparison with line source AAS. Furthermore, it is also possible to use side pixels to decrease the sensitivity [57–60]. Thus, it is easier with this instrumentation to accommodate the sensitivity such that all the elements of interest can be monitored sequentially, but in the same run, without the need for diluting the samples. For all these reasons, HR CS FAAS can be considered as a very suitable tool for performing fast multi-element determinations.

In addition to this, the same advantages noted for GFAAS, monitoring several lines of the same analyte, internal standardization and LSBC, have also been explored for determinations by FAAS.

For instance, Bechlin et al. evaluated the summation of adjacent transitions: for B (249.773 nm and 249.677 nm), for PO (246.400 nm, 247.620 nm and 247.780 nm) and for S (257.595 nm and 257.958 nm), and reported a moderate improvement in the LOD for S using this approach (30.5 mg L⁻¹ using one detector pixel, while using the most

Table 3

Applications reporting on multi-line monitoring by means of high-resolution continuum source flame atomic (or molecular) absorption spectrometry.

Wavelength (nm)	Element or molecule monitored	Limit of detection	Sample	Remarks	Reference
324.754	Cu	5.4 $\mu\text{g L}^{-1}$	Soil extracts	Fast sequential multi-element analysis Use of side pixel registration on the main Fe line (248.327 nm) to reduce sensitivity and increase the linear range for Fe	[57]
248.325	Fe	147 $\mu\text{g L}^{-1}$			
252.744	Fe	55.0 $\mu\text{g L}^{-1}$			
279.482	Mn	3.0 $\mu\text{g L}^{-1}$			
213.875	Zn	4.5 $\mu\text{g L}^{-1}$			
217.001	Pb	10 $\mu\text{g L}^{-1}$			
283.306		17 $\mu\text{g L}^{-1}$	Phosphoric acid	Use of LSBC to solve the spectral overlap caused by PO molecules at 217.001 nm Pb line Use of Co as internal standard to correct for matrix-induced variations in the transport efficiency	[62]
324.754	Cu	4 ng g^{-1}	Lubricating oil	Fast sequential multi-element analysis Evaluation of different sample preparation procedures	[77]
357.869	Cr	23 ng g^{-1}			
248.327	Fe	7.4 ng g^{-1}			
232.003	Ni	5 ng g^{-1}			
217.000	Pb	15 ng g^{-1}			
217.581	Sb	51 ng g^{-1}			
213.857	Zn	3 ng g^{-1}			
309.271	Al	250 ng g^{-1}			
553.548	Ba	10 ng g^{-1}			
313.259	Mo	40 ng g^{-1}			
251.611	Si	40 ng g^{-1}	Steel samples	Estimation of B isotope ratios On the 208.9 nm B line, peak absorption of ^{10}B and ^{11}B differs by 2.5 pm Internal standards (Fe, Ni) used to correct for monochromator instability	[65]
318.398	V	22 ng g^{-1}			
208.959	^{10}B	Not available			
208.957	^{11}B	Not available			
239.856	Ca	0.6 mg L^{-1}	Sugarcane and CRM leaves	Fast sequential multi-element analysis Use of side pixel registration to reduce sensitivity for Mg and increase the linear range Use of LSBC to solve the spectral overlap caused by NO bands on Zn at 213.857 nm	[58]
324.754	Cu	0.0077 mg L^{-1}			
248.327	Fe	0.0077 mg L^{-1}			
404.414	K	0.4 mg L^{-1}			
202.582	Mg	0.1 mg L^{-1}			
279.482	Mn	0.0015 mg L^{-1}			
213.857	Zn	0.0059 mg L^{-1}			
249.773	B	0.001 mg g^{-1}			
239.856	Ca	0.15 mg g^{-1}			
324.754	Cu	0.58 $\mu\text{g g}^{-1}$			
248.327	Fe	1.6 $\mu\text{g g}^{-1}$			
404.414	K	0.12 mg g^{-1}			
202.588	Mg	0.048 mg g^{-1}			
279.482	Mn	0.096 $\mu\text{g g}^{-1}$			
313.259	Mo	0.016 $\mu\text{g g}^{-1}$			
213.618	P	0.14 mg g^{-1}			
258.055	S (as CS)	0.11 mg g^{-1}	Liquid fertilizers and NIST 120c phosphate rock	Fast sequential multi-element analysis Use of side pixel registration to reduce sensitivity and increase the linear range for K Evaluation of atomic and molecular lines for P	[60]
213.857	Zn	0.66 $\mu\text{g g}^{-1}$			
404.422	K	0.2 mg L^{-1}			
213.618	P	55 mg L^{-1}			
246.400	P (as PO)	20 mg L^{-1}			
247.620		17 mg L^{-1}			
247.780		12 mg L^{-1}			
324.616		18 mg L^{-1}			
327.040		20 mg L^{-1}			
257.595	S (as CS)	15.1 mg L^{-1}			
257.958		22.4 mg L^{-1}			
258.056		21.8 mg L^{-1}			
323.658	S (as HS)	2558.3 mg L^{-1}			
324.064		1502.8 mg L^{-1}	Fuel and crude oils	Comparison of approaches to define the baseline Sample dissolution in xylene	[36]
327.990		955.8 mg L^{-1}			
258.056	S (as CS)	18 mg kg^{-1} in solution 450 mg kg^{-1} in sample (dilution 1/25 m/v)			
239.856	Ca	0.012 mg g^{-1}			
202.852	Mg	0.005 mg g^{-1}	Dairy products (yogurt, cow milk and milk powder)	Fast sequential multi-element analysis Slurry sampling	[80]
324.754	Cu	0.12 mg kg^{-1}			
248.327	Fe	0.62 mg kg^{-1}	Soybean, olive and sunflower oils	Fast sequential multi-element analysis Microemulsion preparation with propan-1-ol	[81]
232.003	Ni	0.58 mg kg^{-1}			
213.857	Zn	0.12 mg kg^{-1}			
251.611	Si	8.4 $\mu\text{g L}^{-1}$			
			Lubricant oil	Use of LSBC to solve the spectral overlap caused by CS molecules Use of an internal standard to correct for matrix-induced variations in the transport efficiency Ba, Ti, V and W tested as internal standards W (255.135 nm) provided the best results	[63]

Table 3 (continued)

Wavelength (nm)	Element or molecule monitored	Limit of detection	Sample	Remarks	Reference
324.754	Cu	4.8 $\mu\text{g L}^{-1}$ (IS Bi) 5.2 $\mu\text{g L}^{-1}$ (IS Te)	Distilled alcoholic beverages	Use of an internal standard to correct for matrix-induced variations in the transport efficiency Bi, In, Sn and Te tested as internal standards. Best results with Bi (223.061 nm) and Te (214.281 nm) Dilute-and-shoot approach	[64]
249.773 249.677	B	0.5 mg L^{-1} 2.9 mg L^{-1} $\Sigma = 1.0 \text{ mg L}^{-1}$	Medicinal plants	Fast sequential multi-element analysis Investigation on summation of the absorbance (Σ) of different lines to improve limits of detection	[61]
246.400 247.620 247.780	P (as PO)	28.1 mg L^{-1} 13.7 mg L^{-1} 48.8 mg L^{-1} $\Sigma = 17.4 \text{ mg L}^{-1}$			
257.595 257.958	S (as CS)	34.7 mg L^{-1} 73.8 mg L^{-1} $\Sigma = 30.5 \text{ mg L}^{-1}$			
217.001 212.739	Pb Sb	0.02 mg L^{-1} 5.7 mg L^{-1}	Pewter alloy cups	Fast sequential multi-element analysis	[56]
328.068 228.802 240.206 357.869 324.754 232.003 217.000 213.856	Ag Cd Co Cr Cu Ni Pb Zn	0.18 mg kg^{-1} 0.14 mg kg^{-1} 0.36 mg kg^{-1} 0.25 mg kg^{-1} 0.09 mg kg^{-1} 1.0 mg kg^{-1} 1.4 mg kg^{-1} 0.18 mg kg^{-1}	Soil	Fast sequential multi-element analysis	[82]

sensitive transition only — 257.595 nm and 5 detector pixels a value of 34.7 mg L^{-1} was reported) [61].

Concerning the use of an internal standard, again the requisites differ from those discussed for GFAAS. While in principle it would be preferable to select as an IS an element that could be truly simultaneously monitored, since the signal achieved is very stable with regard to time, authors have selected internal standards (Co for Pb [62], W for Si [63], Bi or Te for Cu [64]) that were actually monitored sequentially. Despite such an asynchronous measurement, the strategy has demonstrated its potential to correct for non-spectral interferences, allowing for the development of straightforward calibration approaches.

A different type of application that also made use of an internal standard was developed by Wiltsche et al. [65], who evaluated the performance of HR CS FAAS for B isotopic analysis. The atomic lines for pure ^{10}B and pure ^{11}B are slightly different: 208.95898 nm for ^{10}B and 208.95650 nm for ^{11}B , as measured by emission techniques. This difference is still too small to observe two fully resolved peaks with an HR CS FAAS instrument. However, what can be appreciated is that the B absorption profile shifts as a function of the boron isotopic ratio: the higher the % of ^{10}B , the higher the wavelength at which the maximum of the boron peak is found. Thus, there is potential to determine the B isotopic composition. However, since the isotopic shift of boron is very small, it is necessary to correct for possible instabilities of the monochromator in order to achieve sufficient precision and accuracy. This can be done using a suitable internal standard that is monitored truly simultaneously. In this case, use of either Fe or Ni appears feasible, as these elements show atomic lines close enough to those of B, and it was found that both elements exhibited a satisfactory performance for this purpose. It must be remembered that, since the internal standard is used to correct for spectral drifts only, it is not necessary that it be absent from the sample for this application. The authors conclude that, while use of HR CS FAAS cannot rival mass spectrometric approaches in terms of accuracy and precision, it is an inexpensive and simple alternative suitable to distinguish different enrichment levels of ^{10}B (within 5%) in steel samples.

Finally, use of LSBC has proved to be as useful as it is in GFAAS to avoid spectral overlaps. Again, it is possible to correct for the interference produced by molecules that are always present in a flame (e.g., OH, or CN and NO in acetylene-nitrous oxide flames), or by molecules

that are formed from compounds present in the matrix, as long as a suitable reference spectrum is obtained. Table 3 highlights some examples where this correction strategy has been deployed. For instance, determination of Pb using its most sensitive line (217.001 nm) in phosphoric acid, which gives rise to overlapping PO transitions [62], becomes possible using LSBC. The same is true for the determination of Si in lubricant oil, which gives rise to the formation of CS molecules, whose transitions overlap with the main atomic line of Si (251.611 nm) [63]. Determination of Zn in plant tissues, which is affected by the overlap between NO transitions and the main atomic line of Zn (213.856 nm), is also feasible providing LSBC is used [58]. Chapter 8 of [3] shows some additional examples, including the determination of Zn in iron and steel samples (interference already discussed in Section 3.3.) or of Zn in high purity copper (Cu and NO interference).

5. Conclusions

The characteristics of commercially available HR CS GFAAS instrumentation (simultaneous monitoring of a narrow spectral bandwidth only) limit its possibilities for multi-element determinations, such that only a few elements, typically including some with many available atomic lines (e.g., Co, Cr, Fe, Ni, and Ti), can be determined in a truly simultaneous way. However, despite these limitations, the potential of the technique for direct analysis of solid samples or very complex liquid samples still makes it appealing in various contexts. In addition, sequential monitoring of elements from the same aliquot has been demonstrated to be feasible, as long as their volatility is sufficiently different to permit their temporal resolution. This latter approach does not require the target elements to have closely adjacent lines, thus further improving the possibilities of monitoring various elements from a sample in a single run.

In addition to multi-element determinations, there are also a number of significant advantages arising from the simultaneous monitoring of various elemental lines or molecular transitions. While some of these advantages have been widely explored in the literature (e.g., use of LSBC), there are still very few papers reporting on the use of an internal standard or exploring quantification using multiple transitions of the same element or molecule.

Finally, it is necessary to state that the situation for HR CS FAAS is rather different, since the stable nature of the signal generated with

this technique makes fast sequential monitoring very appealing, and several authors have demonstrated the potential of such an approach to develop fast multi-element methods.

Acknowledgments

This work has been funded by the Spanish Ministry of Economy and Competitiveness (project CTQ2012-33494) and the Aragón Government (Fondo Social Europeo). MRF thanks the Spanish Ministry of Economy and Competitiveness for her PhD grant (project CTQ2009-08606).

References

- M. Resano, F. Vanhaecke, M.T.C. de Loos-Vollebregt, Electrothermal vaporization for sample introduction in atomic absorption, atomic emission and plasma mass spectrometry—a critical review with focus on solid sampling and slurry analysis, *J. Anal. At. Spectrom.* 23 (2008) 1450–1475.
- B. Welz, Atomic absorption spectrometry—pregnant again after 45 years, *Spectrochim. Acta Part B* 54 (1999) 2081–2094.
- B. Welz, H. Becker-Ross, S. Florek, U. Heitmann, High-resolution continuum source AAS, *The Better Way to Do Atomic Absorption Spectrometry*, Wiley-VCH, Weinheim, 2005.
- A. Walsh, The development of the atomic absorption spectrophotometer, *Spectrochim. Acta Part B* 54 (1999) 1943–1952.
- P.N. Keliher, C.C. Wohlers, High resolution atomic absorption spectrometry using an echelle grating monochromator, *Anal. Chem.* 46 (1974) 682–687.
- A.T. Zander, T.C. O'Haver, P.N. Keliher, Continuum source atomic absorption spectrometry with high resolution and wavelength modulation, *Anal. Chem.* 48 (1976) 1166–1175.
- B.T. Jones, B.W. Smith, J.D. Winefordner, Continuum source atomic absorption spectrometry in a graphite furnace with photodiode array detection, *Anal. Chem.* 61 (1989) 1670–1674.
- C.M.M. Smith, J.M. Harnly, Sensitivities and detection limits for graphite furnace atomic absorption spectrometry using a continuum source and linear photodiode array detection, *Spectrochim. Acta Part B* 49 (1994) 387–398.
- J.M. Harnly, Instrumentation for simultaneous multi-element atomic absorption spectrometry with graphite furnace atomization, *Fresenius J. Anal. Chem.* 355 (1996) 501–509.
- J.M. Harnly, The future of atomic absorption spectrometry: a continuum source with a charge coupled array detector, *J. Anal. At. Spectrom.* 14 (1999) 137–146.
- J.B. True, R.H. Williams, M.B. Denton, On the implementation of multi-element continuum source graphite furnace atomic absorption spectrometry utilizing an echelle/CID detection system, *Appl. Spectrosc.* 53 (1999) 1102–1110.
- H. Becker-Ross, S. Florek, U. Heitmann, R. Weisse, Influence of the spectral bandwidth of the spectrometer on the sensitivity using continuum source AAS, *Fresenius J. Anal. Chem.* 355 (1996) 300–303.
- S. Florek, H. Becker-Ross, T. Florek, Adaptation of an echelle spectrograph to a large CCD detector, *Anal. Bioanal. Chem.* 355 (1996) 269–271.
- H. Becker-Ross, S.V. Florek, Echelle spectrometers and charge-coupled devices, *Spectrochim. Acta Part B* 52 (1997) 1367–1375.
- H. Becker-Ross, S. Florek, U. Heitmann, Observation, identification and correction of structured molecular background by means of continuum source AAS—determination of selenium and arsenic in human urine, *J. Anal. At. Spectrom.* 15 (2000) 137–141.
- B. Welz, High-resolution continuum source AAS: the better way to perform atomic absorption spectrometry, *Anal. Bioanal. Chem.* 381 (2005) 69–71.
- B. Welz, D.L.G. Borges, F.G. Lepri, M.G.R. Vale, U. Heitmann, High-resolution continuum source electrothermal atomic absorption spectrometry—an analytical and diagnostic tool for trace analysis, *Spectrochim. Acta Part B* 62 (2007) 873–883.
- B. Welz, S. Morés, E. Carasek, M.G.R. Vale, M. Okrus, H. Becker-Ross, High-resolution continuum source atomic and molecular absorption spectrometry—a review, *Appl. Spectrosc. Rev.* 45 (2010) 327–354.
- M. Resano, E. Garcia-Ruiz, High-resolution continuum source graphite furnace atomic absorption spectrometry: is it as good as it sounds? A critical review, *Anal. Bioanal. Chem.* 399 (2011) 323–330.
- H. Becker-Ross, S. Florek, U. Heitmann, M. Huang, M. Okrus, B. Radziuk, Continuum source atomic absorption spectrometry and detector technology: a historical perspective, *Spectrochim. Acta Part B* 61 (2006) 1015–1030.
- M. Resano, E. Bolea-Fernández, E. Mozas, M.R. Flórez, P. Grinberg, R.E. Sturgeon, Simultaneous determination of Co, Fe, Ni and Pb in carbon nanotubes by means of solid sampling high-resolution continuum source graphite furnace atomic absorption spectrometry, *J. Anal. At. Spectrom.* 28 (2013) 657–665.
- L.M.G. dos Santos, R.G.O. Araujo, B. Welz, S. do C. Jacob, M.G.R. Vale, H. Becker-Ross, Simultaneous determination of Cd and Fe in grain products using direct solid sampling and high-resolution continuum source electrothermal atomic absorption spectrometry, *Talanta* 78 (2009) 577–583.
- L.M.G. dos Santos, B. Welz, R.G.O. Araujo, S.C. Jacob, M.G.R. Vale, A. Martens, I.B. Gonzaga Martens, H. Becker-Ross, Simultaneous determination of Cd and Fe in beans and soil of different regions of Brazil using high-resolution continuum source graphite furnace atomic absorption spectrometry and direct solid sampling, *J. Agric. Food Chem.* 57 (2009) 10089–10094.
- F. Vignola, D.L.G. Borges, A.J. Curtius, B. Welz, H. Becker-Ross, Simultaneous determination of Cd and Fe in sewage sludge by high-resolution continuum source electrothermal atomic absorption spectrometry with slurry sampling, *Microchem. J.* 95 (2010) 333–336.
- M. Resano, L. Rello, M. Flórez, M.A. Belarra, On the possibilities of high-resolution continuum source graphite furnace atomic absorption spectrometry for the simultaneous or sequential monitoring of multiple atomic lines, *Spectrochim. Acta Part B* 66 (2011) 321–328.
- A.T. Duarte, M.B. Dessuy, M.G.R. Vale, B. Welz, J.B. de Andrade, Sequential determination of Cd and Cr in biomass sample and their ashes using high-resolution continuum source graphite furnace atomic absorption spectrometry and direct solid sample analysis, *Talanta* 13 (2013) 55–60.
- M. Resano, M. Verstraete, F. Vanhaecke, L. Moens, Evaluation of the multi-element capabilities of electrothermal vaporization quadrupole-based ICP mass spectrometry, *J. Anal. At. Spectrom.* 16 (2001) 1018–1027.
- U. Heitmann, H. Becker-Ross, D. Katskov, Feasibility of filter atomization in high-resolution continuum source atomic absorption spectrometry, *Spectrochim. Acta Part B* 61 (2006) 351–360.
- U. Heitmann, B. Welz, D.L.G. Borges, F.G. Lepri, Feasibility of peak volume, side pixel and multiple peak registration in high-resolution continuum source atomic absorption spectrometry, *Spectrochim. Acta Part B* 62 (2007) 1222–1230.
- M. Resano, A.C. Lapeña, M.A. Belarra, Potential of solid sampling high-resolution continuum source graphite furnace atomic absorption spectrometry to monitor the Ag body burden in individual *Daphnia magna* specimens exposed to Ag nanoparticles, *Anal. Methods* 5 (2013) 1130–1139.
- M. Resano, J. Briceño, M.A. Belarra, Direct determination of Hg in polymers by solid sampling-graphite furnace atomic absorption spectrometry. A comparison of the performance of line source and continuum source instrumentation, *Spectrochim. Acta Part B* 64 (2009) 520–529.
- B. Welz, F.G. Lepri, R.G.O. Araujo, S.L.C. Ferreira, M.-D. Huang, M. Okrus, H. Becker-Ross, Determination of phosphorus, sulfur and the halogens using high-temperature molecular absorption spectrometry in flames and furnaces—a review, *Anal. Chim. Acta* 647 (2009) 137–148.
- F.G. Lepri, D.L.G. Borges, R.G.O. Araujo, B. Welz, F. Wendler, M. Krieg, H. Becker-Ross, Determination of heavy metals in activated charcoals and carbon black for Lyocell fiber production using direct solid sampling high-resolution continuum source graphite furnace atomic absorption and inductively coupled plasma optical emission spectrometry, *Talanta* 81 (2010) 980–987.
- T. Limburg, J.W. Einax, Determination of bromine using high-resolution continuum source molecular absorption spectrometry in a graphite furnace, *Microchem. J.* 107 (2013) 31–36.
- M.-D. Huang, H. Becker-Ross, S. Florek, U. Heitmann, M. Okrus, B. Welz, H.S. Ferreira, High-resolution continuum source molecular absorption spectrometry of nitrogen monoxide and its application for the determination of nitrate, *J. Anal. At. Spectrom.* 25 (2010) 163–168.
- Z. Kowalewska, Feasibility of high-resolution continuum source molecular absorption spectrometry in flame and furnace for sulphur determination in petroleum products, *Spectrochim. Acta Part B* 66 (2011) 546–556.
- M. Resano, M.R. Flórez, Direct determination of sulfur in solid samples by means of high-resolution continuum source graphite furnace molecular absorption spectrometry using palladium nanoparticles as chemical modifier, *J. Anal. At. Spectrom.* 27 (2012) 401–412.
- H.S. Ferreira, F.G. Lepri, B. Welz, E. Carasek, M.-D. Huang, Determination of sulfur in biological samples using high-resolution molecular absorption spectrometry in a graphite furnace with direct solid sampling, *J. Anal. At. Spectrom.* 25 (2010) 1039–1045.
- F.G. Lepri, B. Welz, D.L.G. Borges, A.F. Silva, M.G.R. Vale, U. Heitmann, Speciation analysis of volatile and non-volatile vanadium compounds in Brazilian crude oils using high-resolution continuum source graphite furnace atomic absorption spectrometry, *Anal. Chim. Acta* 558 (2006) 195–200.
- M. Resano, J. Briceño, M.A. Belarra, Direct determination of phosphorus in biological samples using a solid sampling-high resolution-continuum source electrothermal spectrometer: comparison of atomic and molecular absorption spectrometry, *J. Anal. At. Spectrom.* 24 (2009) 1343–1354.
- U. Heitmann, H. Becker-Ross, S. Florek, M.-D. Huang, M. Okrus, Determination of non-metals via molecular absorption using high-resolution continuum source absorption spectrometry and graphite furnace atomization, *J. Anal. At. Spectrom.* 21 (2006) 1314–1320.
- In: U. Kürfurst (Ed.), *Solid Sample Analysis: Direct and Slurry Sampling using GF-AAS and ETV-ICP*, Springer, Berlin, 1998.
- B. Radziuk, N.P. Romanova, Y. Thomassen, Evaluation of internal standardisation in electrothermal atomic absorption spectrometry, *Anal. Commun.* 36 (1999) 13–16.
- A.P. Oliveira, J.A. Gomes Neto, J.A. Nóbrega, P.V. Oliveira, Use of the internal standardization for difficult sampling by graphite furnace atomic absorption spectrometry, *Talanta* 64 (2004) 334–337.
- P.R.M. Correia, P.V. Oliveira, J.A.G. Neto, J.A. Nóbrega, Silver as internal standard for simultaneous determination of Cd and Pb in whole blood by electrothermal atomic absorption spectrometry, *J. Anal. At. Spectrom.* 19 (2004) 917–922.
- P.R.M. Correia, P.V. Oliveira, Evaluation of internal standardization in atomic absorption spectrometry using correlation graphs, *Quím. Nova* 28 (2005) 539–543.
- A. Paiva de Oliveira, J.A. Gomes Neto, J.A. Nóbrega, P.V. Oliveira, Internal standardization in graphite furnace atomic absorption spectrometry: comparative use of As and Ge to minimize matrix effects on Se determination in milk, *Spectrochim. Acta Part B* 60 (2005) 681–686.
- P.R.M. Correia, P.V. Oliveira, Cobalt as internal standard for arsenic and selenium determination in urine by simultaneous atomic absorption spectrometry, *Talanta* 67 (2005) 46–53.

- [49] S.R. de Oliveira, J.A. Gomes Neto, Evaluation of Bi as internal standard to minimize matrix effects on the direct determination of Pb in vinegar by graphite furnace atomic absorption spectrometry using Ru permanent modifier with co-injection of Pd/Mg(NO₃)₂, Spectrochim. Acta Part B 62 (2007) 1046–1050.
- [50] N.M. Caldas, S.R. Oliveira, J.A. Gomes Neto, Feasibility of internal standardization in the direct and simultaneous determination of As, Cu and Pb in sugar-cane spirits by graphite furnace atomic absorption spectrometry, Anal. Chim. Acta 636 (2009) 1–5.
- [51] J. Briceño, M.A. Belarra, K.A.C. De Schampelaere, S. Vanblaere, C.R. Janssen, F. Vanhaecke, M. Resano, Direct determination of Zn in individual *Daphnia magna* specimens by means of solid sampling high-resolution continuum source graphite furnace atomic absorption spectrometry, J. Anal. At. Spectrom. 25 (2010) 503–510.
- [52] R. Evens, K.A.C. De Schampelaere, L. Balcaen, Y. Wang, K. De Roy, M. Resano, M.R. Flórez, P. Van der Meer, N. Boon, F. Vanhaecke, C.R. Janssen, Liposomes as an alternative delivery system for investigating dietary metal toxicity to *Daphnia magna*, Aquat. Toxicol. 105 (2011) 661–668.
- [53] R.G.O. Araujo, B. Welz, F. Vignola, H. Becker-Ross, Correction of structured molecular background by means of high-resolution continuum source electrothermal atomic absorption spectrometry—determination of antimony in sediment reference materials using direct solid sampling, Talanta 80 (2009) 846–852.
- [54] M. Resano, E. Mozas, C. Crespo, J. Briceño, J. del Campo-Menoyo, M.A. Belarra, Solid sampling high-resolution continuum source graphite furnace atomic absorption spectrometry to monitor the biodistribution of gold nanoparticles in mice tissue after intravenous administration, J. Anal. At. Spectrom. 25 (2010) 1864–1873.
- [55] M. Aramendía, M.R. Flórez, M. Piette, F. Vanhaecke, M. Resano, Al determination in whole blood samples as AlF₃ via high-resolution continuum source graphite furnace molecular absorption spectrometry: potential application to forensic diagnosis of drowning, J. Anal. At. Spectrom. 26 (2011) 1964–1973.
- [56] M.B. Dessuy, R.M. de Jesus, G.C. Brandao, S.L.C. Ferreira, M.G.R. Vale, B. Welz, Fast sequential determination of antimony and lead in pewter alloys using high-resolution continuum source flame atomic absorption spectrometry, Food Addit. Contam. A 30 (2013) 202–207.
- [57] J.L. Raposo Jr., S.R. de Oliveira, N.M. Caldas, J.A. Gomes Neto, Evaluation of alternate lines of Fe for sequential multi-element determination of Cu, Fe, Mn and Zn in soil extracts by high-resolution continuum source flame atomic absorption spectrometry, Anal. Chim. Acta 627 (2008) 198–202.
- [58] S.R. de Oliveira, J.L. Raposo Jr., J.A. Gomes Neto, Fast sequential multi-element determination of Ca, Mg, K, Cu, Fe, Mn and Zn for foliar diagnosis using high-resolution continuum source flame atomic absorption spectrometry: feasibility of secondary lines, side pixel registration and least-squares background correction, Spectrochim. Acta Part B 64 (2009) 593–596.
- [59] S.R. Oliveira, J.A. Gomes Neto, J.A. Nóbrega, B.T. Jones, Determination of macro- and micronutrients in plant leaves by high-resolution continuum source flame atomic absorption spectrometry combining instrumental and sample preparation strategies, Spectrochim. Acta Part B 65 (2010) 316–320.
- [60] R. Borges Ferreira, S.R. Oliveira, V.P. Franzini, A. Virgilio, J.L. Raposo Jr., J.A. Gomes Neto, Evaluation of lines of phosphorus and potassium by high-resolution continuum source flame atomic absorption spectrometry for liquid fertilizer analysis, Atom. Spectrosc. 32 (2011) 56–61.
- [61] M.A. Bechlin, J.A. Gomes Neto, J.A. Nóbrega, Evaluation of lines of boron, phosphorus and sulfur by high-resolution continuum source flame atomic absorption spectrometry for plant analysis, Microchem. J. 109 (2013) 134–138.
- [62] J. Raposo Jr., S.R. Oliveira, J.A. Nóbrega, J.A. Gomes Neto, Internal standardization and least-squares background correction in high-resolution continuum source flame atomic absorption spectrometry to eliminate interferences on determination of Pb in phosphoric acid, Spectrochim. Acta Part B 63 (2008) 992–995.
- [63] J.L. Raposo Jr., S.R. Oliveira, J.A. Gomes Neto, J.A. Nóbrega, B.T. Jones, Determination of silicon in lubricant oil by high-resolution continuum source flame atomic absorption spectrometry using least-square background correction and internal standardization, Anal. Lett. 44 (2011) 2150–2161.
- [64] J.L. Raposo Jr., A.P. de Oliveira, B.T. Jones, J.A. Gomes Neto, Internal standardization combined with dilute-and-shoot preparation of distilled alcoholic beverages for Cu determination by high-resolution continuum source flame atomic absorption spectrometry, Talanta 92 (2012) 53–57.
- [65] H. Wiltche, K. Prattes, M. Zischka, G. Knapp, Estimation of boron isotope ratios using high resolution continuum source atomic absorption spectrometry, Spectrochim. Acta Part B 64 (2009) 341–346.
- [66] I.M. Dittert, J.S.A. Silva, R.G.O. Araujo, A.J. Curtius, B. Welz, H. Becker-Ross, Direct and simultaneous determination of Cr and Fe in crude oil using high-resolution continuum source graphite furnace atomic absorption spectrometry, Spectrochim. Acta Part B 64 (2009) 537–543.
- [67] I.M. Dittert, J.S.A. Silva, R.G.O. Araujo, A.J. Curtius, B. Welz, H. Becker-Ross, Simultaneous determination of cobalt and vanadium in undiluted crude oil using high-resolution continuum source graphite furnace atomic absorption spectrometry, J. Anal. At. Spectrom. 25 (2010) 590–595.
- [68] D.P.C. Quadros, E.S. Chaves, F.G. Lepri, D.L.G. Borges, B. Welz, H. Becker-Ross, A.J. Curtius, Evaluation of Brazilian and Venezuelan crude oil samples by means of the simultaneous determination of Ni and V as their total and non-volatile fractions using high-resolution continuum source graphite furnace atomic absorption spectrometry, Energy Fuel 24 (2010) 5907–5911.
- [69] L. Rello, A.C. Lapeña, M. Aramendia, M.A. Belarra, M. Resano, A dried spot test to simultaneously monitor Mo and Ti levels using solid sampling high-resolution continuum source graphite furnace atomic absorption spectrometry, Spectrochim. Acta Part B 81 (2013) 11–19.
- [70] B. Welz, M.G.R. Vale, M.M. Silva, H. Becker-Ross, M.-D. Huang, S. Florek, U. Heitmann, Investigation of interferences in the determination of thallium in marine sediment reference materials using high-resolution continuum-source atomic absorption spectrometry and electrothermal atomization, Spectrochim. Acta Part B 57 (2002) 1043–1055.
- [71] D.L.G. Borges, A.F. da Silva, B. Welz, A.J. Curtius, U. Heitmann, Determination of lead in biological samples by high-resolution continuum source graphite furnace atomic absorption spectrometry with direct solid sampling, J. Anal. At. Spectrom. 21 (2006) 763–769.
- [72] F.G. Lepri, M.B. Dessuy, M.G. Vale, D.L.G. Borges, B. Welz, U. Heitmann, Investigation of chemical modifiers for phosphorus in a graphite furnace using high-resolution continuum source atomic absorption spectrometry, Spectrochim. Acta Part B 61 (2006) 934–944.
- [73] M.B. Dessuy, M.G.R. Vale, F.G. Lepri, B. Welz, U. Heitmann, Investigation of phosphorus atomization using high-resolution continuum source electrothermal atomic absorption spectrometry, Spectrochim. Acta Part B 62 (2007) 429–434.
- [74] M.B. Dessuy, M.G.R. Vale, F.G. Lepri, D.L.G. Borges, B. Welz, M.M. Silva, U. Heitmann, Investigation of artifacts caused by deuterium background correction in the determination of phosphorus by electrothermal atomization using high-resolution continuum source atomic absorption spectrometry, Spectrochim. Acta Part B 63 (2008) 337–348.
- [75] D. Bohrer, U. Heitmann, M.-D. Huang, H. Becker-Ross, S. Florek, B. Welz, D. Bertagnolli, Determination of aluminum in highly concentrated iron samples: study of interferences using high-resolution continuum source atomic absorption spectrometry, Spectrochim. Acta Part B 62 (2007) 1012–1018.
- [76] I.M. Dittert, D.L.G. Borges, B. Welz, A.J. Curtius, H. Becker-Ross, Determination of silver in geological samples using high-resolution continuum source electrothermal atomic absorption spectrometry and direct solid sampling, Microchim. Acta 167 (2009) 21–26.
- [77] V.R. Amorim Filho, J.A. Gomes Neto, Different lubricating oil treatments for the determination of Cu, Cr, Fe, Ni, Sb, Pb and Zn by HR-CS FAAS, Anal. Lett. 41 (2008) 1555–1570.
- [78] V.R. Amorim Filho, J.A. Gomes Neto, Evaluation of lubricating oil preparation procedures for the determination of Al, Ba, Mo, Si and V by high-resolution continuum source FAAS, Anal. Sci. 25 (2009) 95–100.
- [79] A. Virgilio, J.L. Raposo Jr., A.A. Cardoso, J.A. Nóbrega, J.A. Gomes Neto, Determination of total sulfur in agricultural samples by high-resolution continuum source flame molecular absorption spectrometry, J. Agric. Food Chem. 59 (2011) 2197–2201.
- [80] G.C. Brandao, G.D. Matos, S.L.C. Ferreira, Slurry sampling and high-resolution continuum source flame atomic absorption spectrometry using secondary lines for the determination of Ca and Mg in dairy products, Microchem. J. 98 (2011) 231–233.
- [81] L.S. Nunes, J.T.P. Barbosa, A.P. Fernandes, V.A. Lemos, W.N.L. dos Santos, M.G.A. Korn, L.S.G. Teixeira, Multi-element determination of Cu, Fe, Ni and Zn content in vegetable oils samples by high-resolution continuum source atomic absorption spectrometry and microemulsion sample preparation, Food Chem. 127 (2011) 780–783.
- [82] T. Frentiu, M. Ponta, R. Hategan, Validation of an analytical method based on the high-resolution continuum source flame atomic absorption spectrometry for the fast-sequential determination of several hazardous/priority hazardous metals in soils, Chem. Cent. J. 7 (2013) 43–53.



Contents lists available at SciVerse ScienceDirect

Aquatic Toxicology

journal homepage: www.elsevier.com/locate/aquatox

Liposomes as an alternative delivery system for investigating dietary metal toxicity to *Daphnia magna*

Roel Evens^{a,*}, Karel A.C. De Schampelaere^a, Lieve Balcaen^b, Yingying Wang^c, Karen De Roy^c, Martín Resano^d, María del Rosario Flórez^{b,d}, Paul Van der Meer^e, Nico Boon^c, Frank Vanhaecke^b, Colin R. Janssen^a

^a Laboratory of Environmental Toxicology, Ghent University, Belgium

^b Department of Analytical Chemistry, Ghent University, Krijgslaan 281-S12, BE-9000 Ghent, Belgium

^c Laboratory of Microbial Ecology and Technology, Ghent University, Belgium

^d Department of Analytical Chemistry, University of Zaragoza, Pedro Cerbuna 12, E-50009 Zaragoza, Spain

^e Department of Applied Analytical and Physical Chemistry, Particle and Interfacial Technology Group, Ghent University, Belgium

ARTICLE INFO

Article history:

Received 17 May 2011

Received in revised form 1 September 2011

Accepted 10 September 2011

Keywords:

Daphnia magna
Nickel
Liposomes
Dietary metals

ABSTRACT

Dietary metal toxicity studies with invertebrates such as *Daphnia magna* are often performed using metal-contaminated algae as a food source. A drawback of this approach is that it is difficult to distinguish between the direct toxicity of the metal and indirect effects caused by a reduced essential nutrient content in the metal-contaminated diet, due to prior exposure of the algae to the metal. This hampers the study of the mechanisms of dietary metal toxicity in filter-feeding freshwater invertebrates. The aim of the present study was to develop a technique for producing metal-contaminated liposomes as an alternative delivery system of dietary metals. These liposomes are not vulnerable to metal-induced shifts in nutrient quality. Liposomes were prepared by the hydration of phosphatidylcholine in media containing either 0 (control) or 50 mg Ni/L. The liposomes had average diameters of 19.31 (control) and 10.48 μm (Ni-laden), i.e., a size appropriate for ingestion by *D. magna*. The liposome particles were then mixed with uncontaminated green algae in a 1/10 ratio (on a dry wt. basis) to make up two diets that differed in Ni content (i.e., 2.0 μg Ni/g dry wt. in the control and 144.2 μg Ni/g dry wt. in the Ni-contaminated diet, respectively). This diet was then fed to *D. magna* during a 21-day chronic bioassay. The experiment showed that the Ni content and the size distribution of the liposomes were stable for at least 7 days. Also the use of phosphatidylcholine as a liposome component did not affect the reproduction of the daphnids. Exposure to increased level of dietary Ni resulted in 100% mortality after 14 days of exposure and in an increased whole-body Ni concentration in *D. magna* of 14.9 and 20.4 μg Ni/g dry wt. after 7 and 14 days of exposure, respectively. The Ni-exposed daphnids also exhibited a reduced size (i.e., 30% smaller than the control) after 7 days and a completely halted growth between day 7 and day 14. In terms of reproduction, the size of the first brood (number of juveniles) of the Ni-exposed daphnids was significantly reduced (by 85%) compared to the control. None of the Ni-exposed individuals were able to produce a second brood before dying. The algal ingestion rate – after correction for the indirect effect of a reduced size – was increased (by 68%) by dietary Ni after 6 days of exposure compared to the control, but was severely reduced (by 80% compared to the control) after 13 days. These data suggest that an inhibition of the ingestion process may have contributed to the observed effects of dietary Ni on growth and reproduction beyond 6 days of exposure, although the involvement of other mechanisms cannot be excluded. The mechanism(s) which led to the reduced growth during the first week of exposure remain unclear, although inhibition of the ingestion process can likely be excluded here as an explanation. Overall, this paper demonstrates, using this new method of delivering dietary Ni via liposome carriers and thus excluding potential diet quality shifts, that dietary Ni can indeed induce toxic effects in *D. magna*. This method may therefore be a promising tool to help further elucidate the mechanisms of dietary metal toxicity to filter-feeding invertebrates.

© 2011 Elsevier B.V. All rights reserved.

* Corresponding author. Tel.: +32 92643707; fax: +32 92643766.
E-mail address: Roel.Evens@ugent.be (R. Evens).

1. Introduction

Recent studies have shown that exposure to metal-contaminated diets can be harmful to various freshwater invertebrates (De Schampelaere et al., 2004; Wilding and Maltby, 2006; Sofyan et al., 2007a,b; De Schampelaere et al., 2007; Geffard et al., 2008). However, the pre-exposure of the invertebrate's diet to metals – in order to obtain the metal-contaminated diet for use in ecotoxicological experiments – can result in a significant decline of the concentration of essential nutrients in that diet. McLarnon-Riches et al. (1998), for example, showed that Cu, Zn and Cd exposure affects the (essential) fatty acid content and composition of the green alga *Pseudokirchneriella subcapitata*. This potentially confounding factor has, however, been rarely addressed in dietary metal toxicity studies. Adverse effects observed in invertebrates exposed to metal-contaminated food can thus not be unambiguously linked to the metal in the diet itself. For instance, Evens et al. (2009) showed that the reproduction and growth of *Daphnia magna*, after exposure to Ni-contaminated algae (*P. subcapitata*), was not only significantly correlated with an increased Ni content in the diet, but also with a lower concentration of omega-3-polyunsaturated fatty acids (ω 3-PUFA) in that diet. The latter was caused by pre-exposure of the algae to Ni. This example clearly illustrates that, if one wants to obtain (mechanistic) insights in the ecotoxicological effects of dietary metal exposure which are not confounded by nutritional quality shifts, it is necessary to use ingestible dietary metal carriers that are not affected by nutrient quality shifts. The aim of the present study was to develop such a carrier, i.e., metal-contaminated liposomes, and to investigate their effects in chronic *Daphnia* toxicity tests. Liposomes are spherical self-assembled colloidal particles. They are composed of one or several concentric membranes which encapsulate an aqueous solution. Since liposomes resemble cell membranes in structure and composition, they have frequently been proposed as a suitable dietary delivery system of various substances used in ecological and physiological research (Ravet et al., 2003; Ravet and Brett, 2006; Buttino et al., 2006). In the development phase, we prepared control and Ni-containing liposomes and determined the size distribution of the liposomes in suspensions. This provides insight into their stability and to the degree to which they can (theoretically) be ingested following passage over the filtering apparatus of *D. magna*. In the test phase, we prepared control and Ni-contaminated liposomes and added these to the exposure media (along with an algal diet) in a standard chronic *D. magna* ecotoxicity test. We wanted to examine if dietborne Ni administered via the liposomes affects survival, growth, reproduction and/or algal ingestion rates. For comparative purposes, we ensured that the Ni content of the diet wherein Ni was delivered via the liposomes was in the range of the Ni contents of those diets (i.e., 86–837 μ g Ni/g dry wt.) which had previously been shown to reduce *D. magna* growth and reproduction (Evens et al., 2009). Algal ingestion rates were measured to test the hypothesis proposed by Evens et al. (2009), i.e., that reduced feeding rates could be a possible mechanism of dietary Ni toxicity.

2. Material and methods

2.1. Experimental design

Control and Ni-laden liposomes were prepared according to the method developed by Buttino et al. (2006), using control water and Ni-spiked water during their preparation, respectively. These liposomes were then used as a Ni-contaminated diet for *D. magna* during a standard, 21-day chronic toxicity test. Simultaneously,

uncontaminated green algae *P. subcapitata* were daily added to the test media in order to meet the requirement of *D. magna* for essential nutrients. The final diet was thus composed of a mixture of algae and liposomes, and the different treatments only varied in dietary Ni content, but not in nutritional quality. Dissolved Ni concentrations as well as survival, reproduction and size of the daphnids were monitored throughout the 21-day exposure. Algal ingestion rate was determined after day 6 and 13, whereas the dry weight and the Ni body burden of the individual *D. magna* organisms were determined after day 7 and 14 of exposure.

2.2. Development of Ni-contaminated liposomes: chemical procedure

Liposomes were prepared by a mechanized method in accordance with the methodology described in Buttino et al. (2006). Briefly, a lipid mixture containing 150 mg of hydrogenated and homogeneous dipalmitoyl- and distearoyl-soybean phosphatidylcholine (PC) (Epikuron 200 SH, Cargill, United States) was dissolved in 5 mL of a chloroform/methanol solvent mixture (2:1, v/v ratio), and introduced into a 250 mL round-bottomed flask. In contrast with Buttino et al. (2006), we omitted cholesterol as structural component since to our knowledge no critical threshold for the sterol level of *D. magna* was available. The solvent was removed in a rotary evaporator (Büchi B461 and B480 waterbaths) at 25 °C, until a thin and homogeneous lipid film had formed on the wall of the flask. After the evaporation, the lipid layer was gently flushed with a N₂ stream in order to remove potential solvent residues from the flask. The lipid film was then hydrated with 15 mL of sterilized and double deionized water (Chemlab, Zedelgem, Belgium) at a temperature exceeding the transition temperature of the phospholipid mixture (55 °C) by no more than 5 °C. Ni concentrations (NiCl₂·6H₂O; Sigma-Aldrich, Steinheim, Germany) in the water were 0 (control) and 50 mg/L (nominal values) (for generation of the liposomes to be used in the *Daphnia* bioassays). In a preliminary experiment to determine the stability of Ni contents in liposomes over time, liposomes were made by hydration of PC with Ni concentrations of 10, 100 and 500 mg/L. The resulting suspensions were gently mixed in the presence of glass beads (10 g ~ 7 mL) until the lipid layer was removed from the glass wall and the suspensions were completely homogenized. The flask, containing the suspension and the glass beads, was then attached to the evaporator again (without vacuum), and rotated for 60 min in a water bath at 55 °C. The temperature of the waterbath needed to exceed the transition temperature of the PC mixture to ensure that the phospholipid was in its liquid phase. This procedure ensured that the PC compounds could freely migrate and interact, so that a multilamellar membrane could be generated. Afterwards, the resulting suspensions were mixed on a stirring plate at room temperature during 1 h. All liposome preparations were transferred to hermetic bottles, and stored in dark at 4 °C under nitrogen atmosphere. New liposomes were produced every 7 days during the 21-day *D. magna* bio-assay. Ni content and size distribution of these new suspensions were quantified immediately after production.

2.3. Liposome dry weight and metal content

The dry weight of the liposome suspensions was measured as follows. One mL of the suspension (3 replicates) was dried for 24 h at 60 °C in a pre-weighed aluminium cup. Afterwards the cups were weighed again and the dry weight of the suspension was calculated as the difference between dry wt. after and before addition of the liposome suspension. To determine the Ni content of the liposomes, 10 mg of dry sample was centrifuged in triplicate in 2 mL Eppendorf polyethylene vials at 13,000 × g for 15 min in a Mikro 200 R Centrifuge (Hettich Zentrifugen;

Tuttlingen, Germany). The remaining pellet was washed in a 5 mmol/L solution of Na₂EDTA for 5 min and then centrifuged for a second time as described above (Sunamoto et al., 1980). The 'external Ni fraction' was operationally defined as the amount of Ni that was present in the supernatant after this centrifugation step. It contains the Ni ions that were originally adsorbed to the outer liposome layer, but also the fraction of Ni that may have been entrapped in the interstitial phase of the liposome pellet after the first centrifugation. Complete dissolution of metals in these EDTA solutions was guaranteed by adding HNO₃ to a concentration of 0.14 mol/L. The internal Ni concentration of these particles was defined as the quantity of divalent ions dissolved in the internal cavity and adsorbed onto the internal multi-lamellar layers of the liposomes. For this purpose, the dry pellet was resuspended by the addition of 250 µL of ultrapure 14 mol/L HNO₃ (Normatom quality, obtained from VWR Prolabo, Leuven, Belgium), and subsequent agitation on a vortex (MS1 Minishaker, IKA). The suspensions were transferred to polypropylene vials (Laborimpex, Brussels, Belgium). Remaining pellets of liposomes in the Eppendorf vials were transferred repeating the same procedure. Finally, 100 µL H₂O₂ (30% aqueous solution; Merck, Germany) was added to the polypropylene vials to guarantee complete degradation. The phospholipids were completely decomposed by hot acid digestion (60 min, 110 °C) of the acid suspensions in a furnace. The digests were diluted 10-fold with deionized water (Chemlab, Zedelgem, Belgium) before analysis. All Ni determinations were carried out using sector-field ICP-mass spectrometry (Thermo Scientific Element XR sector-field unit, operated at a mass resolution of ~4000), with a detection and quantification limit of 100 and 330 ng/L, respectively.

2.4. Liposome size distribution

Particle size analysis was carried out relying on Laser Diffraction (Malvern Mastersizer S, Malvern Instruments Ltd., United Kingdom). All procedures including sample preparation, dispersion and analysis were carried out according to the practice guide published by the National Institute of Standards and Technology (NIST SP 960-1, Jilavenkatesa et al., 2001). Before analysis, a wet sample dispersion unit (MS-17), attached to the Malvern Mastersizer, was used to dilute the liposome stock suspension to appropriate concentrations. Each sample was diluted 500-fold in deionized water and was homogenized using an automatic stirrer with a rotation speed of 500 rpm. No sonication was used and the dispersion bath was emptied and cleaned between consecutive measurements. The suspension was then pumped through the sample chamber. A monochromatic He–Ne laser with a fixed wavelength of 633 nm was focused onto the chamber and the diffracted light was collected by a series of detectors. An optical model, based on the Mie diffraction theory, was then employed to predict the sizes of the particles responsible for the observed scattering pattern (10 replicates). The model was fitted to the data on the basis of the fitting index "30HD" ("standard wet method"), assuming a refractive index of 1.5295 and 1.3300 for the particles (i.e., liposomes) and the dispersant (i.e., deionized water), respectively. The size distribution was then recorded as the particle volume percent in 63 discrete size ranges between 0 and 879 µm. For the current work a 300RF lens was used, which is capable of measuring particles with sizes between 0.05 and 900 µm. Size distribution was studied for liposomes created at concentrations of 0 and 50 mg Ni/L in the hydration medium. This was done immediately after the liposome production and after a 7-day storage period.

2.5. Algae culture and *Daphnia* exposure

The green alga *P. subcapitata* was obtained from the Culture Collection of Algae and Protozoa (CCAP 278/4, Argyll, Scotland) and

maintained under conditions as described in De Schampheleere et al. (2004). A quantity of algal biomass sufficient to fully sustain a 21-day *D. magna* experiment was obtained using a 12 L culture. The algae were cultured in modified Provasoli's ES enrichment medium (Provasoli et al., 1957) buffered at pH 8, using an initial concentration of 10⁶ algal cells/mL. The medium was also supplied with 1.4 mg/L FeSO₄·7H₂O, 15 mg/L NaH₂PO₄·2H₂O, 150 mg/L NaNO₃ and 2.35 mg/L MnCl₂·4H₂O. Details on algal growth and harvesting conditions, the determination of algal dry weight, cell concentrations, Ni burdens (control treatment) and storage conditions after harvest can be found in Evens et al. (2009). The 21-day exposure of *D. magna* to dietary Ni was performed according to OECD guideline No. 211 for testing of chemicals (OECD, 1998). More information on the origin and culture conditions of this test species are given in Evens et al. (2009). The exposures were performed in M4 medium (Elendt and Bias, 1990), wherein the Zn concentration was based on research performed by Muysen et al. (2006) (i.e., adjusted to 26 µg/L). The pH of the medium at the start of the test was 8.0. The strong metal chelator EDTA was replaced by 4 mg/L DOC, as explained in De Schampheleere et al. (2003). Before onset of the experiment, the medium was filtered (0.45 µm) for avoiding potential blockage of the Flow Cytometry instrument (see Section 2.6). At the start of the *D. magna* experiment, 30 juveniles (<24 h old) per treatment were transferred individually to polyethylene cups containing 50 mL of test medium. *D. magna* were exposed to a diet composed of a mixture (10:1 (w/w)) of control algae and Ni-contaminated liposomes at two concentrations, representing a diet with unaffected nutritional quality and varying only in Ni contents. The choice for a 10:1 (w/w) mixture of algae and liposomes was made to create a diet with Ni contamination levels similar to the ones used in Evens et al. (2009). Thus, in practice the daphnids were fed daily with 250 + 25, 500 + 50 and 750 + 75 µg dry wt. of algae + liposomes during weeks 1, 2 and 3 of the experiment, respectively. A preliminary experiment was conducted to test the side effects of these daily additions of PC on the performance of *D. magna*. The 21-day reproduction (10 replicates) was assessed for a control treatment, consisting of daphnids that were fed with only control algae, and daphnids that were fed with a mixture of control algae and control liposomes in the above-mentioned proportions. During the main experiment, the test medium was renewed every other day and the pH of the old medium was measured. The pH values were required for the calculations of Ni bioavailability in the dissolved phase of the exposure with the BLM (see further). Survival and reproduction, in terms of the number of juveniles released from the brood pouch, were recorded daily. At the end of every week (at maximum) 10 surviving parent organisms were used to determine their individual dry weight (Sartorius analytical balance, 0.01 mg) and Ni bioaccumulation. Five organisms of these 10 had previously been used to determine the algal ingestion rate (see Section 2.6). Immediately after being sampled from the exposure medium, daphnids were gut-depurated by feeding them with uncontaminated algae in control M4 medium (no Ni added) and in the absence of liposomes for 4 h (Gillis et al., 2005). Ni bioaccumulation was then assessed by solid sampling high resolution-continuum source graphite furnace atomic absorption spectrometry (SS-HR-CS GFAAS), using a Ni atomic line located at 228.999 nm and a standard (approx. 2 min/sample) temperature program (700 °C pyrolysis temperature; 2400 °C atomization temperature). This novel and sensitive technique permits the direct analysis of individual *D. magna* specimens with a very low detection limit (8.3 pg) and quantification limit (27.7 pg), and requires no sample pretreatment other than drying. Also its resolution (approx. 1 pm) and potential to correct for spectral overlaps makes a reliable analysis of complex samples feasible. For more details on the application of this technique to the direct analysis of solid samples, we refer to Welz et al. (2007) and to Resano et al. (2008). Its

performance for the direct determination of Zn in *D. magna* has recently been discussed by Briceno et al. (2010). Simultaneously, the carapax length of the selected as well as the remaining organisms was determined, defined as the linear distance between top of the head and base of the apical spine. At the end of each week, old test medium was sampled and filtered (PALL Life Sciences Acrodisc, pore size 0.45 μm). The Ni concentration was determined to assess the quantity of Ni eliminated and/or desorbed from the algae and liposomes into the *Daphnia* exposure medium, as well as the quantity of Ni that was inadvertently added from the dissolved phase of the liposome suspensions. Indeed, since the hydration medium of the liposomes was not substituted after preparation, the Ni remaining in solution (i.e., not encapsulated in the cavity nor adsorbed onto the membranes of the liposomes) will also have entered in the daphnids' test medium as dissolved Ni. All Ni determinations were carried out using sector-field ICP-mass spectrometry (Thermo Scientific Element XR sector-field unit, operated at a mass resolution of ~ 4000).

2.6. Algal ingestion rates

One of the objectives of this study was to determine if dietary Ni toxicity, as observed in Evens et al. (2009), could be the result of reduced algal ingestion rates. Traditionally this endpoint is measured as the difference in algal cell concentrations in control suspensions (i.e., without daphnids) and suspensions containing one or more test organisms. Routinely applied methodologies like the use of particle counters, however, cannot be used as they cannot distinguish between the signals of algae and liposomes that co-occur in suspension (preliminary analysis, data not shown). We developed a methodology using Flow Cytometry (FC), in order to selectively quantify algal cell concentrations based on their relation to chlorophyll fluorescence. To this end, a series of suspensions of the green alga *P. subcapitata* was prepared in 0.2 μm filtered modified M4 medium, i.e., 0, 1.19×10^5 , 2.17×10^5 , 3.93×10^5 , 9.10×10^5 and 1.70×10^6 cells/mL. A Sedgwick-Rafter counting cell was applied to quantify the cell concentrations by microscope. Corresponding analytical signals were determined using a Cyan™ ADP Flow Cytometry facility. Algal suspensions were homogenized and the cells were quantified and detected by specific excitation of chlorophyll at 488 nm with a 50-mW Sapphire solid state diode laser. Red fluorescence emission was collected with photomultiplier tubes using 613/20 bandpass filters. Forward angle light scatter was detected with a type BP 488/10 bandpass filter. For each sample run, data for 50,000 events were collected. Five replicates were analyzed for each sample (Boon et al., 2006). In parallel, we also examined the FC signal of liposome suspensions in this test medium without algae. Red fluorescence emission of algal chlorophyll as a function of Forward Scatter (FS) could be explicitly distinguished from the background signal, as indicated by the polygon in Fig. 1. Finally, these results were used to formulate a linear equation that correlates FC signals to effective cell concentrations in the medium:

$$\text{Counts}_{\text{FC}} = \text{Intersection}_{\text{FC}} + \text{Slope}_{\text{FC}} \times [\text{algae}] \quad (1)$$

wherein $\text{Counts}_{\text{FC}}$ stands for the analytical signal of the FC application, and $\text{Intersection}_{\text{FC}}$ and Slope_{FC} are the parameters derived from the calibration line. The ingestion rate of *D. magna* was weekly determined. On day 6, 13 and 20, 5 organisms of each treatment were transferred to exactly 50 mL of the filtered modified M4 medium, containing algae and liposomes in a 10:1 ratio (w/w). Together with 5 control treatments (i.e., without *D. magna*), the test vessels were maintained under the conditions prescribed by OECD guideline No. 211 for testing of chemicals (OECD, 1998). After exactly 24 h, the media were homogenized with a syringe and algae concentrations were quantified using the methodology mentioned

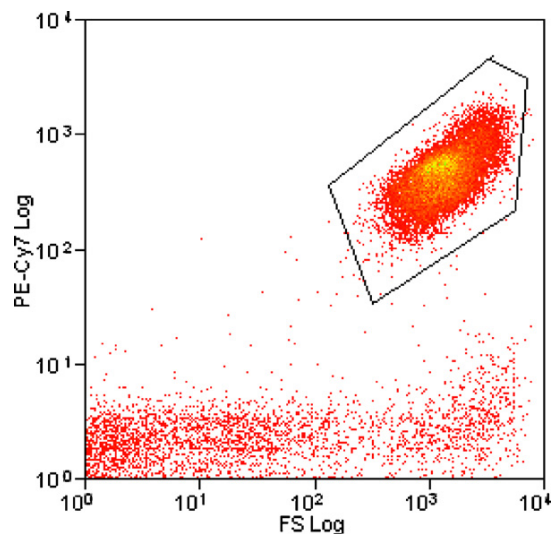


Fig. 1. Flow cytometry diagram: relation between Red Fluorescence Emission of chlorophyll and Forward Scatter signal (FS). The polygon encloses the signals originating from algal chlorophyll, which can be easily discerned from the background signal (scatter at bottom). The signal obtained from liposomes was very weak and was situated in the background scatter.

above. *D. magna* ingestion rates were subsequently determined following the equation:

$$\text{Ingestion rate} = \frac{([\text{algae}]_{\text{control}} - [\text{algae}]_{\text{Daphnia}}) \times V}{t} \quad (\text{cells/h}) \quad (2)$$

wherein $[\text{algae}]_{\text{control}}$ and $[\text{algae}]_{\text{Daphnia}}$ are the concentrations of algae (cells/mL) in the control medium (i.e., without *D. magna*) and the medium with *D. magna*, respectively, V is equal to 50 mL and t is 12 h (± 15 min).

2.7. Data treatment and statistics

All observations related to algae, liposomes and *D. magna* are expressed as mean \pm standard deviation. All statistical comparisons between exposure and control treatment were performed with the Mann-Whitney- U test (MWU; $p = 0.05$; Siegel and Castellan, 1988) and Anova (Student's t -test). All statistical comparisons as well as correlation analyses were performed with Statistica 6.0 software (Statsoft, Tulsa, OK, USA).

3. Results

3.1. Liposome properties

Our preliminary investigation clearly demonstrated the stability of the Ni-content in the liposomes over 7 days. Indeed, hydration of PC with 10, 100, and 500 mg Ni/L created liposomes that had Ni contents of 191 ± 11.5 , 1730 ± 181 , and 5488 ± 223 μg Ni/g dry wt., respectively, immediately after preparation; the Ni contents 7 days later were 198 ± 6.9 , 1876 ± 168 , and 5523 ± 154 μg Ni/g dry wt., respectively. Given this clear stability, Ni concentrations in the liposomes during the *Daphnia* bioassay were only measured weekly in freshly prepared liposome suspensions.

The Ni concentrations in the algae, liposomes and mixed diet (i.e., a 10/1 (w/w) mixture of algae and liposomes) for each week of the exposure are given in Table 1. External Ni represents the concentration of Ni bound to the outer surface of the liposomes, in addition to the concentration of the interstitial liquid of the vesicles. Sorption of external Ni to the liposomes is likely due to the

Table 1

Ni burdens ($\mu\text{g Ni/g dry wt.}$) of control algae and liposomes produced after hydration of phosphatidylcholine with 0 and 50 mg Ni/L in the hydration medium. The burdens of the mixed diet, used as a diet for *D. magna*, were calculated based on a 10/1 (w/w) proportion of algae and liposomes, respectively.

		Week 1	Week 2	Week 3
Liposomes Control	Internal Ni	1.9 ± 0.3	2.1 ± 0.1	1.5 ± 1.4
	External Ni	0.3	0.5	0.7
	Total Ni	2.1	2.6	2.2
Ni-contaminated	Internal Ni	1403 ± 170	1661 ± 103	1348 ± 45
	External Ni	70	100	109
	Total Ni	1474	1761	1457
Algae	Internal Ni	1.5 ± 1.4	0.8 ± 0.1	1.1 ± 0.1
	External Ni	0.9	1.4	0.2
	Total Ni	2.4	2.2	1.3
Mixed diet Control	Internal Ni	1.5	0.8	1.1
	External Ni	0.9	1.4	0.2
	Total Ni	2.3	2.2	1.3
Ni-contaminated	Internal Ni	129	153	124
	External Ni	7	10	10
	Total Ni	136	162	134

interaction of Ni with the anionic P-moieties of the external PC layer (McLaughlin et al., 1978; Sunamoto et al., 1980). Throughout the experiment, concentrations of externally adsorbed Ni were on average 0.5 ± 0.2 and $92.8 \pm 20.1 \mu\text{g Ni/g dry wt.}$ for the liposomes created under control and Ni-contaminated hydration conditions, respectively. Internal Ni is the fraction of metal encapsulated in the internal aqueous cavity and the fraction of Ni adsorbed to the P-moieties present in the interstitial phases of the internal multilamellar membrane (McLaughlin et al., 1978; Sunamoto et al., 1980). Concentrations of this fraction were on average 1.8 ± 0.7 and $1470.8 \pm 166.9 \mu\text{g Ni/g dry wt.}$ for the control and Ni-contaminated liposomes, respectively. Thus, on average 94% of the Ni present in the Ni-contaminated liposomes was encapsulated in the cavity and adsorbed in the internal interstitial phases of the vesicles. The addition of control algae to the liposomes to obtain the mixed diet (see Section 2.5) resulted in a final Ni concentration in the mixed diets of 2.0 and $144.2 \mu\text{g Ni/g dry wt.}$ for the control and Ni-contaminated diet, respectively (Table 1). Fig. 2 shows the size distribution of the control and Ni-contaminated liposome suspensions immediately after preparation and after 7 days of storage. New liposomes were prepared every 7 days during the 21-day chronic toxicity test

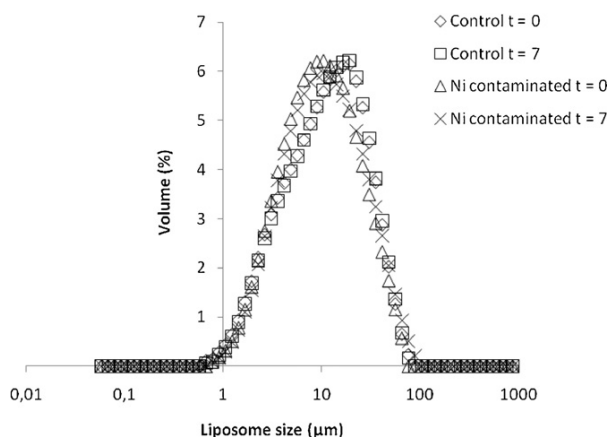


Fig. 2. Size distribution (Malvern Mastersizer 2000) of control and Ni-contaminated liposomes immediately after production and after 7 days of storage on 4°C in the dark under nitrogen atmosphere.

with *D. magna*. The size of control and Ni-contaminated liposomes was log-normally distributed. No differences between new and 7-day old suspensions could be observed. The control liposomes were all between 0.7 and $76.3 \mu\text{m}$ (diameter), with a distribution mode at $19.3 \mu\text{m}$. A slight shift of the distribution to smaller particle diameters was observed for the Ni-contaminated liposomes. All particles were between 0.8 and $88.9 \mu\text{m}$, with a distribution mode at $10.5 \mu\text{m}$.

3.2. Effects on *D. magna* ingestion rates

When using Flow Cytometry, the red fluorescence emission of excited algal chlorophyll (polygon in Fig. 1) could be explicitly distinguished from the background signal. Since PC has no fluorescent properties, its signal was very weak and belonged to the background scatter. In this way the integrated FC signal in the polygon section could be related to the algal cell concentration in a relatively straightforward manner (Uyttendaele et al., 2008). A linear relation ($R^2 = 0.999$) was observed between the FC analytical signal and the algal cell concentration determined with the Sedgwick Rafter counting grid (see Section 2.6):

$$\text{Counts}_{\text{FC}} = 248232 + 0.6054 \times [\text{algae}] \quad (3)$$

with [algae] equaling the algal density (cells/mL). The FC measurements and Eq. (3) enabled us to calculate the concentrations of algae in the suspensions of the feeding assay (with and without added *Daphnia*) to determine ingestion rates (see Section 2.6) according to Eq. (2). The *per capita* algal ingestion rates (i.e., expressed as cells ingested/individual/h; Table 2) were significantly reduced in the daphnids fed with the Ni-contaminated diet by 31% and 94%, after 6 and 13 days of exposure, respectively (Student's *t*-test, $p < 0.05$). Due to 100% mortality at day 15, no ingestion rates after 20 days of exposure could be obtained. It is important to note that *D. magna* ingestion rates are intrinsically proportional to the area of the filtering setae on their thoracic limbs, and that this area in turn is related to the square of the body length (Brooks and Dodson, 1965; Egloff and Palmer, 1971). Since body length was also affected by dietary Ni (see Section 3.3) it is thus important to correct ingestion rates accordingly to discriminate between a merely indirect effect of daphnid size (length) on ingestion rate and a true, direct effect of dietary Ni on the ingestion process (see also De Schampelaere et al., 2007). Given an average cell mass of $2.83 \times 10^{-11} \text{g/cell}$, we calculated that dietary Ni exposure resulted in a significant (Mann–Whitney *U* test, $p < 0.05$) increase of the size-corrected algal ingestion rate from 0.40 ± 0.08 to $0.67 \pm 0.15 \mu\text{g mm}^{-2} \text{h}^{-1}$ (i.e., by 68%) at day 6, but in a significant decrease (Mann–Whitney *U* test, $p < 0.05$) from 2.50 ± 1.18 to $0.49 \pm 0.97 \mu\text{g mm}^{-2} \text{h}^{-1}$ (i.e., by 80%) at day 13 (Table 2). The latter calculations suggest a direct inhibitory effect of dietary Ni exposure on the ingestion process at day 13 (compared to the control).

3.3. *D. magna* internal exposure and effects on growth and reproduction

The preliminary experiment showed that the presence of PC liposomes didn't affect the performance of *D. magna*. The 21-day offspring of the control (56.7 ± 14.7 juveniles) and daphnids exposed to PC (38.8 ± 24.6 juveniles) was not significantly different ($p > 0.05$; Mann–Whitney *U* test). The results of the 21-day exposure of *D. magna* to dietary Ni are given in Table 2. Biomass growth rate of the algae was 1.03d^{-1} . pH did not deviate more than 0.4 units from the start value. The addition of Ni-contaminated liposomes to the test medium resulted in a slight increase of dissolved Ni, but concentrations never exceeded $6.10 \mu\text{g/L}$. Exposure to dietary Ni resulted in 100% mortality after 14 days. Hence, comparisons of all other endpoints could only be made up to day 14. Whole body Ni

Table 2
Experimental conditions and results of the chronic exposure of *D. magna* to a Ni-contaminated diet.

	Control	Exposure
Dietary Ni burden ($\mu\text{g/g}$ dry wt.) ^a	2.0	144.2
Average pH	7.6	8.1
Dissolved Ni at day 7 ($\mu\text{g/L}$)	0.73	1.50
Dissolved Ni at day 14 ($\mu\text{g/L}$)	2.63	6.10
Dissolved Ni at day 21 ($\mu\text{g/L}$)	1.18	–
<i>D. magna</i> 21-day mortality (%) ^b	10	100
<i>D. magna</i> time to mortality ^{c,d}	5.0	12.7 \pm 1.8
<i>D. magna</i> Ni body burden at day 7 ($\mu\text{g/g}$) ^{d,e}	1.7 \pm 0.7	11.9 \pm 6.0*
<i>D. magna</i> Ni body burden at day 14 ($\mu\text{g/g}$) ^{d,e}	0.7 \pm 1.1	20.4 \pm 9.1
<i>D. magna</i> Ni body burden at day 21 ($\mu\text{g/g}$) ^{d,e}	0.4 \pm 0.08	–
Length at day 7 (mm) ^{d,e}	2.85 \pm 0.15	2.00 \pm 0.18*
Length at day 14 (mm) ^{d,e}	3.71 \pm 0.22	2.08 \pm 0.14*
Length at day 21 (mm) ^{d,e}	3.98 \pm 0.15	–
Time to first brood (days) ^{b,d}	8.1 \pm 0.6	10.0 \pm 2.8
1st brood size ^{b,d}	10.3 \pm 2.3	1.5 \pm 0.7*
2nd brood size ^{b,d}	20.6 \pm 2.2	–
14 day reproduction (sum of 3 broods) ^{b,d}	58.2 \pm 9.4	–
Total reproduction (# juveniles/daphnid) ^{b,d}	98.9 \pm 15.3	–
Algal ingestion rate (cells/h) at day 6 ^{b,d}	114,000 \pm 22,000	79,000 \pm 18,000
Algal ingestion rate (cells/h) at day 13 ^{b,d}	1,170,000 \pm 550,000	80,000 \pm 150,000*
Algal ingestion rate (cells/h) at day 20 ^{b,d}	640,000 \pm 240,000	–
Algal ingestion rate ($\mu\text{g/h}$) at day 6 ^{b,d}	3.22 \pm 0.63	2.23 \pm 0.51
Algal ingestion rate ($\mu\text{g/h}$) at day 13 ^{b,d}	33.13 \pm 15.59	2.15 \pm 4.30*
Algal ingestion rate ($\mu\text{g/h}$) at day 20 ^{b,d}	18.07 \pm 6.90	–
Algal ingestion rate ($\mu\text{g/mm}^2$ h) at day 6 ^{b,d}	0.40 \pm 0.079	0.67 \pm 0.15*
Algal ingestion rate ($\mu\text{g/mm}^2$ h) at day 13 ^{b,d}	2.50 \pm 1.18	0.49 \pm 0.97*
Algal ingestion rate ($\mu\text{g/mm}^2$ h) at day 20 ^{b,d}	1.14 \pm 0.44	–

^a Dietary Ni burden is the weighted average of the algal and liposome Ni burdens, taking into account a 10:1 (w/w) dry weight ratio for algae and liposomes, respectively.

^b *D. magna* total reproduction, individual brood size, time to first brood, total mortality and algal ingestion rate are statistically compared with the Mann–Whitney *U* test.

^c *D. magna* time to mortality could not be statistically compared to the control treatment.

^d Data on exposure parameters and toxicological endpoints are presented as mean \pm standard deviation ($n=5$ for algal and liposome Ni burdens, algal ingestion rates, $n=10$ for *D. magna* survival, body burden, length, 21-day reproduction, and size of 1st and 2nd brood).

^e *D. magna* Ni burdens and body length are statistically compared with the Student's *t*-test.

* Significant differences between the control exposure and elevated dietary Ni exposures ($p < 0.05$).

in control daphnids were 1.7, 0.7 and 0.4 $\mu\text{g/g}$ dry wt. after 7, 14 and 21 days, respectively. Whole body Ni in daphnids exposed to dietary Ni was significantly higher and was 11.9 $\mu\text{g/g}$ dry wt. after 7 days which further increased to 20.4 $\mu\text{g/g}$ dry wt. after 14 days. The accumulation of Ni was accompanied by a reduced daphnid length (by 29.8%) after 7 days. Between day 7 and day 14, no further growth occurred in the Ni-exposed daphnids, while the control daphnids still grew by 30% (in length) during the same period. In terms of reproduction, the size of the first brood (number of juveniles) of the Ni-exposed daphnids was significantly reduced compared to the control, i.e., by 85%. None of the Ni-exposed individuals was able to produce a second brood before dying. Maturation rate, expressed

as the time required to release the first brood, was not significantly affected by dietary Ni, but this is mainly due to the high variability of this endpoint among individuals.

4. Discussion

4.1. Liposome Ni concentrations and implications on dissolved Ni

The experiment showed that the Ni content of the liposomes was stable for at least 7 days. This is important since it ensures that the daphnids are exposed to constant dietary Ni levels for at least this time span. Internal Ni in the liposomes accounted for 79 and 94% of the total measured Ni (i.e., internal + external) associated with the control and Ni-contaminated liposomes, respectively. This is in contrast with similar research on Zn (Sunamoto et al., 1980), where 70% adsorbed onto the outside of the liposome bilayer. The latter study was performed using very similar methodologies, fatty acid resources and PC concentrations, except for a metal concentration that was much higher (i.e., 294-fold the molarities we applied). On the basis of this difference, we would have expected an internal Ni fraction not exceeding 70%; until now we have no explanation for this discrepancy. Given a PC molecular weight of 760 g/mol, we calculated that a concentration of 10 mg PC/mL corresponds to 1.32×10^{-5} mol PC/mL or 1.32×10^{-5} mol of anionic phosphate moieties or negative charges (per mL). The Ni concentrations we applied (8.51×10^{-7} mol/mL) are thus far below the maximum sorption capacity – assuming a 1/1 binding – in contrast with the study of Sunamoto et al. (1980). Nevertheless, since mass balance calculations pointed out that the maximum achievable internal Ni content of the liposomes (i.e., when all Ni added would end up inside the liposomes) was 5000 μg Ni/g dry wt., the encapsulation efficiency of the Ni-contaminated liposomes was not higher than 31%, with the rest of the Ni remaining in the solution phase of the suspension. This implies that the addition of liposomes to *D. magna* test media could in theory result in a significant addition of Ni into the waterborne phase of the test-medium. However, taking into account that at maximum 3 doses of liposomes are added to test medium in-between two media renewals, the waterborne Ni added in this way would never exceed concentrations of 5, 10 and 15 μg Ni/L during the first, second and third week of the exposure, respectively. This is confirmed by the measured dissolved Ni concentrations on day 7 (1.50 $\mu\text{g/L}$) and day 14 (6.10 $\mu\text{g/L}$) in the test media to which Ni-contaminated liposomes were added. The Biotic Ligand Model for chronic waterborne Ni toxicity (Deleebeek et al., 2008) predicted that a concentration of 160 μg Ni_{dissolved}/L was needed to reduce total reproduction by 10%. It seems thus very unlikely that a 85% reduction of the first brood size, and the inability of the exposed daphnids to reproduce afterwards in the current study could have been caused by the concentrations reported above. The impact of waterborne Ni on *D. magna* under the current test conditions (i.e., the composition of the test water) can thus be considered negligible. This implies that the contribution of dietary Ni to both accumulation and toxicity in this experiment must have been far more important, and that the unwanted addition of dissolved Ni, along with the liposomes, does not have any consequences on the interpretation of the observed accumulation and toxicity data.

4.2. Liposome size distribution

Determination of liposome size distribution is an instructive quality control assay as it provides insight into the physical consequences of storage time and of the exposure of the PC compounds to Ni. Additionally, size distribution is important in terms of the fraction that can be ingested by *D. magna*. The filtration apparatus of *D. magna*, responsible of capturing suspended particles from the

water, is composed of range of setulae that act as filter meshes. The in-between distance of these bristle-like structures is representative for the minimal particle size that can be captured (Geller and Müller, 1981). The presence of Ni resulted into a slight shift of the log-normal size distributions, with modal diameters varying from 19.3 μm (control liposomes) to 10.5 μm (Ni-contaminated liposomes). This shift probably did not have important consequences on the potential “ingestability” of liposomes created under different Ni concentrations as *D. magna* can ingest particles over a wide size-range from 0.6 to 40 μm by mechanical sieving over their setulae (Geller and Müller, 1981). Based on the log-normally size distribution function, we calculated that 86.0% (on day 0 and 7) of the control liposomes and 86.7% (on day 0) and 83.0% (on day 7) of the Ni-contaminated liposomes could be retained by the filtering apparatus of *D. magna* and could thus be ingested. This implies that the conditions during liposome preparation (e.g., in terms of lipid mixture composition, hydration conditions and lack of sonication), allowed us to obtain vesicles in a size range that was suitable to be retained by the filtering apparatus of *D. magna*.

4.3. Bioaccumulation and effects on *D. magna*

D. magna was exposed to dietary Ni levels in the mixed diet containing 2.0 (control) and 144.2 $\mu\text{g Ni/g dry wt.}$ Whole body Ni content in the Ni-exposed *D. magna* increased gradually with time, reaching 11.9 $\mu\text{g Ni/g dry wt.}$ and 20.4 $\mu\text{g Ni/g dry wt.}$ after 7 and 14 days, respectively. The observed effects parallel this time trend as they were more severe between day 7 and 14 than prior to day 7. Although it should be noticed that the slightly (by 16%) higher Ni content of the mixed diet in the second week may have contributed somewhat to this trend, possible physiological explanations should not be disregarded either, and these are explored in what follows. Until day 7, no mortality occurred and size-corrected algal ingestion rate (i.e., *per capita* algal ingestion rate corrected for size) was not inhibited by Ni. After day 7, mortality began to occur in the Ni-exposed daphnids, and size-corrected algal ingestion rate in those individuals that survived until day 13 was severely decreased compared to the control (i.e., by 80%). The latter mechanism may be one possible explanation as to why no significant growth was observed in the Ni-exposed daphnids between day 7 and day 14. On the other hand, this mechanism can most likely not explain the reduced length at day 7, since the feeding process was not affected until day 7 in the Ni-exposed daphnids. This is in line with observations with *D. magna* exposed to elevated dietary Cu (De Schampelaere et al., 2007). These authors reported that the Cu-induced adverse effects on the feeding process only started to occur after 12 days of exposure.

From the perspective of energy budget theories (e.g., Nisbet et al., 2000), two other mechanisms may explain the reduced growth observed during the first exposure week. The first is that, even if the ingestion process itself is not affected, the assimilation of nutrients across the digestive epithelial tract may be inhibited. Ptashynski et al. (2001), for example, showed that dietary Ni exposure of lake whitefish (*Coregonus clupeaformis*) and lake trout (*Salvelinus namaycush*) caused aberrations of the digestive epithelial tract, which were the direct cause of reduced nutrient absorption. Analysis of gut epithelial morphology may confirm whether this also applies in *D. magna* following dietary Ni exposure. A second possibility is that exposure to and bioaccumulation of Ni may have reduced the amount of energy that is available for investment in somatic growth; possibly in two ways. First, there may have been a need for additional energy expenditure to detoxify Ni, for instance through energy needed for production of detoxifying metallothioneins, although only shown in other organisms for Ni (Srivastava et al., 1993; Sun et al., 2007). Various metals, among them Cd (Frayse et al., 2006) are detoxified by *D. magna*

through the production of metallothioneins. Second, there may have been an overall reduction of the available energy charge (i.e., ATP levels) in the Ni-exposed daphnids. Pane et al. (2003, 2004) have shown that waterborne exposure to Ni^{2+} (a Mg^{2+} antagonist) reduces whole body Mg^{2+} in *D. magna* as well as their ATP content. They speculated that these two observations were linked because Mg^{2+} is a co-factor of ATP on a 1:1 molar basis and its decrease caused the overall depression of the daphnids' metabolic health. It would be interesting to investigate if this effect would also be observed following dietary Ni exposure. Beyond day 7, the two mechanisms explained above (reduced nutrient assimilation and reduced available energy for growth) may also have acted together with the reduction of ingestion rate (observed on day 14, Table 2) to result in the completely halted growth (between day 7 and day 14).

Along with growth, the reproductive process was also severely inhibited (Table 2). The Ni-exposed daphnids exhibited a reduction by 85% of the number of offspring in the first brood (compared to the control), and none of them were able to produce a second clutch of offspring at all. All of the energy-budget related mechanisms described above, which are potentially involved in effects on growth, may also have contributed to the effects on reproduction. Obviously, there is more research required to discriminate between or to determine the relative importance of the above-postulated mechanisms of dietary Ni toxicity.

In the context of the present study, it is important to recognize that the method of delivering dietary Ni via liposome carriers has revealed unambiguously that dietary Ni can induce toxic effects in *D. magna*. Since this method excludes the potentially confounding factor of a diet quality shift, it may therefore be a promising tool to help further elucidation of the mechanisms of dietary metal toxicity to daphnids and other invertebrates. However, one limitation of this method is that metals in liposomes likely do not reflect metals in natural contaminated diets, such as live metal-contaminated algae. Thus, a comparison with results from dietary exposures with natural diets is still highly recommended if one wants to address the issue of ecological relevance of dietary metal toxicity. For instance, a comparison with our earlier study (Evens et al., 2009) reveals that adverse effects on daphnid growth and reproduction following exposure to a Ni-contaminated algal diet occurred at accumulated whole body Ni contents of 49.6 $\mu\text{g Ni/g dry wt.}$ and higher. Since in the present study, using Ni-contaminated liposomes, a lower accumulation was needed to invoke toxicity (i.e., 11.9 $\mu\text{g Ni/g dry wt.}$, Table 2), it may be suggested that the daphnids' whole body accumulation of Ni in Evens et al. (2009) was indeed high enough to contribute to the reduced growth and reproduction, and that the diet quality shifts likely only played a minor role (as already suggested in Evens et al., 2009). At the same time, however, the same data illustrate that Ni accumulated in *D. magna* via Ni-laden liposomes produces a stronger effect than via Ni-laden algae, suggesting that the bioreactivity of Ni (i.e., the toxic activity of Ni once absorbed), may be higher when accumulated from liposomes. While care obviously has to be taken in making conclusive inferences from comparing results of bioassays that are conducted separated in time, the comparison supports, to some extent, our earlier point that metal-contaminated liposomes are likely not 100% predictive of the effects that natural metal-contaminated diets can cause. Therefore, it is recommended that bioassays with liposomes as metal carriers should preferably be conducted in parallel and simultaneously with bioassays with natural diets to make more conclusive inferences about mechanisms and ecological relevance of the observed effects.

5. Conclusion

Ni-laden liposomes have been shown to be a valuable alternative to algae for studying dietary metal toxicity to *D. magna*.

The methodology used in this study was appropriate for creating dietary Ni levels that are comparable to those in algal diets used in previous studies. Moreover, the Ni contents in liposomes were shown to be stable over at least 7 days. It was demonstrated that the size distribution of these particles is not affected by storage time nor Ni exposure and that the particles are suitable to be ingested by *D. magna*. The use of PC as a basic compound of the liposomes did not affect the performance of the daphnids. The method of delivering dietary Ni via liposome carriers has revealed unambiguously that dietary Ni can indeed induce toxic effects in *D. magna*, since this method excludes the potentially confounding factor of a diet quality shift. Our results indicate that inhibition of the algal ingestion rate may be one possible toxicity mechanism involved in growth and reproduction impairment. More research is required to investigate if the other mechanisms that have been proposed are involved as well. Also, in order to gain more insight into mechanisms of dietary Ni toxicity under natural exposures, a comparison with the results from simultaneous dietary Ni exposures using natural diets is still recommended.

Acknowledgements

Roel Evens is supported by a Ph.D. grant of the Institute for the promotion of Innovation through Science and Technology in Flanders (I.W.T. Vlaanderen). We would like to acknowledge the Spanish Ministry of Science and Innovation for financial support (project CTQ2009-08606) and Marlies Bulckaert, Emmy Pequeur, Gisèle Bockstael and Geert Van De Wiele for technical assistance.

References

- Boon, N., Depuydt, S., Verstraete, W., 2006. Evolutionary algorithms and flow cytometry to examine the parameters influencing transconjugant formation. *Federation of European microbiological society. Microbiology and Ecology* 55, 17–27.
- Briceno, J., Belarra, M.A., De Schampelaere, K.A.C., Vanblaere, S., Janssen, C.R., Vanhaecke, F., Resano, M., 2010. Direct determination of Zn in individual *Daphnia magna* specimens by means of solid sampling high-resolution continuum source graphite furnace atomic absorption spectrometry. *Journal of Analytical Atomic Spectrometry* 25 (4), 503–510.
- Brooks, J.L., Dodson, S.L., 1965. Predation, body size, and composition of plankton. *Science* 150 (3692), 28–35.
- Buttino, I., De Rosa, G., Carotenuto, Y., Ianora, A., Fontana, A., Quaglia, F., La Rotonda, M.I., Miralto, A., 2006. Giant liposomes as delivery system for ecophysiological studies in copepods. *The Journal of Experimental Biology* 209, 801–809.
- Deleebbeck, N.M.E., De Schampelaere, K.A.C., Janssen, C.R., 2008. A novel method for predicting chronic waterborne nickel bioavailability and toxicity to *Daphnia magna* in artificial and natural waters. *Environmental Toxicology and Chemistry* 27 (10), 2097–2107.
- De Schampelaere, K.A.C., Canli, M., Van Lierde, V., Forrez, I., Vanhaecke, F., Janssen, C.R., 2004. Reproductive toxicity of dietary Zn to *Daphnia magna*. *Aquatic Toxicology* 70, 233–244.
- De Schampelaere, K.A.C., Forrez, I., Dierckens, K., Sorgeloos, P., Janssen, C.R., 2007. Chronic toxicity of dietary copper to *Daphnia magna*. *Aquatic Toxicology* 81 (4), 409–418.
- De Schampelaere, K.A.C., Vasconcelos, F.M., Heijerick, D.G., Tack, F.M.G., Delbeke, K., Allen, H.E., Janssen, C.R., 2003. Development and field validation of a predictive copper toxicity model for the green alga *Pseudokirchneriella subcapitata*. *Environmental Toxicology and Chemistry* 22 (10), 2454–2465.
- Egloff, D.A., Palmer, D.S., 1971. Size relations of filtering area of 2 *Daphnia* species. *Limnology and Oceanography* 16 (6), 900–905.
- Elendt, B.P., Bias, W.R., 1990. Trace nutrient deficiency in *Daphnia magna* cultured in standard medium for toxicity testing: effects of the optimization of culture conditions on life history parameters of *D. magna*. *Water Research* 24 (9), 1157–1167.
- Evens, R., De Schampelaere, K.A.C., Janssen, C.R., 2009. The effects of dietary nickel exposure on growth and reproduction of *Daphnia magna*. *Aquatic Toxicology* 94 (2), 138–144.
- Frayse, B., Geffard, O., Berthet, B., Quéau, H., Biagiatti-Risbourg, S., Geffard, A., 2006. Importance of metallothioneins in the cadmium detoxification process in *Daphnia magna*. *Comparative Biochemistry and Physiology, Part C: Toxicology and Pharmacology* 144 (3), 286–293.
- Geffard, O., Geffard, A., Chaumot, A., Vollat, B., Alvarez, C., Tusseau-Vuillemin, M., Garric, J., 2008. Effects of chronic dietary and waterborne cadmium exposures on the contamination level and reproduction of *Daphnia magna*. *Environmental Toxicology and Chemistry* 27 (5), 1128–1134.
- Geller, W., Müller, H., 1981. The filtration apparatus of cladocera: filter mesh-sizes and their implications on food selectivity. *Oecologia* 49, 316–321.
- Gillis, P.L., Chow-Fraser, P., Ranville, J.F., Ross, P.E., Wood, C.M., 2005. *Daphnia* need to be gut-cleared too: the effect of exposure to and ingestion of metal-contaminated sediment on the gut-clearance patterns of *D. magna*. *Aquatic Toxicology* 71 (2), 143–154.
- Jillavenkatesa, A., Lum, L.H., Dapkunas, S., 2001. NIST Recommended Practice Guide: Particle Size Characterization.
- Nisbet, R.M., Muller, E.B., Lika, K., Kooijman, S.A.L.M., 2000. From molecules to ecosystems through dynamic energy budget models. *Journal of Animal Ecology* 69 (6), 913–926.
- McLarnon-Riches, C.J., Rolph, C.E., Greenway, D.L.A., Robinson, P.K., 1998. Effects of environmental factors and metals on *Selenastrum capricornutum* lipids. *Phytochemistry* 49 (5), 1241–1247.
- McLaughlin, A., Grathwohl, C., McLaughlin, S., 1978. The adsorption of divalent cations to phosphatidylcholine bilayer membranes.
- Muyssen, B.T.A., De Schampelaere, K.A.C., Janssen, C.R., 2006. Mechanisms of chronic waterborne Zn toxicity in *Daphnia magna*. *Aquatic Toxicology* 77, 393–401.
- Organisation for Economic Co-operation Development, 1998. OECD Guidelines for Testing of Chemicals. Guideline 211: *Daphnia magna* Reproduction Test. Publication Service OECD, Paris, France.
- Pane, E.F., Smith, C., McGeer, J.C., Wood, C.M., 2003. Mechanisms of acute and chronic waterborne nickel toxicity in the freshwater cladoceran, *Daphnia magna*. *Environmental Science and Technology* 37, 4382–4389.
- Pane, E.F., McGeer, J.C., Wood, C.M., 2004. Effects of chronic waterborne nickel exposure on two successive generations of *Daphnia magna*. *Environmental Toxicology and Chemistry* 23 (4), 1051–1056.
- Provasoli, L., McLaughlin, J.J.A., Droop, M.R., 1957. The development of artificial media for marine algae. *Archiv für Mikrobiologie* 25 (4), 392–428.
- Ptashynski, M.D., Pedlar, R.M., Evans, R.E., Wautier, K.G., Baron, C.L., Klavervkamp, J.F., 2001. Accumulation, distribution and toxicology of dietary nickel in lake whitefish (*Coregonus clupeaformis*) and lake trout (*Salvelinus namaycush*). *Comparative Biochemistry and Physiology Part C* 130, 145–162.
- Ravet, J.L., Brett, M.T., Müller-Navarra, D.C., 2003. A test of the role of polyunsaturated fatty acids in phytoplankton food quality for *Daphnia* using liposome supplementation. *Limnology and Oceanography* 48 (5), 1938–1947.
- Ravet, J.L., Brett, M.T., 2006. Phytoplankton essential fatty acid and phosphorus content constraints on *Daphnia* somatic growth and reproduction. *Limnology and Oceanography* 51 (5), 2438–2452.
- Resano, M., Vanhaecke, F., de Loos-Vollebregt, M.T.C., 2008. Electrothermal vaporization for sample introduction in atomic absorption, atomic emission and plasma mass spectrometry – a critical review with focus on solid sampling and slurry analysis. *Journal of Analytical Atomic Spectrometry* 23 (11), 1450–1475.
- Siegel, S., Castellán, N.J., 1988. *Nonparametric Statistics for the Behavioral Sciences*. McGraw-Hill.
- Sofyan, A., Price, D.J., Birge, W.J., 2007a. Effects of aqueous, dietary and combined exposures of cadmium to *Ceriodaphnia dubia*. *Science of the Total Environment* 385 (1–3), 108–116.
- Sofyan, A., Rosita, R., Price, D.J., Birge, W.J., 2007b. Cadmium uptake by *Ceriodaphnia dubia* from different exposures: relevance to body burden and toxicity. *Environmental Toxicology and Chemistry* 26 (3), 470–477.
- Srivastava, R.C., Hasan, S.K., Jyotsana, Gupta, S., 1993. Protective role of metallothionein in nickel induced oxidative damage. *Biochemistry and Molecular Biology International* 30 (2), 261–270.
- Sun, H., Zhou, Q., Tang, W., Shu, Y., Zou, Z., Zhang, G., 2007. Metallothionein expression induced by nickel accumulation in the midgut of *Spodoptera litura Fabricius* larvae exposed to nickel. *Chinese Science Bulletin* 52 (23), 3227–3232.
- Sunamoto, J., Shironita, M., Kawachi, N., 1980. Liposomal membranes. V. Interaction of Zinc(II) ion with egg phosphatidylcholine liposomes. *Bulletin of the Chemical Society* 53, 2778–2781.
- Uyttendaele, M., Rajkovic, A., Van Houteghem, N., Boon, N., Thas, O., Debevere, J., Devlieghere, F., 2008. Multi-method approach indicates no presence of sub-lethally injured *Listeria monocytogenes* cells after mild heat treatment. *International Journal of Food Microbiology* 123, 262–268.
- Welz, B., Borges, D.L.G., Welz, B., Vale, M.G.R., Heitmann, U., 2007. Progress in direct solid sampling analysis using line source and high-resolution continuum source electrothermal atomic absorption spectrometry. *Analytical and Bioanalytical Chemistry* 389 (7–8), 2085–2095.
- Wilding, J., Maltby, L., 2006. Relative toxicological importance of aqueous and dietary metal exposure to a freshwater crustacean: implications for risk assessment. *Environmental Toxicology and Chemistry* 25 (7), 1795–1801.



Contents lists available at SciVerse ScienceDirect

Aquatic Toxicology

journal homepage: www.elsevier.com/locate/aquatox

The use of liposomes to differentiate between the effects of nickel accumulation and altered food quality in *Daphnia magna* exposed to dietary nickel

Roel Evens^{a,*}, Karel A.C. De Schampelaere^a, Lieve Balcaen^b, Yingying Wang^c, Karen De Roy^c, Martin Resano^d, M. Flórez^d, Nico Boon^c, Frank Vanhaecke^b, Colin R. Janssen^a

^a Laboratory of Environmental Toxicology, Ghent University, Belgium

^b Laboratory of Analytical Chemistry, Ghent University, Belgium

^c Laboratory of Microbial Ecology and Technology, Ghent University, Belgium

^d Department of Analytical Chemistry, University of Zaragoza, Pedro Cerbuna 12, E-50009 Zaragoza, Spain

ARTICLE INFO

Article history:

Received 2 September 2011

Received in revised form

27 November 2011

Accepted 29 November 2011

Keywords:

Daphnia magna

Dietary metals

Nickel

Molar C:P ratio

Omega 3 polyunsaturated fatty acids

Liposomes

ABSTRACT

A potential drawback of traditional dietary metal toxicity studies is that it is difficult to distinguish between the direct toxicity of the metal and indirect effects caused by altered concentrations of essential nutrients in the metal-contaminated diet. In previous studies it has become clear that this can hamper the study of the real impact of dietary metal exposure and also complicates the analysis of the mechanisms of dietary metal toxicity in filter-feeding freshwater invertebrates like *Daphnia magna*. This problem has been partly circumvented by the production of liposomes, since these vectors are invulnerable to metal-induced food quality shifts and as such can be applied to study the mechanisms of dietary metal toxicity without the confounding effect of nutritional quality shifts. The aim of current study was to evaluate if there is relevance for dietary Ni toxicity under natural exposures, i.e., when *D. magna* is exposed to dietary Ni via living algae, and secondly, to quantify how nutritional quality shifts contribute to the toxic effects that are observed when algae are used as contaminated food vectors. For this aim, liposomes were prepared by the hydration of phosphatidylcholine in media containing 0 (control), 10, 50, 100 and 500 mg Ni/L. The liposome particles were then mixed with uncontaminated green algae in a 1/10 ratio (on a dry wt basis) to make up diets with constant nutrient quality and varying Ni contents (i.e., 1.2 µg Ni/g dry wt in the control and 18.7, 140.3, 165.0 and 501.6 µg Ni/g dry wt in the Ni-contaminated diet, respectively). A second food type was prepared on the basis of a 1/10 mixture (on a dry weight basis) of control liposomes and Ni-contaminated algae, representing a diet that differed in Ni content (i.e., 1.2, 26.8, 84.7, 262.3 and 742.7 µg Ni/g dry wt) and concentrations of essential nutrients (in terms of P and omega 3 poly-unsaturated fatty acids like eicosapentaenoic acid and α-linolenic acid). Both diets were then simultaneously fed to *D. magna* during a 21-day chronic bioassay, using reproduction, growth, survival, ingestion rate and Ni bioaccumulation as endpoints. Ni delivered by liposomes caused a significant inhibition of reproduction and growth when the metal accumulated to minimum levels of 11.9 and 20.0 µg Ni/g dry wt after 7 and 14 days, respectively. Using algae as Ni vector, similar effects of dietary Ni exposure occurred when algae had been pre-exposed to concentrations of at least 133 µg/L of bioavailable Ni (i.e., Ni²⁺), which is similar to the reproductive EC50 of waterborne Ni exposure for *D. magna* (115 µg Ni²⁺/L). While this may have some consequences for predicting chronic Ni toxicity in this range of Ni concentrations with the biotic ligand model – which could be further improved by including the dietary toxicity pathway in this model, the occurrence of such high concentrations in the field is very rare. Hence, there seems to be very little environmental relevance for dietary Ni toxicity to *D. magna*. Finally, besides the direct effects of Ni there was no evidence that nutritional quality shifts could have affected daphnids' growth, but it is very likely that the impairment of reproduction at toxic exposure levels of Ni was also partly the result of reduced fatty acid levels.

© 2011 Elsevier B.V. All rights reserved.

1. Introduction

Several studies reported that the exposure of freshwater invertebrates to metal-enriched diets can cause adverse effects. The model crustacean *Daphnia magna*, for instance, exhibits reduced

* Corresponding author. Tel.: +32 92643707; fax: +32 92643766.
E-mail address: roel.evens@ugent.be (R. Evens).

fitness under exposure to algal diets, contaminated with Zn, Cu, Cd and Ni (De Schampelaere et al., 2004, 2007; Geffard et al., 2008; Evens et al., 2009). Recent research, however, demonstrated that it cannot always be ruled out that the observed effects are at least partly due to an alteration of the nutritional quality of the contaminated algal diets, induced by the pre-exposure to metals. Indeed, Evens et al. (in press) found that the alleged reproductive effects of dietary Zn exposure to *D. magna* may also be attributed to a reduced availability of dietary phosphorus (P). With respect to dietary Ni, Evens et al. (2009) observed that the reproduction and growth of *D. magna* significantly decreased with increasing Ni concentrations in the diet and increasing bioaccumulation of Ni in the organisms, but this study also showed that the reproduction decreased when the concentration of essential polyunsaturated omega 3 fatty acids (ω 3-PUFAs) in the food was lower. Since the ω 3-PUFA content and internal Ni concentration of the algae were inversely correlated, the cause of dietary Ni toxicity to *D. magna* could not be unambiguously related to either dietary Ni exposure itself or to the correlated change of the food quality. Thus, the real mechanisms of Ni toxicity with natural diets have yet to be elucidated. A first attempt to circumvent this problem was made by Evens et al. (2011), who used Ni-contaminated liposomes as an alternative dietary metal carrier. Liposomes are spherical self-assembled colloidal particles, composed of a multi-lamellar phospholipid membrane which encapsulates a cavity holding an aqueous solution (Ravet et al., 2003; Ravet and Brett, 2006). In accordance with Sunamoto et al. (1980), Evens et al. (2011) produced liposomes that could be contaminated with Ni up to concentrations comparable to the levels under contaminated field conditions. These carriers, composed of the phospholipid phosphatidylcholine, had a chemical composition that was not vulnerable to Ni exposure and were applied in proportions that neither influenced the performance of *D. magna*. The use of liposomes thus offered the advantage that the effects observed in this study could be directly related to Ni exposure without the need to take nutritional quality shifts into account. A main drawback of this method was, however, that the effects caused by metal-contaminated liposomes are very likely not fully predictive for the effects that similar Ni concentrations in natural diets can cause. A possible explanation could be that the bioreactivity of Ni, i.e., the toxic activity of Ni once absorbed by the organisms, may be higher when accumulated from liposomes (Evens et al., 2011). Also, this methodology could not elucidate whether the nutritional quality shifts as previously observed (Evens et al., 2009) are important from a toxicological point of view nor to what extent they would contribute to the observed effects. The major aim of this study was therefore to evaluate if there is ecological relevance for dietary Ni toxicity to *D. magna*, i.e., whether dietary Ni toxicity can occur when the metal is administered via living algae that were previously contaminated at realistic exposure levels. Secondly, we wanted to quantify to what extent Ni-induced nutritional quality shifts alter the fecundity of this test organism.

In the present study, we exposed *D. magna* during 21 days to dietary Ni via two food types. One diet was composed of a combination of the green alga *Pseudokirchneriella subcapitata* (basic nutrient supply) and various concentrations of Ni in liposomes, representing a diet that varied only in Ni content. The other diet consisted of a combination of control liposomes and algae contaminated with varying concentrations of Ni, representing a diet with gradual variations of the Ni content and (possibly) a differential food quality. *D. magna* Ni burden, body length and algal ingestion rate were assessed on a weekly basis, whereas reproduction and survival were monitored daily. We expect that a comparison of both treatments in this parallel design enables the assessment of the ecological relevance of dietary Ni toxicity, whereas (potential) discrepancies between the effects of both food types

will have been caused by nutritional quality shifts in the natural diet.

2. Materials and methods

2.1. Liposome preparation and properties

Control and Ni-laden liposomes were prepared by a mechanized method in accordance with the methodology as described in Evens et al. (2011). Briefly, a homogeneous fatty acid mixture containing 150 mg of dipalmitoyl- and distearoyl-soybean phosphatidylcholine (Epikuron 200 SH, Cargill, United States) was hydrated with water containing Ni concentrations of 0 (control), 10, 50, 100 and 500 mg/L (nominal values). More information on the preparation and storage conditions can be found in Evens et al. (2011). External Ni was operationally defined as the metal quantity desorbed from the outer surface of the liposomes and the interstitial liquid of the vesicles after 5 min of washing in 5 mmol/L Na₂EDTA. The remaining fraction, i.e., internal Ni, was the concentration of metal encapsulated in the aqueous cavity and the Ni present in the interstitial phases of the multi-lamellar membranes. This could be quantified by an acid digestion in HNO₃/H₂O₂ followed by ICP-based Ni analysis (Thermo Scientific Element XR sector-field unit, operated at a mass resolution of ~4000; detection limit = 100 ng/L; quantification limit = 330 ng/L). Liposomes were prepared every 7 days and their body burden was determined immediately afterwards. More details on the metal analysis can be found in Evens et al. (2011, in press).

2.2. Algae exposure and characteristics

The green alga *P. subcapitata* was obtained from the Culture Collection of Algae and Protozoa (CCAP 278/4, Argyll, Scotland) and maintained under conditions as described in De Schampelaere et al. (2004). A quantity of algal biomass sufficient to fully sustain a 21-day *D. magna* experiment was obtained using a 12 L culture. The algae were cultured in a pH buffered (pH 8) growth medium to which the modified Provasoli's ES enrichment medium at half strength (Provasoli et al., 1957) and 1.4 mg/L FeSO₄·7H₂O, 15 mg/L NaH₂PO₄·2H₂O, 150 mg/L NaNO₃ and 2.35 mg/L MnCl₂·4H₂O were added. Algae were inoculated in concentrations of 10⁶ cells/mL, and exposed to concentrations of 0 (control), 225, 450, 900 and 1800 μ g Ni_{dissolved}/L (nominal values). Details on algal growth and harvesting conditions, determination of algal dry weight, cell concentrations, Ni burdens and storage conditions after harvest can be found in Evens et al. (2009). All Ni determinations were carried out using sector-field ICP-mass spectrometry.

After harvest, two food quality parameters were quantified that are known to be of importance for *D. magna* performance, i.e., P (often expressed as the molar C:P ratio) and the concentration of essential ω 3-PUFAs like eicosapentaenoic acid (EPA; 20:5(ω -3)) and alfa-linolenic acid (ALA; 18:3(ω -3)) (Sundbom and Vrede, 1997; Weers and Gulati, 1997; Wacker and von Elert, 2001; Faerovig and Hessen, 2003; Becker and Boersma, 2003; von Elert, 2004; Becker and Boersma, 2005; Ravet and Brett, 2006; Brett et al., 2006). These parameters were determined following the methods described in Evens et al. (2009) and De Schampelaere et al. (2007), respectively.

2.3. *Daphnia magna* exposure and Ni bioaccumulation

The 21-day exposure of *D. magna* to dietary Ni was performed according to OECD guideline No. 211 for testing of chemicals (OECD, 1998). More information on the origin and culture conditions of this test species are given in Evens et al. (2009). The exposures were

Table 1
Series of suspensions of *Pseudokirchneriella subcapitata* in 0.2 μm filtrated modified M4 medium.

$\mu\text{g Ni/L}$	Contr.	1	2	3	4	5	6	I	S	Cell mass ($\times 10^{-05}$ μg)
0	0	1.19	2.17	3.93	9.10	16.96		0.61	2.48e05	2.83
225	0	0.67	1.15	2.41	6.68	12.70	20.64	0.82	1.32e05	2.76
450	0	0.67	1.52	2.78	7.10	14.73		0.62	8.31e04	3.05
900	0	0.57	0.94	1.95	5.31	8.69	1.44	0.54	3.31e04	4.02
1800	0	0.87	1.01	1.98	4.01	9.33	11.96	0.46	−234.6	8.38

Actual concentrations (10^5 cells/mL) were determined by Segwick-Rafter microscope analysis. Corresponding analytical signals were obtained by a Cyan™ ADP Flow Cytometry facility, generating calibration lines with intersection I and slope S for automatic detection.

performed in M4 medium (Elendt and Bias, 1990), with the modifications as described in Evens et al. (2009). Before onset of the experiment, the medium was filtered (0.45 μm) to avoid potential blockage of the Flow Cytometry instrument (see Section 2.4). At the start of the *D. magna* experiment, 30 juveniles (<24 h old) per treatment were transferred individually to polyethylene cups containing 45 mL of test medium.

D. magna was exposed to two diet types with varying concentrations of Ni and (possibly) varying molar C:P ratios and ω 3-PUFA concentrations. The first diet was composed of a mixture (10:1, w/w) of control algae and Ni-contaminated liposomes at 5 different concentrations, representing a diet with unaffected nutritional quality and variable Ni contents. The second diet was composed of a mixture (1:10, w/w) of control liposomes and algae with 5 different Ni concentrations, representing a diet varying in both the Ni content and (possibly) nutritional quality. As the control of both food types was identical, the experiment comprised a total of 9 different treatments. A 10:1 (w/w) mixture of algae and liposomes was chosen to create overlapping Ni concentrations in both diets. Thus, in practice the daphnids were fed 250+25, 500+50 and 750+75 μg dry wt of algae + liposomes during weeks 1, 2 and 3 of the experiment, respectively. Every other day, the test medium was renewed and the pH of the old medium was measured. Survival and reproduction, in terms of the number of juveniles released from the brood pouch, were recorded daily.

At the end of every week (at maximum) 10 surviving parent organisms were used to determine their individual dry weight (Sartorius Digital Micro Balance, type 2405; Germany) and Ni bioaccumulation. Five organisms of these 10 had previously been used to determine the algal ingestion rate (see Section 2.4). Ni bioaccumulation was assessed by solid sampling high resolution-continuum source graphite furnace atomic absorption spectrometry (SS-HR-CS GFAAS; detection limit=8.3 pg; quantification limit=27.7 pg). More details on the application of this technique are given in Evens et al. (2011). Carapax length of the selected as well as the remaining organisms was determined, defined as the linear distance between top of the head and base of the apical spine.

At the end of each week, old test medium was sampled and filtered (PALL Life Sciences Acrodisc, pore size 0.45 μm). The Ni concentration was determined to assess the quantity of Ni eliminated and/or desorbed from the algae and liposomes into the *Daphnia* exposure medium. Since the hydration medium of the liposomes was not substituted after preparation, the Ni remaining in solution (i.e., neither encapsulated in the cavity nor adsorbed onto the liposome membranes) will have entered in the daphnids' test medium. Mass balance calculations pointed out that an extra waterborne Ni exposure involved with these additions would be maximal 25, 50 and 75 $\mu\text{g Ni}_{\text{dissolved}}/\text{L}$ during week 1, 2 and 3, respectively. An additional monitoring experiment was performed simultaneously with the dietary exposures, to assess the implications of this inadvertent side exposure. Similar to the main experiment, daphnids (10 replicates) were fed control algae and control liposomes, and were exposed to waterborne concentrations of 25, 50 and 75 $\mu\text{g Ni}_{\text{dissolved}}/\text{L}$ (nominal values) during weeks 1, 2 and 3, respectively. Dissolved Ni and *D. magna* body length were

measured weekly. Reproduction was recorded daily. *D. magna* body burden was quantified at the end of the exposure (i.e., day 21). Ni concentrations in the solution phase were quantified with sector-field ICP-mass spectrometry.

2.4. Ingestion rate

The ingestion rate of algae by daphnids is measured as the difference in algal cell concentrations in a control suspension (i.e., without daphnids) and the suspensions containing the daphnids from the above-mentioned treatments. We applied a methodology using Flow Cytometry (FC) to quantify the algal cell concentrations based on their relation to chlorophyll fluorescence. For each of the 5 Ni concentrations to which the green alga *P. subcapitata* was exposed, a series of suspensions was prepared in 0.2 μm filtered modified M4 medium (Table 1). Corresponding analytical signals of these suspensions (5 replicates) were determined using a Cyan™ ADP Flow Cytometry facility. A calibration line relating chlorophyll fluorescence to cell concentration could be developed, so that unknown cell concentrations in the treatments could be quantified in a relatively straightforward manner. More details on this technique and the calculation of the ingestion rate are reported in Evens et al. (2011).

2.5. Data treatment and statistics

All observations related to algae, liposomes and *D. magna* are expressed as mean \pm standard deviation. All statistical comparisons between exposures and control treatment were performed with the Mann-Whitney-U test (MWU; Siegel and Castellan, 1988) for reproduction, and ANOVA for body length, Ni burden (Tukey) and algal ingestion rate (Duncan). Level of significance $p=0.05$. All statistical comparisons as well as correlation analyses were performed with Statistica 6.0 software (Statsoft, Tulsa, OK, USA).

3. Results

3.1. Diet properties: Ni burdens and food quality

The Ni concentrations in the algae, liposomes and mixed diet (i.e., a 10:1, w/w mixture of algae and liposomes) are given in Table 2. Internal Ni in the contaminated liposomes varied from 2.0 to 5505.8 $\mu\text{g Ni/g}$ dry wt. Over all treatments, at least 74% of Ni in the contaminated liposomes was present in the internal phase, i.e., encapsulated in the aqueous cavity and adsorbed to the internal P-moieties of the vesicles. The addition of control algae to the Ni-laden liposomes, to obtain a mixed diet with constant nutrient quality (see Section 2.3), resulted in an internal Ni concentration ranging between 1.2 (control) and 501.6 $\mu\text{g Ni/g}$ dry wt (Table 2). Internal Ni concentrations in the exposed algae varied from 1.1 (control) to 816.7 $\mu\text{g Ni/g}$ dry wt. Thus, the addition of the control liposomes to these algae, to create a diet with variable Ni concentrations and food quality, ranged between 1.2 and 742.7 $\mu\text{g Ni/g}$ dry wt.

The molar C:P ratio of the algae significantly decreased ($p < 0.05$) from 56 to 87% with increasing Ni exposure (Table 2). For

Table 2
Data on algae exposure and properties of the algal diets cultured in 5 different Ni concentrations. Ni burdens of the liposomes are given after exposure of phosphatidylcholine to 5 different Ni concentrations in the water. The properties of the mixed diet were calculated based on a 10:1 (w:w) proportion of algae:liposomes, respectively. All data are reported as mean ± standard deviation.

Diet	Variable Ni – constant food quality					Variable Ni – variable food quality				
	Control	Control	Control	Control	Control	Control	Control	Control	Control	Control
Algae exposure (µg Ni/L)	1.03	1.03	1.03	1.03	1.03	0.96	0.89	0.44	0.85	0.85
Biomass growth rate (d ⁻¹)	1.1 ± 0.5	1.1 ± 0.5	1.1 ± 0.5	1.1 ± 0.5	1.1 ± 0.5	29.3 ± 3.3	92.9 ± 3.9	288.3 ± 14.8	816.7 ± 146.5	816.7 ± 146.5
Internal Ni (µg/g dry wt)	1.1 ± 0.3	1.1 ± 0.3	1.1 ± 0.3	1.1 ± 0.3	1.1 ± 0.3	15.2 ± 1.4	41.2 ± 6.3	136.3 ± 9.2	323.8 ± 12.8	323.8 ± 12.8
External Ni (µg/g dry wt)	1843 ± 352	1843 ± 352	1843 ± 352	1843 ± 352	1843 ± 352	1949 ± 877	803 ± 66*	309 ± 17*	244 ± 10*	244 ± 10*
Molar C:P ratio	18.43 ± 0.31	18.43 ± 0.31	18.43 ± 0.31	18.43 ± 0.31	18.43 ± 0.31	12.62 ± 0.35*	6.93 ± 0.06*	5.02 ± 0.10*	0.58 ± 0.99*	0.58 ± 0.99*
ω3-PUFA (mg/g dry wt)	1.51 ± 0.04	1.51 ± 0.04	1.51 ± 0.04	1.51 ± 0.04	1.51 ± 0.04	1.65 ± 0.09	1.56 ± 0.03	1.44 ± 0.03	0.17 ± 0.27	0.17 ± 0.27
α-Linolenic acid	Control	Control	Control	Control	Control	Control	Control	Control	Control	Control
Eicosapentaenoic acid	Control	Control	Control	Control	Control	Control	Control	Control	Control	Control
Liposome hydration concentration (mg Ni/L)	Control	Control	Control	Control	Control	Control	Control	Control	Control	Control
Internal Ni (µg/g dry wt)	2.0 ± 0.1	194.5 ± 5.1	1532.1 ± 182.0	1803.2 ± 103.6	5505.8 ± 24.7	2.0 ± 0.1	2.0 ± 0.1	2.0 ± 0.1	2.0 ± 0.1	2.0 ± 0.1
External Ni (µg/g dry wt)	0.4 ± 0.2	12.1 ± 3.0	85.0 ± 20.9	320.6 ± 74.3	1885 ± 553.6	0.4 ± 0.2	0.4 ± 0.2	0.4 ± 0.2	0.4 ± 0.2	0.4 ± 0.2
Molar C:P ratio ^a	42	42	42	42	42	42	42	42	42	42
ω3-PUFA (mg/g dry wt)	–	–	–	–	–	–	–	–	–	–
Mixed diet	Control	Control	Control	Control	Control	Control	Control	Control	Control	Control
Internal Ni (µg/g)	1.2	18.7	140.3	165.0	501.6	26.8	84.7	262.3	742.7	742.7
Molar C:P ratio ^b	260	260	260	260	260	262	225	162	145	145
ω3-PUFA (mg/g dry wt)	16.75	16.75	16.75	16.75	16.75	11.47	6.30	4.56	0.53	0.53
α-Linolenic acid	1.38	1.38	1.38	1.38	1.38	1.50	1.42	1.31	0.15	0.15
Eicosapentaenoic acid	–	–	–	–	–	–	–	–	–	–

^a Liposome molar C:P ratio of 42 is the average C:P of dipalmitoyl phosphatidylcholine (42) and distearoyl phosphatidylcholine (44).

^b Molar C:P ratio and ω3-PUFA content of the mixed diet are calculated on the basis of a 10:1 ratio (w:w) of algae:liposomes, given the carbon content of algae is 0.4 g C/g dry wt.

* Significant difference after comparison with Mann-Whitney U test (p < 0.05).

the liposomes, a molar C:P ratio of 42 was calculated on the basis of the structural formulae of dipalmitoyl- and distearoyl-phosphatidylcholine. The presence of relatively high and constant P concentrations in the liposomes leveled out the large differences between the Ni-contaminated algae when both vectors were put together: weighted averages of the molar C:P in the mixed diet (based on a 10:1, w/w mixture of algae:liposomes) varied between 262 and 145 mol/mol. Concentrations of the essential ω 3-PUFA EPA were significantly reduced ($p < 0.05$) only at the highest exposure to Ni (by 89%). ALA levels significantly decreased ($p < 0.05$) from 32 to 97% with increasing Ni exposure. Since these ω 3-PUFAs were not present in the liposomes, their concentrations in the mixed diets were 9.1% lower (on mass basis) than in the algae.

3.2. *Daphnia* exposure: effects on survival, growth and reproduction

3.2.1. Exposure to Ni via liposomes

The addition of Ni-contaminated liposomes to the test medium resulted in a slight increase of dissolved Ni in most of the treatments, and was maximal 76 $\mu\text{g/L}$ at the end of the second week (Table 3). This is higher than the concentration we expected to occur based on mass balance calculations and the concentrations that were applied in the monitoring experiment (see Section 3.2.3). Exposure to dietary Ni resulted in 100% mortality after 14 days. Hence, comparisons of all other endpoints could only be made up to day 14. Whole body Ni in the control daphnids was 1.7, 0.7 and 0.4 $\mu\text{g/g}$ dry wt after 7, 14 and 21 days, respectively. Whole body Ni in the daphnids exposed to dietary Ni was significantly higher and increased linearly with increasing Ni concentrations in the diet after day 7 ($p = 0.0002$; $R^2 = 0.99$) and up to day 14 ($p = 0.002$; $R^2 = 0.97$). The accumulation of Ni ≥ 11.9 $\mu\text{g/g}$ dry wt was accompanied by a decrease of the 7-day daphnid length by at least 21.4%. Between day 7 and day 14, no further growth occurred in the Ni-exposed daphnids, while the control daphnids still grew by 30% (in length) in this time span. The first brood size (expressed as number of juveniles) of the Ni-exposed daphnids was significantly reduced by minimum 40%. None of the Ni-exposed individuals were able to produce a second brood before dying. Maturation rate, expressed as the time required to release the first brood, was not significantly affected.

3.2.2. Exposure to Ni via algae

The addition of Ni-contaminated algae to the test medium also resulted in a gradual increase of dissolved Ni, but concentrations never exceeded 25 $\mu\text{g/L}$ (Table 3). Exposure to dietary Ni resulted in 100% mortality after 21 days in only the highest exposure (i.e., 742.7 $\mu\text{g Ni/g}$ dry wt). Similar to Ni administered via liposomes, whole body Ni in the daphnids increased linearly with increasing Ni concentrations in the algae after day 7 ($p = 0.004$; $R^2 = 0.96$) and day 14 ($p = 0.006$; $R^2 = 0.94$). Bioaccumulation of Ni administered via liposomes was, however, more efficient: similar concentrations in the diet resulted in daphnid burdens that exceeded the bioaccumulation of Ni delivered via algae by almost factor 2 (slope of $\text{Ni}_{D. magna}$ vs. $\text{Ni}_{liposomes} = 0.085$; slope $\text{Ni}_{D. magna}$ vs. $\text{Ni}_{algae} = 0.044$). After 7 days of exposure, *D. magna* body length was unaffected when whole body Ni concentrations increased up to 6.7 $\mu\text{g Ni/g}$ dry wt, whereas bioaccumulation up to 34.1 $\mu\text{g Ni/g}$ dry wt resulted in a growth that was significantly reduced by 33% in comparison to the control. Despite this reduction, it is important to note that growth in this treatment still continued between day 7 and 14 (i.e., by 18%), whereas no further growth occurred in the daphnids exposed to Ni-contaminated liposomes, although these organisms accumulated less Ni (i.e., 20.4 $\mu\text{g Ni/g}$ dry wt vs. 133.2 $\mu\text{g Ni/g}$ dry wt). First brood size was significantly reduced (by minimum 40%) when Ni burdens in the daphnids exceeded 6.7 $\mu\text{g Ni/g}$ dry wt. The second, third

and fourth brood size were significantly reduced by 19.4, 62.6 and 74.5%, respectively. Maturation rate was not significantly affected.

3.2.3. Exposure to Ni via dissolved phase

D. magna Ni burdens significantly increased (Mann–Whitney *U* test, $p < 0.05$) as a function of waterborne Ni exposure (Table 4). Maturation rate, expressed as the time to first brood, was significantly ($p < 0.05$) retarded by one day. Other parameters were not affected.

3.3. *Daphnia magna* ingestion rates

A linear relation (minimal $R^2 = 0.998$) was observed between the FC signal and the cell concentration for each of the 5 Ni concentrations to which the green alga *P. subcapitata* was exposed. Intersections and slopes of these calibration functions are reported in Table 1. The FC measurements and the calibration data were used to calculate the concentrations of algae in the suspensions of the feeding assay (with and without added *Daphnia*) and subsequently to determine the ingestion rates (according to Evens et al., 2011). For the diet composed of Ni-laden liposomes and Ni concentrations ≥ 140.3 $\mu\text{g Ni/g}$ dry wt, the *per capita* algal ingestion rates (i.e., expressed as cells ingested per individual per hour; Table 5) were significantly reduced by at least 31% and 94%, after 6 and 13 days of exposure, respectively (Student's *t*-test, $p < 0.05$). Due to 100% mortality at day 15, no ingestion rates after 20 days of exposure could be obtained. For the diet composed of Ni-contaminated algae and containing Ni levels ≥ 26.8 $\mu\text{g Ni/g}$ dry wt, *per capita* algal ingestion rates were significantly reduced by at least 46% and 62%, after 6 and 13 days of exposure, respectively (Student's *t*-test, $p < 0.05$).

Two corrections were performed to obtain data with more toxicological relevance. Firstly, ingestion rates were corrected for the square of the body length to discriminate between a merely *indirect* effect of daphnid length on ingestion rate and a true, *direct* effect of dietary Ni on the ingestion process (also see De Schampheleere et al., 2007; Evens et al., 2011). Secondly, since Ni exposure altered the dry weight of an individual algal cell (Table 1), cell-specific weight was taken into account to express the ingestion rates in terms of biomass. In this way, we calculated that dietary Ni exposure via liposomes did not affect size specific algal ingestion rate at day 6, but exposures ≥ 140.3 $\mu\text{g Ni/g}$ dry wt resulted in a decrease from 2.50 ± 1.18 to at least 0.49 ± 0.97 $\mu\text{g mm}^{-2} \text{h}^{-1}$ at day 13 (i.e., reduction by 80% and higher) (Table 5). For the daphnids fed with Ni-contaminated algae, size specific algal ingestion rates at exposures ≥ 26.8 $\mu\text{g Ni/g}$ dry wt were reduced from 0.40 ± 0.079 to at least 0.23 ± 0.030 $\mu\text{g mm}^{-2} \text{h}^{-1}$ at day 6 (i.e., minimum reduction of 43%) and from 2.50 ± 1.18 to at least 1.16 ± 1.00 $\mu\text{g mm}^{-2} \text{h}^{-1}$ at day 13 (i.e., minimum reduction of 54%).

4. Discussion

4.1. Side exposure to waterborne Ni

Neither *D. magna* body length nor reproduction was affected by dissolved Ni in the monitoring experiment. Except for the daphnids that were exposed to the most contaminated liposomes, it can thus be excluded that the reproduction and growth effects of dietary Ni exposure would have been (partly) caused by a side exposure to Ni via the dissolved phase. Also, the 21-day Ni burden of the organisms exposed via the water (i.e., 1.58 $\mu\text{g Ni/g}$ dry wt) is relatively small in comparison with the bioaccumulation that would have occurred in the daphnids after 3 weeks of exposure to these diets (Table 3). Except for the maturation rate, it can thus be concluded that the contribution of dietary Ni to both accumulation and toxicity in most of these treatments must have been far more important, and that the unwanted addition of dissolved Ni, along

Table 3
Experimental conditions and results of a 21-day chronic exposure of *Daphnia magna* to 9 food types, varying in Ni concentration and/or nutritional quality.

	Control	Ni laden liposomes: variable Ni – constant food quality			Ni contaminated algae: variable Ni – variable food quality		
Algal Ni burden ^{a,e}	1.1 ± 0.5	1.1 ± 0.5	1.1 ± 0.5	1.1 ± 0.5	29.3 ± 3.3	92.9 ± 3.9	288.3 ± 14.8
Lipo Ni burden ^{a,e}	2.0 ± 0.1	1532.1 ± 182.0	1803.2 ± 103.6	5505.8 ± 24.7	2.0 ± 0.1	2.0 ± 0.1	816.7 ± 146.5
Dietary Ni burden ^{b,e}	1.2	140.3	165.0	501.6	26.8	84.7	2.0 ± 0.1
Diss Ni at day 7 ^c	1	1	7	42	2	3	742.7
Diss Ni at day 14 ^e	1	6	12	76	3	5	7
Diss Ni at day 21 ^e	1.2	0.9	–	–	4	7	14
<i>D. magna</i> 21 day mortality (%)	10	100 [*]	100 [*]	100 [*]	60	40	100 [*]
<i>D. magna</i> Ni at day 7 ^{a,c,e}	1.7 ± 0.7 ^A	2.7 ± 1.8 ^{AB}	11.9 ± 6.0 ^C	12.2 ± 4.3 ^C	2.8 ± 1.7 ^A	3.5 ± 3.0 ^A	6.7 ± 2.3 ^{BC}
<i>D. magna</i> Ni at day 14 ^{a,c,e}	0.7 ± 1.1 ^A	12.5 ± 7.1 ^A	20.4 ± 9.1 ^A	20.0 ± 11.1 ^A	1.5 ± 0.3 ^A	4.1 ± 2.2 ^A	15.0 ± 5.1 ^A
<i>D. magna</i> Ni at day 21 ^{a,c,e}	0.4 ± 0.08 ^A	3.3 ± 1.3 ^A	–	–	4.7 ± 2.8 ^A	8.2 ± 7.5 ^A	29.7 ± 14.3 ^B
Length at day 7 ^{a,c,e}	2.85 ± 0.15 ^A	2.77 ± 0.17 ^A	2.00 ± 0.18 ^{BC}	2.22 ± 0.22 ^C	2.81 ± 0.07 ^A	2.84 ± 0.22 ^A	2.56 ± 0.22 ^A
Length at day 14 ^{a,c,e}	3.71 ± 0.22 ^A	3.40 ± 0.18 ^{AB}	2.08 ± 0.14 ^C	2.41 ± 0.52 [*]	3.43 ± 0.24 ^{AD}	3.38 ± 0.37 ^{AE}	3.09 ± 0.19 ^{BDE}
Length at day 21 ^{a,c,e}	3.98 ± 0.15 ^A	3.55 ± 0.25 ^{AB}	–	–	3.73 ± 0.46 ^{AB}	3.77 ± 0.33 ^A	3.17 ± 0.17 ^B
Total reproduction (# juveniles/daphnid ^{a,d})	98.9 ± 15.3	82.4 ± 29.5	–	–	89.3 ± 40.3	92.0 ± 28.9	33.3 ± 5.5 [*]
14 day reproduction (3 broods)	58.2 ± 9.4	50.9 ± 12.3	–	–	60.3 ± 8.1	39.3 ± 4.1 [*]	22.3 ± 3.4 [*]
Time to first brood (days) ^{b,d}	8.1 ± 0.6	8.3 ± 0.7	10.0 ± 2.8	8.9 ± 1.5	8.9 ± 0.4	9.3 ± 0.5	9.1 ± 1.1
1st brood size (juv.) ^{b,d}	10.3 ± 2.3	9.6 ± 2.3	1.5 ± 0.7 [*]	4.0 ± 3.8 [*]	9.8 ± 1.5	9.9 ± 3.3	6.2 ± 3.4 [*]
2nd brood size (juv.) ^{b,d}	20.6 ± 2.2	18.0 ± 3.7	–	1.0	21.1 ± 4.1	16.6 ± 5.5 [*]	10.9 ± 2.4 [*]
3rd brood size (juv.) ^{b,d}	24.3 ± 2.7	24.2 ± 7.9	–	–	25.5 ± 9.7	20.3 ± 12.7	9.1 ± 5.0 [*]
4th brood size (juv.) ^{b,d}	19.6 ± 9.9	13.7 ± 7.6	–	–	18.6 ± 8.8	20.3 ± 7.5	5.0 ± 2.0 [*]
5th brood size (juv.) ^{b,d}	20.6 ± 6.1	15.7 ± 9.4	–	–	22.0 ± 9.6	20.5 ± 6.8	10.0

^a Data on exposure parameters and toxicological endpoints are presented as mean ± standard deviation (n = 5 for algae and liposome Ni burden, n = 10 for *D. magna* body burden, length, total and 14 day reproduction, time to first brood and size of 1st to 5th brood).

^b Dietary Ni burden is the weighted average of the algal and liposome Ni burdens, taking into account a 10:1 (w/w) dry weight ratio for algae and liposomes, respectively.

^c *D. magna* Ni burdens and body length not sharing the same letter are significantly different from each other (One way ANOVA, Tukey, p < 0.05).

^d *D. magna* total reproduction, individual brood sizes, time to first brood and total mortality are statistically compared with Mann–Whitney U test.

^e Ni burdens in algae, liposomes, mixed diet and *D. magna* are expressed as µg/g dry wt. Dissolved Ni expressed as µg/L. *D. magna* length expressed as mm.

^{*} Significant differences between the control exposure and elevated dietary Ni exposures (Mann–Whitney-U test, p < 0.05).

^{**} Treatments comprising one or two replicates were not used for statistical analysis. The limitation of the number of data also puts significant constraint on the accuracy of data-interpretation.

Table 4

Comparison of dissolved Ni, Ni bioaccumulation, *Daphnia magna* body length and reproduction between a control and waterborne exposure of maximal Ni concentration in water.

Nominal waterborne Ni for week 1–2–3 ($\mu\text{g/L}$)	0 (control exposure)	25–50–75
Dissolved Ni at day 7 ($\mu\text{g/L}$)	1	23
Dissolved Ni at day 14 ($\mu\text{g/L}$)	1	44
Dissolved Ni at day 21 ($\mu\text{g/L}$)	1.2	64
<i>D. magna</i> Ni body burden at day 21 ($\mu\text{g/g}$)	0.37 \pm 0.08	1.58 \pm 0.78*
Length at day 7 (mm)	2.85 \pm 0.15	2.85 \pm 0.20
Length at day 14 (mm)	3.71 \pm 0.22	3.56 \pm 0.14
Length at day 21 (mm)	3.98 \pm 0.15	4.07 \pm 0.15
Total reproduction (# juveniles/daphnid)	98.9 \pm 15.3	110.3 \pm 25.3
Time to first brood (days)	8.1 \pm 0.6	9.1 \pm 0.6*
1st brood size	10.3 \pm 2.3	10.0 \pm 2.5
2nd brood size	20.6 \pm 2.2	21.4 \pm 5.0
3rd brood size	24.3 \pm 2.7	25.1 \pm 5.1
4th brood size	19.6 \pm 9.9	28.7 \pm 7.2*
5th brood size	20.6 \pm 6.1	27.3 \pm 6.9

* Significant difference after comparison with Mann Whitney U test ($p < 0.05$).

with the liposomes and algae, does not have any consequences on the interpretation of the observed accumulation and toxicity data. One exception is the treatment in which the daphnids were fed with the most contaminated liposomes (i.e., the composite diet containing 501.2 $\mu\text{g Ni/g dry wt}$), since the dissolved Ni concentrations in these test media were higher than the concentrations investigated in the monitoring experiment. For this treatment it can thus not be excluded *a priori* that the observed toxic effects may also have been due to waterborne Ni exposure. These data should thus be interpreted cautiously.

4.2. Ni bioaccumulation and effects on *Daphnia magna*

When using the liposomes as a Ni vector, *D. magna* body length and reproduction were significantly reduced when the mixed diet contained 140.3 $\mu\text{g Ni/g dry wt}$ (i.e., LOEC) and higher. The whole body Ni content in these organisms increased gradually to at least 11.9 $\mu\text{g Ni/g dry wt}$ after day 7 and to at least 20.4 $\mu\text{g Ni/g dry wt}$ after 14 days of exposure. The observed effects parallel this time trend as they were more severe between day 7 and 14 than prior to day 7. Similar effects were observed in previous studies on dietary Ni (Evens et al., 2011) and dietary Cu (De Schampelaere et al., 2007). A significant reduction of the size-corrected algal ingestion rate between day 6 and 13 may be a possible explanation as to why no significant growth was observed in the Ni-exposed daphnids between day 7 and 14. This mechanism can, however, not account for the observed effects before day 7 of the exposure since size-corrected algal ingestion rates were not inhibited in this time span. Two other mechanisms, although suggestive, may explain the reduced growth during the first exposure week. Firstly, the assimilation of nutrients across the digestive tract may have been inhibited, caused by potential aberrations of the digestive tract. A second possibility is that the exposure to and bioaccumulation of dietary Ni may have reduced the amount of energy that is available to invest in somatic growth, for instance due to increased energy

requirements to detoxify Ni, and/or due to an overall reduction of the available energy charge (i.e., ATP-levels) in the Ni-exposed daphnids (Evens et al., 2011). However, more research is required to test these hypotheses.

4.3. Comparison of artificial and natural exposures

The abovementioned results reveal unambiguously that dietary Ni can induce toxic effects in *D. magna*, without the the potentially confounding factor of diet quality shifts that were observed in previous studies (Evens et al., 2009). In line with this, the major aim of current study was to investigate if there is also environmental relevance for dietary Ni toxicity, so whether toxicity occurs when daphnids are exposed to similar levels of dietary Ni via natural vectors like living algae. A limitation of using liposomes is, however, that the Ni concentrations in contaminated liposomes are likely not 100% predictive of the effects that natural Ni-contaminated diets can cause. Ni-laden liposomes produced a much stronger effect to *D. magna* than the Ni-laden algae, although similar Ni concentrations in the mixed diet (i.e., the composite diet) were present. This is likely due to the fact that the bioaccumulation of Ni in *D. magna* was almost 2-fold higher when the metal was administered via the liposomes than via the algae (see Section 3.2.2). Thus, in order to examine if there is environmental relevance for dietary Ni toxicity (see Section 4.4), not the Ni concentration in the diet but the Ni bioaccumulation in *D. magna* was considered as a common denominator between both exposure modes.

4.4. Is there ecological relevance for dietary Ni toxicity?

The LOEC for dietary Ni exposure via liposomes was 140.3 $\mu\text{g Ni/g dry wt}$, which resulted in a body burden of 20.4 $\mu\text{g Ni/g dry wt}$ after 14 days. Exposure to Ni via algae resulted in a similar burden when the daphnids received a diet with Ni concentrations that must have been situated in the range from 262.3 to 742.7 $\mu\text{g Ni/g dry wt}$ (Table 3). Thus, an exposure to at least 900 $\mu\text{g Ni}_{\text{dissolved}}/\text{L}$ or 133 $\mu\text{g Ni}^{2+}/\text{L}$ was needed to achieve this level in the algal culture medium (see Section 2.2). This concentration is in the same order of magnitude as the reproductive EC50 for *D. magna* (115 $\mu\text{g Ni}^{2+}/\text{L}$), as predicted with the chronic BLM (Deleebeek et al., 2008) for the respective test water applied in this study (see Section 2.3). This may support the earlier made assumption (Deleebeek et al., 2008) that the chronic toxicity observed previously in standard 'waterborne' Ni exposures may have been partly due to an indirect exposure via the diet if algae accumulated those Ni levels from the exposure medium before they were ingested by the daphnids. However, a decisive answer cannot be given since the bioavailability of identical Ni^{2+} concentrations in the modified M4 medium (i.e., daphnids' test medium) and the modified ES&Walne medium (i.e., algal culture medium) was different. Indeed, since the concentration of cations that enter into competition with Ni^{2+} for uptake, like Mg^{2+} and H^+ , were 2.5 and 10 fold higher in the former medium, respectively, it is doubtful if algae in the daphnids' medium could also have accumulated Ni up to the burdens that were acquired after culture in the modified ES&Walne medium. More research is required to tackle this question. Also, although our finding that dietary Ni can cause toxic effects on *D. magna* is important from a mechanistic point of view, it must be acknowledged that the Ni concentrations to which the algal food was exposed, i.e., at least 900 $\mu\text{g Ni}_{\text{dissolved}}/\text{L}$ or 133 $\mu\text{g Ni}^{2+}/\text{L}$, as well as the internal Ni concentration in the algal food that was needed to invoke toxicity in *D. magna*, i.e., 288 $\mu\text{g Ni/g dry wt}$, will not often be found in natural environments. Ambient concentrations in natural surface waters (away from point sources and thus representing diffuse pollution) have been measured recently in 6 European regions, with mean values varying between only 0.33 and

Table 5
Algal ingestion rates of *D. magna* exposed to 9 food types, varying in Ni concentration and/or nutritional quality. In the lower rows, algal ingestion rates were adjusted to the square of the body length of the respective test organisms to take into account size dependency of nutritional requirements.

	Control	Ni laden liposomes: variable Ni – constant food quality			Ni contaminated algae: variable Ni – variable food quality		
Dietary Ni ($\mu\text{g Ni/g dry wt}$)	1.2	140.3	501.6	26.8	84.7	262.3	742.7
Algal ingestion rate (cells/h) ^a							
Day 6	113,797 \pm 22,342 ^A	100,779 \pm 13,836 ^{AB}	68,473 \pm 28,516 ^C	61,442 \pm 7887 ^{CD}	35,822 \pm 52,116 ^{DE}	25,172 \pm 8658 ^{EF}	3010 \pm 3289 ^F
Day 13 ^b	1,171,392 \pm 551,373 ^A	824,157 \pm 519,646 ^{AB}	46,704 \pm 93,407 ^C	443,408 \pm 361,086 ^{BC}	402,560 \pm 345,791 ^{BC}	78,824 \pm 133,729 ^C	17,350 \pm 38,795 ^C
Day 20 ^{b,c}	639,043 \pm 244,032 ^A	150,823 \pm 240,318 ^B	–	87,796 \pm 196,317 ^B	141,565 \pm 235,743 ^B	0 \pm 0 ^B	0
Algal ingestion rate ($\mu\text{g/h}$) ^a							
Day 6	3.22 \pm 0.63 ^A	2.85 \pm 0.39 ^{AB}	1.94 \pm 0.81 ^{CD}	1.70 \pm 0.22 ^{CD}	1.09 \pm 0.16 ^{DE}	1.01 \pm 0.35 ^{DE}	0.25 \pm 0.28 ^E
Day 13 ^b	33.13 \pm 15.59 ^A	23.31 \pm 14.70 ^{AB}	1.32 \pm 2.64 ^C	12.24 \pm 9.57 ^{BC}	12.26 \pm 10.53 ^{BC}	3.17 \pm 5.37 ^C	1.45 \pm 3.25 ^C
Day 20 ^{b,c}	18.07 \pm 6.90 ^A	4.27 \pm 6.35 ^B	–	2.42 \pm 5.42 ^B	4.31 \pm 7.18 ^B	0 \pm 0 ^B	0
Algal ingestion rate ($\mu\text{g}/\text{mm}^2 \text{ h}$) ^a							
Day 6	0.40 \pm 0.079 ^A	0.39 \pm 0.053 ^A	0.39 \pm 0.16 ^A	0.23 \pm 0.030 ^{CD}	0.16 \pm 0.023 ^{CD}	0.17 \pm 0.057 ^{CD}	0.09 \pm 0.094 ^D
Day 13 ^b	2.50 \pm 1.18 ^A	1.80 \pm 1.14 ^{AB}	0.21 \pm 0.42 ^C	1.05 \pm 0.86 ^{BC}	1.16 \pm 1.00 ^{BC}	0.39 \pm 0.66 ^C	0.36 \pm 0.80 ^C
Day 20 ^{b,c}	1.14 \pm 0.44 ^A	0.34 \pm 0.50 ^B	–	0.17 \pm 0.39 ^B	0.30 \pm 0.51 ^B	0 \pm 0 ^B	0

^a Algal ingestion rates not sharing the same letter are significantly different from each other (One way ANOVA, Duncan, $p < 0.05$).

^b Algal ingestion rates lower than the detection limit (unidentified) were set to 0.

^c No ingestion rates could be calculated for organisms exposed to the three highest Ni concentrations in liposomes (100% mortality).

5.13 $\mu\text{g Ni}_{\text{dissolved}}/\text{L}$ (Risk Assessment Report on Ni, 2009). Additionally, given the 56% reduced growth rate of the algae (Table 2) at internal Ni burdens causing dietary toxicity to *D. magna*, it could be argued that algal food may disappear from natural systems at Ni concentrations lower than those that could lead to dietary toxicity. For all these reasons, it can be argued that dietborne Ni toxicity is of limited concern in freshwater ecosystems for at least *D. magna* as a key species.

The results presented in this paper are in line with a previous study on dietary Ni (Evens et al., 2009), where total (21-day) reproduction and 21-day length were severely affected when the daphnids were fed algae pre-exposed to 900, 1800 and 3600 $\mu\text{g/L}$, but not when fed algae grown in 225 and 450 $\mu\text{g/L}$. In contrast, reproduction of the marine copepod *Acartiatonsa*, fed with the Ni-contaminated diatom *Thalassiosira pseudonana*, decreased gradually and in a dose-dependent manner and was significant at much lower dietary Ni levels (LOEC = 58.1 $\mu\text{g Ni/g dry wt}$; Bielmyer et al., 2006) than in the current study (LOEC = 262.3 $\mu\text{g Ni/g dry wt}$). Similarly, the waterborne Ni concentrations to which the live phytoplankton species were exposed to obtain these toxic Ni contents were far lower in the study of Bielmyer et al. (2006) than in our study (i.e., 7.60 vs. 900 $\mu\text{g Ni/L}$). This demonstrates that the effects of dietary Ni exposure are species-specific and this is a factor that should preferably be accounted for when evaluating potential risks of dietary Ni exposure in the aquatic environment.

4.5. Importance of nutritional quality shifts

In contrast with the study of Evens et al. (2009), wherein the (direct) effects of Ni uptake and the (indirect) effects of Ni-induced food quality shifts could not be disentangled, current study has provided evidence that the effects of dietary Ni exposure may (at least partly) be the result of Ni bioaccumulation if whole body burdens of the daphnids exceed 20.4 $\mu\text{g Ni/g dry wt}$ (=LOEC of bioaccumulation). To this end a pre-exposure of the algae to concentrations higher than 900 $\mu\text{g/L}$ (\sim EC50 for waterborne Ni toxicity) was required. A recent study (Evens et al., in press) has revealed that metal-induced food quality shifts may have a considerable contribution to the alleged effects of dietary metals. Thus, the traditional way of relating dietary metal toxicity directly to metal uptake does not hold if nutritional quality shifts have not been investigated or ruled out. The second aim of this research was to investigate to what extent nutritional quality shifts may have contributed to or mitigated the effects of Ni when the exposure was performed via this vector.

The key nutritional factor governing growth in *D. magna* and other cladocerans is the molar C:P ratio, representing the phosphorus (P) content of the diet. *D. magna* growth is limited by mineral P only at dietary C:P values >350 (Becker and Boersma, 2003). The fact that (1) all molar C:P ratios of the mixed diet are beneath this threshold and (2) Ni exposure to algae clearly increased the P content of the diet (probably as a detoxification mechanism to include Ni in polyphosphate granules; Wang et al., 2007) leads us to suggest that reduced P-availability was not a relevant mechanism in this study. The increasing level of P in the Ni-contaminated algae could, however, be an explanation for the reduced ingestion rate after 6 and 13 days, since the whole body Ni burdens of *D. magna* were not predictive for this effect (Table 3). Darchambeau and Thys (2005) found that the clearance rate of *D. galeata* was always negatively correlated with the P concentration in the food, and argued that *Daphnia* always reacts to a decrease of food quality (i.e., higher C:P ratio) by an increase of its feeding rate.

When algal C:P ratios are lower than 350, representing a diet that is P-sufficient, *D. magna* growth can be limited by the concentration of essential ω 3-PUFAs. Eicosapentaenoic acid (EPA; 20:5(n-3)) is considered as one of the most important fatty acids

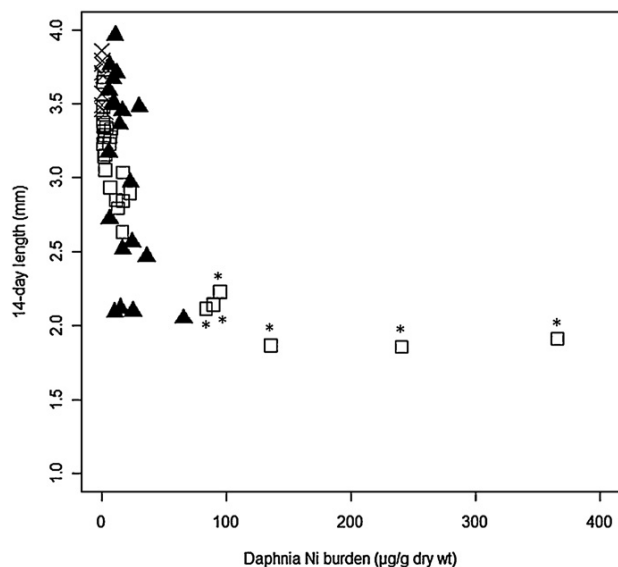


Fig. 1. *Daphnia magna* body length after 14 days in relation to Ni bioaccumulation for organisms fed with a 1/10 (w/w) combination of Ni contaminated liposomes and algae, and a 10/1 (w/w) combination of Ni contaminated algae and liposomes. × = control diet; ▲ = diet with Ni-laden liposomes; □ = diet with Ni-laden algae. (*) Length of daphnids that were fed with algae pre-exposed to 1800 µg/L.

for daphnids (Weers and Gulati, 1997; von Elert, 2004; Becker and Boersma, 2005; Brett et al., 2006), and is known to limit growth if the dietary concentrations <math><2.23 \mu\text{mol/g C}</math> (or 0.27 mg/g dry wt). Since the EPA levels reported in Table 2 are constant and higher than this threshold for algae exposed to 900 µg/L, this study demonstrates that neither a shift of dietary ω 3-PUFA levels could have altered the toxicity of dietary Ni. Thus, there is no evidence that the nutritional quality shifts in the algae may have affected the growth

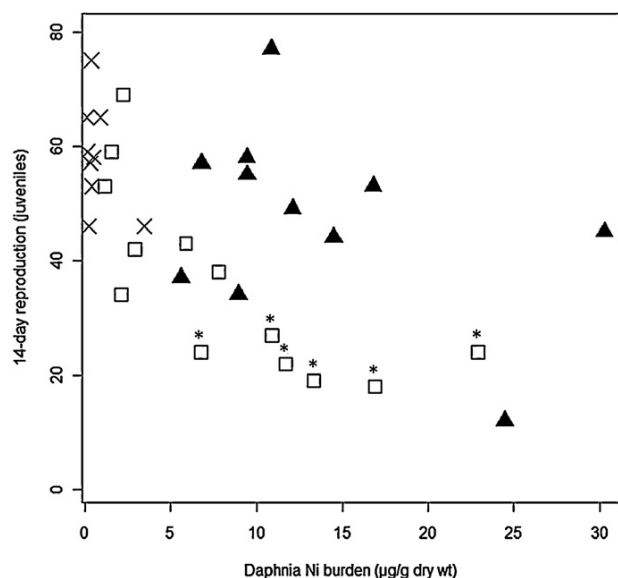


Fig. 2. *Daphnia magna* reproduction after 14 days in relation to Ni bioaccumulation for organisms fed with a 1/10 (w/w) combination of Ni contaminated liposomes and algae and a 10/1 (w/w) combination of Ni contaminated algae and liposomes. Only organisms that produced three broods were selected. (*) Reproduction of daphnids that were fed with algae pre-exposed to 900 µg/L. No juveniles were produced at higher exposure levels. × = control diet; ▲ = diet with Ni-laden liposomes; □ = diet with Ni-laden algae.

for exposures to at least 900 µg Ni/L, so that the growth effects related to this diet can be fully attributed to dietary Ni uptake. This is supported by the fact that the relations between body length and Ni bioaccumulation for the daphnids that were fed with Ni-laden liposomes and Ni-contaminated algae coincide in this concentration range (Fig. 1). In contrast, there is a possibility that the algae exposed to 1800 µg Ni/L may have contained insufficient EPA levels (Table 2: EPA <math><0.27 \text{ mg/g dry wt}</math>). Our data can, however, not confirm this suggestion, since the bioaccumulation of Ni from both food types does not overlap in this concentration range (Fig. 1).

Finally, a significant discrepancy was observed between the 14-day reproduction of daphnids fed with Ni-laden liposomes and algae pre-exposed to 900 µg Ni/L (Fig. 2). It is very unlikely that P-limitation would have occurred, since the P-requirements for reproduction are even lower than for growth, and reproduction is mostly sensitive for varying ω 3-PUFA levels (Urabe and Sterner, 2001; Becker and Boersma, 2003). EPA levels in this treatment were, however, not different from the control (Table 2). We could attribute the additional toxic effect to reduced ALA levels (by 73%) but there are no threshold values available to verify this. To date it remains unclear which parameter could really have been limiting, but these data provide evidence that altered nutritional quality can impair reproduction in addition to a metal related effect of Ni itself.

5. Conclusion

The use of Ni-contaminated liposomes has unambiguously demonstrated that dietary Ni can be toxic to *D. magna*, without the potential interference of nutritional quality shifts. This study revealed that the alga *P. subcapitata* has to be exposed to at least 133 µg Ni²⁺/L if one wants to induce similar effects of Ni delivered by natural vectors. It can thus be concluded that there is little environmental relevance for dietary Ni toxicity in *D. magna*, since the presence of these concentrations is very rare, and also since the algal food may disappear from natural systems at these Ni concentrations. This study also showed that nutritional quality shifts, that co-occur with exposure of algae to Ni, do not significantly contribute to the reduction of daphnids' growth. In contrast, it seems that a Ni-induced reduction of the food quality causes an adverse effect on *D. magna* reproduction, in addition to Ni. Until now, however, it is unclear to which nutrient this deficiency could be related. These results can contribute to the scientific debate on if and how risk assessment of Ni should account for the effects of dietary metal exposure, and also question if metal-induced food quality shifts should be implemented in risk assessments.

Acknowledgements

Roel Evens is supported by a Ph.D. grant of the Institute for the promotion of Innovation through Science and Technology in Flanders (I.W.T. Vlaanderen). Lieve Balcaen is supported by a post-doctoral fellowship from the Flemish scientific research fund (FWO, Vlaanderen, Belgium). Additional funding was obtained from the Spanish Ministry of Science and Innovation (project CTQ2009-08606). We also would like to thank Marlies Bulckaert, Emmy Pequeur, Gisèle Bockstael and Geert Van De Wiele for technical assistance.

References

- Becker, C., Boersma, M., 2003. Resource quality effects on life histories of *Daphnia*. *Limnology and Oceanography* 48 (2), 700–706.
- Becker, C., Boersma, M., 2005. Differential effects of phosphorus and fatty acids on *Daphnia magna* growth and reproduction. *Limnology and Oceanography* 50 (1), 388–397.

- Bielmyer, G.K., Grosell, M., Brix, K.V., 2006. Toxicity of silver, zinc, copper, and nickel to the copepod *Acartia tonsa* exposed via phytoplankton diet. *Environmental Science and Technology* 40 (6), 2063–2068.
- Brett, M.T., Müller-Navarra, D.C., Ballantyne, A.P., Ravet, J.L., Goldman, C.R., 2006. *Daphnia* fatty acid composition reflects that of their diet. *Limnology and Oceanography* 51 (5), 2428–2437.
- Darchambeau, F., Thys, I., 2005. In situ filtration responses of *Daphnia galeata* to changes in food quality. *Journal of Plankton Research* 27 (3), 227–236.
- Deleebeeck, N.M.E., De Schampelaere, K.A.C., Janssen, C.R., 2008. A novel method for predicting chronic nickel bioavailability and toxicity to *Daphnia magna* in artificial and natural waters. *Environmental Toxicology and Chemistry* 27 (10), 2097–2107.
- De Schampelaere, K.A.C., Canli, M., Van Lierde, V., Forrez, I., Vanhaecke, F., Janssen, C.R., 2004. Reproductive toxicity of dietary Zn to *Daphnia magna*. *Aquatic Toxicology* 70, 233–244.
- De Schampelaere, K.A.C., Forrez, I., Dierckens, K., Sorgeloos, P., Janssen, C.R., 2007. Chronic toxicity of dietary copper to *Daphnia magna*. *Aquatic Toxicology* 81, 409–418.
- Elendt, B.P., Bias, W.R., 1990. Trace nutrient deficiency in *Daphnia magna* cultured in standard medium for toxicity testing: effects of the optimization of culture conditions on life history parameters of *D. magna*. *Water Research* 24, 1157–1167.
- Evens, R., De Schampelaere, K.A.C., Janssen, C.R., 2009. The effects of dietary nickel exposure on growth and reproduction of *Daphnia magna*. *Aquatic Toxicology* 94 (2), 138–144.
- Evens, R., De Schampelaere, K.A.C., Balcaen, L., Wang, Y., De Roy, K., Resano, M., del Rosario Flórez, M., Van der Meeren, P., Boon, N., Vanhaecke, F., Janssen, C., 2011. Liposomes as an alternative delivery system for investigating dietary metal toxicity to *Daphnia magna*. *Aquatic Toxicology* 105, 661–668.
- Evens, R., De Schampelaere, K.A.C., De Laender, F., Janssen, C. The effects of Zn-contaminated diets on *Daphnia magna* reproduction may be related to Zn-induced changes of the dietary P content rather than to the dietary Zn content itself. *Aquatic Toxicology*, doi:10.1016/j.aquatox.2011.11.018, in press.
- Faerovig, P.J., Hessen, D.O., 2003. Allocation strategies in crustacean stoichiometry: the potential role of phosphorus in the limitation of reproduction. *Freshwater Biology* 48 (10), 1782–1792.
- Geffard, O., Geffard, A., Chaumot, A., Vollat, B., Alvarez, C., Tusseau-Vuillemin, M., Garric, J., 2008. Effects of chronic dietary and waterborne cadmium exposures on the contamination level and reproduction of *Daphnia magna*. *Environmental Toxicology and Chemistry* 27 (5), 1128–1134.
- Organisation for Economic Co-operation and Development, 1998. OECD Guidelines for Testing of Chemicals. Guideline 211: *Daphnia magna* Reproduction Test. Publication Service OECD, Paris, France.
- Provasoli, L., McLaughlin, J.J.A., Droop, M.R., 1957. The development of artificial media for marine algae. *Archiv für Mikrobiologie* 25 (4), 392–428.
- Ravet, J.L., Brett, M.T., Müller-Navarra, D.C., 2003. A test of the role of polyunsaturated fatty acids in phytoplankton food quality for *Daphnia* using liposome supplementation. *Limnology and Oceanography* 48 (5), 1938–1947.
- Ravet, J.L., Brett, M.T., 2006. Phytoplankton essential fatty acid and phosphorus content constraints on *Daphnia* somatic growth and reproduction. *Limnology and Oceanography* 51 (5), 2438–2452.
- Risk assessment report on Ni-environmental part (2009). Scientific Committee on Health and Environmental Risks (SCHER) (adopted on 13.01.09).
- Siegel, S., Castellan, N.J., 1988. *Nonparametric Statistics for the Behavioral Sciences*. McGraw-Hill.
- Sunamoto, J., Shironita, M., Kawauchi, N., 1980. Liposomal membranes. V. Interaction of Zinc(II) ion with egg phosphatidylcholine liposomes. *Bulletin of the Chemical Society* 53, 2778–2781.
- Sundbom, M., Vrede, T., 1997. Effects of fatty acid and phosphorus content of food on the growth, survival and reproduction of *Daphnia*. *Freshwater Biology* 38, 665–674.
- Urabe, J., Sterner, R.W., 2001. Contrasting effects of different types of resource depletion on life-history traits in *Daphnia*. *Functional Ecology* 15 (2), 165–174.
- von Elert, E., 2004. Food quality constraints in *Daphnia*: interspecific differences in the response to the absence of a long chain polyunsaturated fatty acid in the food source. *Hydrobiologia* 526 (1), 187–196.
- Wacker, A., von Elert, E., 2001. Polyunsaturated fatty acids: evidence for non-substitutable biochemical resources in *Daphnia galeata*. *Ecology* 82 (9), 2507–2520.
- Wang, M., Wang, D., Wang, G., Huang, X., Hong, H., 2007. Influence of N, P additions on the transfer of nickel from phytoplankton to copepods. *Environmental Pollution* 148, 679–687.
- Weers, P.M.M., Gulati, R.D., 1997. Effect of the addition of polyunsaturated fatty acids to the diet on the growth and fecundity of *Daphnia galeata*. *Freshwater Biology* 38, 721–729.

Isotope ratio mapping by means of laser ablation-single collector-ICP-mass spectrometry: Zn tracer studies in thin sections of *Daphnia magna*

Cite this: *J. Anal. At. Spectrom.*, 2013, **28**, 1005

María R. Flórez,^{ac} Maite Aramendía,^{*bc} Martín Resano,^a Ana C. Lapeña,^a Lieve Balcaen^c and Frank Vanhaecke^c

In this paper, the possibilities of LA-single collector-ICP-mass spectrometry for obtaining isotope ratio images of thin sections of *Daphnia magna* specimens exposed to isotopically enriched Zn tracers were evaluated. Zn was selected considering its importance in ecotoxicological studies. All aspects of the analytical methodology deployed were carefully studied and optimized for obtaining the best isotope ratio precision and accuracy. The development of this methodological approach consisted of: (i) evaluation of the performance of two different medium mass resolution exit slits, a conventional one providing a mass resolution of $m/\Delta m \approx 4000$ and triangular shaped peaks, and another (wider) one, offering a lower mass resolution ($m/\Delta m \approx 2000$), but providing enhanced ion transmission and flat-topped peaks; (ii) the use of a wet plasma for improving plasma robustness; (iii) thorough optimization of the ablation conditions (such as laser spot size, repetition rate, scan speed and laser fluence) and data acquisition parameters (such as scan mode, the number of nuclides monitored, mass window, the number of samples per peak and dwell times); and (iv) adequate data treatment including the use of the moving average of 5 individual values. With the methodology developed, isotope ratio images with 30 micrometer spatial resolution scale were obtained for exposed and unexposed *Daphnia magna* individuals. The typical overall uncertainty of the measurements was approximately 5% RSD for the $^{66}\text{Zn}/^{64}\text{Zn}$ and $^{68}\text{Zn}/^{64}\text{Zn}$ ratios, which can be considered as satisfactory taking into account that the amount of Zn present per $30 \mu\text{m} \times 30 \mu\text{m}$ pixel only reached a few picograms in the most favourable cases (giving rise to 10 000–20 000 counts per s for ^{64}Zn). These results open the possibility for tracer studies with stable isotopes to be carried out using single collector instrumentation, a much more widespread analytical technique than multi-collector ICP-MS.

Received 14th March 2013
Accepted 1st May 2013

DOI: 10.1039/c3ja50087j

www.rsc.org/jaas

1 Introduction

During the last 10 years, laser ablation-inductively coupled plasma-mass spectrometry (LA-ICP-MS) has been increasingly used for elemental mapping. An advantage over other imaging techniques, such as micro-X-ray fluorescence or particle-induced X-ray emission,^{1–5} that has not been fully exploited yet, is the capability of LA-ICP-MS for providing isotopic information.⁶ There is an increasing amount of literature on both elemental mapping with high spatial resolution by means of LA-ICP-MS and isotopic analysis *via* ICP-MS, but in contrast, there are not many papers reporting on a combination of both features, *i.e.* mapping of isotope ratio data.⁷

The acquisition of isotope ratio images can be of great interest in a variety of disciplines, such as biochemistry, geology and ecotoxicology, because it provides information on the distribution of specific isotopes of a target element, permitting revelation of isotope fractionation processes that have occurred within a sample, or unravelling the uptake routes and/or body distribution of selected elements *via* tracer experiments with stable isotopes. For instance, in ecotoxicology, several studies have been carried out in which the uptake and bioaccumulation of metals in test organisms (particularly *Daphnia magna*) are investigated to evaluate toxic effects.^{8–13} In these studies, obtaining spatially resolved isotope ratio information for the test organisms could be of great interest for reaching a more profound insight into the uptake routes or the bio-processes involved in the assimilation of the elements under study and the corresponding kinetics.¹⁴

When isotope ratios need to be measured with very high precision, multi-collector (MC) ICP-MS instrumentation is preferred over single-collector (SC) units.¹⁵ However, MC-ICP-MS is much less widespread than SC instrumentation (a couple of hundred *vs.* many thousands of instruments) and, for some

^aDepartment of Analytical Chemistry, University of Zaragoza, Pedro Cerbuna, 12, E-50009, Zaragoza, Spain

^bCentro Universitario de la Defensa de Zaragoza, Carretera de Huesca s/n, E-50090, Zaragoza, Spain. E-mail: maiteam@unizar.es

^cDepartment of Analytical Chemistry, Ghent University, Krijgslaan 281 - S12, B-9000, Ghent, Belgium

applications, the use of SC-ICP-MS is preferred as a result of its better sensitivity and/or higher mass resolution. In the literature, several papers report on the efforts made to achieve the best conditions for measuring isotope ratios with a SC-ICP-MS instrument,¹⁶ also in combination with laser ablation as a means of sample introduction.^{6,17–21} Typically, the data acquisition parameters are selected such that a situation of quasi-simultaneous monitoring of the isotopes involved is obtained, leading to the best precision possible. Due to the amount of variables that have to be taken into account, some of them being interrelated, the initial optimization stage for isotope ratio determination with LA-SC-ICP-MS is far from being straightforward. This process turns out to be even thornier when the final goal is to present the isotope ratio data obtained as an image, as then the spatial resolution also needs to be considered, in combination with other parameters, such as total time of analysis or sensitivity achievable. This complex optimization process may well be the reason why not much work has been done in this particular line to date.

It is the main goal of this paper to try to fill this methodological gap and offer a starting point for the development of tracer experiments with stable isotopes, complemented with isotope ratio images as a more comprehensive data presentation. LA-SC-ICP-MS was optimized and used in the present study for acquiring Zn isotope ratio images for thin sections of *Daphnia magna* individuals, which had been exposed to an increased concentration of dissolved Zn, with an isotopic composition that was varied from natural to strongly enriched in ⁶⁴Zn and ⁶⁷Zn. *Daphnia magna* are small (0.2–5 mm long) planktonic crustaceans that belong to the *Cladocera* suborder. Their high sensitivity to the chemical composition of the freshwater media they inhabit, along with the ease with which they can be cultured in a laboratory, their short lifetime period and their parthenogenetic reproduction place these animals among the most commonly used test organisms for bioassays and eco-toxicological studies.¹¹ Zn was selected as the target element because it is an essential trace element for living organisms due to its role as a cofactor in several types of enzymes and regulatory proteins. However, when present in concentrations above a fixed quality level, it may exert toxicity and put the ecosystem at risk.^{10,14,22}

Moreover, from an analytical point of view, the work developed regarding the measurement of Zn isotope ratios by means of LA-ICP-MS in such small and thin sample surfaces brings about an intrinsic challenge due to the very low counting rates expected to be measured and the presence of significant spectral interference due to the occurrence of polyatomic ions. In this context, the suitability of a new entrance/exit slit combination available for the Thermo Element XR ICP-MS instrument deployed in this study, capable of providing flat-topped spectral peaks when operating at higher mass resolution ($m/\Delta m \approx 2000$)²³ was also explored, and results are presented in the manuscript.

2 Experimental

2.1 Instrumentation

A New Wave Research 193 nm wavelength ArF* excimer-based laser ablation system (UP193HE, New Wave Research, CA, USA)

coupled to a sector field-based ICP-MS instrument (ELEMENT XR, Thermo Scientific, Bremen, Germany) was used. The LA unit is equipped with an ablation cell mounted on a tri-translational stage. A teardrop-shaped ablation cell,²⁴ built by Axel Gerdes at the University of Frankfurt based on the work of Bleiner and Günther,²⁵ was used throughout the work. This cell has an internal volume of *circa* 2.5 cm³, which, compared with the standard cell (30 cm³ volume), reduces the washout time significantly, allowing improved time-resolved elemental and isotopic information²⁶ and, therefore, better spatial resolution.

A quartz dual pass cyclonic spray chamber with two inlet ports (Elemental Scientific Inc., Omaha, NE, USA) was included in the set-up for simultaneous nebulization of a solution with the ablated aerosol (“wet plasma” mode). The aerosols coming from the spray chamber and the laser ablation cell were mixed in a Y-piece connection. The benefits of this setup are discussed in Section 3.2.

A new slit system provided by Thermo Fisher Scientific (Bremen, Germany) for the ELEMENT XR, which generates flat-topped peaks at a mass resolution of $m/\Delta m \approx 2000$ (20% ion transmission of that observed at low resolution -LR- mode),²³ was used. These mass spectral characteristics are realized *via* a wider exit slit than the conventional medium resolution slit (offering a resolution of $m/\Delta m \approx 4000$ at 10% ion transmission of that at LR mode), which generates triangular shaped peaks.

2.2 Reagents and standards

The NIST glass standard reference material SRM 612 (National Institute of Standards and Technology, MD, USA) was used for optimizing the instrument settings with the aim of maximizing the Zn signal intensity at the beginning of every LA-ICP-MS measurement session.

All elemental standard solutions used throughout the study were prepared from mono-element standard solutions purchased from Inorganic Ventures (The Netherlands). Corresponding dilutions were made using ultrapure water (obtained using a Milli-Q Direct Q-3 purification system, Millipore, USA) and 14 mol L⁻¹ HNO₃ (Chem-Lab, Belgium), further purified by sub-boiling distillation. All these operations were performed in a class-10 clean lab, for minimizing Zn contamination to the largest possible extent.

“Wet plasma” conditions were achieved by mixing the aerosols originating from, respectively, the LA unit and the nebulisation of a 5 μg L⁻¹ Cu solution prepared by diluting a 1 g L⁻¹ solution of the NIST SRM976 Cu isotopic reference material with 0.14 mol L⁻¹ HNO₃. The admixed Cu was relied on for mass bias correction (see Section 2.4 for further details).

For checking the behaviour of spectral interferences (Section 3.1), aqueous solutions of 10 mg L⁻¹ of Ca, P and S (matrix elements) were prepared *via* dilution of mono-element standard solutions of 1 g L⁻¹. Cl-based interfering species were checked *via* measuring a 0.12 mol L⁻¹ HCl solution (Chem-Lab, Belgium), prepared from ultrapure 12 mol L⁻¹ HCl, purified by sub-boiling distillation.

All salts and reagents used for preparation of the *D. magna* culture media, dehydration and cleaning were of pro-analysis

Paper

grade and were purchased from Merck (Germany), while the isotopically enriched Zn standards used in the tracer experiment were purchased from Isoflex (USA) as ZnO (stable ^{64}Zn (99.30%) and stable ^{67}Zn (89.60%)). Stock solutions of these enriched isotopes were prepared by dissolving the oxide in 5 mol L^{-1} HCl and diluting the solution with Milli-Q water to obtain a final Zn concentration of 100 mg L^{-1} . Paraffin used for embedding the samples prior to microtoming was obtained from Richard-Allan Scientific (Paraffin Type 9 for infiltration or embedding), Thermo Fisher Scientific (Germany).

2.3 Sample preparation

Several *D. magna* specimens from a monoclonal in-house laboratory population were cultured under normal conditions of diet and water medium.²⁷ Freshwater medium was prepared by adding MgSO_4 , NaHCO_3 , KCl and CaSO_4 to deionized water; the water was kept at a hardness level of $160\text{--}180 \text{ mg L}^{-1} \text{ CaCO}_3$ and a pH between 7 and 8. The temperature was maintained at approximately 23°C , with O_2 aeration and photoperiods of 16 hours of light, followed by 8 hours of darkness. The individuals were fed with lyophilized algae every 2 days. 21 days old offspring individuals of the population were collected and exposed for 24 hours to a water medium fortified with a Zn spike, isotopically enriched in ^{64}Zn and ^{67}Zn (total Zn concentration of 1 mg L^{-1}) and with a culture density of one specimen per 5 mL. The exact isotopic composition of the Zn spike was determined,¹⁵ obtaining relative abundance values of ^{64}Zn (50.52%), ^{66}Zn (2.12%), ^{67}Zn (44.79%), ^{68}Zn (2.52%) and ^{70}Zn (0.05%). These exposures were carried out in separate vessels with no further feeding or aeration. After 24 hours, the *daphnias* were rinsed with a $1 \mu\text{mol L}^{-1}$ EDTA solution (obtained by dissolving an appropriate amount of the corresponding disodium salt), followed by rinsing with deionized water. Afterwards, they were dehydrated with acetone–water mixtures with an increasing acetone fraction and immersed in toluene immediately prior to be embedded in paraffin for subsequent cutting. $20 \mu\text{m}$ thickness sagittal sections of each *D. magna* specimen were cut using a rotary microtome (Slee CUT 4060, Mainz, Germany) and adhered to glass supports for their ablation.

2.4 Experimental setup and instrumental conditions for the acquisition of images

Before starting the LA measurements, determination of the Element XR detector dead time was carried out using the standard pneumatic nebulization sample introduction system, by monitoring the $^{235}\text{U}/^{238}\text{U}$ isotope ratio for solutions of increasing concentration. A value of 14.5 ns, providing constant $^{235}\text{U}/^{238}\text{U}$ ratios, was finally selected.²⁸

Data acquisition for images was carried out under “wet plasma” conditions. For this purpose, a $5 \mu\text{g L}^{-1}$ Cu isotopic standard solution (NIST SRM 976) was nebulized simultaneously with the ablation of the samples, so that the Cu ratio monitored could be used at a later stage as an internal standard for mass bias correction.

Every measurement session was preceded by appropriate tuning of the LA-ICP-MS settings while ablating rasters from

the surface of NIST SRM 612 glass and simultaneously nebulizing a 0.14 mol L^{-1} HNO_3 solution. Particular attention was paid to the RF power and the carrier gas flow rate (He through the LA cell mixed with Ar before the plasma), so as to obtain high sensitivity, good peak shape and a stable U/Th ratio (~ 1), while minimizing the formation of oxides and doubly charged ions.²⁹

For the ablation of the *D. magna* sections, a laser spot size of $30 \mu\text{m}$, a repetition rate of 10 Hz and a scan speed of $60 \mu\text{m s}^{-1}$ were selected. The energy fluence was adjusted to a value between 1.8 and 2.1 J cm^{-2} .

Mass spectrometer settings providing the best precision while avoiding spectral overlap (see Section 3.2) consisted of (i) the use of the modified medium resolution slit system, (ii) measurement in pure E-Scan mode at a fixed magnet mass of 62.929 u, (iii) measurement in a window covering the central 10% of each peak³⁰ and programming 50 samples per peak (thus actually monitoring the signal intensity at 5 points per nuclide) and (iv) selecting a dwell time of 3 ms combined with the minimum settling time allowed by the instrument software for E-Scan mode (1 ms). This resulted in a total dwell time per nuclide of 15 ms. With these settings, 5 data points per nuclide were obtained every approx. 500 ms. The moving average of 5 points was used as the representative value, as discussed in Section 3.4.

The process of ablation and raw data acquisition was automated. Every *D. magna* section was completely ablated with approximately 50 scan lines of about 50 s duration each. Taking into account that every line is preceded by 10 s of laser warm up (ablation with the shutter closed) and followed by 70 s for enabling data handling by the ICP-MS software, data acquisition for each image takes an average time of 2 hours. All measurement conditions and parameters deployed are summarized in Table 1.

2.5 Data handling for obtaining isotope ratio images

For subsequent transformation of the measurement data into the corresponding isotope ratio images, it is first necessary to consider two aspects that will affect precision and accuracy of the results: the appearance of spiky signals and the occurrence of instrumental mass discrimination.

Although the use of wet plasma conditions reduced the occurrence of spiky signals significantly, it was necessary to correct for some remaining spikes (0.5% of the acquired points or less). Rejection of spikes is important in this context, as they usually affect only one of the Zn isotopes measured and hence, result in a significant bias for the isotope ratio recorded. Identification and rejection of spikes was done manually, by checking the raw intensity signals and spotting and rejecting signals (normally one or two isolated points affecting only one of the Zn isotopes) exceeding the level of the 10 adjacent points on each side of the point by more than 3 times the standard deviation. For every measurement, the signal for the first 10 seconds during which the laser is warming up (ablation with the shutter closed) was considered as a gas blank signal and was subtracted from the signal intensity for every data point before

Table 1 Instrument settings and data acquisition parameters

LA unit parameters: New Wave Research UP193HE	
Wavelength	193 nm
Cell volume	≈ 2.5 cm ³
Spot size	30 μm
Repetition rate	10 Hz
Scanning speed	60 μm s ⁻¹
Energy density	1.8–2.1 J cm ⁻²
Laser warm-up time	10 s
ICP-MS instrumental parameters: Thermo Element XR	
Mass resolution, <i>m/Δm</i>	2000
RF power	1120 W
Auxiliary gas flow rate (Ar)	0.70 L min ⁻¹
Nebulizer gas flow rate (Ar)	0.75 L min ⁻¹
Carrier (He) gas flow rate through cell	0.60 L min ⁻¹
Data acquisition parameters	
Scanning mode	E-Scan
Settling time	1 ms
Samples per peak	50
Mass window	10%
Sample time	3 ms
Segment duration (total dwell time per nuclide)	15 ms
Runs/passes	600/1
Nuclides monitored	⁶³ Cu ⁺ , ⁶⁴ Zn ⁺ , ⁶⁵ Cu ⁺ , ⁶⁶ Zn ⁺ , ⁶⁷ Zn ⁺ , ⁶⁸ Zn ⁺

further treatment. Wherever the net Zn signal laid beneath the blank value plus 3 times the standard deviation recorded for the gas blank, the Zn concentration was considered too low for providing reliable isotope ratios. Consequently, and with the purpose of improving readability of the final isotope ratio images, these intensity values were disregarded and were represented in black in the final isotope ratio image. Subsequently, the blank-corrected signal intensities were ratioed for obtaining the four different target isotope ratios that were expected to show the maximum variation with respect to the natural values: ⁶⁶Zn/⁶⁴Zn, ⁶⁸Zn/⁶⁴Zn, ⁶⁶Zn/⁶⁷Zn and ⁶⁸Zn/⁶⁷Zn. For each of these isotope ratios, the instrumental mass discrimination was corrected for point-by-point, using Cu as the internal standard. To do so, the signals monitored for the 5 μg L⁻¹ isotopic Cu standard solution (NIST SRM 976), simultaneously nebulized with the ablation during the whole image acquisition session and thus obviously acquired with the same instrumental parameters, were used. The empirical mass bias correction strategy proposed by Longerich *et al.*³¹ and improved by Maréchal *et al.*³² and Woodhead³³ was used for these calculations. For estimating the K-factor, which relates a measured isotope ratio to its true value, the exponential model of Russell *et al.*³⁴ was chosen.

Next, all of the lines monitored for a single *D. magna* (approx. 50 per *Daphnia*) were combined to form a single image. The images had to be manually scaled according to the real dimensions of the sample. To this aim, additional image-

treatment software was deployed (Aabel 3 20/20 data vision, Gigawiz). Once the images were built, the different regions of interest (*i.e.* eye, egg, gills and gastrointestinal tract) could be visually identified and the average isotope ratios for these regions were calculated.

3 Results and discussion

3.1 ICP-MS measurement of Zn isotopes. Overcoming spectral overlap

Zn has five stable isotopes, with the following natural relative abundances ⁶⁴Zn (49.17%), ⁶⁶Zn (27.73%), ⁶⁷Zn (4.04%), ⁶⁸Zn (18.45%) and ⁷⁰Zn (0.61%),³⁵ all of them with atomic masses below 80 u, the region of the mass spectrum where most spectral interferences due to the occurrence of polyatomic ions occur. For the application considered in this work, problematic elements found at high concentrations within the body of the *D. magna* are P and Ca (particularly conforming the exoskeleton of the crustaceans), and S and Cl (which are essential elements for all living organisms). Ni, on the other hand, with a minor isotope at *m/z* 64 (⁶⁴Ni, 0.93%), is expected to be below 2 μg g⁻¹ in *D. magna* specimens,^{10,11} and is thus not really problematic. Taking this into account, a summary of potential spectral interferences affecting Zn isotopes when measuring *D. magna* specimens is included in Table 2, with the most relevant ones highlighted in bold.

Self-evidently, these interferences need to be avoided if accurate isotope ratios are to be obtained. This can be accomplished by using a SF-ICP-MS instrument operating at medium mass resolution mode (*m/Δm* ≈ 4000).^{37,38} Unfortunately, the use of this increased mass resolution also entails a significant drop in sensitivity, while the mass spectral peaks are no longer flat-topped, but become triangular-shaped instead. Both facts are detrimental for highly precise isotope ratio measurements.⁶ To cope with these three issues (mass resolution, sensitivity and peak shape) in a more efficient way, a new medium resolution

Table 2 Potential S-, P-, Cl- and Ca-based polyatomic spectral interferences that may hinder the determination of Zn in *Daphnia magna* specimens^a

Isotope	Relative isotopic abundance (%) ³⁵	Potential spectral interferences ³⁶
⁶⁴ Zn	49.17	³²S³²S⁺ , ³²S¹⁶O¹⁶O⁺ , ⁴⁸Ca¹⁶O⁺ , ³³S³¹P⁺ , ³¹P¹⁶O²H⁺ , ³¹P¹⁶O¹⁷O⁺ , ³⁴S¹⁶O²+
⁶⁶ Zn	27.73	³²S³⁴S⁺ , ³³S³²S⁺ , ³⁵Cl³¹P⁺ , ³⁴S¹⁶O²+ , ³³S¹⁶O²H⁺ , ³²S¹⁶O¹⁸O⁺ , ³²S¹⁷O²+ , ³³S¹⁶O¹⁷O⁺
⁶⁷ Zn	4.04	³⁵Cl¹⁶O¹⁶O⁺ , ³²S³⁵Cl⁺ , ³³S³⁴S⁺ , ³¹P³⁶Ar⁺ , ³⁴S¹⁶O²H⁺ , ³²S¹⁶O¹⁸O¹H⁺ , ³⁴S¹⁶O¹⁷O⁺ , ³³S¹⁶O¹⁸O⁺ , ³²S¹⁷O¹⁸O⁺ , ³³S¹⁷O²+
⁶⁸ Zn	18.45	³⁵Cl¹⁶O²H⁺ , ³⁴S³⁴S⁺ , ³⁶Ar³²S⁺ , ³⁶S¹⁶O²+ , ³⁴S¹⁶O¹⁸O⁺ , ³⁵Cl¹⁶O¹⁷O⁺ , ³⁴S¹⁷O²+ , ³³S¹⁷O¹⁸O⁺ , ³²S¹⁸O²+ , ³²S³⁶S⁺
⁷⁰ Zn	0.61	³⁵Cl³⁵Cl⁺ , ³⁵Cl¹⁷O¹⁸O⁺ , ³⁷Cl¹⁶O¹⁷O⁺ , ³⁴S¹⁸O²+ , ³⁶S¹⁶O¹⁸O⁺ , ³⁶S¹⁷O²+ , ³⁴S³⁶S⁺ , ³⁶Ar³⁴S⁺ , ³⁸Ar³²S⁺

^a Most significant interferences for this particular application are highlighted in bold.

Paper

slit system was tested. This slit system uses the same entrance slit as deployed for the conventional medium resolution system, but a wider exit slit (wider than the entrance slit). In this way, flat-topped mass peaks are obtained. This change in the shape of mass spectral peaks, however, comes at the expense of a 50% decrease in the mass resolution ($m/\Delta m \approx 2000$) compared to the conventional medium resolution system, but should also provide better sensitivity due to an enhanced ion transmission efficiency.

To further test this possibility, optimization of the actual mass interval measured for each nuclide was carried out in a first stage by nebulizing different Zn standard solutions, containing about $3 \mu\text{g L}^{-1}$ Zn and high concentrations of each of the matrix elements at the origin of polyatomic species included in Table 2 (10 mg L^{-1} for Ca, S, P and 4.25 g L^{-1} for Cl). Only S- and Cl-based species produced a significant signal in the proximity of the signals for ^{64}Zn and ^{68}Zn , respectively. This is illustrated in Fig. 1, which displays mass spectra in the regions of interest obtained in medium resolution with the conventional and with the new (wider) exit slit. As anticipated, the analytical and the interfering peaks are not totally baseline-resolved with the new medium resolution slit ($m/\Delta m \approx 2000$ only), although there is a sufficiently wide plateau (of approx. 30% of the whole peak) in the centre of the peak where the analyte signal can be measured interference-free. On the other hand, the sensitivity obtained is about two times higher than

that obtained with the conventional medium resolution slit. Considering all of the above, it seems clear that the use of the alternative (wider) medium resolution slit should be the best option for our application, providing sufficient mass resolution and enhancing sensitivity, as long as the right portion of the peak is monitored. In any case, further tests using LA for sample introduction (described in Section 3.3) were carried out for quantifying the actual extent of this potential benefit.

3.2 Selection of the conditions for ablation

Before performing further optimization of the ICP-MS acquisition parameters, adequate conditions for ablation of the *D. magna* thin sections had to be selected. In this regard, the most important laser parameters that need to be considered when aiming at generating images are the laser spot size and repetition rate, scan speed (translation rate) and laser fluence. In most cases and also for this application, images are acquired as a sequence of contiguous lines that are afterwards composed offline using adequate software. Data acquisition along these lines is normally carried out in an automated way, by triggering the ICP-MS instrument at the beginning of every ablated line. For ensuring optimum results, the waiting time between the ablation of consecutive lines has to be carefully optimized for keeping the total acquisition time at minimum values while ensuring the absence of memory effects, as well as allowing

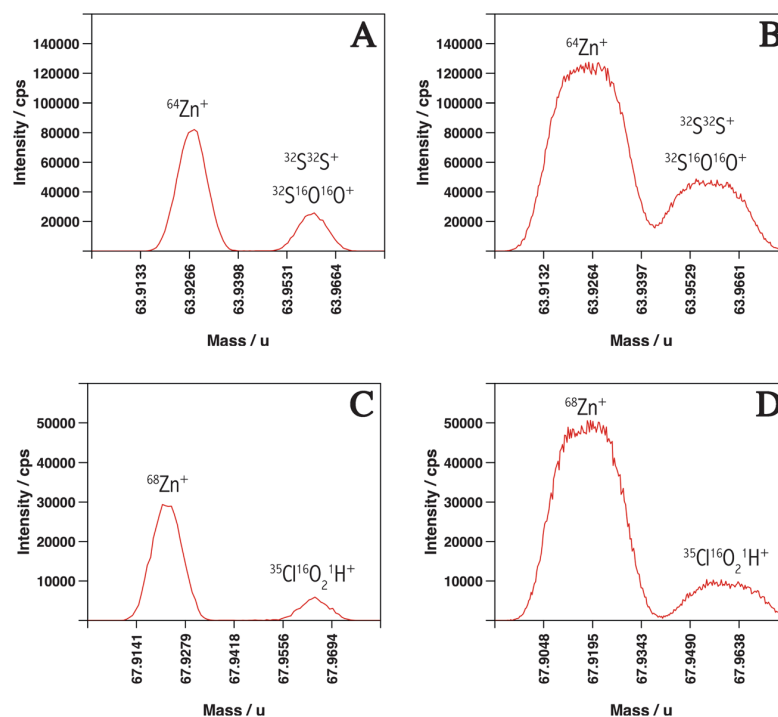


Fig. 1 Mass spectra in the vicinity of ^{64}Zn and ^{68}Zn when simultaneously nebulizing high concentrations of Cl and S, using different mass resolution slit systems. (A) Mass spectrum in the vicinity of ^{64}Zn for a solution containing $3 \mu\text{g L}^{-1}$ Zn and 10 mg L^{-1} S using a conventional medium resolution slit system ($m/\Delta m \approx 4000$). (B) Mass spectrum in the vicinity of ^{64}Zn for a solution containing $3 \mu\text{g L}^{-1}$ Zn and 10 mg L^{-1} S using a new medium-resolution slit system (flat-topped peaks, $m/\Delta m \approx 2000$). (C) Mass spectrum in the vicinity of ^{68}Zn for a solution containing $3 \mu\text{g L}^{-1}$ Zn and 4.25 g L^{-1} Cl using a conventional medium resolution slit system ($m/\Delta m \approx 4000$). (D) Mass spectrum in the vicinity of ^{68}Zn for a solution containing $3 \mu\text{g L}^{-1}$ Zn and 4.25 g L^{-1} Cl using a new medium-resolution slit system (flat-topped peaks, $m/\Delta m \approx 2000$).

enough time for the ICP-MS instrument to handle the data generated while ablating the sample according to a line.

Choosing the best combination of these parameters is not straightforward, as all of them are interrelated and images take too long to be acquired for conventional mono-variant optimization experiments to be carried out. First, the spot size of the laser beam is closely related to the spatial resolution and the sensitivity. The smaller the spot size is, the higher the spatial resolution would be, but at the expense of decreasing the signal intensity. Sensitivity issues are especially important for this particular application, as we were forced to work under medium resolution mode; thin sections were only 20 μm thick (an adequate compromise between sensitivity and spatial resolution), and Zn concentration in the samples was expected to be low. In fact, experiments carried out using solid sampling high-resolution continuum source graphite furnace atomic absorption spectrometry⁸ permitted us to calculate the total amount of zinc present in *D. magna* specimens, which varied between 25 and 50 ng. That translates into 0.5 to 1.0 ng of Zn for a whole 20 μm section.

The achievable sensitivity was therefore studied by varying the spot size and repetition rate while ablating one of the *D. magna* sections at locations where, according to previous investigations,⁹ most Zn was supposed to be accumulated.

On the other hand, the scan speed needs to be adjusted in order to minimize the sample acquisition time without considerably sacrificing the signal intensity and spatial resolution.³⁹ Increasing the scan rate results in a shorter ablation time at each point and therefore the sensitivity per pixel is negatively affected. This can be counteracted to some extent by adjusting the laser energy and increasing repetition rate.

Taking all these parameters and their correlations into account, the set of conditions finally chosen consisted of: (i) a laser spot size of 30 μm , for ensuring adequate resolution considering the small dimensions of the sample type studied, while maintaining a sufficiently high signal intensity; (ii) 10 Hz repetition rate at a laser fluence of 1.8–2.1 J cm^2 , for ablating the total thickness of the sample on a single pass without inflicting any significant damage to the glass support, and (iii) a scan (translation) speed of 60 $\mu\text{m s}^{-1}$ for maintaining the total acquisition time at reasonable levels.³⁹ Under these conditions, the maximum count rate for ⁶⁴Zn was ~10 000–20 000 cps for exposed specimens, while the background level signal was reached in approximately 1 second from the maximum signal intensity, minimizing image blurring. The waiting time between lines was finally set at 70 s to allow the ICP-MS instrument enough time for handling the data generated. With these acquisition parameters, the total acquisition time for gathering the data to plot an image of each *D. magna* section varied between 2 hours and 2 and a half hours.

3.3 Optimization of the ICP-MS acquisition parameters and comparison of the different mass resolution slit systems

When it comes to carrying out isotope ratio measurements by means of SC-ICP-MS, attention must be paid to several aspects of the acquisition method in order to improve the uncertainty

attainable. When LA is used as the sample introduction system, additional sources of uncertainty are introduced due to the noisy nature of the signal. Moreover, when the purpose is to obtain a 2D image of the distribution of isotope ratios on the surface of a sample, *i.e.*, when the best uncertainty is needed for *each pixel* of the image, selection of the operating conditions that provide the best possible results is of course even more important as well as challenging. An insight into the factors affecting uncertainty when measuring isotope ratios by means of SC-LA-ICP-MS is given in ref. 6, where different hints and approaches to be kept in mind when developing a method for the determination of isotope ratios in bulk materials are provided. From that work, three main factors to be taken into account for the development of our particular method can be identified: (i) maximization of sensitivity and selection of detector mode; (ii) reduction of the occurrence of spiky signals through the use of more robust plasma conditions (*e.g.*, wet plasma conditions) and (iii) achievement of quasi-simultaneous measurement conditions for suppressing potential noise sources to the largest possible extent so as to improve measurement precision.

Concerning point (i), as previously mentioned, the use of the new medium resolution slit system with enhanced sensitivity should bring an advantage. In any case, and considering that the images were mapped for 20 μm thickness sections of the *D. magna* individuals, in which Zn is unevenly distributed and very low signals are expected for most pixels, this sensitivity enhancement was not enough to warrant the use of the analog detection mode, thus the counting detection mode was used.

As for point (ii), it has been described in the literature that wet plasmas are more robust towards matrix effects^{6,40} and the occurrence of spiky signals (probably resulting from the introduction of larger particles into the plasma) is considerably reduced for many sample types. For this particular application, admixture of a nebulized solution to the ablated material brings an additional advantage, as it will be possible to introduce an isotopic reference material for mass bias correction purposes. The only significant question that needs to be considered when applying this strategy for the acquisition of images is the experimental set-up deployed, which should avoid signal expansion and mixing of the material ablated at slightly different locations.

In fact, washout time is the most influential parameter affecting image resolution, and this is the reason why the tear-drop ablation cell, with a volume of 2.5 cm^3 vs. the 30 cm^3 of a standard cell, was deployed in this work.^{24–26} Avoiding signal expansion is of great importance. With this in mind, different experimental setups for admixing a nebulized aerosol were considered. The setup proposed in ref. 6 (mixing of the LA-generated dry aerosol and the nebulized aerosol *inside* a spray chamber) was disregarded, as it brings about a signal expansion by several seconds. Instead, the experimental setup chosen was adapted from ref. 40. In this system, the Ar flow carrying the liquid aerosol coming from the dual-pass spray chamber, equipped with a 20 $\mu\text{L min}^{-1}$ microflow nebulizer, encounters the He flow carrying the dry ablated aerosol coming from the LA chamber in a Y-shaped joint, where both gas streams merge and

Paper

flow through the third port of the connection towards the plasma torch.

The benefits observed when using this experimental set-up are illustrated in Fig. 2, where a comparison between the signals generated in “dry mode” and “wet mode” (through continuous nebulization of a 0.14 M HNO₃ solution) for the ablation of the NIST SRM 612 glass with the same acquisition parameters is shown. It can be seen that, even though a moderate loss in sensitivity is observed when working under “wet plasma” conditions, the signal appears to be substantially more stable under these conditions (the RSD for the ⁶⁴Zn signal is 9.5% in wet mode and 20.2% in dry mode), while spiky signals are mostly absent. It also can be seen clearly in the figure that shifting to “wet mode” is not accompanied by significant stretching of the washout: after ablation stops, both signals decay to the background level after about 3.5 s. As a result of this, further experiments were carried out under these “wet plasma” conditions. In the final experiments, a 5 μg L⁻¹ solution of the Cu NIST SRM 976 standard reference material in 0.14 M HNO₃, generating a ⁶³Cu⁺ signal of about 20 000 cps, was used for the study.

Finally, and regarding point (iii), optimization of the mass spectrometer acquisition parameters also has to be considered for improving the precision of the measurements by trying to approach as much as possible the simultaneous detection of the measured isotopes. In this regard, aspects such as the number of nuclides monitored, settling time and total dwell time have to be studied. In general terms, the number of nuclides monitored as well as the settling time between nuclides have to be kept to a minimum.⁶ For this purpose, and when using a sequential sector field instrument, it is important to avoid changing the magnet mass for minimizing the settling time needed for obtaining accurate measurements. In such a context, selection of an adequate internal standard for mass bias correction so that all nuclides can be scanned by changing the accelerating voltage only (*i.e.*, staying at a fixed magnet mass, E-Scan mode) becomes crucial. In this particular case, selection of Cu as the internal standard permitted us to work at a fixed magnet mass of 62.929 u, and ⁶³Cu, ⁶⁴Zn, ⁶⁵Cu, ⁶⁶Zn, ⁶⁷Zn and ⁶⁸Zn were sequentially monitored by using pure E-Scanning. Under these working conditions, settling times could be set at 1 ms in all cases, the minimum allowed by the instrument software.

Optimization of the time spent at each of the nuclides monitored was considered next and a comparison of the two available mass resolution slit systems in terms of measurement precision was also performed. When working in the conventional medium-mass resolution mode, as triangular peaks are obtained, it is important to ensure that measurements are carried out at the peak maximum. This requirement is not so stringent in the case of the new medium mass resolution slit system, as a wide plateau at maximum sensitivity is available. Taking this into account, a mass window of 10% was chosen for both resolution slits. The number of samples per peak, on the other hand, was set to 50, so that 5 samples covering the central 10% of the nominal peak width were actually monitored per nuclide. From this situation, the time spent at each sample had to be chosen for obtaining the best measurement precision.

For deciding which setting provides the best point-by-point RSD% values, ablation of a homogeneous sample, thus eliminating potential variations due to sample heterogeneity, was carried out. NIST SRM 612 glass, which is considered to be rather homogeneous for Zn at the μm level,⁴¹ was selected for that purpose. The NIST SRM 612 glass was ablated with a set of laser parameters providing Zn signal intensities not far from those obtained for the *D. magna* thin sections (⁶⁴Zn 10 000–20 000 cps): 200 μm spot size, 20 Hz repetition rate, 10 μm s⁻¹ scan speed and 10 J cm⁻² fluence. The influence of segment duration on the %RSD was then studied with both resolution slit systems by varying the sample time from 1 ms (5 ms total dwell time per nuclide) to 16 ms (83 ms total dwell time per nuclide) and averaging the corresponding data points in order to have a single value for each target nuclide every approximately 500 ms (since the laser scan advances 30 μm in that period of time, thus allowing us to obtain a 30 × 30 μm resolution). Results obtained are summarized in Fig. 3. As expected, the slit system providing flat-topped peaks leads to somewhat improved isotope ratio precisions for all conditions tested, particularly for unfavourable (very different from unity) isotope ratios, probably due to the higher sensitivity provided and the improved robustness with respect to small mass calibration instabilities. As for the mass spectrometer parameters, it seems that the best measurement precision values are provided between 15 ms and 30 ms acquisition time for every isotope

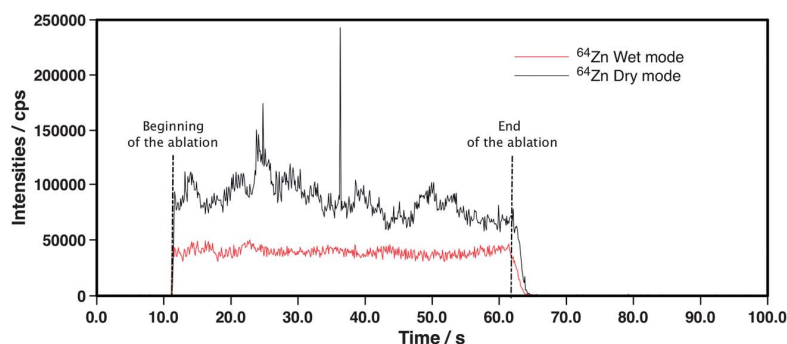


Fig. 2 Comparison between the ⁶⁴Zn signals obtained upon ablation of NIST SRM 612 glass (400 μm, 20 Hz, 10 μm s⁻¹, 10 J cm⁻²) measured under both dry and wet (through nebulization of a 0.14 M HNO₃ solution) plasma conditions.

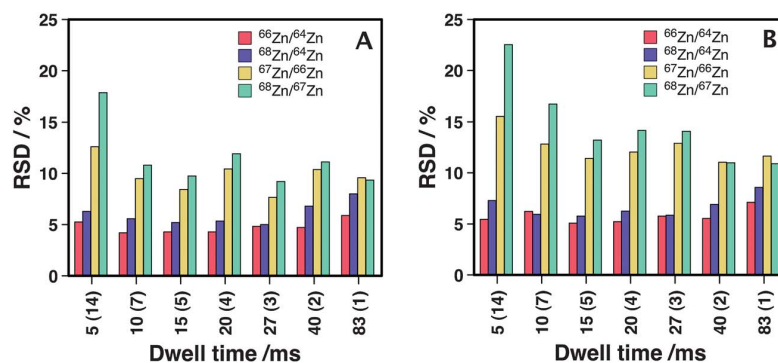


Fig. 3 Measurement precision (%RSD) for Zn isotope ratios as a function of the total dwell time selected per nuclide. (A) Results for a new medium-resolution slit system (flat-topped peaks, $m/\Delta m \approx 2000$). (B) Results for a conventional medium-resolution slit system (triangular peaks, $m/\Delta m \approx 4000$). Signals were obtained for the ablation of NIST SRM 612 glass (200 μm , 20 Hz, 10 $\mu\text{m s}^{-1}$, 10 J cm^{-2}) under wet plasma conditions. The number between brackets next to each dwell time value indicates the number of points averaged for obtaining a single isotope ratio value every 500 ms. Natural values for the isotope ratios shown in the charts: $^{66}\text{Zn}/^{64}\text{Zn} = 0.564$, $^{68}\text{Zn}/^{64}\text{Zn} = 0.375$, $^{67}\text{Zn}/^{66}\text{Zn} = 0.146$, $^{68}\text{Zn}/^{67}\text{Zn} = 4.567$.

ratio tested. As seen from Fig. 3, selection of these working conditions can ensure RSD values in the range of 4–5% for isotope ratios closer to unity, while values around 10% are obtained for the rest. The precision attained is in accordance with results reported in the literature for Zn isotope ratio determination by means of LA-single collector ICP-MS⁴² and could suffice for performing tracer studies like the one attempted in this project. As a consequence, further experiments with the *D. magna* thin sections were carried out. For this purpose and based on the abovementioned results, the flat-topped MR slit with 15 ms total dwell time per nuclide (thus requiring the averaging of 5 points) was selected for acquisition of the images.

3.4 Acquisition of isotope ratio images for *D. magna* thin sections. Validation and interpretation of the results

Once all the experimental parameters had been optimized, acquisition of images for the *D. magna* thin sections was carried out, following the experimental procedures described in Sections 2.4 and 2.5 for ablation of the samples and data handling, respectively. At this point, it may be necessary to make a statement concerning the resolution attained with the conditions selected and the best way to process the data.

The scan speed (60 $\mu\text{m s}^{-1}$) and repetition rate (10 Hz) used mean that the ablation line advances at a pace of 6 μm per shot (0.1 s). On the other hand, with the optimum data acquisition parameters discussed before, a signal intensity value for every nuclide monitored is actually obtained for every laser shot (5 points per nuclide every 0.5 s, so 1 point every 0.1 s). As seen from these data, for this particular application, there is a perfect matching between sampling and acquisition speed for optimum %RSD values. Although, in principle, acquiring data faster than the ablation rate might lead to improved %RSD for other applications, the spatial resolution, ultimately limited by the ablation speed, would not improve by selecting such settings. Acquiring data more slowly, on the other hand, always results in a loss of spatial resolution.

Thus, data for presenting 30 μm (spot size, x axis) \times 6 μm (y axis) are actually attained with our method. However, that does not mean that the true resolution is 30 \times 6 μm , because every new laser shot samples 6 μm of new material, but only together with 24 μm of material from an area ablated before (since 5 laser shots are actually needed for sampling the

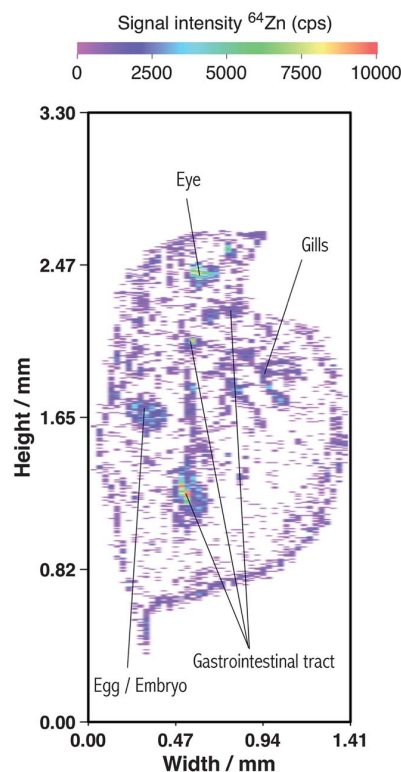


Fig. 4 Image showing the distribution of ^{64}Zn over a 20 μm thick section of a *D. magna* individual exposed to a ^{64}Zn -enriched water medium, obtained following the experimental protocol described in Sections 2.4 and 2.5.

complete layer). Thus, we considered that the best way to process the data is to use the moving average of 5 data points, because in this way the ablation procedure is perfectly mimicked, as every data value represented is affected by the four previous ones. Thus this approach was used.

Fig. 4 shows the distribution of ^{64}Zn in a 20 μm thick section of a *D. magna* specimen exposed to a ^{64}Zn -enriched medium (see Section 2.3 for details). This image clearly allows the body regions where the Zn preferably bio-accumulates to be identified, with four clearly distinguishable areas: the eye, the gastrointestinal tract, the gills and the egg/embryo. The carapace also contains Zn at lower levels, which permits us to identify the shape of the animal. These regions match up with the findings presented in ref. 43, where some images from control and Zn-exposed *D. magna* specimens, obtained with Synchrotron XRF, are shown. From these images, however, it is impossible to determine whether Zn incorporated in the *D. magna* comes from the isotopically enriched water medium or was already incorporated in the body through feeding, an issue of crucial importance within eco-toxicological studies. In fact, although dietary and waterborne Zn toxicity in *D. magna* has been broadly studied before within these eco-toxicological contexts,^{14,22,27} these studies were mainly focused on the determination of total Zn body burdens through digestion and analysis by means of pneumatic nebulization ICP-MS, so that a clear idea could not be given about where and/or why this bio-accumulation takes place.^{9,43} The performance of tracer studies

and acquisition of isotope ratio images instead of elemental distribution images only, as attempted in this work, could help to clarify this issue.

For transforming the elemental images obtained into the corresponding isotope ratio data, the procedure described in Section 2.5 was followed. Fig. 5 shows the isotope ratio images obtained for the same 20 μm section of a *D. magna* specimen presented in Fig. 4. Although the water medium deployed was also enriched in ^{67}Zn , signal intensities for this isotope were very close to the LOD for some of the samples analyzed (especially control specimens) and some of the regions of interest, and therefore, only ^{64}Zn data are discussed. From these images, average isotope ratios were calculated for the different regions of interest (all except the carapace, for which signal intensities were considered too low as to provide reliable results) and for both exposed and non-exposed *D. magna* specimens, following the protocol described in Section 2.5. In order to give an estimation of the analytical uncertainty associated with these values, 4 contiguous sections of the same *D. magna* specimens were ablated in each case (exposed and non-exposed). A typical RSD value is 5%. All of these results are compiled in Fig. 6. To provide an idea of the quality of the data, it needs to be considered that for every thin section analyzed (roughly 0.5–1.0 ng Zn) approximately 3000 pixels of 30 \times 30 μm are obtained. Thus, every pixel would contain 0.15–0.30 pg of Zn. Obviously, the distribution of Zn is not homogeneous, but in the best of cases only a few pg of Zn per pixel are present.

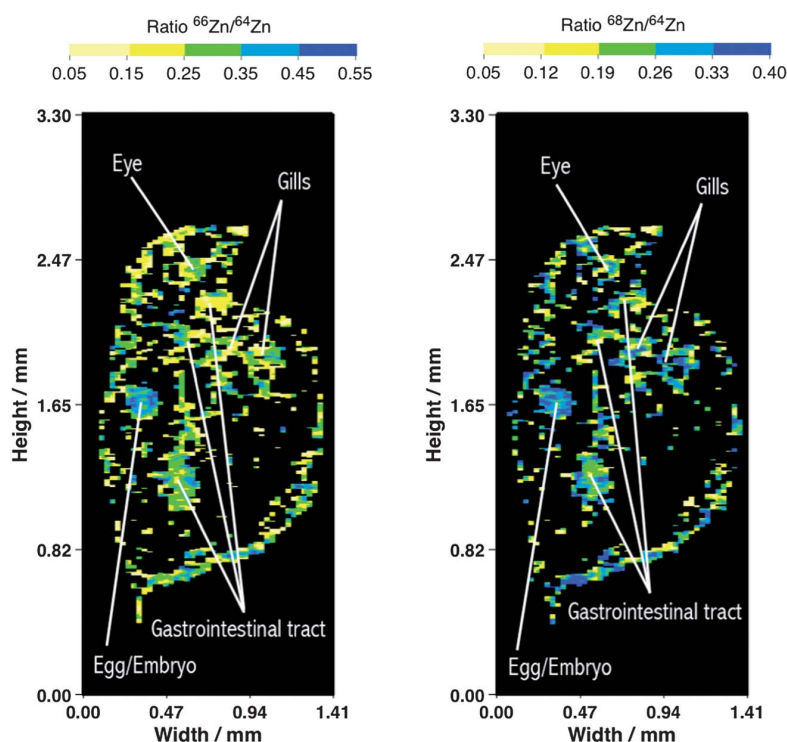


Fig. 5 $^{66}\text{Zn}/^{64}\text{Zn}$ and $^{68}\text{Zn}/^{64}\text{Zn}$ isotope ratio images for the bioaccumulation of Zn in a 20 μm section of a *D. magna* individual exposed to a ^{64}Zn -enriched water medium, obtained following the experimental protocol described in Sections 2.4 and 2.5.

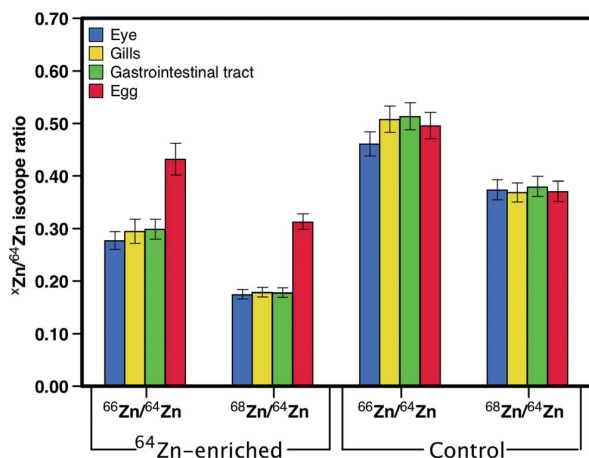


Fig. 6 Mean $^{66}\text{Zn}/^{64}\text{Zn}$ and $^{68}\text{Zn}/^{64}\text{Zn}$ isotope ratio values for the main Zn-accumulating body compartments in four contiguous sections of the same *D. magna* individuals, with one individual exposed to a ^{64}Zn -enriched medium and one control specimen. Analytical uncertainty, u , is given as the standard deviation between sections ($n = 4$). Isotope ratio values expected for Zn of natural isotopic composition: $^{66}\text{Zn}/^{64}\text{Zn} = 0.564$ and $^{68}\text{Zn}/^{64}\text{Zn} = 0.375$, while isotope ratio values for the isotopic spike of Zn added to the water medium are: $^{66}\text{Zn}/^{64}\text{Zn} = 0.042$ and $^{68}\text{Zn}/^{64}\text{Zn} = 0.050$.

As seen from this figure, the difference between the four body areas is not significant in the case of the control (non-exposed) specimens, with ^{64}Zn -related isotope ratios close to the values expected for Zn of natural isotopic abundance (0.564 for $^{66}\text{Zn}/^{64}\text{Zn}$ and 0.375 for $^{68}\text{Zn}/^{64}\text{Zn}$). For exposed specimens, on the other hand, isotope ratios close to the natural values are only obtained for the embryo, while the eye, gills and gastrointestinal tract show significantly lower ^{64}Zn -related isotope ratios, indicating that these regions are richer in the ^{64}Zn coming from the enriched water medium (spike ratios: 0.042 for $^{66}\text{Zn}/^{64}\text{Zn}$ and 0.050 for $^{68}\text{Zn}/^{64}\text{Zn}$). This can also be seen in Fig. 5, as the embryo is clearly bluer (natural ratio) than the other preferential areas, where yellow and green (thus, lower ratios) predominate.

Although interpretation of these experimental findings is beyond the scope of this paper, the fact that the embryo does not seem to be affected by the Zn waterborne exposure could be explained based on the studies of De Schampelaere *et al.*,²² who concluded that Zn assimilated from the diet mainly affects reproduction by accumulating in cells or tissues involved in their parthenogenetic reproduction. Taking into account that no feeding was provided during the 24 hours of exposure to the isotopically enriched water media, it can be presumed that the embryo was already developed prior to the exposure and therefore the enriched medium did not affect the isotopic composition of the Zn present in it.

The results obtained in this paper clearly demonstrate that LA-SF-ICP-MS together with tracer experiments can be deployed for obtaining isotope ratio images in thin sections of biological samples containing very low amounts of the elements of interest (such as Zn), from which important information inaccessible by other analytical techniques can be extracted.

4 Conclusion

This paper discusses all issues that need to be taken into consideration for acquiring isotope ratio images by means of LA-SC-ICP-MS and presents the best conditions found for a particular application: a simple tracer experiment based on the exposure of *Daphnia magna* specimens to a ^{64}Zn -enriched water medium.

An example was given as to how a tracer experiment with a stable isotope followed by isotope ratio imaging can be designed to provide additional information. This approach not only visualizes where the target element is present (as is the case in elemental imaging), but also where specifically the tracer is accumulated. In this way, further spatially resolved and time-resolved information on the element under consideration can be obtained, facilitating the elucidation of, for instance, element uptake routes.

Acknowledgements

This work has been funded by the Spanish Ministry of Economy and Competitiveness (Project CTQ2012-33494) and the Aragón Government (Fondo Social Europeo). M.R.F. thanks the Spanish Ministry of Economy and Competitiveness for her PhD grant (project CTQ2009-08606) and Ghent University for financing her stay at A&MS group (project BOF 01SB0309). M.A. and L.B. thank the FWO for their postdoctoral grants. F.V. thanks UGent for the financial support under the form of a BOF GOA grant. The authors would also like to acknowledge Leen Pieters for arranging the preparation of the histological sections and Thermo Scientific for providing them with the new type of medium resolution slit.

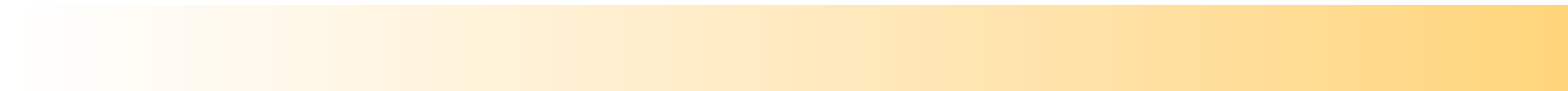
Notes and references

- 1 A. Izmer, D. Gholap, K. De Houwer, F. Cuyckens and F. Vanhaecke, *J. Anal. At. Spectrom.*, 2012, **27**, 413–418.
- 2 J. S. Becker, M. Zoriy, B. Wu, A. Matusch and J. S. Becker, *J. Anal. At. Spectrom.*, 2008, **23**, 1275–1280.
- 3 D. S. Urgast, O. Ou, M.-J. Gordon, A. Raab, G. F. Nixon, I.-S. Kwun, J. H. Beattie and J. Feldmann, *Anal. Bioanal. Chem.*, 2012, **402**, 287–297.
- 4 J. D. Woodhead, J. Hellstrom, J. M. Hergt, A. Greig and R. Maas, *Geostand. Geoanal. Res.*, 2007, **31**, 331–343.
- 5 J. S. Becker, *J. Anal. At. Spectrom.*, 2002, **17**, 1172–1185.
- 6 M. Aramendía, M. Resano and F. Vanhaecke, *J. Anal. At. Spectrom.*, 2010, **25**, 390–404.
- 7 D. S. Urgast, S. Hill, I.-S. Kwun, J. H. Beattie, H. Goenaga-Infante and J. Feldmann, *Metallomics*, 2012, **4**, 1057–1063.
- 8 J. Briceño, M. A. Belarra, K. A. C. De Schampelaere, S. Vanblaere, C. R. Janssen, F. Vanhaecke and M. Resano, *J. Anal. At. Spectrom.*, 2010, **25**, 503–510.
- 9 D. S. Gholap, A. Izmer, B. De Samber, J. T. van Elteren, V. S. Šelih, R. Evens, K. De Schampelaere, C. Janssen, L. Balcaen, I. Lindemann, L. Vincze and F. Vanhaecke, *Anal. Chim. Acta*, 2010, **664**, 19–26.

Paper

- 10 R. Evens, K. A. C. De Schamphelaere, L. Balcaen, Y. Wang, K. De Roy, M. Resano, M. Flórez, N. Boon, F. Vanhaecke and C. R. Janssen, *Aquat. Toxicol.*, 2012, **109**, 80–89.
- 11 R. Evens, K. A. C. De Schamphelaere, L. Balcaen, Y. Wang, K. De Roy, M. Resano, M. del Rosario Flórez, P. van der Meeren, N. Boon, F. Vanhaecke and C. R. Janssen, *Aquat. Toxicol.*, 2011, **105**, 661–668.
- 12 D. M. M. Adema, *Hydrobiologia*, 1978, **59**, 125–134.
- 13 H. C. Poynton, J. R. Varshavsky, B. Chang, G. Cavigliolo, S. Chan, P. S. Holman, A. V. Loguinov, D. J. Bauer, K. Komachi, E. C. Theil, E. J. Perkins, O. Hughes and C. D. Vulpe, *Environ. Sci. Technol.*, 2007, **41**, 1044–1050.
- 14 L. I. L. Balcaen, K. A. C. Schamphelaere, C. R. Janssen, L. Moens and F. Vanhaecke, *Anal. Bioanal. Chem.*, 2008, **390**, 555–569.
- 15 F. Vanhaecke, L. Balcaen and D. Malinovsky, *J. Anal. At. Spectrom.*, 2009, **24**, 863–886.
- 16 D. R. Bandura and S. D. Tanner, *At. Spectrosc.*, 1999, **20**, 69–72.
- 17 M. Resano, P. Marzo, J. Pérez-Arategui, M. Aramendía, C. Cloquet and F. Vanhaecke, *J. Anal. At. Spectrom.*, 2008, **23**, 1182–1191.
- 18 S. A. Crowe, B. J. Fryer, I. M. Samson and J. E. Gagnon, *J. Anal. At. Spectrom.*, 2003, **18**, 1331–1338.
- 19 L. A. Allen, J. J. Leach, H. M. Pang and R. S. Houk, *J. Anal. At. Spectrom.*, 1997, **12**, 171–176.
- 20 M. Resano, M. P. Marzo, R. Alloza, C. Saéñz, F. Vanhaecke, L. Yang, S. Willie and R. E. Sturgeon, *Anal. Chim. Acta*, 2010, **677**, 55–63.
- 21 M. E. Kylander, D. J. Weiss, T. E. Jeffries, B. Kober, A. Dolgoplova, R. Garcia-Sanchez and B. J. Coles, *Anal. Chim. Acta*, 2007, **582**, 116–124.
- 22 K. A. C. De Schamphelaere, M. Canli, V. Van Lierde, I. Forrez, F. Vanhaecke and C. R. Janssen, *Aquat. Toxicol.*, 2004, **70**, 233–244.
- 23 T. Lindemann, M. Hamester, J. Hinrichs, L. Rottmann and J. D. Wills, *Federation of Analytical Chemistry and Spectroscopy Societies (FACSS)*, 2009.
- 24 D. Frei and A. Gerdes, *Chem. Geol.*, 2009, **261**, 261–270.
- 25 D. Bleiner and D. Günther, *J. Anal. At. Spectrom.*, 2001, **16**, 449–456.
- 26 M. S. A. Horstwood, G. L. Foster, R. R. Parrish, S. R. Noble and G. M. Nowell, *J. Anal. At. Spectrom.*, 2003, **18**, 837–846.
- 27 B. T. A. Muysen, K. A. C. De Schamphelaere and C. R. Janssen, *Aquat. Toxicol.*, 2006, **77**, 393–401.
- 28 S. M. Nelms, C. R. Quétel, T. Prohaska, J. Vogl and P. D. P. Taylor, *J. Anal. At. Spectrom.*, 2001, **16**, 333–338.
- 29 B. Hattendorf, C. Latkoczy and D. Günther, *Anal. Chem.*, 2003, **75**, 341A–347A.
- 30 F. Vanhaecke, L. Moens, R. Dams, I. Papadakis and P. Taylor, *Anal. Chem.*, 1997, **69**, 268–273.
- 31 H. P. Longerich, B. J. Fryer and D. F. Strong, *Spectrochim. Acta, Part B*, 1987, **42**, 39–48.
- 32 C. N. Maréchal, P. Télouk and F. Albarède, *Chem. Geol.*, 1999, **156**, 251–273.
- 33 J. Woodhead, *J. Anal. At. Spectrom.*, 2002, **17**, 1381–1385.
- 34 W. A. Russell, D. A. Papanastassiou and T. A. Tombrello, *Geochim. Cosmochim. Acta*, 1978, **42**, 1075–1090.
- 35 M. Berglund and M. E. Wieser, *Pure Appl. Chem.*, 2011, **83**, 397–410.
- 36 T. W. May and R. H. Wiedmeyer, *At. Spectrosc.*, 1998, **19**, 150–155.
- 37 F. Vanhaecke and L. Moens, *Anal. Bioanal. Chem.*, 2004, **378**, 232–240.
- 38 L. Moens, P. Verrept, R. Dams, U. Greb, G. Jung and B. Laser, *J. Anal. At. Spectrom.*, 1994, **9**, 1075–1078.
- 39 J. Lear, D. Hare, P. Adlard, D. Finkelstein and P. Doble, *J. Anal. At. Spectrom.*, 2012, **27**, 159–164.
- 40 C. O'Connor, B. L. Sharp and P. Evans, *J. Anal. At. Spectrom.*, 2006, **21**, 556–565.
- 41 S. M. Eggins and J. M. G. Shelley, *Geostand. Newsl.*, 2002, **26**, 269–286.
- 42 B. Fernández, F. Claverie, C. Pécheyran, J. Alexis and O. F. X. Donard, *Anal. Chem.*, 2008, **80**, 6981–6994.
- 43 B. De Samber, R. Evens, K. De Schamphelaere, G. Silversmit, B. Masschaele, T. Schoonjans, B. Vekemans, C. R. Janssen, L. van Hoorebeke, I. Szalóki, F. Vanhaecke, G. Falkenberg and L. Vincze, *J. Anal. At. Spectrom.*, 2008, **23**, 829–839.

General outline and conclusions
Resumen y conclusiones generales
Algemeen overzicht en conclusies



GENERAL OUTLINE AND CONCLUSIONS

The development and the introduction of commercially available high-resolution continuum source atomic absorption spectrometers had represented a significant step forward in the trajectory of AAS. The instrumental improvements regarding the high intensity continuum light source, the monochromator system and the CCD array detector implied the overcoming of important drawbacks historically associated with LS AAS, particularly focused in the fact that a spectral window is monitored in each measurement recording not only the line of interest but also its spectral environment, with a high resolution (down to 1 pm). Derived benefits imply the resolution of spectral interferences, the potential for multi-element analysis and the possibility of developing analytical methods for the determination of elements for which no HCLs were available (such as non-metals). All these benefits are particularly important when **direct analysis of solid samples or complex matrices** is aimed at. In this context, several aspects concerning the high spatial resolution features offered by the HR CS AAS technique are presented and discussed in the current PhD dissertation:

- The capacity for **monitoring multiple lines** within a given spectral window was explored. A limitation still exists due to the reduced number of pixels of the CCD array detector devoted to signal recording (200). Currently, a range of 0.2-0.3 nm can be monitored in the far-UV region, 0.5 nm in the visible up to approximately 1 nm at a 800 nm wavelength. In this way, in order to be simultaneously recorded, lines need to appear sufficiently close one to another, but separated enough not to suppose a spectral interference due to possible line-broadening effects depending on the amount, and with a suitable sensitivity for the sample content. When

the lines recorded respond to different analytes, possibilities for simultaneous multi-element determination are presented, and the thermochemical behaviour of the target elements need to be considered in order to adequately establish a set of optimal parameters. If, on the other hand, the lines monitored respond to the same species, enhancement of the analytical figures can be attained, depending on the relative sensitivity of the different lines: if the sensitivity is very different, the linear range might be expanded, permitting to analyse samples of different concentrations with ease, while if the sensitivity is similar the lines can be combined so to improve limits of detection and the precision. A general article discussing the possibilities of HR CS AAS for multi-line monitoring, addressing the direct multi-element analysis of solid samples, and a critical review including the findings on the previous work as well as other approaches found in literature are presented in this thesis.

- The advantages of HR CS AAS in terms of **background correction** are further discussed all along most of the articles of this compendium. Being able to record the analytical environment of the lines of interest means a great improvement for detecting spectral interferences. Moreover, the fact that three-dimensional time- and wavelength-resolved absorbance spectra are recorded permits to track the interference during optimization, to find the optimum condition in which it may be avoided or resolved in time. If this is not possible, a mathematical correction based on the application of a least-squares algorithm may be applied whenever a clean reference spectrum of the interfering species is available for subtraction. This strategy permits the direct determination of elements in some samples (*e.g.* Ni in *D. magna*) that would be hardly feasible otherwise.

- The monitoring of molecular absorption bands enables the determination of elements that might pose a problem for atomic absorption spectrometry. **Determination of non-metals** represent a clear example of this situation, as all of them have the principal resonant absorption lines occurring in the vacuum-UV region, inaccessible for the currently available spectrometers. However, some of them (like the halogens, N, P, S) are able to form stable diatomic molecules in gas phase at relatively high temperatures, giving rise to molecular absorption signals of different structures that may be optimized with views to develop quantitative methods. In this work the absorption spectrum of the CS molecule was explored for direct S determination, paying special attention to the use of modifiers for obtaining a signal independent from the chemical form in which the analyte is present within the samples. A suspension of Pd nanoparticles proved to be fit for purpose for a variety of solid samples of different nature (biological, petroleum coke, polyethylene and steel CRMs). Moreover, a method was developed permitting the direct determination of Br in different plastic materials by monitoring the CaBr molecular species. Lastly, AlF molecular absorption band was studied with the aim of presenting a method for direct Al determination in blood samples, free of spectral and non-spectral interferences. A critical review is also included on the current progress of metalloids and non-metals by means of HR CS MAS, covering all the previous studies as well as many other achievements found in the literature of this field.
- The suitability of GFAAS for the **direct analysis of solid micro-samples** has also been demonstrated taking advantage of the benefits of HR CS AAS previously described, giving rise to methods of not only good spatial but high spectral resolution. In this context, a

method was developed for simultaneously determining the total body burden of Cd and Ni in *D. magna* individuals, pointing out the interest of multi-element determination methods when dealing with unique individual micro-samples. Complementarily, another method for micro-samples analysis is presented based on laser ablation sampling followed by ICPMS determination, focusing on the capabilities of LA-ICPMS for gathering isotope information with high spatial resolution. The process of optimization for designing a tracer experiment that may be followed by isotope ratio imaging is illustrated by the acquisition of Zn isotope ratio images of thin sections of *D. magna* specimens. The method proposed enables a resolution of 30 μm and precision values around 5% RSD to be achieved. It is important to stress that such methodology permits visualizing not only where the target element is found, but also where the tracer is really accumulating, a feature that may be of great interest for the elucidation of elemental uptake routes and is beyond the potential of most elemental techniques not based on mass spectrometry.

RESUMEN Y CONCLUSIONES GENERALES

El desarrollo y la disponibilidad comercial de espectrómetros de absorción atómica de alta resolución con fuente continua (HR CS AAS), ha supuesto un avance significativo en la trayectoria de la espectrometría de absorción atómica (AAS). Las mejoras instrumentales en cuanto a la fuente de radiación de alta energía, el sistema de monocromación y el detector con dispositivos de acoplamiento de carga (CCD), han permitido la superación de varios inconvenientes importantes asociados históricamente a la AAS con fuente de línea (LS AAS), debido al hecho de que en cada medida se monitoriza, con una elevada resolución (por debajo de 1 pm), una ventana espectral que engloba no sólo la línea de interés sino también su entorno espectral. Los principales beneficios derivados de este hecho incluyen la resolución de interferencias espectrales, el potencial para llevar a cabo análisis multielementales y la posibilidad de desarrollar métodos analíticos para la determinación de elementos para los cuales no existen lámparas de cátodo hueco disponibles (como es el caso de los no metales). Todas estas ventajas son particularmente importantes cuando se pretende llevar a cabo el análisis **directo de muestras sólidas o matrices complejas**. En este contexto, la presente tesis doctoral evalúa todos los aspectos relacionados con la alta resolución espacial que ofrece la técnica de HR CS AAS:

- Se ha explorado la capacidad para **medir múltiples líneas** dentro de una ventana espectral dada. Sigue existiendo una limitación debida al reducido número de píxeles del detector CCD dedicados al registro de la señal (200). Actualmente, es posible monitorizar un intervalo de 0.2-0.3 nm en la región del UV lejano, 0.5 nm en la región del visible y hasta 1 nm a una longitud de onda de 800 nm. De esta manera, a fin de ser registradas simultáneamente, las líneas

deben aparecer lo suficientemente cercanas una de otra (pero también suficientemente distanciadas para evitar interferencias espectrales debidas a posibles efectos de ensanchamiento de línea que se producen con cantidades de analito elevadas) y con una sensibilidad adecuada al contenido en la muestra. Cuando las líneas registradas corresponden a distintos analitos, se presenta la posibilidad de llevar a cabo la determinación multi-elemental simultánea, y será necesario considerar el comportamiento térmico de los elementos de interés con el fin de establecer un conjunto de parámetros óptimo. Si, por el contrario, las líneas monitorizadas responden a una misma especie será posible obtener una mejora de los parámetros analíticos, dependiendo de la sensibilidad relativa de las diferentes líneas: si la sensibilidad es muy distinta, puede expandirse el rango lineal, lo cual permitirá analizar fácilmente muestras de distinta concentración, mientras que si la sensibilidad es similar, la señal de las distintas líneas puede combinarse para mejorar la precisión y los límites de detección. En esta tesis se presenta un artículo general discutiendo las posibilidades de la técnica de HR CS AAS para la medida de múltiples líneas, abordando el análisis multi-elemental directo de muestras sólidas, y un review crítico que incluye todos estos aspectos y discute todos los estudios encontrados en la literatura.

- Las ventajas de la técnica de HR CS AAS para la **corrección de la señal de fondo** se discuten ampliamente a lo largo de la mayoría de los artículos de este compendio. El hecho de que se pueda registrar el entorno de las líneas de interés constituye una gran mejora a la hora de detectar interferencias espectrales. Además, dado que se registran espectros de absorbancia tridimensionales (resueltos en tiempo y longitud de onda), es posible apreciar la evolución de las

interferencias a lo largo de las etapas de optimización, siendo más sencillo encontrar las condiciones óptimas en las cuales dicha interferencia pueda ser evitada o resuelta en el tiempo. Si la interferencia no pudiera ser resuelta temporal ni espectralmente, es posible aplicar una corrección matemática basada en la aplicación de un algoritmo de mínimos cuadrados siempre y cuando se disponga de un espectro de referencia limpio (libre de la señal analítica de interés) para la sustracción. Esta estrategia permite la determinación directa de elementos en algunas muestras (por ejemplo, Ni en *D. magna*) que de otra manera no sería factible.

- La medida de bandas de absorción molecular habilita la determinación de elementos que siempre han sido problemáticos para AAS. La **determinación de no metales** representa un ejemplo claro de esta situación ya que todos ellos muestran sus principales líneas de absorción en la región del UV lejano, inaccesible para los espectrómetros disponibles comercialmente. No obstante, algunos de ellos (como los halógenos, N, P, S) son capaces de formar moléculas diatómicas estables en fase gas a temperaturas relativamente altas, dando lugar a señales de absorción molecular con diferentes estructuras que pueden ser optimizadas y utilizadas para el desarrollo de métodos cuantitativos de análisis. En este trabajo, se exploró el espectro de absorción de la molécula CS para la determinación directa de S, prestando especial atención al uso de modificantes para obtener una señal independiente de la forma química en la que el analito se encuentra en la muestra. El empleo de una suspensión de nanopartículas de Pd demostró ser adecuado para el análisis directo de una gran variedad de muestras sólidas de diferente naturaleza (CRMs biológicos, de coque de petróleo, de polietileno y de acero). Además, se desarrolló un método para llevar

a cabo la determinación directa de Br en diferentes materiales plásticos mediante la medida de la especie molecular CaBr. Por último, se estudió la banda de absorción molecular de AlF con el objeto de presentar un método, libre de interferencias espectrales y no espectrales, para la determinación directa de Al en muestras de sangre. Se incluye también un review crítico basado en el progreso actual de la determinación de metaloides y no metales por medio de HR CS AAS, abarcando todos los estudios previamente descritos así como otros aportes encontrados en la literatura científica.

- La idoneidad de GFAAS para el **análisis directo de micro-muestras sólidas** ha quedado patente haciendo uso de los beneficios de la técnica de HR CS AAS descritos anteriormente, dando lugar a métodos de alta resolución no sólo espacial, sino también espectral. En este contexto, se desarrolló un método para la determinación simultánea de la bioacumulación total de Cd y Ni en individuos de *D. magna*, resaltando el interés de los métodos de determinación multielemental cuando se trabaja con micro-muestras que sólo se pueden analizar una única vez. De manera complementaria, se presentó otro método para el análisis de micro-muestras basado en el muestreo por ablación láser seguido de la determinación por ICPMS, centrándose en la capacidad de la técnica de LA-ICPMS para recabar información isotópica con alta resolución espacial. El proceso de optimización para el diseño de un experimento con trazadores que puedan ser seguidos mediante el cálculo de relaciones isotópicas es ejemplificado mediante la adquisición de imágenes de relaciones isotópicas de Zn en secciones muy delgadas (20 μm) de especímenes de *D. magna*. El método propuesto hace posible obtener una resolución de 30 μm y valores de precisión alrededor de 5% RSD. Es importante destacar que tal

metodología permite visualizar no sólo dónde se encuentra el elemento de interés, sino dónde se está acumulando realmente el trazador, una característica que puede ser de gran interés para elucidar rutas de absorción de elementos y que queda fuera de las posibilidades de la mayor parte de las técnicas elementales que no estén basadas en espectrometría de masas.

ALGEMEEN OVERZICHT EN CONCLUSIES

De ontwikkeling en commerciële introductie van hoge-resolutie continu bron atoomabsorptiespectrometrie (continuum source atomic absorption spectrometry of CSAAS) betekenden een beduidende stap voorwaarts voor AAS. De technische verbeteringen aan de hoog-intense continu lichtbron, het monochromatorsysteem en de CCD-array detector lieten toe belangrijke nadelen, historisch geassocieerd met lijnbron AAS, te overwinnen. Dit is in de eerste plaats te danken aan het gegeven dat bij elke CSAAS meting niet alleen de betreffende atoomlijn, maar ook de directe spectrale omgeving met hoge resolutie (tot 1 pm) wordt geobserveerd. De voordelen die daaruit voortvloeien omvatten onder meer het resolveren van spectrale interferenties, mogelijkheden tot multi-elementanalyse en de bepaling van elementen waarvoor geen holle kathode lamp (HKL) bestaat (bv. niet-metalen). Deze voordelen zijn bijzonder belangrijk wanneer **vaste monsters** direct worden geanalyseerd (solid sampling) of wanneer **complexe matrices** voorliggen. In dit doctoraatsproefschrift worden verscheidene aspecten gelinkt aan de hoge resolutie geboden door CSAAS belicht en besproken:

- De mogelijkheid tot **observatie van verschillende lijnen** binnen een geselecteerd spectraal venster werd verkend. Deze aanpak is nog steeds gelimiteerd door het beperkte aantal pixels in de CCD-array detector waarmee CSAAS apparatuur is uitgerust (200). Dit betekent dat momenteel een spectrale breedte van 0,2-0,3 nm simultaan kan worden geobserveerd in het verre UV-gebied, van 0,5 nm in het zichtbaar gebied van het spectrum en van 1 nm bij een golflengte van 800 nm. Voor simultane meting moeten de betreffende atoomlijnen bijgevolg enerzijds voldoende dicht bij elkaar gelegen zijn, maar anderzijds ook niet zo dicht dat

spectrale interferentie optreedt ten gevolge van de lijnverbreding, die afhankelijk is van de elementconcentratie. Ook moeten de betrokken lijnen een voldoende intensiteit vertonen om bepaling bij de voorliggende concentraties toe te laten. Wanneer atoomlijnen afkomstig van verschillende analieten aan deze voorwaarden voldoen, ontstaan mogelijkheden voor simultane multi-elementanalyse. Om tot een set van optimale instellingen te komen, moet met de thermochemische eigenschappen van de betrokken elementen rekening worden gehouden. Wanneer de lijnen binnen het spectrale venster van hetzelfde element afkomstig zijn, kunnen de analytische karakteristieken worden verbeterd. Als de lijnen een groot verschil in gevoeligheid vertonen, kan het lineair dynamisch bereik worden uitgebreid, waardoor het makkelijker wordt om stalen met sterk verschillende analietconcentraties te analyseren. Vertonen de lijnen daarentegen een gelijkaardige gevoeligheid, dan kunnen hun intensiteiten worden opgeteld, wat tot een verbeterd detectievermogen en een hogere precisie leidt. Deze thesis bevat een tijdschriftartikel betreffende het gelijktijdig meten van verschillende analietlijnen in de context van de directe analyse van vaste materialen (solid sampling) en een critical review die, naast bevindingen uit eigen solid sampling werk, ook andere benaderingen gerapporteerd in de literatuur bespreekt.

- De voordelen van hoge-resolutie CSAAS in de context van **achtergrondcorrectie** worden geïllustreerd en besproken in de meeste artikels opgenomen in deze doctoraatsverhandeling. De mogelijkheid de directe spectrale omgeving van de analytische lijn te bestuderen, laat toe op eenvoudige wijze het voorkomen van spectrale interferentie na te gaan. Gezien bovendien de spectrale

gegevens in drie dimensies – intensiteit, golflengte en tijd – kunnen worden weergegeven, kan een optredende interferentie in detail worden gekarakteriseerd, zodat optimale condities kunnen worden geselecteerd die toelaten de interferentie te vermijden door het kiezen van een geschikt tijdsinterval voor de meting. Indien dit niet mogelijk is, kan mathematische correctie steunend op een kleinste kwadraten benadering worden doorgevoerd, indien een zuiver referentiespectrum van de interferentie beschikbaar is. Op deze wijze worden bepalingen (bv. Ni in *Daphnia magna*) mogelijk, die anders nauwelijks haalbaar zouden zijn.

- De observatie van moleculaire absorptiebanden laat de bepaling van elementen toe, die anders moeilijk of niet met AAS te bepalen zijn. De **bepaling van niet-metalen** is hier een belangrijk voorbeeld van, vermits voor al deze elementen de belangrijkste resonantielijnen in het vacuüm-UV gebied gelegen zijn, een spectrale range die voor de huidig beschikbare spectrometers niet toegankelijk is. Sommige van deze elementen, zoals de halogenen, N, P en S, vormen echter stabiele diatomische moleculen in de gasfase bij relatief hoge temperatuur, waarvoor moleculaire absorptiesignalen met verschillende structuren worden waargenomen. Methodes werden ontwikkeld voor kwantitatieve elementbepaling steunend op observatie van deze moleculaire absorptiebanden. In dit werk werd het gebruik van het absorptiespectrum van de CS-molecule voor de directe bepaling van S in vaste materialen verkend. Hierbij werd vooral aandacht besteed aan het gebruik van een modifier, die moet verzekeren dat het signaal onafhankelijk is van de chemische vorm waarin het analietelement voorkomt in het monster. Er werd aangetoond dat

een suspensie van nanopartikels van Pd geschikt is als modifier voor een wijde variëteit aan monsters (materiaal van biologische oorsprong, cokes, polyethyleen en staal referentiematerialen). Ook een methode voor de bepaling van Br in verschillende types polymeren werd ontwikkeld, steunend op de observatie van CaBr moleculaire species. Ten slotte werd ook de interferentievrije bepaling van Al in volbloed gerealiseerd via observatie van de moleculaire band van AlF. Dit proefschrift bevat tevens een critical review die de vooruitgang beschrijft inzake de bepaling van halfmetalen en niet-metalen via hoge-resolutie continu bron molecuulabsorptiespectrometrie. Daarin worden niet alleen de analyseprotocollen ontwikkeld in dit doctoraat beschreven, maar ook vele andere vorderingen gerapporteerd in de literatuur.

- Ook de inzetbaarheid van GFAAS voor de **analyse van vaste micro-stalen** werd gedemonstreerd. Bij de ontwikkeling van deze methodes werd gesteund op de eerder vermelde voordelen van hoge-resolutie CSAAS en konden hoge ruimtelijke en hoge spectrale resolutie aan elkaar worden gekoppeld. In deze context werden methodes ontwikkeld voor de gelijktijdige bepaling van de “totale belasting” (totaal gehalte in het lichaam) van Cd en Ni in individuele *Daphnia magna* organismen. Het simultaan karakter van de bepaling is in deze context cruciaal omdat een individueel organisme vanzelfsprekend maar één keer kan geanalyseerd worden. Voor de analyse van individuele *Daphnia magna* organismen werd ook een alternatieve aanpak op basis van bemonstering via laser ablatie (LA) en detectie met ICP-massaspectrometrie (ICP-MS) ontwikkeld, met als doel het verwerven van informatie inzake de isotopische samenstelling van een targetelement met hoge ruimtelijke resolutie. Na optimalisatie

van een tracerexperiment, werd LA-ICP-MS ingezet voor de visualisatie van de verdeling van Zn-isotopenverhoudingen over dunne secties van *Daphnia magna*. Met het ontwikkelde protocol werd een ruimtelijke resolutie van 30 μm en een precisie van 5% RSD gerealiseerd. Deze aanpak laat niet alleen toe te ontrafelen hoe het bestudeerde is verdeeld, maar ook waar de tracer na opname accumuleert. Deze informatie kan van groot belang zijn om inzicht te verwerven in de opnameroutes en is ontoegankelijk voor de meeste methodes voor elementbepaling die niet op massaspectrometrie gebaseerd zijn.

Appendix



APPENDIX

The current PhD dissertation is structured as a compendium of nine already published articles. Complete references of these articles are listed below (in chronological order), along with the impact factors and subject categories of each of the journals in which they were published.

1. On the possibilities of high-resolution continuum source graphite furnace atomic absorption spectrometry for the simultaneous or sequential monitoring of multiple atomic lines

M. Resano, L. Rello, M. Flórez, M.A. Belarra

Spectrochimica Acta Part B 66 (2011) 321-328

Journal impact factor 2012 (JCR ISI): 3.141

Subject categories (Journal ranking): Spectroscopy (8/43, Q1)

2. Al determination in whole blood samples as AlF *via* high-resolution continuum source graphite furnace molecular absorption spectrometry: potential application to forensic diagnosis of drowning

M. Aramendía, M.R. Flórez, M. Piette, F. Vanhaecke, M. Resano

Journal of Analytical Atomic Spectrometry 26 (2011) 1964-1973

Journal impact factor 2012 (JCR ISI): 3.155

Subject categories (Journal ranking): Analytical Chemistry (17/75, Q1), Spectroscopy (7/43, Q1)

3. Liposomes as an alternative delivery system for investigating dietary metal toxicity to *Daphnia magna*

R. Evens, K.A.C. De Schamphelaere, L. Balcaen, Y. Wang, K. De Roy, M. Resano, M.R. Flórez, P. Van der Meeren, N. Boon, F. Vanhaecke, C.R. Jansen

Aquatic Toxicology 105 (2011) 661-668

Journal impact factor 2012 (JCR ISI): 3.730

Subject categories (Journal ranking): Marine and Freshwater Biology (4/100, Q1), Toxicology (15/85, Q1)

4. The use of liposomes to differentiate between the effects of nickel accumulation and altered food quality in *Daphnia magna* exposed to dietary nickel

R. Evens, K.A.C. De Schamphelaere, L. Balcaen, Y. Wang, K. De Roy, M. Resano, M.R. Flórez, N. Boon, F. Vanhaecke, C.R. Jansen

Aquatic Toxicology 109 (2012) 80-89

Journal impact factor 2012 (JCR ISI): 3.730

Subject categories (Journal ranking): Marine and Freshwater Biology (4/100, Q1), Toxicology (15/85, Q1)

5. Direct determination of sulfur in solid samples by means of high-resolution continuum source graphite furnace molecular absorption spectrometry using palladium nanoparticles as chemical modifier

M. Resano, M.R. Flórez

Journal of Analytical Atomic Spectrometry 27 (2012) 401-412

Journal impact factor 2012 (JCR ISI): 3.155

Subject categories (Journal ranking): Analytical Chemistry (17/75, Q1), Spectroscopy (7/43, Q1)

6. Isotope ration mapping by means of laser ablation-single collector-ICP-mass spectrometry: Zn tracer studies in thin sections of *Daphnia magna*

M.R. Flórez, M. Aramendía, M. Resano, A.C. Lapeña, L. Balcaen, F. Vanhaecke

Journal of Analytical Atomic Spectrometry 28 (2013) 1005-1015

Journal impact factor 2012 (JCR ISI): 3.155

Subject categories (Journal ranking): Analytical Chemistry (17/75, Q1),
Spectroscopy (7/43, Q1)

7. High-resolution continuum source atomic absorption spectrometry for the simultaneous or sequential monitoring of multiple lines. A critical review of current possibilities

M. Resano, M.R. Flórez, E. García-Ruiz

Spectrochimica Acta Part B 88 (2013) 85-97

Journal impact factor 2012 (JCR ISI): 3.141

Subject categories (Journal ranking): Spectroscopy (8/43, Q1)

8. Direct determination of bromine in plastic materials by means of solid sampling high-resolution continuum source graphite furnace molecular absorption spectrometry

M.R. Flórez, M. Resano

Spectrochimica Acta Part B 88 (2013) 32-39

Journal impact factor 2012 (JCR ISI): 3.141

Subject categories (Journal ranking): Spectroscopy (8/43, Q1)

9. Progress in the determination of metalloids and non-metals by means of high-resolution continuum source atomic or molecular absorption spectrometry. A critical review

M. Resano, M.R. Flórez, E. García-Ruiz

Analytical and Bioanalytical Chemistry 406 (2014) 2239-2259

Journal impact factor 2012 (JCR ISI): 3.659

Subject categories (Journal ranking): Analytical Chemistry (9/75, Q1),
Biochemical Research Methods (18/75, Q1)

Justification of the contribution of the PhD student

The PhD student, Ms. María del Rosario Flórez García, has carried out the whole experimental work gathered in the current doctoral thesis and has actively collaborated in the experimental design, evaluation of results and realization of the previously presented publications.




RENUNCIA DE LOS COAUTORES DE LOS TRABAJOS PRESENTADOS COMO PARTE DE UNA TESIS DOCTORAL EN LA MODALIDAD DE COMPENDIO DE PUBLICACIONES

1.- Datos personales del coautor		
Apellidos: Rello Varas	Nombre: Luis	
DNI/Pasaporte/NIE: 29102441N	Teléfono 636412106	Correo electrónico luisrello@gmail.com

2.- Tesis Doctoral
Título: High spectral and spatial resolution for the direct elemental and isotopic analysis of solid samples and complex matrices
Autor: María del Rosario Flórez García
Programa de doctorado: Ciencia Analítica en Química (RD 1393/2007)

3.- Publicaciones que formarán parte de la tesis y de las que el firmante es coautor
On the possibilities of high-resolution continuum source graphite furnace atomic absorption spectrometry for the simultaneous or sequential monitoring of multiple atomic lines M. Resano, L. Rello, M. Flórez, M.A. Belarra Spectrochimica Acta Part B 66 (2011) 321-328

RENUNCIA:
Renuncio a que las publicaciones anteriores puedan ser presentadas como parte de otra tesis doctoral en la modalidad de compendio de publicaciones.
<lugar>, <fecha> ZARAGOZA, 27 de mayo de 2014
 Firma: